



The 11th International Conference of Young Scientists on Energy Issues

Kaunas, Lithuania, May 29–30, 2014

Organized by

Lithuanian Energy Institute

In cooperation with:

AGA

HNIT-BALTIC

Reo Investment

Chairman of the Conference

prof. Eugenijus Ušpuras

Chairman of the Organizing Committee

dr. Diana Meilutytė-Lukauskienė

INTERNATIONAL SCIENTIFIC COMMITTEE

Andres Siirde	Estonia	Mantas Marčiukaitis	Lithuania
Andris Kreslins	Latvia	Namejs Zeltins	Latvia
Alessandro Petruzzi	Italy	Pierre-Etienne Labeau	Belgium
Bernhard Peters	Luxemburg	Panos M. Pardalos	USA
Bjørn C. Hauback	Norway	Ralf Ebinghaus	Germany
Darius Milčius	Lithuania	Sten Bergstrom	Sweden
Enn Mellikov	Estonia	Sigitas Rimkevičius	Lithuania
Eugenijus Ušpuras	Lithuania	Sergej Zhdanok	Belarus
Finn Ravndal	Norway	Victor A. Zhovyansky	Ukraine
Florentin Paladi	Moldova	Vaclovas Miškinis	Lithuania
Luis E. Herranz	Spain	Virginijus Radziukynas	Lithuania
Myriam Lazard	France	Vytautas Martinaitis	Lithuania

The Board of Reviewers was formed from experts in the field of the Conference topics.

Board of Reviewers

Alessandro Petruzzi	Italy	Liudvikas Pranevičius	Lithuania
Algirdas Gulbinas	Lithuania	Linas Miknius	Lithuania
Algirdas Jasinskas	Lithuania	Liutauras Marcinauskas	Lithuania
Andres Siirde	Estonia	Luis E. Herranz	Spain
Andris Kreslins	Latvia	Mantas Marčiukaitis	Lithuania
Artur Rogoža	Lithuania	Marija Eidukevičiūtė	Lithuania
Arturas Klementavičius	Lithuania	Marijus Šeporaitis	Lithuania
Artūras Šmaižys	Lithuania	Martynas Lelis	Lithuania
Arvidas Galdikas	Lithuania	Marius Aleinikovas	Lithuania
Arvydas Adomavičius	Lithuania	Mindaugas Ažubalis	Lithuania
Asta Malakauskaitė	Lithuania	Mindaugas Jakubčionis	Lithuania
Aleksandras Iljinas	Lithuania	Mindaugas Vaišnoras	Lithuania
Asta Narkūnienė	Lithuania	Mindaugas Valinčius	Lithuania
Audrius Jonaitis	Lithuania	Myriam Lazard	France
Aurimas Lisauskas	Lithuania	Namejs Zeltins	Latvia
Aušra Pažėraitė	Lithuania	Narimantas Listopadskis	Lithuania
Bernhard Peters	Luxemburg	Nerijus Pedišius	Lithuania
Bjørn C. Hauback	Norway	Nerijus Striūgas	Lithuania
Brigita Abakevičienė	Lithuania	Panos M. Pardalos	USA
Česlovas Christauskas	Lithuania	Pierre-Etienne Labeau	Belgium
Dainius Martuzevičius	Lithuania	Raimondas Bliūdžius	Lithuania
Dalia Grigaliūnienė	Lithuania	Raimondas Pabarčius	Lithuania
Dalia Jankūnaitė	Lithuania	Ralf Ebinghaus	Germany
Dalia Štreimikienė	Lithuania	Ramūnas Gatautis	Lithuania
Dalius Tarvydas	Lithuania	Reda Čerapaitė-Trušinskienė	Lithuania
Danas Ridikas	Austria	Regina Kalpokaitė-Dičkuvienė	Lithuania
Darius Albrektas	Lithuania	Ričardas Krikštolaitis	Lithuania
Darius Biekša	Lithuania	Rimantas Levinskas	Lithuania
Darius Milčius	Lithuania	Rolandas Jonynas	Lithuania
Darius Virbukas	Lithuania	Robertas Alzbutas	Lithuania

Diana Meilutytė-Lukauskienė	Lithuania	Robertas Navakas	Lithuania
Diana Adlienė	Lithuania	Robertas Poškas	Lithuania
Diana Šarauskienė	Lithuania	Rolandas Urbonas	Lithuania
Egidijus Norvaiša	Lithuania	Romualdas Kėželis	Lithuania
Egidijus Saulius Juodis	Lithuania	Romualdas Škėma	Lithuania
Egidijus Urbonavičius	Lithuania	Saulė Milčiuvienė	Lithuania
Eglė Biekšienė	Lithuania	Sergej Zhdanok	Belarus
Eglė Jaraminienė	Lithuania	Sigitas Kadiša	Lithuania
Enn Mellikov	Estonia	Sigitas Rimkevičius	Lithuania
Ernestas Narkūnas	Lithuania	Stanislovas Vrubliauskas	Lithuania
Eugenija Farida Dzenajavičienė	Lithuania	Stasys Šinkūnas	Lithuania
Eugenijus Perednis	Lithuania	Sten Bergstrom	Sweden
Eugenijus Ušpuras	Lithuania	Tomas Sabonis	Lithuania
Finn Ravndal	Norway	Vaclovas Kveselis	Lithuania
Florentin Paladi	Moldova	Vaclovas Miškinis	Lithuania
Giedrius Laukaitis	Lithuania	Vaidas Matuzas	Lithuania
Giedrius Šiupšinskas	Lithuania	Valdas Girdauskas	Lithuania
Gintautas Miliauskas	Lithuania	Valdas Ragaišis	Lithuania
Grigorijus Duškesas	Lithuania	Valentinas Klevas	Lithuania
Inga Konstantinavičiūtė	Lithuania	Victor A. Zhovyansky	Ukraine
Inga Radžiūnienė	Lithuania	Vidas Lekavičius	Lithuania
Inga Stasiulaitienė	Lithuania	Viktorija Grigaitienė	Lithuania
Inga Valuntienė	Lithuania	Vilma Čipinytė	Lithuania
Irina Kliopova	Lithuania	Violeta Makarevičienė	Lithuania
Jolanta Dvarionienė	Lithuania	Violeta Motuzienė	Lithuania
Jonas Baltrušaitis	USA	Violeta Vaitkevičienė	Lithuania
Juozas Gudžinskas	Lithuania	Virginijus Radziukynas	Lithuania
Jūratė Karbauskaitė	Lithuania	Virginijus Vileiniškis	Lithuania
Jūratė Kriaučiūnienė	Lithuania	Vitas Valinčius	Lithuania
Jurij Tonkonogij	Lithuania	Vykintas Šuksteris	Lithuania
Justas Kažys	Lithuania	Vytautas Janilionis	Lithuania
Karolina Čepurnienė	Lithuania	Vytautas Martinaitis	Lithuania
Karolis Banionis	Lithuania	Vytis Kopustinskas	Italy

Kęstutis Čiuprinskas	Lithuania	Vladislovas Algirdas Katinas	Lithuania
Kęstutis Valančius	Lithuania	Žaneta Stasiškienė	Lithuania
Kęstutis Venslauskas	Lithuania	Žilvinas Nakutis	Lithuania
Kristina Brinkienė	Lithuania	Živilė Rutkūnienė	Lithuania
Kristina Ukvalbergienė	Lithuania	Žydrė Kadžiulienė	Lithuania

Dear Reader of the Conference proceedings,

We are glad to continue a work, which has started a decade ago and became a nice annual tradition, and proud to bring together talented young scientists to participate in the 11th International Conference of Young Scientists on Energy Issues 2014 (CYSENI 2014). We expect that this will contribute to improved knowledge of young researchers, development of their acquired abilities and contribute to increasing level of exercised scientific research activities.

The initiative for such an event came from young and enthusiastic researchers of Lithuanian Energy Institute (LEI). They realised that there are a lot of young, smart and science-oriented young people who do research in the energy area and they do need a place and time to meet each other to share their views, generated ideas and present the latest research results.

The first Conference was organized by young researchers with the supervision of experienced scientists from LEI in 2004.

In 2005, it became a national Conference with participants from Kaunas University of Technology, Vilnius Gediminas Technical University, Vilnius University, Vytautas Magnus University – in fact from all science and education institutions of Lithuania involved in energy-related topics.

The next year (2006) was devoted to strengthening the status of the Conference among young researchers and their experienced supervisors. We tried to bring them the message that targets can be reached with joint efforts and collaboration in a small country.

In 2007, the Organising Committee decided to put emphasis both on regional and international dimensions of the Conference. The participants from neighbouring countries – Belarus and Poland participated in the Conference for the first time. We realised that young researchers facing challenges in energy research need to be brought together as much as possible to create a critical mass, to be competent and competitive for the future research. Thus, the Conference was not only intended for the increase of the participants' competence by involvement of the best experienced scientists as peer reviewers, involvement of the participants in the review process of their colleagues (educational exercise), but also to expand geographically.

In 2008, we welcomed the participants from Belarus, Estonia, India, Latvia, Lithuania and Russia.

In 2009 the outcomes of the Conference (in terms of scientific papers) was contributed by the young scientists from Belarus, Estonia, Italy, Latvia, Lithuania, Nigeria and Ukraine.

With a growing attention to this annual event the Conference proceedings included the papers with scientific results of researchers from various Lithuanian science and research institutions and foreign institutions (Belarus, Estonia, Germany, Italy, Latvia, Nigeria, Norway and Ukraine) in 2010.

In total 69 papers of young scientists' from various Lithuanian science and research institutions and foreign institutions in Belarus, Estonia, Germany, Latvia, Nigeria, Poland, Taiwan and Ukraine were reviewed and accepted for the publication in 2011.

In 2012, even 81 young scientists took part in the conference (CYSENI 2012) and presented the results of their research.

Conference celebrated its 10 years anniversary in 2013. This time there were submitted 130 abstracts, 100 papers were reviewed and 80 papers were accepted to the Conference. The authors were not just from Lithuanian institutions, but also from neighbouring countries – Latvia, Estonia, Poland, Belarus, Ukraine, Moldova, Georgia, Romania, Nigeria, Indonesia and Taiwan.

This year we are pleased that young scientists further found the Conference valuable to present their up to date research results and share scientific experience.

This event in Institute is usually full of pleasant atmosphere, interesting and valuable discussions and cheerful social programme. The greetings and acknowledgments of the participants encourage us to keep these moments in mind and improve the future CYSENI Conferences. Regarding the next year we already invite you to the 12th International Conference of Young Scientists on Energy Issues 2015 (CYSENI 2015), which will be held in 27-28 May, 2015 in Kaunas, Lithuania.

Sincerely,
Conference Organizers

CONTENT

I HYDROGEN AND FUEL CELLS (1)

M. Urbonavičius, D. Milčius

Hydrogen generation from reaction between plasma activated aluminum powder and water I-1

II RENEWABLE ENERGY SOURCES (12)

I. Murauskaitė

Interaction between district heating producers and consumers: the case of the use of large-scale renewable energy II-9

I. Pučka, D. Lazdiņa

Radial growth changes in *salix caprea* l. and *salix alba* l. stands II-17

Iłona Alisauskaite-Seskiene

Renewable energy sources technology assessment and promotion..... II-27

A. Kalnacs, J. Kalnacs, A. Mutule, V. Entins

Ways to increase the efficiency of hydrokinetic devices and their evaluation II-38

N. Urbonas, A. Kanapickas

Analysis of the impact of climate change on wind energy resources II-46

S. Alyokhina, O. Senetskyi

The use of turbines that work on organic rankine cycle for small enterprises II-56

P. Pikk, A. Annuk

PVT cooling and hot water solar fraction in northern latitudes II-63

B. Butkutė, J. Cesevičienė, E. Norkevičienė

Development of low-cost and Rapid method for the evaluation of organic and inorganic components in switchgrass biomass II-69

K. Meile, A. Zhurinsh, B. Spince

Periodate oxidation for the determination of levoglucosan and total sugars in pyrolysis liquids II-79

G. Gecevičius, M. Marčiukaitis

Technical and economic evaluation of wind turbines in different regions of Lithuania II-86

J. Guilbaud

Economic assessment of hybrid solar/battery power generation system for the mining industry II-96

A.V. Lozhachnik, V.V. Sauchyn, A.N. Nikanchuk, G.V. Dolhonenka

Technology of rubber waste treatment..... II-106

III SMART ENERGY NETWORKS (4)

A. Pensini, A. Mammoli

Feasibility of optimizing large utility electricity customers on a distribution feeder III-112

L.Grackova, I. Oleinikova, G. Klavs

Role of electrical vehicles for improvement of electrical networks efficiency III-120

Y.K. Bhateshvar, H.D. Mathur

Inter-area oscillation control with super conducting magnetic energy storage in thermal-hydro power system using optimized intelligent controller..... III-129

V. Jurkans, J. Blums

Impact of Peltier element supplied power characteristics on short term cooling performance III-140

IV ENERGY EFFICIENCY AND RELIABILITY (6)

A.A. Brin

Optimization of the mechanical draft cooling tower performance IV-149

G. Fridenbergs, A. Lešinskis

Experimental stand device modeling for IEAC thermal performance study IV-158

S.C. Nwanya, O.V. Ekechukwu

Energy efficiency and carbon footprint for the brewery industry in Nigeria IV-169

T. Iešmantas, R. Alzbutas

Bayesian methodology for fusion plant reliability data analysis IV-181

K. Vagolinš

Using straw for high efficiency district heating systems IV-194

M.Yu. Liakh, A.P. Tsitovich, A.A. Khartonik

Experimental and numerical investigation of the thermal conditions of plasma lamp IV-205

V KNOWLEDGES FOR ENERGY POLICY MAKING (7)

J. Juozaitis

Possibilities to use Lithuania's membership in the international organizations as an instrument in neutralizing the threats to state's energy security V-213

J. Paškevičius

The energy charter process V-224

J. Lunytė,

EU Energy: security in unity V-232

Z. Gachechiladze, I. Pirveli, N. Sumbadze

Strategic planning of sustainable energy development for Georgia V-242

O. Ruksans, I. Oleinikova

Electricity market integration and monitoring V-252

A. Lvovs

Study on customer costs of reliability as key prerequisite for power supply reliability level performance-based regulation V-259

A. Obushevs, I. Oleinikova

Transmission expansion planning considering electricity market and integration of renewable generation V-270

VI INVESTIGATIONS IN THE FIELDS OF THERMAL PHYSICS, FLUID MECHANICS AND METROLOGY (1)

P.S. Grinchuk, N.I. Stetukevich

Minimum of effective thermal conductivity coefficient in fibrous materials at high temperatures: theoretical explanation of experimental results VI-281

VII MATERIALS SCIENCES AND TECHNOLOGY (7)

R.Vessart, T.Unt, A. Mere, M.Krunks

Structural and electrical properties of P-type NiO thin films deposited by spray pyrolysis heterostructures VII-290

I. Gromyko, T. Dedova, M. Krunks, V. Mikli, T. Unt, I. Oja Acik, A. Mere

Zinc oxide rods on different tco substrates and seed layers by electrochemical deposition VII-298

P.S. Grinchuk, S.M. Danilova-Tretiak, N.I. Stetukevich

Force chains as the main mechanism of thermal conductivity of granular matter under stress VII-306

D.V. Solovej, E.V. Batirev, S.A. Filatov, G.S. Kuczynski

Thermal transformation and raman structural investigation of the nanoporous tin oxide VII-314

<u>A. Kiyanitsa, S. Gaidukov, E. Zukulis, I. Juhnevica</u>	
Preparation and properties of polyethylene oxide composites	VII-322
<u>Š. Varnagiris, D. Milčius</u>	
Ageing and surface characteristics investigation of expanded polystyrene treated in air and argon plasma	VII-333
<u>V.V. Sauchyn, A.V. Lozhachnik, Hr.V. Dalholenka, D.V. Skamarokhau</u>	
Plasma system for ash residues processing	VII-339

VIII INVESTIGATIONS OF COMBUSTION AND PLASMA PROCESSES (5)

<u>A. Tamošiūnas, P. Valatkevičius, V. Grigaitienė, V. Valinčius</u>	
Diagnostics of the atmospheric pressure thermal arc plasma by enthalpy probe method	VIII-348
<u>A. Saliamonas, N. Striūgas, R. Navakas</u>	
Spectroscopic analysis of syngas generated from wooden pellets addition to natural gas combustion.....	VIII-353
<u>S.I. Dmitriev, P.S. Grinchuk, N.V. Pavljukovich</u>	
Carbon black production from different types of raw material: Experiments and mathematical modelling	VIII-361
<u>R. Paulauskas, A. Džiugys, N. Striūgas</u>	
Experimental investigation of wood pellet shrinking during pyrolysis	VIII-373
<u>K. Zakarauskas, N. Striūgas</u>	
Experimental investigation of additional reforming process of syngas using biomass char	VIII-379

IX GLOBAL CHANGE AND ECOSYSTEMS (1)

<u>M. Ruduks, A. Lešinskis</u>	
Generation of a typical meteorological year for Alūksne, Latvia	IX-384

XI NUCLEAR FISSION AND RADIATION PROTECTION (3)

<u>X.C. Arnoult, M.Zychova, E. Krecanova, J. Berka, F. Di Gabriele, O. Srba</u>	
New nuclear advanced facilities at CVRZ	XI-392
<u>S. Alyokhina, A. Feshchenko</u>	
The definition of maximum temperature in ventilated container with spent nuclear fuel	XI-400
<u>A. Šutas</u>	
Analysis of the fuel rods degradation in Ignalina NPP spent fuel pools in case of loss of coolant accident	XI-406

HYDROGEN GENERATION FROM REACTION BETWEEN PLASMA ACTIVATED ALUMINUM POWDER AND WATER

M. Urbonavičius, D. Milčius

Lithuanian Energy Institute

Breslaujos str. 3, LT-44403 Kaunas – Lithuania

ABSTRACT

Reaction of aluminum with water ($2\text{Al} + 3\text{H}_2\text{O} \rightarrow \text{Al}_2\text{O}_3 + 3\text{H}_2$) is of interest for hydrogen generation for a wide range of applications. Gravimetric hydrogen capacity from this reaction is 3.7 wt. %. Aluminum is appropriate material because of its availability, environmental safety, low price and high efficiency. According to literature, 1245 cm^3 of H_2 could be generated when 1 g of Al completely reacts with water. Although this concept is not new but it has some challenges. Aluminum-water reaction is thermodynamically favorable (exothermic) but does not proceed due to passivation of aluminum surface by a protective oxide layer which prevents from direct contact between water and aluminum metal particles. The aim of this research is activation of aluminum powder and disruption of oxide layer under hydrogen plasma treatment on purpose to produce hydrogen from water.

Aluminum powder was activated under hydrogen plasma using magnetron for 1 and 3 hours. Al-water reaction is more effective using promoters. Fast and significant hydrogen generation was observed after aluminum powder immersion into alkaline water, while reaction did not proceed with untreated Al. Such concept could be used to provide hydrogen for H_2 powered portable devices. All samples were characterized by SEM (scanning electron microscopy), EDS (energy dispersive X-ray spectroscopy) for elemental analysis, XRD (X-ray diffraction) for microstructure analysis, and gas (O, N, and H) content analyzer.

Keywords: aluminum, plasma, hydrogen generation, water

1. INTRODUCTION

Hydrogen is one of the best energy carriers that can be consumed converting chemical energy into electrical energy with high performance [1]. Fuel cells which use hydrogen have the real potential to a future sustainable energy system with zero CO_2 emission. Although hydrogen has a high calorific value and its reaction byproduct is environmentally friendly but expensive and technologically complicated methods for hydrogen production and storage must be employed [2]. Hydrogen gas is mainly produced by steam reforming of hydrocarbons (usually methane). Also hydrogen can be extracted by means of various methods including biological process, photo-electrochemical methods, coal gasification, and water electrolysis [3].

In order to use hydrogen in microfuel cells for application in portable electronics, there is a need for hydrogen storage. Therefore in-situ hydrogen generation materials are sought [4]. Currently, various metal hydrides (MgH_2 , LiH , NaH , LiBH_4 , NaBH_4) are used for reaction with water. But most of them are very expensive, for example 1 kg of NaBH_4 costs US\$ 55, also some are unstable and have limited solubility [5].

Another approach is provided by use aluminum (Al) for hydrogen production on-board. Hydrogen is generated through the following basic aluminum oxidation reactions: (1) $2\text{Al} + 6\text{H}_2\text{O} \rightarrow 2\text{Al}(\text{OH})_3 + 3\text{H}_2$; (2) $2\text{Al} + 4\text{H}_2\text{O} \rightarrow 2\text{AlO}(\text{OH}) + 3\text{H}_2$; (3) $2\text{Al} + 3\text{H}_2\text{O} \rightarrow \text{Al}_2\text{O}_3 + 3\text{H}_2$ [6]. All byproducts (bayerite- $\text{Al}(\text{OH})_3$, boehmite- $\text{AlO}(\text{OH})$ and aluminum oxide- Al_2O_3) of these reactions are solid. Hydrogen generation from this reaction becomes interesting because of its low cost, simplicity of H_2 generation system, pure hydrogen generation with high humidity and relatively high gravimetric hydrogen capacity (3.7 wt. %) [7]. According to before mentioned reaction, about 1245 cm^3 of hydrogen could be collected after complete

reaction between 1 gram of Al and water. The byproducts are stable and non-corrosive. Aluminum hydroxide can be used as an effective absorbent in chromatography or flame retardant. Alumina (Al_2O_3) can be used as catalyst, an additive of paints and pigment, etc [8]. Aluminum is one of the most widespread metals in the crust [9].

Although the reaction is thermodynamically favorable and aluminum is one of the most reactive metals, it is passivated by formation of thin, coherent about 5 nm thickness oxide film (Al_2O_3) after exposure to air [10]. This oxide film on the surface prevents aluminum-water reaction.

There are many techniques of removing aluminum oxide layer, such as adding alkaline catalysts, using oxide or inorganic salts additives (KCl, NaCl), forming aluminum alloys with other metals (Ga, In, Sn, Bi, Ni etc.), mechanical activation (milling) [7–9]. Also hydrogen generation rate depends on aluminum particle size, water temperature and Al/water mass ratio [11].

In present research aluminum powder was activated under hydrogen plasma treatment where surface energy of powder has been increased. Further activated aluminum powder was immersed in water with small amount of NaOH promoter dissolved and hydrogen generation was investigated. Therefore sodium hydroxide acts as catalyst to produce hydrogen in the reaction: $2\text{Al} + 6\text{H}_2\text{O} + 2\text{NaOH} \rightarrow 2\text{NaAl}(\text{OH})_4 + 3\text{H}_2$ [1].

2. METHODOLOGY

2.1. Activation technique

Aluminum powder (with size 10–75 μm) was placed in vacuum chamber under the circular magnetron (Al cathode) which was used as a source of plasma (Fig. 1). A vacuum system including rotary and diffusion pumps enabled a base pressure of 1.1 mTorr ($\sim 1.5 \cdot 10^{-1}$ Pa). Plasma activation was performed at 12 Pa of hydrogen as working gas. DC power supply was used to generate plasma. The power dissipated in plasma was approximately 300 W. Al powder was treated under hydrogen plasma for 1 and 3 hours.

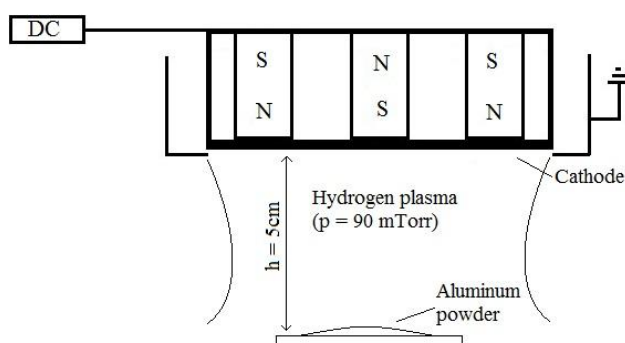


Fig. 1. The experimental scheme

2.2. Analysis methods

The microstructure of aluminum powder samples was characterized by X – ray diffraction (XRD) method using Bruker diffractometer (Bruker D8). The measurements were performed at 2θ angle in the range $20\text{--}70^\circ$ using Cu $K\alpha$ radiation ($\lambda = 0.15406$ nm) in steps of 0.01° . The identification of peaks has been done using *EVA Search – Match* software. The powder views before and after hydrogen plasma treatment was investigated by the scanning

electron microscopy (SEM, Hitachi S-3400N). Concentrations of oxygen, nitrogen and hydrogen within the samples were measured using gas analyzer (HORIBA EMGA 830).

3. RESULTS

3.1. XRD analysis

Fig. 2 includes X – ray diffraction patterns of untreated aluminum powder – curve 1 and plasma treated at power 300 W for 1 hour – curve 2 and 3 hours – curve 3. Aluminum peaks with cubic crystallographic orientation (111), (200) and (220) were registered at $2\theta = 38.3^\circ$, 44.6° and 65° , respectively in all samples. Moreover it was observed that intensity of predominant peak Al (111) increased after plasma activation meanwhile intensity of Al (200) and Al (220) peaks decreased. Small peaks of tetragonal aluminum oxide Al_2O_3 (104) and orthorhombic aluminum hydroxides $\text{Al}(\text{OH})_3$ (121) and $\text{AlO}(\text{OH})$ (111) were identified at $2\theta = 34.5^\circ$, 41.8° and 43° , respectively in sample activated for 3 hours. Aluminum hydride was not registered at all.

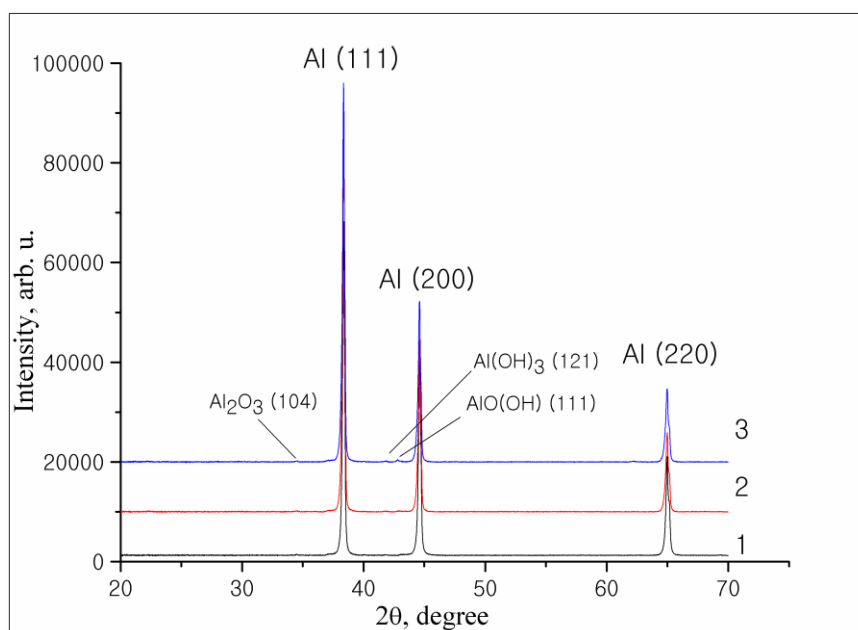


Fig. 2. XRD patterns of untreated Al powder (curve 1) and after plasma treatment at 300 W for 1 hour (curve 2) and 3 hours (curve 3)

3.2. SEM analysis

Fig. 3 shows SEM views of untreated aluminum powder (a-b) and plasma activated aluminum powder (c-d) at power 300 W for 3 hours. Views of 1 hour activation look quite similar as after 3 hours treatment. Untreated powder surface seems to be relatively smooth (Fig. 3(a-b)). Size of single particles varies from 10 to 75 μm . Higher charge accumulation at the edges of untreated Al powder demonstrates the presence of oxygen.

Surface of plasma activated powder was cracked (Fig. 3c) and it was registered blisters in some areas (Fig. 3d). Presumably bubbles are tending to form after hydrogen molecules accommodation in the bulk of aluminum without hydride formation. These bubbles can distinguish aluminum and aluminum oxide layer. Moreover stored hydrogen generates high stresses and lattice expansion which lead to formation of cracks and defects [12].

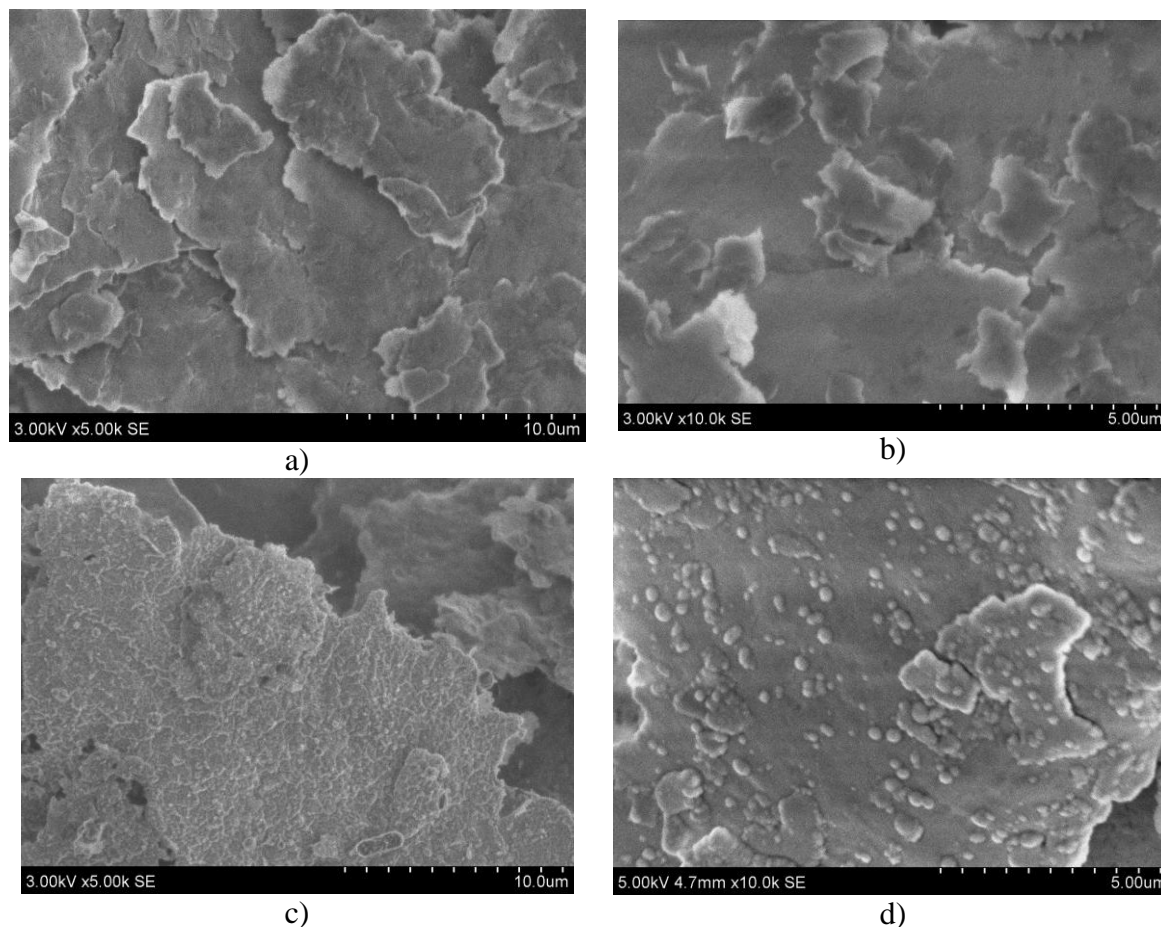


Fig. 3. SEM views of aluminum powder: (a-b) – untreated, and (c-d) – plasma treated at 300 W for 3 hours

3.3. Gas analyzer (HORIBA EMGA 830) results

Several plasma activated and untreated samples were measured using gas content analyzer. Results are presented in Table 1, where Al powder was activated under before mentioned conditions (3 hours, 300 W power). Untreated powder contains more nitrogen and oxygen than activated. Oxygen amount indicates the presence of oxide layer which is removed under plasma activation. Certainly, activated aluminum, upon exposure to air, forms a thin oxide layer again. Hydrogen concentration of untreated samples is higher as well. It was rather unexpected finding. Untreated aluminum powder was kept in the ceramic vessel under ambient conditions. Such powder with large surface area interacts with air and some moisture which leads to oxygen and water molecules absorption as well higher surface passivation [13]. Therefore, not only thin layer of natural oxide Al_2O_3 is formed but also this passive layer is enriched with OH groups and nitrogen molecules.

Plasma cleans this layer and introduces hydrogen into aluminum. Aluminum oxide layer is transparent for energetic hydrogen ions. Though hydrogen content becomes lower but it is not adsorbed on the surface but is sufficient for powder activation.

Table 1. Gas content in various samples

Activated Al powder	mass, g	Oxygen, wt. %	Nitrogen, wt. %	Hydrogen, wt. %
Sample 1	0.0464	1.5954	0.0480	0.1290
Sample 2	0.0463	1.4593	0.0259	0.1249
Sample 3	0.0564	1.1692	0.0415	0.1137
Untreated Al powder	mass, g	Oxygen, wt. %	Nitrogen, wt. %	Hydrogen, wt. %
Sample 4	0.0461	3.0208	0.2673	0.3265
Sample 5	0.0484	2.7882	0.1336	0.3246
Sample 6	0.0585	2.8165	0.2178	0.2816

3.4. Hydrogen generation

Activated aluminum powder, for 1 hour and 3 hours at 300 W, was immersed into alkaline water for hydrogen production. Fig. 4 shows hydrogen yield after full aluminum powder reaction with water. Present experiment was performed according to the scheme from reference [5]. 0.034 grams of activated aluminum powder were used in both cases. Sodium hydroxide (NaOH) was used as a promoter of process. Small amount of NaOH (1 tablet equals mass of 0.207 g) was dissolved in 50 ml of pure water resulting pH = 13.8.

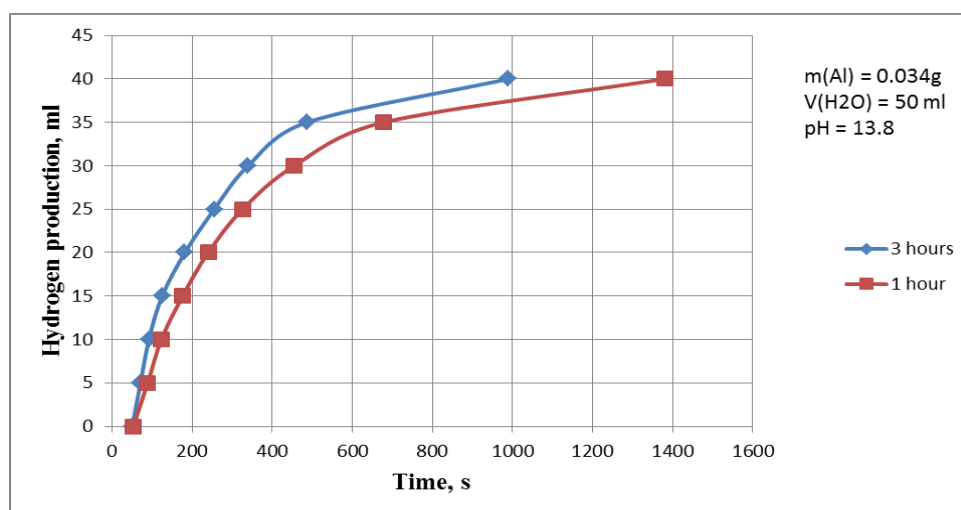


Fig. 4. Hydrogen yield after reaction between aluminum and alkaline water

After immersion activated Al powder went to the bottom of vessel because of high surface energy and increased hydrophilicity. Meanwhile untreated Al powder floated on the top of water and hardly reacted with water [14]. Reaction started after 53 seconds and lasted till 990 s and 1380 s for 3 h and 1 h activated samples respectively. 40 ml of hydrogen was produced. It is evident that plasma activation for 3 hours is more efficient.

Approximately 1200 cm³ of hydrogen could be obtained from reaction between water and 1 g of plasma activated aluminum powder. Same result is achieved by other authors after alloying Al with Ga, In, Sn, Li, etc. or activating aluminum by mechanically milling process [15–17]. These activation routes are more complex and expensive.

4. DISCUSSION

Obviously, aluminum powder exposed to air forms thin oxide layer. It is in agreement with gas analyzer results (Table 1). During activation in plasma oxide layer is removed and

surface defected by ballistic processes induced by hydrogen ions bombardment. Hydrogen ions are adsorbed and trapped in the region between Al and natural Al_2O_3 . Further they diffuse into the bulk and back to the surface without formation of aluminum hydride (Fig. 2) and occasionally accumulate in the bubbles as H_2 gas (Fig. 3d). It was observed that hydrogen plasma treatment leads to aluminum oxide and hydroxides formation (Fig. 2, curve 3). Due to high temperature in plasma, it seems that simultaneous processes of surface sputtering and new phase formation take place. Where hydrogen atoms with defected aluminum oxide surface form $\text{AlO}(\text{OH})$ compound. Presumably the following reaction occurs and hydrogen bubbles are generated: $6\text{AlOOH} + 2\text{Al} \rightarrow 4\text{Al}_2\text{O}_3 + 3\text{H}_2$ [18]. Moreover hydrogen generates high stresses which leads to surface irregularities (energy increases) and formation of defects (Fig. 3c). Although surface of activated powder oxidizes after taking out from vacuum chamber, it still stays activated. Hydrogen can be located between Al and Al_2O_3 [4]. It was noticed that even after 3 months since plasma treatment aluminum powder remains active.

After immersion into alkaline water, aluminum powder sinks, which means high surface energy. Reaction starts after 53 s (Fig. 4). It is induction period while hydroxide ions destroy aluminum oxide layer [19]. OH groups diffuse through the oxide layer and approach aluminum surface [20]. Alkaline water accelerates the reaction effectively. It is easier to reach aluminum metal surface because of micro cracks. As the reaction starts, presumably trapped H_2 bubbles break the oxide film and more area for $\text{Al-H}_2\text{O}$ reaction is opened (allowing water to come into contact with aluminum).

After oxide layer is completely disrupted, the fast reaction and hydrogen generation proceed until 455 s and 487 s for 1 hour and 3 hours activated powder respectively (Fig. 4). The size of aluminum grains decreases as the reaction proceeds.

Next, fast reaction is replaced by slow reaction. As thickness of byproducts (Al_2O_3 , $\text{Al}(\text{OH})_3$ or $\text{AlO}(\text{OH})$) which covers Al grains, increases, the resistance of hydroxide diffusion increases as well [20]. Therefore the $\text{Al-H}_2\text{O}$ reaction rate becomes limited due to OH transfer through Al_2O_3 .

Hydroxides help to disrupt the passive oxide layer and make the openings to pass water molecules. But Al hydration produces byproduct which obstructs the openings.

5. CONCLUSIONS

According to the results aluminum powder after hydrogen plasma treatment becomes highly active and hydrophilic. Surface irregularities and some bubbles were observed by scanning electron microscopy. XRD analysis of activated Al powder registered intensity increase of predominant cubic Al peak (111) and decrease of (200) and (220) cubic Al peaks. Small tetragonal Al_2O_3 (104) peak and orthorhombic $\text{Al}(\text{OH})_3$ (121) and $\text{AlO}(\text{OH})$ (111) peaks were identified after 3h plasma activation. Oxygen concentration of Al decreases after H_2 plasma treatment. Hydrogen generation rate depends on powder activation conditions and treatment time. Hydrogen generation rate was demonstrably higher after 3h activation than 1h activation time. As well it highly depends on hydroxide ions concentration dissolved in water. About 1200 ml of hydrogen can be collected after water reaction with 1 g of plasma activated Al powder. Whereas untreated Al powder hardly reacted with water. This research will be continued by looking for optimal activation conditions to obtain maximum hydrogen evolution and applying process to generate electrical energy in the system: hydrogen generation reactor and low temperature hydrogen fuel cell (e.g.: PEMFC – proton exchange membrane).



ACKNOWLEDGEMENT

This research was funded by a grant (2012-08-13 No. 31V-137) from the Lithuania Agency for Science, Innovation and Technology.

REFERENCES

1. KANEHIRA S., KANAMORI S., NAGASHIMA K., SAEKI T., VISBAL H., FUKUI T., HIRAO K. Controllable hydrogen release via aluminum powder corrosion in calcium hydroxide solutions. *Journal of Asian Ceramic Societies*, 2013, Article in press.
2. WANG CH., CHOU Y., YEN CH. Hydrogen generation from aluminum and aluminum alloys powder. *Procedia Engineering*, 2012, Vol. 36, p. 105–113.
3. FRANZONI F., MILANI M., MONTORSI L., GOLOVITCHEV V. Combined hydrogen production and power generation from aluminum combustion with water: Analysis of the concept. *International Journal of Hydrogen Energy*, 2010, Vol. 35, p. 1548–1559.
4. GAI W., LIU W., DENG Z., ZHOU J. Reaction of Al powder with water for hydrogen generation under ambient condition. *International Journal of Hydrogen Energy*, 2012, Vol. 37, p. 13132–13140.
5. MACANAS J., SOLER L., CANDELA A.M., MUNOZ M., CASADO J. Hydrogen generation by aluminum corrosion in aqueous alkaline solution of inorganic promoters: The AlHidrox process. *Energy*, 2011, Vol. 36, p. 2493–2501.
6. PETROVIC J., THOMAS G. Reaction of Aluminum with Water to Produce Hydrogen. *U.S. Department of Energy*, 2008, p. 1-26.
7. HUANG X., GAO T., PAN X., WEI D., LV CH., QIN L., HUANG Y. A review: Feasibility of hydrogen generation from the reaction between aluminum and water for fuel cell applications. *Journal of Power Sources*, 2013, Vol. 229, p. 133–140.
8. RAZAVI-TOUSI S.S., ALI NEMATOLLAHI GH., EBADZADEH T., SZPUNAR J.A. Modifying aluminum-water reaction to generate nano-sized aluminum hydroxide particles beside hydrogen. *Powder Technology*, 2013, Vol. 241, p. 166–173.
9. SHKOLNIKOV E.I., ZHUK A.Z., VLASKIN M.S. Aluminum as energy carrier: Feasibility analysis and current technologies overview. *Renewable and Sustainable Energy Reviews*, 2011, Vol. 15, p. 4611–4623.
10. CZECH E., TROCZYNSKI T. Hydrogen generation through massive corrosion of deformed aluminum in water. *International Journal of Hydrogen Energy*, 2010, Vol. 35, p. 1029–1037.
11. ELITZUR S., ROSENBAND V., GANY A. Study of hydrogen production and storage based on aluminum-water reaction. *International Journal of Hydrogen Energy*, 2014, Vol. 39, p. 6328–6334.
12. PRANEVICIUS L., MILCIUS D., PRANEVICIUS L.L., THOMAS G. Plasma hydrogenation of Al, Mg and MgAl films under high-flux ion irradiation at elevated temperature. *Journal of Alloys and Compounds*, 2004, Vol. 373, p. 9–15.
13. TENG H., LEE T., CHEN Y., WANG H., CAO G. Effect of Al(OH)₃ on the hydrogen generation of aluminum-water system. *Journal of Power Sources*, 2012, Vol. 219, p. 16–21.
14. Reactions of activated Aluminum with Water to produce Hydrogen. Feb. 2014. <http://inovatas.lt/figa.serveriai.lt/en/uncategorized-en/reactions-of-activated-aluminum-with-water-to-produce-hydrogen/>.
15. ZIEBARTH J., WOODALL J., KRAMER R., CHOI G. Investigation on microstructure and hydrogen generation performance of Al-rich alloys. *International Journal of Hydrogen Energy*, 2010, Vol. 35, p. 12011–12019.



16. ZIEBARTH J., WOODALL J., KRAMER R., CHOI G. Liquid phase-enabled reaction of Al-Ga and Al-Ga-In-Sn alloys with water. *International Journal of Hydrogen Energy*, 2011, Vol. 36, p. 5271–5279.
17. FAN MQ., XU F. SUN L. Studies on hydrogen generation characteristics of hydrolysis of the ball milling Al-based materials in pure water. *International Journal of Hydrogen Energy*, 2007, Vol. 32, p. 2809–2815.
18. YAVOR Y., GOROSHIN S., BERGTHORSON J., FROST D.L., STOWE R., RINGUETTE S. Enhanced hydrogen generation from aluminum-water reactions. *International Journal of Hydrogen Energy*, 2013, Article in Press, p. 1–11.
19. WANG H.Z., LEUNG D.Y.C., LEUNG M.K.H., NI M. A review on hydrogen production using aluminum and aluminum alloys. *Renewable and Sustainable Energy Reviews*, 2009, Vol. 13, p. 845–853.
20. DUPIANO P., STAMATIS D., DREIZIN E.L. Hydrogen production by reacting water with mechanically milled composite aluminum-metal oxide powders. *International Journal of Hydrogen Energy*, 2011, Vol. 36, p. 4781–4791.

INTERACTION BETWEEN DISTRICT HEATING PRODUCERS AND CONSUMERS: THE CASE OF THE USE OF LARGE-SCALE RENEWABLE ENERGY

L. Murauskaitė

Lithuanian Energy Institute

Breslaujos str. 3, LT-44403 Kaunas – Lithuania

ABSTRACT

Lithuania has ambitious target to increase the use of renewable energy sources three times in district heating sector by 2020. Unstable state energy policy and changes of incentive measures destabilize investments initiatives. The lack of both sides economic evaluation is the main challenge during the way to achieve target. This paper analyses socio-economic and environmental consequences of interaction between district heating producers and consumers and possible solutions in state policy. Moreover, the case of Varena city is taken into account to compare different incentives for renewable energy sources, such as biomass boilers on producer's side and solar collectors and heat pumps on the consumer's side. The solar collector field to produce hot water during summer time on the producer's side is also taken into consideration. Macroeconomic benefit of both sides' investments in renewable energy on district heating system is analysed. Solutions to improve interaction between producers and consumers in district heating sector are given, when analysing the case of the use of large-scale renewable energy.

Keywords: district heating, renewable energy, heating producers, heating consumers

1. INTRODUCTION

The scientific problem is evaluation of the social utility of renewable energy sources (RES) that can show the advantages, which is underestimated in investment decisions; for example, RES inexhaustibility and possibility to ensure sufficiency of energy resources for future generations at the same time. Utilization of some of the RES technologies, such as solar energy, also solves environmental issues. Therefore they may be additionally financed from other sources. The main issue is diversity of RES utilization opportunities and incentives. Moreover, it is transfer of their economic interpretations on uniform rules and economic laws into specified dimension, in this case trying to reduce different opinions as much as possible.

Phenomenon of energy is RES that could change exhausted types of energy such as oil, natural gas and could be realized by few types of energy. This could be solar, wind, geothermal energy. On the other hand, social utility of RES differs from oil and natural gas, because RES guarantee for future generations the supply of energy resources, but this benefit does not have methodological evaluation. This is one of the main accents of the concept of sustainable energy development. Sustainable energy development - it is energy production and consumption that ensure long-term humanity objectives of each country's development in all social, economic and environmental aspects.

Energy resources that are got from the result of economic activity depend on continuity of economic activity. Moreover, in all cases it is necessary to take into account multifunctional utilization. Utilization of economic activity and municipal waste by the use of RES technologies is a good measure for solving problems of environmental management and nature protection. However, the key question is realization of energy. Energy status (technical, economic and financial) have greater impact on the overall feedback to the

economic situation, than it is estimated. Energy consumption and energy efficiency have to meet the various aspects of the country's economy.

Authors usually take into analysis modelling of the future district heating system by integrating RES [1–7], analysis of energy policy for district heating [8, 9], competition aspect in district heating [10, 11], environmental, economic or energy efficiency aspects of district heating [12, 13]. The use of solar collectors and heat pumps in district heating sector is widely spread in Denmark [1, 3, 6, 7] and Sweden [2, 5, 14, 15] countries, that have similar climatic condition as Lithuania. Scientific literature analysis has shown the gap of deeper analysis of interaction between district heating producers and consumers. Such interaction is caused by the use of RES on the consumer side, the example could be solar collectors or heat pumps for producing hot water and space heating.

The aim of this paper is to analyse socio-economic and environmental consequences of interaction between district heating producers and consumers and possible solutions in state policy. Moreover, the case of Varena city is taken into account to compare different incentives for renewable energy sources, such as biomass boilers on producer's side and solar collectors and heat pumps on the consumer's side. The solar collector field to produce hot water during summer time on the producer's side is also taken into consideration. Macroeconomic benefit of both sides' investments in renewable energy on district heating system is analysed. Solutions to improve interaction between producers and consumers in district heating sector are given, when analysing the case of the use of large-scale renewable energy.

2. METHODOLOGY

The main methods used in this paper are analysis of available scientific literature and qualitative survey method. The results are compared with the previous initial calculations of solar thermal and heat pump use in the apartment building of 45 flats [16]. Modelling was being done by evaluating the heating demand in apartment building, working period of flat plate solar collectors in a year, their efficiency. Depending on the solar collectors' area, heat loss parameters the program calculated the price of hot water made by collector, the payback period of the system, NPV, IRR, etc. Moreover, large scale solar collector field in Varena city [17] is taken as an example of possible, but still not used heat production technologies in Lithuanian district heating sector. Modelling assumptions was made using various sources, available statistical data of solar collectors' fields in Denmark, studies, reports, papers, and websites. The previous paper dealt with the possibility to install the solar collectors' field that is connected directly to district heating network in Varena city. Solar collectors were selected taking into account the intensity of solar radiation and fluctuation of hot water system needs in district heating.

This paper continues previous research with the case study of Varena city. Qualitative survey method is used for the analysis of existing RES integration on the production and consumption sides in Varena city. Unique apartment building in Varena city that has already installed solar collectors for the preparation of hot water and heat pumps for the space heating is taken into account. This 5 floors apartment building is the only one in Lithuania that uses both types of RES technology for heating purposes. New biomass boiler and new economizer was visited in district heating company of Varena city. Previous study of possibility to use solar collectors' field on the production side was presented for the headquarter of Varena district heating company. The purpose of the use of qualitative survey method is not to gain quantify data or to measure the incidence of various views. Qualitative research is focused to providing insights into a problem, generating ideas and/or hypotheses for later quantitative

research. Survey method is used for the revealing the advantages and disadvantages of RES integration on the demand and supply sides in district heating sector.

3. RESULTS AND DISCUSSIONS

District heating sector was subsidized by the government; consumers paid only a small part of the costs associated with the real costs of heat supply in "transition" economies during the period of planned economy. The exact accounting for consumed energy or regulation was not necessary; expenditure on heating accounted for a relatively small burden on consumers, and the state made collective decisions. The situation completely changed when the former "socialist" countries have started to develop a free market economy, moved to the international market price, eliminated subsidies, etc. Then were revealed the true costs of energy, efficiency of buildings and energy supply systems. District heating sector, especially in "transition" economies, is highly socially sensitive because it affects many inhabitants; the payments for the thermal energy is relatively high; and consumers have a poor ability to regulate the heat consumption [18].

The current Lithuanian state support for the heating of apartment buildings, according to the results of survey, has the following *characteristics*:

- Individual social support is given mostly for heating old, energy-inefficient buildings, and discourage their renovation, because social payments are not associated to energy savings;
- A preferential 9% rate of value-added tax rate is applied to all amount of heat that is bought by the households. Therefore 12 percentage points (from the standard VAT rate of 21%) support mostly gets owners of large flats (presumably potentially richer residents) and energy-intensive buildings. This is unfair to both social solidarity and economic terms.
- The beneficiaries of the social compensation for heating often prevents energy-saving initiatives, because their payments for heating has a little dependency on the quantity of thermal energy consumption.
- Social compensation for heating and VAT exemption will only increase with fuel prices and will discourage renovation of apartment buildings, therefore more rational use of the taxpayers' contributions to state budget should be taken.

Almost all EU countries have *incentives* for RES in the heating sector, such as subsidies for investment, soft loans, and various tax incentives. For example, in Denmark and in Sweden, the biomass is exempted from the CO₂ tax. In many EU countries, the promotion of RES in the heating sector have subsidies from the various national and EU Structural Funds.

Lithuania supports district heating producers with investment subsidies for biomass boilers up to 10 MW capacity and economizers; intensity of support is not more than 50 percent. Consumers of district heating has investment subsidies for the use of RES (solar, geothermal, etc.); intensity of support is 30 percent. Interaction of district heating producers-consumers occurs, when consumption for heating decrease significantly because of installed solar collectors and heat pumps, shows the case of Varena. In this case producers should play „reserve“ role for the apartment buildings that have solar collectors and heat pump installed. However, the price for such a „reserve“ is significantly to low according to expenses of district heating network. If solar collectors and heat pumps are used in a large-scale for apartment buildings, producers should increase the price of district heating. The main reason for price increase is that expenses of district heating network remains the same, but the consumption decrease in a significant manner.

Key *measures* to reduce the negative environmental impacts of energy are abolishment of subsidies for traditional types of energy and integration of external costs into energy prices,

also introduction of pollution taxes or tradable emissions permit scheme. These measures are often used on the supply side of district heating. An example of the demand side measures could be subsidies to consumers that reduce the interest in energy savings or optimization of living space. Therefore arises twofold problem: burden on the state budget and neighbors in apartment buildings. The problem arise when individuals, who are receiving subsidies, tend to waste energy and not to take saving measures, especially related with modernization of multi-family building. VAT exemption also contributes to market signals, because consumers are less interested in efficient use of energy or decrease of consumption.

Social policy decisions mixed with energy policy distort *market signals* to consumers. Support that is given for the use of heat decrease the incentives and possibilities for reducing the consumption of heat, and to look for more efficient ways of using heat, as it would be under market conditions. If the state decides to support the less wealthy citizens, direct payments that is not related to consumption will have significantly less impact to the the market signals and will allow users to make more effective decisions.

Heat consumers in various countries, where district heating has been developed adequately to the needs of consumers, positively evaluate this technology for the following reasons:

- Risk of fire, which is available from the combustion of any fuel in the building, is eliminated. Gas is more dangerous because it can cause an explosion. Even the electric heating pose a potential fire hazard;
- Residents do not have to worry about fuel or to operate the heating device, therefore there is no indoor pollution;
- Buildings requires no installation and maintenance of the chimney, and there is no smell of smoke in the city;
- Useful area of the premises is unoccupied with fuel-burning equipment;
- Buildings are unoccupied with boiler house, therefore space can be rationally used for other purposes;
- Lower capital investment in the space heating equipment and low maintenance costs;
- Building with modern space heating and hot water system, which is acting in automatic mode, ensure the needs of the heating and hot water parameters;
- District heating suppliers are responsible for all troubles experienced by the individual heat users;
- Practical data shows that the district heating price is lower compared to other heating methods, if all services provided by the suppliers of district heating is taken into account [19].

Heat demand does not depend on the macroeconomic indicators. This is primarily due to the the fact that the intensity of heating in apartment buildings is increasingly regulated by automatic devices that respond only to the physical parameters of the environment. On the other hand, the greatest part of the apartment buildings is supervised and administered by the municipalities, which are not interested in efficient use of energy.

The transition to a wider use of biomass in the district heating sector has a negative impact on the consumption of natural gas. However, this has only a slight affect to the employment and the value added that is created in natural gas sector in Lithuania, because this type of fuel is imported. Projections of utilization of RES give unreasonable excessive role for biomass. Meanwhile, the usage of a huge potential of solar and geothermal energy is significantly too small.

The largest *macroeconomic positive effects* could be seen directly in the production and use of biofuel related industries, while the overall increase in added value is evaluated 33 million Litass. The increase in the employment is evaluated nearly 700 workplaces. The situation of trade balance is improved because of the refusal of imported natural gas. Overall

positive effect on the trade balance is around 27 million Litass, as was calculated in huge study [20].

Budgetary impact could be evaluated depending on the personal income tax, profit tax, deductions from income in accordance with the Law of Forests and not deductible value added tax (VAT) and net taxes on products. The total sum of the expected budget revenues from those sources is around 4 million Litass. These revenues could be allocated to the wider use of biofuel in the district heating sector without damage of the budget income.

It should be noted that the analysis presented in study [20] is based on 2005 data, and underestimate all the additional effects (such as further use of the increase of the value added in Lithuania). It is assumed that the assessment of the increase in the prices of energy resources and other factors might be stated in even more significant positive socio-economic effects of transition to widespread use of biofuel in district heating sector. However, even taking into account the limitations of the analysis presented here suggests that a wider use of biofuels is beneficial for society as new jobs are created, local production is increasing, and trade balance is improved.

For example, if direct support is applied for RES or environmental technologies, the impact would depend on the volume of support and source of funding. For example, if the direct assistance is financed from the state budget, the promotion measures would increase the budget deficit in addition to the above mentioned positive aspects. It is therefore essential that the promotion would be a cost-effective: the benefits exceed the negative effects. The fact that in the implementation of European Union directives Lithuania fulfills the obligations related to the objectives of the Union, it would be logical to give the support from the Structural Funds of the EU, because it is encouraged in Directive 2009/28/EC of Renewable Energy. Lithuania pays less money to the EU budget than receives from it, thus it can be argued that in this case the overall effect would be positive for our state. On the other hand, the use of the Structural Funds for investment in district heating sector has positive effect too, because this is an effective way to distribute support to many users, so there are also positive social effect. Soft loans may be as relatively less resource intensive instrument, therefore the burden on public finances is less than for direct support. Moreover, the payment are located over a longer period of time in this case.

Abandonment of fossil fuel imports from foreign countries would improve the *trade balance*, but the final effect would also depend on what part of renewable energy resources and technology are imported. It is difficult to assess in the current situation, because it might be that the expansion of the use of biofuels across Europe (other EU countries also have quite ambitious obligations of the increase of renewable energy in final consumption; the use of biofuels for the supply of district heating is one of the most attractive options) will increase the efficiency of the biofuel market and will expand international trade. Lithuania has sufficient potential of biofuel (not only wood, but also straw, grass and energy crops), therefore it is important that it would be effectively exploited. Positive impact on the trade balance might be expected in this case. Biofuel would not have such a positive impact on the trade balance if the vast majority of the biofuel is imported.

The implementation of the incentive mechanisms would have a positive impact on the *environment*. All of the measures provided in this paper are directly or indirectly related to the environmental protection. The wider use of RES in the district heating sector would let to reduce pollution of the atmosphere relative to greenhouse gases (assuming that carbon dioxide emissions of biofuel is equal to zero). On the other hand, there will be an increase of cities pollution by other compounds (e.g. solid particles), but their quantities do not exceed the limits. Renewal of district heating networks would contribute to enhancing the effectiveness of the system, which is directly related to lower fuel consumption, while at the same time with lower environmental pollution. The introduction of measures for atmospheric pollution from

large combustion plants would have a direct positive impact on the environment. Integration of renewable energy projects (such as solar collectors) into district heating systems may create external positive effect to the whole society concerning environmental and other regional development goals. Consumers' need for hot water or space heating is satisfied without burning natural gas or biomass, therefore the pollution is avoided. Moreover, import of natural gas from Russia is reduced, or the forest conservation is increased.

The case study of Varena district heating company has shown that the subsidies for biofuel boiler significantly reduces the price of heating. Varena city has one of the lowest district heating price in Lithuania. The reason of a low price of heating is the price of fuel. Biomass is almost double cheaper than imported natural gas. It should be noted, that Lithuania will have LNG terminal at the end of 2014; therefore, the changes of natural gas prices is expected. The instalment of economizer was the best choice for district heating company that reduced the price as well. The presented possibility to use solar collector's field for the preparation of hot water mostly during summer time made an impression for headquarters. Initial calculation of sensitivity analysis has shown that if investment subsidies of 30 percent is used, solar collectors field has positive NPV (Net Present Value) even if the price of district heating decrease 20 percent. Therefore, solar collectors' field might be a very good alternative for the cities, where expensive natural gas is used for the production of heat. Subsidy for investment of solar collectors field on the production side is not enacted at the moment. Unfortunately, the financial situation in the district heating company of Varena is still complicated. Biofuel boiler was installed with investment subsidy, but the rest of investment was covered by the loan from bank. Economizer also was financed by the soft loan. Therefore company does not have an extra equipment that could be suggested for a bank.

The interview with unique 5 floors apartment building that has installed solar collectors and heat pumps revealed the disadvantages of bureaucracy in Lithuania. This building got soft loan for the renovation and subsidies for the investment of solar collectors and heat pump. However, it is difficult to finish official registration of the building and to have money paid. The building saved 55 percent of energy. Therefore the payment for consumers hot water and space heating reduced significantly. On the other hand, even without RES technologies the payments for this buildings would be reduced more than twice. For this reason and for the lack of statistical data economic evaluation of alternatives for district heating becomes complicated. Moreover, the interaction between district heating producers and consumers is not clearly indicated in the state policy documents, if the use of solar collectors and heat pumps increase in large-scale. Solution for this gap might be changes in district heating price, including "reserve" part for almost energy-independent apartment houses.

In conclusion, the main problems of Lithuanian district heating are related to the old and energy-inefficient buildings, the state's compensation for heating and insufficient possibility to use different type of RES during the modernisation of heat networks. The relative cost for district heating in Lithuania is one of the largest in the European Union and the main reasons for this are the relatively harsh climatic conditions, the low-quality of buildings in terms of energy efficiency, predominance of expensive imported natural gas, and low economic power of consumers. The increase of natural gas prices affects the higher cost for district heating supply and the growing demand for social compensations for heating and greater burden to the state and to all taxpayers. Existing social compensation for heating system does not encourage the efficient use of heat, because it is not associated to the consumption of thermal energy and energy savings, but only with incomes. One of the ways to solve these problems is the wider use of diversified types of RES in the district heating sector, which would help to solve environmental problems, would increase employment mainly in smaller towns, where relatively higher unemployment rates, would improve the trade balance, and would increase revenues to the budget.

4. CONCLUSIONS

RES sector is distinguished by a unique specificity. There exist a set of problems that can be attributed to specifics of RES market. The main idea is to highlight organization of support for RES utilization and who gets the benefit from existing measures.

Integration of renewable energy projects (such as solar collectors) into district heating systems may create external positive effect to the whole society concerning environmental and other regional development goals. Consumers' need for hot water or space heating is satisfied without burning natural gas or biomass, therefore the pollution is avoided. Moreover, import of natural gas from Russia is reduced, or the forest conservation is increased.

Projections of utilization of RES give unreasonable excessive role for biomass. Meanwhile, the usage of a huge potential of solar and geothermal energy is significantly too small. The possibilities to use solar collectors and heat pumps on the demand and supply side in district heating system were analysed. Renewable energy development in district heating requires large investments; however the use of RES for the generation of district heating would let to diversify the fuel and energy sources. Subsidies for investments of solar and geothermal energy technologies would let to use them in district heating system as economically attractive alternatives.

Moreover, if ecological, economic and social benefit is comprehensive evaluated in a long term period and on that basis would be given support for RES energy, the demand for advanced RES technologies would increase noticeably.

ACKNOWLEDGEMENTS

This research was supported by the Research Council of Lithuania (IEP-01/2012).

REFERENCES

1. NIELSEN, S., MÖLLER, B. GIS based analysis of future district heating potential in Denmark. *Energy*, 2013, Vol. 57 p. 458–468.
2. ÅBERG, M., HENNING, D. Optimisation of a Swedish district heating system with reduced heat demand due to energy efficiency measures in residential buildings. *Energy Policy*, 2011, Vol. 39, No. 12, p. 7839–7852.
3. NIELSEN, S., MÖLLER, B. Excess heat production of future net zero energy buildings within district heating areas in Denmark. *Energy*, 2012, Vol. 48, No. 1, p. 23–31.
4. DALLA ROSA, A., CHRISTENSEN, J.E. Low-energy district heating in energy-efficient building areas. *Energy*, 2011, Vol. 36, No. 12, p. 6890–6899.
5. PERSSON, U., WERNER, S. Heat distribution and the future competitiveness of district heating. *Appl. Energy*, 2011, Vol. 88, No. 3, p. 568–576.
6. LUND, H., MÖLLER, B., MATHIESEN, B.V., DYRELUND, A. The role of district heating in future renewable energy systems. *Energy*, 2010, Vol. 35, No. 3, p. 1381–1390.
7. LUND, H., MATHIESEN, B.V. Energy system analysis of 100% renewable energy systems—The case of Denmark in years 2030 and 2050. *Energy*, 2009, Vol. 34, No. 5, p. 524–531.
8. CANSINO, J.M., PABLO-ROMERO, M. DEL P., ROMÁN, R., YÑIGUEZ, R. Promoting renewable energy sources for heating and cooling in EU-27 countries. *Energy Policy*, 2011, Vol. 39, No. 6, p. 3803–3812.
9. HOLMGREN, K., GEBREMEDHIN, A. Modelling a district heating system: Introduction of waste incineration, policy instruments and co-operation with an industry. *Energy Policy*, 2004, Vol. 32, No. 16, p. 1807–1817.

10. GROHNHEIT, P.E., GRAM MORTENSEN, B.O. Competition in the market for space heating. District heating as the infrastructure for competition among fuels and technologies. *Energy Policy*, 2003, Vol. 31, No. 9, p. 817–826.
11. SÖDERHOLM, P., WÅRELL, L. Market opening and third party access in district heating networks. *Energy Policy*, 2011, Vol. 39, No. 2, p. 742–752.
12. COSMI, C. ET AL. Environmental and economic effects of renewable energy sources use on a local case study. *Energy Policy*, 2003, Vol. 31, No. 5, p. 443–457.
13. AGRELL, P.J., BOGETOFT, P. Economic and environmental efficiency of district heating plants. *Energy Policy*, 2005, Vol. 33, No. 10, p. 1351–1362.
14. MAGNUSSON, D. Swedish district heating – A system in stagnation: Current and future trends in the district heating sector. *Energy Policy*, 2012, Vol. 48 p. 449–459.
15. ERIKSSON, M., VAMLING, L. Future use of heat pumps in Swedish district heating systems: Short- and long-term impact of policy instruments and planned investments. *Appl. Energy*, 2007, Vol. 84, No. 12, p. 1240–1257.
16. MURAUSKAITĖ L. The significance of district heating for the promotion of renewable energy sources demand // 10th international conference CYSENI: Kaunas, Lithuania, May 29–31, 2013. Kaunas: LEI, 2013. ISSN 1822-7554, p. 294–301.
17. MURAUSKAITĖ L. Presumptions for increasing the use of renewable energy sources in large scale in district heating // Digital proceedings: 8th conference SDEWES, Dubrovnik, Croatia, September 22–27, 2013. Croatia, 2013. ISSN 1847-7178, p. 1–9.
18. LUKOŠEVIČIUS, V. Quickly implemented measures to improve the accessibility for district heating of Lithuania. Vilnius, 2011. [in Lithuanian].
19. GUDZINSKAS, J., LUKOŠEVIČIUS, V., MARTINAITIS, V., TUOMAS, E. (2011) Heat User's Guide. Vilnius, 2011. 294 p. ISBN 978-609-95258-0-8 [in Lithuanian].
20. LUKOŠEVIČIUS, V. et. al. (2011) Complex investment program for the development of district heating sector and the creation of implementing measures during 2011–2020. Vilnius, 2011 [in Lithuanian].



RADIAL GROWTH CHANGES IN *SALIX CAPREA* L. AND *SALIX ALBA* L. STANDS

I. Pučka

*Latvia University of Agriculture
Liela street 2, LV 3001 – Latvia*

D. Lazdiņa

*Latvian State Forest Research Institute "Silava"
Rīgas street, LV 2169 – Latvia*

ABSTRACT

Interest about renewable energy sources, including timber production from willows have been growing in recent years. The use of willow crops for energy production will improve energy security. It is therefore important to make assessment of willow stands to obtain various types of information. Tree-ring dating was performed on wood discs sawed down at different tree heights (0 m, 1.3 m, 3 m and 5 m). The number of growth rings is used to calculate for how long time (years) the tree has reached the established height. An average age of measured *Salix alba* trees was estimated to have achieved 10.2 m height in 9.9 years and *Salix caprea* trees achieved 9.3 m height in 11.7 years. Measured trees have not steady growth each year. There was not found direct correlation between the width of a ring and the climatic factors.

Keywords: willows, tree-ring dating, radial growth

1. INTRODUCTION

Variability of radial growth is caused by seasonal changes. However, it also depends on internal factors, for example, tree age and external factors, such as climate, geographic location, pests and disease impact etc. Climate is one of the most important external environmental factors [1, 2, 3, 4].

The theoretical framework of tree-ring dating is dependence of annual tree ring width and annual growth on climate factors, their changes and intensity. Each region has specific growing conditions, so time series are different and characteristic for each tree [5].

Use and accuracy of tree-ring dating method is based on the analysis of the specific tree growth rates. Radial growth of trees occurs each growing season, but the number of cells, chemical structure and other parameters varies. The increment of a tree differs in any year and depends on climatic and environmental factors. Tree-ring provide information about weather conditions dominate during the growing season [6], about local, regional, and even global environmental history [2, 3] and about the effects of anthropogenic factors (farming, agricultural pollution etc.) [5].

Nowadays tree-ring dating is used in different research areas, including climatology, ecology, forestry, geography and biology [7, 8]. Tree-ring techniques have been widely used for identifying forest growth trends [9] and to assess the quality of the environment.

Determination of the similarities between narrow and wide rings and establishment of population growth models can be done through selecting samples from one population [6].

A study conducted by the Latvian State Forest Research Institute "Silava" (2008) claims that trees on agricultural lands have wider tree rings [10].

Tree age information is important in different forest growth models, such for projections of expected timber yield [11]. Additionally, tree age is an indicator for a tree's ecological value [12].

Woody plants with tree rings can be found almost everywhere on earth, but the number of species with clear visible of tree rings is directly related to the seasonality of climate [13]. The tree-ring record is defined by organismal processes. Changes in the tree-ring record to changes in the environment can be determined using environmental observation and statistics [2]. Tree rings within a series vary in response to climatic conditions during the current growing season [2] and contain information about the changes in growth over a long period of time [14].

I.Liepa (1996) has used tree-ring analysis as a tool for tree radial growth assessment [15]. Tree-ring dating is based on the fact that annual tree growth changes have been associated with climate change. These changes could be determined by tree ring or wood density changes [16]. Weather conditions and environmental data are unique for each year and are different in regional and time scale [3]. Using of tree-ring chronology can synchronize each increment in wood samples with calendar year [6].

Radial growth changes of trees depending on the weather and climate changes have been studied in many countries around the world [3, 4, 9, 16]. Coniferous trees (e.g. Scots Pine (*Pinus sylvestris* L., Norway spruce (*Picea abies* (L.) H.Karst.) are more often used species in dendroclimatological studies. From deciduous trees the more commonly used species are oaks and birches.

Monthly temperatures and precipitation during the dormant and vegetation period vary from year to year [17]. Ring width is most often measured in tree-ring series, but latewood width and wood density can give valid information and be a more sensitive recorder of climate than ring width [2].

Only few experimental data are available on the studies about growth process of *Salix* spp. specie [13, 18, 19]. A good adaptation of some *Salix* clones to soil and climate conditions could be expressed in growth rhythm and high biomass production [20]. Yearly average 20–25 m³ of biomass can be achieved from willow plantations within 3 years rotation period in Latvia [21].

Many countries show an interest in energy production from willows biomass during the last 10 years. Willow natural stands and the forest plantations are subject to forest management planning [20]. Willows are widely planted bioenergy crops in Europe for heat and power production [22, 23, 24, 25, 26, 27]. Swedish willow plantations are considered as a good example in the field for bioenergy production in Europe. Various policy measures were implemented in order to promote willow plantations and expand the areas of willows [28].

Replacing fossil fuels with biomass for energy production is an important strategy for the European Union. Bioenergy production is being contributed through several EU Directives and national policies in many European countries [29, 30]. Short-rotation woody crops can be grown on abandoned, contaminated land and less fertile soils, thus biomass production does not compete with food or feed production [31].

The aim of this research is determination of radial growth rate of *Salix caprea* L. and *Salix alba* L.

Research objectives:

1. Measurement of tree ring width of each disk sample from different heights and clarification of relation between tree age, radial growth and tree ring width.
2. Description of changes of weather parameters (precipitation, mean temperature) of study site.
3. Clarification of relationship between weather conditions and tree rings width.

2. MATERIALS AND METHODS

2.1. Study site description

The study site is located in the central part of the Latvia, in Ķeguma district, Rembate parish, about 50 km from Riga. Experimental plantation of oak and birch were overgrown with osiers (*Salix alba*, *Salix caprea*), and stand tending was carried out. Trees of *S.alba* and *S.caprea* reached heights of five metres, were harvested and measured.

2.2. Field research

The field work was carried out in February 2013. The height was determined after cutting by measuring trunk width with tape measure. A total of 19 trees radial growths were measured (*S.alba* – 10, *S.caprea* – 9).

In order to obtain the data about tree height growth process, trunk discs (2–3 cm thick) were sawn at different heights above the ground level (stump height, breast height, 3 m and 5 m height). Discs must be selected from the entire stem length thus reducing missing rings and facilitating the measurement of tree ring width [18].

The sawing discs are perpendicular to the stem axis. Before the tree felling, north direction was marked on the bole. After felling, plot and sample number, the height at which each disc is taken were recorded on the top of disc.

Tree age was determined by counting the rings on disc from the root collar (0.0 m). Tree-ring analysis was done through 73 stem discs collected from different heights of trees. The number of rings of each disc was counted to determine the age at which the tree reached that disc height level. Tree diameter was measured in two perpendicular directions.

2.3. Laboratory methods

Wood discs were oven-dried in a Memmert UNB 500 chamber for one week in a 50⁰C. All disks were surfaced using progressively finer sandpaper, treated with glicerol to obtain a better contrast for the following image analysis and scanned /photographed (600 dpi). On each disk was measured tree-ring width on four radii (south, east, north, west), using the LignoVision Software v.1.38e [32]. The accuracy of ring width measurement is 0.01 mm.

2.4. Meteorological data analysis

Temperature and precipitation are often analysed as an influencing factors of growth changes because of the wide availability of these data [33].

Climate data were obtained from the nearest observation station “Skrīveri” 20 km south-east of the study site. Data were obtained from Latvian Environment, Geology and Meteorology Centre [34].

The data about mean daily temperatures (degrees Celsius) and annual precipitation (millimeters) time series selected from 2001 until the 2012. Temperature was recorded every hour and precipitation was recorded eight times a day. The monthly mean temperature is calculated from the average of daily temperature using Microsoft Office Excel software. Air temperature and precipitation data were collected for the vegetation period (April to October).

2.5. Statistical data analysis

Statistical analysis of obtained data realized using Microsoft Excel, SPSS software tools. A set of sample statistics including the highest, the smallest and average values, average tree-ring width, variance and mean were computed using methods of describing statistics and correlation analysis [35].

3. RESULTS AND DISCUSSIONS

Analysis of tree rings was performed for trees with height at least 5 metres. According to The Law of the Republic of Latvia Forest law (2000), forested areas are defined as areas where trees have reached, or can reach, at least heights of 5 meters. Therefore, it is important to find out, in what period of time trees grow up to five meters in height.

3.1. Tree age analysis

Growth process of a tree described through tree ring measurement in different heights. The number of rings at each disc show period of time during which trees reach heights of 1.3, 3 and 5 meters.

The age of trees was determined by the number of annual rings at the neck of a root.

An average age of all measured *S.alba* trees was estimated to have achieved 9.9 years and average height is 10.2 m

Table 1 shows that *S.alba* trees have been measured to reach 3 m in four years and 5 m in five years.

Table 1. *Salix alba* height development

Height (m)	Average number of rings	Age
0.0	Stump (9.9)	0
1.3	7.8	2
3	6.3	4
5	5.1	5

S.caprea trees have achieved 11.7 years with average height 9.3 m. *S.caprea* trees have been measured to reach 3 m in four years and 5 m in six years (Table 2).

Table 2. *Salix caprea* height development

Height (m)	Average number of rings	Age
0.0	Stump (11.7)	0
1.3	10	2
3	7.9	4
5	6.1	6

The number of rings decreased gradually with height from stump to top of the tree. The difference between the numbers of rings at different height shows the number of years taken to reach specific height. Obtained data show, that measured trees have not steady growth each year.

Salix spp. species are characterised as fast growing species, with potential to grow on different habitats. Relatively intensive overgrowing of agricultural lands is observed in

Latvia, including overgrowth with *Salix spp.* species. Fast-growing tree plantations could be established in areas not suitable for agriculture.

3.2. Radial growth rates

Obtained data show, that ring widths at different stem heights do not differ significantly (Fig. 1.). Highest average tree ring width of *S.caprea* trees (3.8 ± 0.49 mm) was observed on the height of 3 m above the ground, but *S.alba* trees – 1.3 m (4.6 ± 0.45 mm).

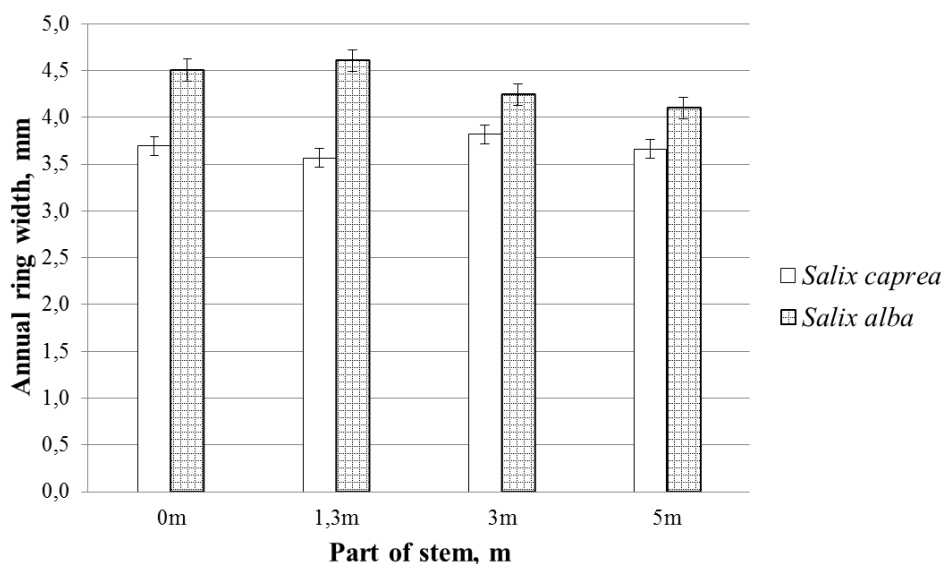


Fig. 1. Annual ring width of *Salix caprea* L. and *Salix alba* L. trees within different stem heights

Growth rate models of many tree species are characterized by an increasing growth rate in young age. Therefore significant variations of tree ring width in different periods can be explained by effect of tree age [14]. It is possible, that later in the growing season relevance of age on growth rate decrease. In the present study it is difficult to assess the effects of age, measured trees are relatively young, reach a maximum age of 12 years.

3.3. Changes in the thickness of the tree rings

Mean annual ring width of each tree was calculated as sapwood width divided by the number of annual sapwood rings. As tree ring measurement was carried out to 5 m height, variance of tree ring width represented until this height (Fig. 2).

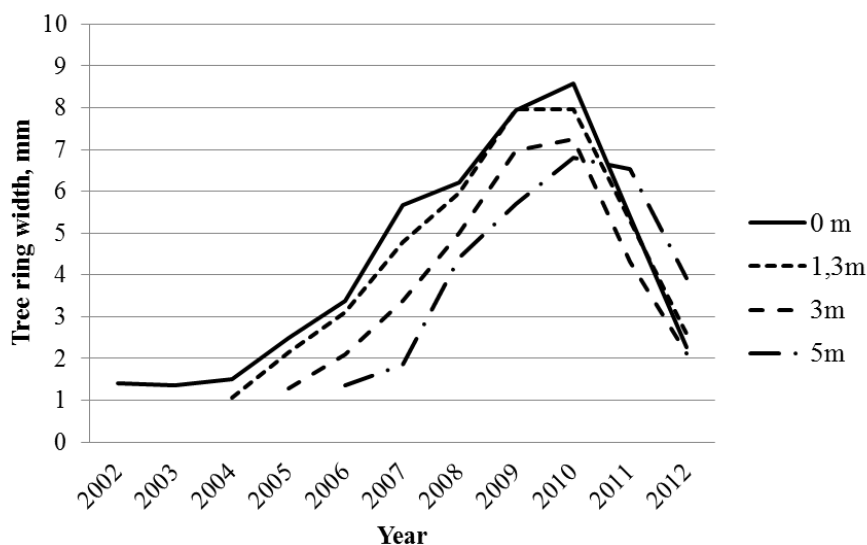


Fig. 2. Average tree ring widths of *Salix alba* at different heights

This curve shows the variation in annual ring increment from one year to another in different heights. Rapid rate of extension of the tree ring width was observed during the first 8 years of growth and then a sharp decrease of ring width occurs. At the age of 8–9 years trees have widest tree rings. Maximum tree ring width of *Salix alba* trees was 14.5 mm, and minimal – 0.5 mm.

Variances between tree ring widths of *S. caprea* trees in different height are less pronounced (Fig. 3).

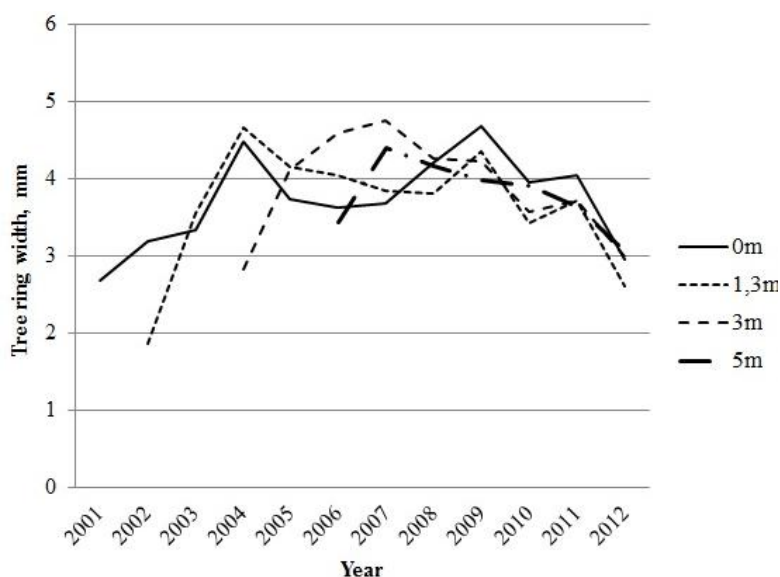


Fig. 3. Average tree ring widths of *Salix caprea* at different heights

Tree ring variability observed in rings of *S. caprea* tree is similar throughout the entire tree radius. Average ring width ranged between 2.1–2.3 mm.

Individual trees differ in growth rates along their life-span. *Salix alba* trees have larger amount of ring-width variability within the trees of the site.

3.4. Climate and tree-ring widths

The climatic conditions of the territory of Ķeguma district are characterized as transition zone between maritime and continental climate (in Latvia scale) [36].

The average temperature varies between 11.8 °C in 2003 and 13.5 °C in 2006 and 2011 (Fig. 4)

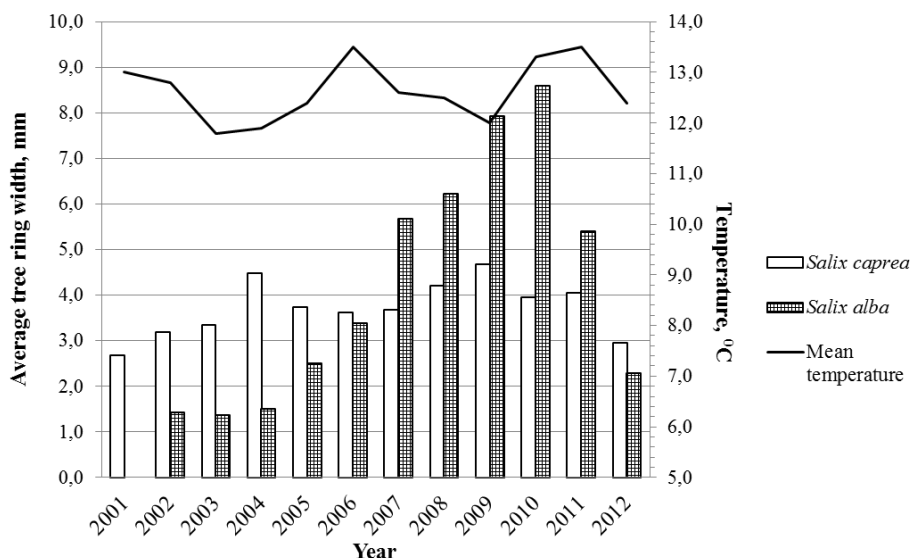


Fig. 4. Observation station “Skrīveri” meteorological data about average air temperature in vegetation period (April to October) [29] and average tree ring width

The climate in vegetation period is characterized by annual precipitation 513 mm (Fig. 5). The highest precipitation amount recorded in 2012 (653 mm). 2006 was the year with smallest precipitation, only 353.6 mm in seven months.

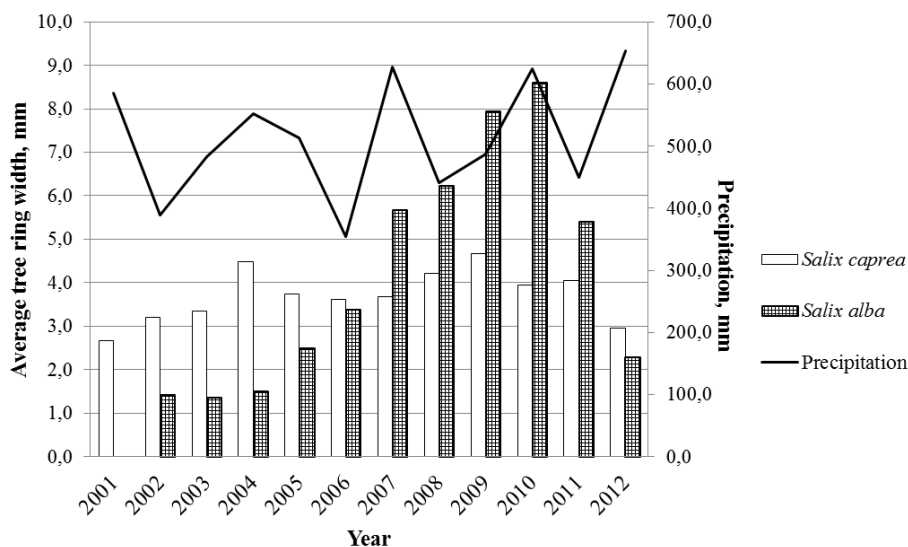


Fig. 5. Observation station “Skrīveri” meteorological data about precipitation in vegetation period (April to October) [29] and average tree ring width

There was not found direct relationship between the width of a ring and the climatic factors.

No significant correlations between *Salix alba* average tree-ring width (at the neck) and climate parameters (mean temperature and precipitation) is observed. Pearson's correlation coefficient between tree ring width and average temperature of vegetation period of *S.alba* trees ($r=0.33$), *S.caprea* trees ($r=-0.14$), $p>0.05$.

Pearson's correlation coefficient between annual precipitation in vegetation period and tree ring width of *S.alba* trees ($r=0.2$), *S.caprea* trees ($r=0.07$), $p>0.05$ also do not show significant correlation.

There was not found relationship between precipitation per month, and month temperature and tree ring width of *S.alba* and *S.caprea* trees in specific year. In a similar study [37], using *Salix fragilis*, were found positive influence of precipitation and temperature on annual radial increment.

It is possible that the results will be different if older trees, at least 20 years of age, will be selected.

4. CONCLUSIONS

Salix alba trees have larger amount of ring-width variability within the trees of the site.

The largest tree ring widths of *Salix alba* trees were observed in height of 1.3 m (4.6 mm), and decrease gradually from stump to top of the tree.

Highets tree rings width (3.8 mm) of *Salix caprea* trees was observed in 3 m height.

Average tree ring width of *Salix alba* trees is 4.2 mm, *Salix caprea* trees – 3.7 mm.

Measured trees do not show a sensitive reaction to changing growth conditions (average temperature and precipitation).

REFERENCES

1. VAGANOV, E.A.; HUGHES, M.K.; SHASHKIN, A.V. *Growth dynamics of conifer tree rings. Images of past and future environments*. Berlin, Heidelberg, Springer-Verlag, 2006, 354 p.
2. SMITH, K.T. An organismal view of dendrochronology. *Dendrochronologia*, 2008, Vol. 26, p. 185–193.
3. HORDO, M., HENNTTONEN, H.M., MAKINEN, H., HELAMA, S., KIVISTE, A. Annual growth variation of Scots Pine in Estonia and Finland. *Baltic Forestry*, 2011, Vol. 17, No. 1, p.35–49.
4. SOHAR, K., LÄÄNELAID, A., ECKSTEIN, D. Climatic signal in tree-ring widths of pedunculate oak (*Quercus robur*L.) in Estonia. BALTDENDRO 2012. Materials of the 2nd international conference of Baltic States dendrochronologists. Šventoji: Lithuania. 2012 August 30 – September 2.
5. LIEPA, I. Dendrochronoloģija (Dendrochronology). In book Broks J. (red.) *Meža enciklopēdija* (Forest encyclopedia). Rīga, Zelta grauds, 2003, 76 p. (in Latvian).
6. ZIELSKI, A., KRAPIEC, M. *Dendrochronologia*. In: Falinski J. B. (red.). Warszawa, Wydawnictwo naukowe PWN, 2004, p.17–287.
7. BRAKER, O.U. Measuring and data processing in tree-ring research - a methodological introduction. *Dendrochronologia*, 2002, Vol. 20, No. 1–2, p.203–216.
8. ZUNDE, M. Par senseniem kokiem (About ancient trees). *Vides vēstis*, 2005, Vol. 4, No. 79, p. 22–24 (in Latvian).

9. LOPATIN, E., KOLSTRÖM, T., SPIECKER, H. Approaches for the Identification of long-term Trends in Growth of Siberian Spruce and Scots Pine in North West of Russia. *Baltic Forestry*, 2007, Vol. 13, No. 1, p. 17–27.
10. SILAVA, *Sakņu trupes uzraudzība un ierobežošana skujkoku mežos* (Monitoring and restriction of root rot within the coniferous forests), Latvian State Forest Research Institute – Silava, 2008, 57 p. (in Latvian).
11. HALL, D.B., CLUTTER, M. Multivariate multilevel nonlinear mixed effects models for timber yield predictions. *Biometrics*, 2004, Vol. 60, p. 16–24.
12. MICHEL, A.K., WINTER, S. Tree microhabitat structures as indicators of biodiversity in Douglas-fir forests of different stand ages and management histories in the Pacific Northwest, U.S.A., *Forest Ecology and Management*, 2009, Vol. 257, p. 1453–1464.
13. OWCZAREK, P. *Dendrogeomorphological potential of Salicaceae from SW Spitsbergen (Norway)*. Proceedings of the Dendrosymposium 2008. Zakopane: Poland. 2008 April 27–30.
14. TJARVE, D. Parametric analysis of radial increment of scots pine for environmental assessment. Resume of the PhD paper, Riga, 2013, 117 p. (in Latvian).
15. LIEPA, I. *Pieauguma mācība* (Growth increment lessons). Jelgava, LLU, 1996, 123 p. (in Latvian).
16. FRITTS, H.C. *Tree rings and climate*. Blackburn Press, Caldwell, New Jersey, 2001. 567 p.
17. LEBOURGEOIS, F. Climatic signals in earlywood, latewood and total ring width of Corsican pine from western France. *Annals of Forest Science*, 2000, Vol. 57, p.155–164.
18. WOODCOCK, H., BRADLEY, R.S. *Salix arctica* (Pall.): its potential for dendroclimatological studies in the High Arctic. *Dendrochronologia*, 1994, Vol. 12, p. 11–22.
19. GARTNER-ROER, I., HEINRICH, I., GARTNER, H. Wood anatomical analysis of Swiss willow (*Salix helvetica*) shrubs growing on creeping mountain permafrost. *Dendrochronologia*, 2013, Vol. 31, p. 97–104.
20. Poplars and willows culture and utilization during 2008–2011. National poplar and willow commission. Country report. Bucharest, 2012, 29 p.
21. LAZDIŅA, D., *Using of wastewater sewage sludge in short rotation willow coppice*. Summary of Promotion Thesis, Jelgava, 2009, 58 p. (in Latvian).
22. BERNDES G., HOOGWILK M., VAN DEN BROEK R. The contribution of biomass in the future global energy supply: a review of 17 studies. *Biomass Bioenergy*, 2003, 25, p. 1–28.
23. DIMITRIOU, I., ARONSSON, P. Willows for energy and phytoremediation in Sweden. *Unasylva*, 2005, Vol. 221, No. 56, p. 46–50.
24. MOLA-YUDEGO, B., ARONSSON, P. Yield models for commercial willow biomass plantations in Sweden. *Biomass and Bioenergy*, 2008, Vol. 32, No. 9, p. 829–837.
25. MOLA-YUDEGO, B. Regional potential yields of short rotation willow plantations on agricultural land in Northern Europe. *Silva Fennica*, 2010, Vol. 44, No. 1, p. 63–76.
26. MOLA-YUDEGO, B. Trends and productivity improvements from commercial willow plantations in Sweden during the period 1986–2000. *Biomass and bioenergy*, 2011, Vol. 35, p.446–453.
27. ADEGBIDI, H.G., VOLK, T.A., WHITE, E.H., ABRAHAMSON, L.P. Biomass and nutrient removal by willow clones in experimental bioenergy plantations in New York State. *Biomass and Bioenergy*, 2001, Vol. 20, p. 399–411.

28. MOLA-YUDEGO, B., GONZÁLEZ-OLABARRIA, J. Mapping the expansion and distribution of willow plantations for bioenergy in Sweden: lessons to be learned about the spread of energy crops. *Biomass and Bioenergy*, 2010, Vol. 34(4), p. 442–448.
29. GASOL, C.M., BRUN, F., MOSSO, A., RIERADEVALL, J., GABARRELL, X. Economic assessment and comparison of acacia energy crop with annual traditional crops in Southern Europe. *Energy Policy*, 2010, Vol. 38, p. 592–597.
30. KUNDAS, S., RODZKIN, A., POZNIAK, S., ROMANOVSKY, C. Assessment of the environmental benefit of fast growing willow cultivated for biomass supplying. *Protection*, 2008 Vol. 8, p. 1–8.
31. DJOMO, S.N., EL KASMIQUI, O., CEULEMANS, R. Energy and greenhouse gas balance of bioenergy production from poplar and willow: a review. *GCB Bioenergy*, 2011, Vol. 3, p. 181–197.
32. RIN, F. *LignoVision – Scanning of wood and tree-ring recognition*. Version 1.38e for Microsoft Windows 98, 2000, XP. User Reference. Heidelberg, Germany, 2006, 24 p.
33. PARN, H. Changes in radial growth of two consecutive generations of scots pine (*Pinus sylvestris* L.) stands. *Baltic forestry*, 2012, Vol. 18, No. 1, p. 12–24.
34. Latvian Environment, Geology and Meteorology Centre, 2014. Link to the internet <<http://www.meteo.lv/meteorologija-datu-meklesana/?nid=461>>
35. ARHIPOVA, I.; BĀLIŅA, S. *Statistika ekonomikā. Risinājumi ar SPSS un Microsoft Excel* (Economic statistics. Solutions using SPSS and Microsoft Excel). Datorzinību centrs, 2003. 349 p. (in Latvian).
36. The Spatial Development Plan of Ķeguma district 2003-2015, 2009. Link to the internet <http://www.kegums.lv/upload/attistibas_plani/planojums_2010/5.dala_vides_parskats.pdf>
37. VITAS, A. Dendroecological research on *Salix fragilis* L. in the Nevėžis Botanical-Landscape Reserve. *Ekologija*, 2004, Vol. 3, p. 43–46.



RENEWABLE ENERGY SOURCES TECHNOLOGY ASSESSMENT AND PROMOTION

Ilona Alisauskaite-Seskiene
Lithuanian Energy Institute
Breslaujos str. 3, Kaunas, LT-44403, Lithuania

ABSTRACT

While the demand of energy is increasing around the world, the traditional energy resources are depleting and their acquisition methods are damaging to the environment. Renewable energy sources (RES) are an attractive alternative to traditional energy. The issue of RES and its usage promoting has been addressed by the European Union long ago and is one of the Lithuanian energy policy objectives set out in the National Energy Strategy and in the Law of Energy of the Republic of Lithuania. Lithuania has sufficient reserves of RES in order not only to meet its commitments to the EU, but also exceed them, thereby increasing the country's energy security. But one of the reasons that prevent achieving the objectives – insufficient incentives for the use of RES development and untapped potential for increasing the use of RES by combining the interests of producers, suppliers and consumers, as well as untapped potential of science of Lithuania. In Lithuania the issue of RES assessment and promotion went under consideration relatively recently, in most cases talking just about incentives for manufacturers of RES technology. Currently there is no instrument in Lithuania that would encourage consumers to use RES technology – all functioning incentives are applicable to manufacturers or suppliers. Until now such holistic RES technology promotion method, when incentives of RES technology for producers would be combined with those designated for consumers, has not yet been examined. The paper aims to analyse the experience of other countries in the area of RES technology incentives in households in order to achieve the main task – to review, which RES technology incentives in households can be adapted in Lithuania.

Keywords: renewable energy sources, incentives of RES technology, the interests of producers, suppliers and consumers

1. INTRODUCTION

While the demand of energy is increasing around the world, the traditional energy resources are depleting and their acquisition methods are damaging to the environment. Renewable energy sources (RES) are an attractive alternative to traditional energy. As it is specified in the Law on Renewable Energy of Republic of Lithuania [1] renewable energy is the energy from renewable non-fossil sources: wind, solar, aerothermal, geothermal, hydrothermal and ocean energy, hydropower, biomass, biogas, including landfill and sewage treatment plant gas as well as other non-fossil renewable resources, the use of technology is now available or will become available in the future, energy. RES technology not only helps to solve the problems of climate change, but also makes it possible to fight against poverty, exclusion, energy and economic challenges.

The issue of RES and its usage promoting has been addressed by the European Union long ago and is one of the Lithuanian energy policy objectives set out in the National Energy Strategy [2] in the Law of Energy of the Republic of Lithuania [3]. Because of the lack of primary energy resources, Lithuania's economy depends on the import of these resources and is vulnerable, especially in the event of supply disruptions, or in case of price fluctuation. The goal of RES sector development is to maximize the use of these resources and thus reduce fuel imports and the use of gas for electricity and district heating production, create new jobs and reduce greenhouse gas emissions.

In 2010 the National Audit Office found that Lithuanian energetics, based on the use of RES, could be an effective tool not only for solving the problem of particular relevance – ensuring energy independence, environmental issues, as Lithuania in the RES species and their abundance is sufficient volume to achieve this. In addition, Lithuania has sufficient reserves of RES to not only meet its commitments to the EU: making energy from RES, by 2020 increase to 23% and the share of RES used by all modes of transport, at least 10%, but also exceed them, thereby increasing the country's energy security. But one of the reasons that prevent achieving the objectives – insufficient incentives for the use of RES development and untapped potential for increasing the use of RES by combining the interests of producers, suppliers and consumers, as well as untapped potential of science of Lithuania.

Currently there is no instrument in Lithuania that would encourage consumers to use RES technology – all functioning incentives are applicable to manufacturers or suppliers. Until now such holistic RES technology promotion method, when incentives of RES technology for producers would be combined with those designated for consumers, has not yet been examined. The aim of this paper is to review, which RES technology incentives in households can be adapted in Lithuania. In order to achieve this, the following tasks are being raised:

- to review existing literature of Lithuanian and foreign researchers about RES technology incentives;
- to analyse the experience of other countries in the area of RES technology incentives in households.

These tasks will be achieved using the methodology of analysing, systemizing and generalizing selected scientific literature.

2. EXPERIENCE OF RES ASSESSMENT AND PROMOTION IN LITHUANIA AND WORLD'S LITERATURE

In Lithuania the issue of RES assessment and promotion went under consideration relatively recently, in most cases talking just about incentives for manufacturers of RES technology:

- Jankauskas V. [5] – analyzed various promotion methods for RES using electricity generation.
- Streimikiene D., Bubeliene J. [6] – introduced reader with the common EU framework for the promotion of RES development in the Baltic countries.
- Streimikiene D., Klevas V. [7] – presented and reviewed in detail the means by which renewable energy sources to support policy in the Baltic countries is being implemented.
- Streimikiene D., Pusinaite R. [8] – estimated the awareness of Lithuanian citizens ' of "green " energy benefits.
- Klevas V., Streimikiene D. [9] – particular part of the the book " Lithuanian energy economy" is dedicated to analysing the promotion of renewable energy economy, including the financial and economic promotion measures.
- Klevas V., Streimikiene D., Griksaite R. [10] – analyzed how the improvement of energy efficiency in the Baltic countries could be increased.
- Streimikiene D., Klevas V., Bubeliene J. [11] – made a comprehensive overview of the new EU Member States' capacity to use EU structural funds for sustainable energy projects and the disposal of market failures associated with negative side effects of pollution.
- Katinas V. ir kt. [12] – examined the ways in which assistance can be maximized to infiltrate RES Lithuanian electricity sector and their potential impact on the environment.

- Streimikiene D., Sivickas G. [13] – an overview of indicators system for monitoring the key EU directives and other policy documents related to sustainable energy development.
- Ciegis R., Zeleniute R. [14] – discussed the economic development aspect of sustainability of Lithuania.
- Klevas V., Streimikiene D., Kleviene A. [15] – examined the methodological issues arising from the integration of sustainable energy into regional development procedures.
- Galinis A., Lekavičius V., Miskinis V. [16] – analyzed the wider exploitation of RES.
- Streimikiene D. [17] – analyzed the greenhouse gas life cycle and private expenditure on major future power generation technologies.
- Streimikiene D., Mikalauskiene A., Zaikiene J. [18] – assessed the electricity generation technology coherence in the EU.
- Streimikiene D. [19] – made several transport technologies comparative assessment under the various international climate change scenarios for 2020 and 2050, singling cheap, fuel and vehicles in terms of prices and greenhouse gas terms.
- Streimikiene D. ir kt. [20] – clarified the multiple criteria decision system, choosing the most sustainable energy technologies.

The issue of RES technology assessment and promotion in the world is addressed much more versatile. On this subject in their latest works are debating:

- Taylor M. [21] – described in detail the renewable solar energy policies on innovation in California, with emphasis on the interface between technology producers and users.
- Strbac G. [22] – a research paper discusses the major renewable energy demand management strengths and challenges.
- Langniss O., Diekmann J. ir Lehr U. [23] – the researchers examined three different improvement options of German Renewable Energy, that wouldn't repress or slow down the RES technology.
- Liao C., Ou H. ir Yu Y. [24] – studied renewable energy policy of Taiwan, analyzing renewable energy promotion methods for consumers, producers and investors' side.
- Del Rio P. [25] – a research paper investigated the interaction between energy efficiency measures and the promotion of RES.
- Paulus M. ir Borggreffe F. [26] – investigated the technical and economic feasibility of energy-intensive industries, the potential to provide consumers with electricity in 2030.
- Clastres C. [27] – examined innovative energy systems, which not only encourages competition, increases electrical systems security, the fight against climate change, however, poses a number of economic issues.
- Battle C. [28] – a research paper presented and analyzed an innovative distribution method of grants for the promotion of RES.
- Wood G. ir Dow S. [29] – explored the British renewable energy promotion policy, analyzing the different mechanisms induced by internal and external problems.
- Schmid G. [30] – examined the RES development in India and which forms of politics are most effective.
- Doukas H. ir kt. [31] – analyzed the most common RES techniques, which would be possible to adapt in the Tajik energy sector.
- Moe E. [32] – analyzed the renewable energy sector of Japan.
- Marques A. C. ir Fuihnas J. A. [33] – analyzed various existing forms of politics, which promote renewable energy technologies, in different European countries.
- Boute A. [34] – a research paper analyzed the alternative to the support schemes of RES – promotion of RES technologies by increasing the capacity of the overall energy market.

– Trypolska G. [35] – an overview of Ukraine's adoption of legislation on renewable energy feed-in tariff, the pros and cons, as well as the related challenges.

3. THE REVIEW OF RES TECHNOLOGY ASSESSMENT AND PROMOTION

Economic theory and practice shows that there are significant market barriers and disadvantages of hindering the development of renewable resources [9]:

- commercial barriers, arising from new technologies competitive with conventional technologies;
- market failure in terms of RES social benefits and the negative external effects of traditional energy sources;
- market barriers, such as inadequate information, access to capital constraints, change of initiatives between home owners and renters, and high transaction costs of making small purchases, and institutional barriers.

In order to remove these barriers the necessity of state measures appears. In order to boost the popularity of renewable energy, the world's governments have developed and implemented a variety of mechanisms to promote new technology creators and producers and investors to be more involved in the renewable energy market [9]. However there are no universal RES support schemes. Each EU country has its own system of incentives established in accordance with its tasks, taking into account the situation of their country's power industry [4].

According to Lithuanian researchers [9], RES assessment measures could be divided into groups, such as:

- legal and institutional, specified in the number of EU and Lithuanian legislation and the law;
- guarantees of origin, which are used for electricity generation from RES volume set to show the end user related to the origin of the electricity and help power from RES to demonstrate that the electricity they sell is produced from renewable energy sources;
- economic. They are divided into fiscal (various taxes), financial assistance (grants, tax incentives) and a flexible, market mimic climate change mitigation measures.

All these measures in Lithuania are applied for RES developers, manufacturers or investors, however, the external cost, associated with energy production, is being paid by society [16].

Nevertheless there are a number of prepared detailed works of foreign scientists on applying innovative methods to promote RES on the user side. As it has been already mentioned, there are no universal RES support schemes, however, in order to achieve the objective of this paper, the three different examples in literature are analysed: the experience of non-EU country, the experience of EU country and the general, researcher proposed, method.

The article “Analysis of renewable energy policies in Taiwan”, prepared by National Taiwan University researchers Ching-Hu Liao, Hsin-Hung Ou and Yue-Hwa Yu [24], investigated innovative promotion methods of RES technologies for users. According to scientists, state government must ensure that the renewable energy sector results are consistent with economic, social and environmental objectives raised by the parties, and, in order to achieve this, there are approved incentives and subsidies. The researchers note that in 2008 RES support policies in many countries around the world have been developed and improved and green energy users (as households and firms) in the world has increased to more than 5 million. An increase of the interest of the local authorities to actively plan and implement the policy of promoting the use of RES contributed to this, and also the aim to introduce carbon dioxide emission reduction system. Although in 2004 the Energy Commission, established by the Taiwanese government in 1979, was reorganized and

renamed the Energy Office, pursuing sustainable energy policy, which aimed to achieve positive results in all areas of economic, energy, environmental and public, according to data, in 2008 Taiwan renewable energy accounted for only 0.4% total energy consumption, which was lower than the 2.2% worldwide average.

In cited article the researchers describe energy policy as the government response to the activity of prevailing circumstances in a given energy-related field. For example, the government has to choose whether to maintain the prevailing circumstances in which it is in line with current social objectives or change these circumstances through policies. In this way, the government assumes the responsibility of ensuring that the results of energy sector matches with the economic, social and environmental objectives. According to the article, main energy policy objectives consists of:

- Cost-effectiveness of energy supply;
- Energy consumption efficiency;
- Diversity of energy sources;
- Consistency between energy policy and other policy objectives, such as environmental policy;
- Energy safety;
- Cost and availability of energy resources for low-income earners;
- Energy resources transformation;
- Energy supply technology research;
- A sustainable supply of energy.

In order to achieve these goals, the Taiwanese government established the RES technology incentives and subsidies, which are defined in the Table 1.

Table 1. Promotion programs of RES development

Areas	Beneficiary objects	Fiscal incentives	Non-fiscal incentives
Research, development, demonstration	<ul style="list-style-type: none"> • The Government • Electrical Manufacturers • RES technology manufacturers 	<ul style="list-style-type: none"> • Subsidies for research and development • Capital Grants • Third-party finance 	<ul style="list-style-type: none"> • Legislation and International Agreements • Research, development and demonstration • Energy-saving guidelines • Public investment
Investments	<ul style="list-style-type: none"> • The Government • Electrical Manufacturers • RES technology manufacturers 	<ul style="list-style-type: none"> • Capital Grants • Bidding System • Subsidies for investments • Third-party finance • Investment tax credits • Accelerated depreciation 	<ul style="list-style-type: none"> • Voluntary programs • Administrative Regulation
Manufacturing and Distribution	<ul style="list-style-type: none"> • Electrical Manufacturers • RES technology manufacturers 	<ul style="list-style-type: none"> • Guaranteed price • Production tax credits • Negotiable Certificates 	<ul style="list-style-type: none"> • Voluntary programs • Liabilities
Consumption	<ul style="list-style-type: none"> • The Government • Consumers 	<ul style="list-style-type: none"> • Grants / rebates to consumers • Excise tax exemptions • Net (net) measurement • Fossil fuel taxes 	<ul style="list-style-type: none"> • Liabilities • Government Purchases • Green Energy Costing • Public awareness - education

Source: Ching-Hui Liao and others, 2010

Incentives and subsidies in Taiwan are provided for business and individual businesses in order to be able to install and use RES technologies. However, as can be seen in Table 1, current Taiwanese alternative energy incentives are focused on production, but not on consumption subsidies. Researchers attribute that to the government's initial test to increase the use of RES in the market as quickly as possible. The article states that the RES market is still limited because of its two key properties: a high unit cost of production and a slow return on investment compared to traditional energy sources. RES producers face financial, economic, institutional, political, technical, media and information barriers during market development process. Therefore, incentives – the most commonly used instrument for the government to influence the market development of RES. The article stressed that RES incentives has several important advantages:

- Security of supply: in order to ensure the internal power supply and reduce dependence on imports;
- Improving the environment: reduction of environmental pollution, including different emissions and the implementation of international commitments (such as the Kyoto Protocol);
- Economic benefits: grants, in the form of reduce price, are used to promote specific economic sectors or groups of people, such as reducing poverty and increasing access to energy in developing countries;
- Employment and social benefits: save jobs, especially in the period of transition economies.

The authors stress that the subsidy, that reduces prices of certain energy technologies, may affect the excessive rise of consumer demand for energy or energy dissipation. There are other negative effects of mentioned promotion: government finances can be an intolerably high burden, and also, because of the increased and turned into a waste consumption of fossil energy, incentives become contrary to the objectives of sustainable development. So the abuse of RES technology incentives can increase toxic and greenhouse gas emissions in the RES market, which cause irreparable damage to resources and environment as a whole. However, according to authors of the article, it would be possible to avoid that by calculating the promote efficiency of RES policy. This efficiency is calculated by comparing the amount of renewable energy that goes to the public and the optimum amount of energy needed to produce the energy using RES technologies. Such a difference would show the wasted amount of energy and the less it would be, the more correct is the existing policy that promotes the use of RES.

Ultimately researches conclude that rational policy, which promotes the use or RES, should allow the consumers to choose the use of renewable energy, in spite of the fact that it is more expensive, and to encourage them to buy green power products. Therefore, in the policy of RES as important as economic efficiency should also be the ambition for social equity and justice, and addressed issues of environmental and sustainable development. In addition, RES policies should be consistent with other policies such as transport, industry, tax, social.

In the article of German scientists O. Langniss, J. Diekmann and U. Lehr “Advanced mechanisms for the promotion of renewable energy – Models for the future evolution of the German Renewable Energy Act” [23] it is stated that the mentioned act was a very successful renewable energy technology promotion tool in Germany. Nevertheless, because of the growing integration of the electricity markets and increasingly frequent fluctuations in electricity production, the document needs improvement. In this article, the researchers described the different options for the improvement of the Act: offering appropriate and flexible measures to promote RES and quantitative compensation scheme, which would not slow down the RES technology.

In Germany the share of renewable energy in total energy production continues to grow, and the challenge is to maintain the share of renewable energy resources to consumers at as low rates as possible. Focusing on economic stimulus measures in the light of quantitative compensation system resulting negative impact, the author suggests three alternative German Renewable Energy Act of opportunities for improvement: the so-called “retailer model”, “market mediator model” and “optional bonus model”. The researchers stressed, that in order to achieve the objective firstly one must answer the question – who should realize the renewable energy in the market?

German Renewable Energy Act – is the system of feed-in tariff based on the lowest price standard, which requires the distribution network operators to connect renewable electricity-producing power plants and buy their electricity at a fixed price. Pay depends on the cost of the influence of technology, equipment capacity and other factors. In order to insure investors, the reward is determined for twenty years, and for newly connected companies it is declining each year. The Act provides for priority of RES connection to the network, thus avoiding obstacles to the alternative energy producers supplying energy to consumers.

The article emphasizes that, despite the apparent growth of renewable energy, there is need to increase competitiveness of RES technology manufacturers and suppliers. It is expected that the increase of the competitiveness would reduce the cost of promoting of renewable energy generation and thereby reduce their price. Thus, the authors argue that incentives are necessary in order to support the deployment of renewable energy and these incentives should have a positive impact not only for producers, but also consumers. Integration of renewable energy promotion should be assessed in two ways:

1) Improving the integration of renewable energy production systems in the energy supply system. Energy production and distribution flows should correspond as closely as possible with the actual energy demand in the long and short term, in the long run creating the capacity value.

2) Strengthening the commercial integration of renewable energy in the electricity market. Raising the question of who and under what conditions should sell renewable energy?

In scientists described “retailer model” the promoting measure of RES technologies is a competitive advantage that drives the traders as possible to effectively combine their energy sales to the actual demand. In this way, renewable energy prices for consumers would be reduced.

The essence of “market mediator model” – one or more market intermediaries become responsible for renewable energy integration and trade, but the distribution companies would still be forced to buy renewable energy by paying a fee for it provided the act. After that, distribution network operators would resell the energy for the market intermediaries distributor resold energy market intermediaries for the same price, and market intermediaries would seek to maximize their benefits while selling energy. It may happen that the market intermediaries received pay would not cover costs from purchasing energy from the distribution network operators. That is way the premium paid payment? is needed. The premium paid would be made by consumers in the form of tax to the electricity transmission system operators, who later would return it to market intermediaries. In this model, it is essential that market intermediaries operate as profit disciples, thus the market would create a strong incentive for the integration of renewable energy in the most efficient and most favorable economic measures.

Third scientists proposed “optional bonus model”, which is based on business equipment operators promoting greater integration of their products, i.e. energy from RES. Bonuses are differentiated according to the technology and each year it decreases for the

newly formed energy companies. Plant operators should take care of energy market sales and the receipt of income, excluding bonuses, by themselves. This model forces operators of companies to adjust the supply of generated energy to the existing demand. In this way, users can be also, albeit indirectly, encouraged to choose green energy.

In the end researches state that each of these models (promotional techniques) has some disadvantages, so each of the models involved (operators, manufacturers, consumers, investors, business operators) need to understand the risks of their actions, and the state has to decide which promotion model it is appropriate to choose under different circumstances.

In the research paper of C. Battle “A method for allocating renewable energy source subsidies among final energy consumers” [28] it is stated that there is a need for methodology for allocating the cost of RES subsidies that ensures an optimal balance between compliance with the main regulatory principles of tariff design and each state’s specific policy is of cardinal importance in the current context. Application of the new method would take into account the fact the proportions consumers use energy in spite of its type (liquid fuel, gas, electricity or coal).

The author emphasizes that the RES can help solve problems such as the preservation of the natural environment and national energy security, it is now possible to observe the world to promote the use of RES growth trends in both energy supply and transport. Despite the innovation of RES technology sector and lower investment costs, RES technology is still not able to compete with conventional energy sources. Therefore use of RES technology is dependent on the promotional methods designed for investors, in order to guarantee their return on investment, but ultimately the cost of subsidies is redeemed by the final consumers and/or taxpayers.

The utility of distribution method describes a situation where the production costs are the lowest, and the price is equal to marginal cost. Thus consumers’ marginal utility of buying the product is equal to its alternative costs of supply. In this way, according to market participants’ preferences, production technology maximizes the benefits, in other words, the maximization of energy production efficiency influences the reduction of costs of production.

The researcher described the method in a stylized mathematical model and concluded that the solution that he proposes is consistent with the basic principles that should govern tariff design, maximizing allocative efficiency and equity. Thus, according to the author, the RES subsidy-driven extra costs distribution is ruled according to the marginal cost pricing and cost-causality principles. The author emphasizes that the methodology entails that all final fuel consumers should pay the costs of RES promotion programmes in proportion to their final consumption, regardless of the origin of renewable energy (such as biofuels or wind or solar energy).

RESULTS

As can be seen after literature analysis, although all researchers agree upon the importance of RES usage and the benefits that it provides, even economically strong countries are struggling with obstacles in the area of RES technology promotion in consumers’ side. And though it is difficult to compare these three described examples, the portrayed experiences suggests that no methods of RES promotion on consumers side could be adapted in Lithuania before further investigation in order to clarify certain key issues, such as:

- The government has to decide, what will be its role in pursuance to encourage households to use RES.
- Who and under what conditions should sell renewable energy?
- Who will implement renewable energy in the market?

- It is highly important to increase competitiveness of manufacturers and suppliers in that case the cost of promoting RES and its price will be lower. However this requires particularly close cooperation of manufacturers and suppliers.
- The higher mentioned lower than it is now price of RES technology for consumers is not a promotional tool itself, but it can become one when combining it with consumers awareness.
- Nevertheless, next to promotion methods for households using RES, its policy should cooperate with social policy in such a way that every household would be informed about their options to choose between traditional energy resources and RES and they would deliberately choose to use RES.

CONCLUSION

1. Renewable energy sources (RES) are an attractive alternative to traditional energy since it might help to solve many climate change and economic problems and also to ensure the country's energy independence.

2. Insufficient incentives for the use of RES development and untapped potential for increasing the use of RES by combining the interests of producers, suppliers and consumers, as well as untapped potential of science of Lithuania, prevent achieving the main – making energy from RES by 2020 increase to 23%.

3. Many Lithuanian scientists in their work analyzed the use of RES technologies and examined their incentive problems mainly oriented to the approach of investors and producers, regardless the fact that households, also being the economic players, as well may contribute to the development of RES.

4. After the foreign scientists works review it can be said that the aim of the article is only partially achieved, yet it can be confidentially stated that each country has its own promotion methods and apply them in different ways, therefore, using the good practice, it would be possible to complete the analyzes of renewable energy resources – to identify new renewable energy incentives aimed to consumer sector in Lithuania, however it only can be done when firstly identifying certain fundamental issues.

REFERENCES

1. Lietuvos Respublikos atsinaujinančių išteklių energetikos įstatymas. *Valstybės žinios*. 2011, Nr. 62-2936.
2. Lietuvos Respublikos nacionalinė energetikos strategija. *Valstybės žinios*. 2007, Nr. 11-430.
3. Lietuvos Respublikos energetikos įstatymas. *Valstybės žinios*. 2011, Nr. 160-7576.
4. Lietuvos Respublikos valstybės kontrolės 2010 m. sausio 15 d. valstybinio audito ataskaita Nr. VA-P-20-2-1 „Atsinaujinančių energijos išteklių potencialo naudojimas Lietuvoje“.
5. JANKAUSKAS V. Elektros energijos, pagamintos naudojant atsinaujinančius energijos išteklius, rėmimo būdai. *Energetika*. 2004, 4, p. 1–11.
6. STREIMIKIENE, D.; BUBELIENĖ, J. Policies and Measures to Enhance the Use of Renewable Energy Sources in the Baltic States. *Aplinkos tyrimai, inžinerija ir vadyba*. 2005, 2(32), p. 63–74.
7. STREIMIKIENE, D.; KLEVAS, V. Promotion of Renewable Energy in Baltic States. *Renewable and Sustainable Energy Reviews*. 2005, 11, p. 672–687.
8. Streimikiene, D.; Pušinaitė, R. Lietuvos vartotojų preferencijos ir pasirengimas mokėti už „žaliąją“ energiją. *Ekonomika*. 2006, 74, p. 78–90.

9. KLEVAS, V.; STREIMIKIENE, D. 2006. *Lietuvos energetikos ekonomikos pagrindai*. Kaunas: Lietuvos energetikos institutas.
10. KLEVAS, V.; STREIMIKIENE, D.; GRIKŠTAITĖ, R. Sustainable Energy in Baltic States. *Energy Policy*. 2007, 35, p. 76–90.
11. STREIMIKIENE, D.; KLEVAS, V.; BUBELIENĖ J. Use of EU Structural Funds for Sustainable Energy Development in New EU Member States. *Renewable and Sustainable Energy Reviews*. 2007, 11, p. 1167–1187.
12. KATINAS, V., et al. Governmental Policy and Prospect in Electricity Production from Renewables in Lithuania. *Energy Policy*. 2008, 36, p. 3686–3691.
13. STREIMIKIENE, D.; ŠIVICKAS, G. The EU Sustainable Energy Policy Indicators Framework. *Environment International*. 2008, 34, p. 1227–1240.
14. ČIEGIS, R.; ZELENIŪTĖ, R. Lietuvos ekonomikos plėtra darnaus vystimosi aspektu. *Taikomoji ekonomika: sisteminiai tyrimai..* 2008, 2(2), p. 11–28.
15. KLEVAS, V.; STREIMIKIENE, D.; KLEVIENĖ, A. Sustainability Assessment of the Energy Projects Implementation in Regional Scale. *Renewable and Sustainable Energy Reviews*. 2009, 13, p. 155–166.
16. GALINIS, A.; LEKAVIČIUS, V.; MIŠKINIS, V. *Atsinaujinančių energijos išteklių platesnio vartojimo kryptys*. Mokslas ir technika [interaktyvus]. Vilnius, 2010 [žiūrėta 2012-06-10]. <<http://www.mokslasirtechnika.lt/mokslo-naujienos/atsinaujinanci-energijos-istekli-platesnio-naudojimo-kryptys.html>>
17. STREIMIKIENE, D. Comparative Assessment of Future Power Generation Technologies Based of Carbon Price Development. *Renewable and Sustainable Energy Reviews*. 2010, 14, p. 1283–1292.
18. STREIMIKIENE, D.; MIKALAIŠKIENĖ, A.; ZAIKIENĖ, J. Elektros energijos gamybos technologijų darnumo vertinimas, taikant integrutous rodiklius. *Energetika*. 2011, 3, p. 147–153.
19. STREIMIKIENE, D. Comparative Assessment of Future Motor Vehicles Under Various Climate Change Mitigation Scenarios. *Renewable and Sustainable Energy Reviews*. 2011, 15, p. 3833–3838.
20. STREIMIKIENE, D., et al. Prioritizing Sustainable Electricity Production Technologies: MCDM Approach. *Renewable and Sustainable Energy Reviews*. 2012, 16, p. 3302–3311.
21. TAYLOR, M. BEYOND Technology-Push and Demand-Pull: Lessons from California's Solar Policy. *Energy Economics*. 2008, 30: 2829–2854.
22. STRBAC, G. Demand Side Management: Benefits and Challenges. *Energy Policy*. 2008, 36, p. 4419–4426.
23. LANGNISS, O; DIEKMANN, J.; LEHR, U. Advanced Mechanisms for the Promotion of Renewable Energy – Models for the Future Evolution of the German Renewable Energy Act. *Energy Policy*. 2009, 37, p. 1289–1297.
24. Liao, C.; Ou, H.; Yu, Y. Analysis of Renewable Energy Policies in Taiwan. *Environmental Engineering and Management Journal*. 2010, 20(3): 195–201.
25. DEL RIO, P. Analysing the Interactions between Renewable Energy Promotion and Energy Efficiency Support Schemes: The Impact of Different Instruments and Design Elements. *Energy Policy*. 2010, 38, p. 4978–4989.
26. PAULUS, M.; BORGGREFE, F. The Potential of Demand-Side Management in Energy-Intensive Industries for Electricity Markets in Germany. *Applied Energy*. 2011, 88, p. 432–441.

27. CLASTRES, C. Smart grids: Another Step Towards Competition, Energy Security and Climate Change Objectives. *Energy Policy*. 2011, 39, p. 5399–5408.
28. BATLLE, C. A Method for Allocating Renewable Energy Source Subsidies among Final Energy Consumers. *Energy Policy*. 2011, 39, p. 2586–2595.
29. WOOD, G.; DOW, S. What Lessons have been Learned in Reforming the Renewables Obligation? An Analysis of Internal and External Failures in UK Renewable Energy Policy. *Energy Policy*. 2011, 39, p. 2228–2244.
30. SCHMID, G. The Development of Renewable Energy Power in India: Which Policies have been Effective? *Energy Policy*. 2012, 45, p. 317–326.
31. DOUKAS, H., et al. Promoting Renewables in the Energy Sector in Tajikistan. *Renewable Energy*. 2012, 39, p. 411–418.
32. MOE, E. Vested Interests, Energy Efficiency and Renewables in Japan. *Energy Policy*. 2012, 40, p. 260–273.
33. MARQUES, A. C.; FUINHAS, J.A. Are Public Policies Towards Renewables Successful? Evidence from European Countries. *Renewable Energy*. 2012, 44, p. 109–118.
34. BOUTE, A. Promoting Renewable Energy Through Capacity Markets: An Analysis of the Russian Support Scheme. *Energy Policy*. 2012, 46, p. 68–77.
35. TRYPOLSKA, G. Feed-in Tariff in Ukraine: The Only Driver of Renewables' Industry Growth? *Energy Policy*. 2012, 45, p. 645–653.



WAYS TO INCREASE THE EFFICIENCY OF HYDROKINETIC DEVICES AND THEIR EVALUATION

A. Kalnacs, J. Kalnacs, A. Mutule

*Institute of Physical Energetics
Aizkraukles street 21, LV-1006, Riga – Latvia*

V. Entins

*LLC „Environment, Bioenergetics and Biotechnology Competence centre”
Aizkraukles str. 21, LV-1006, Riga – Latvia*

ABSTRACT

River flow hydrokinetic devices have several advantages, but there is also one major drawback of this technology compared to other hydrokinetic technologies. The density of the energy is relatively low in the flow of a river. Channelling devices such as diffusers and ducts are the means that allow for efficient concentration of this energy as well as provide other benefits that enable more efficient energy production with hydrokinetic devices. This work serves as the concise overview of the benefits, challenges and opportunities that channelling devices offer. A method for evaluation and comparison of the gains that use of different channelling devices may offer is proposed based on the overview. Conclusions regarding further research and development of channelling devices are drawn.

Keywords: Hydroelectric power generation, microhydro power, hydrokinetic device, flow velocity, diffuser, duct, channelling device

1. INTRODUCTION

Hydrokinetic technology have seen much attention and had developed rapidly during the last decade [1, 2, 3, 4]. It enables extraction of energy from waves and free flow of water in seas, oceans and rivers. According to the source of the energy hydrokinetic technologies can be distinguished into wave, tidal and free flow. Most concentrated energy is in waves and tidal streams. This explains why there are more attention is devoted to and research conducted regarding wave and tidal hydrokinetic technologies. The least concentrated energy is in river streams. However river flow technologies have their advantages too. Some of the most important ones are:

- it is much less complicated to extract energy from free flow than from waves;
- there are many consumers of electricity located next to or near the rivers (as oppose to big enough waves, tides and flows in the sea or ocean);
- wave, tidal and marine free flow power plants need to be placed at a considerable distance from the coast, making their connection to the grid and maintenance more complicated and expensive;
- the river environment is much more friendly to technical power plant equipment, than sea or ocean which allows river devices to be less complicated, and less expensive;
- tidal (and in many cases also marine) flows change in direction and velocity, whereas river flows are unidirectional and usually does not change much in velocity. This again allows river technology to be less complicated.

In case of Latvia, when there is no tidal energy available, river free flow devices can be utilized for the power supply for stand-alone objects or object groups of up to 1 MW. Wave

power plants in Latvia can be used for generation of larger amounts of power and supplying it into the grid.

The potential of the river free flow hydrokinetic energy is considerable.

Taking into account how many kilometres of rivers are there, hydrokinetic (free flow) devices may become one of the main local electricity production choices compared to other types of renewable energy sources, especially ones that does not produce emissions.

In Latvia the density of rivers is 0.6 km on each square kilometre [5]. Assuming that 10 square meters of such river are used for electricity production (1m average depth and 10 m average width), very rough estimate, using assumptions and other data from the work described further, shows that 100 MWh of electricity can be produced per year in Latvia on each square kilometre. Multiplied by the Latvia territory of 64589 km² it gives a total of 6.46 TWh. It should be stressed that this is renewable and sustainable energy source. This energy is produced without emissions, while keeping rivers available for other uses and with negative impact on environment close to zero.

Given the indications of the considerable potential of hydrokinetic energy from rivers and the comparatively lower concentration of this energy, two major questions deserving research are how to increase the concentration of the energy and how to evaluate its potential and the effect from increasing its concentration.

2. CHANNELING DEVICES AND NEED FOR EVALUATION

As it was described the only major disadvantage of the river free flow hydrokinetic technologies, compared to other hydrokinetic technologies is the lowest concentration of the energy.

The power of a single hydrokinetic device as well as the power that can be obtained from one cross-section of the river with this type of devices is calculated by the same formula:

$$N = k \cdot v^3 \cdot S \cdot \rho, \quad (1)$$

where:

k is an empirical coefficient depending on the device;

v is the flow velocity before (upstream) the device or cross-section (m/s);

S is the cross-sectional area of the flow (m²);

ρ is the flow (water) density, kg/m³;

$m=(v \cdot S \cdot \rho)$ is the mass of water per second which runs through the device or cross-section.

Flow velocity has the most substantial impact on the power output of the hydrokinetic free flow power plants. Concentration of the energy in the free flow grows together with the flow velocity and to the third degree faster than the flow velocity. It impacts the output of the power plant not only directly (see (1)), but also indirectly by changing efficiency coefficient that is included in the constant k in (1).

Flow velocity usually transforms into the rotational speed of the turbine and the efficiency coefficient of the generators increases together with the rotational speed as well. This gives opportunities to increase the efficiency of the free flow hydrokinetic power plants. Using Bernoulli law the opportunities to concentrate kinetic energy and to rise the efficiency of device are exploited with different kind of channelling devices [6, 7, 8, 9, 10]. While increasing the flow velocity, channelling devices also reduce the available area that the active parts of the hydrokinetic devices (such as propellers, blades or other like parts) can cover. This area is equal to the area that is covered by the channeling device itself and thus cannot be covered with the active parts of the hydrokinetic device (HKD). The result is reduction in S (see (1)) that causes linearly reduction into the output power of the device. Since the gain in

velocity increases the power proportional to the third degree, gains in power are higher than the losses due to area (S) reductions.

Channeling devices are simpler and require less maintenance than HKD and does not have moving parts. Therefore a HKD equipped with a channeling device usually is less costly to produce and maintain than a HKD without channeling device that would cover the same area.

Use of channelling devices can also increase costs in some aspects, but they are strongly outweighed with the achieved gains. Since channeling devices are clear obstacles for the flow, they are subject to considerable drag forces [10, 11]. Thus major aspect of increase in costs to consider is mooring of the channelling devices. It is also an aspect to consider when choosing dimensions and shape of the channeling device as well as when developing new channelling devices. Pair of words “channelling device” seems the most universal name from reviewed in literature for all devices of this nature. There are plenty of other terms used in literature to name the channeling devices, but they as a rule refer to some specific kind of channeling device or specific part of a channeling device. The most popular of such words are concentrator, diffuser and duct. Diffuser refers to a channeling device which have an outlet (or nozzle) after (downstream) the HKD which has larger or the same cross-section area than inlet which is all covered by the active parts of HKD. Duct usually refers to the same things as “channeling device” but, since this word has the meaning on its own, using it without proper definition can create confusion. Pair of words “channeling device” is chosen to refer to the devices here and is suggested as most appropriate from reviewed ones to refer to all devices of this kind. Fig. 1 for examples of channelling device.

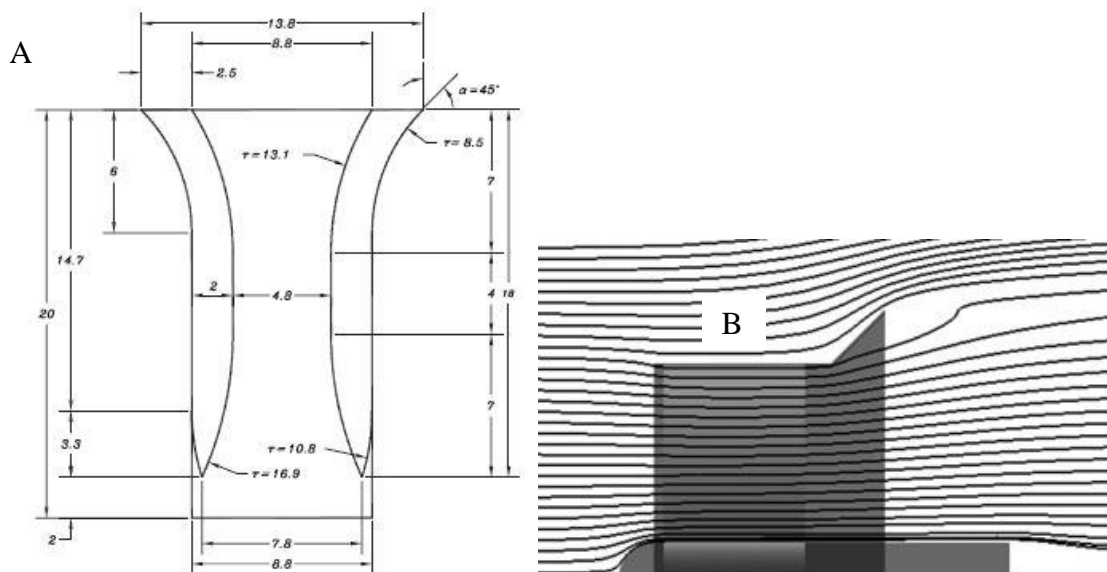


Fig. 1. Examples of channelling device (A taken from [16]; B taken from [10])

As it is revealed in several works [12,13] channelling devices can be very different and provide for very substantial increase in velocity of the flow that operates a hydrokinetic device. Consequently, channeling devices can be used to increase the energy concentration in the free flow efficiently. As the river free flow is the one with the least power concentration, it can gain the most from channeling devices, compared to other hydrokinetic technologies.

Channelling devices also provide opportunities to extract power from a free flow beyond the Betz limit [10, 14, 15]. According to the Betz limit the maximum power that can be extracted from the free flow equals to 60% of the kinetic energy in the flow, but this is

stated with the assumption that the entire inlet area of the flow is swept by the active parts of turbine and ignores the presence of channeling device.

The efficiency of channeling devices in concentrating the free flow kinetic energy increases when this concentration of energy becomes lower [16]. This provides more opportunities for adopting free flow HKD in plain regions with many calm rivers such as in Latvia, all Baltic countries and many other parts of the world. Flow velocity measurements in the rivers of Latvia show that in most of the places which are best suitable for operation of hydrokinetic devices flow velocity is between 0.4 and 0.9 m/s. For efficient operation of hydrokinetic devices, it is advisable to place them into at least two to three times faster flows. Possible designs and operation of channeling devices for rivers with flow velocities around and below 1 m/s are least researched and have highest potential to give good results.

River hydrokinetic devices represent rather new technology and most of them, especially most promising, are only on their initial stages of the development. Thus their potential is usually evaluated only in theoretical or very specific, but not in real circumstances.

There is a wide variety of rivers, hydrokinetic devices and channeling devices to choose from. Thus it is essential to be able to evaluate the potential of a river in general and for use of a specific HKD and channelling devices. It would be very helpful for choosing the best places for the deployment of the hydrokinetic devices as well as choosing the best HKD and channelling devices for the particular segment of a river.

Mentioned needs can be satisfied with a method that allows both the evaluation of the rivers energy in general and evaluation of the results of use of some specific hydrokinetic technology.

3. EVALUATION METHOD

Method for the evaluation of the energy potential of a river for the development of power plants based on hydrokinetic devices were developed to assess the potential of specific spans of a river Daugava in Latvia [17]. However it can be used for evaluation of any river or span of a river where it is possible to move by boat or any similar floating device and keep this floating device motionless against the banks of the river. Method covers also the validations of the obtained flow velocity, bed depth and other measurement data against the statistical data of the flow rate. Full description of the method is available at [18].

The method consists of the following consecutive steps:

1. Measurements of the flow velocity and depth of the river bed in the several river cross sections.

2. Validation of the obtained measurement data. Calculated data of the flow rate at the time when measurements were performed must be compared with statistical averages of the flow rate. For rivers in Latvia required statistical data can be obtained from the internet [19].

3. To reduce unnecessary workload, river segments where bed depth, flow velocity or other obtained critical characteristics are not satisfactory need to be excluded from further evaluation and analysis.

4. Explored spans of the river should be rearranged into segments based on flow velocity and other critical characteristics. Spans that have been explored and are retained for further analysis should be arranged into continuous segments with relatively equal critical characteristics throughout the entire segment. There could be several such characteristics, when performing the evaluation for some specific technology. For example, average bed depth and/or cross section width in addition to flow velocity could be considered. Thus segments where specific count of devices can be set up in a single cross section (next to and/or above/below each other) will be established.

5. For all segments defined during step 4 a potential for production of electrical energy should be calculated based on formula (1). To calculate this potential energy, following parameters should be defined:

- a. cross-sectional area of the river that is used by hydrokinetic devices,
- b. efficiency ratio of the hydrokinetic devices,
- c. efficiency ratio of the electricity generator,
- d. the distance between the devices in the direction of the river flow,
- e. idle standing days in a year.

To enable evaluating the use of a channeling device the described methodology is updated with two additional parameters to those described in the step 5.

- f. area ratio of the channeling device (calculated as outlet area/inlet area of the channeling device) [10]: this parameter takes into account the area that the channeling device occupies and thus reduces the S (see (1)),
- g. efficiency ratio of the hydrokinetic devices, if used together with the channeling devices: this parameter takes into account gains in v and N (see (1)).

4. RESULTS

The final results table for the evaluation is also updated with several columns to allow comparison between different segments of a river, different HKD and their performance without and with the channelling devices (see columns 10–15 in Table 1).

The flow velocity and bed depth data for the Table 1 are taken from [17]. All the calculations and analysis of data that does not concern the channelling devices can be obtained from the respective work. The data for the channelling device A is taken from [16] and the data for channelling device B is taken from [10] regarding the channelling device E1A6 profile. Descriptions and other information regarding the channelling devices A and B can be obtained in the respective works. The channelling devices are pictured in Fig. 1.

The data in the Table 1 shows that the use of channelling device A can increase electricity production in the given circumstances by 47% while channelling device B can increase it by 110%. The performance data of channelling device A has been obtained from empirical experiment. It is a device that have the best practically proved results as found by the internet research performed for this work. The channelling device B has more than two times better performance, but it is only a theoretical device and its performance is theoretical.

The results show that channelling devices can increase the electricity production substantially and thus can increase the efficiency of HKD. Channelling devices are least researched for use with flow velocities at about 1 m/s and below, but their efficiency is higher at these lower flow velocities. This provides opportunities for use of HKD with channelling devices especially in slower rivers. Provided that there is a theoretical possibilities to increase the efficiency of channelling devices to at least 110%, it is even more prospective field of research for countries with many relatively slower rivers.

The theoretical data regarding performance of the channelling devices at the flow velocities below 1 m/s should be verified in an experiment where the optimal dimensions of the channelling device are also found for each particular HKD.

Table 1. Evaluation of the potential for electrical energy production with hydrokinetic devices in the explored spans of Daugava

							No channeling device				Channeling device A [16]		Channeling device B [10]	
1	2	3	4	5	6	7	8	9	10	11	12	13	14	15
#	Location in Daugava (number of cross-section or point)		Length (m)	Flow velocity (m/s)	Cross-section area (m ²)	Flow energy potential of the whole cross-section(W)	Attainable electrical power from cross-section (W)	Amount of electrical energy per year (MWh)	Power from 1 km of the river (KW)	Amount of electrical energy per year from 1 km (GWh)	Power from 1 km of the river (KW)	Amount of electrical energy per year from 1 km (GWh)	Power from 1 km of the river (KW)	Amount of electrical energy per year from 1 km (GWh)
	Start	End												
1	45	41	750	2.416	n/d	n/d	n/d	n/d	n/d	n/d	n/d	n/d	n/d	n/d
2	38	30	4000	0.759	n/d	n/d	n/d	n/d	n/d	n/d	n/d	n/d	n/d	n/d
3	29	24	4400	0.534	697.7	53041	2254.24	1596.072	198.373	0.363	292.232	0.534	457.783	0.837
4	24	21	3000	0.454	1167.5	54671	2323.51	1121.671	139.410	0.374	205.372	0.551	321.716	0.863
5	21	10	850	n/d	n/d	n/d	n/d	n/d	n/d	n/d	n/d	n/d	n/d	n/d
6	10	n/d	n/d	below 0,45	n/d	n/d	n/d	n/d	n/d	n/d	n/d	n/d	n/d	n/d
7	9	5	2150	0.800	557	142529	6057.49	2095.711	260.472	0.975	383.713	1.436	601.089	2.249
8	5	3	3000	0.677	772	119848	5093.55	2458.906	305.613	0.820	450.212	1.207	705.260	1.891
9	3	1	4000	0.479	1181.7	64987	2761.96	1777.776	220.956	0.444	325.501	0.655	509.900	1.026
10	1	n/d	n/d	below 0,41	n/d	n/d	n/d	n/d	n/d	n/d	n/d	n/d	n/d	n/d

5. CONCLUSIONS

Based on the results of this work following conclusions regarding use of channelling devices together with HKD can be made:

- Calculations show that channelling devices can increase efficiency of electricity production with HKD by 50% to 110%.
- Channelling devices is a prospective solution to increase efficiency of especially river free flow as well as other free flow HKD.
- Effects of using the channeling device can be evaluated using the method proposed in this work.
- More research should be done to develop channeling devices for the river with flow velocities around and below 1 m/s as they are least researched so far and promise the best increases in the efficiency of HKD.
- Reducing drag that channeling devices create and efficient mooring solutions to withstand the drag forces shall be among top priorities in further research and development of channelling devices.

ACKNOWLEDGEMENT

This work has received a financial support of the European Regional Development Fund according to the agreement between LLC „Environment, Bioenergetics and Biotechnology Competence Centre” and “Investment and Development Agency of Latvia” from April 11, 2011 regarding implementation of the project # L-KC-11-0005. Complete research results are available at www.vbbkc.lv

REFERENCES

1. KHAN M.J., BHUYAN G., IQBAL M.T., QUAICOE J.E. Hydrokinetic energy conversion systems and assessment of horizontal and vertical axis turbines for river and tidal applications: A technology status review. *Applied Energy*, 2009, Vol. 86, p. 1823–1835.
2. LAGO L.I., PONTA F.L., CHEN L. Advances and trends in hydrokinetic turbine systems. *Energy for Sustainable Development*, 2010, Vol. 14, Iss. 4, p. 287–296.
3. SURNES K. Small-scale Water Current Turbines for River Applications. ZERO – Zero Emission Resource Organisation 2010. Link to the internet <www.zero.no>
4. KHAN M.J., IQBAL M.T., QUAICOE J.E. River current energy conversion systems: Progress, prospects and challenges. *Renewable and Sustainable Energy Reviews*, 2008, Vol. 12, No. 8, p. 2177–2193.
5. RUDOVICS A. *Latvijas fiziskā ģeogrāfija*, Zvaigzne ABC, 1996.
6. MUKRIMIN S.G. Evaluation and measures to increase performance coefficient of hydrokinetic turbines. *Renewable and Sustainable Energy Reviews*, 2011, Vol. 15, p. 3669–3675.
7. WANG SH., XU CH., YUAN P., WANG Y. Hydrodynamic optimization of channelling device for hydro turbine based on lattice Boltzmann method; *Computers and Mathematics with Applications*, 2011, Vol. 61, p. 3722–3729.
8. MALIPEDDI A.R., CHATTERJEE D. Influence of duct geometry on the performance of Darrieus hydroturbine. *Renewable Energy*, 2012, Vol. 43, p. 292–300.

9. SHIOMI N., SETOGUCHI T., KINOUE Y., KANEKO K., OHYA Y. Development of Two-Way Diffuser for Tidal Energy Conversion System. Proceedings of The Thirteenth (2003) International Offshore and Polar Engineering Conference. Honolulu, Hawaii, USA, 2003 May 25–30.
10. GADEN DAVID L.F., BIBEAU ERIC L. A numerical investigation into the effect of diffusers on the performance of hydrokinetic turbines using a validated momentum source turbine model. *Renewable Energy*, 2010, Vol. 35, p. 1152–1158.
11. SETOGUCHI T., SHIOMO N., KANEKO K. Development of two-way diffuser for fluid energy conversion system. *Renewable Energy*, 2004, Vol. 29, p. 1757–1771 [technical note].
12. LAWN C.J. Optimization of the power output from ducted turbines. Proceedings of the Institution of Mechanical Engineers, Part A (Journal of Power and Energy) 2003, Vol. 217, p. 107–117.
13. PHILLIPS D.G., NASH T.A., OAKLEY A., FLAY R.G.J., RICHARDS P.J. Computational fluid dynamic and wind tunnel modelling of a diffuser augmented wind turbine. *Wind Engineering*, 1999, Vol. 23, p. 7–13.
14. BETZ A. *Wind-Energie und ihre Ausnutzung durch Windmuehlen*. GoÖttingen: Bandenhoeck & Ruprect, 1926.
15. JAMIESON P. Generalized limits for energy extraction in a linear constant velocity flow field. *Wind Energy*, 2008, Vol. 11, p. 445–457.
16. PONTA F., JACOVKIS P. Marine-current power generation by diffuser-augmented floating hydro-turbines. *Renewable Energy*, 2008, Vol. 33, p. 665–673.
17. KALNACS J., KALNACS A., MUTULE A., PĒRSIS U. Potential of the lower Daugava for sitting hydrokinetic turbines. *Latvian journal of physics and technical sciences*, 2013, Vol. 50, p. 3–14.
18. KALNACS A., KALNACS J., MUTULE A., PĒRSIS U. Methods for estimation of the riverflow potential for hydrokinetic power generation. *Latvian journal of physics and technical sciences*, 2014, Vol. 51, p. 26–36.
19. State Limited Liability Company "Latvian Environment, Geology and Meteorology Centre": Link to the internet <www.meteo.lv>

ANALYSIS OF THE IMPACT OF CLIMATE CHANGE ON WIND ENERGY RESOURCES

N. Urbonas, A. Kanapickas

*Department of Physics, Vytautas Magnus University
Vileikos 8, LT-44404, Kaunas – Lithuania*

ABSTRACT

The variability of wind speed is the most important issue that determines the reliability of wind electricity generation in short-term time scales. For long time scales the energy produced by wind farms is based on the data about typical wind speeds averaged over at least 30 year time period. However, because of climate change environmental parameters including wind speed have drastically changed during the last century. Therefore, the overall performance of wind farms can be affected by these changes. In the present work, the changes of wind speed in Lithuania as well as in some neighboring regions are analyzed. Monthly mean wind speed data of Lithuania (Klaipėda, Laukuva and Kaunas) was acquired from Lithuanian Hydrometeorological Service; of Germany (Bremen, Schleswig, Greifswald) and Estonia (Voru, Vilsandi) regional monthly mean wind speed data was acquired from the Association of the European Climate. It was found that for the most sites average wind speed decreased during the analyzed time period. For instance, mean wind speed in Kaunas decreased by 0,7 m/s in 1977-2013 (about 22 %). A similar tendency was observed in Estonia where mean wind speed declined by about 1 m/s. Potential energy loss due to the decrease of wind speed was calculated by using RETScreen program model; wind turbine Enercon E82 2 MW was chosen as a sample. It was revealed that potential annual energy generated in Klaipėda and Kaunas sites would have decreased by 2100 MWh and 1200 MWh respectively. That amounts for about 40% of reduction in potentially generated energy at these sites. The same analysis was applied to a region in Germany where potential amount of energy generated would have decreased by 16-19 %. Obtained results show that climate change induced wind speed reduction and may have an adverse effect on the amount of energy generated by the wind power plants.

Keywords: climate change, wind speed, wind energy resources

1. INTRODUCTION

Renewable energy share of global final energy consumption currently meet approximately 19 % of energy demand world-wide [1], only 1.1% of this amount comes from the wind power generation. In 2012, almost 45 GW of wind power capacity began operation thus reaching the number of 283 GW and increasing global wind capacity by 19% [1]. Total wind power capacity by the end of 2012 was enough to meet at least 2.6–3% of global electricity consumption. In the EU, wind capacity operating at year's end was enough to cover 7% of the region's electricity consumption in a normal wind year [1]. Wind power accounted for 32% (11.2 GW) of new installations of power generating capacity in 2013 [2]. The wind power capacity installed in the EU would produce 257 TWh of electricity in an average wind year, enough to cover the 8% of the EU's total electricity consumption [2].

Wind energy remains a relatively small fraction of worldwide electricity supply and its growth has been concentrated in Europe, Asia and North America [3]. According to International panel on Climate Change (IPCC) forecast (Assessment Report [4] or Special Report Renewable Energy Sources [3]), on- and offshore wind energy could contribute from 4.8 to 7% of global electricity supply by 2030 depending on the policy scenario. Wind energy's contribution to the global electricity supply could rise to 13–14% by 2050 if the median scenario for greenhouse gas concentration stabilization was taken up [1].

Nevertheless, the current trend of wind energy technology development can largely contribute to the environmental protection measures, climate change mitigation and security of energy supply.

Wind energy may also be susceptible to climate change because it depends on the global energy balance and resulting atmospheric motion. What impact may global climate change have on the wind energy industry – this question remains open because there are few studies devoted to this problem [5]. All tools that help to design wind farms, such as freely available RETScreen Clean Energy Project Analysis [6], System Advisor Model [7] or more sophisticated professional WindPRO software [8], implicitly assume that climate from which the mean wind resource is derived is stationary at least during the period that is appropriate for the projected wind farms. Therefore the main task of the present study is to analyze the changes of wind speed in three Lithuanian meteorological stations and in some stations in neighboring countries over time periods longer than 30 years. Since wind energy depends on the cube of wind speed, a small change in speed has significant increase in produced energy. To evaluate the extent of changes in produced electricity induced by wind climate variation RETScreen program model was selected, whereas wind turbine Enercon E82 2 MW was chosen as a sample.

2. METHODOLOGY

2.1. Wind speed data

Since such meteorological parameters as temperature, wind speed or precipitation are highly variable, at least a 30 year period has to be considered, as it is long enough to filter out any interannual variation or anomalies. To elucidate possible wind speed trends induced by climate change even longer data sequences should be taken into consideration. Monthly mean wind speed data from the sites in Lithuania (Klaipėda, Laukuva and Kaunas) was obtained from Lithuanian Hydrometeorological Service [9]; data from other sites analyzed in the present work (namely, Bremen, Schleswig, Greifswald in Germany and Voru, Vilsandi in Estonia) were acquired from the Association of the European Climate [10]. All wind speeds were measured at the height of 10 m above the ground in periods of 3 hours.

The sites in Lithuania chosen for the analysis are located in regions that are being exploited with wind power plants. Vilsandi (Estonia) met-station is in the island in the Baltic sea and the data from Voru (Estonia) represents winds in the continental part of Estonia. Germany is a leading European country in employing wind energy for electricity generation, most of wind power plants in this country are installed in the coastal region. All three meteorological stations are located in this region thus providing wind speed data that are important for the evaluation of wind energy potential.

Table 1. Characteristics of monthly mean wind speed data of the sites analysed in the work

Site		Latitude, N	Longitude, E	Elevation, m	Period of record used, years	Pearson correlation coefficient, <i>r</i>	Statistical significance
Kaunas	Lithuania	54°53'	23°53'	77	1977-2013	-0.71	< 0.001
Klaipėda	Lithuania	55°43'	21°07'	8	1977-2013	-0.54	< 0.001
Laukuva	Lithuania	55°61'	22°23'	166	1977-2013	-0.25	0.144
Vilsandi	Estonia	58°22'	21°48'	7	1966-2012	-0.70	< 0.001
Võru	Estonia	57°50'	27°01'	108	1966-2012	-0.80	< 0.001
Bremen	Germany	53°52'	8°48'	12	1966-2012	-0.33	0.026
Schleswig	Germany	54°31'	9°33'	20	1966-2012	-0.38	0.008
Greifswald	Germany	54°06'	13°22'	1	1978-2012	0.35	0.042

2.2. Wind energy analysis

In order to evaluate the trends of meteorological data, monthly and annual averages as well as other statistical parameters were calculated by using Statistica software package. Pearson product-moment correlation coefficients are presented in Table 1 to give a general indication of coincidence between met-station and index time series - the points in time at which the time has a specific value.

Significance levels are also presented in Table 1. It should be noted that when the significance level is less than 0.05 then the result is considered statistically significant. Analysis of meteorological data is presented in the next section where the statistical parameters are shown in appropriate graphs.

The energy in the wind depends on the cube of wind speed

$$E = \frac{1}{2} \rho V^3, \quad (1)$$

here E – energy density, W/m^2 ; ρ – air density, kg/m^3 ; V – wind speed at hub height, m/s . Therefore, a small change in the wind speed can result in a considerable increase of the wind energy resource. For example, a change in wind speed by 10% causes the energy density to increase by over 30%. It means that the wind speed tendency over time does not represent correctly the energy amount generated by a wind plant. To analyze the changes in the amount of generated electricity induced by the change of mean wind speed a sample wind turbine was chosen and annual amount of electricity was calculated with regard to the time span that corresponds to meteorological data. To carry out these calculations freely available RETScreen Clean Energy Project Analysis [6] software was used. User interface window for data input and calculation is shown in Fig. 1. It can be seen that monthly averaged wind speed values are used for the evaluation of electricity produced during particular month.

Other technical parameters of a sample wind turbine Enercon E82 are shown in Table 2. Power curve data are included in the RETScreen database; other parameters such as array losses, airfoil losses (such things as bugs or ice build-up), availability were chosen according to the data of wind farms projects in Lithuania [11].

Table 2. Technical parameters of a wind turbine Enercon E82

Parameter	Unit	Value
Rated capacity	MW	2
Cut-in wind speed	m/s	3
Cut-out wind speed	m/s	30
Number of blades		3
Rotor diameter	m	82
Hub height	m	85

Resource assessment				
<input checked="" type="checkbox"/> Show data				
Resource method	Month	Wind speed m/s	Klaipeda m/s	Electricity export rate \$/MWh
	January	5,8	5,8	120,0
	February	5,1	5,1	120,0
	March	4,6	4,6	120,0
	April	4,0	4,0	120,0
	May	3,7	3,7	120,0
	June	3,8	3,8	120,0
	July	3,8	3,8	120,0
	August	3,9	3,9	120,0
	September	4,5	4,5	120,0
	October	5,1	5,1	120,0
	November	5,3	5,3	120,0
	December	5,6	5,6	120,0
	Annual	4,6	4,6	120,0
Measured at	m	10,0	10,0	
Wind shear exponent		0,14		
Wind turbine				
Power capacity per turbine	kW	2.000,0		
Manufacturer		Enercon		
Model		ENERCON - 82 E2 2MW - 85m		
Number of turbines		1		
Power capacity	kW	2.000,0		
Hub height	m	85,0	6,2 m/s	
Rotor diameter per turbine	m	82		
Swept area per turbine	m²	5.281		
Energy curve data		Standard		
Shape factor		2,0		
				Electricity exported to grid MWh
				628
				458
				410
				284
				235
				242
				247
				264
				362
				488
				516
				590
				4.723

Fig. 1. RETScreen parameter input window

Variability of wind speed is accounted by fitting a measured wind speed probability distribution in a particular location over a certain period of time by the Weibull distribution. The probability density function of the Weibull, $f(v)$, wind speed, v , during any time interval is given

$$f(v) = \left(\frac{k}{\alpha} \right) \left(\frac{v}{\alpha} \right)^{k-1} e^{-\left(\frac{v}{\alpha} \right)^k} \quad (2)$$

Here, k (m/s) is the Weibull scaling parameter and α is the dimensionless Weibull parameter.

Functions, which have been developed to describe the change in average wind speed with height, are based on experiments. One of these functions is as follows:

$$v(z) = v_0 \left(\frac{z}{z_0} \right)^\beta \quad (3)$$

Here, z is the height above ground, v_0 is the wind speed at the reference height, z_0 above ground level, $v(z)$ is the wind speed at height z ; β is an exponent which depends on the roughness of the ground. RETScreen requires wind speed values at the height of 10 m, then wind speed is recalculated for the required height using (3) Equation.

Another important parameter which actually describes performance of a wind turbine is the power curve. The power curve of a wind turbine is a curve that indicates amount of the electrical power output for the turbine at different wind speeds. The power curve is an individual characteristic of a turbine. It may be obtained from the manufacturer. Power curve of Enercon 82 which is used by RetScreen for electrical power output calculation are shown in Fig. 2.

Electricity produced by a wind component of $[v, v+\Delta v]$ is equal

$$E_v = f(v)P(v). \quad (4)$$

Here, $f(v)$ is Weibull frequency distribution of wind speed v and $P(v)$ is electrical power of a wind turbine at a particular wind speed. Total annual electrical output, E_e , can be calculated by a simple sum of electrical power of individual wind components multiplied by number of hours in a year, N :

$$E_e = N \sum_v f(v)P(v). \quad (5)$$

Here, N is a number of days multiplied by a number of hours in a day, i.e. $N=365 \cdot 24$ [h]. When using units, as it is indicated, the unit of final result is kWh which is appropriate for economic calculations.

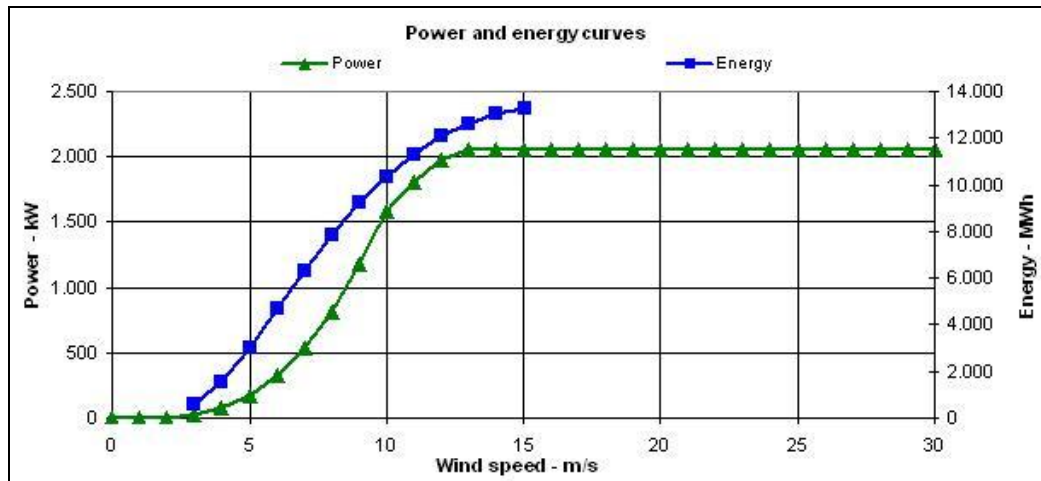


Fig. 2. Power curve of wind turbine Enercon 82

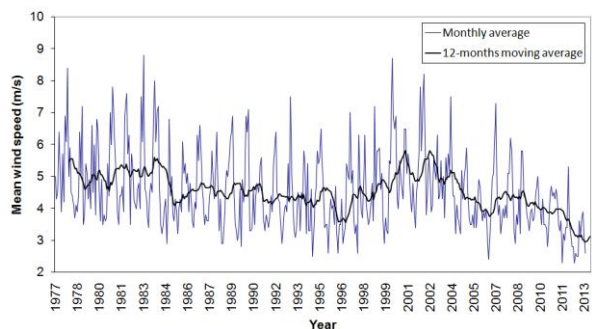
3. RESULTS

3.1. Wind speed analysis

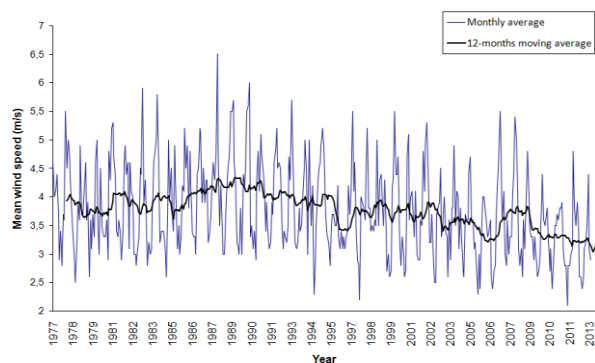
In this section, the wind speed data of Lithuania's meteorological station are analyzed in greater detail; the results of the data analysis of other sites are presented only for reference.

Wind speed data at 10 m height above ground level for the time period 1977–2012 is shown in Fig. 1. The data were statistically analysed by using Statistica software package in order to elucidate possible tendency over time. Next to corresponding Fig. 3 graphs wind speed linear regression trends (Fig. 4) are arranged with 95% confidence intervals shown in dotted lines. Pearson correlation coefficients r are shown in each image (in Table 1 as well) which give a general indication of coincidence between annual mean wind speed (m/s) values for corresponding meteorological stations being analyzed and the values of index time for the period 1977–2012. The p-value for the F-test is smaller than 0.01, hence, it can be concluded

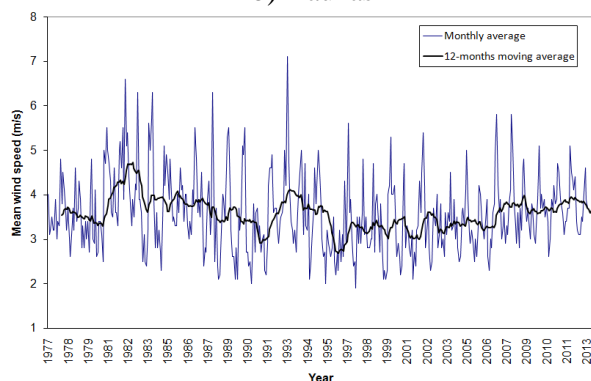
that strong statistical evidence (given a 5% significance level) to reject the null hypothesis of the test exists [12]. The dotted lines shows confidence limits of values and the line indicates the best fit of the data for annual mean wind speed correlation within the time period [13].



a) Klaipėda

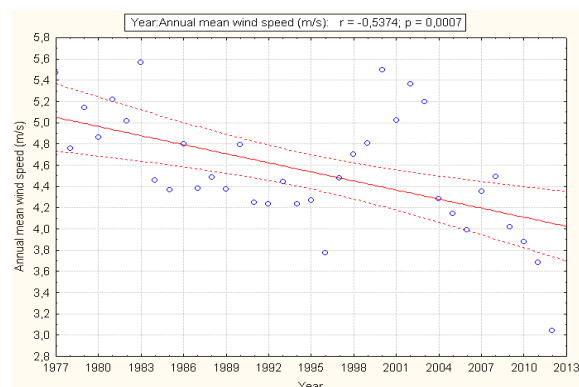


b) Kaunas

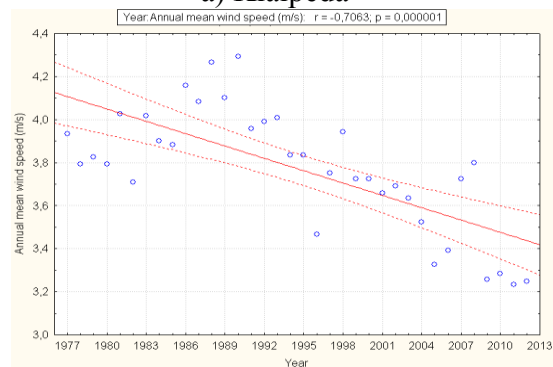


c) Laukuva

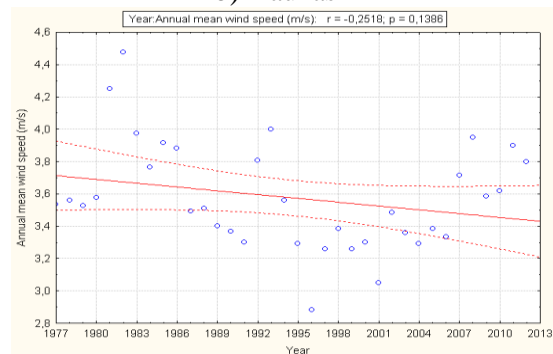
Fig. 3. Wind speed data at the 10 m height for the time period 1977–2012



a) Klaipėda



b) Kaunas



c) Laukuva

Fig. 4. Annual wind speed linear regression trend with 95% confidence intervals shown in dotted lines

The obtained results show clearly that, in 1977–2012, mean wind speed decreased in all three meteorological station sites being analyzed. The change of the average annual wind speed was evaluated as the difference between the first and the last values of the regression curve for the analyzed time interval. Reductions of mean wind speed extracted from appropriate linear trends for 36 year time span are as follows, in m/s: $\Delta V_1 = -0.95$ (Klaipėda), $\Delta V_2 = -0.70$ (Kaunas) and $\Delta V_3 = -0.25$ (Laukuva). These results correspond to the recent findings of Lithuanian Hydrometeorological Service [14], which indicate that new observed

values (1981–2010) of annual averages of wind speed are less than current climatic norm (1961–1990) by 0.3–1.5 m/s depending on the observation site.

The variation of mean wind speed during year-seasons plays an important role in wind energy production process. Monthly mean wind speed distributions during a year averaged for time periods 1977–1989, 1989–2001, 2001–2012 are presented in Fig. 5. It follows from these graphs that more wind energy is available during the cold season, whereas in summer wind speed is lower. These results correspond to the general trend of monthly wind speed distribution in Lithuania [15]. High variability of wind speed does not allow to analyze these results with satisfactory statistical reliability, the data is required to be averaged over a longer time period.

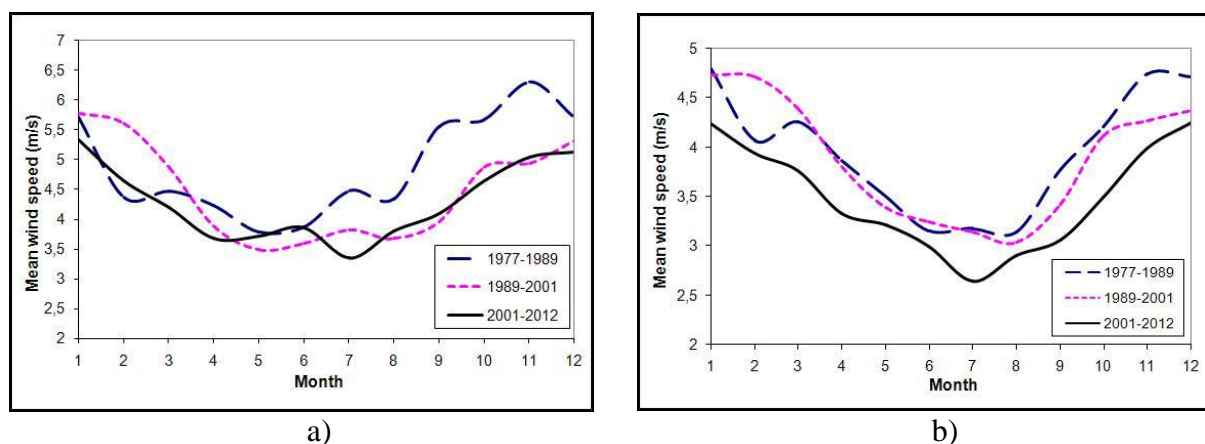


Fig. 5. Monthly mean wind speed averaged for the time periods of 1977–1989, 1989–2001, 2001–2012: a) Klaipėda; b) Kaunas

The wind speed data observed in Estonia (Vilsandi, Võru) and Germany (Bremen, Schleswig, Greifswald) for the time period 1966–2012 are presented in Fig. 6. The data was obtained from the Association of the European Climate [10]. Data description indicates that wind speeds were measured at the height 10 m above the ground with 3 hour intervals. Further transformation of the data includes the calculation of annual mean wind speed and following linear best fit.

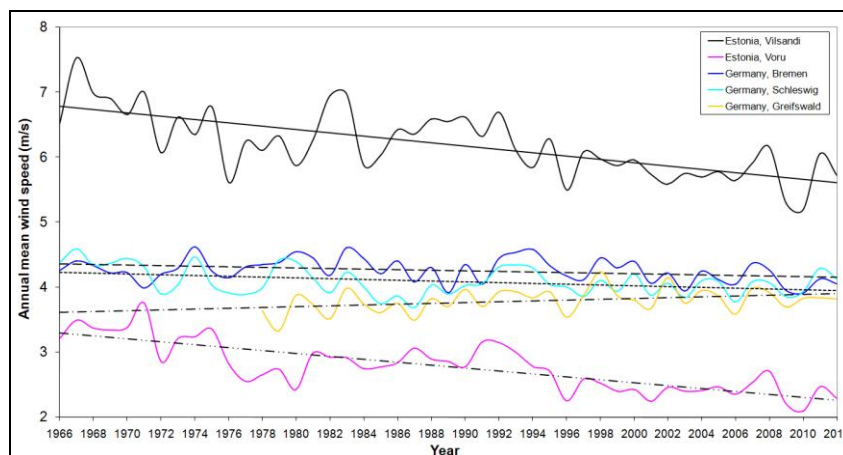


Fig. 6. Annual mean wind speed in meteorological stations in Estonia (Vilsandi, Võru), Germany (Bremen, Schleswig, Greifswald) in the time period 1966–2012 and best fit functions

It follows from the Fig. 6 that wind speed in Vilsandi site is higher than that in Voru (both Estonia) – this result is obvious because the first of them is located in the Baltic sea island where winds are stronger, and the second – deeper in continental part where the wind climate is milder. More importantly, the decrease of mean wind speed in both sites at similar rate and the manifestation of this observed reduction is more evident than in the sites in Lithuania analyzed previously.

The character of wind speed variations in three Germany's meteorological station sites is different. From the statistical point of view, the values of correlation and significance (Table 1) suppose quite reliably that there are some changes (the wind speed decreases in two sites, whereas it increases in the third one). However, the observed trends are so slight that deeper investigation should be carried out in order to draw reasonable conclusions. It is possible to summarize at this point that in the observed sites in Estonia the mean wind speed decreases with obvious trend, in the sites in Germany, the long-term changes of wind speed are very small.

The obtained results lead to three conclusions. Wind climate in the territory where wind turbines are planned to be installed is usually considered as steady. This obviously is not true, therefore wind atlases [16] which are used for the calculation of wind energy production should be constantly renewed. Secondly, to evaluate the economic and energetic value of installed wind turbines, wind speed changes should be foreseen because these wind plants are going to operate for 20–25 years – the shift of wind speed can be significantly high during this period. Thirdly, the patterns of wind speed in the near future should be analyzed in greater detail since the regions which are favorable for wind energy development may change their borders because of the climate change.

3.2. Changes in annually generated electricity

As it was noted above, the variations of the amount of generated electricity induced by the change of mean wind speed were calculated using the sample plant which is included in the RETScreen database. Enercon E82 (2 MW) was chosen as a sample plant, all technical parameters were the same for all sites, wind speed was the only parameter that varied from site to site.

Using wind data discussed in previous section, annually generated electricity was evaluated for all sites. Fig. 7 presents variation of annual generated electricity in 1977–2012 in the case when sample plant would be located at the sites that have a wind speed typical of the meteorological sites in Klaipėda, Kaunas, Laukuva. Dotted lines show the linear function that fits the variations best.

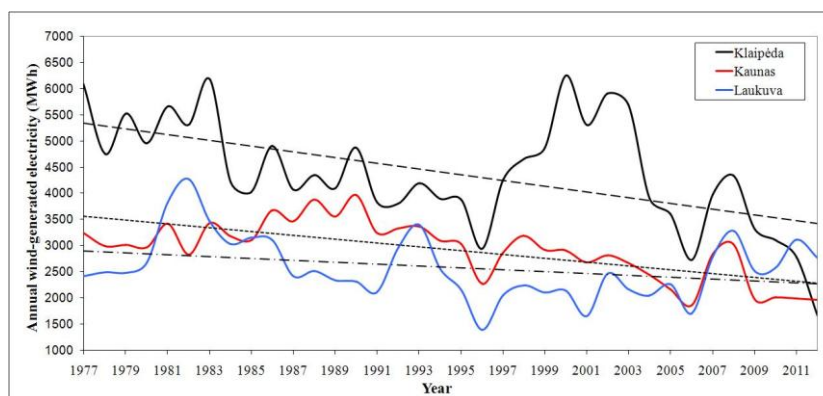


Fig. 7. Annually generated electricity (MWh) for wind speed typical of the meteorological station sites in Klaipėda, Kaunas, Laukuva in the time period 1977–2012

Since mean wind speed decreased during 1977–2010, the amount of the produced energy also decreased. However, the reduction is more considerable: -39 %, in Klaipėda site, -38 %, in Kaunas site, -24 % in Laukuva site. The obtained results could be compared to the real change of the amount of produced wind electricity, but the time that passed since the beginning of wind energy exploitation in Lithuania is too short: the first wind turbine in Lithuania was installed in Vydmantai only in 2006. However, the obtained values are quite large and encourage to carry out deeper investigations.

Similar evaluation of the produced energy was carried out for other sites presented in this study. One may expect that the changes in the amount of produced electricity follow the variation of mean wind speed. However, due to the fact that wind energy depends on wind speed, the changes in the produced energy are more significant. The statement is illustrated in Fig. 8, which shows the amount of the generated electricity during 1966–2012 calculated for the wind climate typical of Bremen, Schleswig, Greifswald (Germany) sites. Slight changes in wind speed noted in previous section caused the changes in produced energy in these sites as it follows: -15% (Schleswig), -11% (Bremen), +17% (Greifswald). It should be noted that the time period is different, so, the comparison should be made by initially normalizing the obtained values for the same period.

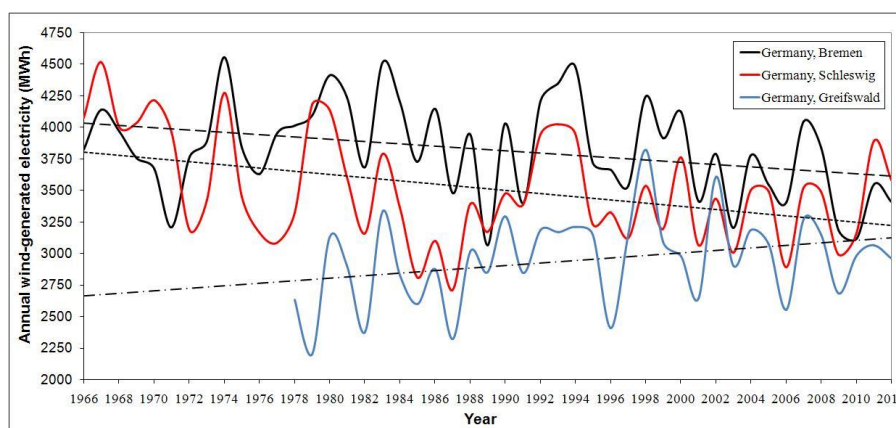


Fig. 8. Annually generated electricity (MWh) for the meteorological station sites in Bremen, Schleswig, Greifswald (Germany) during the time period 1977–2012. Dotted lines show the linear function that fits the variations best

4. CONCLUSIONS

The analysis of wind speed variations during the past decades has shown that wind speed decreases in most meteorological sites investigated in the present work. For analyzed Lithuanian sites the reductions of mean speed during 1977–2010 are as it follows: -0.95 m/s (Klaipėda), -0.70 m/s (Kaunas) and -0.25 m/s (Laukuva). Since wind energy depends on the cube of wind speed the changes in the amount of produced energy are more considerable: -39 % in Klaipėda site, -38% in Kaunas site and -24% in Laukuva site during the same time period. Obtained changes are substantial; therefore, the planning of wind power plant distribution should consider additional measures. First of all, wind atlases have to be constantly renewed. The assessment of a wind farm project should include the forecast of wind speed changes for the time period a power plant is to operate, i.e. at least 20–25 years. Climate change induced variations of meteorological parameters have to be analyzed in greater detail to obtain more appropriate information about wind energy exploitation.



REFERENCES

1. International Energy Agency I. World energy outlook: 2013 (London: OECD/IEA, 2013), p. 49–51
 2. The European wind energy association. Wind in power: 2013 European statistics 2014 February 14. (Europe: EWEA, 2013), p. 15.
 3. IPCC, 2011: IPCC Special Report on Renewable Energy Sources and Climate Change Mitigation. Prepared by Working Group III of the Intergovernmental Panel on Climate. Cambridge University Press, Cambridge, United Kingdom and New York, NY, USA. p. 1075
 4. IPCC, 2007: Climate Change 2007: Synthesis Report. Contribution of Working Groups I, II and III to the Fourth Assessment Report of the Intergovernmental Panel on Climate Change. IPCC, Geneva, Switzerland, p. 104.
 5. PRYOR S.C, BARTHELMIE R.J. (2010) Climate change impacts on wind energy: a review. Renewable and Sustainable Energy Reviews 14, p. 430–437.
 6. RETScreen Software 2006: Online User Manual. Clean Energy Decision Support Centre. Natural Resources Canada. p. 110 [referred on the 21th of March in 2013]. Link to the internet <<http://www.etscreen.net>>
 7. National Renewable energy laboratory. System Advisor Model (SAM).[referred on the 18th of February in 2013]. Link to the internet <<https://sam.nrel.gov/>>
 8. Professional WindPRO software for wind energy project design and planning.[referred on the 10th of February in 2014]. Link to the internet <<http://www.emd.dk/WindPRO>>
 9. Lithuanian Hydrometeorological Service under the Ministry of Environment.[referred on the 15th of March in 2013]. Link to the internet < www.meteo.lt>
 10. The European Climate Assessment & Dataset project. [referred on the 13th of February in 2013 y.]. Link to the internet <<http://eca.knmi.nl/dailydata/customquery.php>>
 11. United Nations Framework Convention on Climate Change (UNFCCC). Ministry of Environment of the Republic of Lithuania: JI Projects. [referred on the 26th of February in 2013].Link to the internet <https://ji.unfccc.int/JI_Parties/DB/U1TU09IG05C2669GVJJE9CR9DQM8MZB/viewDFP>.
 12. ANASTASIADES G., McSHARRY P.E. (2013) Extreme value analysis for estimating 50 year return wind speeds from reanalysis data. University of Oxford, Oxford, UK. Wind Energy, p. 15.
 13. PRYOR S.C., BARTHELMIE R.J., KJELLSTROM E. (2005). Potential climate change impact on wind energy resources in northern Europe: analyses using a regional climate model. Climate Dynamics 25, p. 815–835.
 14. Lithuanian Hydrometeorological Service under the Ministry of Environment. 2013. Climate averages for Lithuania 1981–2010: Vilnius, p. 24.
 15. BUKANTIS A. 2008. Lithuanian natural environment, condition, processes and developments. Journal of the Environmental Protection Agency. Vilnius: Petro ofsetas, p. 238.
 16. The Wind power. Wind turbines and wind farms database. [referred on the 26th of February in 2013]. Link to the internet <http://www.thewindpower.net/country_maps_en_43_lithuania.php>
- RETScreen international 2004: Wind energy project analysis. Natural Resources Canada. p 30. [referred on the 21th of March in 2013]. Link to the internet <www.etscreen.net/download.php?ang\19\0\Textbook_WIND.pdf>



THE USE OF TURBINES THAT WORK ON ORGANIC RANKINE CYCLE FOR SMALL ENTERPRISES

S. Alyokhina, O. Senetskyi

*A.N. Podgorny Institute for Mechanical Engineering Problems of the
National Academy of Sciences of Ukraine
Dm. Pozharsky st. 2/10, UA-61046 Kharkiv – Ukraine*

ABSTRACT

High prices of traditional fuel and energy resources and increasing demands for environmental protection increase the interest for use as fuel renewable energy sources, including biomass. The only drawback of such fuel is lowest calorie (the twice as smaller than fossil fuels). Majority of industries such as agriculture, woodworking and other industries, which have this type of fuel, want to produce their own heat and electric energy. The low power cogeneration installations with closed cycle schemes are widely used at the present time. Their usage allows efficiently produce thermal and electrical energy for their own needs through the usage of vapor turbines with low-boiling working fluids by implementing the so-called Organic Rankine Cycle (ORC).

The A.N. Podgorny Institute for Mechanical Engineering Problems of the National Academy of Sciences of Ukraine solves the problems of energy saving by using an ORC. The working fluid for the closed contour vapor turbine is chosen depending on the amount and the calorific value of the combusted fuel. The working fluid has the appropriate chemical, physical and exploitation properties at the given operating conditions. Numerical researches of thermal schemes depending on the selected working fluid are conducted. Heat exchanging devices and turbines are modeled.

Realization of this type of vapor turbine cycles will allow small enterprises using local types of renewable fuel resources for their own needs in thermal and electric power. Excess energy can be sold allowing the generation of more revenue for small enterprises.

Keywords: energy saving, low-boiling working fluid, Organic Rankine Cycle, vapor turbine, renewable fuel resources

1. INTRODUCTION

The question of increasing of efficiency of fuel usage and energy resources in order to implement energy-saving technologies becomes extremely important. The production technologies of thermal energy and electric energy from burning of renewable fuel resources (biomass, peat, etc.) currently acquire the special significance.

The main reasons for the biomass usage as fuel are: the cost parameters of fuel resources and the degree of ecological impact. Ecology aspect is important for consumers but in developing countries there are very few energy producers worried about the ecological situation. Unfortunately this approach can lead to irreversible ecological changes worldwide. For all participants in the energy sector the question of the economy is also very important. Calculations and analysis of basic fuels prices indicate that the biomass in many cases equals to the cost of traditional fuels (natural gas and coal) [1]. In perspective while retaining existing tendency of the developing energy industry the cost of traditional fuels will exceed the cost of renewable fuel resources, so biofuels will be more required.

One of the effective ways to use renewable fuel energy resources is the electricity production based on vapor turbines with low-boiling working fluids (LWF) [2–9]. In these installations the so-called Organic Rankine Cycle is implemented.

The power installations with LWF usually are projected at a predetermined temperature of the heating medium which starts from 80 °C. The changing of this temperature by more

than 20–30 °C leads to a significant change of efficiency and economic indicators of power installation [10, 11].

The realization of thermal scheme where the LWF used as working fluid is considered in this paper. In this scheme so-called cogeneration installation is implemented in which unlike the condensation installation the latent heat of vaporization is useful used for hot water. The variant of the condensation thermal scheme which improves the production of electric energy is also examined. The quantity of fuel flow rate remains constant for the two schemes.

2. BURNING OF RENEWABLE FUEL RESOURCES

Currently there is a large amount of literature on the use of renewable fuel resources [12–17 and others]. In this case we want to note the perspective and expediency of development of this direction.

Considering of the energy potential to biomass includes all forms of raw materials of vegetable origin which can be used to generate energy: wood, grass and cereals, waste of forestry etc. Since the biomass is a solid fuel it can be compared with coal (Table 1).

Table 1. Energy capacity of various fuels [17]

Type of fuel	Moisture content, %	MJ / kg	(kWh) / kg
Anthracite coal	4.0	30.0-35.0	8.3
Brown coal	20.0	10.0-20.0	5.5
Stove fuel	–	42.7	11.9
Rapeseed oil	–	37.1	10.3
Peat	15.0	18.1-23.6	5.8
Oak	20.0	14.1	3.9
Straw	15.0	14.3	3.9
Crops	15.0	14.2	3.9
Pine	20.0	13.8	3.8

The moisture content of the fuel renewable resources is higher than coal therefore energy density of biomass is lower (Table 1). On the other part the biomass has advantages from the point of view of the chemical composition. The ash content of biomass is much lower than coal. Furthermore, ash of biomass generally does not contain heavy metals and other pollutants, so it can be used as a fertilizer. Systems which use biomass for energy purposes provide economic development without increasing the greenhouse effect, since biomass is neutral with respect to CO_2 emissions into the atmosphere if its production and usage is carried out reasonably. Biomass has a sparing ecological properties (low emission of sulfur and nitrogen oxides).

Biomass provides greater flexibility in energy supply because of the large number of fuel types that can be produced from it. Biomass energy can be used to produce thermal and electrical energy by the burning in modern devices thereby provide energy independence of consumers. Currently, the energy sector the awareness is growing that the biomass usage in large commercial systems is based on sustainable accumulated resources and wastes so it can improve the management of natural resources in general.

3. CHOOSING OF WORKING FLUID

At the choosing of low-boiling working fluids (freons) for ORC turbines the working fluids must satisfy the ecological, thermodynamic, operational and economic requirements. It is almost impossible to find freons which fully meet the necessary requirements. Therefore in

each individual case the freon is selected with taking into account the specific conditions operation of the plant and preference should be given to those which meet most of the requirements [7, 18].

The properties of some working fluids that can be used in a closed cycles of turbine installations of this type are presented in Table 2.

Table 2. Basic properties of some freons [19 – 21]

Substance	Molecular mass, g/mol	$T_{b.p.}^*$, °C	T_{cr}^{**} , °C	P_{cr}^{**} , bar	ODP	GWP
R-123	152.93	27.1	182.0	35.6	0.02	90
R-124	136.48	-12.0	122.3	36.2	0.02	480
R-134a	102.03	-22.5	101.10	40.67	0	1300
R-142b	100.49	-9.2	136.8	41.5	0.065	2000
R-236fa	152.04	1.4	124.9	32.0	0	6300
R-406a	89.6	-32.7	116.5	48.8	0.043	8500
R-600	58.12	-11.8	150.80	37.18	0	20
R-600a	58.12	-11.8	135.92	36.84	0	20

* – boiling point at atmospheric pressure;

** – critical value.

Depending on the critical parameters of the working fluid and of potential of heat source the working fluid is selected. List of used working fluids is not limited by the list which is presented in Table 2.

4. METHODOLOGY

Calculation of thermal schemes with low-boiling working fluids includes the following sequence [22].

1. Calculation of thermal schemes begins with the determination of the parameters of the working fluid at the outlet of the steam superheater by compiling thermal and material balances.

Enthalpy at the inlet and outlet of the of heat exchangers at given pressure P and temperature T is determined

$$i = i(P, t).$$

2. In a continuously operating heat exchanger (Fig. 1) the heat transfer carries out between two running fluids which are separated by heat transfer wall. The thermal balances compiles on the basis of the fact that the amount of heat Q_1 , which comes into the apparatus per unit time with the incoming fluids is equal to quantity of heat from the outgoing fluids from the apparatus during the same time

$$Q_1 = G_1 i_{1up} + G_2 i_{2up} = G_1 i_{1d} + G_2 i_{2d}, \quad (1)$$

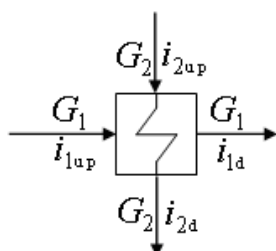


Fig. 1. The principal scheme of heat exchanger

i_{1up} , i_{2up} and i_{1d} , i_{2d} – enthalpy of substances, respectively incoming and outgoing of apparatus.

Thermal balance compiles on external factors: before and after apparatus.

From the equation (1) the amount of heat Q which is transferred from one medium to another can be determined as the difference between the enthalpies

$$Q = G_1 (i_{1up} - i_{1d}) = G_2 (i_{2d} - i_{2up}). \quad (2)$$

Flow rate of secondary fluid is found from the material and heat balances

$$G_2 = \frac{G_1(i_{1up} - i_{1d})}{(i_{2up} - i_{2d})}, \quad (3)$$

G_1, G_2 – flow rate of heating and heated medium, kg/s.

This approach is typical for heat exchangers when the flow rate of the working fluid determines and energy balances compiles.

3. Calculation of heat drop on the turbine is made depending on the functional purpose of the thermal scheme (condensation or cogeneration scheme). As the initial data the pressure and temperature of the stream at the inlet and outlet of the turbine, the working fluid flowrate and efficiency of mechanical and generator are used.

$$H_T = i(P_{in}, t_{in}) - i(P_{out}, t_{out}), \quad (4)$$

H_T – heat drop on the turbine.

Electric power of turbine

$$N_E = H_T \cdot G_2 \cdot \eta_{oi}^T \cdot \eta_m \cdot \eta_g, \quad (5)$$

$\eta_{oi}^T, \eta_m, \eta_g$ – efficiency of turbine flowing part, mechanical efficiency and generator efficiency.

Calculation of thermal scheme is carried out with taking into account the features of thermodynamic characteristics of the considered low-boiling working fluids.

The model will be improved in the future for obtaining better technical characteristics of heat exchange equipment.

5. RESULTS

The thermal scheme of cogeneration installation in closed cycle that uses low-boiling working fluid is designed (Fig. 2).

The closed ORC contour includes: boiler (1) for the evaporation and superheat the LWF till the required parameters, turbine (2) with an electric generator (3), the heat exchanger for heating water for hot water supply (4) and condensate pump (5).

In the boiler as the fuel the renewable fuel resources are burned. Amount of heat which is input by the working fluid in the boiler is 370 kW. The cogeneration scheme in a closed cycle, which used low-boiling working fluid is used.

In the majority of cases the subcritical turbine cycles are realized because the costs of implementation of the supercritical cycle is greater than the gain on the power. Feature of the ORC turbines is the expansion process in the turbine is finished in the field of superheated vapor that excludes erosive wear of the blades and has a positive effect on its performance.

In the thermal scheme the condensation heat of the working fluid after the turbine is effectively used in the hot water heater.

The option of installation of condenser after the turbine is also examined (Fig. 3).

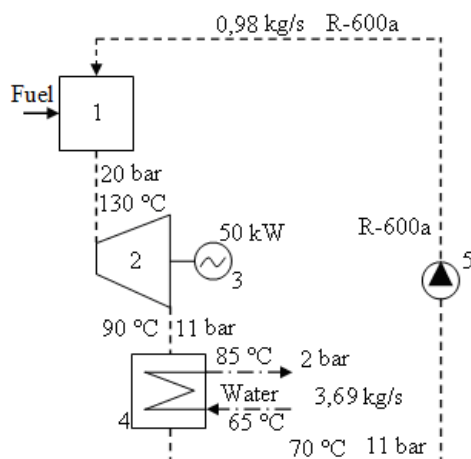


Fig. 2. The principal thermal scheme of cogeneration unit

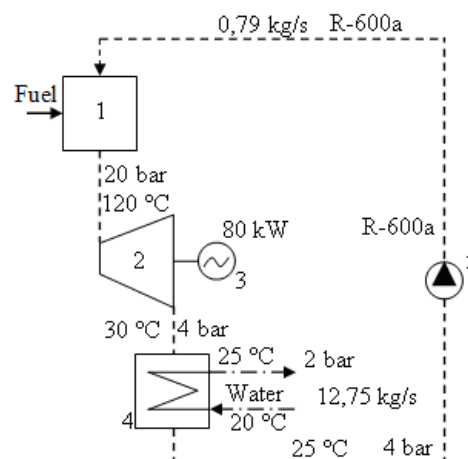


Fig. 3. The principal thermal scheme of condensation unit

According to the results of thermal and material balances of heaters and preliminary calculations of the thermal scheme the electrical power of cogeneration unit amounted to ≈ 50 kW and of the condensing unit ≈ 80 kW.

Flow rate and parametric characteristics of selected low-boiling working fluids are obtained on base of numerical researches and the power of installation depending of used working fluids is calculated (Table 3).

Table 3. Summary results for electrical power and efficiency

Working fluid	Cogeneration thermal scheme			Condensation thermal scheme	
	Heat capacity, kW	Electrical power, kW	Electrical efficiency, %	Electrical power, kW	Electrical efficiency, %
R-124	309	35	6.22	80	16.22
R-134a	—	—	—	60	11.78
R-142b	318	40	7.34	70	14.0
R-236fa	330	30	5.11	80	16.22
R-600a	309	50	9.56	80	16.22

Depending on the used working fluid and availability of hot water supply the power of installation varies from 30 to 50 kW. In such case it is resonable to use as working fluid the R-600a and the power of installation will be 50 kW.

6. CONCLUSIONS

The analysis of low-boiling working fluids is conducted. The selection criteria for the working fluid at implementing of a closed thermal scheme are defined.

The perspectives of realization of thermal schemes for solving problems of energy saving by using turbines with LWF are shown. In condensation regime the power of turbines more (60–80 kW) than at presence of hot water system (30–50 kW). In this case the freon R-600a is selected. In case of necessity necessary of the realization of the condensation thermal scheme the freon R-600a can be replaced by R-124 or R-236fa depending on the requirements for the operating conditions.

This direction would be developed in the future. Heat exchangers and turbines with considering the thermodynamic properties of the working fluids will be modeled. Analysis of the literature and numerical research has shown that prospects use of energy installations with

ORC is a perspective direction in the energy industry which requires further development and conducting additional research.

REFERENCES

1. *Technological aspects of biofuel combustion*. Dnepropetrovsk (Ukraine): OOO «PKF «VISTA-Dnepr» [referred on the 16th of January in 2014 y]. Link to the internet <vistapellets.com.ua/page.php?p=stat1>
2. BILEKA, B., VASILIEV, E., IZBASH, V. and others. Utilization waste heat of GPU in power installations with low-boiling working fluids. *Gas turbine technologies*, 2002, No. 5, p. 6–10.
3. REDKO, A.A. Thermodynamic parameters of geothermal power plant with supercritical binary cycle. *Integrated technologies and energy saving*, 2009, No. 4, p. 81–85.
4. PYATNICHKO, V.A., KRUSHNEVICH, T.K., PYATNICHKO, A.I. Utilization of low potential heat to produce electricity by using pentane as the working fluid. *Ecological Technologies and Resource Saving*, 2003, No. 4, p. 3–6.
5. SCHWARTZ, G.R., GOLUBEV, S.V., LEVYKIN, B.P. and others. Produce recycling power installations with organic coolants. *Gas Industry*, 2000, No. 6, p. 14.
6. LEGMANN, H., DAVID, C. Recovery of low grade heat by means of the ORC process in the cement industry. *Official website of the company ORMAT International, Inc.* [2010]. [Referred on the 16th of January in 2014 y.]. Link to the internet <www.ormat.com>
7. BAZAEV, A.R. Research of thermodynamic properties of mixtures of technically important substances as effective heat transfer fluids in power plants. *PHYSICS*, 2007, CILD XIII, № 1–2, p. 57–60.
8. GREENMAN, M.I., FOMIN, V.A. Prospects of application of low-power power installations with low-boiling working fluids. *Power machine building*, 2006, No. 1, p. 63–69.
9. SHUBENKO, A.L., BABAK, N.Y., ROGOVOY, M.I. and others. Economic efficiency of utilization of of low potential secondary energy resources by installing turbines at low boiling working fluid. *Energy saving. Energetic. Energy audit*, 2010, No. 6, p. 18–26.
10. RUSTAMOV, N.A., ZAITSEV, S.I., CHERNOV, N.I. *Biomass – energy source*. [Referred on the 16th of January in 2014 y.]. Link to the internet <<http://cbio.ru/page/43/id/1771/>>
11. *Official website of the company*. Kiev (Ukraine): Green energy T. [Referred on the 16th of January in 2014 y.]. Link to the internet <<http://www.greenenergyt.com.ua>>
12. *Belarusian web portal on renewable energy*. Minsk (Belarusian): Renewable energy sources. [Referred on the 16th of January in 2014 y.]. Link to the internet <<http://re.buildingefficiency.info/>>
13. *EurObserv'ER*. Solid biomass barometer, 2011- [Referred on the 16th of January in 2014 y.]. Link to the internet <www.eurobserv-er.org>
14. BAIN, R.L., OVEREND, R.P. Forest Product Journal. *Biomass for Heat and Power*, 2002, Vol. 52, No. 2, p. 12–19.
15. *Biomass*. Electronic Journal of Energy Service Company of Ecological systems, 2009, No. 4. [Referred on the 16th of January in 2014 y.]. Link to the internet <http://www.esco-ecosys.ru/2009_4/art024.htm>



16. SHUBENKO, A.L., BABAK, N.Y., SENETSKYI, A.V. and others. Disposal of waste heat of technological processes industrial enterprises in order generate electricity. *Energy saving. Energetic. Energy audit*, 2012, No. 07(101), p. 23–29.
17. *ANSI/ASHRAE Standard 62.1-2007*. – Ventilation for Acceptable Indoor Air Quality – 2007 (46 p., 1041-2336), PDF (Scan).
18. *Refrigerants*: Electronic data (1 PDF file), 26 p. [referred on the 16th of January in 2014 y.]. Link to the internet
<http://www.ozoneprogram.ru/upload/files/r/ruk/8_rukovodstvo_unido.pdf>.
19. *Reference Fluid Thermodynamic and Transport Properties* (REFPROP). Version 9.0. This program, developed by the National Institute of Standards and Technology Boulder, CO.
20. *Clean energy ahead Turboden*: Official website of the company. – Electronic data (1 PDF file). [referred on the 16th of January in 2014 y.]. Link to the internet
<http://www.turboden.eu/en/public/downloads/Presentation_of_Turboden_ORC_Technology_Russian.pdf>
21. De Biasi Victor. Cascade waste heat recovery for gas turbine power and efficiency. *Gas Turbine World*, 2008 September-October, p. 22 – 25. Official website of the company. – Electronic data (1 PDF file). [referred on the 16th of January in 2014 y.]. Link to the internet <[www.wowenergies.com/GTW% 20%2022-25%20Simple%20Cycle%20Power%20Recovery.pdf](http://www.wowenergies.com/GTW%20%2022-25%20Simple%20Cycle%20Power%20Recovery.pdf)>
22. KOSTYUK, A.G., FROLOV, V.V., BULKIN, A.E., TRUHNYY, A.D. Turbines of thermal and nuclear power plants: Textbook for universities. 2nd ed. MEI, Moscow, Russia, 2001, p. 488.

PVT COOLING AND HOT WATER SOLAR FRACTION IN NORTHERN LATITUDES

P. Pikk, A. Annuk

*University of Life Sciences
Fr. R. Kreutzwaldi 56 – Estonia*

ABSTRACT

Photovoltaic-thermal (PVT) collectors deliver from solar irradiation electrical energy and additionally provide thermal gains and losses. Through integrated solution the mean average electrical energy production compared to conventional photovoltaic (PV) module increases. At the same time thermal energy gains are lower as part of the falling solar irradiation is turned into an electrical energy. The total energy potential of a PVT collector in northern latitudes (over 50°N) is estimated higher than separate PV and thermal collector energy gains. The suitability of PVT collector for hot water preparation and cooling potential is investigated widely in recent years. The recent work is concentrated to PVT collector absorption cooling potential and economic analysis in southern and equatorial regions of the world. More interesting for northern latitudes is energetic and economic analysis of PVT night radiative cooling potential. Typical dynamical office building simulation is prepared to find building loads. Dynamical simulations of PVT cooling system is prepared to find solar fraction of PVT night radiative cooling for the building. Article analyses the solar fraction of a PVT absorption, PVT compression chiller and PVT night radiative cooling energy and economical potential. Article results with comparison of PVT cooling technologies considering installation, maintenance and yearly energy costs for a typical residential or small office building in northern latitudes.

Keywords: PVT, solar fraction, hot water, cooling

INTRODUCTION

Technologies utilizing solar energy are developed continuously in various fields. Main fields are production of thermal energy and electricity. The share of renewable energy in European Union countries must increase yearly to avoid pollution and energy dependence problems. Facing the situation where all the energy is exported from neighbouring countries or other continents is not acceptable. Large amount of energy is used in building sector and some part of it is used in cooling the buildings. Buildings located in north Europe need in average less cooling energy than buildings in southern Europe. Mainly cooling loads are smaller because of fewer sunny hours and lower global irradiation. As cooling loads in northern Europe (latitude N50° and higher) are not as high, less papers are published about cooling the buildings with solar energy. Cooling load does not take a high share from average total energy demand of a north European building [1]. Still noticeable CO₂ emissions are caused by the ventilation and cooling units during the summer period. In side of existing cooling technologies like absorption, compression chiller and desiccant cooling different new technologies like night radiative cooling emerges. To investigate the economic performance of various cooling technologies in northern latitudes parameters are set and compared.

1. SOLAR POWERED COOLING SYSTEMS

Cooling systems are powered by primary energy sources like gas, coal, sun, waste heat, etc. The biggest difference of technologies is that the secondary energy is supplied as a heat or electricity.

1.1. Electrically powered cooling systems

Electricity for cooling systems is mainly taken from the grid, but also renewable electricity like wind or solar power is used. Both wind and solar energy are fluctuating in time and therefore not as suitable as electricity from grid. Still, solar energy is very suitable for cooling purposes as cooling is needed in times where sun is heating the indoor sections of the buildings. The higher the outdoor temperature and solar irradiation, the higher is the cooling load of the building.

1.1.1. Photovoltaic compression chiller systems

Compression chiller system needs electricity to deliver cooling energy for the buildings. In compression chiller cycle pressurized hot gas is condensed outdoors until it reaches outdoor temperature and guided to expansion valve. In expansion valve the pressure and temperature of the gas drops and gas turns to gas and fluid mixture. The cold mixture is warmed up with the building warm air and guided to compressor. Warm vapour entering the compressor is compressed to higher pressure and guided as a higher temperature vapour to condenser. See Fig. 1.

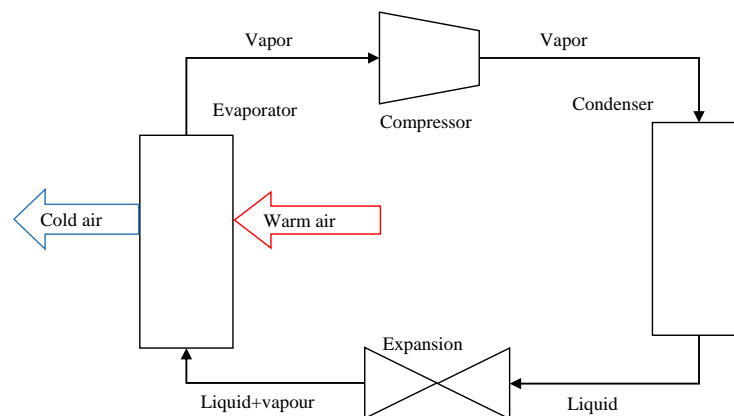


Fig. 1. Principal schematic of vapour or water cooled compression chiller system

Main indicator for compression chiller system performance is coefficient of performance (COP). As found in [2] the yearly average COP of the system is 3.5 or 3.0 in [2]. To deliver 100% of needed electrical energy the power output from the photovoltaic modules must be always higher, than instantaneous power of compression chiller. System used 9.3% less primary energy (2 923 653 kWh) photovoltaic (PV) delivers 299 779 kWh. Costs 4 800 000 €. Cooling consumption 201 322 kWh. In Freiburg simulated compression chiller system resulted primary energy savings of about 0.12 €/kWh [3].

1.2. Thermally powered cooling systems

1.2.1. Absorption cooling systems

Collectors provide 27.91% cooling consumption in summer period [2]. In Oberhausen, Germany absorption cooling plant, which included 37 kW cooling capacity, vacuum tube collectors' area 108 m² and cooling tower of 134 kW. The maximum free cooling was 70%, but during 5 years period only 25% of cooling was covered. COP of the chiller varied from 0.37 to 0.81 [4]. Another installation in Germany, Munich with nominal capacity of 10 kW operated in average COP of 0.7. The suitable relation on heat storage capacity and thermal

storage content was found 10 kW to 120 kWh [5]. Another paper uses methodology described in SACE tool. The installation costs for 50 kW system in Freiburg, Germany are 8 859 €. The cost of primary energy savings is found under collector area of 160 m² 0.38 €/kWh. The COP of solar energy to secondary energy ratio is found in [3] 0.45 for compression chiller.

1.2.2. Desiccant cooling systems

Measurements in France, where honeycomb desiccant cooling wheel was installed showed that COP of 0,55 including the solar installation is reached [6]. Another desiccant cooling plant was installed in Althengstett, Germany. In the specific costs per one year heating, cooling, distribution and solar system installation and maintenance costs were taken into account. The total cost for cooling was found 0,94 €/kWh [7]. As a comparison in Althengstett, Germany the compression chiller system costs 0,65 €/kWh [7]. Another Austrian team compared a district heating powered desiccant cooling system costs with electrical compression chiller system and found that for 960 full load hours the cooling costs are 0.55 €/kWh and for compression chiller at the same time 0.51–0.56 €/kWh [8].

1.2.3. Night radiative cooling systems

Radiative cooling possibilities like roof-top ponds, flat plate collectors are investigated over the years [10]. Study in Norway found that using polymer based radiators on the roof the cooling potential is 50-150W/m². The investment cost of such an installation is in range of 60–100 €/m². Having a residential house with treated floor area of 150 m², radiator area on the roof of 50 m², 2 m³ tank for coolant, in a clear and dry night 22 kWh of energy is stored [10]. In another study of positive energy building and PVT night radiative cooling is experimentally investigated [11]. The building is cooled during the daytime with a reversible heat-pump having a 2.4 kW cooling power. The tank is loaded during the daytime with heat from heat-pump. At night time or times when outdoor temperature is lower than tank temperature the tank is cooled using frameless and not insulated PVT modules. The coolant is circulated at night threw to PVT modules located on the roof and on the wall of the building. The specific cooling power was measured 119 ± 6.3 W/m² in location Stuttgart, Germany. Having higher temperature differences between outdoor temperature and coolant the specific cooling power is over 120 W/m². The exact same system was tested also in Madrid, Spain and as a result the specific cooling power was 43.1 ± 2.9 W/m² and 65.6 ± 3.2 W/m². Investigation in Stanford University have indicated that by mid-IR emitting nano scale terrestrial structures the cooling power of 100 W/m² can be achieved in daytime. The daytime radiative cooling works on wavelength of 8-13µm. Another cooling project is conducted in Australia where cooling area of 10 m² reaches cooling rate of 11 kW (closed system). Inlet temperatures are not known, but heat transfer coefficient is 20 W/(m²·K).

3. MATERIALS AND METHODS

To evaluate the performance of solar cooling systems northern Europe latitudes experimental measurements or dynamical simulation is needed to conduct. As the complexity of dynamical simulations without verifying the actual model cannot be done, the comparison must be based on previously conducted work in countries as close to latitude N50° as possible. Existing results about experimental and dynamical simulation results is presented in paragraph 1. Comparison of solar cooling technologies for buildings is based on cost per produced useful cooling energy (€/kWh).

To compare night-radiative solar cooling technology with existing cooling technologies like compression, absorption, desiccant cooling a dynamical simulation in north European location is prepared. For the dynamical simulation software TRNSYS® and component nr. 203 is used. The PVT component is a laminated and glazed PV module where on the backside metallic fins and tubing is installed. The main schematic of the component is presented in Fig. 2 [12].

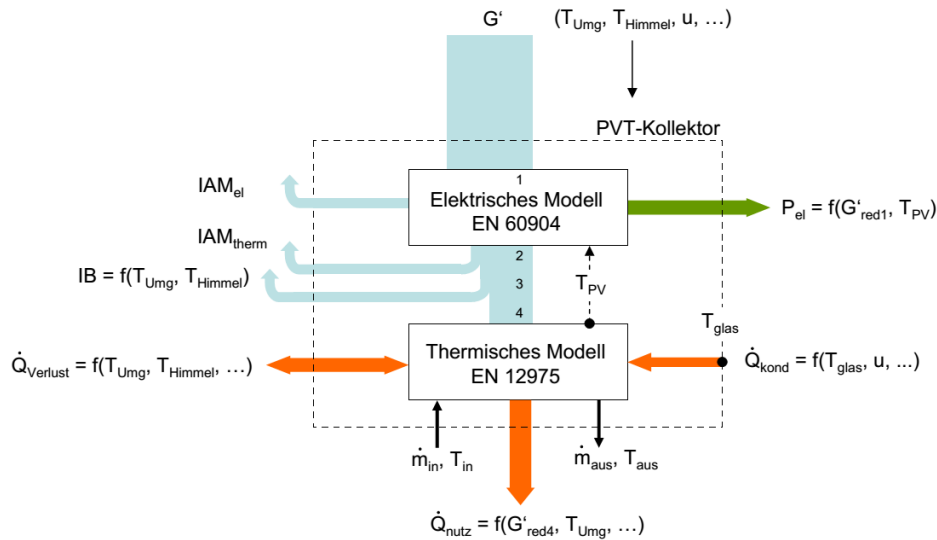


Fig. 2. TRNSYS component energy balance model of the unglazed PVT collector [12]

For the collector default parameters are used except that internal heat transfer coefficient is set to 23 W/(m²·K), overall heat transfer coefficient is set to 10.0 W/(m²·K), inclination angle is set to 0 degrees, azimuth angle to 180 degrees (south), and surface area of the PVT collectors is 10 m².

The inlet temperature is set to 25 °C, and flow rate is set to 25 kg/(h·m²). The annual cooling load is dependent on the building properties. In current article the building cooling load is not in detail analyzed in current article and set to annual value of 5 819kWh. The cooling load is presented in Fig. 3.

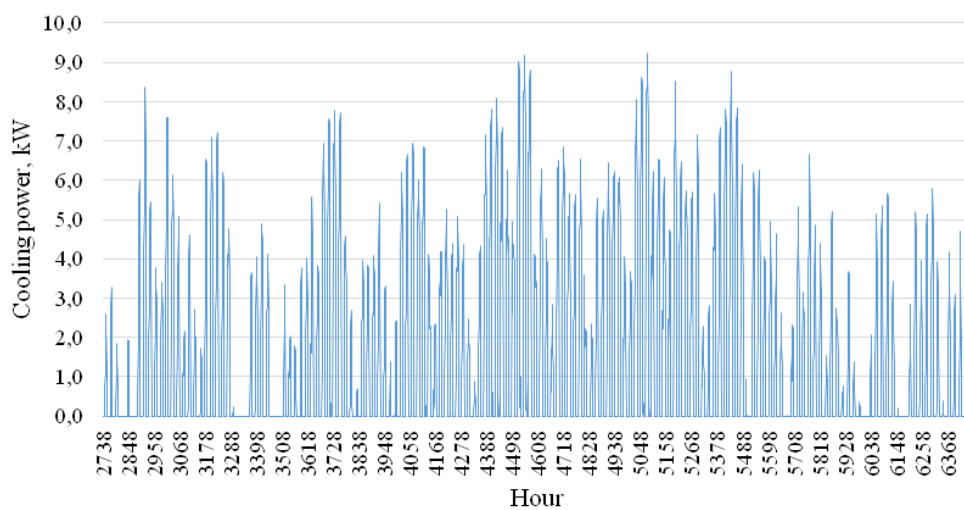


Fig. 3. Cooling load of a residential building in latitude N58°

In timestep of 5 minute the cooling load of the building and the PVT collector is calculated. Solar fraction is calculated and summarized over the simulation period.

4. RESULTS AND DISCUSSION

Cooling potential of the PVT module is over the cooling period 4 481 kWh, 4.48 kWh/m². Taking into account that not all the gains from cooling can be used, the cooling potential reduces 30% to 3137 kWh. The total cooling load of the building is by higher than the possible cooling gains from PVT collectors. The cooling energy needed to generate by compression chiller system is 2 682 kWh. Taking COP of the compression chiller 3.5 [11], the electricity required to cool the building during the daytime is 766 kWh. Following Table 1 illustrates the used parameters for economical calculation. The nominal cooling power of the installation is ca. 7.4 kW. As the nominal power is dependent on the inlet temperature of the PVT module more specific analysis is not conducted. The nominal power is taken as 80% of the maximum cooling load of the building.

Table 1. Used parameters for PVT-compression chiller economical calculations

Description	Value	Unit
Investment cost of a PVT modules, storage, installation	3500	€/kW
Investment cost of a compression chiller, installation	4500	€/kW
Maintenance of the system	50	€/year
Running costs of auxiliary devices	26,325	€/year
Price of electricity	0,13	€/kW

The calculation results that compared to compression chiller cooling system PVT integrated cooling system has a simple payback period of 10.5 years. Internal Rate of Return is 7.0 % and NPV in 20 years period is 595€.

For comparing the absorption, desiccant cooling processes with PVT compression chiller cooling the cost for producing kWh of cooling energy must be specified and compared with the result. During 20 years period 116 380 kWh cooling energy is required. Investment and running cost of PVT-compression chiller system for 20 years is 12 519 €. Cost for cooling is therefore 0,107 €/kWh.

As a reference the 10 kW absorption chiller system costs are 0.38 €/kWh [3]. Other systems have too high capacity to compare with PVT-compression chiller system.

Desiccant cooling systems are also installed in various capacities, but as already referenced previously the Austrian and German desiccant cooling systems had a cost of 0.55 and 0.95 €/kWh respectively. Both absorption and desiccant cooling systems depend how the cooling power and running hours are dimensioned [7], [13]. Dimensioning too large cooling capacity the installation costs are increased and cost of cooling energy increases. In northern latitude higher than N50°, the running hours of the cooling device have an important effect on the cost of cooling energy. As the cooling period is shorter, than in latitudes where experimental results are taken, the cost of cooling energy increases.

Night radiative cooling system with polymer collectors as measured in Norway [10] is promising as collector installation costs around 100 €/m² without installation costs, but with PVT installation during the daytime additionally electricity is produced which will be used to deliver power to compression chiller system. Reducing the costs for electricity reduces even more the cost of cooling.

CONCLUSION

Solar cooling possibilities and economical values were analysed. For northern latitudes over N50° the cooling concepts of the public or residential buildings are different, than in southern regions of Europe and world. Developed and economically viable absorption and desiccant cooling systems have already in latitudes of N45 ° high costs of produced cooling energy. In northern regions where cooling season is even shorter and number of sunny days is smaller, the cooling devices have to be integrated with heating and if possible electricity producing devices like reversible compression chiller and PVT module systems. As the sky temperatures are in northern latitudes lower the costs for produced cooling energy are lower compared to southern Europe regions. Simple and conservative simulation and economical calculation resulted with the costs for cooling energy of 0.107 €/kWh. Compared to costs to absorption and desiccant cooling systems the PVT-compression chiller combination is 2–3 fold cheaper. Low temperature PVT-compression chiller system is therefore promising and needs experimental work to confirm theoretical simulations.

REFERENCES

1. M. Science and P. Engineering, “Analysis of the thermal heating and cooling market in Europe.”
2. FONG K.F., LEE C.K., CHOW T.T. “Comparative study of solar cooling systems with building-integrated solar collectors for use in sub-tropical regions like Hong Kong,” *Appl. Energy*, vol. 90, no. 1, pp. 189–195, Feb. 2012.
3. HARTMANN N., GLUECK C., SCHMIDT F.P., “Solar cooling for small office buildings: Comparison of solar thermal and photovoltaic options for two different European climates,” *Renew. Energy*, Vol. 36, No. 5, p. 1329–1338, May 2011.
4. ALI A.H.H., NOERES P., POLLERBERG C. “Performance assessment of an integrated free cooling and solar powered single-effect lithium bromide-water absorption chiller,” *Sol. Energy*, Vol. 82, No. 11, p. 1021–1030, Nov. 2008.
5. HELM M., KEIL C., HIEBLER S., MEHLING H., SCHWEIGLER C. “Solar heating and cooling system with absorption chiller and low temperature latent heat storage: Energetic performance and operational experience,” *Int. J. Refrig.*, Vol. 32, p. 596–606, 2009.
6. BOURDOUKAN P., WURTZ E., JOUBERT P. “Experimental investigation of a solar desiccant cooling installation,” *Sol. Energy*, Vol. 83, No. 11, p. 2059–2073, Nov. 2009.
7. EICKER U., SCHNEIDER D., SCHUMACHER J., GE T., DAI, Y. “Operational experiences with solar air collector driven desiccant cooling systems,” *Appl. Energy*, Vol. 87, No. 12, p. 3735–3747, Dec. 2010.
8. S. Der Technologie, “Klimaschutz: Technologien, Wirtschaftlichkeit und CO₂ – Reduktionspotenziale,” 2005.
9. ERELL E., ETZION Y. “Radiative cooling of buildings with flat-plate solar collectors,” *Build. Environ.*, Vol. 35, No. 4, p. 297–305, May 2000.
10. MEIR M.G., REKSTAD J.B., LØVVIK O.M., “A STUDY OF A POLYMER-BASED RADIATIVE COOLING SYSTEM,” Vol. 73, No. 6, p. 403–417, 2003.
11. EICKER U., DALIBARD A. “Photovoltaic–thermal collectors for night radiative cooling of buildings,” *Sol. Energy*, Vol. 85, No. 7, p. 1322–1335, Jul. 2011.
12. STEGMANN M., BERTRAM E., ROCKENDORF G., JANßEN S., MODELLE E. “Modell eines unverglasten photovoltaisch-thermischen Kollektors basierend auf genormten Prüfverfahren Modellanforderungen,” No. Fkz 0325952, p. 1–12, 2012.
13. DAOU K., WANG R., XIA Z., “Desiccant cooling air conditioning: a review,” *Renew. Sustain. Energy Rev.*, Vol. 10, No. 2, p. 55–77, Apr. 2006.

DEVELOPMENT OF LOW-COST AND RAPID METHOD FOR THE EVALUATION OF ORGANIC AND INORGANIC COMPONENTS IN SWITCHGRASS BIOMASS

B. Butkutė, J. Cesevičienė, E. Norkevičienė

Institute of Agriculture

Lithuanian Research Centre for Agriculture and Forestry

Instituto ave. 1, LT-58344 Akademija, Kėdainiai district – Lithuania

ABSTRACT

The objective of the present study was to assess the ability of near infrared spectroscopy (NIRS) to predict chemical composition of switchgrass (*Panicum virgatum* L.) biomass as a bioenergy feedstock. The NIRS calibrations were developed for nitrogen (N), carbon (C), sulphur (S), neutral detergent fiber (NDF), acid detergent fiber (ADF), water soluble carbohydrates (WSC), acid detergent lignin (ADL), ash, and minerals (Ca, Mg, P, K, Si, Na) using switchgrass samples of whole aboveground plant part at different plant maturity stage and age (harvest year) as well as biomass samples of separate morphological fractions. Samples were collected during 2012–2013. Reflectance spectra were recorded in the range of 400–2500 nm by NIRS–6500. Chemical composition parameters were determined by reference methods. A modified partial-least-squares (MPLS) statistical technique was used to develop calibration equations. Different spectral pre-processing options were explored to enhance the relation between the spectra and measured biomass properties. Calibration equations were developed successfully for the concentrations of the majority of organic components as well as for some mineral constituents. The best coefficients of determination between the reference and NIRS predicted data in cross-validation (R^2_{cv}) were obtained: for N 0.978; NDF 0.944; ADF 0.959; WSC 0.920; ash 0.931; Si 0.910. The accuracy of the equations designed for C, K assessment in switchgrass biomass is satisfactory and for Na – insufficient. Our findings suggest that NIRS application could be a cost-effective, fast and an environment-friendly method for the analysis of biomass feedstocks.

Keywords: switchgrass, bioenergy feedstock, quality, organic and inorganic composition, NIRS calibration, accuracy of equation

1. INTRODUCTION

One of the key EU policy objectives is to increase energy consumption from renewable sources of energy because of their positive impact on the environment. The European Directive 2009/28/EC emphasizes that Member States should establish a national renewable energy action plan considering the different uses of biomass and therefore it is essential to concentrate new biomass resources. Searching for novel energy crops, an interest in C4 type plant switchgrass (SWG) (*Panicum virgatum* L.) has increased worldwide (especially in USA): SWG as an energy plant is used for solid biofuel, second generation bioethanol and biogas production [1]. Warm season grasses have the potential for biomass production because of their high yield potential and efficient utilization of soil nutrients and water. Approaching SWG as a multi-use energy plant, understanding the physical and chemical properties of switchgrass is an important issue for future utilization of biomass for biofuels and is essential for optimizing pre-treatment technologies for this bioresource [2]. It was found that for high output of methane as well as of second-generation bioethanol yield, in addition to the optimal C:N ratio, the biomass should contain a low lignin and high organic matter and non-structural carbohydrates concentrations [3, 4]. The main indicators of biomass as feedstock for direct combustion are C, N, S, ash and mineral composition [5, 6]. High lignin concentration is a positive character of solid biofuel [7]. The concentration of both

mineral and organic components in biomass depends on the environment, plant species, genotype, harvest time and other factors. [5, 8–10].

Standard methods for chemical composition are slow, labour-intensive, may require a number of reagents, and result in expensiveness of analyses as well as in the generation of hazardous waste. Rapid compositional analysis methods based on near-infrared (NIR) reflectance spectroscopy combined with multivariate statistics are well-established and widely used for the evaluation of chemical composition of agricultural, industrial (petroleum, pharmacy and other) objects [11, 12]. Most chemical and biochemical materials contain unique “fingerprint” information in their spectra that can be used for both qualitative and quantitative characterization. The most noticeable absorption bands occur in the NIR region and are related to overtones and combinations of fundamental vibrations of –CH, –NH, –OH (and –SH) functional groups [13]. Near-infrared (NIR) spectroscopy is a high throughput method that simultaneously provides analysis of a wide number of constituents on virtually any matrix with levels of accuracy and precision that are comparable to primary reference methods [12, 13]. The use of NIR spectroscopy can offer non-invasive techniques requiring little to no sample preparation and no reagents. Although a calibration needs to be done, first using the traditional measurement techniques as a reference [14]. When NIRS equations have been developed, measurements are quick and easy. After performing the standard technique once, future sample parameters can be predicted by inserting spectral data into robust calibration models.

Rapid compositional analysis methods have been developed for a number of different potential bioenergy feedstocks [4, 15]. The goal of this work was to develop NIR calibration model as a rapid analysis tool for the evaluation of organic and inorganic components in the biomass of switchgrass as a multi-use bioenergy feedstock.

2. METHODOLOGY

2.1. Switchgrass trial for biomass quality research

Field experiments were carried out in Lithuanian Institute of Agriculture. Switchgrass germplasm collections were sown in the soil characterized as *Endocalcari-Epihypogleyic Cambisol* (CMg-n-w-can) with the following characteristics of the plough layer (0–25): pH 6.52, humus content 1.82. Experimental collections were set up using the seedlings grown in a greenhouse. Seeds for the germplasm collections of switchgrass were obtained from the Plant Genetic Resource Conservation Unit (PGRCU) of the United States Department of Agriculture and Agricultural Research Service. The SWG biomass samples that were used for NIRS calibrations development represented the potentially wide range of quality. The biomass samples were of different plant age, i.e. harvest year: they were collected from the fields of SWG germplasm collections set up in 2010, 2011 and 2012. Plants were sampled at two stages: simulating the species management under commercial cultivation conditions, the grass was cut twice per season at the beginning of the anthesis and after re-growth of aftermath as feedstock for biogas in the first treatment. In the second treatment, the grass was cut once at seed maturation stage as feedstock for bioethanol of the second generation and for solid biofuel. Separation of the sampled herbage of SWG accessions, promising for growing under Lithuanian conditions into three botanical fractions (leaves: blades+sheaths, stems, and panicles) was additionally performed. Herbage samples weighing 200–300 g were collected for each accession for chemical analysis and NIRS scanning.

2.2. Sample preparation and chemical analyses by reference methods

The harvested samples were dried, ground, and used for chemical analyses and NIRS calibration. Fresh samples, chopped into particles of 3–5 cm, were fixed at 105°C for 15 min, dried at 65±5°C and ground in a cyclonic mill with a 1 mm sieve. The samples were analysed using standard methods for biomass compositional analysis. For the acid detergent fibre (ADF), neutral detergent fibre (NDF) and acid detergent lignin (ADL) the cell wall detergent fractionation method according to Van Soest [16] was used. NDF and ADF extraction was done on an ANKOM220 Fibre Analyzer (ANKOM Technology, USA) using F57 filter bags [17]. Sodium sulphite was added to the neutral-detergent solution and data of NDF are presented as ash-free. Concentrations of water soluble carbohydrates (WSC) in water extracts of dried samples were measured spectrophotometrically on a Camspec M107 (Camspec Ltd., UK; 620 nm) using the sulphur acid - anthrone reagent [18]. Determination of silicon (Si) content was performed spectrophotometrically on a Cary 50 UV-Vis (Varian Inc., USA; 660 nm) according to the method reported by Kraska and Breitenbeck [19] and Dai et al. [20]. The concentrations of P digestates in the sulphuric acid were evaluated by a colouring reaction with ammonium molybdate vanadate [21] on a Cary 50 UV-Vis, at the wavelength 430 nm. Carbon (C), sulphur (S) and nitrogen (N) in the samples were assessed by dry combustion on a CNS analyser (Elementar, Vario EL, Germany). K, Na, Ca, Mg concentration in wet digested samples was quantified by flame atomic absorption (AAS). Parameters of the AAnalyst 200 instrument (Perkin Elmer, USA) were chosen in accordance with the manufacturer's instructions.

2.3. NIRS scanning and calibration procedure by chemometric software

All the grass samples were scanned on a monochromator NIR Systems model 6500 (Perstorp Analytical, USA) equipped with a Spinning Module by using a small ring cup (ø 4.7 cm). The reflectance spectral data collected, covered the range 400 to 2498 nm and were recorded at 2-nm intervals. All samples were scanned in either duplicate or triplicate. Replicate scans were averaged prior to building calibration models. Quality-control material and check-cell were scanned along with the experimental samples to ensure instrument stability; no anomalies were seen with the check scans. Reflectance (R) values were converted into absorbance (A) values using the formula:

$$A = \log(1/R) \quad (1)$$

Calibration development was performed using the chemometric software WinISI II v.1.05 [22]. The spectra were matched with the reference data and calibration models were developed using MPLS regression (modified partial least squares) algorithm and cross-validation technique [11]. Spectra were corrected for scatter and transformed into different mathematical treatment models. Mathematical treatment of spectra is described by four digits, eg. 1,4,4,1. The first means derivative, the second is the gap over which the derivative is calculated, the third is the smooth, i.e. the number of data points in a running average and the fourth is the second smooth: the scatter correction standard normal variate and detrend (SNVD) and no correction (none) were applied to spectra transformation. Spectral data of wavelength intervals of 400–2500, 700–2500 and 1100–2500 nm with spectral data points 8, i.e. when absorbance readings was every 80 nm, were tested in order to optimise the accuracy of calibration. Calibration performances were assessed by the standard error of calibration (SEC), coefficient of determination of calibration (R^2_C), SECV, coefficient of determination of cross-validation (R^2_{CV}).

3. RESULTS AND DISCUSSION

3.1. The characterisation of switchgrass quality and the calibration set

One key component of the NIR prediction model is the size and nature of the population of samples covered by the reference method which will be scanned by the NIRS instrument. Wide ranges in biomass constituents are desirable because greater sample diversity results in more effective NIRS calibration. The sample population should represent the full diversity of plant materials to be scanned. The chemical composition of SWG dried and ground samples determined by conventional methods are given as mean, minimum and maximum values in Table 1. Due to plant stage at harvest and plant part, the data of quality of switchgrass samples differed in a wide range: quality components in individual samples differed 4–24 times, except for C, NDF and ADF. The variation coefficients of values in the calibration samples set were from 5.32% (for C) to 74.3% (for Na). Extremely low contents of N and mineral constituents were found in the SWG stems, and the highest contents in the leaves as well as in young biomass, i.e. in biomass harvested at early heading stage. Conversely, stems were distinguished by the highest NDF, ADF, ADL, C concentration [9, 10]. The content of lignocellulose, referred to as NDF, was higher in the stems (785 g kg⁻¹ DM) and whole plant (741 g kg⁻¹ DM) than in leaves (599 g kg⁻¹ DM) and panicles (673 g kg⁻¹ DM) [9].

Table 1. Variation of data of chemical composition of switchgrass, collected in the database for NIRS calibration

Component of biomass quality	Number of samples (n)	Values of component concentration, % DM			Standard deviation (SD)	Coefficient of variation
		Mean	Min	Max		
NDF	271	69.2	55.8	82.8	5.59	8.08
ADF	271	44.2	32.5	60.1	5.87	13.3
ADL	271	7.33	3.07	17.5	2.82	38.5
WSC	271	6.79	2.66	17.5	2.20	32.4
N	148	1.16	0.225	3.03	0.610	52.6
C	118	45.9	42.5	56.7	2.44	5.32
S	110	0.085	0.051	0.220	0.041	48.2
Ash	297	6.44	2.29	11.6	1.68	26.1
K	162	1.41	0.640	3.34	0.504	35.7
Na	116	0.140	0.033	0.809	0.104	74.3
Ca	162	0.627	0.099	1.68	0.383	61.1
Mg	162	0.370	0.099	0.934	0.179	48.4
P	137	0.194	0.034	0.441	0.076	39.2
Si	100	0.490	0.177	0.871	0.152	31.0

The larger the variation in values of the chemical composition in the calibration database, the more reliable and universal equations, i.e. equations which accurately could predict quality of a wider diversity of samples, can be developed. Thus, the calibration samples set for the development of equations, designed for the determination of SWG quality indicators by the NIRS-6500 instrument, met this requirement; it included samples covering the full range of potential variation.

3.2. Spectral properties of different switchgrass samples

Fig. 1 and 2 show the spectral reflectance curves for the individual SWG samples and standard deviation in the visible and near-infrared regions. SWG samples are biomass of

whole aboveground plant of two maturity stages, as well as samples of different plant parts. Therefore the samples differed in the chemical composition of both organic and mineral components. The raw ($\log 1/R$) spectra of all soil samples had similar shapes with the strongest absorption in the visible region and peaks around 1464 and zone of 1900–2488 nm in infrared region (Fig. 1). The absorption peaks in the visible region at 460–700 nm are associated with the plant pigments such as chlorophylls, carotenoids, anthocyanin, xanthophyll [23]. The absorption peaks observed in the NIR region, are related to C-H, O-H and N-H bonds associated with the water, carbohydrates and protein content of the sample. In the NIR region, the curve of SD of the raw spectra shows only one evident peak at 1932 nm related to water content and some small peaks in the zone around 2000–2300 nm.

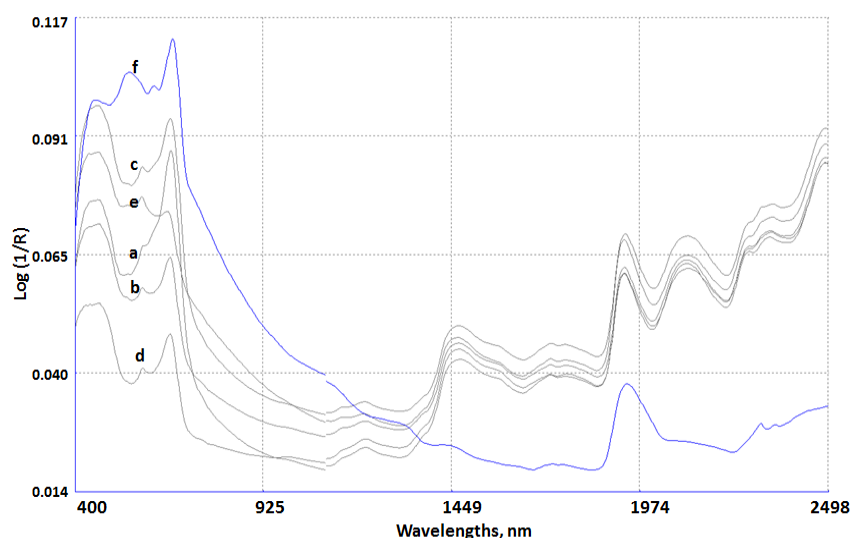


Fig. 1. Raw NIRS spectra of switchgrass (SWG) samples and standard deviation (SD) of the spectra: a – SWG at heading; b – SWG at seed maturation; c – SWG leaves; d – SWG stems; e – SWG panicles; f – SD. Mathematical treatment 0,0,1,1; scatter correction – none

Particle size and structure of a sample can cause spectral differences that are unrelated to chemical composition, and the statistics of accuracy of equations developed by using the raw $\log 1/R$ is often unsatisfactory. The first step for minimisation of the effect of particle size in calibration is subjecting the calibration file to various pre-treatments of the spectral data [24]. These transformations usually include scatter correction that may use standard normal variate procedures for minimization of the interfering effect and mathematical derivative transformations. Fig. 2 demonstrates the second derivative SNVD corrected spectra of the same samples as in fig. 1 and the SD of the spectra. The second derivative also had apparent absorption bands at 450–700 nm. These absorption bands were associated with the Soret absorption band and with plant pigments [25]. Multiple small and sharp absorption peaks are observed also in the NIR region of the derivatised spectra. According to SD curve, the distinctly visible differences between these samples were observed at spectral ranges of 1880–1950 nm and 2200–2350 nm and less definite around 1360–1460 nm and 1650–1750 nm. Most of the absorption peaks in the NIR region are assigned to the various overtone and combination of molecular vibration of organic functional groups such as: C-H, N-H, O-H, S-H, C=O, C=C and etc. Although the spectra are rich in information about the samples organic compounds, the absorption bands in the NIR region are broad and overlap, which means that conventional univariate calibration techniques, using only one wavelength per component for evaluations, cannot be applied in the cases of overlapping bands [24]. The

information has to be extracted statistically by chemometrical calibration of physical and chemical data.

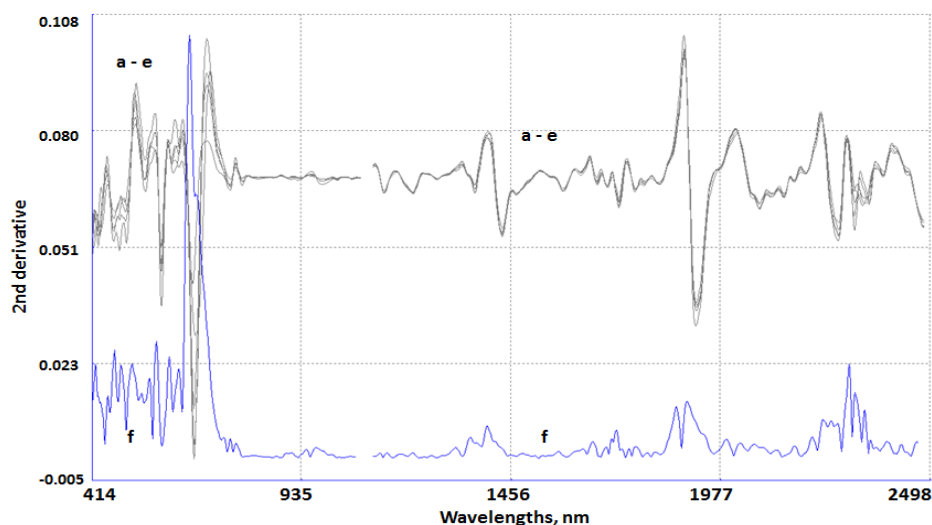


Fig. 2. NIR spectra of switchgrass samples and standard deviation (as in Fig.1) with the application of the spectral data derivatisation by 2,5,5,1 and of scatter correction SNVD

3.3. Effect of the calibration model applied on the robustness of equations

The robustness of calibration for the property of interest can depend on the degree to which this property can be modelled from spectral information of samples within the property domain of the calibration set. The present study has over again demonstrated that the accuracy of NIRS prediction depends on the successful completion of several factors of calibration. Spectra mathematical transformation, scatter correction and calibrating wavelength range of the spectrum have implications for the accuracy of equations both in calibration, as well as cross-validation steps (Table 2).

Table 2. The range of the statistical parameters of the equations accuracy as affected by the calibration model

Component of biomass quality	Range of equation statistics			
	SEC	R^2_c	SECV	R^2_{cv}
NDF	1.18–1.63	0.909–0.958	1.39–1.78	0.893–0.944
ADF	1.00–1.27	0.953–0.971	1.19–1.37	0.945–0.959
ADL	0.679–0.790	0.914–0.939	0.747–0.860	0.898–0.921
WSC	0.535–0.699	0.899–0.947	0.655–0.782	0.873–0.920
N	0.066–0.080	0.977–0.985	0.094–0.080	0.968–0.978
C	0.389–0.505	0.689–0.817	0.496–0.547	0.637–0.702
S	0.010–0.013	0.882–0.925	0.013–0.016	0.814–0.862
Ash	0.348–0.523	0.898–0.973	0.445–0.563	0.883–0.931
K	0.235–0.275	0.710–0.783	0.268–0.303	0.647–0.716
Na	0.0544–0.0572	0.485–0.534	0.0643–0.0654	0.322–0.346
Ca	0.0926–0.129	0.874–0.936	0.123–0.138	0.858–0.887
Mg	0.0469–0.0569	0.880–0.923	0.0532–0.0624	0.862–0.893
P	0.0242–0.0277	0.857–0.889	0.0276–0.0308	0.823–0.855
Si	0.0324–0.0377	0.940–0.956	0.0463–0.0503	0.892–0.910

When adjusting math treatment model of calibrated optical data with wavelength range and especially with composition and volume of the database, the statistics of the accuracy of the developed equations was changed. Depending on the calibration conditions initial equations with different accuracy were developed. Accuracy of the equations varied in the ranges as follows: for the prediction of NDF content $R^2_C=0.909-0.958$, $SEC=1.18-1.63$, $R^2_{CV}=0.893-0.944$, $SECV=1.39-1.78$; for WSC values determination $R^2_C=0.899-0.947$, $SEC=0.535-0.699$, $R^2_{CV}=0.873-0.920$, $SECV=0.655-0.782$; for C concentration assessment in SWG biomass $R^2_C=0.689-0.817$, $SEC=0.389-0.505$, $R^2_{CV}=0.637-0.702$, $SECV=0.496-0.547$; for ash values estimation $R^2_C=0.898-0.973$, $SEC=0.348-0.523$, $R^2_{CV}=0.883-0.931$, $SECV=0.445-0.563$ etc. (Table 2). Previous studies have shown that transformations of spectral data, such as derivatisation allied to scatter correction procedures, can enhance the predictive performance of NIRS techniques [25]. Scatter correction together with mathematical treatment subdues the effect of particle size [24, 26]. Gap size is important in calibration sensitivity to system noise [24].

The discussed spectra pre-treatment affected the accuracy of equations (in calibration, cross-validation) by different intensity subject to analyte (Table 3). The best statistical parameters in most cases are observed when the equations were developed by calibrating spectra of 1000–2500 nm or 700–2500nm interval were scatter-corrected with SNVD followed by second first or derivative (1,5,5,1 or 2,5,5,1). Many NIRS spectroscopists have found also that derivatized and scatter-corrected spectra are preferable to develop applicable equations [24, 26, 27 and others]. Park et al. [26] confirmed also that little improvement in accuracy was obtained by extending wavelength range beyond 1100–2500 nm.

Table 3. Accuracy of equations with the best statistics in the cross-validation, parameters of calibration used for their development and interpretation of the equation application according to P. Williams [28]

Component of quality	SECV	R^2_{CV}	Scatter correction	Math treatment	Wavelength range	Interpretation
NDF	1.39	0.944	SNVD	2,5,5,1	700–2500	Usable in most applications
ADF	1.19	0.959	SNVD	2,5,5,1	1100–2500	Usable in most applications
ADL	0.756	0.921	SNVD	2,5,5,1	700–2500	Usable in most applications
WSC	0.655	0.920	SNVD	1,5,5,1	1100–2500	Usable in most applications
N	0.080	0.978	SNVD	2,5,5,1	700–2500	Excellent, usable for any application
C	0.496	0.702	SNVD	1,5,5,1	1100–2500	Usable for screening and approximate work
S	0.013	0.862	SNVD	2,5,5,1	700–2500	Usable for screening and approximate work
Ash	0.445	0.931	SNVD	2,5,5,1	1100–2500	Usable in most applications
K	0.271	0.716	SNVD	1,5,5,1	700–2500	Usable for screening and approximate work
Na	0.064	0.346	SNVD	1,5,5,1	400–2500	Poor correlation: research the reasons
Ca	0.126	0.882	SNVD	1,5,5,1	1100–2500	Usable with caution for most applications
Mg	0.053	0.893	SNVD	1,5,5,1	700–2500	Usable with caution for most applications
P	0.028	0.853	SNVD	0,2,2,1	1100–2500	Usable with caution for most applications
Si	0.046	0.910	SNVD	1,5,5,1	400–2500	Usable with caution for most applications

NIRS calibrations developed for quality components related to organic matter of SWG biomass display good accuracy. In assessing the equations according to criteria described by P. Williams [28] (Table 3), i.e. on the basis of the coefficient of determination in cross-validation R^2_{CV} of the equations with the best statistic for component, they could be applied as follow: for N is of excellent quality and could be used for any application, NDF, ADF, ADL, WSC and ash prediction by developed equations could be usable in the most cases of the SWG biomass quality investigation. Near infrared spectroscopy primarily detects organic functional groups. Efficacious calibration of N is assuredly explained by the absorption of infrared light by the N-H bonds present in the plant material, mainly in the proteins, good prediction of NDF, ADF, and WSC may be associated with absorbance of compounds with C-H or O-H bonds common for carbohydrates. Successful NIRS determinations of ADL, which in association with structural carbohydrates enters into composition of NDF and ADF, could be linked to aromatic C-H bonds. Meanwhile, minerals generally do not react with infrared light. Nevertheless, there is evidence from publications that the NIRS method is applicable to determine the amounts of macronutrients in plant biomass [14, 29, 30]. Our results presented in Table 3 suggest also, that Ca, Mg, P, Si quantification by NIRS could be performed in many ways, but with some caution, i.e. still together with the analytical verification of selected samples by the reference methods. Equations, developed for C, S, P, K prediction, are usable for SWG screening programs and approximate work only. And finally, the accuracy of that for Na prediction was poor.

A similar level of equation accuracy ($R^2=0.81$) for P prediction in biomass of reed canary grass was developed by Casler et al. [31]. The results published previously confirm the feasibility of using NIRS to predict K, Ca, and Mg concentrations in timothy [32], total ash, Ca, K, and P concentration in lucerne [29]. Lavrenčič et al. [30] showed also, that Ca, P, Mg and K in forage plants of the various cuts and maturity can be predicted with a high degree of accuracy (R^2 of 0.963, 0.884, 0.892 and 0.939, respectively). Like in our work, the prediction of Na concentrations was failed [30, 32]. Although theoretically minerals do not absorb energy in NIR region, prediction of minerals is possible by detecting chelates and complexes. Some well predictable macrominerals are probably closely associated with the organic components, such as plant cell wall (Ca and Mg), chlorophyll (Mg), phytates, phospholipids, phosphoproteins and nucleic acids (P) and organic acids, such as malate (K) [30]. Na is not a significant material in plant nutrition. High concentrations of Na in biomass may be due to mechanical contamination and therefore this item is accompanied by a calibration failure.

4. CONCLUSIONS

Estimation of switchgrass biomass quality by reference methods revealed a high variability in chemical composition of samples.

The present study demonstrated that the accuracy of NIRS prediction depends on the successful completion of several factors of calibration. The best equations were obtained with mathematical treatments that included a derivative of the first or second order and scatter correction with standard normal variate and detrend algorithm. Calibrating of wavelength range 1100–2500 nm or restrictedly extending the interval to VIS zone, i.e. 700–2500 nm generally allowed developing the equations of best accuracy for prediction.

The accuracy of equations ranged: for N determination (R^2_{CV} 0.978) it is of excellent quality, for NDF, ADF, ADL, WSC and ash prediction (R^2_{CV} 0.920–0.959) they are of very good accuracy, for Ca, Mg, P, Si (R^2_{CV} 0.882–0.910) quantification they are of good accuracy, equations developed for C, S, P, K prediction (R^2_{CV} 0.702–0.862) are usable for SWG screening programs and the calibration for Na prediction (R^2_{CV} 0.346) did not succeed.

The use of NIR spectroscopy enable immediate and simultaneous prediction of several components without the use of reagents and is an environment-friendly method which may efficiently decrease the time and cost of switchgrass germplasm screening as a bioenergy crop, thus facilitating the pre-breeding process.

ACKNOWLEDGEMENTS

Separate stages of this research were funded by a grant (No. MIP-073/2012) from the Research Council of Lithuania.

REFERENCES

1. MONTI A. (ed.). *Switchgrass: A Valuable Biomass Crop for Energy*. Series: Green Energy and Technology, Springer-Verlag London, 2012, IX, 209 p.
2. HU Z., SYKES R., DAVIS M.F., BRUMMER E.C., RAGAUSKAS A.J. Chemical profiles of switchgrass. *Bioresource Technology*, 2010, Vol. 101, p. 3253–325.
3. SEPPÄLÄ M., PAAVOLA T., LEHTOMÄKI A., RINTALA J. Biogas production from boreal herbaceous grasses – Specific methane yield and methane yield per hectare. *Bioresource Technology*, 2009, Vol. 100, p. 2952–2958.
4. SLUITER J. B., RUIZ R. O., SCARLATA C. J., SLUITER A. D., TEMPLETON D.W. Compositional analysis of lignocellulosic feedstocks. 1. Review and description of methods. *Journal of Agricultural and Food Chemistry*, 2010, Vol. 58, p. 9043–9053.
5. MONTI A., DI VIRGILIO N., VENTURI G. Mineral composition and ash content of six major energy crops. *Biomass and Bioenergy*. 2008, Vol. 32, p. 216–223.
6. ZHANG K., JOHNSON L., NELSON R., YUAN W., PEI Z., WANG D. Chemical and elemental composition of big bluestem as affected by ecotype and planting location along the precipitation gradient of the Great Plains. *Industrial Crops and Products*, 2012, Vol. 40, p. 210–218.
7. DEMIRBAŞ A. Relationships between heating value and lignin, fixed carbon, and volatile material contents of shells from biomass products. *Energy Sources*, 2003, Vol. 25, p. 629–635.
8. EL-NASHAAR H.M., BANOWETZ G.M., GRIFFITH S.M., CASLER M.D., VOGEL K.P. Genotypic variability in mineral composition of switchgrass. *Bioresource Technology*, 2009, Vol. 100, No. 5, p. 1809–1814.
9. BUTKUTĖ B., LEMEŽIENĖ N., CESEVIČIENĖ J., LIATUKAS Ž., DABKEVIČIENĖ G. Carbohydrate and lignin partitioning in switchgrass *Panicum virgatum* biomass as a bioenergy feedstock. *Zemdirbyste–Agriculture*, 2013, Vol. 100, Iss. 3, p. 251–260.
10. BUTKUTĖ B., LEMEŽIENĖ N., CESEVIČIENĖ J., LIAUDANSKIENĖ I. Dry matter yield and carbon partitioning in the aboveground part of switchgrass (*Panicum virgatum* L.) germplasm. *Agriculture & Food*, 2013, Vol. 1, Part 1, p. 87–97.
11. SHENK J.S., WORKMAN J.J., WESTERHAUS M.O. Application of NIR spectroscopy to agricultural products. In: BURNS D.A., CIURCZAK E.W. (Eds.), *Handbook of Near-Infrared Analysis*, 2nd edition, Marcel Dekker Inc., New York: Basel, 2001. p. 419–474.
12. WORKMAN J.J.R., SHENK J. Understanding and using the near-infrared spectrum and as an analytical method. In *Near-Infrared Spectroscopy in Agriculture*. Eds. ROBERTS C.A., WORKMAN J.J.R., REEVES J.B. ASA, Madison, USA, 2004. p. 3–10.
13. CIURCZAK E.W. Principles of near-infrared spectroscopy. In: BURNS D.A., CIURCZAK E.W. (Eds.), *Handbook of Near-Infrared Analysis*, 2nd edition, Marcel Dekker Inc., New York: Basel, 2001, p. 7–18.
14. WARD A., NIELSEN A.L., MØLLER H. Rapid assessment of mineral concentration in meadow grasses by near infrared reflectance spectroscopy. *Sensors*. 2011, 11, p. 4830–4839.

15. XU F., YU J., TESSO T., DOWELL F., WANG D. Qualitative and quantitative analysis of lignocellulosic biomass using infrared techniques: A mini-review. *Applied Energy*, 2013, Vol. 104, p. 801–809.
16. FAITHFULL N. T. *Methods in agricultural chemical analysis: A practical handbook*. Wallingford: CABI Publishing, 2002. 304 p.
17. BUTKUTĖ B., ŠLEPETIENĖ A. Perdirbimui ir pašarams skirtų fitožaliavų kokybės tyrimų metodai, jų plėtojimas ir tobulinimas. *Mokslinės metodikos inovatyviems žemės ir miškų mokslų tyrimams*. Kaunas: Lututė, 2013, p. 434–447.
18. YEMM E.W., WILLIS A.J. The estimation of carbohydrates in plant extracts by anthrone. *Biochemistry*. 1954, Vol. 57, p. 508–514.
19. KRASKA J.E. BREITENBECK G.A. Simple, robust method for quantifying silicon in plant tissue. *Communications in Soil Science and Plant Analysis*, 2010, Vol. 41, p. 2075–2085.
20. DAI W.M., ZHANG K.Q., DUAN B.W., SUN C.X., ZHENG K.L., CAI R., ZHUANG J.Y. Rapid determination of silicon content in rice. *Rice Science*, 2005, Vol. 12 (2), p. 145–147.
21. CHAPMAN H.D., PRATT P.F. Ammonium vanadate–molybdate method for determination of phosphorus. *Methods of Analysis for Soils, Plants and Water*. California University, Agriculture Division, USA, 1961, p. 184–203.
22. ISI. WinISI 1.5 Near-infrared software, the complete software solution for routine analysis, robust calibration and networking. InfraSoft International LLC, Port Matilda, PA, USA, 2000.
23. SIMS D.A., GAMON J.A. Relationships between leaf pigment content and spectral reflectance across a wide range of species, leaf structures and developmental stages. *Remote Sensing of Environment*, 2002, Vol. 81, p. 337–354.
24. DRYDEN G.M., 2003. Near infrared spectroscopy: Applications in deer nutrition. RIRDC Pub. No. W03/007. Barton, ACT, Australia.
25. COZZOLINO, D. LABANDERA, M. Determination of dry matter and crude protein contents of undried forages by near-infrared reflectance spectroscopy. *Journal of the Science of Food and Agriculture*, 2002, Vol. 82, p. 380–384.
26. PARK, R. S., GORDON, F. J., AGNEW, R. E., BARNES, R. J., STEEN, R. W. J. The use of near infrared reflectance spectroscopy on dried samples to predict biological parameters of grass silage. *Animal Feed Science and Technology*, 1997, Vol. 68, p. 235–246.
27. PERBANDT D. Determination of yield and quality parameters of energy crops applying laboratory and field spectroscopy. Doctoral thesis. Witzenhausen, 2009. 86 p. [Referred 21 10 2013] Link to the internet <http://d-nb.info/1003606652/34/>
28. WILLIAMS P. The application of simple statistics in grains research. [Referred 21 10 2013] Link to the internet <http://projekt.sik.se/traditionalgrains/review/default.htm>.
29. HALGERSON J.L., SHEAFFER C.C., MARTIN N.P., PETERSON P.R., WESTON S.J. Near-infrared reflectance spectroscopy prediction of leaf and mineral concentration in alfalfa. *Agronomy Journal*. 2004, Vol. 96, p. 344–351.
30. LAVRENČIČ A., STEFANON B., OREŠNIK A. Estimation of mineral content in forages by near-infrared reflectance spectroscopy. *Zbornik Biotehniške fakultete Univerze v Ljubljani. Kmetijstvo. Zootehnika*. 2002, 80(1): 41–49.
31. CASLER M.D., UNDERSANDER D.J., JOKELA W.E. Divergent selection for phosphorus concentration in reed canarygrass. *Crop Science*. 2008, Vol. 48, p. 119–126.
32. TREMBLAY G.F., NIE Z., BÉLANGER G., PELLETIER S., ALLARD G. Predicting timothy mineral concentrations, dietary cation-anion difference, and grass tetany index by near-infrared reflectance spectroscopy. *Journal of Dairy Science*, 2009, Vol. 92, p. 4499–506.

PERIODATE OXIDATION FOR THE DETERMINATION OF LEVOGLUCOSAN AND TOTAL SUGARS IN PYROLYSIS LIQUIDS

K. Meile, A. Zhurinsh, B. Spince

Latvian State Institute of Wood Chemistry

Dzerbenes str. 27, Riga LV-1006 – Latvia

ABSTRACT

Biomass, such as wood, can be used to obtain different valuable compounds as a replacement for fossil resources. The liquid products of fast pyrolysis contain a noteworthy amount of sugars and their derivatives. One of the most typical anhydrosugars obtained from wood is levoglucosan, which can be used as a renewable raw material in the production of various polymers and even antibiotics. In this study, various types of sugars have been oxidised with sodium periodate at different pH and temperatures. The kinetic results of the reaction have been used to develop a simple, fast analysis method for the simultaneous determination of sugars and anhydrosugars in pyrolysis liquids for the qualitative control of wood pyrolysis processes. The investigation of the oxidation kinetics of d-glucose and levoglucosan leads to two ways to determine levoglucosan in the presence of glucose or other hexoses: titration of the sample before and after hydrolysis (levoglucosan conversion to glucose) and oxidation at pH 1 for 4 h or titration of the sample before and after hydrolysis and oxidation at pH 9 for 15 min. Both methods showed good accuracy and recovery for mixtures of standard levoglucosan and d-glucose, but only the pH 1 method was suitable for real pyrolysis liquids, because of the complex composition of the samples.

Keywords: renewable resources, wood pyrolysis, anhydrosugars, sugars

1. INTRODUCTION

Biomass, along with sun, wind, water and geothermal resources is one of the sources of renewable energy, but biomass is the only renewable resource of feedstock for the production of carbon containing materials, chemicals and fuels. Wood is a typical biomass example, which can be used as an abundant, low-cost replacement of fossil resources for the production of bio-based chemicals, fuels and energy.

The chemical composition of wood is mostly made up of cellulose (depending on the species 30–50 wt%), hemicelluloses (15–30 wt%) and lignin (10–30 wt%) [1], of which the first two are polysaccharides. Therefore, pyrolysis of wood can yield considerable amounts of sugars and their derivatives. Pyrolysis is the thermal degradation of wood in the absence of oxygen. Cellulose, hemicelluloses and lignin each react differently at different temperatures, so it is possible to fractionate the products of wood pyrolysis. Fast pyrolysis has a characteristically high yield of liquid products (75%), but less solids or char (12%) and gaseous products (13%) [2].

The liquid products of acid pre-treated fast pyrolysis contain a noteworthy amount of levoglucosan or 1,6-anhydro- β -D-glucopyranose [3]. Levoglucosan is an anhydrosugar, with a high potential for applications in the production of biodegradable plastics, and in the synthesis of high value speciality chemicals such as pharmaceuticals, using chiral catalysts incorporating levoglucosan-based ligands [4].

Naturally, a simple analytical method for sugars and their derivatives is required to monitor the process of the production of these compounds. In this study an analytical method based on periodate oxidation has been developed. Periodate oxidation has various applications in sugar chemistry – synthesis [5], quantitative analysis and structure determination [6]. Generally, periodate oxidation is used for α -diols and some other organic compounds, such as

aminoalcohols, but to some extent it has proven to be valuable in inorganic chemistry as well, for example, for the oxidation of manganese II [7]. Many factors influence the periodate oxidation of diols – pH, steric factors, association-dissociation equilibria, temperature, solvents and the concentration of the periodate [8–10]. This paper concerns the influence of pH and temperature on the periodate oxidation of some biomass origin sugars.

Fig. 1 shows the theoretical reaction equations of levoglucosan, d-glucose and its dimer d-cellobiose. Only α -diol groups can be cleaved by periodate, so 1 mole of levoglucosan reduces 2 moles of periodate, giving 1 mole of formic acid [11]. 1 mole of d-glucose reacts with 5 moles of periodate, giving 5 moles of formic acid and 1 mole of formaldehyde [12], but d-cellobiose is oxidised by 11 moles of periodate down to 9 moles of formic acid and 2 moles of formaldehyde [13].

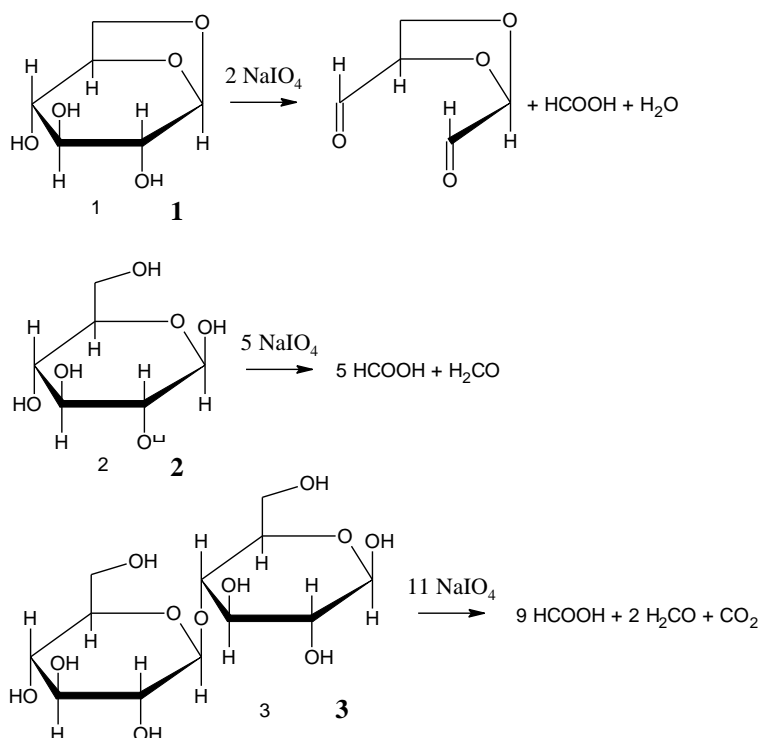


Fig. 1. The reaction equations of levoglucosan (1) d-glucose (2) and cellobiose (3)

The rate of the oxidation reactions can be described by various analytical methods. In this study iodometric titration has been used to determine the iodate ions, which are reduced to iodine by the addition of potassium iodide, and the iodine is titrated with sodium thiosulfate [14]. Formic acid has been determined by potentiometric titration with potassium hydroxide [15].

2. METHODOLOGY

The experimental section of this study includes the procedure of oxidation of different sugars in different conditions with an excess of sodium periodate. Two analytical methods have been used to determine the oxidation products – iodometric titration for iodate ions and potentiometric titration for formic acid. The obtained oxidation curves of levoglucosan and d-glucose have been used to develop the optimal method for determination of sugars and anhydrosugars in wood processing products.

2.1. The oxidation of the sugars

An aqueous solution of the sugars (levoglucosan, d-glucose or d-cellobiose) was oxidised with of 0.2 M sodium periodate at different temperatures (5 °C, 20 °C and 40 °C). The experiments were performed at pH 1, pH 5 and pH 9. 0.1 mL of 15% sulfuric acid was used for pH 1 and 5 mL of borate buffer was used for pH 9. All experiments were performed in triplicate.

2.2. The determination of iodate ions

The excess of periodate was masked with 10% ammonium molybdate solution. Glacial acetic acid and 10% potassium iodide were used to reduce iodate ions to iodine, which was titrated with 0.1 M sodium thiosulfate solution.

2.3. The determination of formic acid

The excess of periodate was reduced with 2% ethylene glycol solution. Formic acid was determined in the neutral samples by potentiometric titration with 0.1 M potassium hydroxide solution.

2.4. The determination of levoglucosan and sugars in pyrolysis liquid samples

In order to determine the amount of levoglucosan and sugars in samples of wood (alder) pyrolysis liquids, the samples were hydrolysed at 120 °C for 90 min in a 7.5% sulfuric acid solution. Afterwards, the hydrolyzed and non-hydrolyzed samples were oxidised at 40 °C pH 1 for 4 h or neutralized with 0.1 M sodium hydroxide and oxidised at 20 °C pH 9 for 1 h. Iodate ions were determined as described in section 2.2.

3. RESULTS AND DISCUSSION

First of all, the kinetics of anhydrosugar and sugar oxidation was examined and the results were used to develop an optimal analysis method. Secondly, various samples were analyzed using the developed methodology.

3.1. The sugar oxidation products

The periodate oxidation of levoglucosan, d-glucose and d-cellobiose was performed at temperatures 5 °C, 20 °C and 40 °C, at pH 1, pH 5 and pH 9 for a period of 4.5 hours. Fig. 2 shows the oxidation curves of levoglucosan. The oxidation rate of the sugars is expressed as periodate moles per one mole of the sugar.

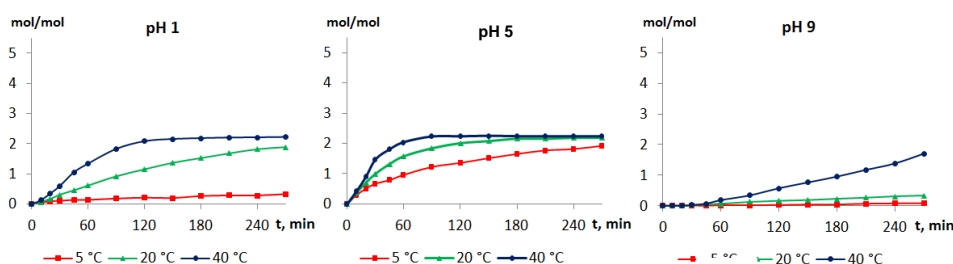


Fig. 2. The oxidation curves of levoglucosan, expressed as periodate moles per one mole of the sugar

Obviously, levoglucosan is oxidised fastest, when there is no catalyst, either an acid or a base, present in the reaction solution (pH 5). This tendency is observed at all temperatures. The reason, why a catalyst is not necessary for the oxidation of levoglucosan, lies in the fact that only two C-C bonds are cleaved in the structure of levoglucosan, and further hydrolysis of the product is not possible. However, it is quite different regarding normal sugars, such as d-glucose. The oxidation curves of d-glucose can be seen in Fig. 3.

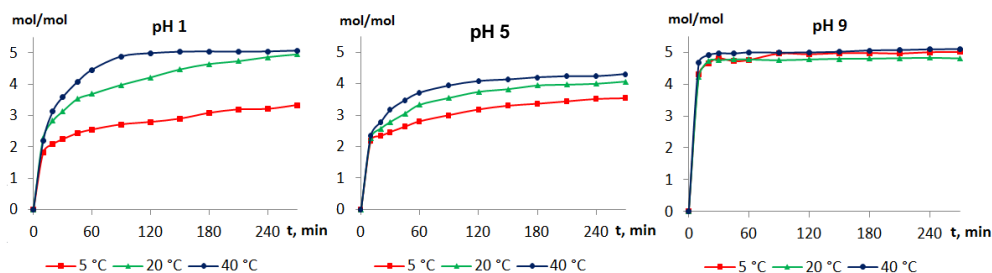


Fig. 3. The oxidation curves of d-glucose, expressed as periodate moles per one mole of the sugar

For a more elaborate study, the periodate oxidation of d-cellobiose was also performed, as shown in Fig. 4. Cellobiose is the dimer of glucose.

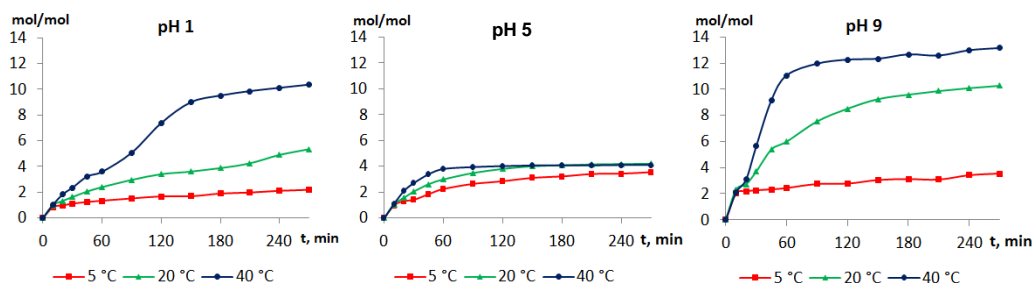


Fig. 4. The oxidation curves of d-cellobiose, expressed as periodate moles per one mole of the sugar

Unlike the anhydrosugar, glucose and cellobiose react most readily in alkaline conditions with the OH^- as a catalyst, however acid conditions (H^+) increase the reaction rate as well. This is due to the fact, that after the initial cleavage of C-C bond in a sugar structure, such as glucose, an intermediate is formed, which can be hydrolysed to a new α -diol, so another periodate oxidation step takes place. Most importantly, a catalyst is necessary for the hydrolysis to be possible. Fig. 5 depicts the reaction steps of the oxidation of d-glucose.

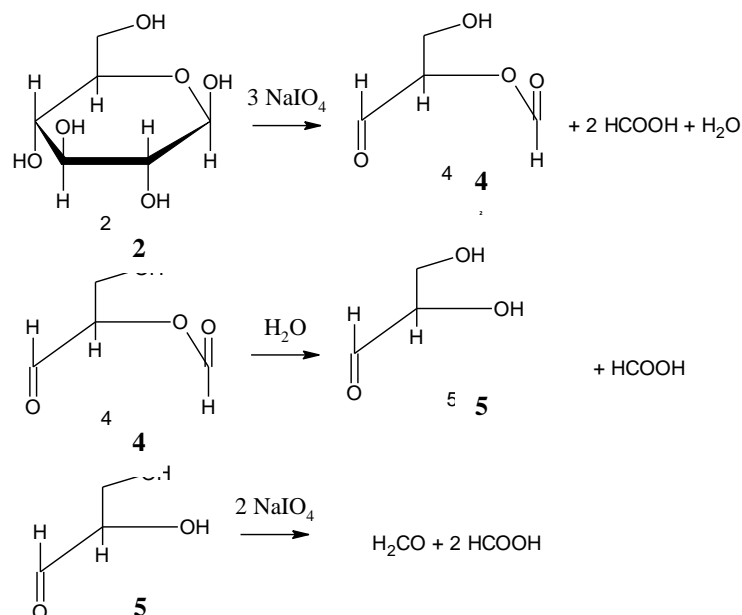


Fig. 5. The oxidation steps of d-glucose (2): intermediate 4 is hydrolysed into a new α -diol 5, which is further oxidised by sodium periodate

The comparison of the oxidation curves of glucose and cellobiose shows that monosaccharides are oxidised faster than oligosaccharides. Furthermore, cellobiose is over oxidised at pH 9, i.e., more periodate is consumed than theoretically expected, which can be attributed to the glycosidic bond.

Additional experiments were performed at 40 °C pH 5 and formic acid was determined potentiometrically. As mentioned before, pH 5 is the perfect pH for levoglucosan to react with periodate according to the stoichiometry shown in Figure 1. However, at pH 5 glucose reacts with 4 moles of periodate giving 4 moles of formic acid and 2 moles of formaldehyde. Cellobiose is only partly oxidised at pH 5; the determined maximum values of formic acid and periodate moles per one mole of cellobiose were 2 and 4, respectively, which do not even come close to the theoretical values – 9 moles of formic acid and 11 moles of periodate.

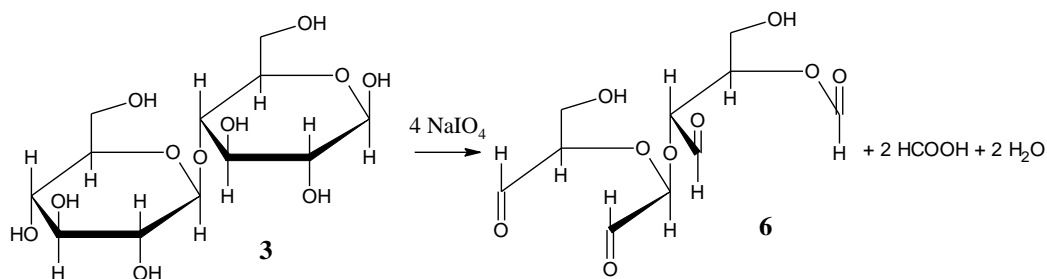


Fig. 6. The oxidation of d-cellobiose at pH 5

It can be assumed, that for cellobiose only bonds between secondary alcohol groups are cleaved at pH 5 and a double dialdehyde (6) is formed as shown in Fig. 6.

3.2. The levoglucosan and sugar content in wood pyrolysis samples

The oxidation curves of levoglucosan and glucose were used to develop methodology for the determination of sugars and levoglucosan in pyrolysis liquids. Two ways of determining levoglucosan in the presence of sugars can be outlined:

- oxidation of a sample for 4 h at 40 °C pH 1 before and after hydrolysis, because both levoglucosan and glucose (representing hexoses) have been completely oxidised according to the stoichiometry;
- oxidation of a sample for 20 min at 20 °C pH 9 before and after hydrolysis, because in these conditions levoglucosan has not started to react yet, but practically 100% glucose have been oxidised.

Naturally, different equations are used to calculate the amount of sugars and levoglucosan in the samples. Equations 1 and 2 are used for the first method (pH 1) and equations 3 and 4 are used for the second method (pH 9). In these equations ‘n’ stands for amount [mol], ‘c’ is molar concentration [mol/L] and ‘V’ is volume [L].

$$n_{\text{levoglucosan}} = \frac{c_{\text{titrant}}(V_{\text{titrant after hydrolysis}} - V_{\text{titrant before hydrolysis}})}{5-2} \quad (1)$$

$$n_{\text{hexoses}} = \frac{c_{\text{titrant}}(V_{\text{titrant before hydrolysis}} - \frac{2}{5-2}(V_{\text{titrant after hydrolysis}} - V_{\text{titrant before hydrolysis}}))}{5} \quad (2.)$$

$$n_{\text{levoglucosan}} = \frac{c_{\text{titrant}}(V_{\text{titrant after hydrolysis}} - V_{\text{titrant before hydrolysis}})}{5} \quad (3)$$

$$n_{\text{hexoses}} = \frac{c_{\text{titrant}} \cdot V_{\text{titrant before hydrolysis}}}{5} \quad (4)$$

Both methods were used to analyse mixtures of standard levoglucosan and d-glucose, and it was found that the recovery of these methods for levoglucosan and glucose was 99–112 %. Table 1 shows the quantitative analysis results of levoglucosan and hexoses in a real sample of pyrolysis liquids.

Table 1. Quantitative analysis results of a real sample of pyrolysis liquids

Method	weight % (levoglucosan) ± standard deviation	weight % (glucose) ± standard deviation
Oxidation at pH 1	51.2 ± 0.1	12.4 ± 0.2
Oxidation at pH 9	48.7 ± 0.4	10.2 ± 0.2

The analysis results of a real pyrolysis liquid show, that the pH 9 method gives lower results, than the pH 1 method. This could be because of the presence of oligosaccharides, which are completely oxidised in 4 hours at pH 1, but not in 20 min at pH 9.

4. CONCLUSIONS

Two methods for the simultaneous determination of levoglucosan and hexoses have been proposed, involving sample oxidation for 4 hours at pH 1 or 20 min at pH 9. Both methods showed good accuracy and recovery for standard samples, but only the method with oxidation at pH 1 is suitable for the analysis of pyrolysis liquids, because of the complexity of these samples. However, the method with oxidation at pH 9 could be applied to wood hydrolysates, where there are no anhydrosugars and only the total amount of sugars has to be determined.

5. ACKNOWLEDGEMENTS

The authors gratefully acknowledge the financial support by the Latvian State Research Programme NatRes.

6. REFERENCES

1. PETTERSEN, R.C. *The Chemistry of Solid Wood*. American Chemical Society, 1984. 614 p. ISBN: 978084122389.
2. DE WILD, P., REITH, H., HEERES, H.J. Biomass pyrolysis for chemicals. *Biofuels*, 2011 Vol. 2, No. 3, p. 185–208.
3. LONGLEY, C.J., HOWARD, J., FUNG, D.P.C. Levoglucosan recovery from cellulose and wood pyrolysis liquids. *Advances in Thermochemical Biomass Conversion*, 1993, p. 1441–1451.
4. LONGLEY, C.J., FUNG, D.P.C. Potential applications and markets for biomass-derived levoglucosan. *Advances in Thermochemical Biomass Conversion*, 1993, p. 1484–1494.
5. KRISTIANSEN, K.A., POTTHAST, A., CHRISTENSEN, B.E. Periodate oxidation of polysaccharides for modification of chemical and physical properties. *Carbohydrate Research*, 2010, Vol. 345, No. 10, p. 1264–1271.
6. ROBYT, J.F. *Essentials of Carbohydrate Chemistry*. Springer, 1998, 399 p. ISBN: 0387949518.
7. DRYHURST, G. *Periodate Oxidation of Diol and Other Functional Groups. Analytical and Structural Applications*. Pergamon Press, 1970, 196 p., ISBN: 080068774.
8. DE WIT, D., VAN DEN BERG, R., JOHANSSON, M., VAN RANTWIJK, F., MAAT, L., KIEBOOM, A.P.G. The periodate oxidation of sucrose in aqueous N,N-dimethylformamide. *Carbohydrate Research*, 1992, Vol. 226, p. 253–260.
9. LI, H., WU, B., MU, CH., LIN, W. Concomitant degradation in periodate oxidation of carboxymethyl cellulose. *Carbohydrate Polymers*, 2011, Vol. 84, p. 881–886.
10. HERMANSON, G.T. *Bioconjugate Techniques*. Academic Press, 1996, 1323 p., ISBN: 0123423368.
11. SPINCE, B., ZANDERSONS, J., ZHURINSH, A. Quantitative analysis of levoglucosan in the presence of glucose and cellobiose using Malaprade reaction and iodometric titration. Proceeding of EWP `10, 2010, p. 381–384.
12. HUGHES, G., NEVELL, T.P. The mechanism of the oxidation of glucose by periodate. *Transatlantic Faraday Society*, 1948, Vol. 44, p. 941–948.
13. HEAD, F.S.H., HUGHES, G. The oxidation of cellobiose by periodate. *Journal of Chemical Society*, 1954, p. 603–606.
14. LIKHOSHERSTOV, L.M., BROSSAR, L.E. Volumetric determination of periodate ion after the oxidation of carbohydrates. *Chemistry of Natural Compounds*, 1967, Vol. 3, p. 5–7.
15. *European Pharmacopoea*. 4th edition, Strasbourg, 2002, 2416 p., ISBN: 9287145873.

TECHNICAL AND ECONOMIC EVALUATION OF WIND TURBINES IN DIFFERENT REGIONS OF LITHUANIA

G. Gecevičius, M. Marčiukaitis
*Lithuanian Energy Institute
Laboratory of Renewable Energy
Breslaujos str. 3, LT-44403, Lithuania*

ABSTRACT

Total installed wind power has reached 282 MW [1] in Lithuania and the target of 500 MW will be reached in next few years (2020). Most of wind farms are situated in the coastal region, but further development of wind power in Lithuania will be related with establishment of new wind farms in regions with lower wind speed. Therefore a thorough estimation of local wind conditions and selection of wind turbines with proper technical parameters will play a vital role.

The purpose of this article is to present the analysis of wind farm performance in different regions of Lithuania and to evaluate technical parameters as well as economic feasibility of different types of wind turbines. Research was carried out by using WAsP 9 software.

Results present the comparison of economic indicators which recognize that wind energy payback time depends on wind turbine tower height, rotor size, investments and wind conditions. Investigation has shown that wind turbines with bigger rotor size would have a significantly better energy yield in regions where average wind speed is comparatively low. Bigger rotors and higher towers mean more investments, therefore the selection of certain type of wind turbine must be based on the balance of technical and economic parameters.

Keywords: wind energy, wind resource assessment, cost benefit analysis

1. INTRODUCTION

Wind energy is a priority renewable energy source in the world. In 2012 installed wind power capacity reached 283 GW and almost 45 GW of wind power capacity began operation, increasing global wind capacity, and it added more capacity than any other renewable energy technology. The main wind energy technologies are developed onshore and just a small part (5.4 GW) is taken by offshore wind turbines [2, 3]. Worldwide only 13 countries had installed offshore wind turbines where more than 90% of this capacity was located off northern Europe. Global biggest onshore wind power capacity is installed in China (75 GW), United States (60 GW) and Germany (31 GW) [4].

Europe 2020 is the main strategy to reach 20% energy, produced from renewable energy sources. Lithuania has target to achieve 23% renewable energy share by 2020. National Energy Independence Strategy of the Republic of Lithuania (2012) presents goals to achieve 500 MW installed wind power capacity. Currently 281 MW of wind power is installed in Lithuania and it is the biggest renewable energy source to produce electricity in Lithuania (in 2012 provided 600 GWh, approximately 6% of total electricity consumption) [1]. In 2013 wind power produced 11.5 percent more electricity than in 2012 [5].

Most of wind farms are situated in the coastal region, but further development of wind power in Lithuania will be related with establishment of new wind farms in regions with lower wind speed. Therefore a thorough estimation of local wind conditions and selection of wind turbines with proper technical parameters will play a vital role.

It is very important to mention that wind conditions and technological research are not very well developed in Lithuania and the main research area is wind turbines in coastal zone

and other regions [6]. As a result of that, in this paper wind farm performance and economical indicators in various regions of Lithuania are analyzed.

1.1. Wind power development in Lithuania.

In Lithuania wind turbines till the March 1st 2013 were separated into 3 categories (according to the law of Renewable Energy Sources): bigger than 350 kW, 30–350 kW and less than 30 kW electric capacities. Since the April 1st 2013 power differentiation was changed, now small power capacity wind turbines are considered up to 10 kW.

Bigger than 350 kW power turbines are the most popular in Lithuania. It is very popular to build stand-alone wind turbines (600–2000 kW) or wind farms with several turbines (2–19 units). In the future, in case positive legislation exists, huge wind farms are planned with more than 100 wind turbines. In Lithuania, leader of wind market is German company Enercon (Fig. 1). These technologies are quite expensive, but also very efficient and installed power capacity unit generates relatively more electricity.

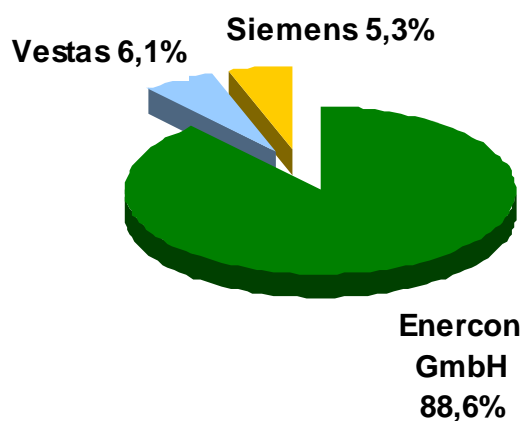


Fig. 1. Wind turbines manufacturers' market in Lithuania
(large wind turbines – more than 350 kW)

Now 15 wind farms operate in Lithuania with total electric power capacity of 282MW. 223 MW are connected to the high voltage transmission grid (110 kV), and 59 MW to the distribution grids (35 and 10 kV) [1].

2. OBJECTS OF INVESTIGATION AND METHODOLOGY

Annual electricity production in wind farms depends on wind conditions, therefore wind turbines is built in the regions where wind has higher energy potential. To reach maximum wind energy generation wind speed of 10–12 m/s is required. It is impossible to find location in the world with such strong and constant winds - wind speed variates, therefore wind turbines use just a part of nominal power. Indicator C_p represents the part of installed wind power which is used in wind turbines or wind farms in a certain period of time.

For the estimation of wind farm efficiency the wind power capacity factor was calculated:

$$C_p = \frac{E_{fact}}{E_{pot}} \cdot 100\%, \quad (1)$$

where C_p – power capacity factor, E_{fact} – generated electricity during the period (GWh), E_{pot} – potential electricity generation during the period if wind turbine worked at its nominal power

all the time (GWh). Maximal C_p factor is 100%, but wind is not permanent, so it is in fact not possible to reach this value. For example in Denmark, where wind conditions are among the best in the world, capacity factor is 42.7 % in 2013 [7].

To estimate economical and technical situation, 13 of 15 wind farms in Lithuania were chosen. These farms are compared by tower height, power capacity and technology (Table 1). Also wind farms are located in various regions of Lithuania (different distance from the Baltic Sea).

For the evaluation and comparison of the efficiency of various rotors WAsP 9 software was used. WAsP stands for the Wind Atlas Analysis and Application Program, it is a tool for wind data analysis, wind climate estimation, and siting of wind turbines.

4 different types wind generators were chosen – Enercon E70-2.3MW, E82-2MW, E82-2.3 MW, E101-3MW, tower height 98 meters. Wind farm electricity production was evaluated for 6 wind turbines in seaside zone in Lithuania. Relative swept area and relative energy production for 1 MW were used in the analysis.

In this paper this indicator is compared among wind farms with different installed capacity and in different wind farm locations in Lithuania.

In part 3 annual electricity generation in wind farms for 1 MW is calculated and WF distance from the Baltic Sea is estimated. Distance was separated to 3 types – less than 10 kilometers (Ciuteliu, Mockiu, Sudenu, Benaiciu WF), less than 50 kilometers (Kreivenu WF) and more than 150 kilometers (Seiriju, Akmeneliu WF).

Table 1. Technical characteristics of wind farms used in the analysis

Tower height	Location	District	Type of wind turbines	Power capacity MW
108	Kreivenu II WF	Taurages	Enercon E82 (2 MW)	10
98	Akmeneliu WF	Pakruojis	Enercon E82 (2 MW)	6
85	Vydmantu WF	Kretingos	Enercon E70 (2 MW)	30
108	Ciuteliu WF	Silutes	Enercon E82 (2,3 MW)	39,1
78	Kreivenu WF	Taurages	Enercon E82 (2 MW)	20
80	Silales WF	Silales	Siemens SWT-2.3-101 (2 MW)	13,8
78	Seiriju WF	Lazdijų	Enercon E82 (2 MW)	6
100	Laukzemes WF	Kretingos	Vestas (5 - 2,75 MW, 1 - 2,25 MW)	16
98	Benaiciu WF	Kretingos	Enercon E82 (2 MW)	34
8 - 108 2 - 78 2 - 73	Didsiliu WF	Kretingos	Enercon E82 (2 MW), E53 (0,8 MW), E48 (0,8 MW)	21,5
78	Sudenu WF	Kretingos	Enercon E82 (2 MW)	8
98	Kreivenu WF III	Taurages	Enercon E82 (2 MW)	15
108	Mockiu WF	Silutes	Enercon E82 (2 MW)	12

3. INVESTIGATION OF WIND FARM ENERGY PRODUCTION

Evaluation of wind sources has been carried out using data of meteorological stations and various analyses in different regions of Lithuania. In Lithuania the windiest areas are in Nida and Klaipėda districts. In other regions annual wind speed differs slightly. Data of wind conditions show, that the biggest wind power potential exists in coastal zone, and the mainland zone is not so favorable for wind power development.

According to the Lithuanian Wind Atlas (Fig. 2), average wind speed at 50 metres height above ground level varies between 3–6 m/s. The highest wind speed is in seaside regions and in Taurage region, (approximately 50 km from the Baltic sea).

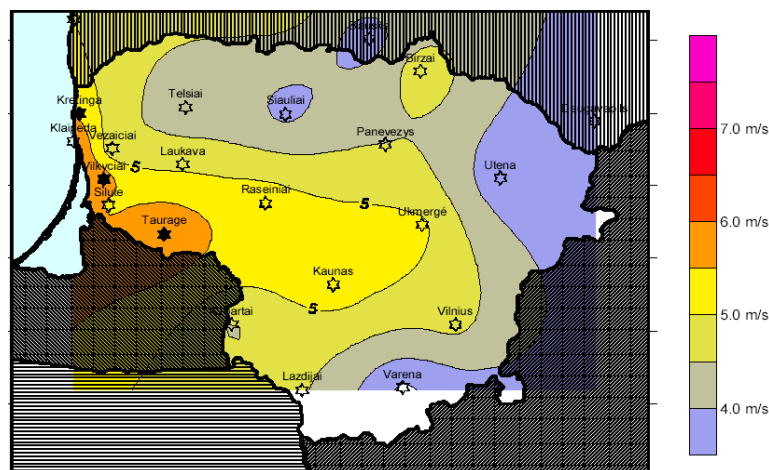


Fig. 2. Wind resource distribution in Lithuania [8]

The main part of wind farms are built in coastal zone and just a few parks further from the sea. Bilgili et al. [9] claims that biggest electricity generation potential is in seaside zone, but the results of the analysis carried out in this work deny that .

To conclude this part it can be claimed that wind energy resources distribution is not very well analysed and can only give a general view about wind distribution tendency in Lithuania. When analysing wind turbine performance it is important to evaluate not only wind speed, but also rotor size, tower height, wind turbines life cycle, profiles of wind speed, areas of roughness, wind parameters changes, etc. [10].

3.1. Analysis of energy production in different locations

Marciukaitis et al. states that due to coastal topography, the average wind speed at the height of 100 m 20 km away from the seacoast decreases by about 22% versus that at the seacoast [11]. This implies that in the coastal region wind resources depend on the distance from the sea and local topography. Also difference between average annual wind speeds in the same height in various sites along the coastal region is found to be less than 10%.

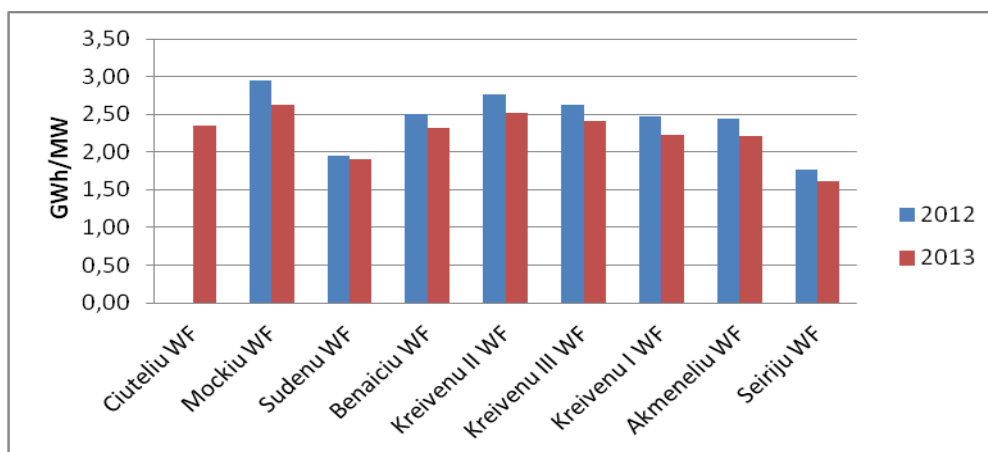


Fig. 3. Electricity production in various wind farms in Lithuania

Fig. 3 presents 9 wind farms in different locations in Lithuania. Results show the comparison of relative annual energy production in GWh for 1 MW. First four wind farms (Ciuteliu, Mockiu, Sudenu, Benaiciu) are situated less than 10 km from the sea, Kreivenu winds farms are less than 50 km, Akmeneliu and Seiriju wind farms stay more than 150 km

from the Baltic Sea. In 2012 year best results are demonstrated by Mockiu wind farm, annual production of which reached 2.96 GWh/MW with tower height of 108 metres. To compare Benaiciu and Sudenu wind farms, lowest results were in Sudenu wind farm (1.96 GWh/MW) with tower height 78 metres. Benaiciu wind farm electricity production reached 2.5 GWh/MW with 98 metres tower height. In 2013 electricity production presents lower scale: Ciuteliu, Mockiu, Benaiciu wind farms produced similar amount of energy, respectively 2.35, 2.62, 2.32 GWh/MW. Sudenu WF shows lowest performance with 1.9 GWh/MW. These results in seaside zone present very different energy production for 1 MW in Sudenu WF and it has clear relation with tower height, because best results exist with tower height 108 and lowest with 78 metres.

Wind energy production in Taurage district (Kreivenai wind farms) demonstrates similar results and correlation between wind farms in 2012 and in 2013 years with the biggest electricity production 2.77 GWh/MW in Kreivenai II wind farm in 2012. Wind farms far from the Baltic Sea (more than 150 km) show poor results (Seiriju WF). There in 2012 and in 2013 energy production reached only 1.77 and 1.61 GWh/MW respectively. To compare the same tower height (78 m) in Sudenu WF, electricity production was 15% better. These data can be explained by the long distance from the sea which is considered to be the main reason for wind power potential decrease. On the other hand, Akmeneliu WF demonstrates better results with 2.44 and 2.21 GWh/MW respectively in 2012 and 2013, but the reason of this difference most likely is the bigger tower height (98 m).

To conclude this part, analysis shows that energy production in wind farms in Lithuania strongly depends on tower height and faintly from the distance from the Baltic Sea.

3.2. Analysis of energy production by rotor size

Electric production in wind farms depends not only on tower height, roughness class or WF distance from the sea, but also very important factor is rotor size. In many cases rotor size option depends on wind conditions.

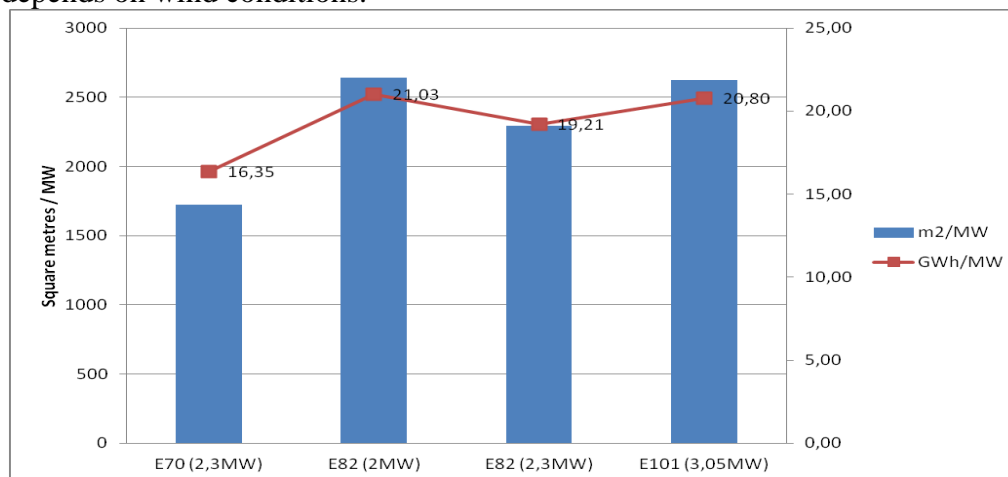


Fig. 4. Electricity production by rotor size for 1 MW

In this part several generators are compared by 3 rotor sizes with tower height 98 metres. These results were prepared by WAsP 9 software and demonstrate various wind farms in the same seaside zone. Figure 4 gives comparison between Enercon E70, E82 and E101 wind turbines rotor size square metres for 1 MW of installed power capacity. Biggest relative swept area is for Enercon E82-2 MW (2627 m²/MW). Also Enercon E82-2MW generates more electricity than E101-3MW. As a result of this, best choice of wind turbines in Lithuania with tower height 98 m is E82-2MW turbines.

3.3 Analysis of wind farms' power capacity factor

Power capacity factor is one of the main indicators which describes effectiveness of wind turbines [12]. Wind power capacity factor describes 6 wind farms effectiveness from January 2012 till December 2013, (Fig. 5, Fig. 6).

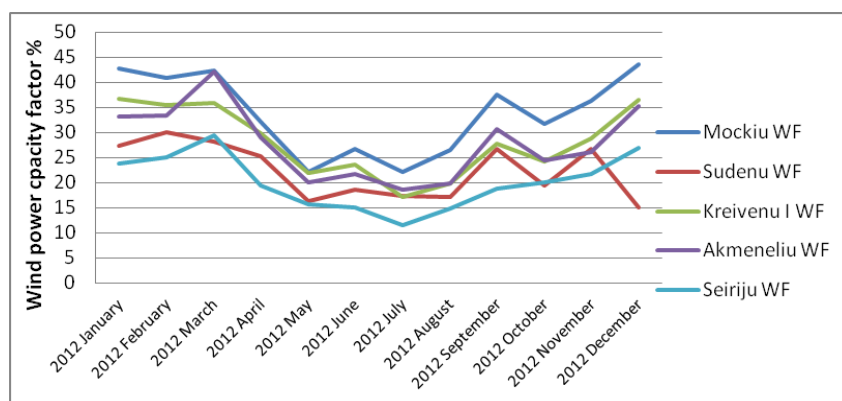


Fig. 5. Wind power capacity factor in different regions of Lithuania in 2012

Results show that power capacity factor is lowest in summer and lowermost point of this factor was in Seiriju WF in 2013 June ($C_p = 8,7\%$). At the same time Silales WF shows $C_p = 18,5\%$ and differences between these parks are approximately 10 percents. To compare tower height Seiriju and Silales WF it is similar –78 and 80 metres. Mockiu WF with tower height 108 metres at the same time show 3% lower results than Silales WF.

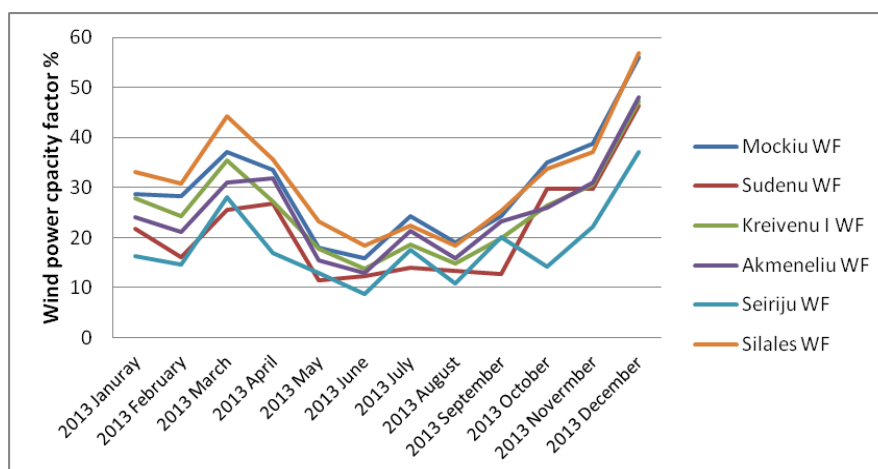


Fig. 6. Wind power capacity factor in different regions of Lithuania in 2013

Best wind power capacity factor results are in winter, in many cases in December. To compare it, Mockiu WF demonstrates best result with $C_p = 43,5\%$ and the lowest Sudenu WF with $C_p = 15,1\%$. In December 2013 Silales and Mockiu WF have shown best results with C_p approximately 56%. Silales WF turbines have larger rotors than E82, therefore C_p is higher than that of the other wind farms. Lowest C_p value at the same time was in Seiriju WF (37%). This can be explained by poor wind conditions in that region and lower tower height.

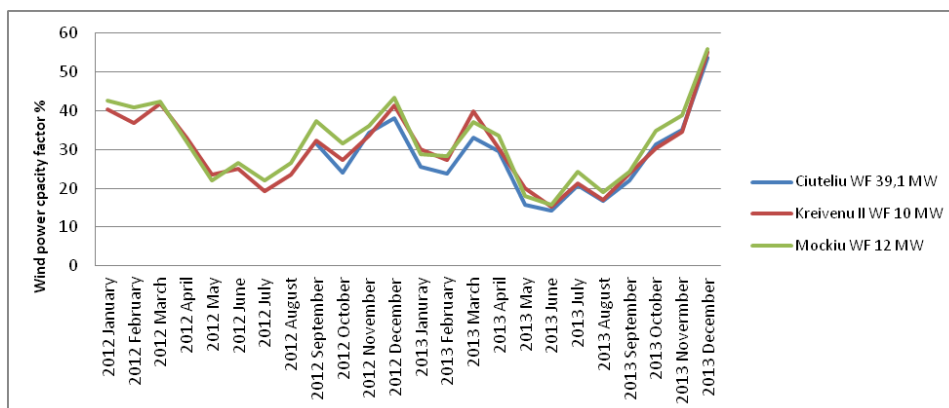


Fig. 7. Wind power capacity factor in wind farms with different installed capacity

Iglesias et al. claim that power capacity factor depends on wind farm's installed capacity, i.e. when capacity is bigger, C_p indicator is higher [13]. Fig. 7 presents the variation of C_p of 3 wind farms with different installed power (tower height 108 m). Ciuteliu WF installed power capacity is approximately 3–4 times bigger than Kreivenu II and Mockiu WF, but in many cases it demonstrates lower efficiency than Ciuteliu and Mockiu. To compare, in 2012 October Ciuteliu WF C_p equals to 24%, Kreivenu II WF $C_p = 27.4\%$, Mockiu $C_p = 31.7\%$. In 2013 average power capacity factor demonstrates similar results: 26.8%, 28.8%, 29.9% respectively for Ciuteliu, Kreivenu II and Mockiu WF. These results prove that wind farms' installed power is not directly related to the power capacity factor in western part of Lithuania.

4. ANALYSIS OF WIND FARMS ECONOMIC FACTORS

The main target of wind systems manufacturers – to optimize wind turbines with aim to generate electric power for the lowest available price [14]. Wind manufacturers usually suggest several WT options optimized for different wind conditions. Optimally chosen wind turbines give maximum amount of annual electric energy. Huge rotors with small generators produce electricity most of the time, but also converts just a small part of wind energy in high winds. On the other hand, powerful generators can generate electricity only in strong winds [15]. Therefore design of wind turbines requires the evaluation of wind conditions and proportions between generator and rotor swept area in different locations. Also tower height has significant influence on annual energy production - wind turbines with higher tower generate more electricity, but they are more expensive, therefore it is important to estimate economic parameters [16].

Recently, there is a tendency to build wind turbines with 100 meters or bigger tower height in Lithuania. Wind farm investments reach 4-7 thousands Lt/ kW (Table 2).

Table2. Economic evaluation of wind farms in Lithuania

Location	Type of wind turbines	Installed power capacity MW	Tower height	Investments mln.lt	Investments mln. Lt/MW	Electricity generation KWh (average 2012-2013)	Applied feed-in tariff Lt/kWh	Payback time	Relative energy price per year Lt/kWh
Kreivenu II WF	Enercon E82 (2 MW)	10	98	68.8	6.9	26444146	0.3	8.7	2.60
Akmeneliu WF	Enercon E82 (2 MW)	6	98	25	4.2	13949504	0.3	8.4	1.79
Vydmantu WF	Enercon E70 (2 MW)	30	85	130	4.3	59946615	0.3	7.2	2.17
Ciuteliu WF	Enercon E82 (2,3 MW)	39.1	108	194	5	65721686	0.3	9.8	2.95
Kreivenu WF	Enercon E82 (2 MW)	20	78	102	5.1	46885822	0.3	7.3	2.18
Silales WF	Siemens SWT-2.3-101 (2 MW)	13.8	80	75	5.4	37656709	0,3	6.6	1.99
Seiriju WF	Enercon E82 (2 MW)	6	78	35.8	6	10131403	0.3	11.8	3.53
Laukzemes WF	Vestas (5 - 2,75 MW, 1 - 2,25 MW)	16	100	98	6.1	35383958	0.3	9.2	2.77
Benaiciu I WF	Enercon E82 (2 MW)	34	98	212	6.2	81836014	0.3	8.6	2.59
Didsiliu WF	Enercon E82 (2 MW), E53 (0,8 MW), E48 (0,8 MW)	21.5	8–108	142	6.6	38999700	0.3	12.1	3.64
			2–78						
			2–73						
Sudenu WF	Enercon E82 (2 MW)	8	78	57	7.1	15667043	0.3	12.1	3.64
Kreivenu III WF	Enercon E82 (2 MW)	15	98	111	7.4	37850737	0.3	9.8	2.93
Mockiu WF	Enercon E82 (2 MW)	12	108	92	7.7	33478398	0.3	9.2	2.75

Comparison of economic indicators gives evaluation of different power capacity and wind tower height. Estimation of wind farms were evaluated by investments and applied feed-in tariffs in 2012 (it was 0.3 Lt/kWh). Payback time of wind farms varies within the range of 7–12 years. The best results of payback time are presented by Vydmantu and Kreivenu WF with 7 years. Tower height of this WF (Vydmantu) shows comparatively small investments for 1 MW and effective location for wind farm. Similar investments – 4.2 mln. Lt/MW is in Akmeneliu WF, but there is 8.4 years payback time. The explanation of this situation can be different location of WF. Akmeneliu WF is located in the North of Lithuania and Vydmantu

WF is in the coastal zone. Akmeneliu and Seiriju WF are located at similar distance from the Baltic sea, but Seiriju WF has 12 years payback time and it is 3-4 years more than Akmeneliu WF. The main reason of that is tower height (respectively 98 and 78 m). These results are confirmed by the economic parameters of Sudenu and Didsiliu WF, located in the coastal zone. Also it is very important to mention that the biggest relative energy price 3.53 lt/kWh is in Seirijai WF and the smallest 1.79 lt/kWh in Akmeneliu WF.

5. CONCLUSIONS

- Electricity generation in wind turbines mostly depends on the geographical location: E82 wind turbines with the same tower height in coastal zone generate 15 % more electricity than those in the midland zone.
- Investigation has shown that for Lithuanian wind conditions turbines with relatively large swept area are most suitable. E82 has largest relative swept area and shows best performance compared to other wind turbine types.
- Results prove that wind farms' installed power is not directly related to the power capacity factor in Lithuania.
- Wind farm capacity factor dynamics show that local wind conditions have stronger impact on wind farm performance than the distance to the Baltic Sea.
- Analysis of economic indicators has revealed that there is no clear dependence between wind farm tower height or installed capacity and the payback time.

REFERENCES

1. Lithuanian electricity transmission system operator (Litgrid), 2014. [Referred on the 25th of February in 2014]. Link to the internet <<http://www.litgrid.eu/index.php?lang=2>>
2. MARKARD, J., PETERSEN, R. The offshore trend: Structural changes in the wind power sector. *Energy Policy*, 2009, Vol. 37, No. 9, p. 3545–3556.
3. HAMEED, Z., VATN, J., HEGGSET, J. Challenges in the reliability and maintainability data collection for offshore wind turbines. *Renewable Energy*, 2011, Vol. 36, No. 8, p. 2154–2165.
4. REN21. *Renewables 2013 Global Status Report, 2013*. ISBN 978-3-9815934-0-2.
5. The Lithuanian Wind Power Association [referred on the 17th of February in 2014] Link to the internet <<http://www.lvea.lt/lt/nv/2013-m-elektros-energijos-gamyba-is-vejo-lietuvoje-augo-daugiau-nei-desimtadaliu->>>
6. KATINAS, V., MARCIUKAITIS, M., MARKEVICIUS, A. Current situation of the wind energy use and investigation of wind resources in the coastal region of the baltic sea in Lithuania. *renewable and sustainable energy reviews*, 2009, Vol. 13, No. 1, p. 201–207.
7. Energy numbers [referred on the 15th of April in 2014] Link to the internet <<http://energynumbers.info/capacity-factors-at-danish-offshore-wind-farms>>
8. Risø National Laboratory. The UNDP/GEF Regional Baltic Wind Energy Programme. Roskilde, 2003. ISBN 87-550-3204-4.
9. BILGILI M., YASAR, A., SIMSE, E. Offshore wind power development in Europe and its comparison with onshore counterpart. *Renewable and Sustainable Energy Reviews*, 2010, Vol. 15, No. 2, p. 905–915.
10. KATINAS, V. Prediction of wind energy and biomass resources usage in energy system. *LEI*, 2011. Report.
11. MARCIUKAITIS, M., ERLICKYTĖ-MARČIUKAITIENĖ, R., TUMOSA, A. Investigation of wind speed dynamics in the Lithuanian coastal region. *Power engineering*, 2009, Vol. 55, No. 1, p. 27–34.



12. TORRES, J.L., PRIETO, E., GARCIA, A., DE BLAS, M., RAMIREZ, F., DE FRANCISCO, A. Effects of the model selected for the power curve on the site effectiveness and the capacity factor of a pitch regulated wind turbine. *Solar Energy*, 2003, Vol. 74, No. 2, p. 93–102.
13. IGLESIAS, G., CASTELLANOS, P., SEIJAS, A. Measurement of productive efficiency with frontier methods: A case study for wind farms. *Energy Economics*, 2010, Vol. 32, No. 5, p. 1199–1208.
14. MOSTAFAEIPOUR, A. Productivity and development issues of global wind turbine industry. *Renewable and Sustainable Energy Reviews*, 2009, Vol. 14, No. 3, p. 1048–1058.
15. HORGAN, C. Using energy payback time to optimise onshore and offshore wind turbine Foundations. *Renewable Energy*, 2013, Vol. 53, p. 287–298.
16. BOLINGER, M., WISER, R. Understanding wind turbine price trends in the U.S. over the past decade. *Energy Policy*, 2012, Vol. 42, p. 628–641.

ECONOMIC ASSESSMENT OF HYBRID SOLAR/BATTERY POWER GENERATION SYSTEM FOR THE MINING INDUSTRY

J. Guilbaud

UCL Energy Institute

14 Upper Woburn Place, WC1H 0NN London – UK

ABSTRACT

The mineral sector is globally responsible for more than 38% of total industrial energy use and 11% of total final energy consumption. The sector is coming under significant pressure to decrease the amount of energy consumed and greenhouse gases emitted. At the same time, the rising trend in the mining industry is the search for cleaner, less carbon-intensive and more efficient energy technologies that can also become new business opportunities to the industry. It is technically feasible for mining companies to power their operations with hybrid renewable systems. A number of low carbon generation options could be implemented but it is unclear whether those technologies can deliver economic benefits to the industry.

This study presents results which aims at understanding the economic potential of hybrid renewable systems for the mining industry. An optimisation model has been developed to search for the least-cost system with regards to optimal system size and optimal system configuration. A case study presents the results for the implementation of NaS batteries and non-tracking solar PV in a Chilean copper mine. Hourly data are used for both the electricity demand of the mine and the total solar irradiance at the mine site. The results show that solar PV is an economically viable option under current market conditions while NaS batteries provide additional benefits for enhancing the output and maintaining stability of the mining power system.

Keywords: hybrid renewable power system, mining, PV, electricity storage, optimisation model

1. INTRODUCTION

The mineral sector is globally responsible for more than 38% of total industrial energy use and 11% of total final energy consumption [1]. This energy consumption could double by 2050 compared to 2009 standards if no policy measures were taken [2]. At the same time, the sector is coming under significant pressure to decrease the amount of energy consumed and greenhouse gases emitted [3]. According to the fifth report of the carbon disclosure project (2007), the main trend in the industry is the search for cleaner, less carbon-intensive and more efficient technologies, that can also become new business opportunities to the industry.

Whereas it is technically feasible for mining companies to power their operations with hybrid renewable energy systems, it is unclear whether those technologies can deliver economic benefits to the industry. Compared with fossil fuels, renewable energies suffer from a number of technical and economical disadvantages such as intermittent supply and higher capital costs. However, energy storage technologies can act as technological enablers, and, in certain conditions, can successfully help renewable technologies to meet power demand and provide a reasonable return on investment [4]. Together, renewable energy sources and energy storage might be able to replace or complement conventional energy sources in the mining industry. The tipping point being the achievement of grid parity in distributed systems and diesel/gas parity in stand-alone systems [5]. That is, when the levelized cost of electricity (LOCE) of hybrid renewable systems is equivalent to the electricity prices of conventional sources.

To date, there is a lack of research to assess the economic value of these systems for mining activities. Previous scientific studies are limited to isolated systems [6, 7] or country-

scale systems [8–10], but no study have done similar investigations for mining settings. Past studies for mining are limited to scoping [11], energy guidelines [12, 13] or global potential [1]. Whilst these past studies have provided initial estimates for alternative energy sources, their results do not account for the context-dependent elements of the mining industry. Alternatively, a number of studies have been published by consulting companies and public organisations, but there is a lack of clarity in reporting technical and economic assumptions, and often little considerations for uncertainty, which have produced a widely diverse set of results [14]. These different degrees of methodological completeness and the use of similar assumptions for different technologies could result in both sub-optimal decisions and missed opportunities for carbon savings. It has therefore become critical to provide a robust economic assessment of these technologies to the industry and its stakeholders.

This paper presents results which aims at understanding the economic potential of hybrid renewable systems for the mining industry. An optimisation model has been developed by the author to search for the least-cost system with regards to optimal system size and optimal system configuration. A case study presents the results of analysis for the implementation of NaS batteries and non-tracking solar PV in a Chilean copper mine.

1.1. Context and limitations

The selected mine for this analysis is the Chuquicamata copper mine in Northern Chile. Chile is the world's largest producer and exporter of copper. The electricity supplied to the mining industry is derived from thermoelectric power for 99.64% – using fossil-fuels – and 0.36% from hydroelectric power [15]. The Chuquicamata mine is the biggest open pit copper mine in the world, owned and operated by Codelco, a Chilean public company. Even though the mine pit is supposed to close in 2017 – due to lowering ore grades – there is the project to expand the mine into the underground mining [16]. This would significantly extend the mine lifetime – probably for several decades - and potentially justify new investments in the energy generation. In 2012, the mine produced 356.000 tons of refined copper and presented a peak electricity capacity demand of 283 MW - which was totally supplied by the grid. Because the mine is located in the area receiving the highest solar irradiance on earth – hourly average of 275 W/m^2 – there is a significant potential for implementing renewable energy technologies such as PV panels or concentrated solar power [17]. As a comparison, the solar irradiance received in the Sahara region are 5% lower – averaging 260 W/m^2 .

In calculations, hourly data have been used for both the electricity demand of the mine and the total solar irradiance at mine site. The economic potential for implementing solar PV and battery storage is calculated based on electricity grid price of US\$ 0.13/kWh. This means that any investment presenting a real LCOE of less or equal than US\$ 0.13/kWh would potentially provide economic benefits to the mine. The implementation of carbon-free technologies can also limit the risk associated with a possible escalation of electricity prices and future implementation of carbon policies. In addition, the implementation of electricity storage presents additional economic and technical benefits (e.g. voltage support, spinning reserves) that will be accounted for in future papers.

At this stage, the modelled storage strategy is limited to capacity firming of solar PV but other strategy – such as off-grid and peak load management – will be considered in the later stages of this research. Considerations for demand shifting and other technologies (e.g. molten salt storage, concentrated solar power) will also be included in the future work. In this paper, the focus is on assessing the economics of replacing a fraction – the optimal amount is calculated by the optimisation model - of the electricity use supplied from the grid by using

renewable power generation at the mine site. The methodology and initial results are provided in the following chapters.

2. METHODOLOGY

2.1. Modelling assumptions

For this exploratory analysis, the following assumptions have been made to derive results:

- Mine demand for electricity varies hour by hour.
- Non-tracking solar PV is implemented at mine site to complement grid supply
- Renewable power generation is intermittent across the year and intra-day.
- A random variation within a range of two standard deviations of the solar radiation was added in order to account for climate uncertainty [18]. This stochastic variation will be reviewed in future work in order to include a more representative distribution of solar radiations [19].
- Energy storage at mine location (NaS Battery).
- Storage is used to firm-up the renewable load by shifting supply S from one time t_1 to another t_2 ; the aim is to ensure that the hybrid system is able to deliver a planned amount of power for each hour of the day.
- There are time varying constraints on when energy can be taken out/in store as defined by the storage strategy. Increases mine demand to $S(1+x)$ because of storage losses.
- System reliability is defined as a modelling constraint (%).

Variables S , t and x are quantified with a dynamic system model as they vary across the hours and days of future years. The list of technical and economic assumptions is provided in Table 1. In particular, the storage cost estimates are given by [20], the PV costs have been estimated by an engineering company (on the basis of previous projects), and the carbon savings are based on the current fuel mix of the grid that supplies the mine [17].

Description	Value	Unit	Description	Value	Unit
PV (Non-tracking)			Batteries (NaS)		
Capital cost	1700	\$/kW	Capital cost	2250	\$/kW
Lifetime	20	years	Lifetime	20	years
Operation cost	0	\$/kW/year	Operation cost	0.07	\$/kWh
Maintenance cost	53	\$/kW/year	Maintenance cost	28	\$/kW/year
PV efficiency	15	%	Round-trip efficiency	72	%
Degradation factor	0.5	%/year	Degradation of efficiency	0.2	%/year
Tilt angle PV modules	22° 180' N				
			Economics		
			Discount rate	10	%
			Inflation (energy & other costs)	2	%
			Grid carbon emissions per MWh	0.266	tons

2.2. Method

The applied method for this exploratory model is the optimisation of the electricity costs, which are represented on the basis of the LCOE [21]. The overall aim of the analysis is to determine the optimal system size that provides the optimal economic benefits for the mine. Specific equations of this model are provided as follow.

2.2.1. Levelized Cost of Electricity (LCOE)

The LCOE represents the cost that, if every unit of energy produced by the system in its lifetime is assigned, will equal the total life cycle cost discounted to the base year [21]. The formula 1.0 expresses this principle.

$$LCOE = TLCC / \left\{ \sum_{n=1}^N \left[Q_n / (1+d)^n \right] \right\} \quad (1.0)$$

Where TLCC is the sum of the life-cycle costs (including capital and operational costs), n is the year of operation, N is the technology lifetime, Q_n represents the energy output in year n , and d is the real discount rate.

2.2.2. PV output

The formula 1.1 was used to calculate the PV load output (PVout, kWh) on an hourly basis while taking into account climate uncertainty.

$$PVout_{m,d,h} = (G_{m,d,h} + \eta_{m,d,h}) * Y * A * PR. \quad (1.1)$$

Where G is the solar irradiance per m² (kW) for the month m , day d , and hour h , η is random climate variation within $\pm 2\sigma$ of G for the month m , day d , and hour h , σ is the standard deviation of G for all hours h over one year of data, Y is the PV efficiency rate, A is the PV installed size (m²), and PR is the performance ratio.

2.2.3. Storage charge/discharge

The storage system and the PV system are sized by the optimisation algorithm in relation to the storage control strategy as well as technical and economic characteristics. Differences between the renewable power output and the electricity demand determines when to charge or discharge the storage system.

The charge quantity of the storage system at time t was determined by [22]

$$E_s(t) = E_s(t-1) + (E_{ga}(t) - E_L(t) / \eta_{inv}) \eta_s. \quad (1.2)$$

The discharge quantity of the storage system at time t was determined by

$$E_s(t) = E_s(t-1) - (E_L(t) / \eta_{inv} - E_{ga}(t)) \eta_s, \quad (1.3)$$

where E_s is the charging quantity of the storage system at time t , E_{ga} is the net amount of energy generated by renewable and available from the grid connection, E_L is the power demand, η_{inv} is the efficiency of the power conditioning unit, and $\eta_s(t)$ is the efficiency of the charging cycle.

Both cycles are subject to a number of constraints:

$$E_{smin} \leq E_s(t) \leq E_{smax}, \quad (1.4)$$

$$E_s(t) \leq E_{spow}, \quad (1.5)$$

where E_{smin} is defined by the maximum depth of discharge (DOD), E_{smax} is the nominal capacity of the storage device, and E_{spow} is the maximum power discharge of the storage device (hourly).

2.2.4. Reliability

Reliability values are expressed according to the energy index of reliability (EIR), which expresses reliability as a function of total system demand. This ensures that large and small systems can be compared on the basis of a common index. The calculation is as follow [23]:

$$EIR = \frac{\sum_{i=1}^n kWh(I_{supply}(t) < I_{needed}(t))}{totalkWh} \quad (1.6)$$

Where $I_{supply}(t)$ represents the hourly supply of electricity by the PV/Battery system, $I_{needed}(t)$ is the required electricity supply from the PV/Battery system to maintain power reliability, and $totalkWh$ is the expected electricity production from the PV/Battery system for a single year.

3. INITIAL RESULTS AND DISCUSSION

In this section, a number of economic results are provided for different value of reliability as well as a brief discussion on the obtained results. This reliability value is representing the ability of the PV/Storage system to supply a fixed amount of electricity. In that sense, the storage system aims at compensating the fluctuation of the PV system. That is, in cases when the solar irradiation is lower than expected, the model assumes that the storage must compensate for this reduced PV output.

The required level of reliability of a mine depends on a number of factor (e.g. time of day, capacity of the grid connection, amount of additional capacity reserve), but it is assumed in this analysis that a mining company would not implement a large amounts of PV if there was no mechanism that could deal with the intermittency. While the grid supply could potentially supply additional capacity to compensate for lower PV outputs, this would come at a high cost as the electricity contracts of large industrial users in Chile are often based on a fixed amount of electricity supply. Ultimately, the cost of marginal electricity purchases as well as the value of lost load will be considered in future research in order to further characterise the optimal level of reliability that brings the highest economic benefits to the mine.

A summary of the results is presented in Table 2, including the optimal system sizes and key performance indicators for the hybrid PV/Battery system.

Table 1 Results for different reliability values

Reliability	99.90%	99%	98%	97%	96%
Optimal energy storage power	55 MW	47 MW	34 MW	30 MW	15 MW
Optimal energy storage capacity	184 MWh	65 MWh	52 MWh	44 MWh	27 MWh
Optimal PV power	270 MW	285 MW	315 MW	332 MW	332 MW
PV capacity factor	22.6%	22.5%	22.1%	21.7%	21.7%
Net present value	- 65 M US\$	- 15 M US\$	1 M US\$	7 M US\$	31 M US\$
Internal rate of return	8.3%	9.6%	10.0%	10.2%	10.7%
Levelized cost of electricity (LCOE)	0.142 US\$	0.132 US\$	0.130 US\$	0.129 US\$	0.124 US\$
Carbon savings (over 20 years)	2.95 MT	3.09 MT	3.41 MT	3.59 MT	3.57 MT
Total system output (% of total demand)	23.6%	25.0%	27.2%	28.4%	28.3%

3.1. Discussion on sizing results

Based on the results presented in Table 2, a number of interesting remarks can be made regarding the optimal system sizes. First, in high reliability scenarios ($\geq 99\%$), the analysis has shown that a large capacity of storage is required in order to handle the intermittency of PV. Second, in scenarios with a lower reliability ($\leq 98\%$), the optimal size of storage capacity and storage power is considerably reduced. In particular, when comparing 98% and 99.9% reliability values, it was found that the storage capacity must be multiplied by more than three in order to reach the high reliability value of 99.9%. These differences in storage capacity have a significant impact on the total investment costs of the battery – which will be discussed in section 3.3. Finally, this analysis also shows that the optimal PV size is different for each reliability scenario. This is because the storage costs are relatively high and it is therefore cheaper to reduce the amount of PV and consequently reduce the size of the storage components in scenarios requiring higher reliability values.

Interestingly enough, as shown on figure 1, the PV capacity factor tends to be reduced for scenarios in which the PV size is significantly superior to the peak electricity demand of the mine (283 MW). This is because the PV peak power output is, in the low reliability scenarios ($< 99\%$), larger than the mine peak demand - which therefore results in electricity spillage.

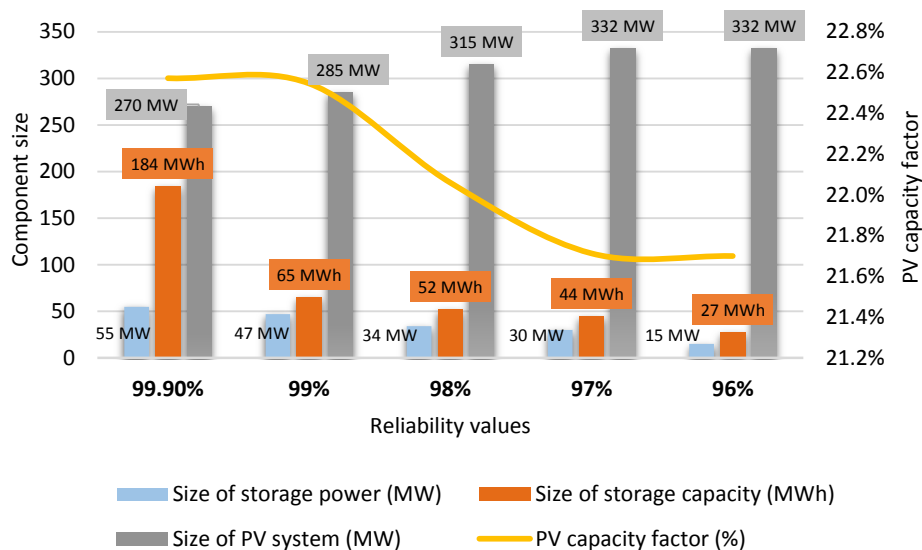


Fig. 1. Sizing results as a function of power reliability

Fig. 2 illustrates the dispatch model developed by the author, including PV input, grid input, and charge/discharge cycles. Specifically, this figure demonstrates that the average capacity level of the battery storage is almost permanently kept above minimum levels in order to be able to provide a reliability of 99.9%.

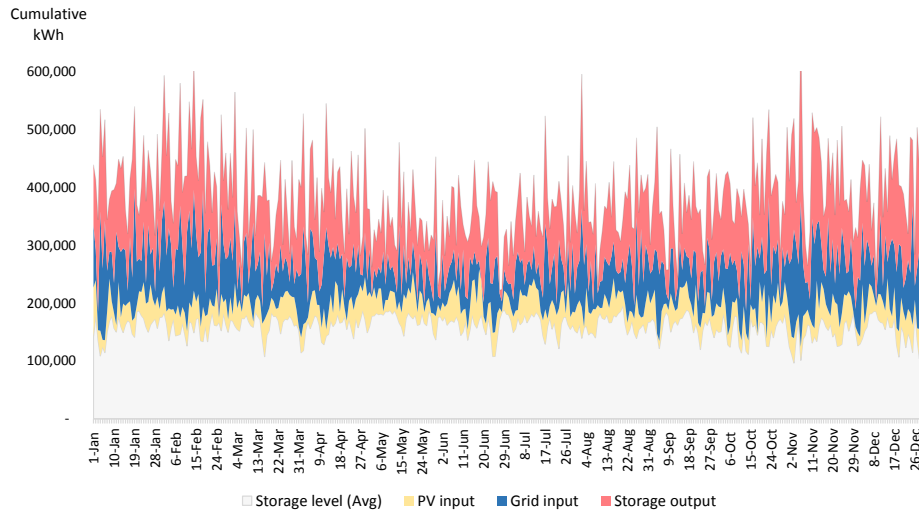


Fig. 2. Storage dispatch for a reliability of 99.9%

3.2. Discussion on economic results

From an economic perspective, the net present value is significantly dissimilar for different reliability coefficients (see Fig. 3). This is due to the additional storage capacities that are necessary to maintain system adequacy in high reliability scenarios. Similarly, the LCOE varies according to different system sizes. The tipping point for economic viability is when the LCOE is able to reach the level of grid prices (the assumption here is US\$ 0.13/kWh).

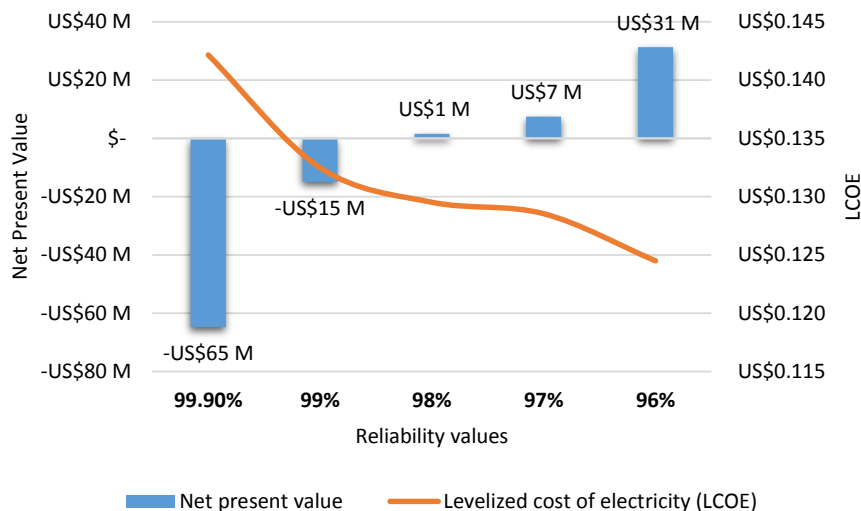


Fig. 1. Net Present Values as a function of power reliability

In particular, this analysis shows that the hybrid PV/Battery is able provide economic benefits for the reliability values equals or inferior than 98%. However, these results are

potentially limited by the value of lost load, which have not been considered in this analysis. That is, the value for each kWh unsupplied by the hybrid PV/Battery due to a lack of reliability. This additional modelling factor will be addressed in future research.

3.3. Sensitivity analyses

Additional sensitivity analyses have been performed to identify the most important factors associated with the economic returns. The most significant factors are presented on Fig. 4 for a reliability of 98%. In this case, the investment cost of PV panels and the discount rate have the biggest impact on the net present value while storage efficiency was found to have the smallest influence. This result is due to the fact that, in this scenario, there is only a small amount of storage and therefore the cost of storage is relatively small in comparison to the overall system cost. As a result, the cost of storage has little impact on the overall system costs. It can be assumed, however, that variations of storage costs will have a much more significant impact on the overall system cost in off-grid applications - requiring larger amounts of storage capacity.

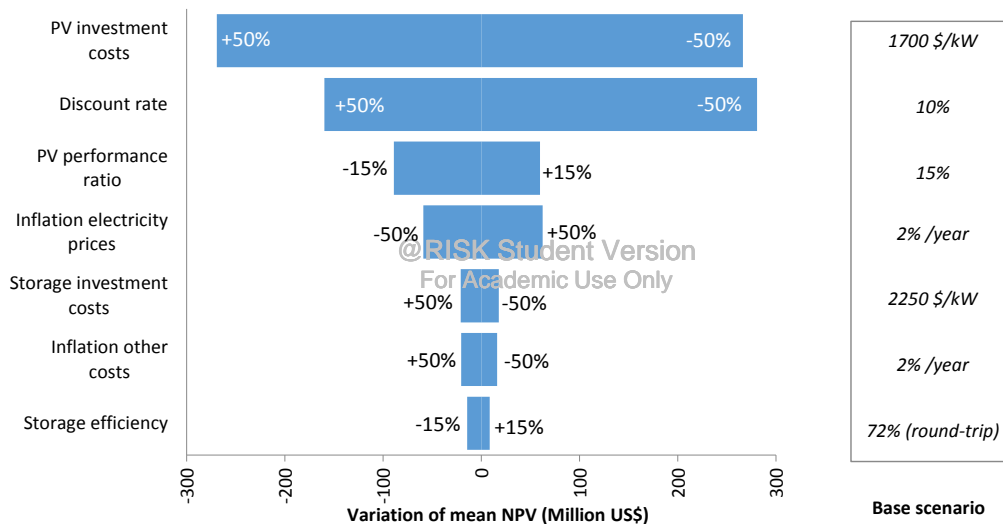


Fig. 2. Sensitivity analysis on modelling factors

4. CONCLUSION

Based on the results of the analysis provided in this paper, a number of conclusions can be made:

- The economic viability of the hybrid Solar PV/Battery energy systems is dependent upon both the grid price and amount of intermittency that the mine is able to handle. Battery energy storage can act as a balancing mechanism that compensates for the intermittency of the PV output. However, it presents high capital and operational costs.
- The economic breakeven point for a grid price of 0.13 US\$/kWh is a PV/Battery system with a reliability of 98%. Higher reliability values are only economically feasible if the grid price is above 0.13 US\$/kWh. More specifically, the grid price must reach 0.142 US\$/kWh in order for the hybrid PV/Battery system to provide economic benefits with a reliability of 99.9%.

Ultimately, this exploratory analyses have identified a number of factors that require further investigations in future work, including: impact of carbon policies; enhanced

modelling of climate uncertainty; consideration for additional storage applications, value of lost load, and marginal electricity purchase from the grid. Accordingly, a research design have been developed to address these current limitations. The future papers of the author will also provide more elements on other technologies (e.g. wind power, molten salt storage, concentrated solar power) as well as investigate the potential for demand-shifting in mining activities.

Funding sources: UCL Impact, M+W Group.

5. REFERENCES

1. McLELLAN, B., et al. *Renewable energy in the minerals industry: a review of global potential*. Journal of Cleaner Production, 2012. 32, p. 32–44.
2. UNIDO, *Global Industrial Energy Efficiency Benchmarking*. 2010.
3. NORGATE, T. and HAQUE N. *Energy and greenhouse gas impacts of mining and mineral processing operations*. Journal of Cleaner Production, 2010. 18(3), p. 266–274.
4. DENHOLM, P., et al. *The role of energy storage with renewable electricity generation*. 2010.
5. BREYER, C. and GERLACH A. *Global overview on grid-parity*. Progress in photovoltaics: research and applications, 2013. 21(1), p. 121–136.
6. WEISSER, D. and GARCIA R.S., *Instantaneous wind energy penetration in isolated electricity grids: concepts and review*. Renewable Energy, 2005. 30(8), p. 1299–1308.
7. ABBEY, C., ROBINSON J., and JOOS G. *Integrating renewable energy sources and storage into isolated diesel generator supplied electric power systems*. 2008.
8. WILSON, I.A.G., MCGREGOR P.G. and HALL P.J. *Energy storage in the UK electrical network: Estimation of the scale and review of technology options*. Energy Policy, 2010. 38(8), p. 4099–4106.
9. IBRAHIM, H., et al., *Integration of Wind Energy into Electricity Systems: Technical Challenges and Actual Solutions*. Energy Procedia, 2011. 6(0), p. 815–824.
10. KORPAAS, M., HOLEN A.T. and HILDRUM R. *Operation and sizing of energy storage for wind power plants in a market system*. International Journal of Electrical Power & Energy Systems, 2003. 25(8), p. 599–606.
11. PARASZCZAK, J. and FYTAS K. *Renewable energy sources—a promising opportunity for remote mine sites?* In Proceedings of the International Conference on Renewable Energies and Power Quality 2012, 2012.
12. AZAPAGIC, A. *Developing a framework for sustainable development indicators for the mining and minerals industry*. Journal of cleaner production, 2004. 12(6), p. 639–662.
13. HILSON, G. and MURCK B. *Sustainable development in the mining industry: clarifying the corporate perspective*. Resources policy, 2000. 26(4), p. 227–238.
14. BRANKER, K., PATHAK M.J.M. and PEARCE J.M. *A review of solar photovoltaic levelized cost of electricity*. Renewable and Sustainable Energy Reviews, 2011. 15(9), p. 4470–4482.
15. FARÍAS, P.C. *Electric demand of the copper mining industry and reduction costs for carbon emissions in the SING*. 2008, Pontificia Universidad Católica de Chile.
16. OLAVARRÍA, S., ADRIASOLA P. and KARZULOVIC A. *Transition from open pit to underground mining at Chuquicamata, Antofagasta, Chile*. in Proceedings of The SAIMM International Symposium on Stability of Rock Slopes in Open Pit Mining and Civil Engineering. 2006.



17. WOODHOUSE, S. *Renewable Energy Potential of Chile*. 2011, San Diego: Global Energy Network Institute.
18. LABED, S. and LORENZO E. *The impact of solar radiation variability and data discrepancies on the design of PV systems*. *Renewable Energy*, 2004. 29(7), p. 1007–1022.
19. BALOUKTSIS, A. and TSALIDES P. *Stochastic simulation model of hourly total solar radiation*. *Solar Energy*, 1986. 37(2), p. 119–126.
20. NREL, *Cost and performance data for power generation technologies*. 2012.
21. SHORT, W., PACKKEY D.J. and HOLT T. *A manual for the economic evaluation of energy efficiency and renewable energy technologies*. 2005: University Press of the Pacific.
22. AI, B., et al. *Computer-aided design of PV/wind hybrid system*. *Renewable Energy*, 2003. 28(10), p. 1491–1512.
23. ALLAN, R. and BILLINTON R. *Probabilistic assessment of power systems*. *Proceedings of the IEEE*, 2000. 88(2), p. 140–162.



TECHNOLOGY OF RUBBER WASTE TREATMENT

A.V. Lozhachnik, V.V. Sauchyn, A.N. Nikanchuk, G.V. Dolhonenka

*A.V. Luikov Heat and Mass Transfer Institute
National Academy of Sciences of Belarus
15 P. Brovka str. Minsk, 220072, Belarus*

ABSTRACT

Technology for organic-polymeric materials treatment is presented. We developed thermal technology for rubber waste processing with the purpose to obtain fuel and raw material for chemical industry. The technology is realized on base of screw reactor with electrical heating. During the process we obtain condensed organic substances which can be used as furnace oil and solid phase (pyrocarbon) which can be used for paints and varnishes, mechanical goods and tires production.

Keywords: rubber waste, screw reactor, technology of treatment, rubber waste

1. INTRODUCTION

One of the main world complicated ecological problems is increasing of industrial and domestic waste volume and bad quality of waste processing [1, 2]. Optimal solving of the problem is to develop and implement low-waste technology in industry. Also we need to take into account social and economic process. Design and application of this kind of technologies is very difficult process and needs more time and financial support.

Among wide range of organic waste rubber waste takes special place, because of its hazard on the environment in the dump or scatters on the surrounding areas, while accumulated in place of use. In addition it has high flammability risk while product of rubber uncontrolled burning render extremely harmful influence on soil, water, air environment and its inhabitants.

General level of secondary processing of rubber waste for most of the countries is no more than 30% of possible collect. Common methods of rubber waste processing can't envelop whole volume of waste. It happens because of the production of tires with metal cord growth.

There are some common methods of useless rubber tires treatment:

- Rubber is crushed in to powder with mechanical (most popular in the world), cryogenic and other methods with separating metal and synthetic cord;
- Pyrolysis of raw material (decomposition at high temperatures $\approx 500^{\circ}\text{C}$). It is possible to obtain low quality technical carbon (because of high contamination of coke, ash, oil and other components), fuel gas which can be used for thermal energy production and metal scrap. Main disadvantages of the method are periodicity of operation, high amount of toxic outgoing gases and burning fuel gases which are harmful for people and environment;
- Rubber dissolution in hot bitumen and oils. According this method raw material for road constructing, as modified bitumen, scrap metal and raw material for producing technical carbon can be obtained. This technology is rather power-consuming. Modified bitumen has a high production cost, that's why it has no chance to substitute analogy from general producing in asphalt concrete mixture production. In addition, extraction and treatment carbon containing residue needed. All of this makes this production not environmentally safe.

- Incompletely crushed auto tires burning (rubber chips). This method is widely spread in the USA where rubber chips are used in a mixture with black coal as fuel for heat electro power station or concrete drying. In general old tires are used as a fuel substitute because it high calorific value. But high toxic of burning product as well as low price level on black coal, especially in coal-mining countries, made unpromising such method.
- Rubber powder devulcanization with devulcanizate (rubber substitute) producing. This method is very complicated and power-consuming. Products are expensive and have low quality.

Combustion of rubber waste can't be considered as method of processing. Polymer and disperse fillers from rubber compound irretrievably loosed and can't be returned to production. Also for realisation such process we need to create complicated units for cleaning outgoing gases.

Presented project supposes creation perspective ecological process for organic waste pyrolysis in continual operation screw reactor with valuable chemical-engineering and energy purpose materials production.

2. EXPERIMENTAL SETUP WITH SCREW THERMOLYSIS REACTOR

Experimental set was designed on the base of experimental results obtained on set with stationary lair data [3, 4]. Set with screw reactor diagram is shown in Fig. 1. Laboratory reactor capacity is up to 10 kg/h.

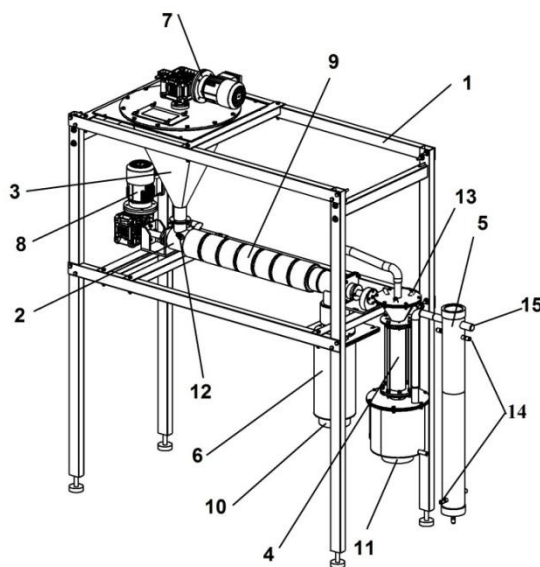


Fig. 1. Scheme of the experimental setup: 1 – supporting frame; 2 – screw reactor; 3 – feeder; 4 – condenser № 1; 5 – condenser № 2; 6 – tank for carbon; 7 – feeder gear-motor drive; 8 – reactor gear-motor drive; 9 – heaters; 10 – carbon tank heater; 11 – condenser № 1 bottom heater; 12 – nitrogen input; 13 – condenser №1 cover with holes for distillate input; 14 – condenser № 2 cooling water input and output; 15 – outgoing gases

According to suggested method material is loaded from feeder with screw to the reactor where material is heated by electrical heaters. Because of high temperature material decomposes and organic vapor is released. Temperature of reactor heating is controlled by thermocouples placed between heaters and heating surface. Inert gas (nitrogen or water steam)

is suoolied to the initial part of the reactor. It used to pull out air from the reactor before start operation and as a carrier gas during decomposition process.

Separation of reaction mixture occurs after destruction process. Solid part is gathered in tank for carbon for cooling and analyses. Collecting condensed organic substances occurs in the condensers №1 and №2.

Operation of the set is controlled by automated control cell with software on PC.

Set is connected to supply systems:

- electricity system;
- water supply system;
- Inert gas (nitrogen) supply system;
- control panel.

3. THERMOLYSIS OF USED TIRES

Thermal rubber waste processing is based on scientific idea of using physical and mechanical properties of disperse system and peculiarity heat treatment of organic material at average temperatures (450–550°C) so as a rubber at a steam-gas medium with further condensation of formed products [5, 6]. As a result of thermal destruction of rubber we obtain liquid (35–50 wt. %) and gaseous (6–8 wt. %) hydrocarbons, 6–10 wt. % of metal and 30–58 wt. % of carbon containing solid residual.

In large-scale developing process realization we are going to compensate energy losses on thermo destruction by using liquid and gaseous hydrocarbons as a fuel. After that all technological scheme will be closed without losses to the environment.

In experiments rubber chips are used. The material has properties listed below:

- Dimension 5x5x2 mm.
- Mass loses while drying at ~150 °C no more than 0.5%.
- Mineral residue while calcination in oxidizing medium up to ~700 °C has 5% level.
- Element analysis: C ~87 %, H ~7.5 %, S ~1 %.

Thermal differential analysis shows that temperature of intensive mass loses in oxidizing medium starts at 260–280 °C. It corresponds to exothermal effect in Fig. 2. Also small exothermal effect with peak on thermogravimetric curve is registered with maximum at 550 °C.

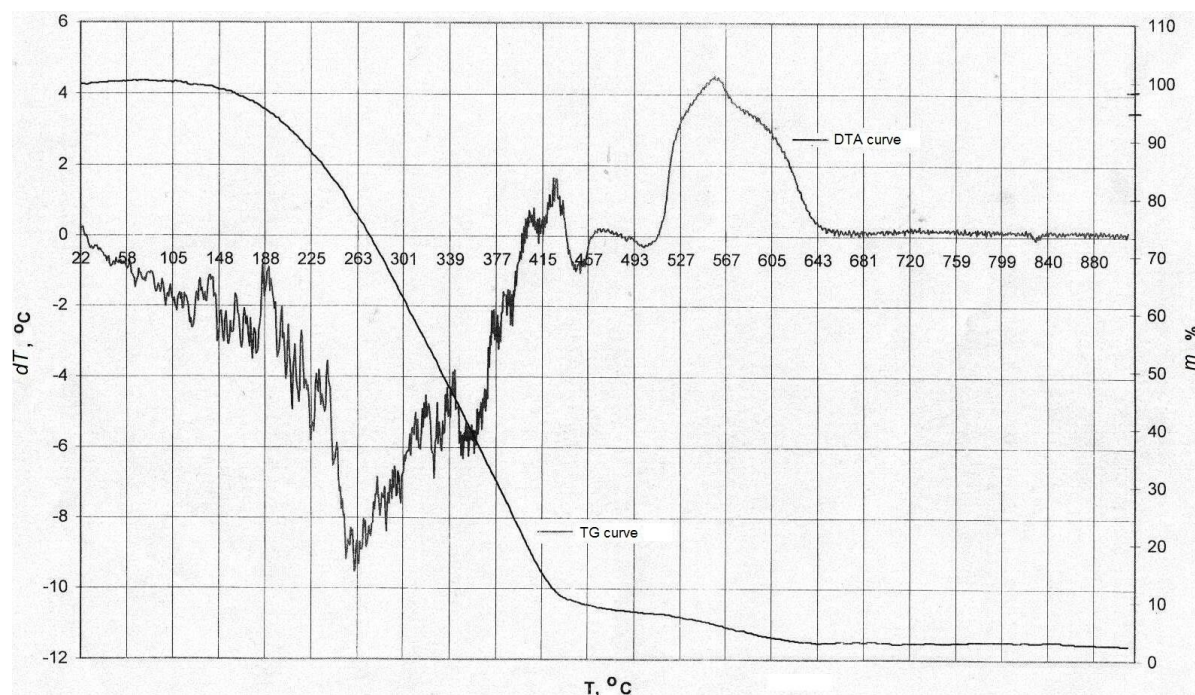


Fig. 2. Differential thermal analysis of rubber waste (oxidizing medium)

4. RESULTS OF THERMOLYSIS

During the processing we obtain products of rubber thermolysis.

Liquid phase (oil condensate) mass ratio is about 54% and depends on parameters of conditions. High temperature ($t_{\text{cond}}=110\text{--}120\text{ }^{\circ}\text{C}$) fraction corresponds to homogeneous black mass with fuel oil consistency with density 0.9 g/cm^3 . Flash temperature of oil condensate in closed cup is $118\text{ }^{\circ}\text{C}$, in open one is $154\text{ }^{\circ}\text{C}$, inflammation temperature is $174\text{ }^{\circ}\text{C}$. Calorific value is 43.5 MJ/kg . Chromatography-mass spectrometry shows discrete maximums at C_{10} , C_{15} , C_{20} , C_{25} , C_{30} that corresponds to isoprene oligomers.

Polytherma of rubber oil evaporation (Fig. 3) shows legible peak at $170\text{ }^{\circ}\text{C}$ which corresponds to $\sim 10\text{ wt.}\%$ losses. So liquid condensate contains relatively low-boiling liquid that corresponds to peak C_{10} on chromatography spectra. Fraction that was extracted with vacuum-thermal distillation is liquid with lemon color, boiling temperature about $170\text{ }^{\circ}\text{C}$ and refractive index about 1.

IR-spectra of light fraction is shown in Fig. 4. There are no additional adsorption lines on this spectrum, in a range of method sensitivity, and it corresponds to test spectra of limonene [7]

Solid phase (pyrocarbon) mass ratio is about 35% and depends on operation parameters. Mineral residue while calcination in oxidizing medium is 6%. It consists of zinc oxide as a main component and some additives of titanium dioxide (according to radiographic-phase analysis). It should be mentioned that existence of mineral residue determined by vulcanized rubber goods producing technology where vulcanize and additives are required component of rubber mixture. It is supposed that initial sulphurous vulcanize is absorbed by mineral filler with sulphide formation during the thermal destruction, as far as after pyrocarbon processing with acid content of sulphur can be decreased up to $0.5\text{ }\%$.

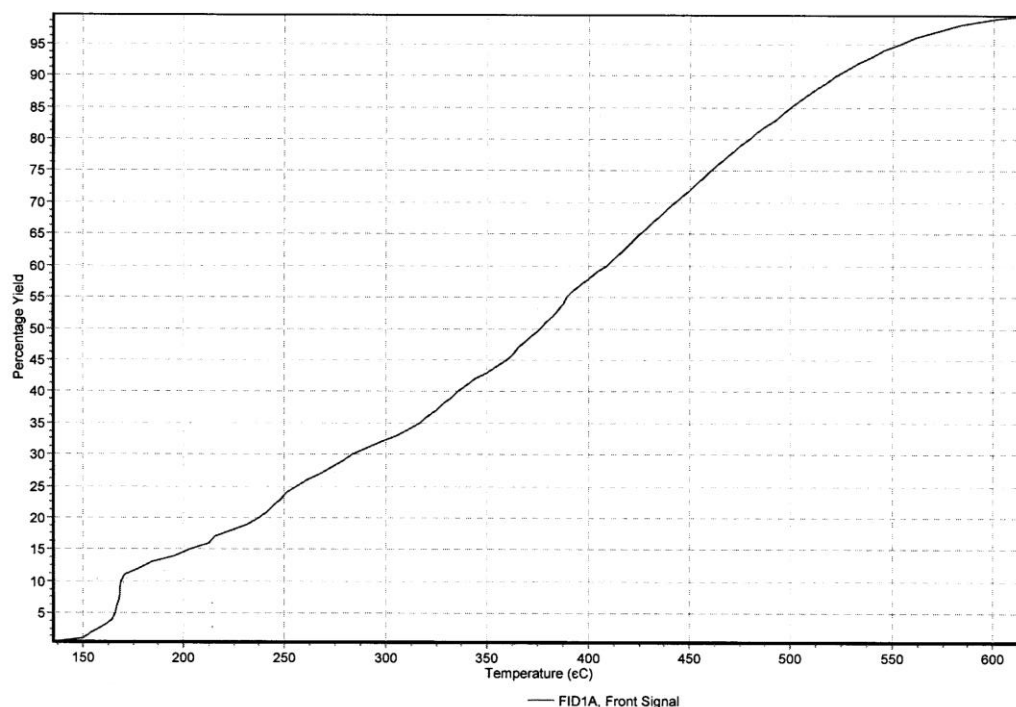


Fig. 3. Polytherma of rubber oil evaporation

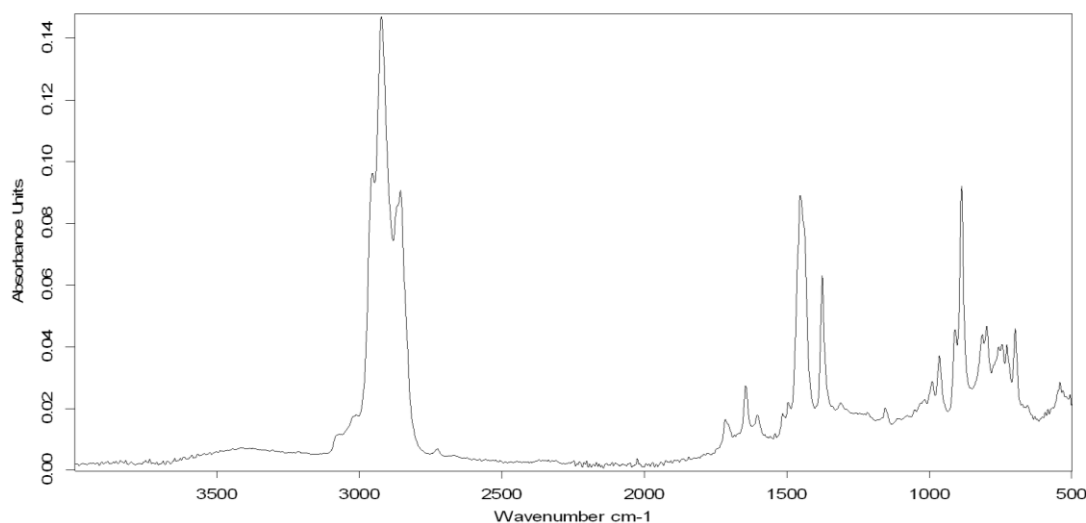


Fig. 4. IR-spectra of light fraction

Element composition of solid fraction is: C – 86–89 %, H – 0.4–0.9 %, S – 1.8–2.5 %. Sorption surface is estimated at a $\sim 15 \text{ m}^2/\text{g}$ (colorant sorption).

Regeneration of mineral residue is out of practical interest. But in case of further application of obtained materials it should be taken into account that in solid phase sulphur main amount is concentrated as a residue of vulcanize additives. Its content in rubber chips is about 1.5 %, and after treatment in solid phase increases up to 2%.

Technical carbon can be used for paints and varnishes, mechanical goods and tires production, in metallurgy and many others fields of industry [8]. In addition carbon residue can be used as a solid fuel, component for asphalt production, at a chemical power source producing and electro-conductive screens of shaft cable.

5. CONCLUSIONS

Efficiency of rubber waste treatment in screw reactor is shown. Such technological processes of thermal destruction permit to treat as useless rubber tires as numerous plastic waste and polymers as well as chlorine and sulphur containing.

It is suggested to separate liquid condensate with purpose to obtain products with cost higher than fuel oil. Designed scheme supposes two step liquid fraction division. Therefore it is reasonable to treat part with high boiling temperature in standard cracked units of petrochemical industry.

In addition we propose not to use solid carbon as a fuel but also regenerate technical carbon. It is possible to increase surface by moving out gum-like additives. So friable disperse material can be obtained.

REFERENCES

1. BOBOVICH B.B.; DEVIATKIN V.V. *Waste treatment of production and consumption: Reference Edition*. M: Intermet Inzhiniring, 2000, 496 p.
2. BELOKOV, V. Methods, technologies and conceptions of carbon industrial solid waste utilization. *Chemical industry*, 2000, Vol. 11, p. 8–25.
3. LOZHECHNIK, A. NIKONCHUK, A. MAKATUN, V. VASILEVICH, A. Steam thermolysis of rubber waste to produce energy-efficient material. Minsk: Belarusian National Technical University. 2012 September.
4. LOZHECHNIK, A. NIKONCHUK, A. MAKATUN, V. Gas-thermal technology for producing fuels and chemical raw materials from organic waste. Minsk: International scientific conference "Aist 2013". 2013 May 28–30.
5. LOZHECHNIK, A., NIKONCHUK, A., MAKATUN, V. Screw reactor for thermolysis of rubber waste. Collection of scientific papers "Heat and Mass Transfer 2012", 2013, p. 196–199.
6. LOZHECHNIK, A. NIKONCHUK, A. SAUCHYN, V. DOLHOLENKA, G. Technology for processing of rubber waste. [CD]. Minsk: International scientific-practical conference "Youth in Science - 2013". 2013 November 19–22.
7. NAKANACY K. *Infrared spectra and structure of organic compounds: Reference Edition*. M: Mir, 1965. 127 p.
8. *Information-analytical agency*. Cleandex: Types of products for recycling of tires waste. [Referred on the 3th of March in 2014 y.] Link to the internet <http://www.cleandex.ru/articles/2010/03/19/tires_recycling_products>

FEASIBILITY OF OPTIMIZING LARGE UTILITY ELECTRICITY CUSTOMERS ON A DISTRIBUTION FEEDER

A. Pensini

*Technical University of Denmark (DTU)
Anker Engelunds Vej, 2800 Lyngby – DK
Lawrence Berkeley National Laboratory (LBNL)
Cyclotron Road, 94720 Berkeley CA – USA*

A. Mammoli

*University of New Mexico (UNM)
University of New Mexico, 87131 Albuquerque NM – USA*

ABSTRACT

The cost of electricity for a building can be lowered by applying optimization strategies that provide optimal purchasing schedules for the building operation under a variable electricity price. From the DSO perspective, this introduces benefits to the grid. The optimal schedule better follows the electricity price, which in turn reflects the DSO requirements. However, most optimization tools are intended for minimizing the costs of a single user and do not take into account the grid operation. If large customers in the same area optimize their schedules, unwanted ‘artificial’ peaks may occur on the feeder that the DSO has to deal with.

Peaks height can be lowered by applying an upper bound to the purchased electricity in the mathematical formulation of the optimization problem. However, introducing a further constraint reduces the economic benefit for optimizing customers. This study assesses the peak reduction potential of introducing the additional constraint while keeping appealing economic benefits for the customers.

DER-CAM, an optimization tool developed at LBNL was used for simulating the operation of three large typical commercial customers over a week. Results prove the peak shaving ability of the proposed model that delivers schedules where the peaks height can be reduced by a given degree. The additional power constraint reduces overload time by 54% while maintaining the electricity bill substantially equal to the optimal unconstrained formulation (1% cost increase).

Reducing overload feeder time allows for larger electric loads to be optimized and fosters the diffusion of microgrids and DERs.

Keywords: smartgrids, microgrids, optimization, energy storage

1. BACKGROUND AND MOTIVATION

Electric utility customers (especially with large heating/cooling demand) can benefit from optimization strategies. Optimized schedules are produced that reduce utility bills by shifting part of the energy demand to periods when the electricity is cheaper. This can be achieved under a variable electricity price when, with matching operation timescales, energy storage is installed at the building level and/or at least part of the load is deferrable. The optimization process is based on load forecasts and takes advantage of the ability of energy storage to shift utilities consumption to cheap tariff periods. From the DSO perspective, this introduces benefits to the grid. The optimal schedule better follows the electricity price, which in turn reflects the grid requirements.

This study was carried out in collaboration with the University of New Mexico (UNM) and the Lawrence Berkeley National Laboratory (LBNL) as part of a study for further enhancing the adoption of microgrids.

A demonstration project at UNM is exploiting an optimization tool for reducing utility bills. The optimized schedule for UNM is produced by the Distributed Energy Resources Customer Adoption Model (DER-CAM) software, in its operation version. DER-CAM is an optimization tool developed by LBNL. The first year of utilizing DER-CAM for controlling energy flows¹ at UNM's Mechanical Engineering Building led to savings up to 30% [1]. However, DER-CAM is a customer oriented tool and does not consider the impact that new schedules have on the electrical distribution system. As long as the controlled load is a single "small" customer, the grid operates without problems. Nevertheless, the distribution system can face problems when "large" shifted loads are optimized. Two aspects of using optimized schedules have to be considered, which may contribute to create high peaks of current on the lines during low tariff periods:

1. Typically, optimized schedules from DER-CAM show peaks during low tariff periods. The height of these peaks mostly depends on the amount and type of storage installed and the original load profile.
2. If more customers in the same area (connected to the same feeder) take advantage of DER-CAM capabilities, their contribution to the total load on the feeder may sum up with each other coincidentally. This situation can occur especially when the customers have similar loads and DERs installed.

During low tariff periods power requirements from non-optimizing customers is on average lower than during high consumption periods. However, under the circumstances given in point 1) and 2) above, there may be moments when the aggregated load profile is significantly high. Distribution grids may not be designed to accommodate such current peaks and issues may arise.

Such current peaks can be reduced by applying maximum power constraints to the purchase schedules. However, this approach with a new additional constraint will inevitably reduce the economic benefit for the customers. Smaller current peaks are achievable against a larger cost increase. A tradeoff between grid overload and attractive cost reduction for utility customers may be found that allows for large consumers to optimize their schedules without negative effects on the grid.

Therefore, for successfully optimizing large loads on a feeder a strategy that addresses both grid and customers' requirements should be implemented. At present, no main studies have been found in literature by the authors that cover such approach.

A feasibility study is needed that assesses the grid operation with large optimized schedules with and without maximum power constraints. Thus, the amount of peak reduction realistically achievable on a typical feeder against a "small" cost increase for the customer introduced by the power constraints has to be assessed.

2. METHODOLOGY

2.1. Input data

This study simulates the summer operation of a feeder rated for 6 MW that serves about 1000 households and three larger consumers that optimize their utility purchase schedules using DER-CAM. The three customers (C1, C2, and C3) are respectively modeled with typical load (electricity, cooling, and refrigeration²) profiles of a large supermarket, a large office building, and a large hotel. Each customer has a set of DER installed, as shown in

¹ Here, the approach used was completely deterministic. The utility price in New Mexico is based on Time of Use (TOU) fixed tariffs and the load forecast was assumed to be a perfect knowledge of the future. Necessary adjustments to the scheduled load to match real time requirements are made one the fly.

² Cooling and refrigeration were converted to the equivalent electricity demands.

Table 1, with the technical characteristics of Table 2, common to all the customers. The cold storage can be charged by electric or absorption chillers. Absorption chillers are driven by heat coming from the heat storage which in turn is charged by solar thermal panels. Electric chillers are modeled to be large enough to meet all the cooling load. Electric storage is charged by electricity from either the grid or the PV array. Photovoltaics can also be used directly to meet the load.

Table 1. Installed DERs for the three customers (values in kW and kWh)

	Customer 1	Customer 2	Customer 3
Electric Storage	2530	1671	1650
Cold Storage	3067	9594	4512
Heat Storage	0	0	800
Solar Thermal	0	0	200
Absorption Chiller	0	0	200
PV	100	100	0

Table 2. Storage technological data

	Battery	Heat Storage	Cold Storage
Efficiency Charge	95%	95%	95%
Efficiency Discharge	95%	95%	95%
Decay	1%	1%	1%
Max Charge Rate	20%	17%	17%
Max Discharge Rate	20%	17%	17%
Min State Of Charge	10%	5%	5%

2.2. Optimization setup

One week of operation was simulated with a time resolution of 15 minutes using DER-CAM³. The decision variable is the electricity from the grid at each time step. The optimization algorithm minimizes the cost of utility electricity paid by the customer while satisfying load and technological constraint. The load constraint requires that the demand has to be met at each time step by energy from either the grid or the storage. Technological constraints are maximum storage charge and discharge rate and minimum state of charge. A Time Of Use (TOU) tariff with on-peak (working days, from 8:00 am to 9:00 pm) and off-peak electricity price was used.

Customers provide the software with the weekly electricity demand forecast and receives as output the optimized schedule for purchasing electricity from the grid, as well as operation of the installed DERs during the week. Schedules from DER-CAM allows the customer to minimize its utility bill by shifting electricity consumption to low tariff periods and storing in for later use.

Two formulations of the optimization problem were assessed.

For each customer a first DER-CAM run (FR) was performed based on the original optimization formulation without additional constraints on the utility purchase. The total feeder load P_f^{FR} based on the outcome from FR was then calculated:

³ For more information about DER-CAM and its mathematical formulation see <http://building-microgrid.lbl.gov/projects/der-cam>.

$$P_f^{FR}(t) = P_f^B(t) + \sum_{i=1}^3 P_i^{FR}(t), \quad (1)$$

where P_f^B is the total feeder base load, P_i^{FR} is the customer load from the first DER-CAM run, t is the time step, and i indexes the three customers.

The feeder load so calculated (P_f^{FR}) has peaks occurring during the low price periods, as explained in section 1. In order to reduce peaks height, a second DER-CAM run (SR) for each customer was performed by applying an upper bound to the utility electricity purchase in DER-CAM:

$$P_i^{SR}(t) \leq \max(P_i^{FR}) \cdot \beta_i, \forall t, \quad (2)$$

where $\beta(0,1)$ is a peak shaving factor chosen as shown in section 2.3. Equation (2) was introduced in the DER-CAM code as an additional constraint.

The new total load for the second run (P_f^{SR}) was calculated:

$$P_f^{SR}(t) = P_f^B(t) + \sum_{i=1}^3 P_i^{SR}(t). \quad (3)$$

2.3. Peak shaving factor

The benefit of the additional constraint (Eq. 2) is that it reduces the maximum height of the peaks from each customer to a given value controlled by the peak shaving factor β . As lower β values give shorter peaks, a small β is desirable. However, setting an upper bound to the electricity consumption also has two main side effects that increase the utility cost.

First, while β decreases, off-peak load is spread over a longer period of off-peak time, while on-peak consumption does not deviate from the FR case, which is the optimal (Fig. 1). This slightly increases the energy consumption, due to energy losses from the storage, which stays charged for longer periods. Nonetheless, for the large customers modeled in this study, energy losses from storage are small compared to the total consumption and the cost increase minimal.

A second negative effect can also be introduced by the maximum power constraint. Below a certain threshold value of beta (β^\wedge), the constraint would prevent part of the off-peak consumption to take place at low price periods and shift it to on-peak hours. This noticeably increases the electricity bill for the customers (Fig. 2). The extreme case is reached with the minimum allowable value β^{\min} . For $\beta < \beta^{\min}$ the optimization is infeasible. Fig. 1 shows the effect of the power upper bound constraint with two β values (namely β^\wedge and β^{\min}) against the unconstrained case FR. For $\beta = \beta^\wedge$ the constraint affects only the off-peak consumption pattern (the blue line is overlapped by the red one during on-peak hours). In contrast, using $\beta = \beta^{\min}$ will change also the on-peak demand, leading to a higher utility cost.

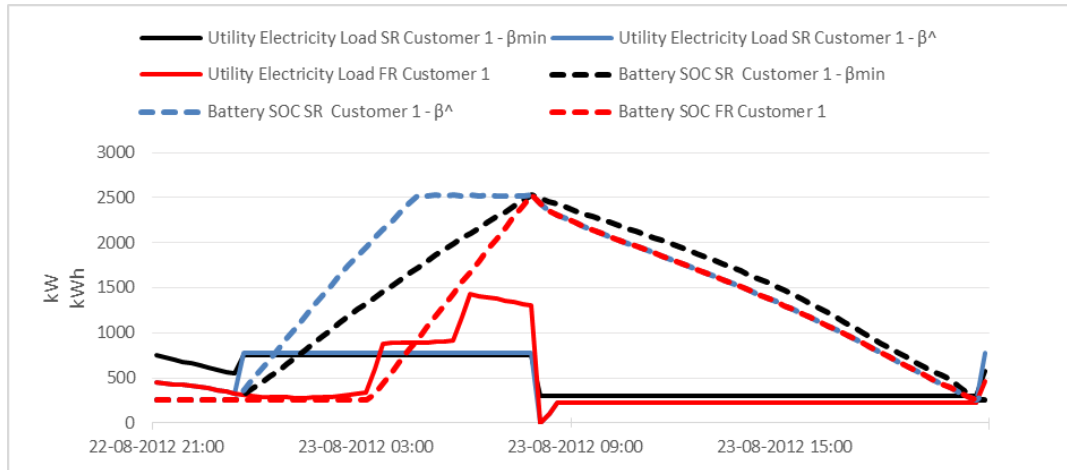


Fig. 1. Utility electricity consumption and battery state of charge for C1 during a 24 hours period (weekday). The first DER-CAM unconstrained run (FR) is shown in red. The second run with maximum power constraint (SR) is shown for two values of β (β^{\wedge} in blue and β^{\min} in black). The off-peak period spans from 22 Aug. 21:00 to 23 Aug. 8:00. The electrical storage state of charge is also shown for the three scenarios with dashed lines

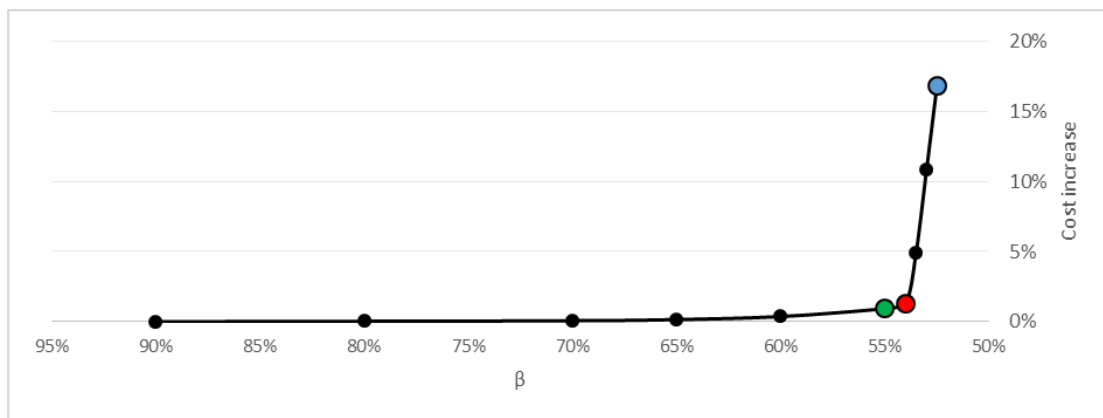


Fig. 2. Utility cost increase vs β for C1. The cost for values of β lower than β^{\wedge} (corresponding to the red marker) increases quickly until the optimization becomes infeasible. The last feasible case is represented by the blue marker that corresponds to β^{\min} . The green marker ($\beta_1=0.55$) is the value used for the simulation which leads to a utility cost 1% higher than the first run

For assessing the peak load ability of the constrained formulation SR, it was assumed that a cost increase of 1% (compared to the unconstrained problem FR) would still keep customers willing to optimize their schedules. The values of β that give 1% of cost increase for each customer were calculated ($\beta_1=0.55$, $\beta_2=0.67$, and $\beta_3=0.51$) and used in the simulation.

3. RESULTS

Results from the simulation are shown in Fig. 3. For the original feeder load without optimization, the peak consumption occurs mostly during on-peak hours (notice that the weekend is 25th and 26th).

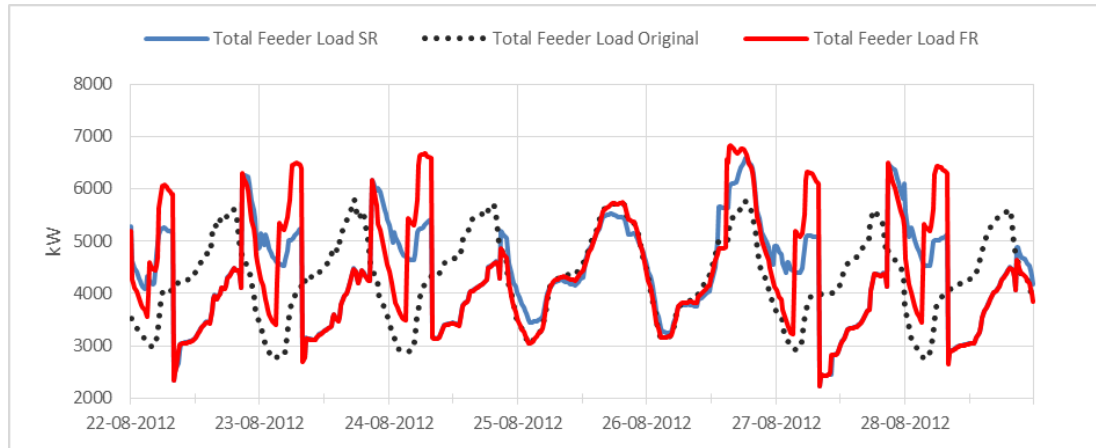


Fig. 3. One week simulation results. The dotted black line represents the original total feeder load, without optimization. The total feeder load from the unconstrained DER-CAM run is shown in red and the blue line is from the optimization with maximum power constraint

When the schedule is optimized without maximum power constraint, part of the on-peak demand is shifted during off-peak. Typically, the optimized schedule during low tariff periods hours presents two peaks, as shown in Fig. 4. This load profile is mostly following the original off-peak demand, which has a minimum in the middle of the night at around 3:00 am. Energy storage charging also contributes to the evening and early morning peaks. The cold storage is charged starting from Oct. 22nd at 21:00 pm while the electrical battery from Oct. 23rd 3:30 am (as shown in Fig. 4 for customer 2).

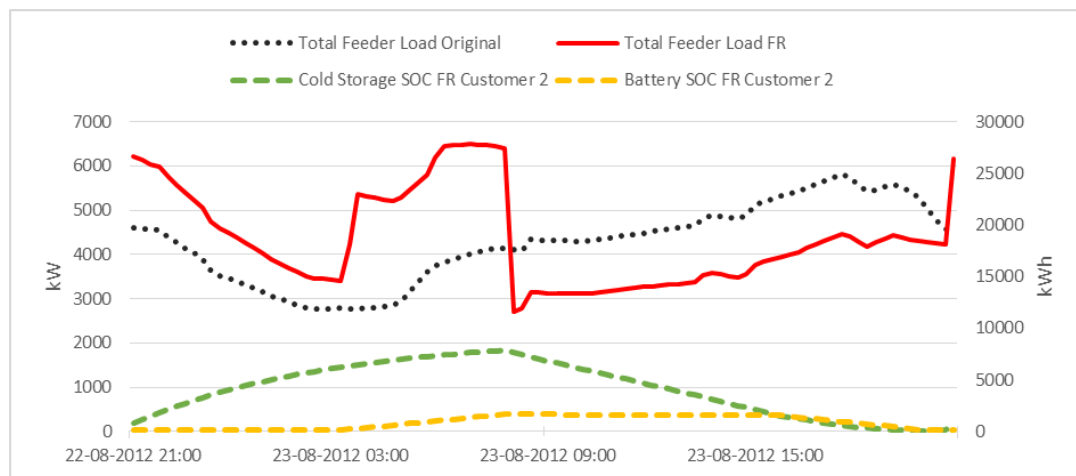


Fig. 4. Feeder original load (dashed black line) and first DER-CAM run (red line) for 24 hours period (weekday). Energy storage state of charge for the case of C2 (cold storage in green and battery in yellow dashed lines) is also shown on the secondary axis

Input power to the storage is the flexible load that is shifted to lower consumption periods when the maximum power constraint is applied, resulting in a more flat load profile (Fig. 3). In particular, the second run is very effective in reducing early morning peaks that during working days drop to about 5 MW.

A similar effect cannot be achieved for evening peaks, which are mostly driven by the charging of the large cold storage of customer 2 that has to be full before the on-peak period begins. The cold storage is modeled in such way that it can be charged by a given percentage (charging rate) of the available energy (maximum capacity minus current capacity). Thus, when the cold storage is empty, the charging power can be as high as its capacity divided by

the charging rate. As the cold storage is filled, the maximum charging power diminishes (Fig. 5) and the time required to store a certain amount of energy increases. Customer 2 has a large cold storage rated for 9600 kWh and takes 11 hours to be charged from 8% to 80% of its capacity. The charging period begins in the evening, during the first off-peak time step. Here the charging power is above 1500 kW (Fig. 5), which is most part of the difference between the total feeder load and the feeder base consumption in that particular moment (Fig. 1).

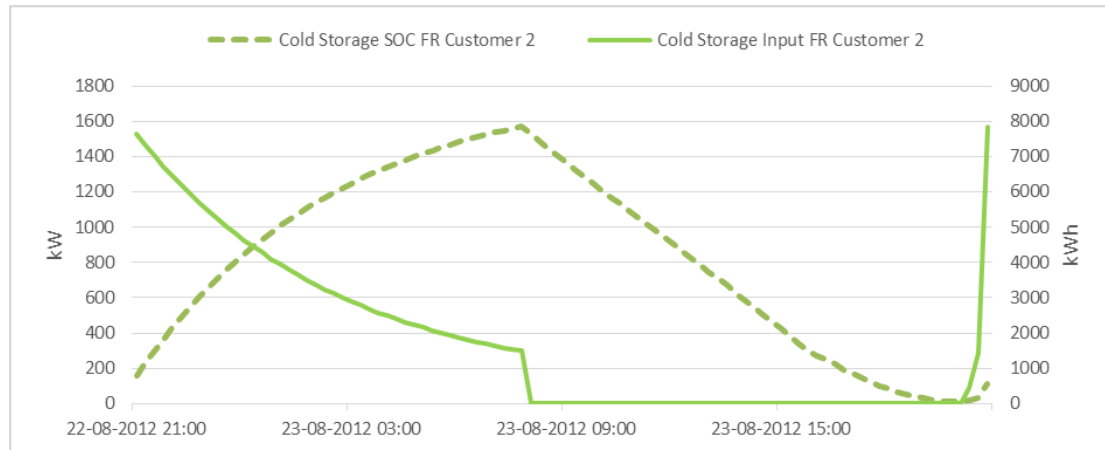


Fig. 5. Cold storage charging power (solid line) and correspondent state of charge (dashed line) during 24 hours for C2

For determining the peak shaving ability, the percentage of time when the feeder is overloaded was calculated for the two optimization cases and for the original load profile with no optimization. In the latter case, the total power never exceeds the rated capacity of 6 MW. When the large customers optimize their schedules concurrently, feeder overload occurs. In particular, the power constraint can reduce the overload from 11.5% to 6.3% of the time.

4. CONCLUSIONS

Scheduling optimal utility consumption allows customers to reduce their utility bills. Traditional optimization tools are intended for minimizing utility cost that customers pay. However, they do not take into account the distribution grid operation and optimized schedules of large customers may cause overload of the electric distribution grid. As the penetration of DERs increases and optimized scheduling is applied, current distribution systems may not be ready to handle the new load profiles.

It is possible to define the optimization problem with an additional upper bound constraint on the electricity consumption that allows for reducing current peaks on the feeder. However, this approach lessens the economic benefit for the optimizing customers depending on the peak reduction that is achieved. For large electric loads to be optimized, two requirements have to be fulfilled. First, overload of the distribution network has to be avoided or kept as low as possible. Second, cost reduction for customers has to be attractive. This study simulates the optimization of large electricity consumers with and without the additional constraint on the maximum electricity consumption. The goal was to determine the peak reduction potential of introducing the new constraint while keeping the utility cost close to the unconstrained problem formulation which gives the optimal economic performance.

DER-CAM optimization software was used for evaluating the operation of a distribution feeder with three large utility customers optimizing their electricity purchase schedules. It was shown that part of the peaks introduced with the optimal load profile can be

reduced by applying a maximum power constraint to the optimization algorithm. The cost increase, compared to the unconstrained simulation, was kept within reasonable limits for the customers (in this study 1%). The overload time of the constrained simulation is kept as low as 6.3% against 11.5% if the traditional optimization formulation. Overload time reduction is consistent (about 45%), however, the strategy is less effective when large amount of energy storage is installed that requires several hours to be charged and has limited flexibility.

This study has to be intended as a first feasibility assessment of optimizing large customers on existing distribution networks and proposes a simple modification of the optimization algorithms that may allow more customers to exploit optimized schedules and enhancing the penetration of smartgrids and DERs.

Expanding on this study, a multi-stage approach can be adopted for avoiding other critical grid operation than feeder overload (such as voltage drop). A feeder model will simulate the grid operation based on the first optimization run and provide the basis for defining a dummy real time price (RTP). The last run is driven by the RTP module and responds to voltage drops along the lines.

5. AKNOWLEDGEMENTS

DER-CAM has been funded partly by the Office of Electricity Delivery and Energy Reliability, Distributed Energy Program of the U.S. Department of Energy under Contract No. DE-AC02-05CH11231. The Distributed Energy Resources Customer Adoption Model (DER-CAM) has been designed at Lawrence Berkeley National Laboratory (LBNL).

REFERENCES

1. MAMMOLI, A., STADLER, M., DEFOREST, N., BARSUN, H., BURNETT, R. and MARNAY, C. "Software-as-a-Service optimized scheduling of a solar-assisted HVAC system with thermal storage." Proc. Microgen 3–3rd International Conference on Microgeneration and Related Technologies, Naples, 15–17 April 2013.

ROLE OF ELECTRICAL VEHICLES FOR IMPROVEMENT OF ELECTRICAL NETWORKS EFFICIENCY

L.Grackova

*Riga Technical University
21, Aizkraukles Street, LV-1006 –Latvia*

I. Oleinikova, G. Klavs

*Institute of Physical Energetics
21, Aizkraukles Street, LV-1006 –Latvia*

ABSTRACT

This research focuses on a relevant issue of electric vehicles implementation with an aim to improve efficiency of electric networks, includes seasonal and daily load curves typical electricity consumption estimation in Latvia from 2010 to 2013. During this study, the possible electricity consumption load curves have been considered for 2020. Simultaneously, the coefficient of non-uniformity of the load curve was calculated - to estimated total power consumption per hour at night. Two scenarios were considered. In scenarios, estimation of electricity consumption at night depended on the number of electric vehicles, a fully charged battery, and the average daily mileage per car. Created scenarios represent the possibilities for electricity consumption increasing and to providing balancing services for the electric networks. Assuming fulfilment of any of the scenarios, the daily household electricity consumption was also examined for 2020.

Keywords: Electric vehicles, load curve, electrical networks

1. INTRODUCTION

The development of electric vehicles (EVs) is a subject widely discussed due to their integration into modern power networks. As for example, in 2010, the European Commission established a European strategy for clean and energy efficient vehicles. It presented a forecast that by 2020 with the market share of sales of new electric cars increasing to 2% a half million of the charging stations for electric vehicles will be located in the EU [1].

There are numerous already existing extensive researches in the field. The interest in electric vehicles appeared with the introduction of Smart Grid technology (SGT) [2].

A SGT is an electrical network that incorporates a combination of traditional and advanced information and communication technologies that monitor and manage the transport of electricity from all generation sources, and supervise the varying electricity demands of end-users. [3] Introduction of SGT has a great opportunity to increase energy efficiency and consistency of power supply for the power system. [4].

Smart Grid technology allows creating mutually beneficial relationships with other industries, for example – with the automobile industry, in particular – with car manufacturers – plug-in hybrid (PHEV), electric vehicles (EV) and vehicle-to-grid (V2G) technology.

Electric vehicles are considered to be a promising solution for coordination of power supply for the power system, and in general – reduce carbon emissions (thus, achievement objectives, adopted by the European Union Climate and Energy Package) and the growth of oil prices. [5].

PHEV, EV and V2G technology can consume electricity at any time of day. Still, for the electrical networks and the car owners, electricity consumption is most profitable at night.

As a result, electric power stations save on fossil fuels, and also – the owners of electric vehicles are able to easily charge the batteries due to favourable electricity tariffs, differentiated by time zones. In turn, V2G can also act as a generator during the day, thus, providing a more efficient and reliable power supply for the society.

PHEV and EV technology has a factual prospect, as they are already present on the roads of the country. As to V2G technologies – they are currently not implemented in Latvia.

A certain amount of PHEV and EV, charging at night, are able to act as energy storage devices. To make this a reality a critical number of EV is required.

Hence, a smart charging policy is required in order to ensure the network stability and also to optimize the charging cost of the EVs.

Aim of this research was to consider the daily power consumption in Latvia in 2020, determine the number of electric vehicles (PHEV, EV technology) required for increasing power consumption during the night at off-peak period, examine the motivation the involve the society (consumers) in participation of power market development.

2. EV CHARGING POLICY

2.1. Load profile estimation

In order to model properly the electrical vehicles behaviours, estimate their impact on electrical network reliability, and create proper EV charging policy, the load consumption, losses and network constraints at a mid-term outlook (typically one year) were analyzed. Detailed power consumption estimation by annual, seasonal and daily load curves from 2010 to 2013 was made during this study (data Latvian Transmission System Operator) [6].

The examined annual graphs indicate that power consumption has increased by 3.7% in 2013 with regard to 2010 (Fig. 1).

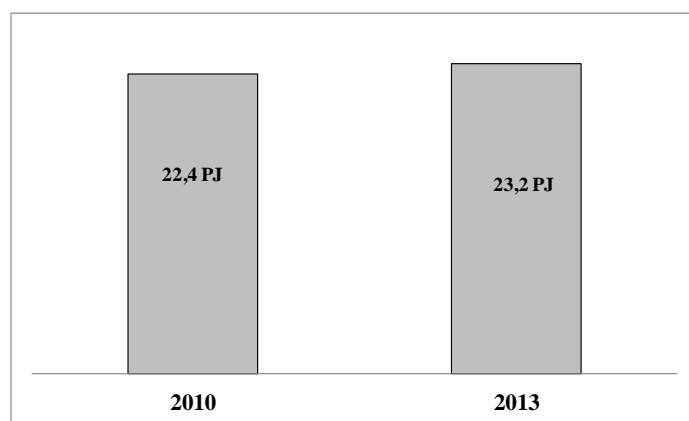


Fig. 1. Annual power consumption, PJ

Seasonal electricity consumption profile shows that the maximum power consumption occurs during the winter season (Fig. 2), whereas minimum consumption occurs during the summer season. (Fig. 3).

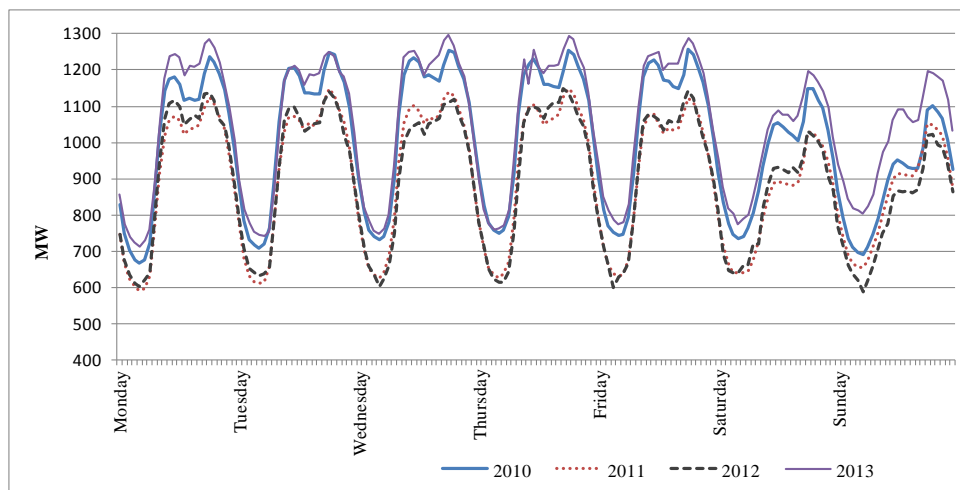


Fig. 2. Seasonal electricity consumption profile (winter), 2010–2013

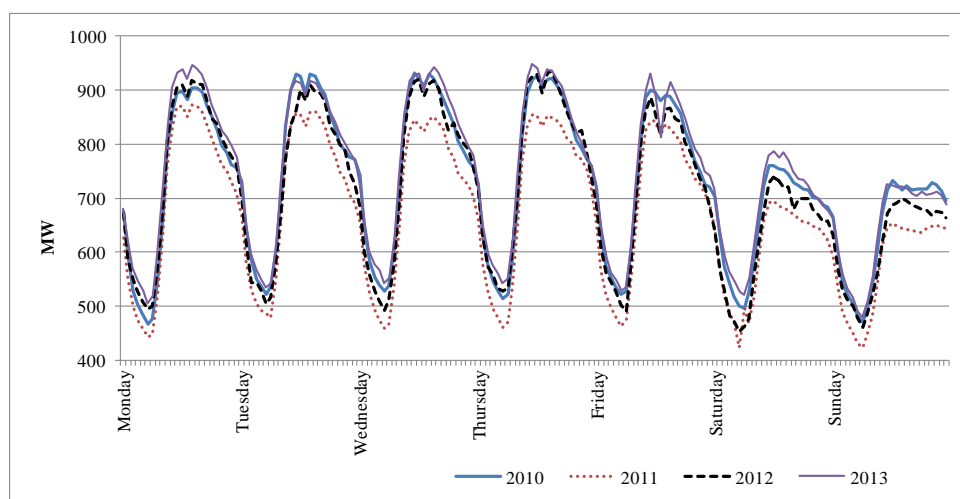


Fig. 3. Seasonal electricity consumption profile (summer), 2010–2013

This analysis was made to evaluate the average daily electricity consumption profile (curve) from 2010 to 2013 and calculate the average daily electricity consumption profile for 2020.

Analysing daily electricity consumption profile from 2010 to 2013, the following conclusion can be mentioned:

- In winter season: from Wednesday to Friday – power consumption maximum, on Saturday and Sunday – power consumption minimum.
- In summer season: from Monday to Thursday – maximum, on Saturday and Sunday – minimum.
- In autumn and spring seasons: from Monday to Thursday – maximum, on Saturday and Sunday – minimum.

From this we can conclude that throughout the whole year, maximum power consumption load can be observed from Mondays to Thursdays, whereas minimum load would be during weekends.

2.2. Charging policy

On the basis of the given data analysis and of made researches of the Institute of Physical energetics (“Latvian energy scenarios (up to 2030) modelling, taking into account economic, environmental and political aspects”), we can highlight that the average daily power consumption load curve for 2013 and the forecast presumed daily load for 2020 were successfully calculated [6].

In comparison to 2013, the total average daily power consumption will increase by 2.4% in 2020 (Fig. 4).

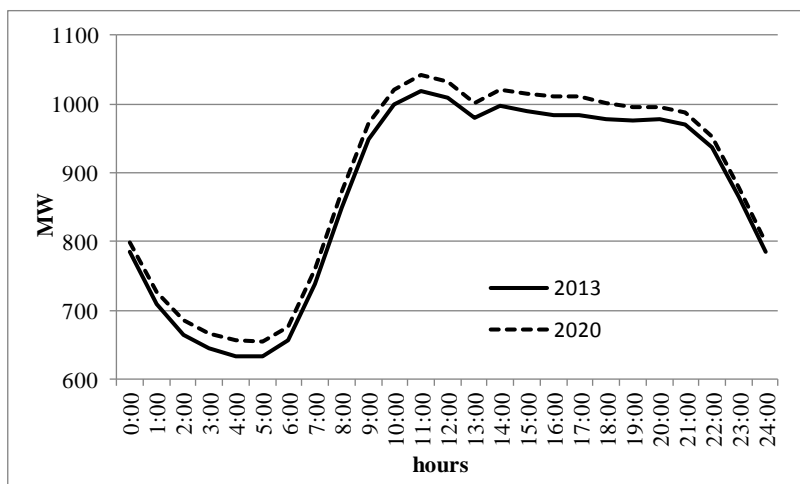


Fig. 4. Average daily electricity consumption profile, 2013 and 2020

According to the above-mentioned graph, we can specify three characteristic zones for any typical daily electricity consumption schedule: maximum load area, middle load area and minimum load area (Fig. 5).

Moreover:

- Maximum load area has a maximum peak load P_{\max} (on peak). Usually, there are one or two maximum power consumptions periods: morning and evening.
- Middle load area – characterized by a significant one-time during the day increase of the load – in the morning, and its substantial recession at the end of the day.
- Minimum load area has a minimum load P_{\min} (off peak). Usually, this occurs at night.

Overall, the daily graph has alternating power system: rises, peaks and valleys, which generally determine its irregularity. Basically, it presents the sum of daily load curves of different consumers.

An important indicator of the daily load curve is the load curve irregularity factor $K_{P_{\min}/P_{\max}}$. Absolutely equal daily load forms of power systems do not exist. $K_{P_{\min}/P_{\max}} = 0.9$ is considered very close to an equal graph load.

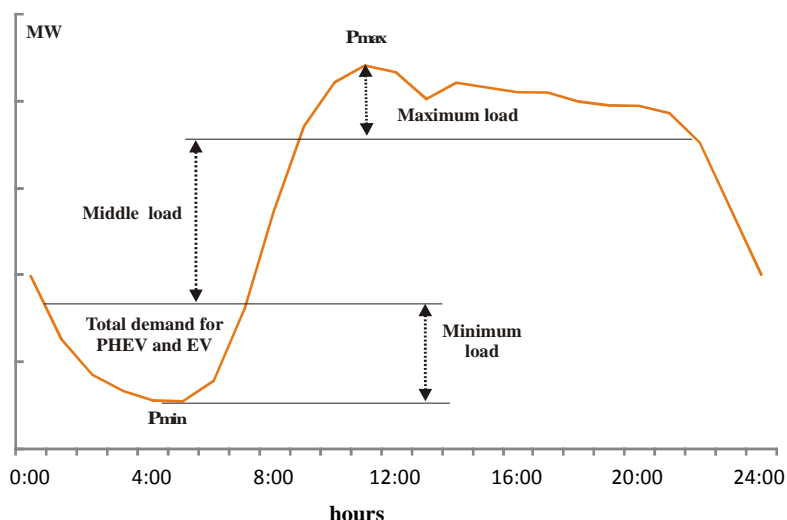


Fig. 5. Typical daily electricity consumption schedule

These are the results of the performed calculations for 2020:

$$P_{\max} = 1041.31 \text{ MW},$$

$$P_{\min} = 655.04 \text{ MW},$$

$K_{P_{\min}/P_{\max}} = 0.63$, what indicate significant daily fluctuations in electricity consumption.

Assuming that exists a sufficient number of EVs in country and the EVs owners are economically interested, for example, by installing a double-rate watt-hour metre, that directly stimulate consumers to use electricity in the economical mode, that as subsequently leading to equalizing the daily load curves. The necessary additional average hourly load on the network at night from 0:00 to 7:00 pm is 124.38 MWh for 2020.

3. EV INCORPORATION SCENARIOS

According to statistics of Road Traffic Safety Directorate of the Republic of Latvia (CSDD), there are 540 102 passenger cars registered in total (01.01.2014), 11 070 out of which are new cars. The number of registered PHEV cars is – 3, and as to EV – there are 15 vehicles in total [7].

Based on the forecast of fuel consumption by vehicles, the possible number of passenger cars in future was established. In 2020, the total number of cars will be – 619 683, out of which, 24 787 will be new cars (4% of the total number of passenger cars) [8].

To analyse the possible equalisation of the daily electricity consumption schedule of Latvian power system through the use of PHEV and EV technologies in 2020, the following two scenarios were proposed (Fig. 6):

- Scenario 1 – the number of PHEV and EV technology promoted by the spontaneous development.
- Scenario 2 – the number of PHEV and EV technology promoted by the government support (they account for 50% of all sold new cars).

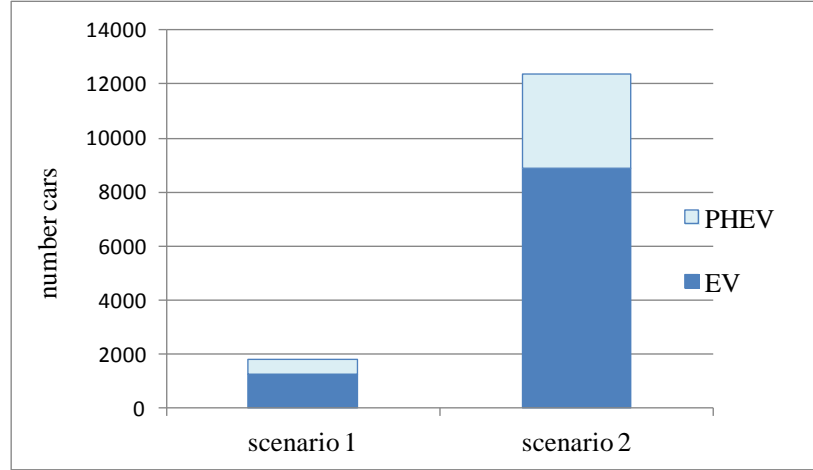


Fig. 6. Number of PHEV and EV technology, 2020

The average electricity consumption of PHEV and EV for one charge was calculated on the basis of the technical characteristics of the most popular EV brands, currently available in the European Union.

For a PHEV to cover 20 to 40 kilometres, a sufficient charge would be from 3 to 5 kWh (the gasoline or diesel engine ensures the autonomy of a conventional vehicle). The battery capacity of a fully charged electric vehicle from electric vehicle automakers, such as Ford Focus Electric is about 20 kWh, Nissan LEAF is about 18.1 kWh and Tesla Model S is about 22.5 kWh, thus, providing an electrical autonomy for about 100 kilometres.

The average electricity consumption of a fully charged battery is 4 kWh for PHEV, 19.4 kWh for EV.

For PHEV and EV are optimal via slow charge in night time for 2–8 hours. Used charging device: Power supply – Single phase – 3.3 kW; Voltage 230 VAC; Max current – 16 A.

The total fuel electricity consumption of PHEV at night time is calculated as follows:

$$P_{PHEV} = E_{PHEV} \times N_{PHEV} / \eta_{charger}, \quad (1)$$

where:

E_{PHEV} – electricity consumption of a single vehicle during a two-hour time period

N_{PHEV} – the number of PHEV electrical cars;

$\eta_{charger}$ – efficiency of the battery charge = 0.9 [9].

The total fuel electricity consumption of EV at night time is calculated as follows:

$$P_{EV} = E_{EV} \times N_{EV} / \eta_{charger}, \quad (2)$$

where:

E_{EV} – electricity consumption of a single vehicle during a seven-hour time period;

N_{EV} – the number of EV electrical cars;

$\eta_{charger}$ – efficiency of the battery charge.

Calculation results, acquired from both scenarios analyses are illustrated in Fig. 7. With an everyday charge, Scenario 1 can only provide about 24% of the required load demand.

Scenario 2, however, meets the necessary load demand completely and even with 66% margin.

All calculations were made assuming that a fully charged battery for distance per 100 km everyday. Since the average driving distance for a Latvian is 43.5 km per day, there will not be a reason to charge EV battery on the everyday. As a result, we obtain Z-zone, which is not constant value. So the Z-zone will depend on the need to charge EV battery (this may be everyday or 2–4 times a week). For that reason, considering the outcomes, we can state that to clarify the Z-zone, additional research is a necessity, since, as a result, that Z-zone will decrease the total load demand in Scenario 2.

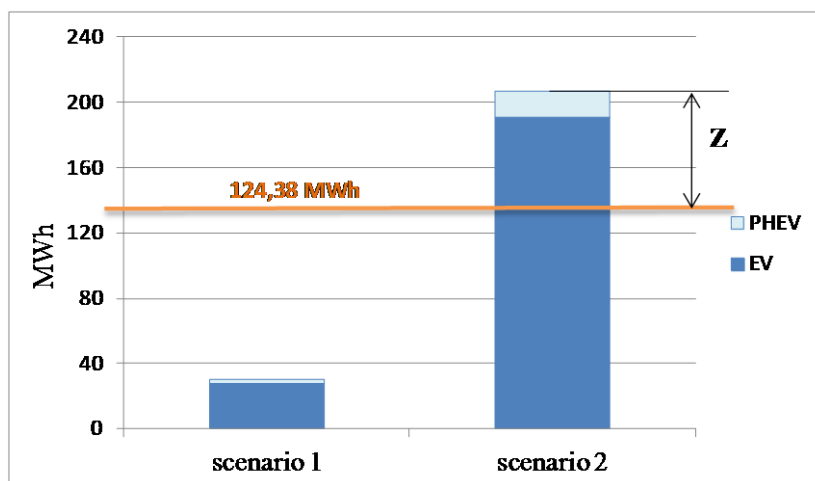


Fig. 7. Results on load demand to two scenarios, 2020

As a result of this research, we can state that 2% PHEV and EV of the total number of passenger cars (Scenario 2) is sufficient for implementation of the electricity consumption increase at night.

Comparing these results with similar research, as example, the thesis "Analysis of Integration of Plug-in Hybrid Electric Vehicles in the Distribution Grid", which the investigated the effects of integration of plug-in vehicles with different electricity consumption profile, consider three urban district of Stockholm (Sweden) with unequal daily load profiles and different numbers of electric vehicles till 2050. The model for estimation of the car number in each area was based on the forecast number of inhabitants. Average daily electricity consumption for these areas will increase by 0.7%, 1.4% and 3.4% in 2020. This percentage depends on the number of cars in the area under consideration [10].

In our model of the cars number depends on the forecast Gross domestic product (GDP). Average daily electricity consumption will increase by 4% in 2020.

Comparison of the results showed that increasing the number of electric vehicles leads to an increase in electricity consumption.

4. AVERAGE DAILY HOUSEHOLD ELECTRICITY CONSUMPTION

Over the past five years in Latvia, there has been a decrease in the number of households and their average daily consumption of electricity (Fig. 8). The average daily consumption of electricity for one household decreased on 8% for 2012 in compare to 2008.

The average daily consumption of electricity was 5.96 kWh for one household in 2012.

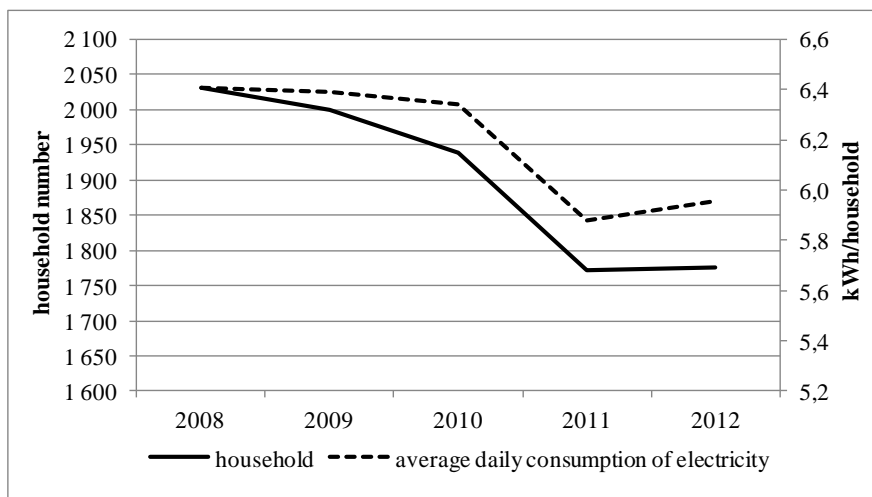


Fig. 8. Number of households and average daily consumption of electricity, 2008–2012

Assuming fulfilment of Scenario 1, the electricity consumption by a single household will increase by 0.5% (5.97 kWh/day) in 2020. If Scenario 2 is fulfilled, the electricity consumption by a single household will increase by 3.4% (6.15 kWh/day) in 2020.

As a result of this research, we can presume that the considered number of electric vehicles will lead to average increase electricity consumption per household.

5. CONCLUSIONS

This study considered PHEV and EV as consumers of electricity in off-peak hours at night as one of the promising ways to save energy resources and providing efficient power supply for the Latvian people.

The study showed that the 2% of the electric vehicles number of the total number of passenger cars will increase the average daily electricity consumption by 4% and will influence the balancing of daily load curve in 2020.

The implementation of electric vehicles allows:

- to improve on the efficiency of electrical distribution networks, by controlled distributed load;
- to increase the load in the network;
- to provide the load balancing grid at night.

For widespread use of electric vehicles in Latvia:

- no developed networks of charging stations in public places;
- government support for the purchase of electric vehicles (electric vehicle prices are quite high) is missing.

Also, to manifest people's interest, it is suggested to develop supplementary rules of installing safe and convenient charging devices near a residential house, a more flexible energy supplier's policy (electricity tariffs, differentiated by time day) and installation of smart meters and demand-side management system (DSM) [11, 12].

The next step of this research would be to create a model of the electrical network in order to study the influence on the distribution networks of electric vehicles charging during the day, as well as specify possible limitations in the medium term outlook.

REFERENCES

1. http://ec.europa.eu/enterprise/sectors/automotive/competitiveness-cars21/energy-efficient/communication_en.htm
2. CHAMMAS, M., CHICHE, A., FOURNIE, L., FIDALGO, J., COUTO, M. A multi-scale optimization model to assess the benefits of a smart charging policy for electrical vehicles. PowerTech (POWERTECH), 2013 IEEE, Grenoble, 16–20 June 2013, 6 p.
3. INAGE S. "Modelling Load Shifting Using Electric Vehicles in a Smart Grid Environment," IEA Energy Papers, No. 2010/07, OECD Publishing, Paris, 2010. doi:10.1787/5km7v0bsmw7k-en
4. MORGAN, T. Smart grids and electric vehicles: Made for each other? Discussion Paper No. 2012-02. International Transport Forum. United Kingdom, Menecon Consulting, 11 April 2012. 28 p.
5. http://ec.europa.eu/clima/policies/package/index_en.htm
6. http://www.ast.lv/eng/power_system/current_situation_in_power_system/planned_and_actual_demand_net_exchange_and_production/
7. http://www.csdd.lv/eng/information_and_services/
8. Latvijas enerģētikas attīstības scenāriju (laikā līdz 2030.gadam) modelēšana, ņemot vērā ekonomiskos, vides un politiskus aspektus 23.lpp. FEI, Rīga 2012. Novembris, 61 p. http://www.em.gov.lv/images/modules/items/Latvijas_energetikas_attistibas_scenariji_2030.pdf
9. http://en.wikipedia.org/wiki/Electric_car
10. KARNAMA A. Analysis of Integration of Plug-in Hybrid Electric Vehicles in the Distribution Grid. Master of Science Thesis, Stockholm, Sweden 2009, 92 p. <http://www.diva-portal.org/smash/get/diva2:610066/FULLTEXT01.pdf>
11. OLEINIKOVA, I., TURCIK, M., MUTULE, A., OBUŠEVŠ, A. Active End-users' Energy Management Possibilities in Market Environment. Conference: Experimental research and DER integration in the EU Energy System. Poster session. 10–11 October 2013. Milan, Italy.
12. OLEINIKOVA, I., TURCIK, M., KOLCUN, M. End-users' Energy Management Strategies in Market Environment. Proceedings of the 7th International Scientific Symposium "Elektroenergetika 2013". Stará Lesná, High Tatras, Slovak Republic, September 18–20, 2013. – Symposium Proceedings, P. 252-255. ISBN 978-80-553-1441-9.

INTER-AREA OSCILLATION CONTROL WITH SUPER CONDUCTING MAGNETIC ENERGY STORAGE IN THERMAL-HYDRO POWER SYSTEM USING OPTIMIZED INTELLIGENT CONTROLLER

Y.K. Bhateshvar, H.D. Mathur

*EEE Department,
BITS, Pilani Campus,
Pilani, India*

ABSTRACT

This paper presents the design and optimization of a Fuzzy Logic Controller (FLC) for Load Frequency Control (LFC) of two-area power system with superconducting magnetic energy storage (SMES) unit. SMES is capable of storing electric energy and releases it as per system requirement. The multi-area power system considered for study comprises of one reheat type thermal unit and a hydro unit of same capacity in each area. Optimization of FLC is done in four different steps; the first step is for optimization of range of input and output variables, second one for optimization of membership function, third and fourth steps for rule base optimization. Genetic Algorithm (GA) technique is utilized for this step-by-step optimization process of FLC. In general, either the upper and lower bounds of membership functions are obtained or only rule base is optimized using any optimization techniques, but proposed method is more effective to get optimal results than existing methods. Further the comparison between a conventional GA optimized PID controller, GA optimized FLC and four steps optimized FLC is carried out. Simulation results show the validation for proposed optimized FLC in terms of less frequency deviations as well as tie-line error. Results are further quantified by two performance indices peak undershoot and settling time.

Keywords: Multi-Area Power System, Load Frequency Control, Fuzzy Logic Controller, Genetic Algorithm, SMES

1. INTRODUCTION

Continuous balance between generation and load is main requirement of power grid. LFC is system for controlling of generation from generators as per fluctuating load demand as well as to ensure the quality of power supply.

Fuzzy logic based controllers have widely accepted for different engineering and industrial applications. FLC is an appropriate choice for linear as well as non-linear system, complex or ill defined system. Already FLC for LFC is explored [1], [2], but proper FLC design required detailed knowledge and experience. For better dynamic performance with the help of optimization algorithms FLC can be tuned easily without detailed mathematical system knowledge. Already many efforts have been made in this direction [3], [4], but still they deliver oscillatory solution.

In order to effectively damp oscillations in interconnected power system, apart from effective intelligent controller additional energy resources provides better results. SMES is one of favourable choice for it for fast response and large storage capabilities. SMES plays significant role to improve power system dynamic performance. In an interconnected power system SMES might be connected to any of the control area or area based on system requirement. Apart from frequency oscillation damping, it also helps in damping tie-line power oscillations.

2. SYSTEM EXAMINED

2.1. Load Frequency Control for Two-Area Power System

The system examined consists of two control areas and having reheat type thermal generating company in control area-1 and hydro generating company in control area 2 and these two control areas are connected by tie-lines.

In LFC, the difference between actual generation and scheduled generation is termed as area control error (ACE) for interconnected power system.

$$ACE_i = \sum_j \Delta P_{tie,ij} + b_i \Delta f_i. \quad (1)$$

Where, b_i is frequency bias constant, Δf_i is frequency deviation, $\Delta P_{tie,ij}$ is change in tie-line power and subscript i & j indicates area1 or 2.

So, scheduled tie line power flow between area-1 and area-2 is:

$$\Delta P_{tie12,sch} = \Delta P_{L,A1 \rightarrow A2} - \Delta P_{L,A2 \rightarrow A1}. \quad (2)$$

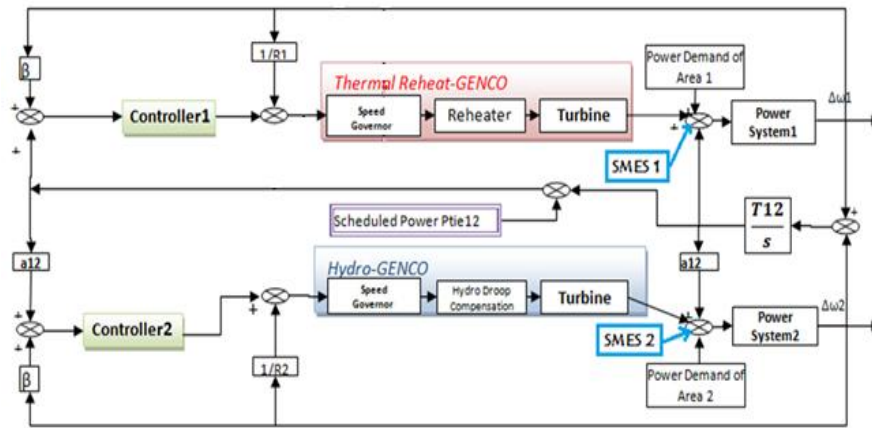


Fig. 1. Complete System model of LFC of Two Area Thermal-Hydro Power System

2.2. Superconducting Magnetic Energy Storage

SMES as energy storage system can charge and discharge very fast with high quantity of power for short span of time. SMES system includes four parts superconducting coil, power conditioning system, refrigeration system and control unit. The power conditioning system incorporates with inverter/rectifier circuit for conversion of AC to DC and vice versa. Charging and discharging of SMES occurs through Power Conditioning System. Refrigeration system maintains superconducting coil below to critical temperature. Control unit is only responsible for mode of operation.

2.2.1. Operating Modes of SMES

Operating mode selection is done by controller based on inter-area oscillation; Area Control Error (ACE) is fed as input signal to SMES control unit. SMES operates in three mode of operation; these are charging, discharging and charge sustain mode. During charging mode superconducting coil is charged to a set value of charge from utility grid. In discharging mode, the stored energy is released. Whenever there is a sudden release in a load then SMES comes to charging mode and it immediately gets charged towards full value. As soon as system returns to steady state SMES returns to charge sustain mode[5], [6].

2.2.2. SMES Modeling

SMES is ready to use for LFC, once rated current reached in SMES coil. The ACE_i is controller input of SMES unit and U_{smi} is controller output. Controller output applied to converter and converter output applied to SMES coil, as described below:

$$\Delta V_{sm}(s) = \frac{1}{1+sT_{dc}} U_{smi}(s) - \frac{K_{sm}}{1+sT_{dc}} \Delta I_{sm}(s)$$

And as the voltage applied to SMES coil, the deviation of coil current, as per below:

$$\Delta I_{sm}(s) = \frac{1}{SL} \Delta V_{sm}(s)$$

Finally, deviation of active power output of SMES unit is described as:

$$\Delta P_{sm} = (I_{sm0} + \Delta I_{sm}) \Delta V_{sm}$$

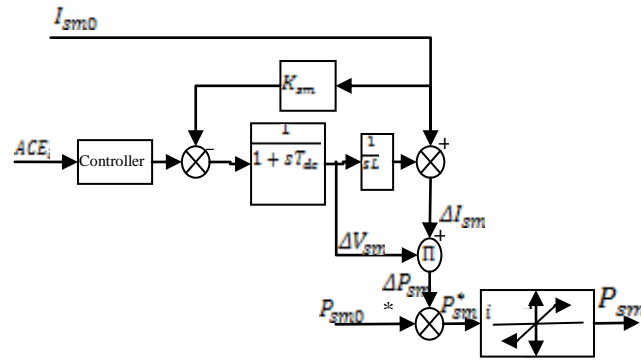


Fig. 2. SMES Unit

3. CONTROL STRATEGY FOR FREQUENCY CONTROL

In this paper, PID controller is selected as controller for LFC. Following tuning and optimization methods are used for selection of gain parameters. PID controller for LFC, in which ACE_i selected as controller input and K_p , K_i and K_d are gains of controller and U_{pid} is output of controller.

$$U_{pid} = K_p(ACE_i) + K_i(\int ACE_i dt) + K_d\left(\frac{dACE_i}{dt}\right). \quad (3)$$

In this paper, PID controller's gain values for LFC are obtained from Zigler Nicholas tuning method and genetic algorithm based stochastic optimization method respectively.

3.1. Zigler Nicholas Tuning

Zigler-Nicholas (ZN) tuning method is a heuristic type approach for PID Controller. This method is based on selection of proportional gain to get sustained oscillation, from which ultimate gain K_u and oscillation period T_u are obtained [7]. In this method, proportional controller is taken as controller and proportional gain value is selected as for which sustained oscillation occurs, this value of proportional gain is called ultimate gain K_u and time period T_u of output response is called oscillation period. PI or PID controller gains can be tuned with formulas based on K_u and T_u . Here PID controller gains are calculated from formulas as shown in Table 1.

Table 1. PID Controller Gains from ZN tuning method

	ZN Tuned PID	Area-1PID Gains	Area-2 PID Gains
K_p	0.6 Ku	1.074	1.074
K_i	2 Kp/Tu	0.74	0.74
K_d	KpTu/8	0.389	0.389

3.2. Genetic Algorithm

GA is stochastic search/optimization algorithm based on natural genetics mechanics, capable of finding optimal solution. This optimization is an iterative procedure, in which every iteration constant population size is maintained [8]. GA utilized different genetic operators for improve the fitness of individual of population solution. These genetic operators are selection, crossover, mutation and elite respectively. By utilizing these genetic different operators, GA improves the fitness of individual population solution. Initially fixed number of random solutions will be generated, and then in next iterations by genetic operators new population of same numbers of solution of improved fitness will be generated. At selection process, the each solution of population is evaluated by its fitness value, which is provided by user defined objective function. In crossover process the pairs of selected solution will be selected by a defined method to generate new solutions. In mutation process the selected solution's is randomly altered with a small probability, this process will help to prevent the GA being trapped in local optimal solution.

Objective function for PID optimization is based on minimization of Integral of Absolute Error (IAE). IAE is an error function, minimization of this function ensure less deviation, smooth and fast response. This objective function selected for GA, is:

$$J_{IAE} = \int_0^T (|ACE_{area-1}| + |ACE_{area-2}|) dt. \quad (4)$$

Here, T is selected 30 sec for present system.

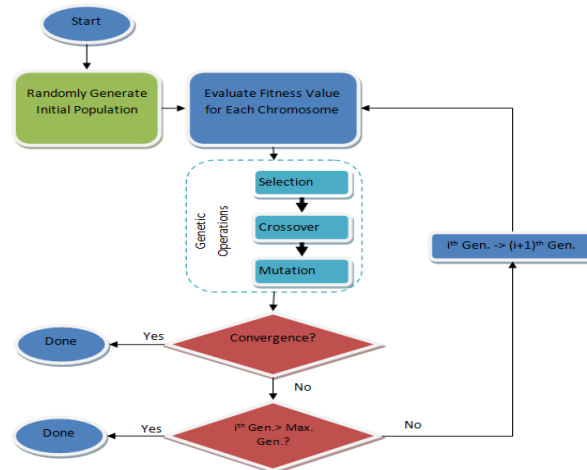


Fig. 3. GA Flow Chart

Table 2. PID Controller gains from GA optimization method

S.N.			Area-1PID Gains	Area-2 PID Gains
1.	<i>GA optimized PID Controller Gains</i>	K_p	1.6823	0.770119
		K_i	1.44188	0.891877
		K_d	0.66441	0.165158

4. FUZZY LOGIC CONTROLLER OPTIMIZED BY GA

4.1. Design of FLC

The FLC modeling consists of three steps i.e. fuzzification, formation of fuzzy control rule base and defuzzification. In the process of fuzzification, input and output variables crisp values converted into linguistic values. The control actions of a FLC are described by sets of linguistic rules. A dual input and single output type FLC is designed for SMES control. These two inputs are ACE_i and $dACE_i/dt$ and one output is U_i for each control area, as shown in Fig. 4. Mamdani type fuzzy logic design is used for FLC design [9], [10]. There are 3 triangular and 2 trapezoidal type membership functions are considered for both inputs, as shown in Fig. 5.



Fig. 4. FLC for SMES Control

Table. 3 presents the view of rules for FLC utilized to design controller. In rule base 25 rules are designed to get the desired response. There are two scaling factors (K_e & K_{ce}) for both input variables (ACE_i , $dACE_i$) respectively and two gain factors K_{pu} & K_{iu} as proportional and integral gains respectively.

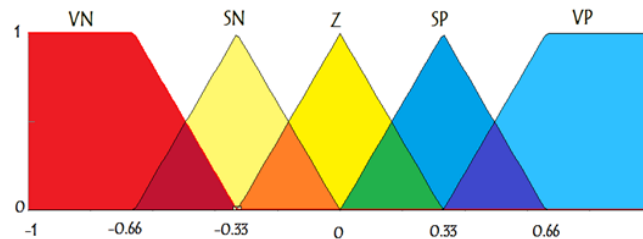


Fig. 5. Membership Functions for input and output variables

Table 3 Rule Base for FLC Controller

	ΔACE					
	VN	SN	Z	SP	VP	
ACE	VN	VN	VN	SN	SN	Z
	SN	VN	SN	SN	Z	SP
	Z	SN	SN	Z	SP	SP
	SP	SN	Z	SP	SP	VP
	VP	Z	SP	SP	VP	VP

VN: Very Negative SN: Small Negative Z: Zero
SP: Small Positive VP: Very Positive

4.2. Optimization of FLC

Optimization of FLC composed of four steps, these are scaling factors optimization, membership functions parameters optimization, rule base optimization and rules weight

optimization respectively. Here GA used for find out optimum values in each step and IAE is selected as objective function for same shown in (4). Matlab/Simulink tool have used for optimization.



Fig. 6. Optimization Process of Fuzzy Logic Controller

After scaling factors optimization, optimum values of scaling and gain parameters are shown in Table 4.

Table 4. Optimum Value of Scaling and Gain Parameters

	Scaling Parameters		Gain Parameters	
	K_e	K_{ce}	K_{pu}	K_{iu}
FLC for Area-1	2.463	2.296	1.792	1.982
FLC for Area-2	1.784	0.111	0.066	0.546

5. RESULTS & DISCUSSIONS

In this paper, optimized FLC Controller is used for LFC for both of areas. New optimization approach is proposed for complete optimization of FLC. The optimization approach is executed in four steps using GA, the best fitness found after every iteration in these step is shown in Fig. 7, 8, 9 and 10 respectively. The dynamic performance of proposed controller compared with ZN tuned PID, GA optimized PID and partially optimized FLC. Frequency deviations of both areas and tie line deviation after a sudden load change of 0.01 p.u. in each area to observe combined impact of thermal as well as hydro power system are shown in Fig.11. Results show that GA optimized FLC is more effective to damp out oscillations. In order to minimize frequency deviation and tie-line deviation the effect of SMES support is also examined with proposed controller, shown in Fig. 12. A comparative analysis is also carried out between LFC without SMES support with ZN tuned PID, GA optimized PID controller, partially optimized FLC and proposed GA optimized FLC and proposed GA optimized FLC with SMES support, as shown in Table 5.

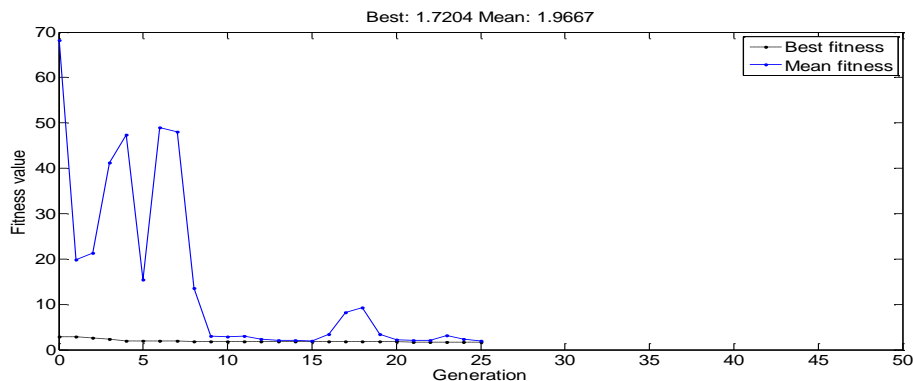


Fig. 7. GA optimization for scaling factor of FLC

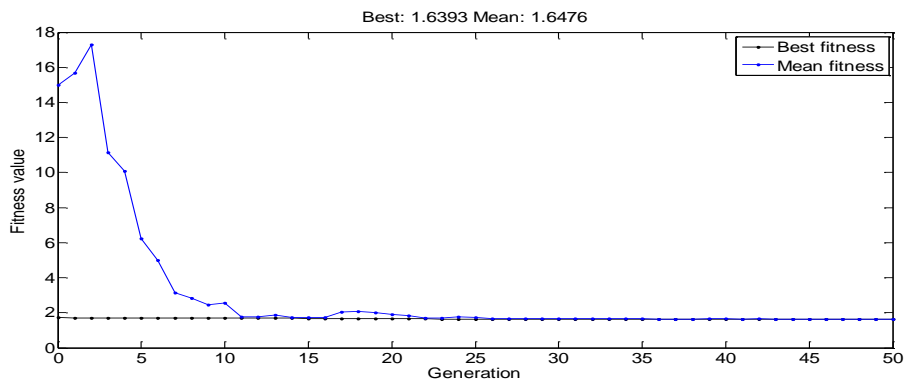


Fig. 8. GA optimization for MF's parameters of FLC

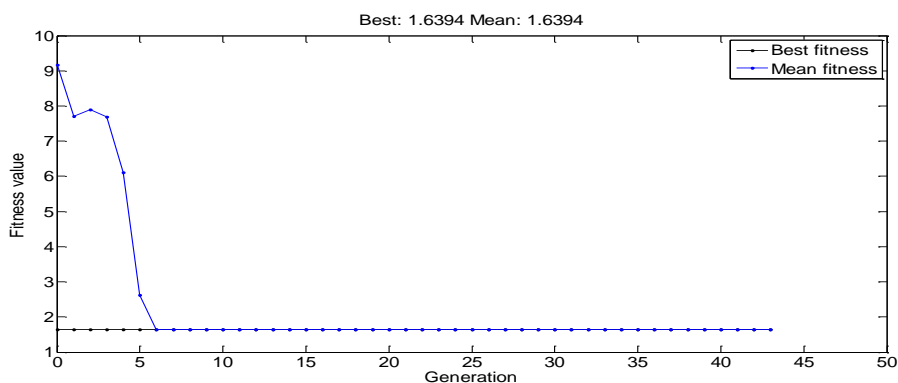


Fig. 9. GA optimization for rule base of FLC

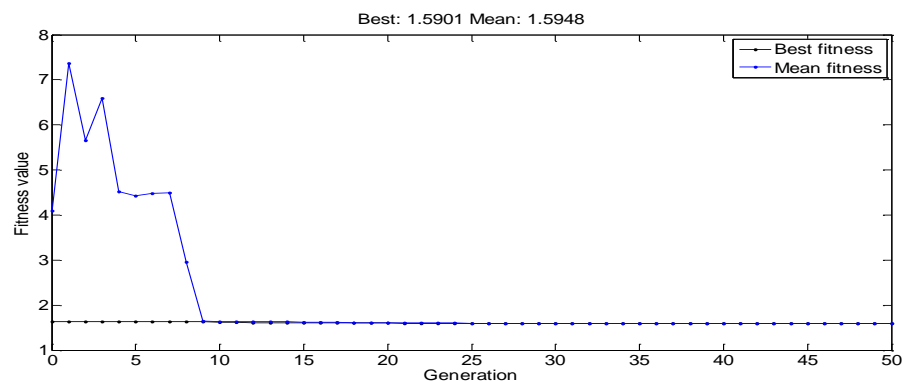
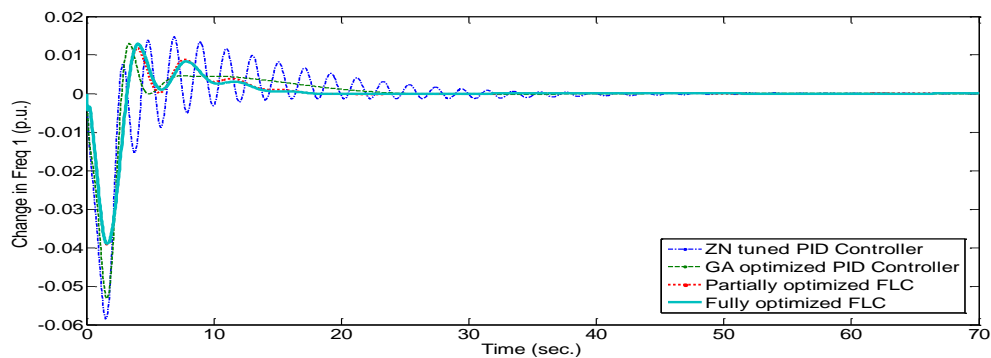
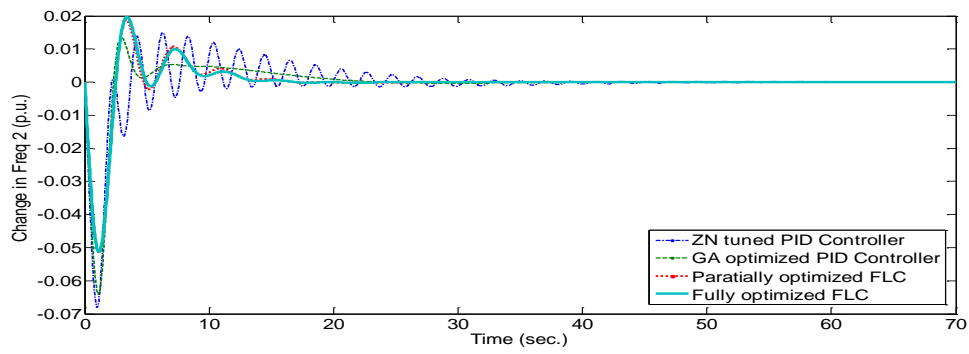


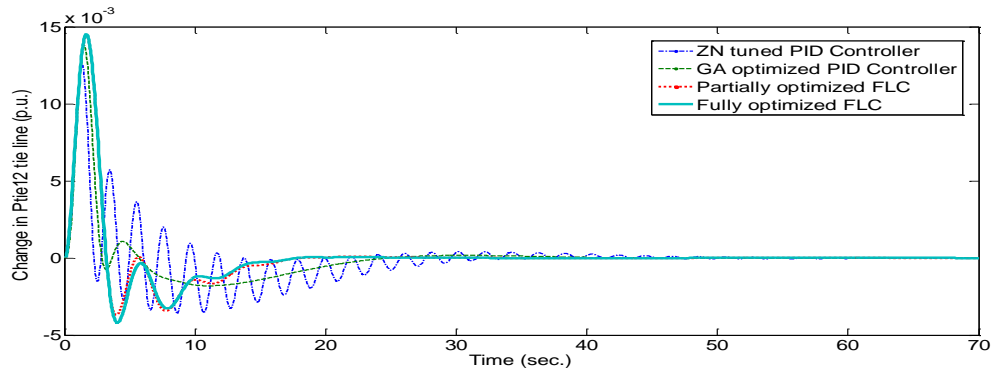
Fig. 10. GA optimization for rules weighting factor of FLC



(a)

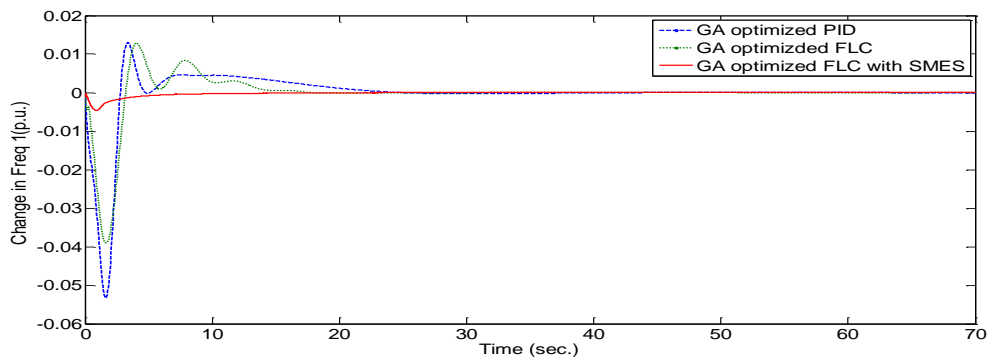


(b)

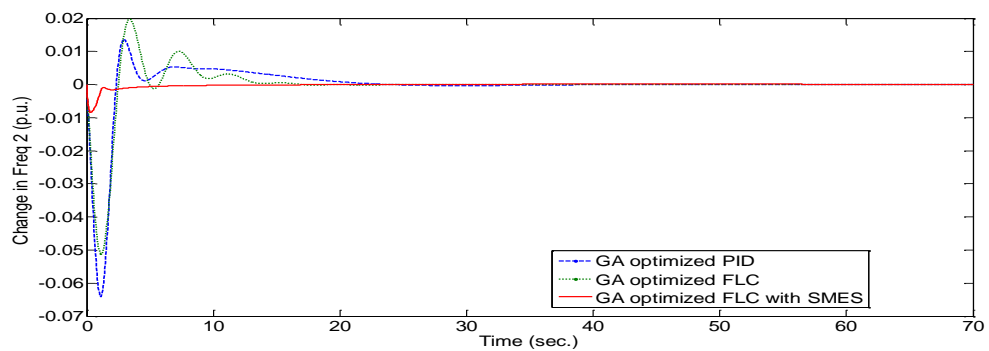


(c)

Fig. 11. Comparison of ZN tuned PID, GA optimized PID, Partially optimized FLC and Fully optimized FLC for two area thermal-hydro power system (a) Δf_1 , (b) Δf_2 , (c) ΔP_{tie12}



(a)



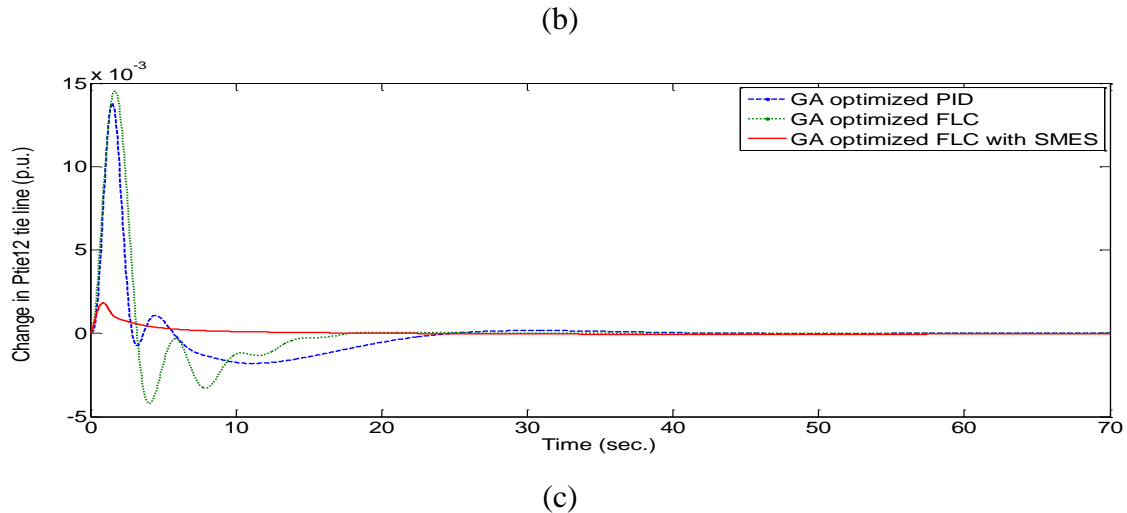


Fig. 12. Comparison of LFC with GA optimized PID, GA optimized FLC and GA optimized FLC with SMES support (a) Δf_1 , (b) Δf_2 , (c) ΔP_{tie12}

Table 5 Comparison of Performance Indices of Δf_1 , Δf_2 and ΔP_{tie12} for different control strategies

		<i>ZN tuned PID Controller</i>	<i>GA optimized PID Controller</i>	<i>GA based Partially optimized FLC</i>	<i>GA based Fully optimized FLC</i>	<i>GA based Fully optimized FLC with SMES</i>
<i>Peak Under Shoot</i>	<i>Frequency of Area-1</i>	0.058541	0.053201	0.039216	0.038982	0.004596
	<i>Frequency of Area-2</i>	0.068018	0.064058	0.051348	0.051284	0.008396
	<i>Tie-line Power</i>	0.003592	0.001806	0.003705	0.004192	0.000061
<i>Settling Time ($\pm 5\%$)</i>	<i>Frequency of Area-1</i>	42.799698	22.262673	16.616575	16.305584	6.722792
	<i>Frequency of Area-2</i>	40.301705	21.305733	15.934718	15.745766	5.853890
	<i>Tie-line Power</i>	27.160380	20.210720	14.295822	13.636988	3.517297

6. CONCLUSION

In this paper, GA based optimization method for FLC is proposed for LFC and it is examined with tuned and optimized conventional PID controller for LFC of interconnected thermal-hydro power systems. Results of simulation show that proposed optimized FLC provides a better performance compared to ZN tuned PID controller, GA optimized PID and partially optimized FLC. Frequency stabilization method is proposed using SMES support as well. A comparative study is also carried out between proposed optimized FLC with SMES support and other control mechanism without SMES support. The simulation results shows that proposed optimized FLC controller with SMES provides less peak undershoot and less settling time in frequency variation in both areas as well as less dip in tie-line power variation.

REFERENCES

- [1] CAM E. and KOCAARSLAN I. "Load frequency control in two area power systems using fuzzy logic controller," *Energy Convers. Manag.*, Vol. 46, p. 233–243, 2005.
- [2] MATHUR H.D. and MANJUNATH H., "Frequency stabilization using fuzzy logic based controller for multi-area power system," *South Pacific J. Nat Sci*, p. 22–29, 2008.
- [3] CHOWN G. and HARTMAN R. "Design and experience with a fuzzy logic controller for automatic generation control (AGC)," *IEEE Trans. power Syst.*, Vol. 13, No. 3, p. 965–970, 1998.
- [4] HEMMATI R., MOJTABA S., BOROUJENI S., DELAFKAR H. BOROUJENI A.S. "Fuzzy load frequency control in multi area electric power system," Vol. 4, No. 7, p. 796–800, 2011.
- [5] TRIPATHY S.C. "Sampled Data Automatic Generation Control with Superconducting Magnetic Energy Storage in Power Syst – Energy Conversion, IEEE Transactions on," Vol. 12, No. 2, p. 187–192, 1997.
- [6] SHEIKH M.I., MUYEEN S.M., TAKAHASHI R., MURATA T., TAMURA J. "Improvement of Load Frequency Control With Fuzzy Gain Scheduled SMES Unit Considering Governor Dead-Band and GRC," No. December, p. 20–22, 2008.
- [7] ZIEGLER J.G., NICHOLS N.B. "Optimum Settings for Automatic Controllers," *Trans. A.S.M.E.*, Vol. 65, No. 5, p. 433–444, 1942.
- [8] GOLDBERG D.E. *Genetic Algorithms in Search, Optimization, and Machine Learning*, vol. Addison-We. 1989, p. 432.
- [9] BHATESHVAR Y.K., MATHUR H.D. "Comparative Dynamic Analysis on Frequency Stabilization for Multi-Area power system in Deregulated Environment," in *2012 IEEE International Conference on Signal Processing, Computing and Control (ISPCC)*, 2012, p. 1–6.
- [10] MATHUR H.D., LEITE L.B.F., SIGUERDIDJANE H., BHATESHVAR Y.K. "Study of impact of wind power penetration on frequency stabilization in multi-area power system," in *2013 8Th International Symposium on Advanced Topics in Electrical Engineering (Atee)*, 2013, p. 1–6.

7. APPENDIX:

7.1. Mathematical Modelling of LFC

Speed Governor:	$\frac{1}{(1 + sT_g)}$
Thermal Reheater:	$\frac{(1 + K_r sT_r)}{(1 + sT_r)}$
Thermal Turbine:	$\frac{1}{(1 + sT_t)}$
Hydro Turbine:	$\frac{(1 - sT_w)}{(1 + 0.5sT_w)}$
Power System:	$\frac{K_p}{(1 + sT_p)}$
Hydro Droop Compensation:	$\frac{1 + sT_r}{1 + s(R_t/R_p)T_r}$



7.2. Parameters of Hydro Thermal System Investigated:

$$P_{r1} = P_{r2} = 2000 \text{ MW};$$

$$K_{p1} = K_{p2} = 120;$$

$$T_{p1} = T_{p2} = 20;$$

$$R_1 = R_2 = 2.4;$$

$$T_{12} = 0.545;$$

$$T_w = 1; T_t = 0.3;$$

$$T_{g1} = 0.08; T_{g2} = 0.02;$$

$$T_r = 5; R_t = 0.38; R_p = 0.05;$$

$$\beta = 0.425; a_{12} = 1.$$

IMPACT OF PELTIER ELEMENT SUPPLIED POWER CHARACTERISTICS ON SHORT TERM COOLING PERFORMANCE

V. Jurkans

*Institute of Radio Electronics
Riga Technical University
Azenes 12, Riga, LV-1048 – Latvia*

J. Blums

*Institute of Technical Physics,
Riga Technical University
Azenes 14, Riga, LV-1048 – Latvia*

ABSTRACT

Peltier elements are widely used in various applications all over the world. Nonetheless a lot of different opinions occur when speaking about how the properties of supplied electrical energy influence the short term performance of Peltier elements and how these elements should be driven. Various sources suggest different approaches and there is a lot of discussion if Peltier elements can be driven with pulse width modulated current or direct current should be used. There is recommendation to not exceed 10% ripple of supplied DC Voltage, but there exists other point of view that pulsed nature of electrical power can be ignored if high frequency pulses are used. Series of experiments were made to find out how does the pulse width, frequency and pulsations of direct current affect the heat conduction ability of Peltier element based cooling system. Dependences are presented and compared to theoretical analysis. Study discusses optimal characteristics for supplied electrical power that is required for reasonable operation.

Keywords: Peltier element, Efficiency, Power Management, Cooling Performance

1. INTRODUCTION

Peltier elements are gaining popularity as very versatile cooling device. They are easy to use as they only require electrical power source to work as a heat pump. Cooling systems based on Peltier effect have no moving parts.

The technology does not require any chlorofluorocarbons or other fluid that may need to be replaced can achieve temperature control to within $\pm 0.1^\circ\text{C}$, is electrically quiet in operation. The modules are relatively small in size and weight and do not import dust or other particles which may cause an electrical short circuit [1].

Development of high density, high power, and high efficiency of electronic components enhances the system efficiency but accompanies with heat dissipation problems. Dramatically increasing heat flux may result in the failure of electronic component or the decrease in efficiency and reliability of system. Therefore, an efficient cooling method is highly desirable to precision electronic components [2].

Nowadays all the electronic devices and systems are pushed to be as small as possible. Technology allows minimizing the size of semiconductor devices and microchips. Although passive components tend to shrink in size they can require relatively high amounts of space in device. There are bunch of solutions to exclude or minimize the use of inductors, as they can be most volume demanding component. For example – charge pump devices, filterless D-class amplifiers, etc.

Peltier elements are mostly used with switching power regulator. It is pretty easy and efficient way to change power that is supplied to cooling device. Simplest regulators require at least 2 reactive components – inductor and capacitor.

Alternative way to regulate supplied power is using unfiltered pulses as it is often done with electromotors and heaters. A lot of recommendations suggest using direct current with minimal ripple/pulsations. Recommendation states: AC power will degrade the operational performance of the thermoelectric modules. The power supply should have a small ripple voltage (maximum of 10% of full output) [3]. 10% ripple of supplied power is pretty common rule of thumb.

Some studies show that pulse current can enhance thermoelectric cooling for a short period of time and enable to offer a sudden over-cooling and strong transient heat pumping capacity compared to the steady state optimum [4].

The present work investigates the impact of unfiltered pulsed electrical power on Peltier element cooling performance, trying to find out if it is possible to maintain effective cooling without using any filtering.

2. THEORETICAL MODEL

If Peltier element has power supply that uses pulsed current, performance of it can be divided into two periods:

1. Cooling state;
2. Stand by state.

In cooling state Peltier element works as it would work if it would be supplied with direct current. Heat that is transported from the cold side of Peltier element (Q) during cooling state depends on three factors:

1. Peltier effect:

$$Q = S \cdot I \cdot T_{mean}, \quad (1)$$

where Q – heat transported from the cold side of Peltier element, S - Seebeck coefficient, I – current that flows through Peltier element, T_{mean} – mean temperature of Peltier element.

2. Joule heating:

$$Q = -\frac{1}{2} \cdot I^2 \cdot R, \quad (2)$$

where Q – heat transported from the cold side of Peltier element, I – current that flows through Peltier element, R – Ohmic resistance of semiconductor in Peltier element.

3. Heat backflow:

$$Q = -\frac{T_h - T_c}{\Theta}, \quad (3)$$

where Q – heat transported from the cold side of Peltier element, T_h and T_c – hot and cold side temperatures of Peltier element, Θ – thermal resistance between hot and cold side of Peltier element.

During stand by state only heat backflow applies to the heat balance of cold side of Peltier element.

Time diagram of pulsed current cooling is shown in Fig. 1. It shows momentary supplied power P_x , average supplied power \bar{P} , duty cycle of current pulse $D = 0 \div 1$,

pulsation period t_p . Q_{c1} and Q_{c2} stands for heat at cold side of Peltier element during cooling and stand by state.

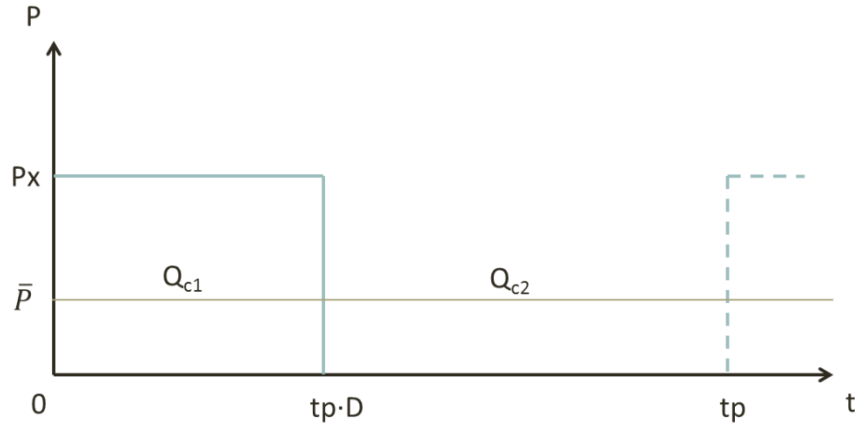


Fig. 1. Time diagram of pulsed cooling with Peltier element

It is important to understand that if average power \bar{P} is constant at every value of duty cycle, momentary power of the pulse Px increases as duty cycle decreases to maintain the same amount of energy in one pulse. Both powers can be described with following equations:

$$\bar{P} = \frac{E}{t_p} = \text{const}; \quad Px = \frac{\bar{P}}{D}; \quad (4)$$

Therefore current of one pulse Ix will be:

$$Ix = \sqrt{\frac{I}{D}}. \quad (5)$$

So if the duty cycle $D = 10\%$ and average current $I = 1 \text{ A}$, we will have momentary current $Ix = 3.16 \text{ A}$.

Fig. 2 (a) shows how much instantaneous current increase compared to average current, but Fig. 2 (b) shows time diagrams of instantaneous current at different duty cycles.

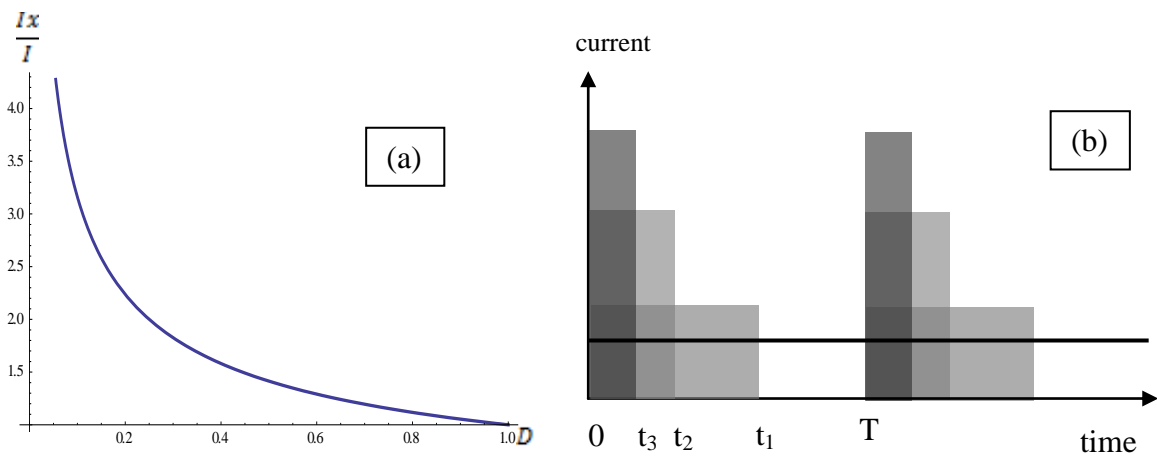


Fig. 2. Momentary current compared to average current

Taking into account equations (1-3) Q_{c1} and Q_{c2} can be described with two equations:

$$Q_{c1} = S \cdot Ix \cdot T_{mean} - \frac{T_h - T_c}{\Theta} - \frac{1}{2} \cdot Ix^2 \cdot R \quad (6)$$

$$Q_{c2} = -\frac{T_h - T_c}{\Theta} \quad (7)$$

If we assume that current can be substituted with equation (8), integral that gathers both periods in heat transported from cold side of Peltier element – Q_c , can be written:

$$Ix = \sqrt{\frac{\bar{P}}{R \cdot D}} \quad (8)$$

$$Q_c = \frac{1}{t_p} \int_0^{t_p} (Q_{c1} + Q_{c2}) dt = \frac{1}{t_p} \left(\int_0^{t_p \cdot D} (Q_{c1}) dt + \int_{t_p \cdot D}^{t_p} (Q_{c2}) dt \right) \quad (9)$$

By integrating Eq. (9) we obtain the following equation:

$$Q_c = -\frac{T_h - T_c}{\Theta} - \frac{1}{2} \cdot \bar{P} + D \cdot \sqrt{\frac{\bar{P}}{R \cdot D}} \cdot S \cdot T_{mean} \quad (10)$$

If constant average power is used and duty cycle is the only argument that is being changed, we can assume that Q_c is proportional to square root of duty cycle:

$$Q_c \propto D \sqrt{\frac{1}{D}} = \sqrt{D} \quad (11)$$

Theoretically we should see that heat Q_c increases and cold side temperature T_c of Peltier element decreases as it is shown in Fig. 3.

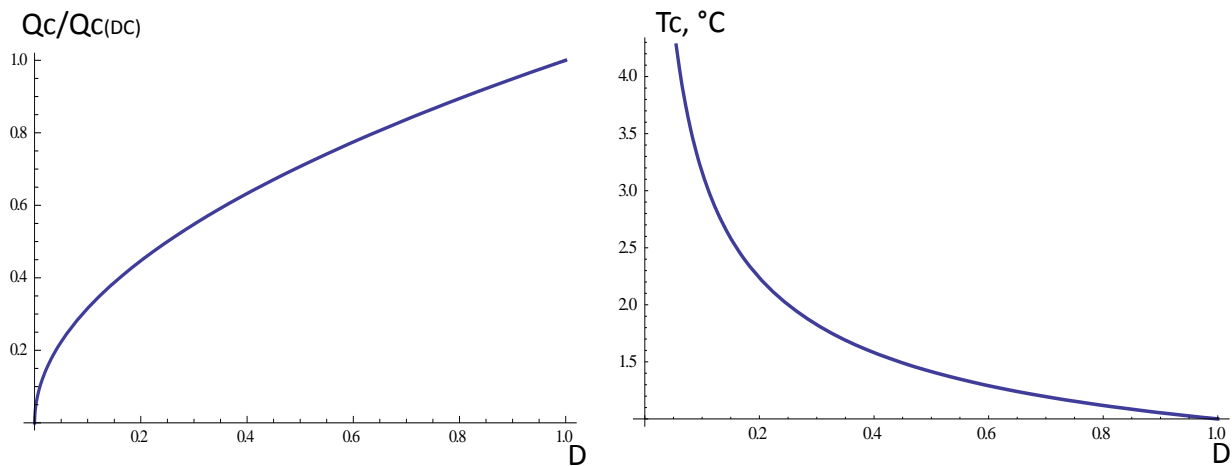


Fig. 3. Theoretically predicted dependence of transported heat from cold side of Peltier element and temperature of cold side in relation to D

There is a problem if we try to describe the Peltier element cooling performance compared to switching frequency. Thermal processes which relates to Peltier element has relatively high thermal inertia so it should not feel any difference between switching frequency as long as it becomes very low. If we talk about frequencies lower than 1Hz it is hard to call it pulsed current. More often this kind of switching refers to thermostatic control which does not include any pulse width modulation. Pulsed current often refers to frequencies in kilohertz range. Main laws that describe thermoelectrical processes do not include any complex components that would cause reactive nature of these processes. So dependence of frequency can only be viewed from electrical perspective. Semiconductors in Peltier element have mostly active impedance. Reactive part in system could be brought by inductance of wires and capacitance of switches and diodes. As frequency is increased different oscillations and delays can occur causing the energy loss.

If we investigate the impact of switching frequency only on the Peltier element it should not feel any difference unless radio frequencies are used.

3. METHODS

To verify the previously described model, experimental setup was set as illustrated in Fig. 4.

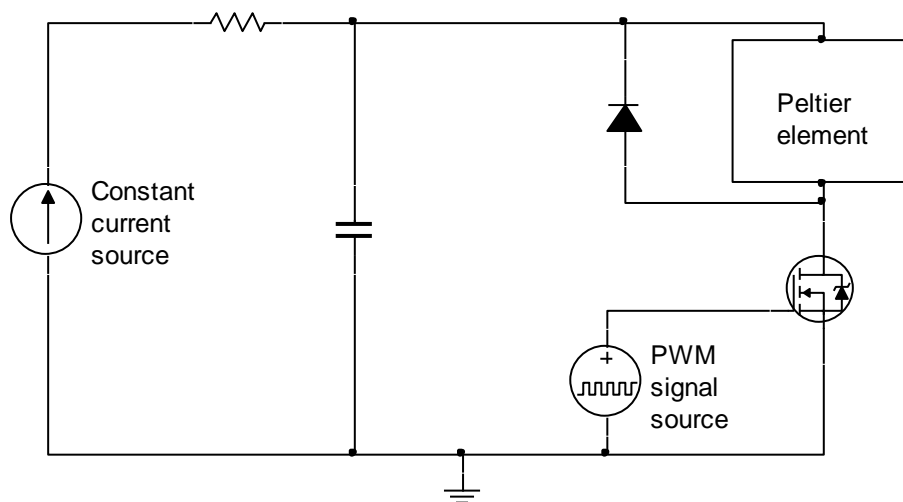


Fig. 4. Schematic of experimental setup

Electrical power is supplied by constant current source which is followed by Resistor-Capacitor filter (RC filter) to keep the average supplied current constant. This filter smoothes the high current pulses that could be felt at the output of current source. Therefore capacitor gives energy required for high current peak at small duty cycles. RC filter is formed with 10 Ω resistor and 10 mF electrolytic capacitor. MOSFET connects the Peltier element to the ground allowing the current flow through it. This flow is controlled by pulse voltage source with changeable pulse width and frequency. Diode in parallel with Peltier element is for minimization of oscillations that can occur due to high frequency switching of load that may have reactive electrical character.

Peltier element is tied to effective heat sink with 0.2 $^{\circ}\text{C}/\text{W}$ thermal resistance and fitted with 6 DS18B20 digital temperature sensors which are placed on both sides of Peltier element. One additional sensor is measuring ambient room temperature. All data is collected with microcontroller and sent to computer for further analysis (see Fig. 5).



Fig. 5. Experimental laboratory setup for Peltier element performance measurements

Cold and hot side temperatures of Peltier element were observed at different duty cycles and frequencies in series of experiments. One pulsed current measurement is 10 minutes long to be sure that temperatures have become stable.

4. RESULTS AND DISCUSSION

First part of experimental series was made using 1A of average current at 40 KHz frequency. This frequency was chosen because frequencies around the 30–50 KHz are often used in power supplies and pulse drivers. This frequency is low enough to bypass radio frequency related problems, such as electromagnetic emissions, skin effect, etc. No parasitic oscillations or peaks were observed during experiment. Duty cycle was changed from 10% to 100% (DC). After collecting all the data, following graph can be drawn (Fig. 6).

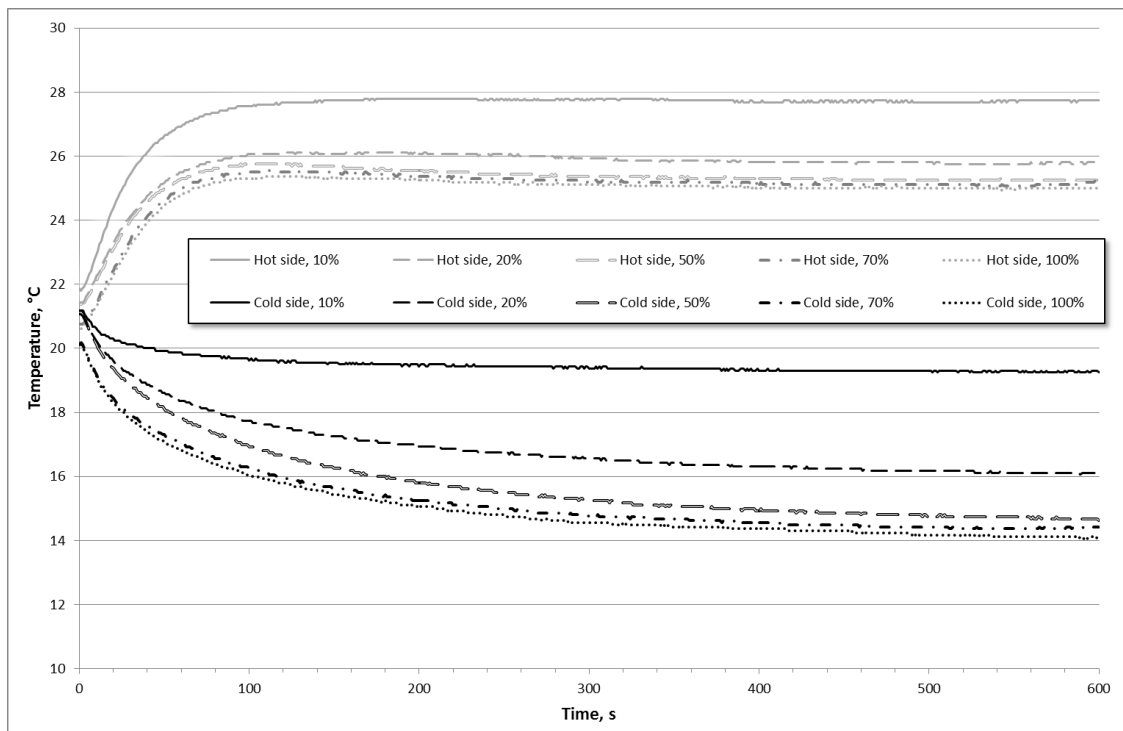


Fig. 6. Time diagrams of experiment

As we can see the process becomes stationary in the course of measurement. Fig. 6. gathers five different duty cycles. Lines that stand out the most are at 10% and 20% duty cycle. If we look at the 10% line we can see that a lot of excess heat is generated as hot side of Peltier element becomes 2°C warmer than in other cases. Cold side shows that almost none of the heat is transported away from cold to hot side. As we move towards direct current (duty cycle = 100%) results become more similar to each other.

As hot side temperature changes, the comparison of performance is showed as temperature difference between hot and cold sides of Peltier element (Fig. 7).

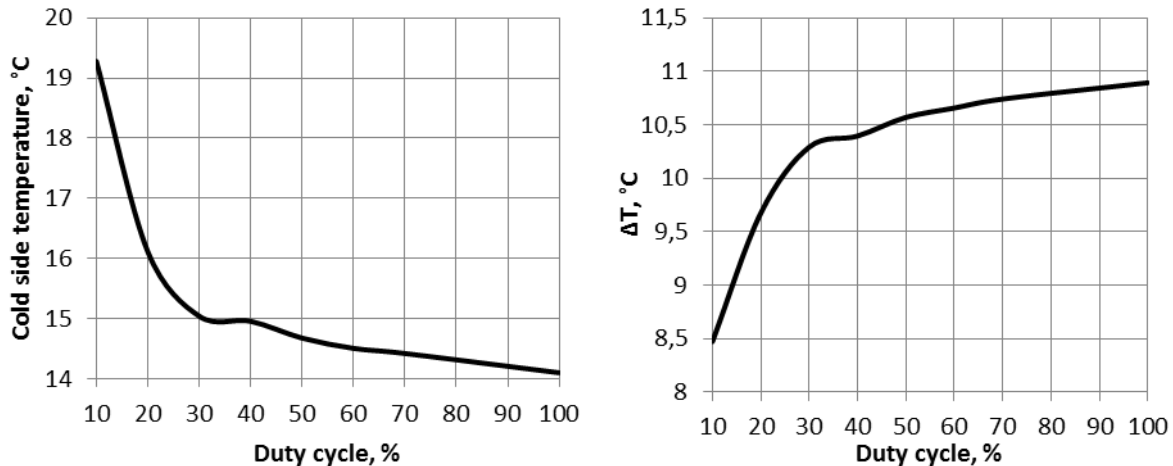


Fig. 7. Cold side temperature and temperature difference between hot and cold side of Peltier element at different duty cycles. Average current is 1A

As we can see cold side temperature falls for about 4 °C if we change duty cycle from 10% to 30% (Fig. 7). Change in performance has square root function just as in theory.

If we change the average current to 0.5A we can see a little bit different picture (Fig. 8). Cold side temperature is decreasing more linearly. Temperature difference still looks as a function of square root, but change in measurements is very small and can be compared to measurement uncertainty. We can see that performance change between 10% and 100% duty cycle could be about 5%. Experiment with 1A had about 20–25% of loss in temperature difference.

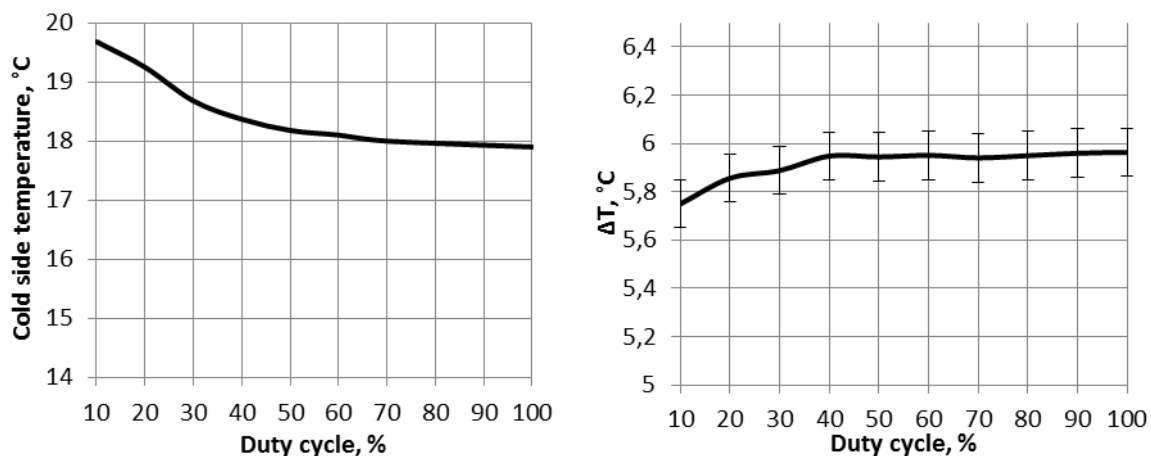


Fig. 8. Cold side temperature and temperature difference between hot and cold side of Peltier element at different duty cycles. Average current is 0.5A

If we return to mathematical model, equation (10) shows that only efficiency of Peltier effect is being changed by duty cycle. Peltier effect is responsible for temperature difference. However cold side temperature depends on the Joule heating, thermal resistance of radiator, thermal conduction between hot and cold side of Peltier element and other parameters too. Therefore we cannot find certain universal point of fast decrease in cooling performance for all situations.

We can try to describe situation from ripple current point of view. Ripple current is amplitude of AC component that persists in DC current. Ripple current can be related to duty cycle using equation (8).

Therefore ripple current is:

$$\frac{I_{AC}}{I_{DC}} = \frac{0.5 \cdot I(D)}{I(100\%)} = \frac{\sqrt{\frac{\bar{P}}{R \cdot 2D}}}{\sqrt{\frac{\bar{P}}{R}}} = \frac{1}{\sqrt{2D}} \quad (12)$$

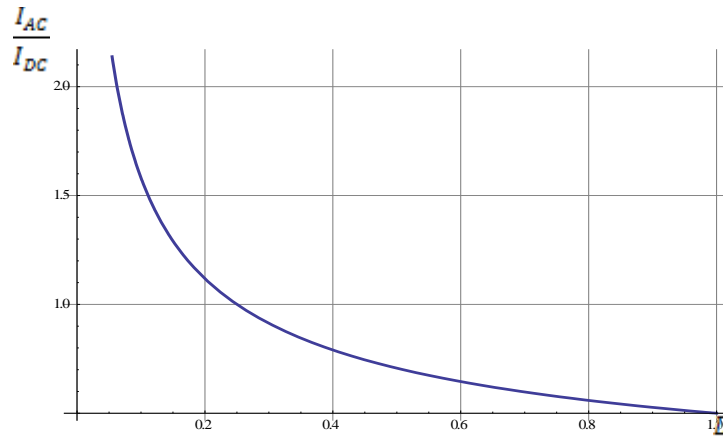


Fig. 9. Amount of ripple current in signal relative to DC

10% ripple current is analog to about 95% duty cycle. If we return to Fig. 7 and Fig. 8 we can see that such changes really ensure negligible change in resulting performance. On the other hand if we look at these experimental results, we can conclude that there is a minimal change in performance even if we move to 50% value. However this conclusion may not apply to all the cases.

To investigate the impact of pulsation frequency on Peltier element short term performance, it was decided to choose 1A of average current and 50% duty cycle. The frequency was changed from 1 Hz to 100 KHz. To provide stable current values at frequencies lower than 100 Hz, RC filter was bypassed and value of current pulse was set to 2A manually.

Experimental results can be seen in Fig. 10.

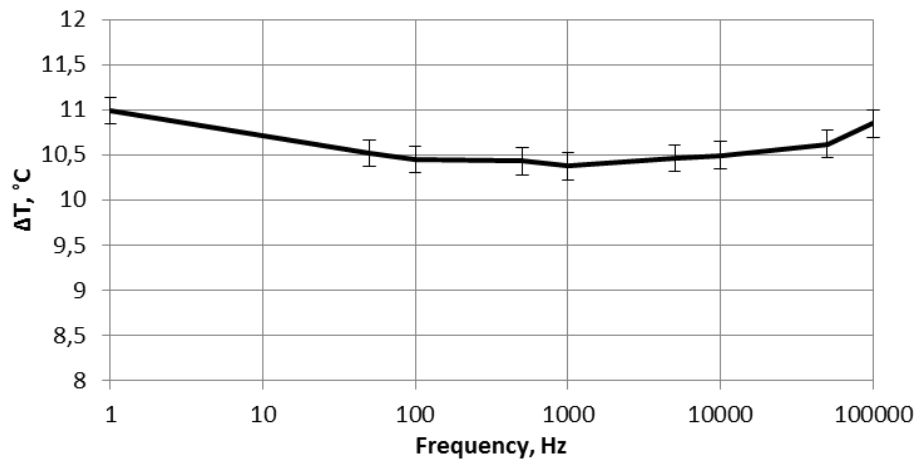


Fig. 10. Temperature difference of hot and cold side of Peltier element at different frequencies

As we can see, changes in performance are minimal. No certain rule can be applied to this case as the deviation of values is about $0.25\text{ }^\circ\text{C}$, which could be some slight change in ambient parameters. Therefore experiment shows that frequency of supplied pulsed current does not impact performance of Peltier element significantly although there could be problems with parasitical parameters of circuit (inductance of wires and capacitance of switches and diodes) as frequency is increased.

5. CONCLUSION

Impact of Peltier element supplied power characteristics on short term cooling performance has been investigated. Theoretical analysis was carried out in order to find factors that influence cooling performance when using pulsed current power supply. It has been found that heat transported from cold side of Peltier element is proportional to square root of duty cycle. This dependence was verified experimentally. Study shows that unfiltered pulse width modulation can be used without significant performance losses if duty cycle is not lower than 50%. It was observed that performance is less influenced if small average current is used. Although change in performance depends on specific factors for each individual cooling system, study shows that pulsed power supply can be effectively used for Peltier elements thus potentially decreasing space and cost of thermoelectric cooling devices.

REFERENCES

1. GOULD, C.A., SHAMMAS, N.Y.A., GRAINGER, S., & TAYLOR, I. (2011). Thermoelectric cooling of microelectronic circuits and waste heat electrical power generation in a desktop personal computer. *Materials Science and Engineering: B*, 176(4), p. 316–325.
2. DU, C. Y., & WEN, C. D. (2011). Experimental investigation and numerical analysis for one-stage thermoelectric cooler considering Thomson effect. *International Journal of Heat and Mass Transfer*, 54(23), p. 4875–4884.
3. Thermoelectric Handbook. Laird Technologies, 2010. [referred on the 11th of November in 2013]. Link to the internet < <http://www.lairdtech.com/temhandbook/> >
4. BAR-COHEN, A. (Ed.). (2012). *Encyclopedia of Thermal Packaging*. World Scientific.

OPTIMIZATION OF THE MECHANICAL DRAFT COOLING TOWER PERFORMANCE

A.A. Brin

*A.V. Luikov Heat and Mass Transfer Institute
National Academy of Sciences of Belarus
15, P. Brovki St., 220072, Minsk – Belarus*

ABSTRACT

A new mathematical model of a mechanical draft cooling tower performance has been developed. The model represents a boundary-value problem for a system of ordinary differential equations, describing a change in the droplets velocity, its radiuses and temperature, and also a change in the temperature and density of the water vapour in a mist air in a cooling tower. The model describes available experimental data with an accuracy of about 3 %. For the first time, our mathematical model takes into account the radiuses distribution function of water droplets. It was shown that the average cube of the droplet radius practically determines thermal efficiency. The relative accuracy of well-defined monodisperse approximation is about several percents of heat efficiency of the cooling tower. A mathematical model of a control system of the mechanical draft cooling tower is suggested and numerically investigated. This control system permits one to optimize the performance of the mechanical draft cooling tower under changing atmospheric conditions.

Keywords: cooling tower, evaporative cooling, mechanical draft, simulation, optimization

1. INTRODUCTION

Mechanical draft cooling towers are widely used in industry for deep cooling of circulating water [1]. The height of the mechanical draft cooling towers can vary from 2 to 12 meters. Basic elements of such cooling towers are shown in Fig. 1: the shell, water distribution system, water collection basin and the fan to create an artificial draft.

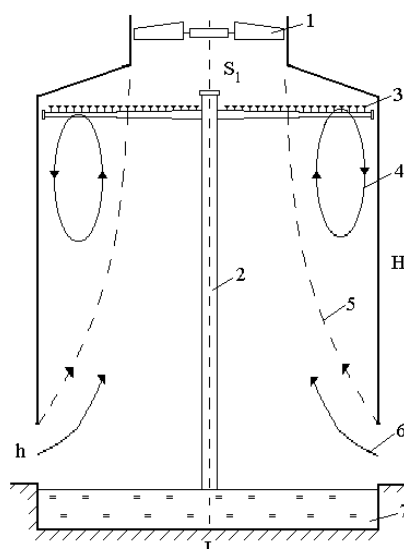


Fig. 1. Scheme of the mechanical draft cooling tower: 1 – fan; 2 – pipeline; 3 – water distribution system with spraying nozzles; 4 – stagnant zone; 5 – edge of stagnant zone; 6 – entering air; 7 – water collection basin

In this paper we consider the heat and mass transfer processes in a mechanical draft cooling tower, where only a water droplet flow takes place, and there are no jet or film flows. In our previous publications, we considered only monodisperse ensemble of droplets [2, 3]. In the cooling tower a polydisperse ensemble of droplets is formed by nozzles, which spray water [4]. In this work, the size distribution of droplets and elements of two-dimensional aerodynamics of a mechanical draft cooling tower are taken into account. This allows one to explain a variety of experimental data.

Although in industry the cooling towers with rather wide distribution of droplet radiuses are used, in the vast majority of simulations of evaporative cooling the approximation of monodisperse ensemble of droplets is used. Our new approach allows one to determine the limits of applicability of this approximation for the problems of evaporative cooling. For simulation of evaporative cooling of water in the mechanical draft cooling tower, we use the results obtained for a natural draft cooling tower [5]. The solution of a boundary-value problem for two phases moving in the opposite directions gives a complete description of evaporative cooling of droplets. As droplets fall down, the water evaporates and convective heat transfer with a colder air occurs. With increase in the velocity of droplets, the time of interaction with a colder air is reduced. On the other hand, as air ascends it is heated and saturated with water vapor. This reduces the intensity of heat and mass transfer of droplets during evaporative cooling.

In a one-dimensional approximation, the average air velocity u is considered constant over the height and section. The air flow velocity u is determined by the fan power and the total aerodynamic drag. In contrast to natural draft cooling towers, where the velocity of convection depends on the degree of air heating and its saturation of it with water vapor.

In a cooling tower the processes of heat and mass transfer depend on the specific mass flow rates of water Q_w and air Q_a , temperature T_{a0} and relative humidity ψ of the air entering into the cooling tower, temperature of the hot water T_{w0} entering into the cooling tower, wind velocity and atmospheric pressure.

We characterize the efficiency of evaporative cooling by means of the dimensionless parameter η :

$$\eta = \frac{T_{w0} - T_{wf}}{T_{w0} - T_{\lim}}, \quad (1)$$

where T_{wf} is an average temperature of the cooled water in the basin of the cooling tower, T_{\lim} is a limiting temperature of evaporative cooling of water for the given air temperature T_a and its relative humidity ψ . The value of T_{\lim} is equal to the wet-bulb temperature and is obtained from the condition:

$$\rho_s(T_a) \cdot \psi = \rho_s(T_{\lim}), \quad (2)$$

where ρ_s is a density of saturated vapor, dependent on temperature and T_a is the temperature of the neighboring cooling tower air.

We note that in the case of monodisperse distribution of droplets the average water temperature T_{wf} coincides with the final temperature of the droplets. When the size distribution of droplets and nonuniformity of air flow in the cooling tower are taken into account, the calculation of the water average temperature in the pool is rather a complex problem.

2. MATHEMATICAL MODEL

For a mathematical model of evaporative cooling of droplets, it is important to know the distribution of the radiuses of the droplets. In a mechanical draft cooling tower droplets are formed by water spraying nozzles. The radiuses of droplets depend on the water flow rate and water temperature in the cooling tower: the larger the water flow rate, the smaller sizes of droplets because of the higher pressure drop in the nozzles. The water temperature affects the surface tension, which substantially determines the character of water spraying. Our calculations show that the dependence of the radius of droplets on hydraulic loading is determined by design features of the spraying nozzle and is not connected with breaking of droplets. Even at the maximum hydraulic load of the cooling tower droplets velocities at nozzle exit are insufficient for their breaking.

In a counter-current cooling tower of any type the maximum and minimum radiuses of droplets are determined, correspondently, by splitting of large droplets and carrying away of small droplets by an air flow. The maximum radius of the droplet falling with the relative velocity v in a humid air flow is determined from the condition of equality of the drag force and surface tension force. Droplets with radius R are not broken, if the following inequality is valid:

$$R \leq 2.3 \frac{\sigma}{\rho_a u^2}, \quad (3)$$

where σ is the surface tension of water, ρ_a is an air density. We note that with increase in the temperature the surface tension of water decreases. The minimum size of the droplets participating in the process of evaporative cooling depends on an upward air flow velocity u . If the drag force due to relative motion of a droplet and air is larger than the gravity, which is valid for rather small droplets, they are carried away by the ascending air flow.

In Fig. 2 the range of possible radiuses of water droplets falling in a mechanical draft cooling tower is shown versus the upward air flow velocity u .

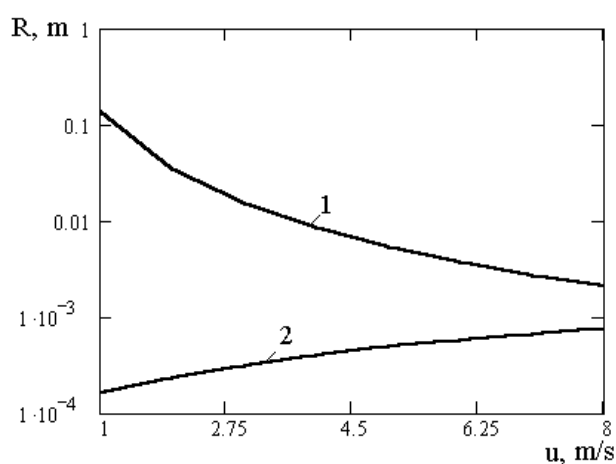


Fig. 2. Possible range of droplets radiuses versus upward flow air velocity:
curve 1 – maximum possible droplets radius; 2 – minimum

The curve 1 corresponds to the largest possible radiuses of droplets, which are found from Eq. (3), and curve 2 is for minimally possible radiuses. As seen from Fig. 2, in the mechanical draft cooling tower the droplets have the radiuses with values between curves 1 and 2. If the radius of a droplet is in the area above curve 1, such a droplet is broken up by air

flow; the droplet is carried away by upward air flow from the cooling tower if the radius of the droplet is in the area below curve 2.

In the case of a polydisperse ensemble of droplets, we have to deal with some size distribution function of droplets as it is shown in Fig. 3.

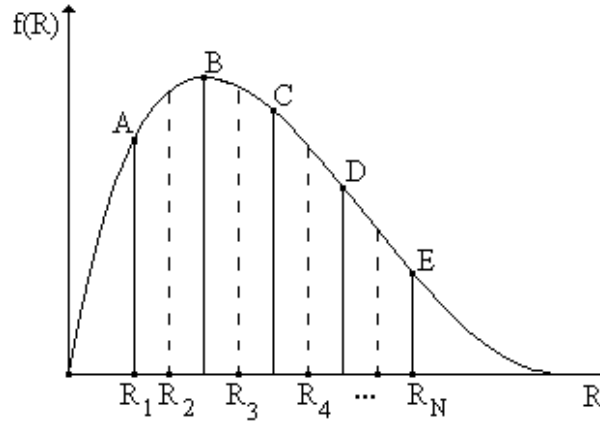


Fig. 3. Radius distribution function of droplets

However, such an approach makes the mathematical description much more complex, therefore, to simplify the problem, we use the following technique. The range of radii of the droplets is divided into N groups, where N is an arbitrary integer parameter. For each intermediate group we replace the actual distribution of droplets by a monodisperse one, with the radius being equal to the average radius for the given group of droplets. The total number of droplets in every group is constant. For two extreme groups, i.e., of the largest and smallest radii, we accept the value of the largest radius and of the smallest one. It is obvious that the smaller the range of change of radius in the group, the more exact is the description of disperse phase behavior.

The following physical assumptions are assumed in our model of evaporative cooling of droplets: droplets have a spherical shape; an approximation of average droplet temperature is used. Besides the semi-empirical dependences of the heat and mass transfer coefficients of a droplet in a gas flow and coefficient of aerodynamic drag, all depending on the Reynolds number for droplets.

Let us now describe the mathematical model of evaporative cooling of water droplets. We direct the z -axis vertically downward and fix the coordinate origin at the point of the beginning of droplet fall. The falling droplet experiences the action of the gravity force and force of aerodynamic drag, which determines the change in the velocity of droplets and their density per volume unit. As a rule, for small size for mechanical draft cooling towers velocities of droplets are increased monotonously during their fall. The system of the differential equations includes N equations that describe a change in the radii of droplets $R_i(z)$ due to evaporation:

$$\frac{dR_i(z)}{dz} = -\frac{\gamma(\text{Re}_i)[\rho_s(T_{wi}(z)) - \rho(z)]}{\rho_w v_i(z)} \quad (4)$$

and N Equations that determine a change in the velocities $v_i(z)$ of the falling droplets:

$$\frac{dv_i(z)}{dz} = \frac{g}{v_i(z)} - C(\text{Re}_i) \frac{\rho_a [v_i(z) - u(z)]^2}{2v_i(z)} \frac{\pi R_i(z)^2}{m_i}. \quad (5)$$

We note that allowance for the accelerated motion of droplets is of great importance for relatively small mechanical draft cooling towers, because the droplets has no time to reach the steady state velocity. For large droplets Eq. (5) can be solved at constant value of droplet radius, because the droplet radius changes less than 1 % due to evaporation.

We have N Equations, describing a change in the volume-averaged temperature of the droplets $T_{wi}(z)$:

$$\frac{dT_{wi}(z)}{dz} = \frac{3\{\alpha(\text{Re}_i)[T_a(z) - T_{wi}(z)] + \gamma(\text{Re}_i)(r - c_w T_{wi}(z))[\rho_s(T_{wi}(z)) - \rho(z)]\}}{c_w \rho_w R_i(z) v_i(z)}. \quad (6)$$

To calculating the change in the temperature of humid air $T_a(z)$ the equation has the form:

$$\frac{dT_a(z)}{dz} = \frac{4\pi}{\rho_a c_a} \sum_{i=1}^N \frac{R_i(z)^2 N_{di}(z)}{(v_i(z) - u(z))} [\alpha(\text{Re}_i)[T_a(z) - T_{wi}(z)]]. \quad (7)$$

It is worth to note that the rate of change of air temperature is directly proportional to the total interfacial surface area $4\pi R_i^2 N_{di}$ and is inversely proportional to the relative velocity of phases.

The equation that describes a change in the density of water vapor $\rho(z)$ in the air-vapor mixture is:

$$\frac{d\rho(z)}{dz} = -4\pi \sum_{i=1}^N \frac{R_i(z)^2 N_{di}(z)}{v_i(z) - u(z)} \gamma(\text{Re}_i) [\rho_s(T_{wi}(z)) - \rho(z)]. \quad (8)$$

The boundary conditions for the system of equations (4)–(8) are:
At $z = 0$ (point of beginning of droplet fall) the following values are defined for:
droplets radiuses

$$R_i|_{z=0} = R_{0i}, \quad (9)$$

temperatures of droplets for each group

$$T_{wi}|_{z=0} = T_{woi}, \quad (10)$$

initial velocities of droplets (for simplicity we consider them to have the same value)

$$v_i|_{z=0} = v_0. \quad (11)$$

At $z = H$:

air temperature

$$T_a|_{z=H} = T_{a0}, \quad (12)$$

density of the water vapor in the air

$$\rho|_{z=H} = \rho_0. \quad (13)$$

Thus, the system of ordinary differential equations (4)–(8) and boundary conditions (9)–(13) represent the nonlinear boundary-value problem.

Attention is to be drawn to the fact that in our model the influence of the number of droplets per unit volume on the parameters of humid air is taken into account. The number of droplets per unit volume $N_{di}(z)$ is defined by the specific water flow rate Q_{wi} , the sizes R_i of droplets and their velocities v_i as:

$$N_{di}(z) = \frac{3Q_{wi}}{4\rho_w \pi R_i^3 v_i(z)}. \quad (14)$$

It follows from Eq. (14) that the number of droplets per unit volume decreases with increase in velocities of droplets at a constant water flow rate. As a rule, for mechanical draft cooling towers the hydraulic loads are such that the average distance between droplets is much greater than their diameter. This fact is taken into account in our mathematical model by using the heat and mass transfer coefficients obtained for a single droplet.

The coefficient of heat exchange of a droplet with the air medium $\alpha(Re_i)$ is determined from the following dimensionless relation:

$$Nu=2+0.5Re^{0.5}. \quad (15)$$

For droplets from the i -th group, the Reynolds number is defined as:

$$Re_i = \frac{2\rho_a R_i |v_i(z) - u(z)|}{\mu_a}, \quad (16)$$

where μ_a is the dynamic viscosity of air. The Nusselt number is calculated as $Nu=2R_i\alpha(Re_i)/\lambda_a$.

Using the analogy between the heat and mass transfer coefficients, the coefficient of mass exchange $\gamma(Re_i)$ for a falling droplet with an ascending air flow is determined as:

$$\gamma(Re_i) = \frac{D(2+0.5Re_i^{0.5})}{2R_i(z)}. \quad (17)$$

The coefficient of aerodynamic drag force of a droplet $C(Re_i)$, is calculated from equation:

$$C(Re_i) = \frac{24}{Re_i} \left(1 + \frac{1}{6} Re_i^{2/3}\right). \quad (18)$$

3. OPTIMIZATION OF THE COOLING TOWER PERFORMANCE

Optimization of the cooling tower performance is one of the most important problems in the theory and engineering practice of evaporative cooling of water. Some aspects of this problem are well known, however it is necessary to carry out great number of theoretical and experimental investigations dealing with creation of a control system for a cooling tower. In this section we consider optimization of the performance of a mechanical draft cooling tower in the following formulation of the problem: it is required to determine the minimum air flow rate through the cooling tower (air flow rate was increased discretely with a given step) for reaching the given constant temperature T_1 of the water leaving the cooling tower. Moreover, the initial circulating water temperature and its flow rate are considered constant, and the temperature and humidity of air are variable quantities. Thus formulation of the optimization problem reflects the practical problem of maintenance of the thermal performance of some technological installation.

For determining the minimum air flow rate, the developed mathematical model (4)–(8) was solved by an iterative method. At the given polydispersity of water the problem of evaporative cooling was solved at an arbitrary initial air flow rate. If the final temperature of water T_w is higher than the given value of temperature T_1 , the air flow rate is increased discretely at a given step. This process was repeated until the condition $T_w \leq T_1$ was met. Some of the calculation results for this optimization problem are presented in Fig. 4 for changing temperature and humidity of the air surrounding the cooling tower.

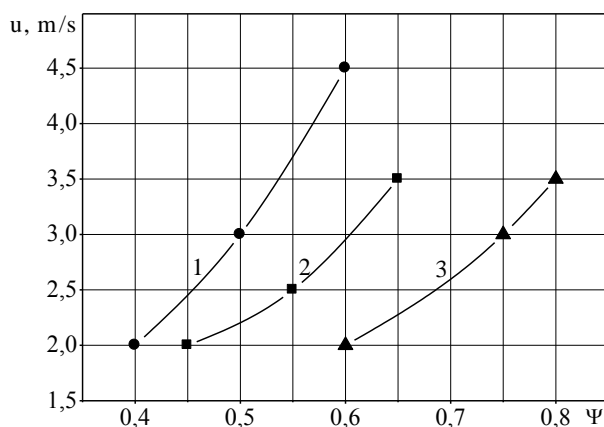


Fig. 4. Optimal air velocity versus its humidity:
curve 1 – air temperature 25 °C; curve 2 – 22 °C; curve 3 – 20 °C

The temperature T_1 was equal to 22 °C; and the air temperature was higher, equal to or lower than T_1 . In the latter case, the role of evaporative cooling is especially great. As it seen from Fig. 4 with increase in the humidity of the atmospheric air it is necessary to increase the air flow rate through cooling tower. The higher the air temperature, the larger should be tangent of the angle of the inclination of curves. This is connected with the increasing of the role of convective heat transfer. Note that the curve corresponding to $T_a = 22$ °C ends when relative humidity is 0.65. This is due to the fact that at large humidity the air flow rate becomes so large that the droplets are entrained blow out by the ascending air flow. This leads to a loss of water in a cooling tower.

4. RESULTS

The system of ordinary differential equations (4)–(8) and boundary conditions (9)–(13) entirely characterizes the process of droplet evaporation in a mechanical draft cooling tower; this system was solved numerically in the MathCAD 14 environment using the reliable and stable Runge–Kutta method of the 4th order.

In numerical calculations we take into account the temperature dependence of the diffusion coefficient of water vapor in air, viscosity and thermal conductivity of air.

In approximation of the average droplet radius, the results of comparison of our calculations with available experimental data [6], obtained for the still air, are shown in Fig. 5.

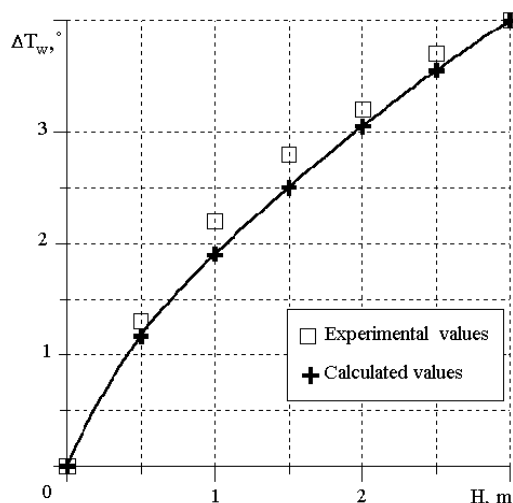


Fig. 5. Droplet temperature drop ΔT_w versus droplet fall height H

As it seen our model qualitatively correctly describes the cooling of the water droplet falling in air. In fact, the ratio of the calculated value of droplet temperature difference $(\Delta T_w)_{\text{theor}}$ and the experimental value $(\Delta T_w)_{\text{exper}}$ for different heights of droplet fall H does not exceed 10 %. Allowance for the weak free convection of air in the laboratory rig always existing during experimental investigation one increases the relative accuracy 3 % even for small heights of fall.

The dependence of the thermal efficiency η on the ratio between the mass flow rates of water and air Q_w/Q_a is shown in Fig. 6.

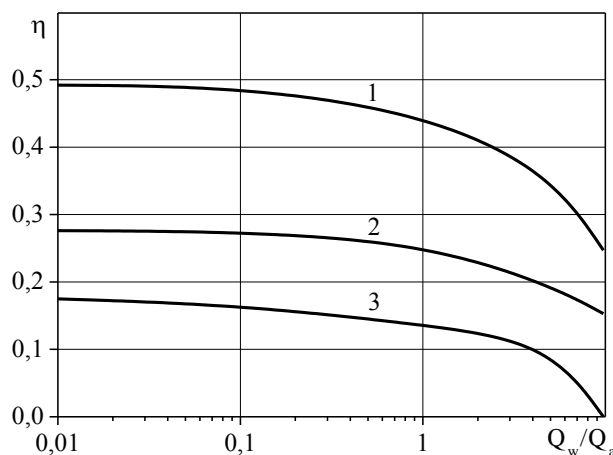


Fig. 6. Thermal efficiency η versus Q_w/Q_a :
curve 1 – $R = 0.5$ mm; curve 2 – $R = 1$ mm; curve 3 – $R = 1.5$ mm

As this ratio increases, the thermal efficiency of a cooling tower decreases. This is typical for all cooling towers. For mechanical draft cooling towers the performance even at small values of the ratio Q_w/Q_a is possible, which corresponds to small hydraulic load or large air flow rate through the cooling tower. The dependence of η on the radius of droplets is rather strong.

5. CONCLUSIONS

For the counter-flow mechanical draft cooling tower a one-dimensional mathematical model has been developed. But, for example, for cross-flow cooling tower [7] it is necessary to use two-dimensional mathematical model due to the more complicated physical processes, which take place in it.

Mathematical model represents the boundary-value problem for a system of ordinary nonlinear differential equations, describing interrelated heat and mass transfer processes and the dynamics of fall of droplets. Moreover, our model includes a distribution function of droplet radiuses. The method for solution of such problem is proposed, computer code is created and numerical simulation is performed.

For a monodisperse ensemble of droplets in a mechanical draft cooling tower, the limits of applicability of this approximation for the description of evaporative cooling are determined. It was found that a variety of effects cannot be described well in approximation of monodisperse ensemble of droplets, and, in particular, the air temperature profile and water temperature fluctuations on the surface of a water collection basin.

The mathematical model of a control system for a mechanical draft cooling tower at varying parameters of air is developed. This model allows optimization of the cooling tower performance adjusting a fan power to changing atmosphere conditions.

The dependence of the thermal efficiency of a mechanical draft cooling tower on the ratio between the mass flow rates of water and air is determined. For mechanical draft cooling towers, this dependence is weaker than for other types of cooling towers. For small values Q_w/Q_a , when they change from 0.01 to 1, the thermal efficiency of the cooling tower practically does not change.

REFERENCES

1. KRÖGER, D.G. Air-cooled Heat Exchangers and Cooling Towers, Begell House, New York, 1998.
2. FISENKO, S.P., PETRUCHIK, A.I. Towards to the control system of mechanical draft cooling tower of film type. *International Journal of Heat and Mass Transfer*, 2005, Vol. 48, p. 31–35.
3. BRIN, A.A.; PETRUCHIK, A.I.; FISENKO, S.P. Mathematical modelling of evaporative cooling of water in a mechanical-draft tower. *Journal of Engineering Physics and Thermophysics*, 2002, Vol. 75, No. 6, p. 68–73.
4. BRIN, A.A.; PETRUCHIK, A.I. Thermal calculation of the ejection cooling tower and method of improving its efficiency. *Journal of Engineering Physics and Thermophysics*, 2011. Vol. 84, No. 2, p. 287–291.
5. FISENKO, S.P., PETRUCHIK, A.I., SOLODUKHIN, A.D. Evaporative cooling of water in a natural draft cooling tower, *International Journal of Heat and Mass Transfer*, 2002. Vol. 45, p. 4683–4694.
6. ERENS, P.J., MERCKER, J.H., DREYER, A.A. Evaporation from accelerating droplets, in: *Proceedings of the 10th Heat Transfer Conference*, Brighton, 1994, p. 305–310.
7. BRIN, A.A.; FISENKO, S.P. Simulation of a cross-flow cooling tower performance. *International Journal of Heat and Mass Transfer*, 2007, Vol. 50, № 15–16, p. 3216–3223.

EXPERIMENTAL STAND DEVICE MODELING FOR IEAC THERMAL PERFORMANCE STUDY

G. Frīdenbergs, A. Lešinskis

*Riga Technical University
Azenes str. 16/2nd floor, LV-1010 – Latvia*

ABSTRACT

This paper reported a review, calculations and measurements based study into Indirect Evaporative Cooling (IEC) stand device parts which have influence on thermal performance, which was undertaken from a variety of aspects including background, history, current status, concept, standardization, system configuration, operational mode, research and industrialization. Experimental stand device parts have been described as equations of heat and mass transfer in primary and secondary air and water flows. Model has been validated with Menerga Sorpsolair device measurements located in Riga Technical university laboratory. The main goal have been to made working stand device for future researches of IEAC device cooling efficiency, which mostly depends on mass flow rates ratios of primary and secondary air flows and spacing between plates of wet and dry passages.

Keywords: IEAC stand device, indirect evaporative air cooler, cooling efficiency, heat and mass transfer from water to air trough thin wall

1. INTRODUCTION

To determine the parameters experimental stand device was studied (Fig. 1). The two main discovered parameters influencing on cooling performace are water consumption and water exchange cycle [1].

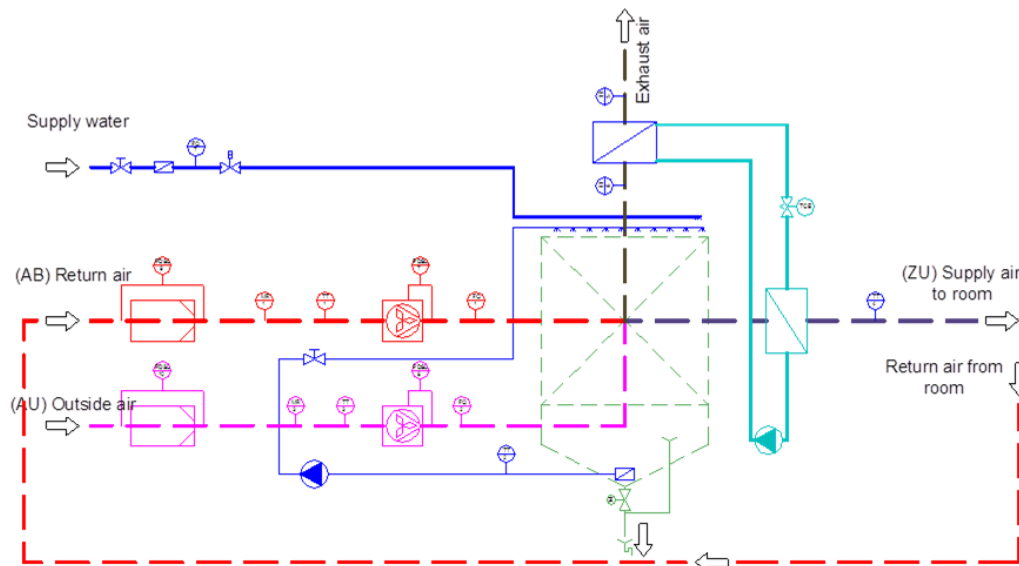


Fig. 1. Practical model of studied device [2]

1. The water consumption of evaporative air conditioners includes the water evaporated to provide the cooling effect.
2. Water exchange cycle – is water dumped off with predicted period of time for the purpose of cleaning and avoiding high salt concentration.

The aim of this paper is to clarify the interaction between the indoor humidity and the thermal performance of an indirect evaporative cooling system where the return air is used as secondary air [4–6].

In the frame of this international project several researchers focused on the interaction between HVAC (heating, ventilation, and air conditioning) systems and the indoor moisture balance, which may be significant especially in buildings with high hygroscopic contents e.g. museums and libraries. Despite of the importance of taking into account moisture buffering in the evaluation of HVAC systems. Only few publications were found in literature: Catalina et al. [7] noted that neglecting the moisture buffering capacity of the indoor environment penalises the evaluation of radiant cooling panels. The authors showed that hygroscopic materials decrease the risk of condensation on the surface of the ceiling and improve the overall performance of the system. Maalouf et al. [8] looked at the effect of taking into account coupled heat and moisture transport through the building envelope on the performance and operation of a desiccant cooling system. Variations in the COP (coefficient of performance) of the system up to 6% were noted between a model taking into account the humidity transport in the walls and one neglecting it. Recently, Woloszyn et al. [9] studied the effect of combining a relative-humidity-sensitive ventilation (RHS) system with indoor moisture buffering materials. By means of Heat, Air and Moisture transfer models the performance of different strategies were analysed in terms of indoor air quality and energy efficiency.

The results demonstrated that RHS-ventilation is able to reduce the building energy demand and confirmed that hygroscopic materials are able to damp the humidity variations in the indoor climate. In a recent study Barbosa and Mendes performed a combined simulation of a HVAC system with a whole – building hygrothermal model [10]. In the simulated case study, disregarding moisture may lead to oversizing the HVAC system by 13% and underestimating the cooling energy consumption by 4%. Osayintola et al. estimated the effect of hygroscopic materials on the energy consumption in buildings [11]. They showed the possibility to reduce the heating and cooling energy consumption respectively up to 5% and 30% when applying hygroscopic materials combined with a well-controlled HVAC-system.

So far no research was found on the interaction between the thermal performance of an indirect evaporative cooling system and the building moisture balance. In this paper an integrated simulation approach is given. The necessary parameters to the model are defined by means of measurements. Next, the potential of IEC-systems to improve the thermal comfort in a typical application in Latvia region will be investigated using dynamic simulations with MS Excel made simulation tool.

2. WATER EVAPORATION

The psychrometric chart in Fig. 2 below illustrates the evaporation process (blue line) when air passes through the wet side of indirect evaporative air conditioner. At given entry air conditions (t_1, t') and evaporation effectiveness (ε_e), the dry-bulb temperature of the leaving air (t_2) can be calculated according the Eq. 1. In ideal conditions the wet-bulb temperature of the leaving air is the same as the wet-bulb temperature of the entering air. Then the humidity ratios of both entering and leaving air can be determined from the psychrometric chart (Fig. 1). The water consumption rate for cooling purpose can be estimated using Eq. 2 [3, 4, 5].

$$t_2 = t_1 - \frac{\varepsilon_e}{100} \times (t_1 - t'). \quad (1)$$

$$\dot{m}_e = \rho \dot{V} (w_2 - w_1) / 1000. \quad (2)$$

Where

\dot{m}_e – water consumption rate, kg/h;

\dot{V} – air volumetric flow rate, m³/h;

ρ – air density, 1.2041 kg/m³;

w_1, w_2 – humidity ratios of entering and leaving air, g moisture/kg dry air.

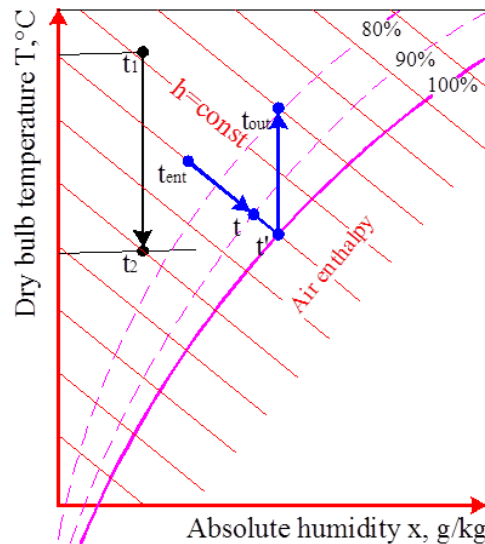


Fig. 2. Psychrometrics of two-stage evaporative cooler [2]

The water consumption rate due to evaporation varies depending on the air flow rate, the temperature and humidity of the outside air and the pad characteristics. Some manufacturers quote indicative figures for water consumption but these can only be used as approximate values. In an effort to provide independent values of the water required for evaporation, the water consumption rates for cooling purposes can be calculated in different locations. The design temperature and humidity can be based on typical historical data and be used to represent the maximum cooling conditions [6].

Furthermore, the amount of water consumption for cooling purpose has been calculated based on hourly weather conditions in a typical hot day and a typical summer day from one available climate data source in Riga, Latvia: (Table 1) data supplied by METEO [6]. It is assumed that cooling to be switched on at full speed during hours when the outside temperature exceeds 27 °C and represents the maximum water consumption on those days in the calculation. The total water consumption and the average consumption rate of the typical summer day are shown in Table 1.

Table 1. Evaporated water consumption in typical days in Riga

Location	Period requires cooling	Total daily water consumption (L/day) for random various air flow rates		Average hourly water consumption rate (L/hr) for random various air flow rates	
		9360(m ³ /h)	16200(m ³ /h)	9360(m ³ /h)	16200(m ³ /h)
Riga typical summer day	10:00am~19:00pm	481.5	833.3	48.1	83.3
	11:00am~20:00pm	538.8	932.5	53.9	93.3

The water consumption rate for cooling purposes is dependent on the humidity ratio difference of the entering and leaving air and the air flow rate. The sizes selected in Table 1 are based on maximum cooling requirements on the hottest part of the day. Typically, the fan utilised in residential evaporative air conditioners has a variable speed and runs on low speeds for the majority of operating time. The evaporated water consumption in Table 1 was calculated based on the maximum fan speed, thus it should be considered as overestimates. Values of air flow rate are average air flow rates of studied air handling unit with indirect evaporative cooling (Fig. 4.)

3. SIMULATION SCHEME

An evaluation procedure is presented which shows that the cooling demand can often be satisfied completely combining direct and indirect evaporative cooling. When return air is used as secondary air, water is evaporated and heat is withdrawn from the air due to latent heat transfer. As a result the return air is cooled. At the same time the supply air is cooled indirectly by sensible heat transport through the heat exchanger walls. The wet bulb temperature of the return air is a measure for the maximum vapour content of the return air at adiabatic saturation, which corresponds to the lowest possible temperature to which the return air may theoretically be cooled. The IEC-effectiveness ε can be defined by the ratio of the actual temperature reduction in the supply air realized by an IEC system to the maximum possible temperature change, which is given by the temperature difference between the dry bulb of the outdoor air and the wet bulb of the return air entering the heat exchanger [3], see Eq. 1:

$$\varepsilon = \frac{Q_{r,1} - Q_{s,2}}{Q_{s,1} - Q_{r,wb,1}} \quad (3)$$

The IEC-effectiveness is mainly characterized by the heat transfer surface, the air flow rate through the heat exchanger and ratio between the supply and return air flow rate. Depending on the geometry of the heat exchanger and the primary and secondary mass flow rates the effectiveness may range from 40 to 80% according to ASHRAE [3].

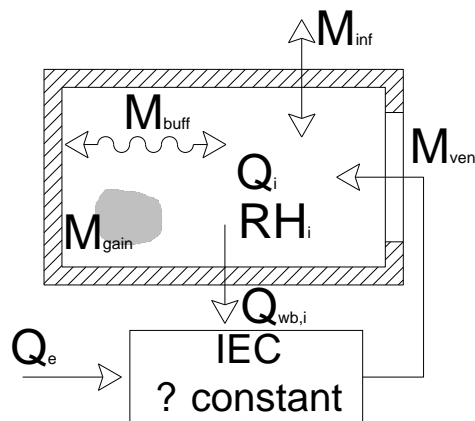


Fig. 3. Scheme of the simulation methodology in MS Excel [7]

As the performance of the installation depends on wet bulb temperature of the return air, the indoor temperature obtained using IEC is defined both by the room heat and moisture balance. Typically the moisture balance includes convective vapour transfer by infiltration and ventilation air $M_{inf/vent}$, moisture gains M_{gain} (e.g. by human activity), water vapour exchange with hygroscopic materials M_{buff} , moisture gains or removals due to humidifying

or dehumidifying systems $M_{de/hum}$ and convective vapour transfer between zones M_{coupl} (Eq. 2).

$$M_{inf} + \sum_k M_{vent,k} + M_{gain} + M_{buff} + M_{hum} - M_{dehum} + \sum_k M_{coupl,k} = V \frac{d\rho_v}{dt} \quad (4)$$

Due to the uncertainty of many parameters related to moisture buffering water vapour Exchange with porous materials is often difficult to assess. As a result building energy simulation (BES) programs such as TRNSYS use simplified models to predict the relative humidity [13]. In this approach a lumped model is used in which the moisture capacity of walls, furniture and room air are combined into one single room moisture capacity. [12]. The effective capacitance C is calculated using Eq. 3 and 4 taking into account the available buffering surface, the material properties and the calculated penetration depth Δ of the porous material. A detailed derivation of the equations is reported in [13]. In the following simulations, the moisture balance can be reduced from Eq. 2 to 5, and is used to define the room vapour pressure at every timestep of the calculation.

$$C = 1 + \left(\frac{R_v T}{V} \sum S \frac{\Delta \rho \varepsilon}{p_{v,sat}(Q_i)} \right) \quad (5)$$

$$\Delta = \sqrt{\left(\frac{\delta_v t p_{v,sat}(Q_i)}{\rho \varepsilon \pi} \right)} \quad (6)$$

$$M_{inf} + \sum M_{vent,k} + M_{gain} = C \frac{dp_v}{dt} \frac{V}{R_v T} \quad (7)$$

The approach used in this paper has the advantage to be able to evaluate the performance of indirect evaporative cooling without the need of numerical models at component level, i.e. describing the wet surface heat exchanger numerically, which may require a large calculation time. The room temperature follows from the heat flow balance of internal and solar gains, infiltration and transmission heat gains or losses, and the convective heat removed by the IEC coupled ventilation system. This latter term couples the heat flow balance to the moisture balance through the definition of IEC-effectiveness (Eq. 1). In order to assess the indoor conditions in a room with an IEC-system by means of BES-models, in every time step the supply air temperature is calculated using Eq.1 assuming a constant IEC-effectiveness (Fig. 3). The correctness of this assumption will be first studied by means of measurements.

4. IEC-EFFECTIVENESS

In order to determine the thermal effectiveness of the technique, measurements were carried out in an air handling unit (AHU) containing an indirect evaporative cooling installation [14]. The evaporative cooling system consists of a double cross flow heat exchanger in polypropylene. Nozzles located upstream of the heat exchanger are wetting the return air in the first part of the heat exchanger. The water is collected in the sump below the heat exchanger and recirculated. Every five minutes temperature and relative humidity in the supply and return air before and behind the heat exchanger were measured [15].

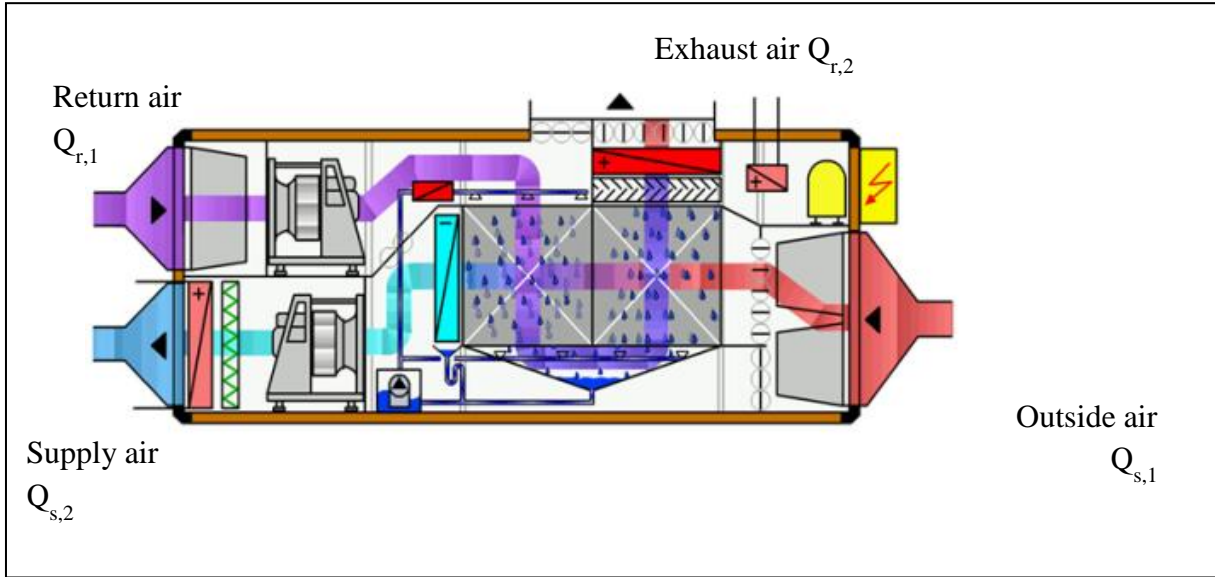


Fig. 4. Operation of studied AHU with indirect evaporative cooling [2]

In Fig. 4. are shown type of air handling unit used in experimental study, it is similar to practical model of studied device (Fig. 1). The negative aspect is that it is not available temperature after IEC heat exchanger and difference with practical model is that refrigeration cooling unit is placed before IEAC heat exchanger.

Difference between the dry bulb temperature of the supply air and the wet bulb temperature of the return air is plotted on the x-axis, the temperature drop in the supply air obtained using IEC is shown on the y-axis. According to Eq. 1, the IEC-effectiveness is given by the slope of the plotted data and could be derived by means of linear regression. The measurements show that the performance of an IEC system is independent of the inlet conditions of temperature and relative humidity of both outdoor air and return air. The total water consumption and the average consumption rate of the typical summer day are given in Table 1. These values are substantially higher than the values mentioned in the introduction which is caused by the specific design of the double heat exchanger.

5. CONTROL STRATEGY

A good control strategy is essential to make the technique perform well. Therefore the control criteria should be carefully chosen to ensure that the evaporative cooling is working properly as long as a cooling demand is present, and no heating of the supply air is occurring especially during colder days. Therefore the different stages in which the AHU (air handling unit) may operate are included in the simulation model:

A. During occupancy hours

- a. $Q_i < Q_{i,set} : V = V_{min}$
- b. $Q_i > Q_{i,set} : V = V_{max}$
- i. $Q_e > 18^\circ\text{C}$ and $Q_e - Q_{i,wb} > 2^\circ\text{C} : Q_{s,2} = Q_{s,1} + \varepsilon(Q_{s,1} - Q_{i,wb})$ (IEC)
- ii. $Q_e < 18^\circ\text{C}$ or $Q_e - Q_{i,wb} < 2^\circ\text{C} : Q_{s,2} = Q_{s,1}$ (Free cooling)

B. Outside occupancy hours

- a. $Q_i > Q_{i,set} : V = V_{max} : Q_{s,2} = Q_{s,1}$

The air flow rate for hygienic ventilation rate min V is calculated to meet the minimal ventilation requirements for a medium indoor air quality (IDA 2) [16]. Because IEC is often combined with free (night) cooling, a maximum ventilation capacity max V based on

conventional cooling load calculations may lead to oversizing of the AHU. Therefore the maximum ventilation capacity can be determined by preliminary simulations. During the following dynamic simulations the maximum ventilation rate $\max V$ is constant. Some additional heating of the supplied air due to the supply fan was not taken into account.

6. PARAMETRIC STUDY

In this part the interaction between the moisture balance and the thermal comfort is studied making use of a typical application in the Latvian climate.

As a case study, a generic room is analysed with a typical geometry of an office or a health care room. The room has a floor surface of 15 m², a height of 2.8 m with a west facing façade containing a window a 3 m². Only the west oriented wall is an external wall, all the other boundaries are adiabatic. No lowered ceiling or raised floor is used and the infiltration rate is 0.4 ach (air changes per hour).

In the base case model the room is occupied during the office hours (08–17h) by one person having a sensible heat production of 65 W and a moisture production of 0.07 kg/h [17]. The same occupancy schedule was applied to all days in the simulation period. Internal gains due to one personal computer (140 W) and lights (10 W/m²) are introduced. The total buffering capacity of the room was five times the capacity of the indoor air ($C=5$), corresponding to 55 m² plastered wall. Simulations were run over an entire year using a 15 – minute time step assuming that besides the IEC there was no other cooling device present. Solar gains are taken into account, no sun shading was present. An extreme warm weather data set, i.e. outdoor temperatures occurring once every 10year. This program constructs the synthetic hourly weather data based on the climatological normals of 1961–1990 for a specific location [18].

During winter the indoor temperature setpoint is 20°C. Based on the measured values of the IEC-effectiveness, a constant IEC-effectiveness equal to 85% (according to experimental stand device data sheet) was chosen in the model. The hygienic ventilation rate $\min V$ for one person is 36m³/h (according to Latvia Building normatives it is lower 15 m³/h per person but chosen much higher value most used for HVAC designing). In order to see the influence of the night cooling on the thermal comfort, the operation of the AHU with and without night cooling is compared for different $\max V$. To compare the number of (weighted) temperature excess hours for an AHU with and without night cooling and shows that night cooling has an important influence on the thermal comfort realized in the building. Some first simulations showed that in the base case $\max V = 3$ ach (125 m³/h) yields to a good thermal comfort.

7. SENSITIVITY ANALYSIS

As the thermal performance of indirect evaporative cooling is influenced by the moisture balance of the room, a sensitivity analysis was performed by changing the parameters from the base case, which influence the indoor humidity (Eq. 5): the maximum ventilation rate $\max V$, the indoor moisture production M_{gain} and the amount of moisture buffering capacity C which is available in the room.

The (weighted) temperature excess hours above 26°C were used as a performance indicator for thermal summer comfort [19]. The amount of time during which the operative temperature exceeds 26°C is multiplied with the temperature difference, in this way the extent of temperature excess is taken into account. Similar to the GTO-method [20] the maximum number of temperature excess hours during one year has been set to 100 h as a criterion for good thermal comfort. The number of temperature excess hours is calculated for the cases with and without IEC. In the latter free cooling with outdoor air is available if there is a

cooling demand. The difference in temperature excess hours gives an indication of the thermal comfort improvement which can be realized using IEC. Furthermore the operation time of the IEC system during one year is derived. It gives an indication of the interaction between the operation of IEC and the indoor moisture balance.

7.1. Maximum ventilation rate $\max V$

First the maximum ventilation rate $\max V$ is varied. It shows that the number of temperature excess hours decreases while increasing the maximum ventilation rate. With higher air flow rates, the operation time for the IEC increases. A high air flow rate causes more moisture to be removed from the room, which lowers the average indoor wet bulb temperature and thus increases the amount of time during which the control conditions for IEC are satisfied. Additionally the influence of free cooling increases due to the higher ventilation rate. Compared to the case with only free cooling, use of IEC is able to improve the comfort by about 25% if $\max V = 60 \text{ m}^3/\text{h}$, and by about 95% if $\max V = 250 \text{ m}^3/\text{h}$, based on the calculated temperature excess hours at both air flow rates.

7.2. Moisture production M_{gain}

Increasing the indoor moisture production M_{gain} has a large influence on the moisture balance of the room and therefore on the thermal performance of IEC. Depending on the number of people and their activity level, the indoor moisture gains in the room may increase. Apart from loads from occupants other gains such as bathing, washing etc. may be introduced. It shows that with higher moisture production M_{gain} the number of temperature excess hours increases from 67 h at 0.07 kg/h to 150 h at 1.5 kg/h , thus approaching the number of temperature excess hours in case the IEC is not in operation. Because of the high indoor humidity, a smaller temperature decrease can be realized in the supply air, which results in a larger number of temperature excess hours. If the indoor air humidity rises, the operation time decreases because the control conditions for IEC are less often fulfilled.

7.3. Moisture buffering capacity C

Moisture buffering is able to contribute to a more comfortable indoor climate since it dampens out humidity variations [10, 11]. Different variations on the base case were simulated: if the walls and ceiling are vapour tight and no other hygroscopic materials are present the effective capacitance is equal to one. In the second variation the moisture buffer capacity from the base case is doubled.

It demonstrates that the number of temperature excess hours decreases with a higher moisture buffering capacity. If the moisture buffering capacity increases, the indoor humidity peaks are damped out and the number of operation hours slightly increases because the control conditions for IEC are more often satisfied. Furthermore, the influence of the moisture buffering capacity on the temperature excess hours is smaller with a higher maximum ventilation rate. In this case less moisture is available to be absorbed and released by the hygroscopic surfaces in the room.

7.4. Results

The result of the calculation is determined by the temperature distribution of the heat exchanger plates, which then will explore the heat transfer across the heat exchanger volume, as well as allow for the calculation of geometrical effects on the final parameters. Below

(Fig. 5) are presented three parameters calculation visualization graphs. The more accurate the data needed for further research.

For this operating condition, the temperature profiles of dry, wet air and the exchanging wall are presented in Fig. 5 a, b, c, the heat flux in Fig. 5 a, b, c, it can be seen that the temperature of supply air in dry channels decreases along its direction of flow, and the temperature of working air in the dry channels.

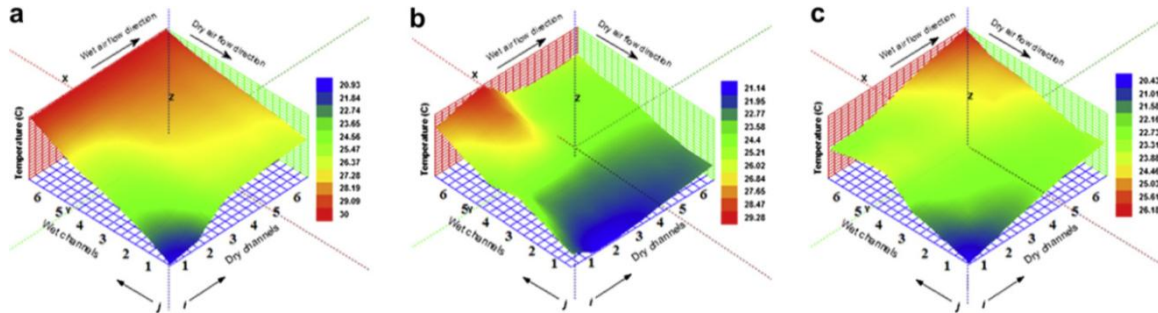


Fig. 5. Temperature distribution across the heat exchanger plate dry side (dry passages) (a), wet side (wet passages) (b) and wall (c)

As shown in Fig. 6 a, the convective heat transfer decreases along the flow path of dry air as a result of the observed (see Fig. 6 a and c) decrease in the temperature difference between the dry channel air and the wall. The heat transfer rate in dry channels is higher if they have bigger air mass flow rates [16–21]. Referring to Fig. 6 b, the wet air is not initially saturated and has a higher temperature than the wet wall close to the entrance of the wet channels (comparison of Fig. 5 b and c). These results in heat being transferred to the water reserved on the wet side of the wall leading to the evaporation of the water. After moving to a critical point, the temperature of wet air is lower than that of the wet wall, so the convective heat flux has become negative (as shown in Fig. 6 b), this means that the wet air picks up both sensible and latent heat from the wall.

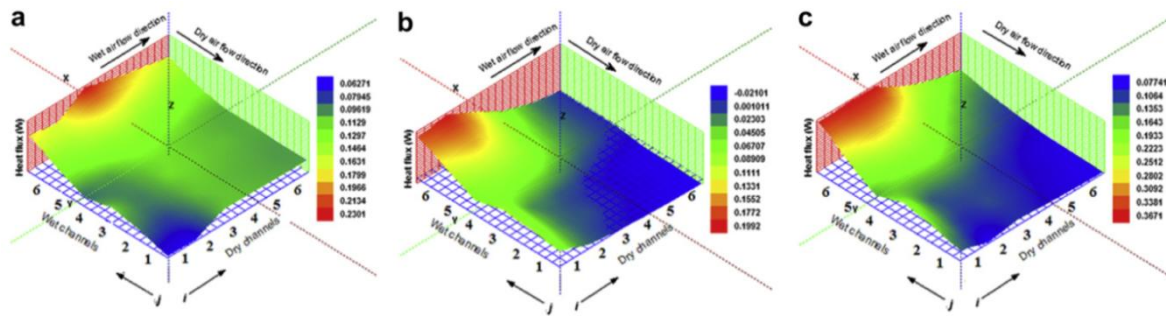


Fig. 6. Heat transfer rate across the heat exchanging plate dry (a), wet (b) side and on the wall (c)

The supply air temperature and the return air temperature just behind the first part of the heat exchanger were in good agreement with the measured data. The model underestimated the temperature of the exhaust air because it does not take into account the fact that the return air is heated by the recirculated water in the second part of the heat exchanger (Fig. 7).

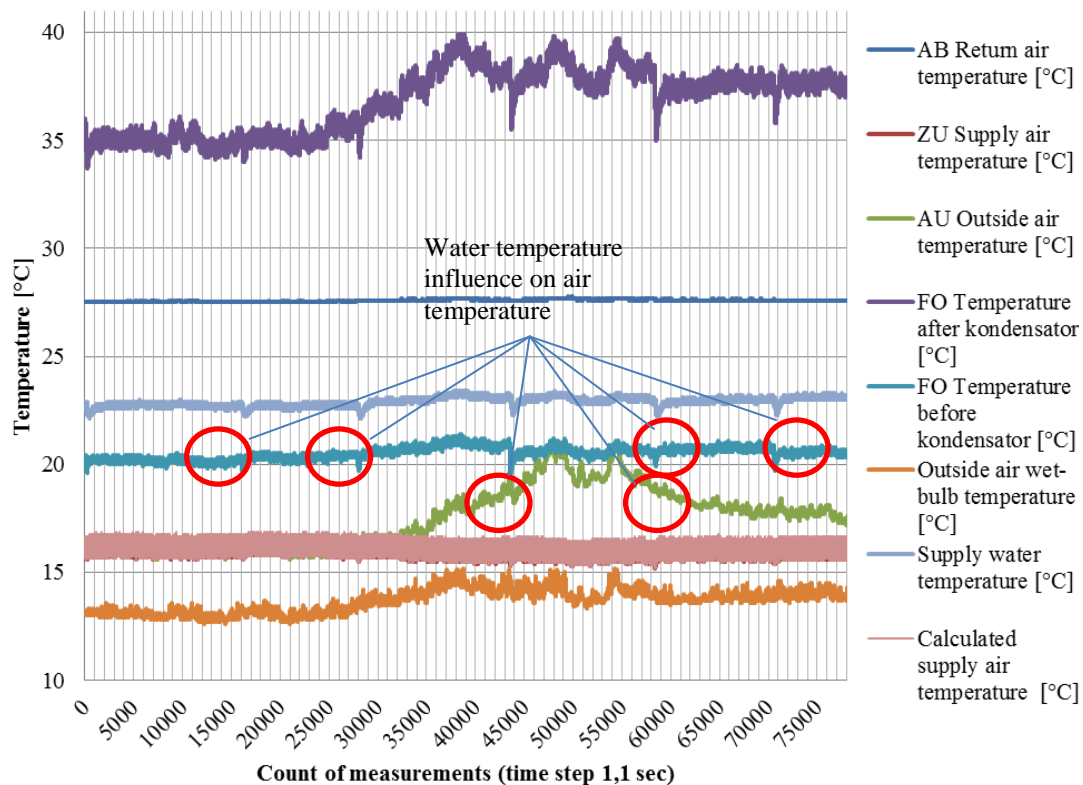


Fig. 7. The observed and calculated water temperature fluctuations on IEAC heat exchanger

CONCLUSIONS

Comparing the two major components of water usage in evaporative air conditioners (water used for the cooling effect and water dumped/bled off), it may be concluded that if the water bleeding/dumping system is well designed, set and maintained, the total water consumption will be largely dominated by the moisture evaporation which is essential in operating the evaporative cooler. However, if not properly adjusted, the water bleeding/dumping rate is of the same order of magnitude as the evaporation rate and can lead to considerable wastage of valuable water.[2].

An integrated simulation methodology of the building with its indirect evaporative cooling installation is necessary in order to take into account both heat and mass balance in building calculations. It is concluded that for future researches isn't important to make calculations because of multiple available publications. In this way it is possible to study the interaction between the thermal performance of an indirect evaporative cooling system and the moisture balance of a room. The IEC-effectiveness was studied using measurements in an AHU containing an indirect evaporative cooling system.

As new aspect in literature [1, 5] is found that the thermal effectiveness is independent of the inlet conditions of the outdoor and return air. It is important for future researches.

REFERENCES

1. SUPPLE, R.G., BROUGHTON, D.R. "Indirect evaporative cooling – Mechanical cooling design", ASHRAE Transactions, Vol. 91, Part 1B – 1985 – p. 319–328.
2. FRĪDENBERGS, G., LEŠINSKIS, A., *Evaluation of indirect evaporative cooler in public buildings*, RTU, 2012 – p. 6–48.

3. HASAN A., SIREN K. *Theoretical and computational analysis of closed wet cooling-towers and its applications in cooling of buildings*. *Energy and Buildings* - 2002 – p. 34.
4. KALS WA. *Wet-surfaces air coolers*, Chemical Engineering – 1971 – p. 68.
5. ZHIYIN, D, CHANGHONG, Z., ZHAN, C., RIFFAT, S.B. *Indirect evaporative cooling: Past, present and future potentials*, Renewable and sustainable energy reviews – 2012. – p. 1–28.
6. Latvijas Metroloģijas centra data base [referred on the 3th of January in 2012 y.]. <www.meteo.lv/pdf_base/meteor_2009.html>
7. ZHAO, X., DUAN, Z., ZHAN, C., RIFFAT, S.B. *Dynamic performance of a novel dew point air conditioning system for the UK climate*. *International Journal of Low Carbon Technology* 2009.
8. HALASZ, B., *A general mathematical model of evaporative cooling devices*, Rev. Gén. Therm., FR, Vol. 37 – 1998 – p. 245–255.
9. COSTELLOE, B., FINN, D. *Indirect evaporative cooling potential in air e water systems in temperate climates*. *Energy and Buildings*, 2003.
10. SETHI V.P, SHARMA S.K. *Survey of cooling technologies for worldwide agricultural greenhouse applications*. *Solar Energy*, 2007.
11. CERCI Y. *A new ideal evaporative freezing cycle*. *International Journal of Heat and Mass Transfer* 2003 – p. 1–11.
12. PARKER R.O., TREYBAL R.E. *The heat-and-mass transfer characteristics of evaporative coolers*, Chemical Engineering Progress Symposium Series – 1961 – p. 57.
13. PETERSON, J.L. *An effectiveness model for indirect evaporative coolers*, ASHRAE Transactions – 1993 – p. 99.
14. CIBSE KNOWLEDGE SERIES: *sustainable low energy cooling: an overview*. Plymouth PL6 7PY, UK: Latimer Trend & Co. Ltd, 2005.
15. STABAAT, P., MARCHIO, D. *Simplified model for indirect-contact evaporative cooling-tower behaviour*, *Applied Energy* 78 (2004), – 2003 – p. 433–451.
16. MACLAINE-CROSS, I.L., BANKS, P.J. *A general theory of wet surface heat exchangers and its application to regenerative evaporative cooling*, *Journal of Heat Transfer*, Vol. 103, No. 3, – 1981 – p. 579–585.
17. MCCLELLAN, C.H. *Estimated temperature performance for evaporative cooling systems in five locations in the United States*, ASHRAE Transactions, 94 (2), – 1988 – p. 1071–1090.
18. MIZUSHINA RIT, MIYASHITA H. *Characteristics and methods of thermal design of evaporative coolers*, *International Chemical Engineering* – 1968 – p. 3–8.
19. MIZUSHINA, RIT, MIYASHITA, H. *Experimental study of an evaporative cooler*, *International Chemical Engineering* 1967 – p. 4–7.
20. NIITSU Y, NAITO K, ANZAI T. *Studies on characteristics and design procedure of evaporative coolers*, *Journal of SHASE*, Japan – 1969. – No. 7 – p. 12–23.
21. SCHIBUOLA, L. *High-efficiency recovery for air-conditioning applications in a mild climate: a case study*, *Applied Thermal Engineering*, Vol. 17, No. 5 – 1997. – p. 447. –454.
22. Rīga's municipal government's corporation "Rīgas Ūdens" data base [referred on the 4th of April in 2013 y]. <<https://www.rigasudens.lv/par-uznemumu/vesture/>>



ENERGY EFFICIENCY AND CARBON FOOTPRINT FOR THE BREWERY INDUSTRY IN NIGERIA

S.C. Nwanya

*Department of Mechanical Engineering
University of Nigeria
410001 Nsukka – Nigeria*

O.V. Ekechukwu

*National Universities Commission
Abuja, Nigeria*

ABSTRACT

The paper assessed and determined energy efficiency and carbon footprint of the brewery industry with the purpose of reducing its carbon dioxide emissions level. The motivating idea is that energy burned in the industry is embodied and passed on at a cost to both consumer and the environment. Two analytical techniques: energy and exergy analyses that focus on identifying improvement opportunities for the system were applied. The first law analysis of the system only accounts for the performance determination by an evaluation of the amount of energy expended. However, the second law analysis (exergy) gives a qualitative description of the system with the critical points where irreversibility (losses) occur are pin-pointed. Hence, the study has combined both the first and second law methods to analyze the boiler system in the brewery. The results showed the energy input to the combustor is at 43846.13kWh while the exergy destruction is calculated to be 10694.16 kWh. The first and second efficiencies are 71.38% and 66.67% respectively. The useful energy gained by the boiler feed-water is at 24784.6 kWh while the exergy destruction in the boiler tube is at 8917.50 kWh, with the first and second law efficiencies at 79.20% and 50.60% respectively. The efficiency of the boiler system is at 64.8%. It concludes that a plausible collaboration of energy efficiency and carbon footprint tools to achieve improved environmental performance is possible.

Keywords: exergetic efficiency, carbon footprint, energy efficiency, brewery, Nigeria

1. INTRODUCTION

The generation of greenhouse gases from Nigerian industrial sector has been observed to increase linearly as a function of increase manufacturing. As a consequence, the increasing energy content of industrial products faces three major long term energy challenges: tackling climate change, product competitiveness, ensuring secure and affordable energy supply. As the industry is heavily dependent on fossil fuel energy for production, the challenges are expected to be on the rise, thus making energy a large component of the total cost of production. The last two challenges are attitudinal in nature, while the first has anthropogenic origin and requires a thorough investigative approach for its solution. The aforementioned challenges are more critical in the food and beverage sector, particularly brewery sub-sector because of their consumption pattern and long supply chain processes that are energy intensive. Also, over 30% of the energy used is wasted on old and obsolete equipment (boilers, generators, etc.), which are inefficient.

According to Worrell et al (2008) large scale production dominates energy intensive industries and such is applicable to the brewery. Curbing the high energy intensity raises questions on kinds of primary energy sources available to the sector and their contributions to global warming. However, Unachukwu et al. (2012) has pointed out that high specific energy contents of produced goods prevailed because of incidence of power outages that compel

industries to embark on self-power generation. A follow up question has been raised on the impact of these sources on the environment if consideration is given to energy quality and efficiency.

On efficiency, primary fossil fuels that are carbon-based characterize the bulk of energy sources in beverage manufacturing industry and they have less efficient conversion processes. The implication is that their potentials are seldom utilized maximally because of losses. These energy sources include commercial fuel such as diesel, oil, natural gas, steam(hydro) and non-commercial ones like air(hydraulic), wood, animal waste and spent grain(bio-fuels). To understand how these energy flows are consumed it is imperative to classify the beverage industry into three segment: (1) those that manufacture nonalcoholic beverages; (2) those that manufacture alcoholic through fermentation; and (3) those that produce distilled alcoholic beverages (NAICS, 2007). Although the classifications are not exhaustive, they point the direction of energy mix for beverage manufacturing. This mix consists of electricity and thermal energy uses. For example, electricity generally goes toward packaging and refrigeration, whereas most thermal energy goes toward the actual brewing process (E-Source, 2010). Looking at the listed non-commercial, it can be inferred that thermal energy is generated from them. On the other hand, electricity is mostly generated from fossil fuels and they contribute greater proportion of the greenhouse effects. However, there is usually a combined mix of electricity and thermal depending upon the type of equipment used, packaging employed and location of beer plant (E-source, 2010).

The involvement of the foregoing factors dictates the need for energy efficiency assessment of core brewery production activity. Energy efficiency describes the ability to use less energy input to generate large economic output consistently. Indirectly, this means reducing CO₂ emissions without loss of economic value. For this reason, EPA (2009) considers energy efficiency as a low-cost resource for achieving carbon emissions reductions. The goal of energy efficiency assessment herein is to build understanding of how energy is used within a brewery factory and to identify ways to reduce costs through the more efficient use of energy. This view is held since industrial energy efficiency is recognized with capacity to afford economic, environmental and social benefits to the society. From literature, several authors have identified the inefficient industrial energy utilization in Nigeria as endemic problem militating against industrialization. Oluseyi et al. (2007) revealed that a part of the problem is low or negligible attention to energy efficiency investments. Sequel to this prevailing energy situation, most strategic industries relocate their production site to neighbouring countries like Ghana, where energy supply is more efficient. But the barriers to energy efficiency measures in Nigerian industries have been documented without feasible solutions. According to Unachukwu et al (2007), the lack of energy efficiency measures result in loss of competitive edge by Nigerian industries.

On energy quality, the level of emissions here if distributed on per capita basis is a worrisome concern to environmentalist. A recent survey has shown in Fig. 1 that gas flaring and combustion of solid, liquid and gaseous fuels account for major sources of GHG emissions. The summary of policy lesson from figure 1 is that energy related activities are lead contributors of the resultant climate change effects. In estimating and selecting strategies to minimize CO₂ emissions, several tools are including carbon footprint have been found useful.

The measurement and evaluation of the emitted greenhouse gases account for the carbon footprint of the sector and it is beneficial for the economy. Carbon footprint refers to quantity of greenhouse gases or the carbon dioxide equivalent produced during a product's life cycle (Cordero, 2013). Carbon footprinting is also an evaluation tool to help increase energy efficiency (Printcity, 2010). In future, to benefit from emission trading and product

labeling schemes carbon footprint assessment is a regulatory requirement. Though, Nigeria has no emission trading scheme now, as a signatory (non-annex I party) to Kyoto Protocol, the future prospects of the scheme looks great and carbon footprint presents a platform through which the greatness can be achieved. This scheme when it takes-off and carbon reduction programmes are implemented, thus will to creating green economy where sale of carbon credit is facilitated. To develop the enabling environment for green economy and sale of carbon credit in a sector like brewery industry energy efficiency and carbon footprint appraisals are imperative as indicators of environmental performance.

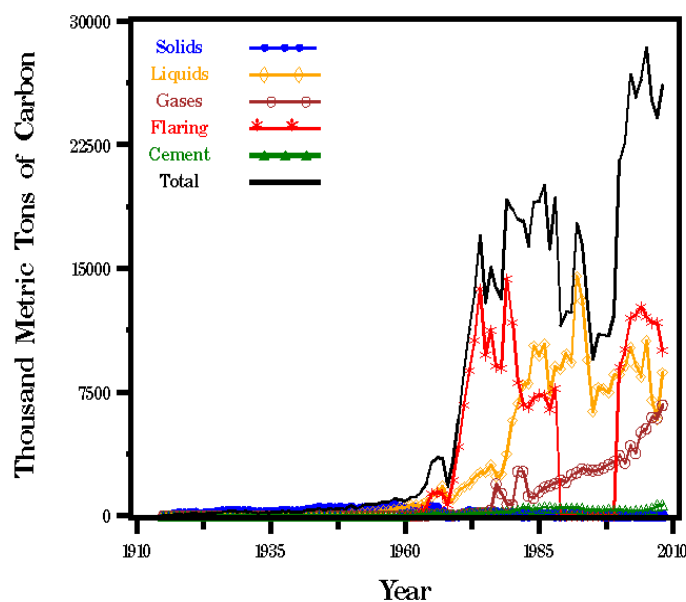


Fig. 1: CO₂ Emissions from Nigeria

Source: [http://cdiac.ornl.gov/trends/emis/ngr.html\(2012\)](http://cdiac.ornl.gov/trends/emis/ngr.html(2012))

On current situation on energy efficiency, it is clear that energy utilization in Nigeria is far from being efficient (NERC, 2013). Igwenagu (2011) has correlated industrial output, energy consumption and manufacturing output with CO₂ emission. According to his findings, there is strong positive correlation between energy consumption and CO₂ emission that exists because of heavy fossil fuel consumption. This view collaborates with NERC (2013) findings. Ogwomike and Aregbeyen (2013) have revealed through a recent survey that industries in Nigeria generally exhibit low level of information on energy efficiency and lack steps to create incentives for investments in energy efficiency. Several studies have examined the influence of distance, retail type, logistics and consumer behavior on CO₂ emissions and carbon footprint measurement due to inefficient industrial energy use. Rizet et al (2011) mapped energy consumption and carbon CO₂ emission of different supply chains to a range of food products with the conclusion that logistics activities exhibit relatively low emissions. The need for a paradigm shift from high carbon intensive fuel to low carbon fuel, to tackle the barriers of efficient energy usage and provide strategies to reduce CO₂ emissions has been recognized in Nigeria. Dayo and Gilau (2012) maintain that the size of Nigeria's global carbon market provides possible potential opportunity for sales of carbon credit if natural gas is used for generation of energy in industries. This is because it contains low carbons and provides great potential for CO₂ emissions reductions. Jackson et al (2013) carried a study on carbon footprint on UK breweries and showed that energy use and footprint are performance

indicators to enable brewers identify areas for improvement. However, there is no literature on carbon footprint of boiler system and this is critical because it is key equipment for conversion of fuels and subsequent release of CO₂.

In this study, the specific objectives include to assess and determine energy efficiency and carbon footprint of the brewery industry with the purpose of reducing its carbon dioxide emissions level. In order to achieve the goals, a bottom-up approach involving detailed energy and exergy analyses techniques were carried out. The scope of this work covers activities under operational control of the organization.

2. METHODOLOGY

In a brewery industry, the boiler is key component in combustion of fuels that releases CO₂ and energy usage is significant contributor of carbon footprint. For this reason, this study combines the methods of energy and exergy analyses of the boiler system with cradle to grave assessment technique in calculating the total CO_{2eq} emission of various stages of production. The assessment includes emissions due to direct and indirect brewing production activities. This is a bottom-up approach for estimating fuel chain emissions (Muller et al, 2007). The method is unique because it enables a feedback information on what should be done or opportunities available to reduce emissions. According to IAEA (1999), it provides framework for comparative assessment of existing and potential fuel chain facilities. Hence, a performance evaluation was carried out based on the relevant operational data obtained from the brewery.

For data collection, the boundaries for the carbon footprint are limited to emissions related to direct and indirect beer production activities. The direct involves energy consumed in brewing and packaging, while indirect concerns consumptions at workshops, canteen, clinics and administrative offices. To determine direct energy flow through the boiler, we take energy mass balance equation as follows:

$$Q + W = m\Delta h \quad (1)$$

For a boiler, $W = 0$ since it neither develops nor absorbs work and energy due to enthalpy is:

$$\therefore Q_{451} = \dot{m}_s (h_1 - h_4) \quad (2)$$

Equation 2 gives us the heat supplied to the steam (through the boiler) per unit mass of fuel and its ideal rankine cycle is shown in Fig. 2.

Where \dot{m}_s = stream flow rate of fuel, h_1 = enthalpy at phase 1, h_2 = enthalpy at phase 4 and Q_{451} = heat supplied.

The T-S diagram is relevant to highlight processes of interest in the study. For this study, process 4-5-1 represents the superheated steam at constant pressure.

For calculation of carbon footprint, the technique used involves having a standard reference emission factors, quantity of energy consumed (electricity, fuel and carbon content) and product yield statistics. Each emission calculated is specific to CO₂, CH₄, N₂O etc. and were summed into carbon equivalent unit after conversion.

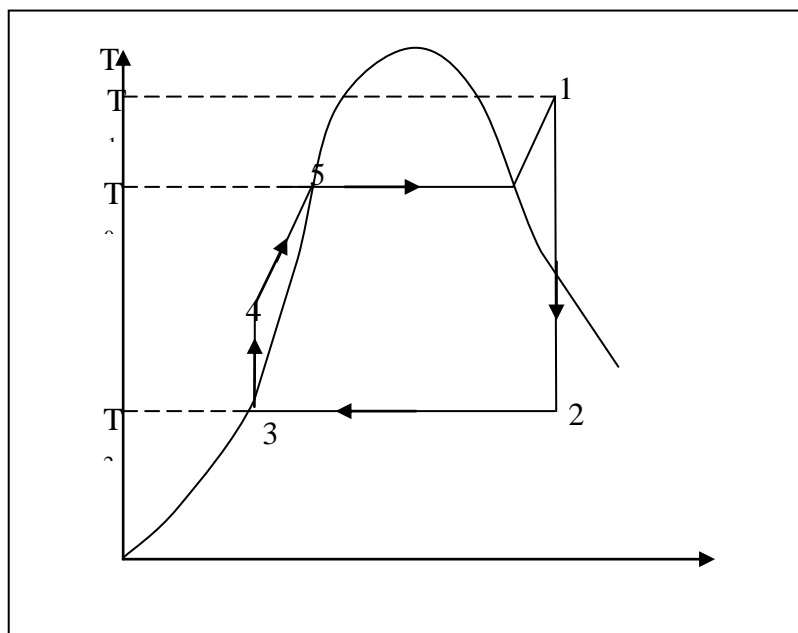


Fig. 2. T – S diagram showing the Rankine cycle

However, for the purpose of analysis, the boiler system was divided into three (3) sub-units shown Fig. 3. The units are (1) an adiabatic combustion process that occurs in the combustor unit of the boiler, (2) a heat transfer process that takes place between the hot flue gas and water (saturated steam) and (3) the mixing of the hot products of combustion (flue gas) with ambient air at the exit of the stack.

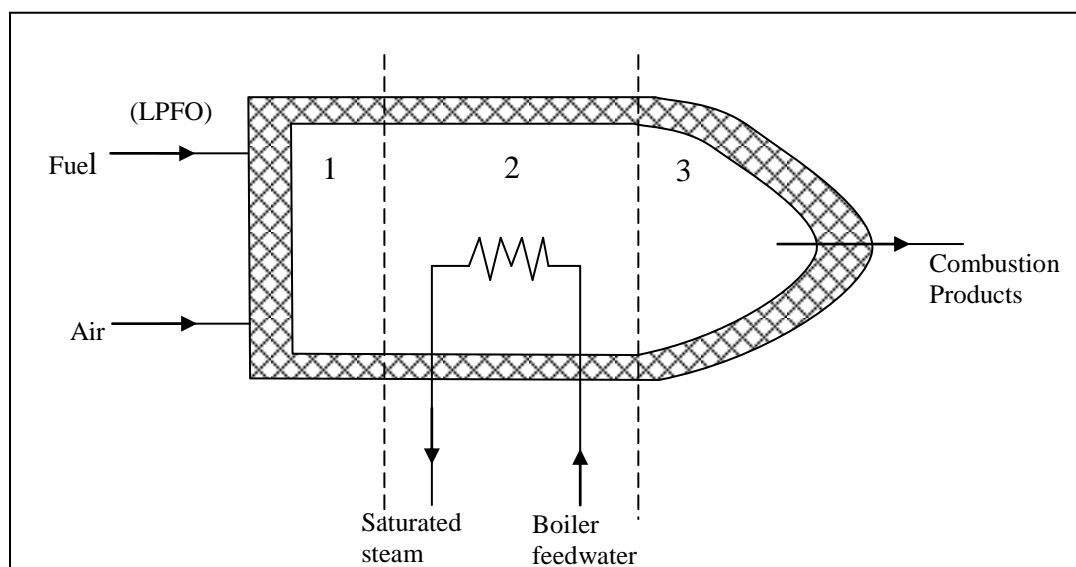


Fig. 3. Schematic diagram of the boiler showing the 3 sub-systems
Source: Abasirim (2013)

2.1 Chemical exergy

According to Dincer (2004) the specific exergy of hydrocarbon fuels reduces to chemical exergy at near ambient conditions as expressed in Equation 3.

$$\xi = \varphi(\text{NCV})^o \quad (3)$$

However, typical values of chemical exergy of selected fuels are shown in Table 1.

Table 1: Typical values of ξ , φ and $(\text{NCV})^o$ of selected fuels

FUELS	HEATING VALUE (NCV) (KJ/Kg)	CHEMICAL EXERGY ξ (KJ/Kg)	EXERGY GRADE FUNCTION, φ
Gasoline	47.849	47.394	0.990
Fuel oil	47.405	47.101	0.994
Kerosene	46.117	45.897	0.995

Source: selected fuels, Saidur (2007)

However, Szargut and Stewart assumed that the ratio of chemical energy, ξ to the net calorific value $(\text{NCV})^o$ for solid and liquid industrial fuels is the same for pure chemical substances having the same ratios of constituent chemicals.

After computing the value of the exergy grade function φ , for numerous pure organic substances containing carbon, hydrogen, oxygen nitrogen and sulphur, correlations expressing the dependence of φ on atomic ratios were derived and extended to cover industrial fossil fuels. The correlations for liquid fuel are given as:

$$\varphi = 1.0401 + 0.1728 \frac{h}{c} + 0.043 \frac{o}{c} + 0.2169 \frac{s}{c} (1 - 2.0628 \frac{h}{c}) \quad \text{Kotas (1985),} \quad (4)$$

where: c, h, o and s are the mass fractions of carbon, hydrogen, oxygen and sulphur respectively.

2.2 Physical exergy

Physical exergy is defined by the maximum amount of work obtained when a stream of substance is brought from its initial state to the environmental state defined by P_o and T_o by physical processes involving only thermal interactions with the environment.

The physical exergy for the analysis of physical process between two states is given in terms of its specific physical exergy as:

$$\Psi = (h - h_o) - T_o (s - s_o). \quad (5a)$$

$$\Psi_{ph1} - \Psi_{ph2} = (h_1 - h_2) - T_o (s_1 - s_2). \quad (5b)$$

Also, the specific physical exergy of a reference gas is given as:

$$\psi_{ph} = c_p (T - T_o) - T_o \left(c_p \int_n \frac{T}{T_o} - R \int_n \frac{p}{P_o} \right) \quad \text{Kotas (1985).} \quad (6)$$

For the purpose of this analysis, T_o is taken to be 25°C or 298K while the pressure, p_o is taken as 1.01325bar or 0.101325 Mpa.

3. ANALYSIS AND DISCUSSION OF RESULTS

3.1 Assumptions

The following assumption are made that: operation of boiler is necessary for fuel combustion and subsequent release of emissions, heat loss to the environment is almost zero (negligible), it has no potential to do work ($W = 0$), the kinetic and potential energies of the fluid (streams) are negligible and steady state conditions exist.

Taking energy balancing

$$\dot{E}_{in} - \dot{E}_{out} = \frac{dE_{system}}{dt} = 0, \quad (7)$$

$$\dot{m}_f h_f + \dot{m}_a h_a - \dot{m}_p h_p = 0, \quad (8)$$

$$\dot{m}_f h_f + \dot{m}_a h_a = \dot{Q}. \quad (9)$$

The energetic efficiency of the combustor is expressed as follows:

$$\eta_c = \frac{\Delta \dot{Q}}{\dot{m}_f h_f + \dot{m}_a h_a}. \quad (10)$$

According to Aljundi (2009), an exergy balance for the combustor is carried out as follows:

$$(\dot{m}_f \psi_f + \dot{m}_a \psi_a) - \dot{m}_p \psi_p - \dot{E}_d = 0, \quad (11)$$

$$\therefore \dot{E}_d = (\dot{m}_f \psi_f + \dot{m}_a \psi_a) - \dot{m}_p \psi_p, \quad (12)$$

where:

\dot{E}_d = Exergy destruction

Therefore, the exergetic efficiency is expressed as:

$$\varepsilon = \frac{\dot{m}_p \psi_p}{\dot{m}_f \psi_f} \quad (13)$$

3.2 Boiler tube analysis

For the boiler tubes located in subunit 2 of Fig. 2, where heat transfer occurs between hot combustion products and the boiler feedwater, we proceed with energetic efficiency as follows:

$$\eta_{Bt} = \frac{\dot{m}_s (h_s - h_L)}{\Delta \dot{Q}} \quad (14)$$

On the other hand, the estimation of exergetic efficiency follows as in Equation (15).

$$\varepsilon_{BT} = \frac{(\psi_s - \psi_L)}{\left(1 - \frac{T_o}{T_i}\right) Q_i} \quad (15)$$

Using the stoichiometric combustion equation the number of moles reactants and products are in Tables 2.

Reactants	No. of moles per unit mass of fuel, n_k (Kmol/Kg of fuel)	Mass fraction, x_k (mass in grams * molar mass)
Carbon, C	0.7166667	0.86
Hydrogen, H	0.06	0.12
Sulphur, S	9.375×10^{-5}	0.003
Oxygen, O	0.116968	0.116968
Nitrogen, N	0.438791	0.116968
Total	0.687519	17.012137

Table 2. Analysis of Reactants and Combustion Products

Products	No. of moles per unit of fuel	Mass fraction (no of moles * molar mass)
CO ₂	0.07166667	3.15333348
H ₂ O	0.06	1.08
SO ₂	9.375×10^{-5}	6×10^{-3}
O ₂	$0.101385419x = 0.0152078$	0.48665001
N ₂	$1.7857143 \times 10^{-4} + 0.381402294 (1 + x) = 0.438791209$	12.28615387
Total	0.5857594	17.01213736

Recalling the correlation for calculating the exergy grade function of liquid fuels:

$$\varphi = 1.0401 + 0.1728 \frac{h}{C} + 0.043 \frac{O}{C} - 0.2169 \frac{S}{C} (1 - 2.0628 \frac{h}{C})$$

Substituting the mass fractions obtained from the ultimate analysis of LPFO fuel, we obtain:

Therefore, the grade function of liquid fuel is $\varphi = 1.140$ fuel and chemical exergy in equation can be obtained as $\dot{\varepsilon} = 1.140 \times 47.405 = 54.041.7$ KJ/kg.

The input energy into the combustor is 4386.13kW, while released heat of combustion is 31299.46 KJ/s. Hence, thermal efficiency applied to combustor, based on equation (10), is 71.38%.

3.3 Exergetic Efficiency of Combustor

Adopting the exergy balance methodology developed by Kotas (1985) and as in Eq. (15) exergetic efficiency is calculated to be 66.67%.

For the boiler tubes, we consider heat gained from the flue gases in order to estimate the energetic efficiency. After calculations this efficiency value is 79.2%, the exergy destruction is 891 KJ/Kg. Based on Eq. (15), the exergetic efficiency is 50.6%.

3.4 Overall boiler efficiency boiler efficiency

From the study, the overall efficiency can be estimated as follows:

$$\text{boiler efficiency} = \frac{\text{energy to steam/ sec}}{\text{energy from fuel /sec}} \quad (16)$$

Using rate of steam generation of 9.6kg/s, specific energy of 2478.46kJ/kg and rate of fuel consumption of 0.978 kg/s , the overall efficiency is 64 %.

3.5 Carbon footprint of brewery industry

The foregoing evaluation of boiler system is an impact pathway approach to track combustion emissions from fuel chain activity. It is technology specific and does not provide sufficient tool for environmental performance indicator for the industry. For an industry-wide performance indicator, the method of carbon footprint is applied. The facility's emissions from different activity areas can be estimated by Equation (17) as follows:

$$E_i = [A \times O_p] Ef_i \times [1 - (CE_i / 100)]. \quad (17)$$

Where E_i = emission rate of pollutant (kg/yr), A = activity rate (tons/hr), O_p = operating hours (hr/yr), Ef_i = uncontrolled emission factor of pollutant and CE_i = overall control efficiency of pollutant (i %). The emission factors for electricity and heat consumptions were used to calculate CO_{2eq} emissions. For Nigeria, electricity specific emission factor is 0.43963136 kg CO_{2eq} /kWh, while heat factor is 0.4034043 kg CO_{2eq} / kWh (Ecometrica, 2011).

The carbon footprint of Nigerian brewery was calculated based on a six-year process data obtained from industry from 2006 through 2007 to 2011 activities. There were difficulties encountered while sourcing data and for this reason, the study focused on direct (brewing and packaging), indirect (workshop, canteen, clinics and offices) and third party (housing and contractors) energy consumption. Therefore, the study did not extend to transport and other logistics emissions.

Results show that CO_2 emissions of 3.864557×10^6 ton/yr, 5.79252×10^6 ton/yr, 6.88988×10^6 ton/yr, 6.56414×10^6 ton/yr, 7.16387×10^6 ton/yr and 9.42036×10^6 ton/yr were recorded from 2006 to 2011, respectively. The percent share of different utilities consumption to the total annual estimated emissions is shown in Table 3. The energy consumed annually for the period under study in brewing and packaging are as follows: 165574686.4 MJ; 214422371.9 MJ; 216 045267.9 MJ; 209306923.9 MJ; 203457155.1 MJ and 204465439.9 MJ, respectively for production capacity (hectolitre, hl) of 1500419 hl; 1728640 hl; 20036639 hl; 1873410 hl; 2097916 hl and 2547244 hl. The results show a corresponding specific energy, an indicator of energy consumption of 110.35 MJ/hl; 124.04 MJ/hl; 10.78 MJ /hl; 111.7 MJ/ hl; 96.98 MJ /hl and 80.26 MJ/hl. The fall in value implies that energy is used efficiently.

Table 3: Share of utilities consumptions from 2006 to 2011

Name	2006	2007	2008	2009	2010	2011
Electricity						
direct	23.0 %	20.3%	17.04 %	21.64 %	15.79 %	21.3%
indirect	3.58 %	7.6 %	11.67 %	5.93 %	15.86 %	12.2%
Third party	1.36 %	0.035%	0.87 %	5.51 %	1.58 %	2.2 %
Heat						
Direct	72.36 %	71.69 %	70.3 %	66.93 %	66.76 %	61.9%

3.6 Discussions

It is evident in table 3 that CO₂ emissions from indirect consumption, though smaller in magnitude, grew by higher rate than direct consumption. It grew faster by 112.2% and 53.55 % in 2007 and 2008, respectively from 2006 and 2007 levels, then experienced decline in 2009. The implication for the industry, if expected beer production volume falls, is that indirect emissions will yet get high because it is independent of volume produced. Also, looking at the boiler efficiencies and the range of emission levels, a plausible inference can be drawn as a consistent measure of relating equipment output performance or technological efficiency and CO₂ emissions for the industry. The foregoing statement supports the argument that to reduce fuel cost and emissions it is important choose the most efficient boilers and install them in suitably designed and controlled systems (Energy Saving Trust, 2008).

Comparatively, the boiler efficiency results indicate that energy is used inefficiently over the years and this collaborates with the range of emission levels. Therefore, the carbon footprint values can be an indication of performance of the boiler, which implies that technological efficiency has a link with or can serve as indicator environmental performance. According to Schipper et al (2001), using simplified methods for estimating the carbon released in direct combustion of fossil fuels, and in electricity and heat production, energy indicators can be extended to carbon emissions. These carbon indicators can play an important role in aiding negotiations over carbon reduction targets and evaluating progress toward meeting abatement goals. The capacity to reduce energy loss through improved efficiency has rebound effect on the reduction of carbon emissions.

There are three main areas where opportunities exist to reduce carbon emissions in brewery industry. These are product strategy (altering product mix), intelligent process scheduling to reduce downtime and equipment upgrade to higher efficiency models.

Accordingly, in the contribution of this work, it propagates combined use of energy efficiency and carbon footprint as catalyst for improved process efficiency and environmental performance. It maintains that boiler efficiency should be a preliminary tool to assess carbon footprint level in brewery industry. In this sense, improvement in efficiency and temporal changes in energy indicator will lead to sustainability and consequently cause reduction in emissions or improved environmental performance.

4. CONCLUSION

The energy efficiency and carbon footprint of brewery industry has been assessed in this study. The following conclusions are drawn:

- The motivating idea is that energy burned in the industry is embodied and passed on at a cost to both consumer and the environment.
- An energy and exergy analyses carried out on the boiler system showed the subunits where losses energy mostly occur.

- The carbon footprint of the brewery was calculated based on a six-year process data obtained from industry from 2006 through 2007 to 2011 activities.
- The combustor was found to have the highest exergy destruction (losses), calculated to be 10690.32KW. The boiler tube losses was found to be 8906.1KW.
- The results show a corresponding energy indicator of 110.35 MJ/hl; 124.04 MJ/hl; 10.78 MJ/hl; 111.7 MJ/hl; 96.98 MJ/hl and 80.26 MJ/hl. The last two years showed an improvement in energy efficiency indicator as implied by decline in value.
- The energetic efficiency of the combustor was calculated to be at 71.32% while the exergetic efficiency was at 61.20%.
- Results show that CO₂ emissions of 3.864557×10^3 ton/yr, 5.79252×10^3 ton/yr, 6.88988×10^3 ton/yr, 6.56414×10^3 ton/yr, 7.16387×10^3 ton/yr and 9.42036×10^3 ton/yr were recorded from 2006 to 2011, respectively. These values are significant and can serve as incentives for initiative on carbon management in the industry.
- Looking at the boiler efficiencies and the range of emission levels, a plausible inference can be drawn between them, which can aid decisions over carbon reduction targets.
- To reduce fuel consumption and emissions level it is imperative to choose efficient boilers and install them to run on biofuels.

The exergy destruction in the combustor is linked to the irreversibility inherent in the combustion processes, heat losses and cases of incomplete combustion. These act as confirmation of level of emissions that enter the atmosphere due to brewery activity.

REFERENCES

1. ALJUNDI I.H. (2009). Energy and exergy analysis of a steam power plant in Jordan". Applied Thermal Engineering Vol. 29, p.324–328.
2. CORDERO, P. (2013). Carbon Footprint estimations for a sustainable improvement of supply chains: state of the art. Journal of Industrial Engineering and Management, Vol. 6 (3). www.jiem.org/index.php/article/view/570/491 (accessed 23 March, 2014).
3. DAYO, F., GILAU A. (2012). Carbon market and clean energy investment opportunities in Nigeria. www.nigeriacan.org/web/download/_1254297.pdf (accessed 30/12/2013).
4. DINCER I. (2004). "Thermoeconomic analysis of power plants. An application to a coal fixed electrical generating station. Internal journal of thermal sciences.
5. Ecometrica, (2011). Technical paper on electricity specific emission factors for grid electricity. www.emissionfactor.com (downloaded 8/3/2014).
6. Energy Saving Trust (2008). Domestic heating by gas: boiler systems guidance for installers and specifiers. 2008 Edition.
7. Environmental Protection Agency, EPA (2009). Energy Efficiency as a low-cost resource for achieving carbon emissions reductions: a resource of the national action plan for energy efficiency. September 2009. www.epa.org/cleanenergy/documents/suca/-ee-and-carbon..pdf. (accessed 8/3/2014).
8. E-Source (2010). Managing Energy costs in Microbreweries. US Environmental Protection Agency, E-Source Companies LLC.
9. IGWENAGU, C.M. (2011). Principal components analysis of global warming with respect to CO₂ emission in Nigeria: an exploratory study. Asia Journal of Mathematics and Statistics 4 (2): 71–80.

10. International Atomic Energy Agency, (IAEA), 1999. Health and Environmental Impacts of Electricity Generation Systems: procedures for comparative assessment. Technical report series No. 394, Vienna.
11. JACKSON, G., FREEMAN G., SHARPE R. (2013). Energy benchmarking survey, carbon footprinting and life cycle analysis. <http://www.ibd.org.uk/cms/file/855> (accessed 23/2/2014).
12. KOTAS T.J. (1985). “The Energy method of thermal plant analysis” Anchor Brendor ltd, Tiptree Essex.
13. MULLER, D.C.A., MARECHAL F.M.A., WOLEWINSKI T., ROUX P.J. (2007). An energy management method for the food industry. Applied Thermal Engineering Vol. 27, p. 2677–2686.
14. Nigerian Electricity Regulatory Commission, NERC (2013). Energy efficiency in Nigeria. Presentation of R & D Division at the 3rd NERC/NARUC/ USAID Training Program 1–10.
15. North American Industry Classification System, NAICS (2007). Manufacturing energy and carbon footprint scope. US Census Bureau, 1–4.
16. OGWUMIKE, F.O., AREGBEYEN O. (2013). Energy use and sustainable development: evidence from the industrial sector in Nigeria.
17. OLUSEYI, P.O., OKORO O.I., CHIKUNI E. (2007). Energy efficiency programme in Nigerian industries: a lesson from India. www.active.cput.ac.za/energy/past_papers/ICUE/2008/ppt. (accessed 23/2/2014).
18. Printcity (2010). Carbon footprint and Energy Reduction for the Graphic Industry Value Chain. Cross Country special report. [www.printcity.de/download.php?-/princity%20carbon%](http://www.printcity.de/download.php?-/princity%20carbon%20) (accessed 23/2/2014).
19. RIZET, C., BROWNE M., CORNELIS E., LEONARDI J. (2011). Assessing carbon footprint and energy efficiency in competing supply chains: review, case studies and benchmarking. Report naXys 27, [http:// www.naxys.be](http://www.naxys.be) (accessed 5/1/2014).
20. SAIDER, R., AHMED J.U, MASJUKI H.H. (2010) “Energy, Exergy and Economic analysis of industrial boilers, Energy Schipper, L., F. Unander, S. Murtishaw, M. Ting (2001). Indicators of energy use and carbon emissions: explaining the energy economy link. Annu. Rev. Energy Environ, Vol. 26; p. 49–81.
21. SZARGUT J. MORIS D.R, STEWART F.R.(2002). “Energy Analysis Thermal chemical and metallurgical processes”. HemispherePublishing co-opration.
22. UNACHUKWU, G.O., ZARMA I.H., SAMBO A.S. (2012). Energy Efficiency and Barriers towards meeting energy demand in Industries in Nigeria.
23. WORRELL, E., BERNSTEIN L., ROY J., PRICE L., HARNISCH J. (2008). Industrial Energy Efficiency and Climate Change Mitigation. Energy Efficiency (doi.10.1007/s12053-008-9032-8).

BAYESIAN METHODOLOGY FOR FUSION PLANT RELIABILITY DATA ANALYSIS

T. Iešmantas, R. Alzbutas
Lithuanian Energy Institute
Breslaujos str. 3, LT-44403, Lithuania

ABSTRACT

In this paper authors present a general methodology for unified analysis of various RAMI (Reliability, Availability, Maintenance, Inspectability) information sources. Methodology is based on Bayesian approach and incorporates analysis of RAMI information coming from different databases, different expert opinions, etc. This methodology enables to use as much fusion RAMI-related data as possible and in this way it allows to make most informed decisions related to DEMO RAMI. In addition, we briefly reviewed databases of most importance for DEMO RAMI assessment and pointed out their strengths and shortcomings.

Demonstration of application was carried out on the case of DEMO HCPB (Helium Cooled Pebble-Bed) water cooling cycle. Our methodology enabled us to use additional information from databases. This would not be possible in classical (frequentist) statistical terms. Due to this additional information posterior distributions had smaller variances, which led to almost ten-fold differences in failure probability estimates as compared to the case, where no additional information was used.

Keywords: Fusion, Bayesian, Reliability, DEMO, RAMI

1. INTRODUCTION

In order to make RAMI (Reliability, Availability, Maintainability, Inspectability) inferences for DEMO (DEMONstration) plant as accurate as possible the amount of statistical information is of crucial importance. The more data we have, the better analysis results can be obtained. However, since DEMO plant is a first of its kind, there are little or no statistical data available. One of possible ways out of this situation is to analyse RAMI data collected at other power plants, at similar systems that will be used in DEMO. In addition, the experience of experts cannot be ignored – elicitation of subjective opinion should be carried out and analysed together with statistical information (if available). Hence, we can see four points of RAMI inference for DEMO:

1. Assessment of available statistical information contained in various databases;
2. Elicitation of prior subjective information;
3. Joint analysis of objective (statistical data) and subjective information;
4. Posterior analysis.

Due to the small number and the innovative aspects of fusion devices, in general, not much information is available in the literature about availability and reliability of their components. To perform probabilistic safety assessment of fusion devices, analysts have to consider use of reliability data originating from different technological experiences [9]. One database has been developed *ad-hoc*, namely the Fusion Component Failure Database [9, 10]. However, this database has some shortcomings and we will discuss it as well as other DEMO RAMI related information resources in further sections.

The purpose of this paper is to develop a methodology for the purpose of assessing DEMO RAMI as accurate as possible with those small data sample that are available. This is achieved by the exploitation of Bayesian approach, which enables to use in statistical

inference not just raw observation but subjective expert judgement as well. It also enables to use additional information that is sometimes provided in the database records.

The structure of this paper is as follows: first we describe and discuss various information sources (T-Book, FCFR, WASH, etc.) in relation to the application of DEMO plant reliability, availability, maintainability and inspectability assessment. Next part of the paper is devoted for the description of the Bayesian approach base methodology for DEMO RAMI assessment, which is able to incorporate various sources of information. The last sections are for a case study. We will show how to use our methodology in real case of Helium cooled pebble bed water cooling cycle unreliability assessment.

2. INFORMATION DATABASES FOR DEMO RAMI ANALYSIS

2.1. The fusion-specific component databases

The Fusion Component Failure Database [9, 10] (further – FCFR database) probably is the most extensive reliability information database developed specifically for the purpose of fusion plant RAMI assessment. It was initiated in the frame of EFDA Fusion Technology Work Programs for the European work and in the frame of the International Energy Agency Agreement on the Environmental, Safety and Economic Aspects of Fusion Power.

In order to have as much relevant statistical information as possible, other non-fission technologies were also considered, like nuclear fission power plants, chemical plants, aeronautic, military and industrial systems. Multiple data sources allow quantifying uncertainties of reliability measures. Hence, addition of new data sources to FCFR database is more than desirable due to the possible increase of accuracy of fusion plant RAMI assessment.

The database already contains statistical information about the buildings reliability (like concrete containment), chemical plants, electric, I&C and mechanic components collected from various reports including sources like IEAE and T-Book, which will be described separately. In addition, there is information about fusion specific devices like magnet system, cryostat system, etc.

High importance of this database is that there are some records in it for fusion-specific components. This information was collected from JET plant as well as provided by Tritium Laboratory of Karlsruhe (TLK). 130 failures/malfunctions have been pointed out since 1995 up to January 2002. Generally speaking, the overall of them do not effect on operations. The largest number of failures/malfunctions (52) concerns “fail to open/close” and “external leaks” of small air actuated valves and solenoid valves, which are easily replaced. There has been a large increase of these valve failures in 1997–1999 due to aging of components as these failures are fatigue failures. For that reasons in 2001, JET Operators started to carry out preventative maintenance on such valves.

TLK Operator pointed out 52 failures/malfunctions which occurred in the facilities of the tritium laboratory..

Although the database is quite extensive in terms of different components, not all records contain the same type of information, e.g. some components/systems are missing the information about the type of probability distribution used to obtain the failure rate estimates. This brings in a bit of uncertainty, since in order to use estimate about such “distribution lacking” components together with those, which has known distribution, we have to make artificial assumptions.

Another issue is multiple records for the same type of components with different failure rates. For example Centrifugal pumps of horizontal flow – there are three records (Table) containing the same information except parameters of probability distribution (which is log-

normal in this particular case). Hence it would be valuable to extend the database with possibility to aggregate such information into one record. More accurate estimate would be obtained as well as uncertainties would be quantified more correctly. One of possible ways to overcome this is to use Bayesian methods.

Table 1. Excerpt for centrifugal pumps data

Type	Failure Mode	Operating Time (h)	Number of Failures	Failure Rate/ Prob. – Mean
Centrifugal Pump	Failure to Run	28.8E+4	8	2.80E-05
		18.1E+4	5	2.30E-05
		4.32E+4	3	6.90E-05

In addition, some information is not parsed into separate columns, like for example operating time and number of failures – this information is placed in the same “sentence” and cannot be manipulated in a straightforward fashion. Having original statistical information rather than just failure rate (or any other reliability-related measure) estimate is more valuable for further more extensive analysis, e.g. updating the failure rate of whole centrifugal pumps population when new data arrives.

2.2. Nuclear component reliability information sources

The lack of fusion-specific RAMI data can partially be alleviated by using the experience of nuclear plants. The extensive knowledge are stored in IAEA databases [1] and WASH report [2] as well as specialized handbooks like T-Book [3].

IEAE lists quite extensive information about the record: operating mode, environmental conditions, generic failure model, original failure mode, failure rates/ probabilities, mean values, repair times, error factors as well as ultimate sources. It is important to notice that ultimate sources sometimes are expert opinion or operating plant experience. As will be discussed later, there is a difference in how expert elicited information and raw statistical data should be treated – these are not sources of identical certainty. However, this database lacks the probabilistic assumptions – seems to be common issue for reliability database.

WASH-1400 [2] although outdated but it is still a significant contribution to the nuclear component reliability knowledge. This report spans over the data of 100 reactor plants. The estimation process is based on Bayesian approach in order to handle the variability between different plants. Log-normal distribution was used as a base model and upper as well as lower bounds for 90% credibility intervals provided.

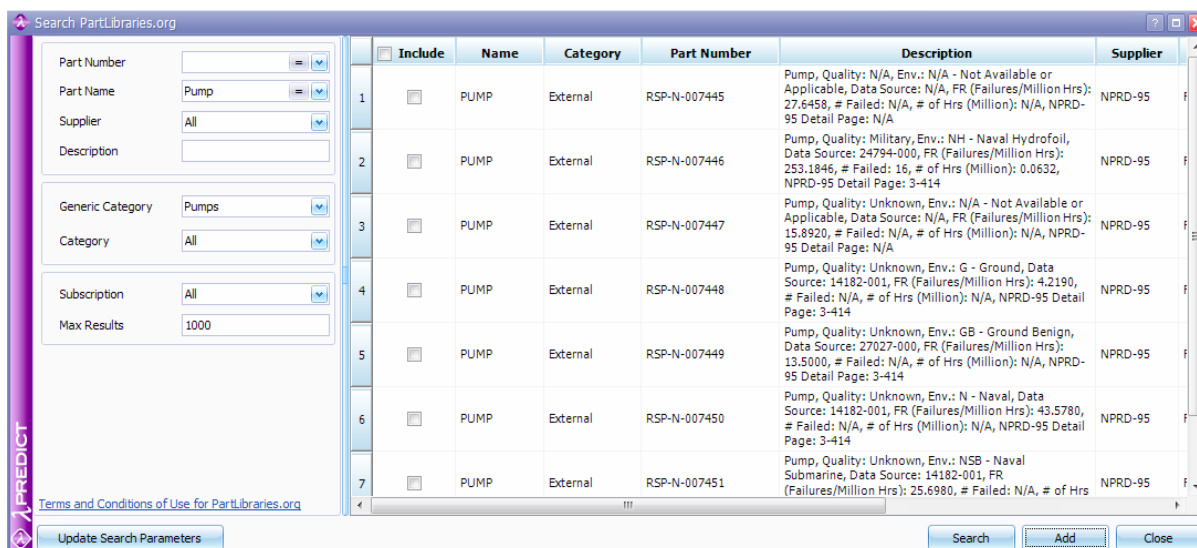
T-Book on the other hand is constructed in more coherent probabilistic manner. Bayesian approach is used to estimate failure rates by assuming gamma distribution for failure rate. The method applied in T-Book is called Bayes Empirical Bayes and provides an easy way to handle quantification of uncertainty, which is present due to the slight variations of identical components functioning in differing environments.

As a result of Bayesian inference on failure rates, for each group of components there are tables, which represents quantiles in addition to the expectation as well as Mean Active Repair Time.

2.3. Other databases

Another database, that can be significant addition to FCFR database, is hosted by PartLibraries.org and available through software Lambda-Predict. PartLibraries.org is a website portal for the collection and dissemination of component data for use in standards based reliability predictions and other reliability analyses, including MIL-HDBK-217 [11], Bellcore/Telcordia, FIDES or NSWC Mechanical reliability prediction analyses [12]. The database provides information for various electronic, electrical, electromechanical as well as mechanical component failure rate. The example of the query results for pump components is as in Fig. 1.

One of the drawbacks of this database is that it can be reached just through Lambda-Predict software and the outputting of the data to another format (e.g. excel) can be a bit tedious. Another issue is the way in which the information is described – it is not parsed into separate columns and just raw failure rate estimate, MTBF and mission time is presented – no assumptions, no number of failures, etc.



Include	Name	Category	Part Number	Description	Supplier
<input type="checkbox"/>	PUMP	External	RSP-N-007445	Pump, Quality: N/A, Env.: N/A - Not Available or Applicable, Data Source: N/A, FR (Failures/Million Hrs): 27.6458, # Failed: N/A, # of Hrs (Million): N/A, NPRD-95 Detail Page: N/A	NPRD-95
<input type="checkbox"/>	PUMP	External	RSP-N-007446	Pump, Quality: Military, Env.: NH - Naval Hydrofoil, Data Source: 24794-000, FR (Failures/Million Hrs): 253.1846, # Failed: 16, # of Hrs (Million): 0.0632, NPRD-95 Detail Page: 3-414	NPRD-95
<input type="checkbox"/>	PUMP	External	RSP-N-007447	Pump, Quality: Unknown, Env.: N/A - Not Available or Applicable, Data Source: N/A, FR (Failures/Million Hrs): 15.8920, # Failed: N/A, # of Hrs (Million): N/A, NPRD-95 Detail Page: N/A	NPRD-95
<input type="checkbox"/>	PUMP	External	RSP-N-007448	Pump, Quality: Unknown, Env.: G - Ground, Data Source: 14182-001, FR (Failures/Million Hrs): 4.2190, # Failed: N/A, # of Hrs (Million): N/A, NPRD-95 Detail Page: 3-414	NPRD-95
<input type="checkbox"/>	PUMP	External	RSP-N-007449	Pump, Quality: Unknown, Env.: GB - Ground Benign, Data Source: 27027-000, FR (Failures/Million Hrs): 13.5000, # Failed: N/A, # of Hrs (Million): N/A, NPRD-95 Detail Page: 3-414	NPRD-95
<input type="checkbox"/>	PUMP	External	RSP-N-007450	Pump, Quality: Unknown, Env.: N - Naval, Data Source: 14182-001, FR (Failures/Million Hrs): 43.5780, # Failed: N/A, # of Hrs (Million): N/A, NPRD-95 Detail Page: 3-414	NPRD-95
<input type="checkbox"/>	PUMP	External	RSP-N-007451	Pump, Quality: Unknown, Env.: NSB - Naval Submarine, Data Source: 14182-001, FR (Failures/Million Hrs): 25.6980, # Failed: N/A, # of Hrs	NPRD-95

Fig. 1. Example of PartLibraries.org database query through Lambda-Predict software

3. BAYESIAN METHODOLOGY FOR RELIABILITY DATA ANALYSIS FOR DEMO PLANT

3.1. Bayesian framework – a way to handle uncertainties in RAMI assessment

The Bayesian approach us to pool information obtained from related experiments into the joint estimation of quantities of interest from each, and it allows us to incorporate expert opinion and subject matter expertise into the analysis of an experiment in a coherent way. Perhaps as importantly, it provides a remarkable degree of flexibility in modelling the phenomena that contribute to reliability and lifetime. In Bayesian reliability analysis, the statistical model consists of two parts: the likelihood function and the prior distribution. The likelihood function is typically constructed from the sampling distribution of the data, defined by the probability density function assumed for the data. In Bayesian analysis, the parameters in the likelihood function are treated as unknown quantities, and we use a probability density function to describe our uncertainty about them.

As a direct consequence of its use of subjective probability, Bayesian methods permit us to incorporate and use information beyond that contained in experimental data. Whether a

reliability analyst does or does not have such test data available, he will often have other relevant information about the value of the unknown reliability parameters. Such relevant information is an extremely useful and powerful component in the Bayesian approach, and thoughtful Bayesian parameter estimates reflect this knowledge. This relevant information is often derived from combinations of such sources as physical/chemical theory, engineering and qualification test results, generic industry-wide reliability data, computational analysis, past experience with similar devices, previous test results obtained from a process development program, and the subjective judgment of experienced personnel.

Because Bayesian posterior distributions are true probability statements about unknown parameters, they may be easily propagated through complex system models, such as fault trees, event trees, and other logic models. Except in the simplest cases, it is difficult or impossible to propagate classical confidence intervals through such models. Features and nuisances of real-world reliability problems, such as complex censoring and random hierarchical effects, can easily be accommodated and modelled by Bayesian methods. Such considerations are often either difficult or impossible to consider when using classical methods [4].

3.2. Updating state of knowledge of DEMO RAMI

As already mentioned, Bayesian approach allow to incorporate various sorts of information, whether it is subjective opinion of expert, or statistical sample observed over some period of time. The nature of Bayesian approach is such that once new data/information becomes available there is no need go incorporate it into previously obtained information and perform inference anew. One can just use previously obtained results as its prior state of knowledge and update it with new information.

Having stated a model for observed reliability data, for elicited subjective insights of experts as well as for information contained in various RAMI data sources, one has to push these parts through the Bayes formula in order to obtain posterior state of knowledge, i.e. RAMI state of fusion devise after all relevant information is taken into account.

Such joint analysis process can be simply visualized as in Fig. 2. This process can be extended to the cyclic procedure, where posterior distribution becomes prior distribution after new statistical data or new expert opinion is available. Then such adjustments of current state of knowledge about RAMI can be repeated over and over again.

Although for engineering use of Bayesian formalism simplicity of posterior calculations is preferred, it can be quite difficult to stick to it however. Taking into account all the information available – expert subjective experiences, raw statistical data – requires different levels of complexity and non-trivial sub-models. Hence, knowledge of computational methods like family of Markov Chain Monte Carlo algorithms is of great advantage. Although, this necessity can be partially relieved with freely available software like OpenBUGS or Stan.

In following sections we will separately present guidelines on how to deal with expert knowledge elicitation, objective analysis of statistical sample, how to use databases as statistical data information sources and which software could be of use in RAMI inference tasks.

3.3. Prior elicitation from group judgement

In this chapter we will describe how Bayesian procedures can be applied to jointly model subjective estimates provided by group of experts. The setup will be closely based on the work of I. Albert et al. [7] and can be graphically encoded as in Fig. 3.

When assessing the reliability of some complex system, we may establish first separate sub-model for each constitutive component. Data are provided to inform some sub-models, while in other sub-models very little data are available so that it is necessary to use expert opinions to supplement the information provide in the other well-informed sub-model. From a Bayesian perspective, this corresponds to constructing informative priors on some of the parameters for which data can provide little information.

With more than one expert, we may elicit from each expert a different prior and in many applications it is desirable to combine these different priors into a single “consensus” prior for parameter q . There are various methods in the literature to achieve this, although most are not entirely satisfactory. The prevailing approaches are averaging [8] and pooling. Averaging emphasizes the consensus on elicited quantities, while linear or logarithmic pooling methods emphasize diversity. The method that will be presented allows to explicitly model the consensus and diversity of expert opinions, whilst acknowledging multiple sources of uncertainty and variation.

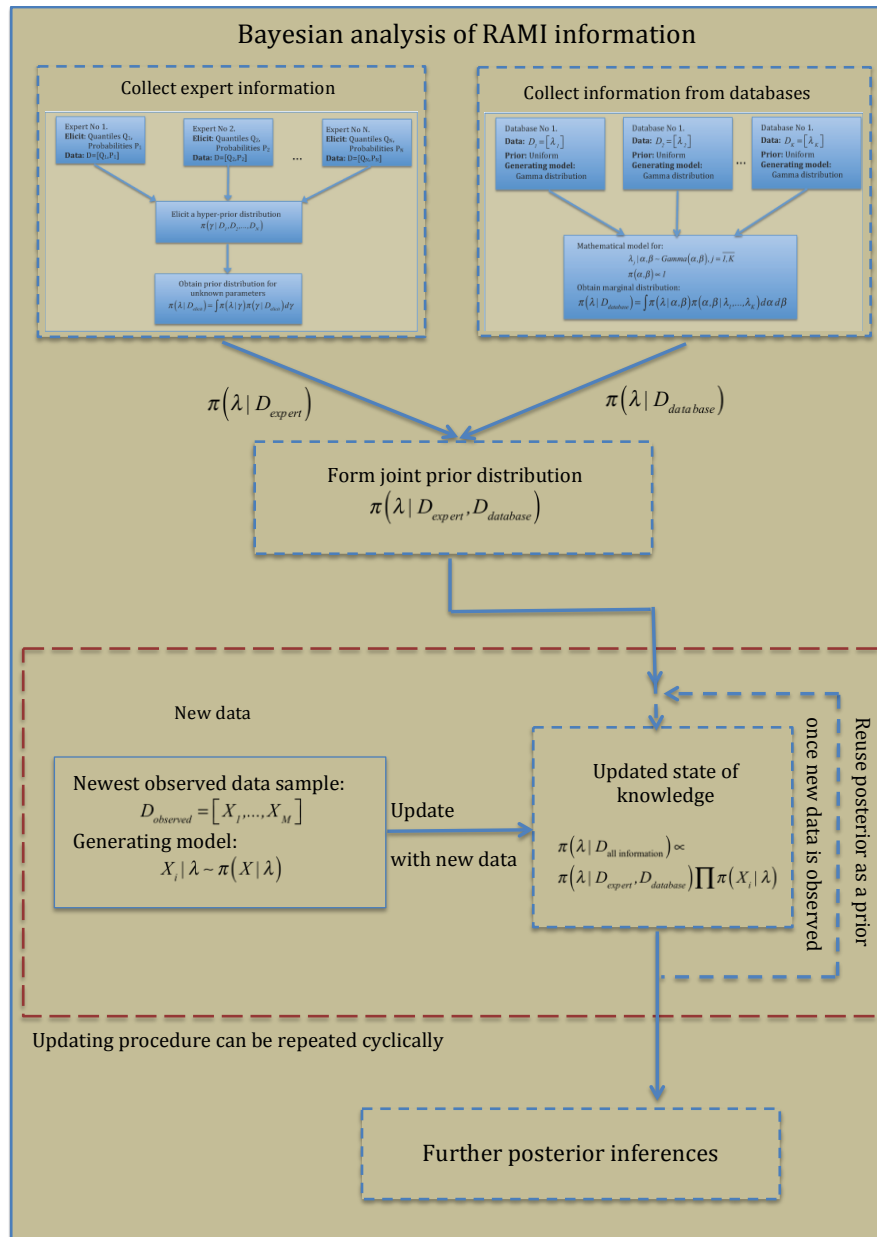


Fig. 2. Scheme of Bayesian analysis of RAMI information procedure

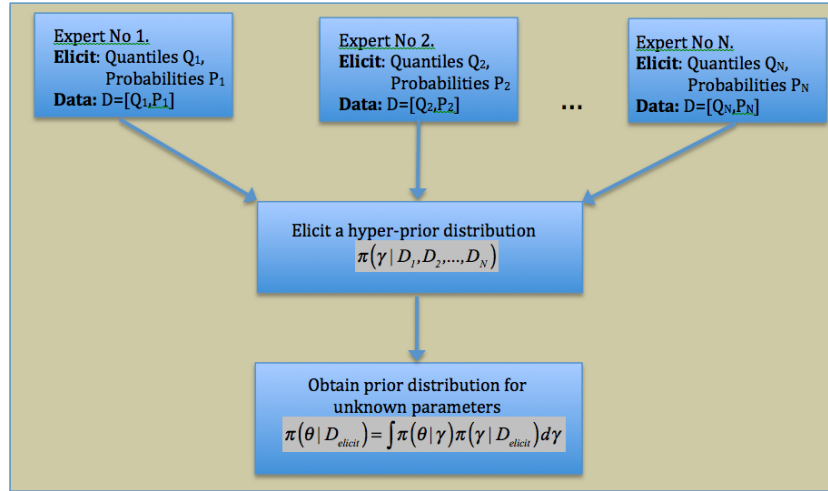


Fig. 3. Expert knowledge elicitation procedure

Let X be a possible vector of observations (e.g. failures, faults, times to failure, etc.) from a distribution, with density $f(X/\theta)$. Each expert may have their own conceptual model about θ , which we parameterize by γ so that $\pi(\theta/\gamma)$ belongs to a parametric class $\{\pi_\gamma, \gamma \in R^p\}$. The aim is to construct an informative prior distribution on q based on expert information denoted by D_{elicit} . Information on g can be obtained using posterior from a Bayesian analysis of the elicited information that begins with a prior π_0 and treats elicited knowledge as data, using the following scheme:

$$\pi(\gamma/D_{\text{elicit}}) \propto f(D_{\text{elicit}}/\gamma) \pi_0(\gamma) \quad (1)$$

Thus the elicited data D_{elicit} is considered conditional on the expert's knowledge, which here is conceptualized as being represented by the distribution π_0 and parameter γ .

The information can be summarized by integrating this posterior over possible parameterizations indexed by γ :

$$\pi(\theta/D_{\text{elicit}}) = \int \pi(\theta/\gamma) \pi(\gamma/D_{\text{elicit}}) d\gamma. \quad (2)$$

About experts and the elicited data

Lets assume that we interview N experts. To the expert e corresponds an unknown hyper-parameter g_e resulting in their own prior distribution $\pi(\theta/\gamma_e)$. To estimate this hyper-parameter, we interview each expert e and encode their knowledge on X . Denote D_e the set of the elicited quantities provided by expert e . Due to higher reliability, we confine our attention to quantiles and probabilities. Hence, D_e consists of a vector of quantiles Q_e and a vector of probabilities P_e .

Let $Q_e = (Q_{ek}, k = \overline{1, \dim Q_e})$ be the vector of elicited quantiles of the distribution $f(X/\theta)$ corresponding to specified cumulative probabilities $(p_{ek}, k = \overline{1, \dim Q_e})$ for expert e . Then $Q_{\text{elicit}} = (Q_e, k = \overline{1, N})$ is the vector of all the elicited quantiles for all experts.

Similarly we denote cumulative probabilities by $P_e = (P_{ek}, k = \overline{1, \dim P_e})$ the set of the elicited probabilities of $f(X/\theta)$ at the specified quantiles $(q_{el}, l = \overline{1, \dim P_e})$. Then $P_{elicit} = (P_e, e = \overline{1, \dim N})$ is the vector of all the elicited probabilities for all experts. We denote the complete set of elicited data by $D_{elicit} = (P_{elicit}, Q_{elicit})$. Each block of answers can be used as separate sources to provide the elicited distribution.

For each question t , the expert e also provides a measure of uncertainty in their answer in the form of a number $c_{et} \in (0, 1)$ quantifying the expert's confidence in their response.

This information allows building a measurement error model to quantify expert's individual accuracy. The main idea is to assume that the error (on the appropriate scale) with which experts specify elicited quantities are conditionally independent, given the expert's conceptual model γ_e . The ε_{et} are therefore independent and have a known distribution constructed by the assessor from the expert's measures of uncertainty c_{et} , together with measures of individual coherence and precision considered by the assessor, based for instance on the training of the expert or on previous expertise.

3.4. Bayesian assessment of RAMI databases information

The estimates contained in various databases can be also treaded as observable data, which was generated according to some stochastic model. Hence, we can perform Bayesian updating step for this kind of data and then after proper marginalization obtain a distribution that can be further processed as a distribution containing some prior knowledge about the parameters of interest. The most important question that should be asked is what is the generating model?

As the estimates contained in databases cannot be treated as directly observable, stating generating stochastic model is quite artificial in that we cannot justify it by any natural laws or any reasoning based on observable world. All we can do is to select a distribution based on some fitness measures. So, for example, if we are analysing failure, we can put gamma distribution on its values, since failure rate is strictly positive, etc. Further figure illustrates such case.

This database information analysis is performed by Bayesian tools as well. However, in order to have a legit prior distribution elicited from databases, we have to perform marginalisation over additional gamma parameters step.

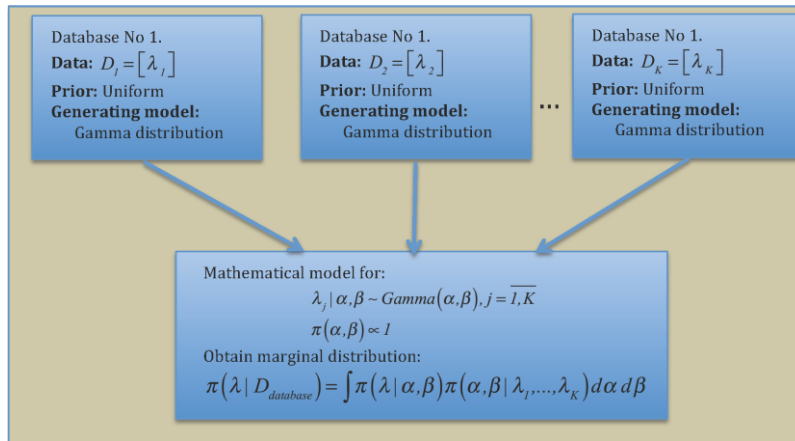


Fig. 4. Failure rate distribution elicitation from various databases

4. CASE STUDY: HELIUM COOLED PEBBLE BED WATER COOLING CYCLE UNRELIABILITY

4.1. Data description

The data, extracted from FCFR database is presented in the Table is failure rates of pipelines of various diameters (generic failure mode). This data will be used to estimate failure probability of HCBP water cooling cycle. Entries with upper and lower bounds give additional information about the probabilistic mechanism that, assumingly, produced respective failure rate. Hence, we could divide the available data into two parts: the one, with complete information about the stochastic nature of the data, and the part where just family of probability distributions is known. The second part could be easily assumed as data coming from parameterized distribution and we just have to estimate parameters of it. We could drop the information about upper and lower bounds in the first part and merge failure rate with the second part. We would loose some amount of information but would not have to bother ourselves any more with the question of how to use that additional information.

Another way could be to see that partial information as some kind of opinion elicited from a set of “virtual experts”. Lets assume that the failure rate estimates are distributed according to log-normal distribution with unknown parameters (μ, σ^2) . And the bounds are given for this distribution. Hence, we will view these quantiles as provided by different (subjective) experts. According to our methodology, we will produce a prior distribution obtained from these quantiles and will use it together with failure rate estimates to obtain a posterior distribution and related estimates.

Table 2. Failure rate and related data

Failure rate [1/(m*h)]	Source	Model	Lower bound	Upper bound
2.78E-10	IAEA-TECDOC-478	Log-Normal	3.00E-12	3.00E-09
2.50E-10	INEEL/EXT-98-00892	Exponential	1.25E-10	5.00E-10
2.50E-11	INEEL/EXT-98-00892	Exponential	8.33E-13	7.50E-10
8.86E-09	AICHE	Log-Normal	4.70E-10	1.00E-07
6.56E-08	RAGUSA	NA	NA	NA
2.78E-10	WASH 1400	Log-Normal	3.00E-12	3.00E-09
2.86E-11	INEL EGG-FSP-8709	Log-Normal	NA	NA
2.86E-10	INEL EGG-FSP-8709	Log-Normal	NA	NA
7.00E-10	INEL EGG-FSP-8709	NA	NA	NA
3.75E-09	INEL EGG-FSP-8709	Log-Normal	NA	NA

4.2. Prior distribution elicitation

Quantiles can easily be converted to the lognormal distribution parameters:

$$\sigma = \frac{1}{\Phi^{-1}(p_1) - \Phi^{-1}(p_2)} \log \left(\frac{F^{-1}(p_1)}{F^{-1}(p_2)} \right), \quad (3)$$

$$\mu = F^{-1}(p_1) - \sigma \cdot \Phi^{-1}(p_1)$$

where $\Phi^{-1}(p)$ is a p-quintile of standard normal distribution, $p_1=0.05$ and $p_2=0.95$, $F^{-1}(p)$ p-quintile of lognormal distribution.

To make our lives a bit easier, let's take a natural logarithm of σ^2 . Hence, the data from which we will form a prior is as in table:

Table 3. Data for prior formation

P (μ)	Q ($\log(\sigma^2)$)
-24.2	1.1306
-22.1	-2.0769
-24.4	1.1078
-19.9	0.6296
-24.2	1.1306

We further assume independency of parameters (μ, σ^2) and models for two sets of data:

$$\begin{aligned} P_i | \alpha_1, \beta_1 &\sim N(\alpha_1, \beta_1^2), i = \overline{1, n} \\ Q_i | \alpha_2, \beta_2 &\sim N(\alpha_2, \beta_2^2) \end{aligned} \quad (4)$$

Then the final prior for $(\mu, \log(\sigma^2)) = (\mu, \gamma)$ will be obtained as follows:

$$\begin{aligned} \pi(\mu, \gamma) &= \pi(\mu) \pi(\gamma) = \int_{-\infty}^{+\infty} \int_{-\infty}^{+\infty} \int_0^{+\infty} \int_0^{+\infty} \pi(\mu, \gamma | P, Q) \pi(P, Q | \alpha_1, \beta_1, \alpha_2, \beta_2) d\alpha_1 d\alpha_2 d\beta_1 d\beta_2 = \\ &= \int_0^{+\infty} \int_0^{+\infty} \pi(\mu | P) \pi(P | \alpha_1, \beta_1) d\alpha_1 d\beta_1 \cdot \int_0^{+\infty} \int_0^{+\infty} \pi(\gamma | Q) \pi(Q | \alpha_2, \beta_2) d\alpha_2 d\beta_2 \end{aligned}$$

After mathematical manipulations we obtain following prior distribution expressions:

$$\pi(\mu, \gamma) \propto \left[\left[(n+1)(\mu^2 + C_1^2 + 2b_1 - 2C_1\mu) + 2b_1 \right] \left[(n+1)(\gamma^2 + C_2^2 + 2b_2 - 2C_2\gamma) + 2b_2 \right] \right]^{-(n+2)}$$

or in original parameters:

$$\begin{aligned} \pi(\mu, \sigma^2) &\propto \sigma^{-2} \left[\left[(n+1)(\mu^2 + C_1^2 + 2b_1 - 2C_1\mu) + 2b_1 \right] \right. \\ &\quad \left. \cdot \left[(n+1)(\log^2(\sigma^2) + C_2^2 + 2b_2 - 2C_2 \log(\sigma^2)) + 2b_2 \right] \right]^{-(n+2)}, \end{aligned} \quad (5)$$

where $C_1 = \frac{n}{n+1} \bar{P}$, $C_2 = \frac{n}{n+1} \bar{Q}$, $b_1 = \frac{1}{2} \sum (P_i - \bar{P})^2 + \frac{n\bar{P}^2}{2(n+1)}$, \bar{P} and \bar{Q} are empirical averages of each data sample.

Hence, this prior distribution represents general prior opinion as given by group of “virtual” experts. In such a way we can exploit that additional information that some records failure rate databases have: we simply treat this information as an independent source of information provided by group of experts, while failure rate estimates are hold to be data sample in the usual sense.

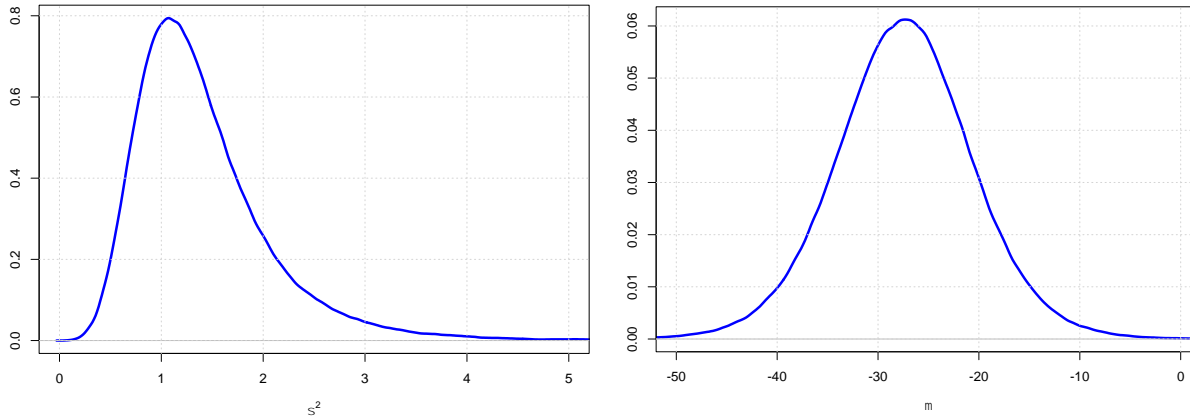


Fig. 5. Prior distributions as obtained from “virtual” expert elicitation procedure for lognormal distribution parameters

As can be visually inspected from prior distributions plots Fig. 5, the variances, especially for parameter m , are quite high. This is because the number of “virtual” experts is low.

4.3. Posterior analysis: combining different types of data

In this section we will give two posterior distributions: the one where prior distribution formulated in previous section is used, and another where prior distribution is uninformative in Laplace sense, i.e. flat prior distribution. We would like to compare these posterior distributions to gain insight into how different inferences would be if we would just drop that additional information about lognormal distribution quantiles.

Just to remind, our main assumption was that failure rates are data points generated from lognormal distribution:

$$\lambda_i | \mu, \sigma^2 \sim N(\mu, \sigma^2); \quad (6)$$

while prior distributions to be used are either:

$$\pi(\mu, \sigma^2) \propto \sigma^{-2} \left[\left[(n+1) \left((\mu - C_1)^2 + 2b_1 \right) + 2b_1 \right] \cdot \left[(n+1) \left((\log \sigma^2 - C_2)^2 + 2b_2 \right) + 2b_2 \right] \right]^{-(n+2)}, \quad (7)$$

or flat prior:

$$\pi(\mu, \sigma^2) \propto 1. \quad (8)$$

Although as indicated in methodological part, there could be many forms of non-informative prior distribution, our experience however shows that flat priors are well suited for samples of moderate size.

Even though variances for expert elicited prior distributions are quite high, still significant influence can be observed (see figure) on posterior distributions as compared to flat priors.

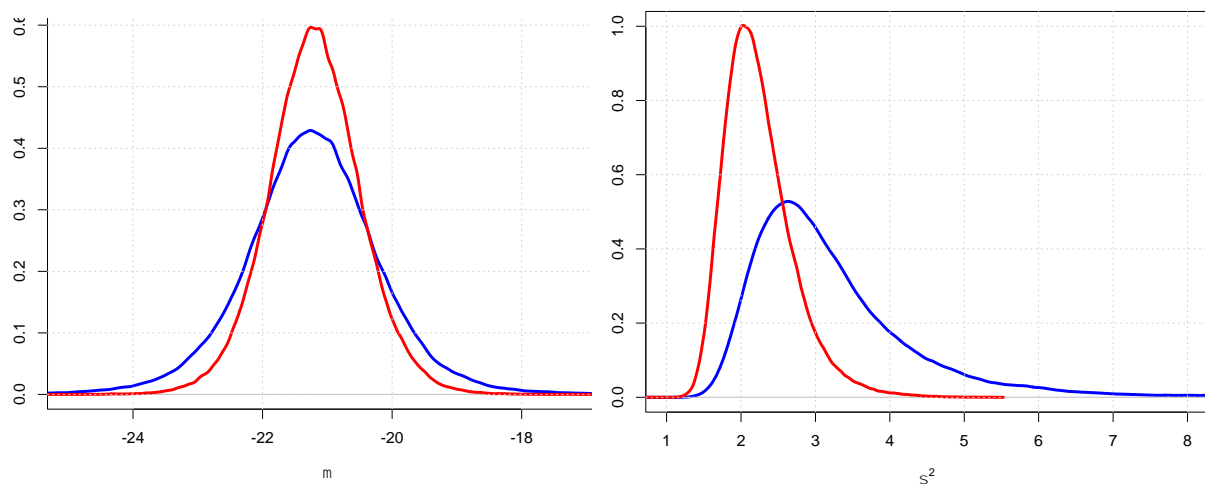


Fig. 6. Posterior distributions of parameters when no prior information is used (blue colour) and when prior form out of expert subjective opinion (red colour)

Such effect of informative prior distribution directly is transferred to pipeline failure probability estimates (see Table)

Table 4. Posterior estimates for parameters and probability of accident in pipelines.

	Mean	0.05	0.95	
Miu	-21.24	-22.92	-19.54	Non-Informative prior
Sigma	3.18	1.66	7.78	
Miu	-21.33	-22.52	-20.15	Informative prior
Sigma	2.26	1.98	5.14	
Probability	1.85E-05	2.00E-09	7.90E-05	Non-informative prior
Probability	7.70E-06	9.90E-09	2.70E-05	Informative prior

5. CONCLUSIONS

In this paper we were concentrating on the issue of handling various type of RAMI information: raw data, database records, expert subjective opinions. The unifying methodology were proposed and demonstrated.

The necessity of such methodology were concluded from the analysis of various reliability data sources, like WASH, lambda-predict, IAEA, T-Book, TKI, etc. Inconsistencies in records information, varying level of mathematical assumption justifications, non-existent data for DEMO, different experiences of experts – these aspects hinders the whole RAMI assessment process for the DEMO plant. And classical statistical methods does not give a hand here – this class of methods simply isn't suited for such differences in information. Hence, we proposed a methodology built entirely on Bayesian statistical notions. It enabled to create a scheme of workflow, by which those different information sources can be easily integrated into one analysis. In such way the methodology is able to extract much more information for the sake of RAMI assessment as compared to classical tools.

On the other hand there are some issues that needs to be resolved. Like the difficulty in obtaining prior distributions based on expert opinion elicitation. There are some mathematical notions at work, which might put off practitioners from applying Bayesian methods.

However, it is possible to provide some worked out examples of most common cases, so that one would not have to perform mathematical calculations (e.g. marginalization) by itself.

We demonstrated proposed methodology for a real case on HCBP water cooling cycle pipelines. By extracting additional information from databases we were able to improve posterior inferences. Out of 10 records, 5 of them had additional information about the probability distributions supposedly generating failure rates. This information was expressed in terms of quantiles. We assumed that this information was provided by virtual experts and out of this information prior distribution were formed.

Posterior results showed that the influence of this additional information translated into almost ten-fold differences in pipeline failure probability as compared with non-informative prior distribution.

REFERENCES

1. IAEA TECDOC 478. Component reliability data for use in probabilistic safety assessment. Vienna: International Atomic Energy Agency; 1988.
2. U.S. Nuclear Regulator Commission, Reactor Safety Study: An Assessment of Accident Risks in U. S. Commercial Nuclear Power Plant. WASH-1400 (NUREG-75/014), October 1975.
3. T-Book Reliability Data of Components in Nordic Nuclear Power Plants, 5th ed., Vattenfall AB, Vallingby, Sweden, 2000.
4. HAMADA, M.S.; WILSON, A.G.; REESE, C.S., MARTZ, H.F. Bayesian Reliability. Springer, 2008;
5. GOLDSTEIN M. Subjective Bayesian analysis: principles and practice. *Bayesian Analysis* 1(3):403–20, 2006;
6. PRESS, S.J. Subjective and Objective Bayesian Statistics: Principles, Models, and Applications, 2nd Edition. New York: John Wiley & Sons, 2003.
7. ALBERT, I., S. DONNET, GUIHENNEUE-JOUYAUX C., LOW CHOY S., MERGERSER K., ROUSSEAU J. Combining expert opinions in prior elicitation. *Bayesian Analysis* 7:503–532, 2012.
8. BURGMAN, M.A., McBRIDE, M., ASHTON, R., SPEIRS-BRIDGE, A., FLANDER, L., WINTKE, B., FIDLER, F., RUMP, L., TWARDY, C. Expert Status and Performance. *PLoS ONE*, 6(7): e22998: 1–7. 504, 526, 2011.
9. PINNA, T., CADWALLADER, L.C. Component failure rate data base for fusion applications. *Fusion engineering and design*, Vol. 51–52: 579–585, 2000.
10. PINNA, T., IZQUIERDO, J., PORFIRI, M.T., DIES, J. Fusion component failure rate database (FCFR-DB). *Proceedings of the Seventh International Symposium on Fusion Nuclear Technology. Fusion engineering and design* Vol. 81, Issue 8–14: 1391–1395, 2006.
11. MORRIS, S.F. Use and application of MIL-HDBK-217. *Solid State Technology*. 33, 65–69, 1990.
12. NSWC07 Handbook of Reliability Prediction Procedures for Mechanical Equipment. 2007.

USING STRAW FOR HIGH EFFICIENCY DISTRICT HEATING SYSTEMS

K. Vagoliņš

*Institute of Heat, Gas and Water technology,
Riga Technical University
Azenes str. 16, LV-1010 – Latvia*

ABSTRACT

The paper „Using straw for high efficiency district heating systems” contains an information of common and different things in between using a gas, woodchip and straw fired boilers in district heating systems. In the paper types of straw boilers and ways for using straw as fuel for heating is collected.

The main parameters which describe the heating system are gathered and analyzed. At the moment natural gas boiler is used as a primary energy source. The main problems that could appear after changing the energy source from natural gas to straw are gathered.

The main goal of the paper is to make it possible for the model show the parameters of the heating system after changing the energy source taking in account the possibilities to regulate the boiler parameters, fluctuations of the temperatures and energy production as well as heat demand by the consumers.

Keywords: Straw fired boiler, district heating systems, energy production, biomass boiler

1 INTRODUCTION

In terms of sustainable energy development in Latvia, as well as in the whole world, there is a growing need for using the alternative energy sources. Alternative energy sources are, in most cases, renewable: biomass, wind power, solar energy, hydro-power and geothermal energy. A need for the utilization of this kind of energy sources is dictated by the market, on one side, as well as by environmental protection, on the other. Prices of fossil fuels grow proportionally to the decreasing of fossil fuel reserves. Since available reserves of fossil fuels in Latvia, especially those of high quality, are relatively limited, this problem becomes even more emphasized [7, 8].

The straw fired boiler plants are rare used in Latvia because you have to spend a lot of time and money for preparing the fuel, building storage for it etc. In this case the situation is easier with wood biomass, there are a lot of woodchip suppliers in the market and you just have to sign the contract and the material will be delivered in your plant by desired schedule. So this means that owner doesn't have to build high capacity storages, organize material logistics etc.

Of course it is much easier to work with oil or gas boiler, because you don't have to look after the burning process, don't have ash in the plant etc., but according to customer data (the customer owns natural gas boiler plant and a straw fired boiler plant) by year 2013 the self-costs for energy production of natural gas boiler plant is 47 EUR/MWh and self-costs of straw fired boiler plant is 16 EUR/MWh, which means that straw fired boiler plant is almost 3 times cheaper in maintenance than natural gas boiler plant and about 1,5 times cheaper than chip fired boiler. [2]

Biomass is one of key renewable energy sources [10]. This is the reason for the development of cheap thermal devices (boilers and furnaces) burning biomass from agricultural production as quite available and cheap energy source. These devices could be used primarily in villages, small towns and small businesses processing agricultural goods

(greenhouses, dairy farms, slaughterhouses etc.) [11,8]. Devices could also be used for heating schools, hospitals, prisons and other institutions.

Mostly two technologies are currently used for the combustion of biomass bales. The first is based on whole-bale combustion in the combustion chamber, while the second considers combustion of biomass bales in “cigar” burners. The “cigar” firing technology provides better quality of the combustion process, resulting in lower pollutant emissions and increased plant efficiency. This technology was found to be very suitable for straw combustion and was deemed not to be associated with any process limitations.

In work is overview of different combustion types. It is made for future researches. There are made data collection from experimental stand device, determination of analyze methodology and prediction of results.

2 METHODOLOGY

2.1. Straw fired boilers and systems description

The boiler rating is fixed on the basis of the maximum heat amount to be supplied to the distribution net on the coldest day of the year. The heat amount can be divided into the net heating requirements of the houses (space heating and hot water) and piping loss in the distribution net. The sum of these two figures yields the heat production ex plant. As an example, the maximum district heating load for a town where the heat production ex plant is 11.200 MWh/per annum can be calculated. This is equal to the heating requirement of 400–450 single-family houses [1].

The various types of boiler plants have different firing principles that require different equipment for transport of straw and handling of straw from storage to boiler. The plants can be grouped in 5 typical systems: [2, 11]

- Boiler plant for chaffed straw;
- Boiler plant for shredded straw;
- Boiler plant for sliced bales;
- Boiler plant for cigar firing;
- Boiler plant for whole bales.

There are 2–3 manufacturers in the market that deliver all-in-one systems. The main components are both manufactured by themselves or they purchase sub-contracts in the form of filters, chimney, crane, and electric equipment etc. All boiler plants consist of the same main components:

- Straw storage with straw scales;
- Straw crane and straw conveyor (straw table);
- Chaff cutter/shredder/slicer (the 3 first-mentioned types);
- Firing system and boiler;
- Combustion air fans;
- Flue gas cleaning and ash/slag conveyor;
- Chimney and flue gas fan;
- Control and regulation equipment [11].

2.2. Boiler Plants for Continuous Firing of Whole Bales

Instead of cutting strings, chaff cutting/shredding of the straw, the whole bales are pushed into the boiler in an endless line where they burn from the end. The crane places the bale in a

feeder box, and a hydraulic ram stoker forces the bale into a tunnel from where it via carriers are carried towards the burner in the boiler wall. The volatile gases are driven out in the burner and are burnt by means of a large number of secondary nozzles. Then the bale is still pushed forward, and the unburnt straw and ash fall on to a water cooled grate for final combustion [1].

“Cigar firing principle”. Big bales are pushed continuously into the combustion chamber where they burn from the end. Combustion air is introduced via nozzles in the inclined burner front. Ash and partly burnt straw fall on to the inclined grate and burns out before being pushed towards the slag hopper farthest below in the picture.

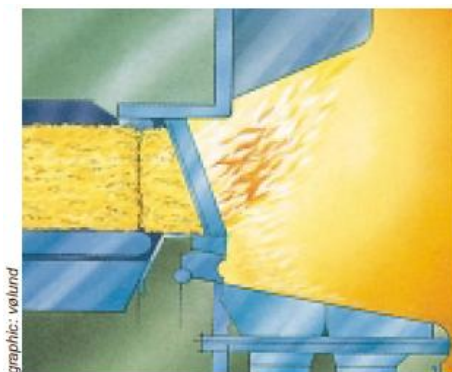


Fig. 1. Cigar firing principle

2.3. Flue Gas Cleaning

The flue gas from the combustion should be cleaned in order to comply with statutory requirements. The Latvian Environmental Protection Agency has suggested the following limit values concerning biomass-fired boilers above 1 MW: Dust emission: Maximum 150 mg/ Nm³ (Nm³=normal cubic meter, i.e. at 0°C). Carbon monoxide percentage maximum 0.05% (volume percentage at 11% oxygen in the flue gas). In Latvia aren't limited more emissions as NO_x, CH₄, CO₂ for straw fired boiler. It will be described in future researches. For plants below 1 MW, there are no well-defined requirements, but the authorities that grants certificates of approval normally use the above values in respect of district heating plants below 1 MW. Flue gas cleaning reduces the amount of fly ash, thereby avoiding particles spreading over the surrounding buildings. The carbon monoxide content is set out in more detail under the section on environmental conditions [4].

Flue gas cleaning equipment may consist of:

Multicyclone: Cleaning, thereby extracting dust particles from the flue gas by centrifugal action taking place in vertical tubes.

Bag filter: The flue gas passes through fine-meshed/pored bags that trap the suspended solid particles.

Electrostatic filter: The flue gas passes through an electric field, and the particles precipitate on electrodes.

Flue gas scrubber: The flue gas passes through a shower so that the particles are trapped/caught in the water.

Flue gas condensation: The flue gas is cooled to below the dew point, and the particles are absorbed/trapped by the dew. The normal equipment is a multicyclone to serve as spark arrester and for coarse particles followed by a bag filter. The multicyclone cleans the flue gas from 1.000–2.000 mg dust/Nm³ to 500–600 mg/Nm³. Much of the fly ash from straw firing is so fine-grained (below 0.01 mm) that the filter bags are the best and cheapest solution for

complying with the requirement of 40 mg dust/ Nm³. The particle content of the dust after filter is under normal operation 20–30 mg dust/ Nm³ with bags without cracks. See also the section on environmental conditions. Electrostatic filters may give problems in connection with straw fired plants. Two plants that originally had electrostatic filters have replaced them with bag filters. The dust particles are difficult to ionize in the electrostatic filter, and it is difficult to make them leave the electrodes and fall off to the ash system due to the very small mass. Some of the particles therefore condense and deposit like coating in the chimney, and, in particular, when the plant is started up, lumps of soot are carried along and fall down in the neighborhood of the plant. A few heating plants have installed a flue gas scrubber. The principle is that the flue gas passes through a “waterfall” of atomized water, thereby absorbing the dust particles, thereby transporting them with the water. This method creates a waste-water problem for the plant instead of an ash deposition problem. As something new, the district heating plant Hals Fjernvarme has installed a flue gas condenser. Experiences gained over the first years are good despite the low water content of straw. The operating costs for electrical power are approx. 5% lower for the entire plant. The costs of maintenance are 1/3–1/4 compared to the filter bags.

2.4. Ash (products of combustions)

Straw contains 3–5% ash. Part of the ash falls off the grate into a hopper under the boiler and passes via the chain scraper to the ash container. The chain scraper usually lies in a water bath where an automatic water addition takes place simultaneously with the water evaporating and being carried together with the ash to the container. Wet transport of the ash is the most normal procedure at the plants, and a water bath in the chain scraper is an efficient trap so as to prevent the introduction of false air to the boiler through the ash conveyor system. The fly ash consists of the suspended solids that follow the flue gas through the boiler and are separated in cyclone and filter. From there, the particles are transported via worm conveyors to the chain scraper [6].

2.5. Control, Regulation and Monitoring/Supervision

The system usually consists of two computers:

- A PLC (Programmable Logic Computer) that collects operating data from the plant and keeps the plant to chosen values for pressure, temperature, flow etc.
- An ordinary PC that shows the operator the actual data from the PLC on a visual display screen and via printouts. The chosen values can be changed on the PC, and the plant operating conditions can be changed via the PLC.

The system is divided into three main functions covering the following:

- The control takes care that the entire process takes place in a pre-set sequence. The crane, e.g., is programmed not to pick up a new straw bale until the preceding bale has been fed into the boiler and the boiler working thermostat calls for more heat.
- The regulation takes care that the values chosen for pressure, temperature etc. are maintained.
- The monitor signals malfunctions. The alarm can via a bleep be transmitted to the person on duty in or outside the plant. Usually the plant is manned from 08:00–16:00 hours during the 5 working days of the week [5].

3 SYSTEM MODEL

For creating a model and simulating the situations the shortened PLC program can be used to simulate how the boiler reacts to the changes of the parameters in the system as well as malfunctions in the system according to average statistical data and human factor, which could be:

- 1) Missing material for burning;
- 2) Dusty water boiler heat surface;
- 3) Blockages in the flue gas system;
- 4) Ash container exchange schedule;
- 5) Reaction times on the malfunctions in the plant.

The same upgraded visualization program only upgraded can be used for watch after the plant model, where other menu can be invented for giving the parameters to the system of which does the user want to see the plant reaction for. For example, rapidly give a heat demand from minimum 30% of the boiler nominal heat production to nominal 100%. The user could see how fast could the boiler raise it's power to provide the nominal power, what could be the fuel consumption at the situation and to understand if it's more efficient to raise the power of the plant rapidly or to raise it step by step.

4 EXPERIMENTAL STAND DEVICE SCHEME

In order to assess the combustion quality and to obtain data for the design of a mixed straw-fired hot water boiler, a demo furnace with thermal power of 7 MW has been designed (by Agro) and built. The appearance of the furnace, with the thermocouple probes, the primary air fan and channel, and the fuel feeding channel is shown in Figure 2. This furnace has been adopted for cylindrical bales, with 1.2–1.5 m in diameter which were available at that time. The boiler plant is built in 2012. The boiler plant consists of: 1) Material hydraulic conveyer; 2) Firebox; 3) Automatic ash discharge system; 4) Vertical 3-way firetube boiler; 5) Multicyclone; 6) Flue gas recirculation system; 7) Chimney.

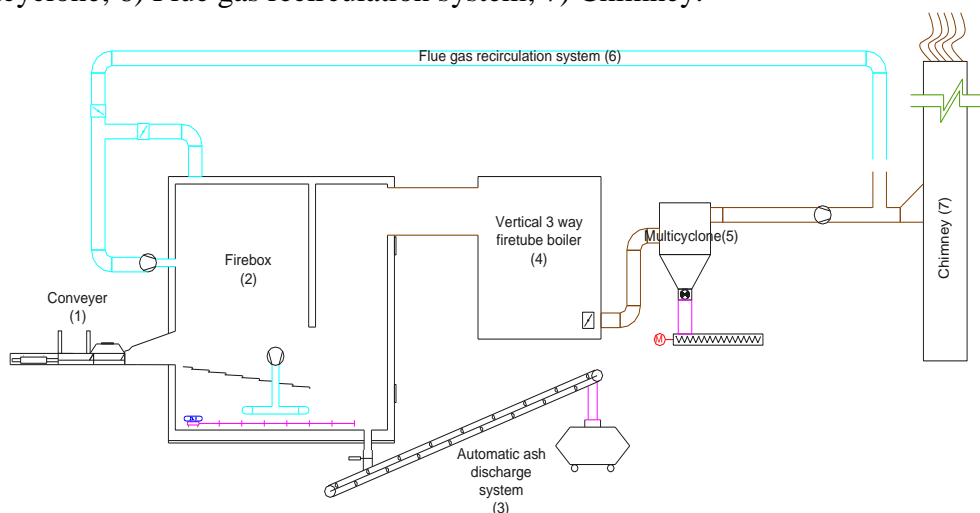


Fig. 2. Straw-fired boiler plant components

** any other flue gas cleaning system is not used because latvian laws do allow the maximum amount of particles in the flue gas up to 150 mg/Nm^3 , an this amount is reachable with using a multicyclone only*

Thermal scheme of distribution facilities is shown in Fig. 3. From it can be seen following thermal circles: a) Hot water from the boiler goes directly into a building that is heated, b) Hot water from the boiler goes into heat only tank, c) Hot water from the boiler

going at the same time in the building and heat reservoir, d) Hot water tank from the heat goes into the building. Also, the boiler is equipped with appropriate management and control system

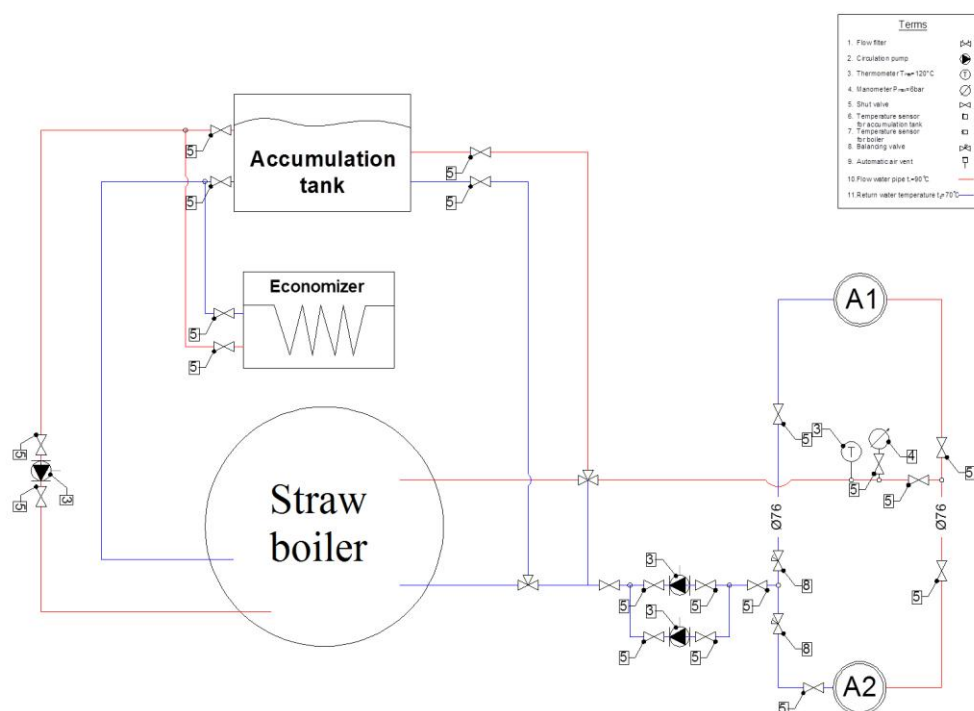


Fig. 3. Experimental stand device scheme

5 RESEARCH OF DEMO FURNACE

In the research the values of following sensors were gathered Fig. 4.

- 1) Straw moisture, %;
- 2) Three temperatures in the firebox:
 - a. Temperature under the moving grates, °C;
 - b. Temperature in the firebox, °C;
 - c. Temperature in the afterburning chamber, °C.
- 3) Amount of the primary air given, %;
- 4) Amount of the secondary air given, %;
- 5) Flue gas temperature, °C;
- 6) Remaining amount of the oxygen in the flue gas, %;
- 7) Amount of the flue gas fan, %.
- 8) Flow and return temperature of the boiler and the grid, °C [1, 8].

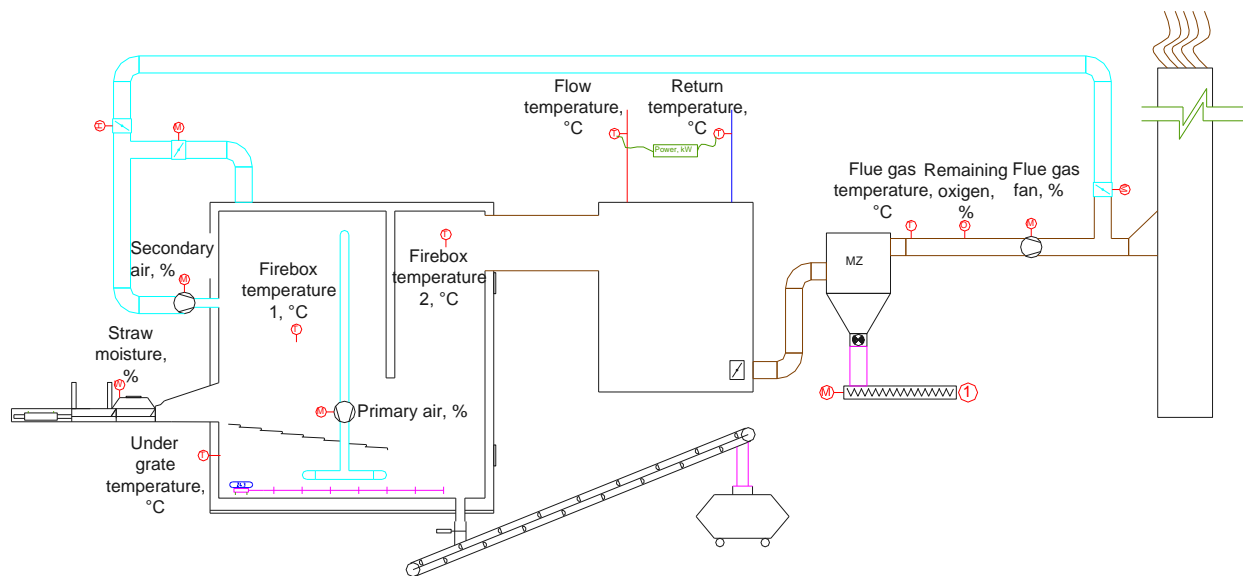


Fig. 4. Sensors placed in the straw-fired boiler plant

Different tests were made. Test 1 was conducted with one bale of straw placed in the feeding channel. Only temperature measurements (example of results in Table 1) were done, and the results showed that the temperature in the combustion zone, in steady conditions, was quite stable (730–830°C, Fig. 8) for a reasonable period of time (40 minutes). It was noted that the amount of tertiary air did not contribute much to overall combustion conditions, and that in fact this air over-cooled the flue gases in the combustion zone.[11]

In test 2, along with temperatures, gas composition was continuously measured. Less air was supplied as tertiary than in test 1. In the initial, start-up period, gas samples were taken directly from the combustion zone, and very high levels of CO in the flue gases were noted. After the choking of the gas sampling probe and its cleaning, and also in all following tests, gas samples were taken only from the top of the furnace. As the temperature in this period increased to approximately 1000°C, bale feeding was slowed down, and this corresponds to the temperature downfall (min. 50–75). Soon after that, stable conditions were obtained, primarily by adjusting bale feeding [8].



Table 1. Example of data received from the PLC

Time	Flue gas fan, %	Primary air, %	Secondary air, %	Flue gas temperature, °C	Firebox temperature 1, °C	Firebox temperature 2, °C	Temperature under grate, °C	Remaining amount of O ₂ , %	Straw moisture, %	Boiler flow temperature, °C	Boiler return temperature, °C	Grid flow temperature, °C	Grid return temperature, °C	Power, kW
1:04:00.916	20,00	21,33	49,86	158,2	834,0	948,0	171,6	14,69	37,37	101,9	85,6	74,3	56,1	2914,4
1:05:00.742	20,00	23,78	46,67	170,9	830,8	911,6	172,4	11,34	37,37	101,9	85,5	74,5	56,2	2956,0
1:06:00.570	20,00	23,74	44,99	179,8	828,4	891,6	173,2	11,34	37,37	101,8	85,2	74,1	56,3	2881,9
1:07:00.395	20,00	23,85	44,00	182,6	827,2	880,0	173,2	10,71	37,37	101,6	85,8	74,0	56,3	2888,9
1:08:00.227	20,00	23,97	43,28	182,5	825,6	871,6	173,2	10,50	37,83	101,2	85,6	73,9	56,5	2872,7
1:09:00.050	20,00	26,26	43,45	184,0	824,0	873,6	172,8	9,14	37,83	100,7	85,3	73,9	56,4	2838,0
1:10:00.887	20,00	26,37	43,73	186,1	823,6	876,8	172,8	9,45	37,83	100,5	85,7	73,9	56,4	2856,5
1:11:00.715	20,00	26,42	43,55	186,2	824,0	874,8	172,4	9,35	37,83	100,4	85,6	73,8	56,6	2780,1
1:12:00.544	20,00	26,46	43,25	184,4	824,8	871,2	172,0	9,56	37,83	100,3	85,5	73,8	56,4	2814,8
1:13:00.367	20,00	26,37	42,90	182,5	826,4	867,2	171,6	9,25	36,85	100,4	85,8	73,9	56,6	2747,7
1:14:00.193	20,00	26,42	42,77	180,7	826,4	865,6	171,6	9,25	36,85	100,3	85,1	73,8	56,5	2770,8
1:15:00.020	20,00	26,47	42,66	179,7	826,4	864,0	171,2	9,35	36,85	100,2	85,1	73,9	56,6	2763,9
1:16:00.860	20,00	26,38	42,39	178,0	826,0	861,2	171,2	9,56	36,85	100,3	85,5	73,9	56,7	2770,8
1:17:00.687	20,00	26,36	41,94	175,5	826,0	856,0	170,8	9,98	36,85	100,3	85,6	73,8	56,6	2763,9
1:18:00.515	20,00	26,42	41,39	172,2	826,0	849,6	170,8	10,09	36,15	100,2	84,9	73,8	56,6	2738,4
1:19:00.340	20,00	26,76	40,78	169,7	824,8	842,4	171,2	11,02	36,15	99,7	86,0	73,8	56,7	2738,4
1:20:00.167	20,00	26,92	39,95	166,7	822,8	832,4	171,2	11,65	36,15	99,5	85,5	73,8	56,8	2729,2
1:21:00.879	20,00	27,17	39,10	163,8	819,2	822,8	171,2	12,28	36,15	99,2	85,7	73,6	56,7	2713,0
1:22:00.778	20,00	28,46	38,48	162,4	814,4	815,6	171,2	11,76	36,15	98,8	85,5	73,4	56,7	2680,6
1:23:00.660	20,00	30,37	38,34	162,8	810,4	814,0	171,6	10,71	35,90	98,6	85,1	73,3	56,6	2638,9
1:24:00.489	20,00	31,23	38,38	163,8	805,2	814,4	171,6	10,61	35,90	98,0	85,1	73,0	56,8	2578,7
1:25:00.256	28,80	31,57	38,31	163,9	800,0	814,0	171,6	10,92	35,90	97,7	85,3	73,0	56,8	2604,2
1:26:00.144	28,45	31,91	38,00	162,9	796,0	810,0	172,0	11,76	35,90	97,3	85,3	72,8	56,7	2562,5
1:27:00.768	28,70	32,21	37,55	161,7	792,0	804,8	172,8	11,65	35,92	97,2	85,7	72,8	56,8	2511,6
1:28:00.806	28,37	32,67	36,90	159,9	787,2	797,2	172,8	12,18	35,92	96,8	85,3	72,5	56,7	2495,4

Table 2. Tests made for straw fired boiler

Test	1	2	3
Number of bales in the feeding tube	1	2	2
Amount of straw [kg]	134,6	280	327.97
Primary air [m ³ /h]	1548	1548	1548
Secondary air [m ³ /h]	-	-	234
Tertiary air [m ³ /h]	504	252	108
Calculated thermal power [kW] ⁺	485,2	529.3	556.5
Average air excess coefficient λ [-]	not measured	4.71	2.61
Test duration [min]	47	89	99

High level of CO concentration at the furnace top in test 2 urged the introduction of a small amount (approximately 10% of total air) of secondary air in the combustion zone, which would cool down the movable cross at the same time. It was also noted that tertiary air flow rate should be decreased, and therefore secondary air was introduced to the detriment of tertiary air. This change in design was examined in test 3, with two bales placed in the feeding channel. [8, 11]

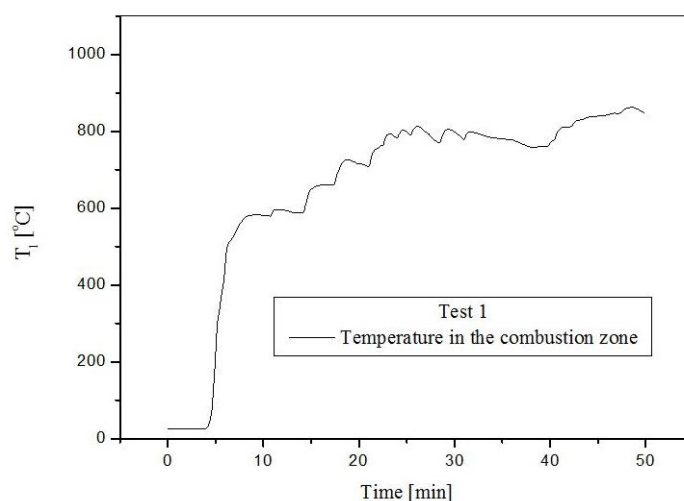


Fig. 5. Test 1 results

The supply of the secondary air through the cross provided excellent conditions for combustion – the concentration of CO was equal to zero for most of the time during the test. The air distribution (82% primary air, 12% secondary, 6% tertiary) was found to be well suited for maintaining steady conditions inside the furnace. On the other hand, the stability of the thermal output was found to depend largely on the active length of the bale immersed into the furnace [8, 9].

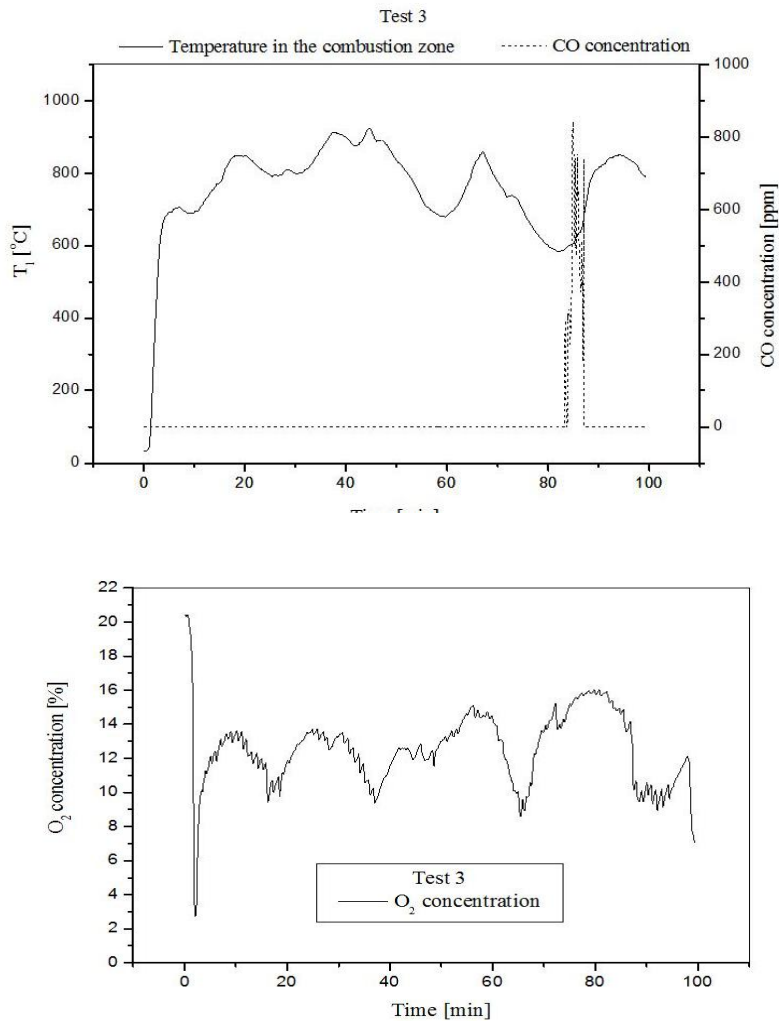


Fig. 5. Test 3 results

Therefore, it is of great importance to feed the bale uniformly in accordance with the combustion process, and to maintain this length as stable as possible, by moving the cross accordingly. The temperature instabilities (from the minute 45 further on, Fig. 5) during this test are a consequence of changes of this length. The only peak in CO concentration coincided expectedly with low temperatures during this period. Nevertheless, this test proved that the adopted concept of the furnace provided good conditions for efficient combustion of soya straw bales, with O₂ concentration ranging from 10–14% (Fig. 5), and an optimal average value of λ [8].

6 CONCLUSION

During experimental investigation of the boiler occasionally came to some minor problems in boiler operation. The problem was detected in the poor biomass burning. It is assumed that the main cause of problems is uneven quality of bales. Therefore, it is examined in detail the quality and moisture in bales that are stored and used in regular plant operation. It is assumed that poor bales quality could come from two reasons: a) rainy season in the period of collection of soybean straw in the fields; b) The increase in moisture content during bales storage up to their use.

Analyzed combustion system promises a more competitive use of renewable for “green” heat and power generation as well as their use in various industrial applications. In the same time, biomass combustion in cigar burners need to be modeled by appropriately developed numerical model. The model need to be developed enabled the effect of fuel moisture content on the temperature distribution in the furnace to be analyzed, as well as related emissions of harmful combustion products into the environment. Research investigation conducted has demonstrated that high combustion temperatures can be achieved. CO and NO_x emission levels are lower than the regulatory emission limit values defined by Latvian legislation.

The end users could invent the boiler plant virtually in their district heating system and see if the desired plant will give the necessary reaction on the changes in the parameters and choose the right for them. Especially this would help the user which are using natural gas or oil boiler plants and want to use biomass boiler plants in the future.

7 REFERENCES

1. NIKOLAISEN, L. *Straw for Energy production*. Centre for Biomass Technology, Copenhagen: 1998, 53 p.
2. *Ecoenergy, Wood fuelled boiler biomass energy services district heating*. Ecoenergy Limited: British Gas – 2009, 4 p.
3. Būvniecības, enerģētikas un mājokļu valsts aģentūra; *Atjaunojamo energoresursu potenciāls Latvijā*. Rīga, SIA “Gandrs”: 2010, 60 p.
4. ADAMOVIČS, A, DUBROVSKIS, V, PLŪME, I, JANSONS, Ā, LAZDIŅA, D., LAZDIŅŠ, A. *Biomassas izmantošanas ilgtspējības kritēriju pielietošana un pasākumu izstrāde*. Rīga: 2011, 146 p.
5. REAY DAVID, KEW PETER. *Heat pipes. Theory, design and applications* - Butterworth – Heinemann. Fifth edition, 2006–130 p.
6. *Ecoenergy, Wood fuelled boiler biomass energy services district heating*. Ecoenergy Limited – British Gas – 4 p.
7. DODIĆ S., ZEKIĆ V., RODIĆ V., TICA N., DODIĆ J., POPOV S. 2010 Situation and perspectives of waste biomass application as energy source in Serbia. *Renewable and Sustainable Energy Reviews*, 2010 – p. 1–23.
8. BRANISLAV S. REPIĆ, DRAGOLJUB V. DAKIĆ, ALEKSANDAR M. ERIĆ, DEJAN M. ĐUROVIĆ, STEVAN D.J. NEMODA AND MILICA R. MLADENOVIĆ. *Development of the Technology for Combustion of Large Bales Using Local Biomass*, Belgrade, Serbia – 2012 – p. 1–34.
9. REPIC, B., DAKIC, D., DJUROVIC, D., & ERIC, A. (2010). Development of a boiler for small straw bales combustion. Nathwani J., Ng AW, editors. *Paths to sustainable energy*, Rijeka, InTech, p. 647–664.
10. KAVALOV, B., & PETEVES, S.D. (2004). *Bioheat applications in the European Union: Ananalysis and perspective for 2010*. European Commission, Directorate-General Joint Re-search Centre, Institute for Energy.
11. DAKIĆ, D., REPIĆ, B., ERIĆ, A., DJUROVIĆ, D., & PAPRIKA, M. (2011). Development of small balle feeding devices for use in agricultural biomass combustion systems. *Contemporary Agricultural Engineering*, 37, p. 165–174.

EXPERIMENTAL AND NUMERICAL INVESTIGATION OF THE THERMAL CONDITIONS OF PLASMA LAMP

M.Yu. Liakh, A.P. Tsitovich, A.A. Khartonik

*Luikov Heat and Mass Transfer Institute
P. Brovka, 15, 220072, Minsk – Belarus*

ABSTRACT

Experimental and numerical investigations of plasma lamp were performed. The temperature field distribution in the system was obtained. The most heated areas at stationary operating conditions of the instrument were determined. On the basis of experimental and numerical data the most critical places were found. Most thermally loaded components of the plasma lamp are AC/DC-converter, light emitter and driver. All of these components of the lamp are the most important elements of the system, and proper work depends on the operation of these parts. There were drawn conclusions to improve cooling of the mentioned objects.

Keywords: plasma lamp, lightning system, plasma lightning systems, heat transfer, numerical modelling, experimental investigation.

1. INTRODUCTION

With the increase in energy consumption and environmental pollution, especially associated with the use of lighting devices, a growing need to explore new save and energy efficient lighting products. For this reason, various types of lamps are currently actively studied and improved, for example plasma lamps PLS (Plasma Lighting System) are of great practical interest. Such lamps are driven by the energy of the radio waves generated by the magnetron. The principle of operation of the plasma lamps is microwave gas ionization. Magnetron emits microwave radiation which excites the sulphur vapor inside the lamp bulb filled with argon and when the temperature reaches a certain value, the gas goes into a plasma state, which constantly emits light.

Interest in the study of such devices caused by a number of advantages [1]:

- a) lamps are characterized by a high color rendering index (from 80 to 85) and reproduce the light close to natural sunlight ;
- b) productivity is much higher than other sources of artificial daylight: 120 lm/W in the afternoon and up to 200 lm/W at night ;
- c) in the visible emission spectrum is completely absent flicker or ripple of light, colour distortion of images;
- d) are able to work up to 25 000 hours (mercury lamps from 4000 to 12000 hours, fluorescent light sources from 3000 to 17000 hours , halogen lamps up to 5000 hrs) .
- e) under the light of plasma lamps processes of photosynthesis is possible, which makes opportunity of using in greenhouses;
- f) plasma light sources (like LED) do not contain environmentally harmful substances.

However, in addition to the many benefits of using PLS- lamps have to face some difficulties in the operation of this device. An important issue is the sensitivity of some of the individual elements of the lamp to a high level of operating temperatures, so for example, the work of the hardware driver amplifier, located in the electronics block of PLS-lamp, at temperatures exceeding 85 °C leads to a reduction in the service life of the whole system. Therefore, when the operating temperature exceeds the threshold value equal to 95 °C device is forcibly de-energized. It is also extremely important to cool the light emitting bulb, for the

reason that at high temperatures there is a risk that sulphur can lose its polymorphic properties. As a result, the emission will have a line spectrum.

Due to the complexity and laboriousness of experimental research in this area, computer simulation is a matter of great scientific and practical significance as an alternative research method. Numerical simulation of the test fixture allows you to get the temperature distribution on the optical and electronic components and reveals the most thermally loaded areas of lamps. The results obtained make it possible to develop recommendations for the optimization of the test fixture.

The task for this research was experimental and numerical investigation of the lamp, prepared for serial production, to avoid dangerous thermal conditions.

2. EXPERIMENTS

Plasma lamp is a lighting device, where the light source is a bulb with a gas being in an electromagnetic field of high frequency. For producing of the light emitting device must be supplied with electricity of high frequency different from the electricity network. For this purpose, a current converter AC/DC is used. Terms of plasma ignition and operation of the plasma lamp is electronically controlled by the driver.

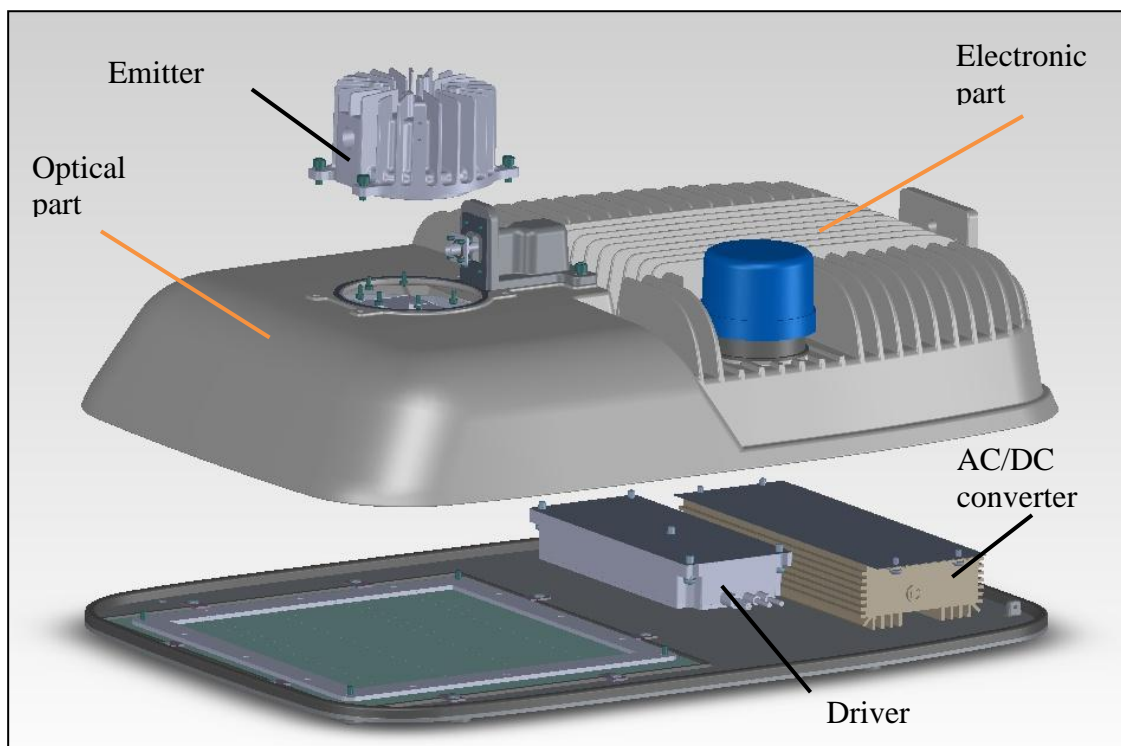


Fig. 1. The structure of the plasma lamp

Experimental study of the plasma lamp is conducted using thermocouples (type-K), Fig. 2. Thermocouples were placed on the surface of the plasma lamp housing in the vicinity of the main functional units. Temperatures in the emitter, AC/DC converter, electronic control module are measured. The signal from the thermocouples went to the measuring device Agilent 48970A. The received data is stored and processed on a PC.

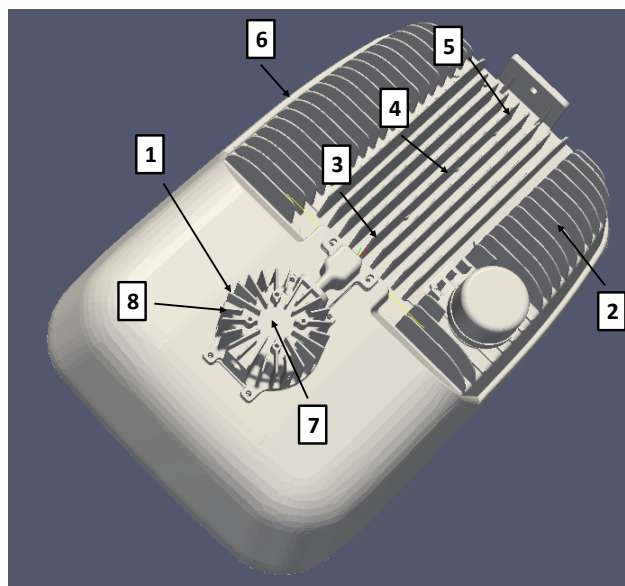


Fig. 2. The placement of thermocouples (1, 7, 8 – emitter, 2, 5 – AC/DC converter, 3, 4 – electronic control unit, 6 – side of the case)

As a result of experiments, Fig. 3, it was found that the most thermally loaded parts are the lamp emitter, AC/DC converter and an electronic control unit. Moreover, the emitter is heated to temperatures up to 120 °C in approximately 400–500 seconds.

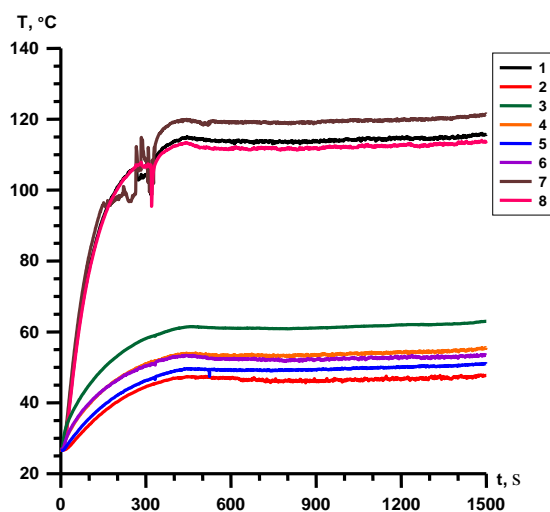


Fig. 3. Experimental data

3. CAD-MODEL AND APPLICATION OF COMPUTATIONAL GRID

CAD – model of plasma light was created in SolidWorks and imported into OpenFOAM for further calculations. With utility SnappyHexMesh, provided with the package OpenFOAM, complex hexahedral and split hexahedral elements of the object are automatically created. Created grid is used for the final calculation of thermal fields in the electronic and optical blocks of the plasma lamp.

All system consists of a large number of parts, which differ from each other not only in form and material, but also in its functional orientation. That is why calculating grids were created for each element individually to avoid any problems, e.g. automatic deletion of some

internal surfaces, surfaces combining of various parts, which are in contact with each other, in a common surface, or combine several parts into a single piece. Three-dimensional view of the computational grid is shown in Fig. 4.

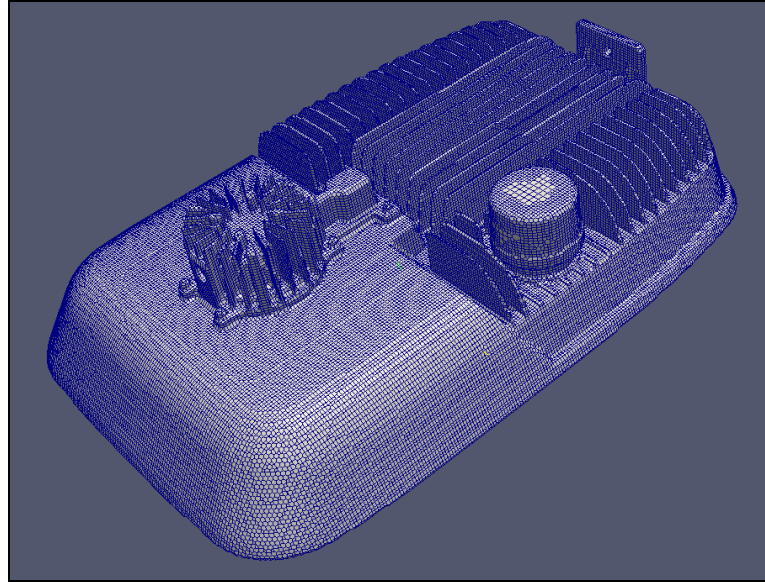


Fig. 4. The lamp with simulated grid

For the thermophysical calculations of the test plasma lamp we used a standard solver chtMultiRegionFoam. This solver allows solving complex problems of heat transfer in systems composed of solids, washed by liquid or gas. In operation of any lighting devices all kinds of heat transfer occur: convection, conduction and radiation heat transfer. However, the above-mentioned standard solver allows for only two types of heat transfer – conduction and convection. Therefore, the code solver chtMultiRegionFoam was changed to use radiation too.

4. THE MATHEMATICAL MODEL

All above-mentioned types of heat transfer are considered during solution. The conservation equations for thermal energy in the task are as follows [2]:
for the areas of air-filled:

$$\rho C_p \frac{\partial T}{\partial t} + \rho C_p \vec{u} \cdot \nabla T + \nabla \cdot (-k \nabla T) = Q, \quad (1)$$

for solid-state areas:

$$\rho C_p \frac{\partial T}{\partial t} + \nabla \cdot (-k \nabla T) = Q, \quad (2)$$

where $Q = 0$ for elements without heat sources.

In areas of radiative heat transfer (optical block plasma illuminator), Q includes heat flux, which is calculated by the formula [3]:

$$Q = aG - 4(e\sigma_{SB}T^4 + E), \quad (3)$$

where the intensity of the incident radiation G is determined from the following expression:

$$\nabla \cdot \gamma \nabla G - aG = 4(e\sigma_{SB}T^4 + E), \quad (4)$$

$$\gamma = 1 / (3\alpha + \sigma_{Eff}). \quad (5)$$

For areas filled with air, the velocity field and pressure are to be found. The calculation of these parameters uses the continuity Equation and the equation of conservation of momentum in the form:

$$\frac{\partial \rho}{\partial t} + \nabla \cdot (\rho \vec{u}) = 0, \quad (6)$$

$$\rho \frac{\partial \vec{u}}{\partial t} + \rho \vec{u} \cdot \nabla \vec{u} = \nabla \cdot \left[-p \vec{I} + \mu (\nabla \vec{u} + (\nabla \vec{u})^T) \right] + \rho \vec{g}. \quad (7)$$

At the initial time temperature of the entire lamp assumed to be equal to the ambient temperature (25 °C).

$$T_{si}|_{t=0} = T_0 \quad (8.1)$$

$$T_{fi}|_{t=0} = T_0 \quad (8.2)$$

Air pressure in the lamp is considered equal to atmospheric pressure, and velocity of air is neglected, i.e.

$$p|_{t=0} = 10^5 \text{ Pa} \quad (8.3)$$

$$\vec{u}|_{t=0} = 0 \text{ m/s} \quad (8.4)$$

Boundary conditions for thermal energy conservation equations are set so that the gradients of temperature and the temperature at the boundaries of elements in contact were equal to each other:

$$T_{si}|_b = T_{sj}|_b, i \neq j \quad (9.1)$$

$$T_{si}|_b = T_{fi}|_b \quad (9.2)$$

$$q_{si}|_b = q_{sj}|_b, i \neq j \quad (9.3)$$

$$q_{si}|_b = q_{fi}|_b \quad (9.4)$$

Air velocity at the boundaries assumed to be zero

$$\vec{u}|_b = 0 \text{ m/s} \quad (9.5)$$

5. SIMULATION RESULTS

As a result of computer simulation of heat transfer in the plasma lamp temperature fields in the electronic and optical unit were obtained (Fig. 5). On the basis of numerical calculations were found that the most thermally loaded regions are situated in the optical block (~150 °C). Despite the fact that the optical unit is separated structurally from the electronic revealed that heat transfer takes place from one block to another due to thermal conductivity of the case that would negatively affect the operation of the lighting device as a whole system.

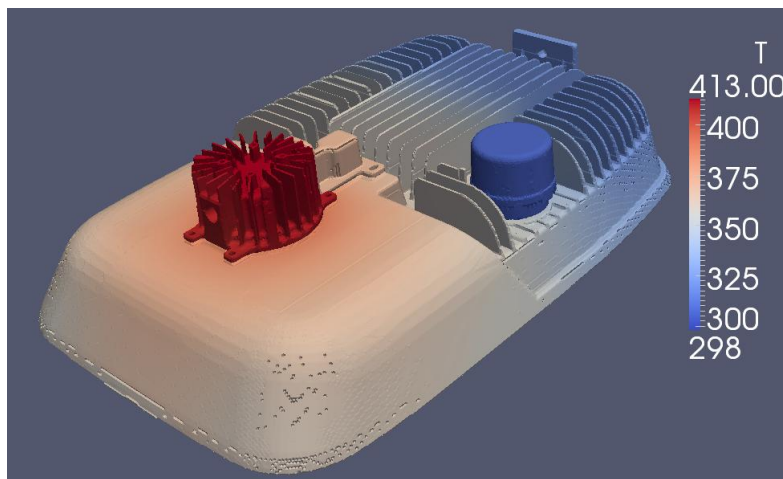


Fig. 5. Three-dimensional illustration of the temperature distribution on the structure of the plasma light (temperature in degrees Kelvin) at steady state (reached after 30 minutes)

Fig. 6 shows the calculated temperature data on the most thermally loaded areas of the plasma lamp depending on the time. As shown on the figure and noticed previously the highest temperature in the device centered in the optical block, namely in the areas of contact between the lamp housing to the emitter ($\sim 150^\circ\text{C}$). Also areas with sufficiently high temperatures are observed in the regions bordering with the driver ($\sim 85^\circ\text{C}$). Casing wall in contact with the converter AC/DC has a temperature of about 45°C .

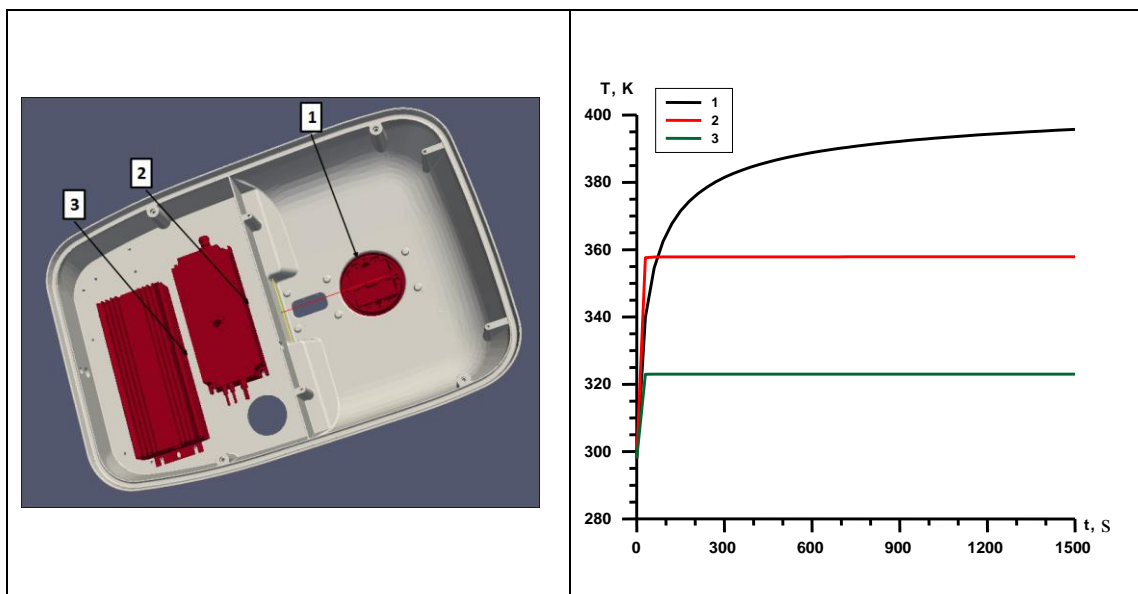


Fig. 6. Temperature versus time plots for plasma lamp, which correspond to the area of contact between the housing and the heat-loaded elements (1 case / emitter, 2 case / driver, 3 case / converter)

Fig. 7 shows the numerical data and temperature versus the time for different sections of the outer surface of the plasma lamp. As it can be seen from the figure, the experimental results are slightly different from the calculated data. This error can be explained by the fact that in the calculations as the properties of the material of construction of the plasma lamp (aluminum alloy) are taken properties of pure aluminum. Also cause discrepancies between the calculated and experimental data can be reference with temperature ideal boundary conditions at the solid / air border.

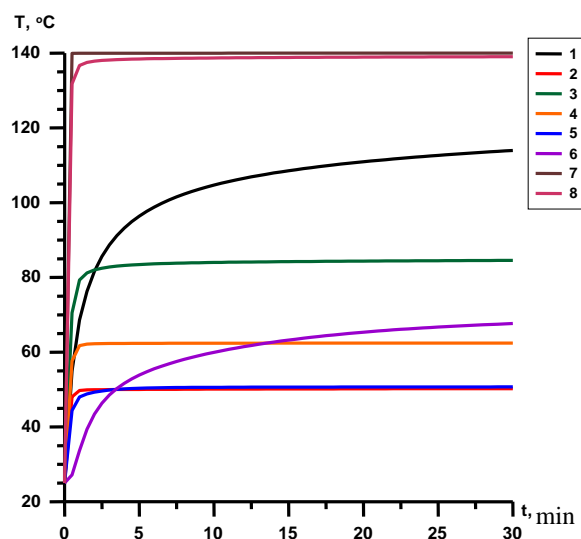


Fig. 7. Temperature versus time plots for different sections of the outer surface of the plasma lamp, obtained by numerical simulation

6. CONCLUSIONS

Experiments and mathematical modeling of the plasma lamp for obtaining the temperature field distribution in his case were made and the most heated parts at stationary operating conditions of the instrument were determined. The most thermally loaded components of plasma illuminator are converter AC/DC, emitter and driver. These components of the fixture are the most important elements of the lamp and their operational conditions have a big influence to the function of the device, so, the cooling of these elements is recommended.

The results of the numerical heat transfer process modeling of the plasma lamp and the environment were compared with the experimental data. The comparison showed good agreement of these results. However, it should be noted that the main reason for the discrepancies in the results is using the thermal characteristics of pure aluminum as the case material in calculations, whereas the body of the lamp is made of aluminum alloy whose properties may vary significantly

Based on these studies and dependencies found, recommendations on optimizing the design of plasma lamp were made. It is recommended to reduce the level of operating temperatures by not combining the electronic block with optical part in the same case. It is recommended to change a bulk case obtained by hot casting aluminum into a lighter thin sheet of metal (aluminum), manufactured by bending, with the aim to reduce weight and dimensions, and consequently the cost. In this situation the driver must be equipped with a compact highly efficient heat sink to protect electronics from overheating during operation.



REFERENCES

1. COURRET, G., CALAME, L., CROCI, M., EGOLF, P. Environmental friendly high efficient light source proceeding of: 14 Schweizerisches Status-Seminar 2006 Energie und Umweltforschung im Bauwesen, Zurich, Switzerland. September 2006.
2. *Theory of heat and mass transfer*. Ed. A.I. Leontiev. Moscow: Bauman MSTU publishing, 1997. 683 p. ISBN 5-7038-1365-8 (in Russian).
3. *Heat exchanger design handbook. Heat exchanger theory*. Translation from English. Ed. B.S. Petukhov, V.K. Shikov. Moscow: Energoatomizdat, 1987. 560 p. (in Russian).

POSSIBILITIES TO USE LITHUANIA'S MEMBERSHIP IN THE INTERNATIONAL ORGANIZATIONS AS AN INSTRUMENT IN NEUTRALIZING THE THREATS TO STATE'S ENERGY SECURITY

J. Juozaitis

Vytautas Magnus University

K. Donelaičio str. 58, LT-44248 Kaunas – Lithuania

ABSTRACT

Lithuania's legal framework indicate that the membership in international organizations is perceived as an instrument to be used for the enhancement of state's energy security. The main condition for such an enhancement is the neutralization of state's major energy security threats – the likelihood of energy supply disruption, and uncontrollable price fluctuations. However, Lithuania's official documents and contemporary scientific literature does not distinguish concrete means to eliminate them in relation to Lithuania's membership in OSCE, NATO, WTO, and the UN. Therefore, the article aims to determine the extent of possibilities for Lithuania to utilize its membership in the already mentioned organizations as a subsidiary instrument in neutralizing the most relevant threats to Lithuania's energy security. The possibilities are determined by analyzing legal frameworks of Lithuania, OSCE, NATO, WTO, and the UN. The application of such a method defines energy security threats as they are understood by state's energy policy makers, and determines the concrete scope of possibilities for Lithuania to utilize its membership in the analyzed organizations for tackling the determined threats. The results of the research indicate that membership in these organizations cannot directly benefit Lithuania's struggle in removing energy security threats. However, few indirect benefits are identified. First of all, membership in the aforementioned organizations serve as platform for informing the international community about Lithuania's energy security threats, and their sources. Furthermore, the research has shown that decision making procedures in OSCE, and NATO enables Lithuania to block any kind of legislation which could be harmful to the energy security of Lithuania. Moreover, the establishment of NATO's Energy Security Centre of Excellence creates conditions for Lithuania's vision of energy security to be included into NATO's legal framework.

Keywords: Energy security, threat, Lithuania, international organizations

1. INTRODUCTION

With the exception of International Energy Agency establishment in 1974, energy security threats have been mostly considered as a matter of individual states to deal with throughout the 20th century. However, contemporary events such as nuclear disaster in Fukushima (2011), Russian – Ukrainian natural gas disputes (2006, 2009), combined with the constant fuss over the increasing greenhouse gas emissions, dwindling global reserves of fossil fuels, and oil price fluctuations have determined the increased attention of international organizations to the energy security issues. The Common Energy Policy was firmly established in the framework of the European Union, energy security issues were included into NATO's newest Strategic Concept, energy trade disputes have started to be investigated by WTO's Dispute Settlement Body, concrete aims, and means for the improvement of energy security among OCSE's members have been included in its official documents, while the energy security threats have constantly been debated within the United Nations [1].

The official documents of Ministry of Energy, and Ministry of Foreign Affairs of the Republic of Lithuania indicate that Lithuania considers its membership in international organizations as a subsidiary instrument for neutralizing state's major energy security threats presented in the National Energy Independence Strategy: the likelihood of natural gas supply

disruptions, and price fluctuations of electricity, and fossil fuels [2]. Furthermore, scientists argue that Lithuania's aims in neutralizing these threats are doomed to fail if they are addressed only by national means [3]. However, the aforementioned statements made by the academia, and the official information provided by Lithuania's energy policy makers do not distinguish the concrete possibilities for Lithuania in using its membership in OSCE, NATO, UN, and WTO to tackle state's energy security threats. Therefore, the article aims to define concrete possibilities for Lithuania to utilize its membership in OSCE, NATO, UN, and WTO¹ as an instrument in neutralizing its energy security threats.

2. THEORETICAL AND METHODOLOGICAL CONSIDERATION

The purpose of theoretical framework is to clarify the confusion emanating from a great deal of energy security definitions, and to define concept of threat, its sources, and its neutralization process by the means of international organizations. After the theoretical framework is firmly established, the article shall consider concrete methods for achieving the aim of the research.

2.1. Theoretical framework

In the context of energy security definition, it should be noted that its diversity is determined by the diverging conception of energy security in various scientific disciplines, and countries (45 energy security definitions are found in the contemporary scientific literature [4]). Political science, economics, engineering, complex and natural science [5] has their own version of energy security, which understanding is further confused by different perception of energy consuming, transit, and exporting countries towards the definition [6]. Since this particular paper is focused on a concrete state – Lithuania, and its possibilities in utilizing its membership in the international organizations to neutralize the energy security threats, hereafter the article shall use Lithuania's official definition of energy security, which is understood in terms of energy independence: “Ability to freely choose the type of energy resources and the sources of their supply (including local production) so that they best meet state's energy security needs and Lithuanian consumers' interests to procure energy resources at the most favorable prices” [7].

On the contrary to the energy security definition, there is a consensus among the scientists over the definition of threat, its sources, and its neutralization procedures. Threat is defined as the capabilities, and intent of actor A to inflict damage to the actor B. The threat is caused by two groups of sources: ones that emanate from the capabilities to inflict damage, and the ones coming from the intention to do so. In order for the threat to be neutralized, its sources has to be eliminated or deterred [8] (prevention of undesired behavior by contemplating that such an action will exceed any possible gain [9]).

Threat neutralization through international organizations is achieved not by the national means, but by the means of international organizations, even though the same process applies –

¹European Union is deducted from the analysis. By now it is more than clear that Lithuania's membership in the EU is already being utilized to neutralize energy security threats of the country. Lithuania has used EU's organizational, financial, and legal capabilities to decrease the likelihood of energy price fluctuations, and supply disruptions: Baltic Energy Market Interconnection Plan (BEMIP) provides a clear framework for regional cooperation; concrete funding was assigned to finance the construction of “Nordbalt” 750 MW electricity interconnector with Sweden (452, 3 million LT), the expansion of national renewable energy production capacity (607, 5 million LT), renovation of apartment buildings in order to increase their energy effectiveness (164, 8 million LT), etc., and antitrust proceedings of “Gazprom” have been initiated by the European Commission [10]. On the contrary possibilities emanating from Lithuania's membership in OSCE, NATO, UN, and WTO are blurred to say the least.

sources of threats has to be eliminated [11]. For example: Lithuania's policy makers advocated for EU's support in linking Lithuania's electricity, and natural gas infrastructure to the European Union network. The natural gas disputes between Russia and Ukraine have created good conditions for Lithuania to impact the decision making process of the EU in relation to the infrastructural isolation², and Lithuania was labeled as an "energy island" in the legal framework of the EU. After gaining such title, Lithuania was assisted by the EU in developing the BEMIP, received concrete funding for construction of "Nordbalt" power line, and enormous political support from the European Commission.

As it could be observed from the example, Lithuania's national problem was turned into an EU one, and the threats of energy supply disruptions, and price fluctuations were started to be neutralized by concrete means of the international organization. Furthermore, the example identifies that the scope for possibilities for a country to achieve its national goals by the means of international organizations is expressed by their legal framework, and state's abilities to change it for the sake of its national interests.³

2.2. Application of methods

Corresponding to the statement above, analysis of legal framework is chosen as a main method for achieving the aim of the article. The advantages of such a method are the following: a) it is capable of defining Lithuania's energy security threats as they are perceived by state's officials⁴; b) the method can objectively determine concrete possibilities of the membership in international organizations for neutralization of threats; c) it is capable of distinguishing the procedures, which define the alteration of legal framework; d) primary sources are analyzed. However, the method has two minor disadvantages: a) it might fail to illustrate the extent of Lithuania's energy security threats; b) possibilities of Lithuania in changing the legal framework of international organizations are also related to the balance of interests among the decision makers. In order to tackle such limitations, the article shall include additional statistical information in determining threats to Lithuania's energy security, and the research conducted by other scientists in relation to the balance of interests among the decision makers in the international organizations.⁵ The additional means shall be invoked only if the results reached by the analysis of legal framework require additional clarification.

The method is operated as follows. Firstly, sources of Lithuania's energy security threats are determined. Secondly, the possible instruments to neutralize Lithuania's energy security threats by the means of OSCE, NATO, WTO, and UN are distinguished. Finally, the article checks wherever legal framework of such organizations could be changed in accordance with Lithuania's interests.

The selection of the methods, and the research design is based on their successful applicability in the similar studies conducted by: Professor Ramūnas Vilpišauskas [12], ex Vice Minister of Energy of the Republic of Lithuania Žygimantas Vaičiūnas [14], and Dr. Tomas Janeliūnas [15]. The first two aforementioned scientists have analyzed Lithuania's success in forming the policies of European Union according to the national interests. The

² The interruption of natural gas supply in 2009 have lasted nearly for two weeks and had a direct effect to 12 EU countries: Bulgaria, Slovakia, Greece, Austria, the Czech Republic, Slovenia, Hungary, Poland, Romania, Germany, Italy, and France [13].

³ In the context of European Union Lithuania had both possibilities, and effectively used them. EU's funds were utilized to finance Lithuania's energy infrastructure projects, Competition law was applied in antitrust proceedings against the "Gazprom", while the dissatisfaction of EU's members caused by the Ukraine – Russia gas crises was utilized to pass the favorable legislation for Lithuania in the framework of EU's Common Energy Policy.

⁴ It is crucial to define how the threats are perceived by Lithuania's energy policy makers because the threats are likely to be neutralized in relation to the threat perception itself.

⁵ Ones that have the power to change the law of the organization.

analysis of legal framework was chosen as the main method in their research: the authors have framed Lithuania's national interests⁶ through state's official documents, while Lithuania's potential to change the framework was evaluated by the changes in the legal framework of the EU. Dr. Tomas Janeliūnas sought to determine the regional implications of Lithuania's energy interests. In doing so, the interests of Lithuania were also framed by analyzing legal documents concerning Lithuania's energy policy. Moreover, the aforementioned author has brought the descriptive statistical analysis as a complimentary method to better explain Lithuania's goals in the energy sector, and displayed the interests of Lithuania's neighbors. This shows that the chosen method set is appropriate for achieving the aims off the article.

3. RESULTS OF THE RESEARCH

3.1. Sources of threats to Lithuania's energy security

In relation to the operated energy security definition, it is observed that three segments of Lithuania's energy security can be threatened: ability to freely choose energy resources, ability to freely choose energy suppliers, and the ability to acquire energy at the most favorable prices. Lithuania's National Energy Independence Strategy indicate that the second, and the third segments are under a constant threat: "Risk of electricity or natural gas supply interruption or large fluctuations of fossil – fuel prices". These threats are caused by four well known sources: domination of one external primary energy supplier, isolation of natural gas, and electricity infrastructure from the rest of continental Europe, Russia's ability to manipulate with electricity, and fossil fuel prices in Lithuania, and its overall perception of energy trade as means to achieve the goals of foreign policy [16]. The extent of Lithuania's reliance on a single energy supplier is illustrated in the first table.

Table 1. Russia's share of Lithuania's supply of primary energy by sector in 2012 [17]

Energy sector	Primary production (ktoe)	Import (ktoe)	Russia's share (ktoe) ⁷
Natural Gas	0	2655.6	2655.6 – 100%
Crude oil	103.6	8647.8	8510 – 97.25%
Solid fuels	17.1	229.6	196. 2 – 79.53%
Renewables	1197.9	152.1	n/a
Nuclear	Ignalina's NPP closed since 2009	0	0

Russia's supply share is absolutely dominant in natural gas, and oil sectors, while renewables is the only primary energy sector dominated by Lithuania's indigenous production, which accounts for 90, 84 % of total primary energy produced in Lithuania as of the data of 2012. The dominance of Russia's share in the natural gas sector is determined by the infrastructural limitations, which leaves Lithuania with no other options in acquiring its natural gas supply. Such reliance intensifies the threat to state's energy security given the following precedents, which illustrate Russia's unreliability as an energy supplier: Russia – Ukraine natural gas disputes in 2006, and 2009, Russia – Belarus energy disputes in 2004, 2007, 2010, and the closure of "Druzhba" oil pipeline in an attempt to purchase the refinery of "Mažeikių nafta" in 2006, etc. Furthermore, Lithuania is part of IPS/UPS electricity system which is centrally controlled by Russia. Such a control enables Russia either to decrease or to

⁶ The whole scope of Lithuania's interests in the energy sector is not analyzed in the article due to too wide nature of such an analysis. Therefore, article limits itself to the analysis of energy security threats.

⁷ % of Russia's energy supply as of Lithuania's total primary production quantity + total import quantity.

increase the transfer capacity of the “BRELL” ring, and in addition to decrease or to increase the electricity prices according to its interests. As far as the price factor is considered, it should be noted that Lithuania’s electricity prices are lower than EU’s average, but they are considerably higher than the ones of Estonia and Latvia – countries being connected to the same electricity ring.⁸ However, the prices of natural gas in Lithuania are not only higher than the ones of Latvia, and Estonia, but also considerably higher than the countries with biggest purchasing power: Germany, UK, France, and Italy.

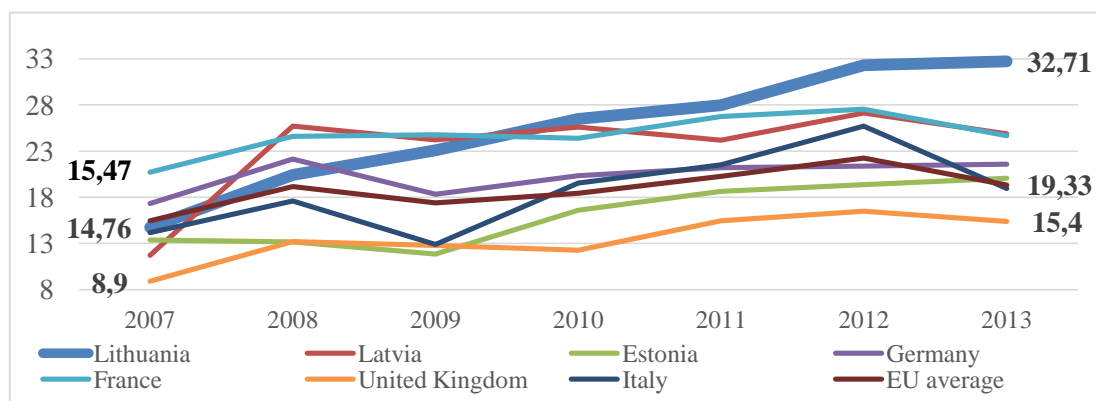


Fig. 1. Natural gas prices for domestic consumers in a comparative view (PPS/GJ) [18]

Having distinguished the sources of threats to Lithuania’s energy security, the paper shall determine the possibilities to neutralize them by utilizing Lithuania’s membership in OSCE, UN, NATO, and WTO.

3.2. International organizations as an instrument in neutralizing Lithuania’s energy security threats

3.2.1. Organization for Security and Co – operation in Europe

The analysis of OSCE’s legal framework indicate that energy security aims raised by OSCE are directly linked with Lithuania’s energy security threats, and might contribute to their elimination. However, the means of the implementation of such aims are declarative, and cannot be utilized to neutralize the threats to Lithuania’s energy security. Moreover, the decisions taken in OSCE reflect the political will of its members, and are not legally binding in contrast to the ones of UN, NATO, and WTO, therefore, they do not guarantee for the compliment. Analysis of OSCE’s legal framework in relation to energy security is summarized in the second table.

⁸ In 2013 electricity price for domestic consumers was 18, 86 in Lithuania, 13, 91 in Latvia, 14, 22 in Estonia, while the EU average was 22,2. Prices are measured in PPS – purchasing power standard per kWh. All national taxes, and levies are excluded from the price.

Table 2. Energy security goals, and means of implementation in the legal framework of OSCE [19]

Document, goals for energy security	Means of implementation
<i>Decision No. 12/06:</i> a) Increase of global transparency, predictability, and stability in the energy markets; b) improvement of investment environment in the energy sector; c) increase of energy effectiveness and savings; d) physical protection of critical energy infrastructure; e) decrease of energy poverty; f) attention to climate change and sustainability.	a) Facilitation of dialogue at the expert level between energy supplying, transit, and consuming states; b) raising awareness and enhancing dialogue on the G8 Plan of Action on climate change, clean energy and sustainable development (facilitation of energy effectiveness, extension of scientific studies, financial support for the sustainable energy development, liquidation of consequences caused by global warming, curb of illegal forestry) and the G8 Plan of Action on global energy security (goals mentioned in the left side of the table);
<i>Decision No. 6/17:</i> Protection of critical energy infrastructure from terrorist attack	a) Intergovernmental cooperation; b) cooperation between private, and public sector; c) cooperation with other international organizations, especially with International Energy Agency; d) exchange of good practice; e) facilitation of discussions;
<i>Decision no. 6/09:</i> Repetition of goals established in Decisions No. 12/06 and 6/17.	a) Consultations on the expert level; b) exchange of practice within the areas of energy efficiency, savings, and the development of renewable energy.

The conditions for changing the framework for the sake of Lithuania's interests are unfavorable to Lithuania. The decisions are taken by the autonomous vote [20], hence all 57 members have to reach a consensus on a certain legal issue. Since Russia is one of the members, it is very unlikely that Lithuania could pass any favorable legislation because its interests directly oppose to the ones of Russia.

In sum, OSCE's legislation does not allow to neutralize Lithuania's energy security threats by the means of the organization, and no potential to change that legislation is observed. However, there is one benefit in this regard. Being a member of international organization with such a decision making procedure allows Lithuania to block any kind of legislation taken within OSCE, which could be harmful to Lithuania's energy security.

3.2.2. United Nations

The analysis of UN legal framework formulates identical conclusion: Lithuania's membership in the organization does not have a direct impact towards the threats to state's energy security. The energy security initiatives found in UN's legal framework concentrate on energy poverty, and global warming issues [21], which cannot add any significant value to the elimination of Lithuania's energy security threats. As far as the decision making procedures are concerned, binding international security related resolutions are discussed in the Security Council. Lithuania is a temporary member of the Council, therefore, having a right to propose security related legislation. However, Lithuania's possibilities for passing favorable legislation are constrained in the context of energy security. Lithuania could claim that under the article 24 of the Charter of the United Nations Russia's manipulation with energy trade are a threat to international peace, and security, therefore, requiring UN's intervention. The analyzed data indicate that such an attempt cannot be successful. Russia has a right to veto

any kind of legislation passed in the Security Council, and will not allow to harm itself [22]. Moreover, the Security Council of United Nations have already shown its inability to solve a crisis of larger scale: Russian – Ukrainian natural gas dispute in 2009 [23].

3.2.3. North Atlantic Treaty Organization

Analysis of NATO's legal framework illuminates similar findings as the ones determined in OSCE's case. NATO's aims in the field of energy security are relevant to Lithuania's energy security threats. However, the organization does not offer concrete instruments to achieve them, and emphasize the role of individual efforts by organization's members which fundamentally opposes the idea of utilizing the international organizations for the sake of national interests (see table no 3).

Table 3. Energy security goals, and means of implementation in the legal framework of NATO [24]

Document, goals for energy security	Means of implementation
<i>Riga Summit Declaration 2006:</i> Protection of energy infrastructure	Analysis of the most immediate risks in the field of energy security, in order to define those areas where NATO may add value to safeguard the security interests of the Allies and, upon request, assist national and international efforts;
<i>Bucharest Summit Declaration 2008:</i> a) Protection of critical energy infrastructure; b) promotion of stability in the energy sector;	a) Information fusion, and sharing; b) extension of international, and regional cooperation; c) consultations with other international organizations.
<i>Strategic Concept 2010:</i> a) Protection of critical energy infrastructure; b) protection of energy supply routes; c) creation of possibilities for NATO to add – value to the energy security of its members;	a) Consultations with NATO member – states, and partners; b) Strategic analysis;
<i>Chicago Summit Declaration 2012:</i> a) Stable, and reliable energy supply; b) diversification of energy suppliers, resources, and supply routes; c) increase of energy effectiveness of NATO's armed forces.	a) Individual efforts by NATO's member states; b) increase of competence through consultations with NATO's partners; c) Efforts by NATO Energy Security Centre of Excellence.

The decision making procedure of NATO is not favorable to Lithuania. Decisions in the organization are made by the autonomous vote, and since many influential countries like Germany do not desire to further expand energy security issues into NATO's agenda, it is very unlikely that legal framework could be changed in Lithuania's favor. Alternatively, being a member of NATO creates same possibility for the country as the ones in OSCE: blockage of harmful legislation to Lithuania's energy security. However, the analysis have spotted an alternative possibility. NATO Energy Security Centre of Excellence is operational in Lithuania, which is responsible of strategic research and analysis, exercise organization, and concept development in the framework of NATO, and the field of energy security [25]. Since the director of the Centre, and the head of Strategic Analysis and Research division are Lithuanians, there is a possibility to slowly frame the NATO's vision of energy security according to Lithuania's perception given the fact that the leadership will remain as it is.

3.2.4. *World Trade Organization*

The analysis of WTO's legal framework have determined that organization is not directly engaged in the energy security issues. However, WTO's fundamental purpose is to facilitate free international trade, and remove its barriers. The organization accomplishes such aims by prohibiting the discrimination of exports or imports of goods, and services either by the countries of origin, or the countries of destination. If one member believes that another one uses discriminative trade measures, it can initiate a dispute settlement process by suing the discriminator to the WTO's Dispute Settlement Body. The decisions of this institution are legally binding, and might come by the form of sanctions or fine. Even though there is no separate indication of energy in the legal framework of organization, but the engagement of Dispute Settlement body in energy trade disputes shows that it is also understood in terms of trade in goods and services [26]. Therefore, the article assumes that Russia could be sued for its discriminative measures in natural gas trade with Lithuania, and that possibility should deter Russia from doing so.

However, there are three shortcomings in this regards, which suggest that such an assumption is wrong. Firstly, dispute settlements usually last no shorter than a year. If Russia would stop its natural gas supply to Lithuania or set a very high price throughout the whole period of dispute settlement, Lithuania's fertilizer industry would collapse, and high social tensions will arise. Furthermore, the latest available data shows that natural gas was the most commonly used fuel for electricity and heat production in Lithuania (65, 3 % - 2012), which consequentially expands Russia's leverage in pressuring the country, therefore, these reasons should deter Lithuania in proceeding with the dispute settlement procedure [27]. Moreover, WTO's history marks only four precedents in the field of energy trade disputes, and none of them have considered the case of disruption of energy supply, or non-market based price for such supply.⁹ Therefore the outcome of such dispute settlement can be very hard to forecast. Finally, the highest penalty possible to be given if Russia would be ruled out as guilty – sanctions issued by all WTO's members in the corresponding sector of goods, and service where the violation took place. This would imply that all WTO's members should stop purchasing natural gas from Russia [28]. However, such sanctions are simply impossible due to the infrastructural limitations of WTO's member states.¹⁰ These arguments show that WTO cannot be utilized to tackle Lithuania's major energy security threats.

4. CONCLUSIONS

Legal framework analysis of NATO, OSCE, WTO, and the UN suggests that these organizations could offer no direct instruments to Lithuania for eliminating its energy security threats: the likelihood of energy supply disruptions, and price fluctuations. Furthermore, decision making procedures of the analyzed organizations, and the interests of its members reveal that Lithuania has no possibilities to change the legal framework in the favor of national energy security interests. Nevertheless, the analysis has distinguished few indirect benefits brought by Lithuania's membership in these organizations. Firstly, it serves as a platform for informing the members of these organizations about Lithuania's energy security threats, and their causes. Secondly, decision making procedures in OSCE, and NATO enables Lithuania to block undesired legislation in accordance with Lithuania's energy security. Finally, establishment of NATO's Energy Security Centre of Excellence creates positive

⁹ The cases mostly considered hi-tech trading.

¹⁰ There are numerous countries which could not acquirer sufficient amount of natural gas from other sources if Russia is sanctioned. Lithuania, Latvia, and Estonia would belong to that group of countries.

conditions for Lithuania's vision of energy security to be included into NATO's legal framework.

The findings of such analysis could add value for the member states of the analyzed organizations, which face similar energy security threats as Lithuania does. The results have a clear message: threats of energy supply disruptions, and price fluctuations cannot be eliminated by the means of OSCE, NATO, WTO, and the UN. These threats have to be tackled either by national means, or by the means of other international organizations, such as European Union for example.

REFERENCES

1. ANDOURA, S. HANCHER, L. WOUDE. *Towards a European Energy Community: a Policy Proposal*. Paris: Notre Europa, 2009. P. 85 – 92. NATO. *Strategic Concept for the Defence and Security of the Members of the North Atlantic Treaty Organization*. Lisbon: NATO. Art 13, 15, 19. – [Referred on the 24th of January in 2014]. Link to the internet <http://www.nato.int/cps/en/natolive/official_texts_68580.htm>; OSCE. *Decision No. 12./06 Energy Security Dialogue in the OSCE*. Brussels: Ministerial Council, 2006. P.2. – [Referred on the 15th of January in 2014]. Link to the internet <<http://www.osce.org/mc/23354>>;
2. RICHARDS, J.T. HERMAN, L. *Relationship between International Trade and Energy*. Brussels: World Energy Task Force, 2010. P. 3; United Nations. *Energy Knowledge Network. Activities*. New York: United Nations. – [Referred on the 8th of January in 2014]. Link to the internet <<http://www.unenergy.org/activities/overview>>
3. Ministry of Energy of the Republic of Lithuania. *National Energy Independence Strategy of the Republic of Lithuania*. Vilnius: Ministry of Energy of the Republic of Lithuania. P. 17, 23, 24. Lietuvos Respublikos Užsienio Reikalų Ministerija. *2012 m. veiklos ataskaita*. Vilnius: Lietuvos Respublikos Užsienio Reikalų Ministerija. P. 4.
4. MOLIS, A. Rethinking EU-Russia energy relations: What do the Baltic States want? *SPES Policy Papers*. No. 1, p. 1–44.
5. SOVACOL, B. K. *The Routledge Handbook of Energy Security*. London and New York: Routledge, 2011. P. 3.
6. CHERP, A. JEWELL, J. The three perspectives on energy security: intellectual history, disciplinary roots and the potential for integration. *Current Opinion in Environmental Sustainability*, 2011, Vol. 3. No. 1, p. 1–11.
7. ČESNAKAS, G. Energetinio saugumo sistemos konstravimas: lygmenys, elementai ir jų ryšių analizė. *Politikos mokslų almanachas*, 2009, Vol. 6, No. 1, p. 59–89.
8. Ministry of Energy of the Republic of Lithuania. *National Energy Independence Strategy of the Republic of Lithuania*. Vilnius: Ministry of Energy of Republic of Lithuania. P. 9.
9. BRAUCH, G.H. *Concepts of Security Threats, Challenges, Vulnerabilities and Risks*. Berlin: Springer Verlag, p. 62–63.
10. LEBOW, R N. *Between Peace and War: The Nature of International Crisis*. Baltimore, John Hopkins University Press, 1981. P 83.
11. European Commission. *European Energy Programme for Recovery*. Brussels: European Commission. – [referred on the 8th of January in 2014]. Link to the internet <http://ec.europa.eu/energy/eepr/index_en.htm>; Europos Sąjungos struktūrinė parama. *Igyvendinami projektai*. Vilnius: Europos Sąjungos struktūrinė parama. [Referred on the 9th of January in 2004] link to the internet <<http://www.esparama.lt/igyvendinami-projektai;jsessionid=353831F171F6FA2EF8F261613C29698F>>

12. ABBOT, K.W. SNIDAL, D. Why states act through formal international organizations? *The Journal of Conflict Resolution*, Vol. 42, No. 1, 1998, p. 3–32.
13. VILPIŠAUSKAS R. National Preferences and Bargaining of the New Member States since the Enlargement of the EU: the Baltic States- Still Policy Takers? *Lithuanian Foreign Policy Review*, 2011. Vol. 23, No. 25, p. 9–32.
14. PIRANI, S. JOHNATAN, S. *The Russo Ukrainian Gas Dispute of January 2009: a Comprehensive assessment*. Oxford: Oxford Institute for Energy Studies, 2009. P. 55.
15. VAIČIŪNAS, Ž. Europos Sąjungos bendros energetikos politikos formavimasis ir Lietuvos interesai. *Politologija*, 2009. Vol. 55, No. 3.2009, p. 89–120.
16. JANELIŪNAS, T. *Lithuanian Energy Strategy and its Implications on Regional Cooperation*. Zinante: Latvian Institute of International Affairs, 2009, p. 190–222.
17. Ministry of Energy of the Republic of Lithuania. *National Energy Independence Strategy of the Republic of Lithuania*. Vilnius: Ministry of Energy of the Republic of Lithuania. P. 9, 17, 18, 19, 21.
18. EUROSTAT. *Energy statistics – quantities, annual data*. Brussels: European Commission. – [Referred on the 16th of February in 2014] link to the internet <<http://epp.eurostat.ec.europa.eu/portal/page/portal/energy/data/database>>
19. EUROSTAT. *Energy statistics – energy prices, annual data*. Brussels: European Commission. – [Referred on the 16th of February in 2014] link to the internet <<http://epp.eurostat.ec.europa.eu/portal/page/portal/energy/data/database>>
20. OSCE. *Decision No. 12./06 Energy Security Dialogue in the OSCE*. Brussels: Ministerial Council, 2006. P. 2. – [Referred on the 15th of January in 2014]. Link to the internet <<http://www.osce.org/mc/23354>>; OSCE. *Decision No. 6/07 Protecting Critical Energy Infrastructure from Terrorist Attack*. Madrid: Ministerial Council, 2007. P. 2. – [Referred on the 15th of January in 2014]. Link to the internet <<http://www.osce.org/mc/29482>> OSCE. *Decision No. 6/19 Strengthening Dialogue and Co – operation on Energy Security in the OSCE area*. Athens: Ministerial Council, 2009. P. 2, 3. – [Referred on the 15th of January in 2014]. Link to the internet <<http://www.osce.org/cio/40708>>; G8 Countries. *G8 Plan of Action for Global Energy Security*. St. Petersburg, 2006. – [Referred on the 18th of January in 2014]. Link to the internet <<http://en.g8russia.ru/docs/11.html>>. G8 countries. *G8 Plan of Action for Climate Change, Clean Energy, and Sustainable Development*, 2005. P. 1. Gleneagles, 2005. [Referred on the 20th of January in 2014]. Link to the internet <https://www.gov.uk/government/uploads/system/uploads/attachment_data/file/48584/gl-eneagles-planofaction.pdf>
21. OSCE. *Rules of Procedure of the Organization for Security and Co – operation in Europe*. Vienna: Ministerial Council. Art. II(a) 3. – [Referred on the 12th of January in 2014]. Link to the internet <http://eeas.europa.eu/delegations/vienna/documents/eu_osce/rules_of_procedure_en.pdf>.
22. UN. *Energy Knowledge Network. Activities*. New York: United Nations. – [Referred on the 8th of January in 2014]. Link to the internet <<http://www.un-energy.org/activities/overview>>
23. UN. *Charter of the United Nations*. New York: United Nations, art. 24. – [Referred on the 17th of February in 2014] link to the internet <<http://www.un.org/en/documents/charter/chapter5.shtml>>.
24. PIFER, S. Crisis between Ukraine and Russia. *Contingency Planning Memorandum*, No. 3, 2009. P. 6.

25. NATO. *Riga Summit Declaration*. Riga: NATO, 2006. Art. 45. – [referred on the 22nd of January in 2014]. Link to the internet <<http://www.nato.int/docu/pr/2006/p06-150e.htm>>; NATO. *Bucharest Summit Declaration*. Bucharest: NATO, 2008. Art. 48. – [Referred on the 22nd of January in 2014]. Link to the internet <http://www.nato.int/cps/en/natolive/official_texts_8443.htm>; NATO. *Chicago Summit Declaration*. Chicago: NATO, 2012. Art. 52. – [Referred on the 22nd of January]. Link to the internet <http://www.nato.int/cps/en/natolive/official_texts_87593.htm?mode=pressrelease>; NATO. *Strategic Concept for the Defence and Security of the Members of the North Atlantic Treaty Organization*. Lisbon: NATO. Art 13, 15, 19. – [Referred on the 24th of January in 2014]. Link to the internet <http://www.nato.int/cps/en/natolive/official_texts_68580.htm>.
26. NATO ENSECO COE. *Concept of the NATO Centre of Excellence for Energy Security*. Vilnius: NATO ENSECOE, art 14. – [Referred on the 20th of February in 2014]. Link to the internet <<http://www.enseccoe.org/resources/downloads?download=10:concept-of-the-nato-centre-of-excellence-for-energy-security>>
27. PPO. *Pasaulio Prekybos Organizacijos steigimo sutarties 2 Priedas Susitarimas dėl ginčų sprendimo taisyklių ir tvarkos*. Ženeva: Pasaulio Prekybos Organizacija, 2001, art. 5. – [referred on the 20th of February in 2014]. Link to the internet <<http://www.infolex.lt/lite/ta/76524>>; DAUKŠIENĖ, I. Pasaulio Prekybos Organizacijos Ginčų Sprendimo Tarybos Sprendimai Europos Sąjungos Teisės Sistemoje. *Jurisprudencija*, Vol. 9. No. 3. P. 905–920; RICHARDS, J.T. HERMAN, L. *Relationship between International Trade and Energy*. Brussels: World Energy Task Force, 2010. P. 3; MARCEU, G. *The WTO in the emerging energy governance debate*. Geneva: WTO, 2010. P. 2.
28. Lietuvos Šilumos Tiekėjų Asociacija. Šilumos tiekimo bendrovių 2012 m. ūkinės veiklos apžvalga. Vilnius: LŠTA, 2013. – [Referred on the 14th of April in 2014]. Link to the internet <http://www.lsta.lt/files/statistika/19493_LSTA_Ukines%20veiklos%20apzvalga_2012_WEB.pdf>
29. WTO. *Understanding of the WTO: Settling Disputes*. Geneva: WTO. – [referred on the 20th of February in 2014]. Link to the internet <http://www.wto.org/english/thewtoe/whatis_e/tif_e/displ_e.htm>; WTO. *Dispute Settlement, index of disputes*. Geneva: WTO, 2014. – [Referred on the 21st of February in 2014]. Link to the internet <http://www.wto.org/english/tratop_e/dispu_e/dispu_subjects_index_e.htm#selected_subject>

THE ENERGY CHARTER PROCESS

J. Paškevičius

*Vytautas Magnus University, Faculty of Law
E. Ožėškienės str. 18, Kaunas – Lithuania*

ABSTRACT

In pursuance to ensure energy security in Europe the political declaration Energy Charter came into light. Later on in 1994 the international multilateral legally binding instrument the Energy Charter Treaty was signed which entered into legal force four years later. Defining the most important aspects that ensure energy security, the Energy Charter Treaty covers investment, trade, transit and dispute settlement. The objective of the article is to identify more effective options aiming the Energy Charter Process objectives. In the first part of the article presented investment concerns in the energy sector. The investment environment is of great concern among the constituencies prompting most disputes on the ground of discriminating treatment. Later on is examined common rules issue in the energy sector. Ultimately presented the advantages of international cooperation between organizations that enables to prevent energy flows disruption, anticipate energy market correction in term of supply and demand, create more effective dispute settlement mechanisms and etc.

Keywords: energy charter, investment, international instrument, energy treaty

1. INTRODUCTION

Energy sector being at the heart of economic growth and development abolished previous political divisions between East and West developing the most important multilateral legal-binding instrument regarding trade, investment, transit and environment in energy sector. In 1990's countries encountered with the energy security issues. Energy as a commodity has a direct effect on social, economic and political stability. Supply volatility may lead to civil unrest threatening countries national security from inside and outside. Against this background, energy exporting countries and energy importing countries were struggling to find a solution for all parties on the principles of mutual benefit, non-discrimination, cooperation and etc. Later on in 1994 the international multilateral legally binding instrument the Energy Charter Treaty (the Treaty) was signed which entered into legal force four years later.

The Process is constantly changing trying to balance investors and host governments' perspectives. Provision regarding the reflection of constant changes in technologies, economy and policies was implemented in the Treaty: in 1999 and thereafter at intervals (of more than five years) to be determined by the Charter Conference. The Charter Conference shall thoroughly review the functions provided for in this Treaty in the light of the extent to which the provisions of the Treaty and Protocols have been implemented [6]. Despite ongoing Reviews every five years some issues must be promptly addressed using this platform as a multilateral legally binding instrument or as a policy forum.

The outcome of the last Review was the document named the Rome Statement. It put forward an idea of expansion and consolidation in order to improve the effectiveness of the Process. The new policy called CONEXO designed to set future directions for the Process consisting of consolidation, expansion and outreach. First, consolidation is intended to facilitate for existing signatories to ratify. Second, expansion relates to support for countries to accede to the Treaty. Third, outreach stands for promotion of the principles beyond the existing geographical scope of the Treaty's constituencies [2]. The same principles were later implemented into the proposal to update the Treaty.

The Treaty is unique in three ways. First, it is designed to deal exceptionally with energy sector. Second, it has wide geographical scope with members and observers in all continents. Third, it is signed by 53 parties including European Community (now part of EU) and Euratom comprising energy producing, consuming and transit countries.

Andrei Belyi & etc. in his article *Modernizing the Energy Charter Process? The Energy Charter Conference Road Map and the Russian Draft Convention on Energy Security* assesses future developments in international energy governance in light of the Road Map and Draft Convention. Andrei Konoplyanik and Thomas Wälde article *Energy Charter Treaty and its Role in International Energy* describes its multifaceted role in improving international energy security. Danae Azaria article *Energy Transit under the Energy Charter Treaty and the General Agreement on Tariffs and Trade* argues that the transit provision of the Energy Charter Treaty should influence the interpretation of, as well as efforts to revise, Article V of the General Agreement on Tariffs and Trade, within the current Doha negotiations in the World Trade Organization.

The objective of the article is to identify more effective options aiming the Energy Charter Process (the Process) objectives.

The article explores questions: (i) what impediments investment faces in the energy sector; (ii) what energy market rules may represent all actors' interests; (iii) how cooperation between international organizations can be beneficial to all parties.

In the paper analyses method was used to separate each component of the affecting elements and on this background the consideration was made.

2. INVESTMENT CONCERNS

Firstly, investor-state disputes in the energy sector. In the lifetime of the Process the investment issue prompted most disputes among the constituencies on the ground of discriminating treatment. Over fifty cases are registered by the Secretariat of the Energy Charter in investor-state dispute settlement cases [23]. This number still may not be taken for granted because not all disputes are officially published. The significant growth in cases appeared in recent years. The reason why investment issues prompted most disputes is allocation of the financial benefits. Investor and host governments views most times are adversarial when it comes to determine what yield should be acceptable. This problem may be seen in EU regarding legal reforms affecting the renewable energy sector. [24] Changing feed-in tariff which is design to promote renewable energy due to its competitiveness in the free market environment has direct effect to the rentability of the investments. Other cases arise out of investment in mining and exploration disputes [25]. These cases shows what type of challenges companies are faced in pre-investment and post investment stages. Thus, lack of legal certainty escalates conflicts between parties.

Secondly, the Treaty do not covers pre-investment stage until investments are actually being made. This issue may be addressed in two ways: applying International law principles and broadening the Treaty's interpretation. The International law generally accepts that governments dispose right of sovereignty over natural resources [5]. Nevertheless member states undertake to facilitate access to energy resources by allocating in a non-discriminatory manner on the basis of published criteria authorizations, licenses, concessions and contracts to energy resources. [21] International principles of non-discriminatory, transparency and etc. must be applied for Foreign direct investment (FDI) regardless of sovereignty right in pre-investment stage. These general principals of law are established in different areas of law. Another way is examine the Treaty that states that each country shall limit to the minimum the exceptions in favour to the own investors or any third party [20.] Defining the term "minimum exceptions" can be very ambiguous due to the failure to present a definition in the

Treaty as well as the difficulty to encompass under this term all possible options. This lack of clarity in the pre-investment stage do not compose level playing field for all energy sector participants. These issues were addressed in the Road Map determining the significance of protection and transparency regarding investment legal field pursuing to strengthen energy security between member states [14].

Thirdly, post investment stage. Unfolding issues regarding implementation of the Treaty was of great concern. Investment related disputes were seen as a major impediment for the Process. The mechanisms must be put in place dealing with these issues otherwise the Process credibility as a platform for international cooperation in the energy sector would be substantially damaged. In fact, the Treaty provides provisions ensuring investment protection. The reference to domestic law was made to provide effective remedies for the assertion of claims and the enforcement of rights with respect to investments, investment agreements, and investment authorizations [26]. Despite that the growing number of arbitrational disputes indicates disadvantages of the Treaty's broad provisions leading to extenuating the effectiveness. The subsequent steps were taken to address this issue through adopting new policies in the Road Map. It suggested that effectiveness improvement can be achieved by tracking the record of cases by arbitration, setting consistency in arbitration decisions, advert the balance of investors and host government perspectives [14]. The strategic document adopted as a political declaration does not legally bind any member state. Therefore the Road Map must be seen as having no concrete consequences because of the lack of consensus.

Fourthly, conduct constant review of investment protection. Since the 1991 when the Charter was born major technological, market structural and political changes have occurred. The substantial reforms are needed to reflect the changes in the energy sector in the past years. Although the Process is under constant Review, the major disagreements among states remain unsolved, in particular, favourable investment environment issue. In 2004 was conducted the second Review and the first comprehensive Review which examined investment issues [9]. Few years later the Secretary General affirmed the same weaknesses in the investment protection system emphasizing the lack of transparency, the lack of cooperation among contracting parties, and the lack of resort to conciliation as an alternative method for the resolution of investment disputes [11]. In 2012 the Annual Report focused on reducing investment risk such as discriminatory treatment and expropriation [2]. In every subsequent review or report since the Treaty has been born investment protection issue establishes itself as prompting most disputes. The Treaty is not just about investment protection in upstream resource-rich countries, it has substantial legally binding provisions covering different types of investments as the increasing number of cases in the EU show [18]. The same issues will be examined until the end of the year in pursuance to adopt an updated version of the 1991 Energy Charter special focus giving to investment protection and investor-state dispute settlement [16].

3. COMMON RULES IN THE ENERGY SECTOR

Energy market structure should be understood as acting in two tiers – nationally and globally. This analyses helps to determine impediments in pursuance to greater energy security. On the national level countries use free market structure or government regulated framework, in particular, energy exporting countries. However government regulated market globally looks hardly envisage. On the other hand free market structure in energy sector in a short term creates more risks then advantages. Especially, major resistance for free energy market appears form energy exporting countries.

In pursuance to create common rules in the energy sector special market structure has to be determined that represents the interest of free market and regulated market adherent

interests. Most energy producing states hardly regulate natural resources extraction as such income constitutes major piece of the national budget. For example, in Russia commodities contribute officially around 60%, in reality 75–80% of the federal budget [10]. Other big energy exporting nondemocratic regimes in the Middle East, Africa or Asia are even more dependent from energy export income. The significance of market structure is an example of Saudi Arabia which is the largest exporter of oil in the world with oil and gas export comprise up to 90% of the government revenue [19]. Fifth largest exporter Nigeria generated 80% of the national budget from energy export [18]. These numbers shows the vitality of incomes from energy resources for some governments that definitely have to be taken in to account determining the energy market structure. It may be assumed that oil producers in the Middle East and Africa recognize the Charter as the more appealing legal instrument for energy consuming states [15]. This division may be defined as ideological as well as economical concern.

Other virtues of international cooperation are that this framework enables to prevent energy flows disruption, anticipate energy market correction in terms of supply and demand, create more effective dispute settlement mechanisms and etc. On the grounds of mutual benefit for all parties the Treaty is designed to reflect the need for investment in energy supply chain from upstream to downstream. Whereas energy investment is mostly capital intensive and long term, close cooperation between host government and private companies is seen as inevitable. Energy being of great importance for countries economy and security makes national governments reluctant to give too many rights to private enterprises.

The reasons why the Treaty has effectiveness problems relates substantially to different market structures. One of the reasons is fair and free competition principles have to be expanded in the post-socialist world on the other hand the state ownership of resources distort the market for private investments in East European and Eurasian energy economies [11]. The balance must be reached between two sides going away with some of the rights. The Process objective to develop an open and competitive market does not play in everyone's interest [4]. Europe private enterprises looking forward to invest in Russian natural resources, but despite great endeavour to convince Russia to commit itself to establish free market in the energy sector, private investments are vulnerable against state owned giant Gazprom and Rosneft.

The Russian case illustrates the willingness of some Process constituencies to greater market regulation. In 2009 Russian president Dmitry Medvedev issued Conceptual Approach that determines recognition of security of supply (delivery) and demand (transparent and predictable marketing) as key aspects of global energy security [8]. Next year Vladimir Putin has submitted a proposal called Draft Convention aiming to maintain an optimal sustainable balance between energy supply and demand providing progressive socio-economic development of countries in accordance with the model of development chosen by them [3]. Thus, these proposals clearly indicate that it is not in the Russian government interest to lose control of the main stream of cash flow into their federal budget. In this case the threat is not only for energy security, in fact, it is more of the national security and stability of the political regime.

Otherwise some level of openness is needed for Russia itself. Restriction to investments would have contrary effect to stable development of natural resources, because it is closely linked to the transfer of new technology. The lack of up-to-date technologies hinders exploration of the new fields. In pursuance to evade technological impediments Russia suggested to establish 'energy Union' with Europe on the basis of asset swap [7]. The proposal of asset swap was designed to assist Gazprom to acquire a share in European downstream in exchange of the accession of FDI to the upstream market in Russia. The questions concerning a need for predictable markets and asset swaps in the energy industry will be discussed later this year in Moscow Energy Charter Forum [12]. Today's political

situation appears to be a huge impediment in closer Russian and EU cooperation in the energy sector.

While the Draft Convention stands in potential contradiction to the multilateral spirit of the Treaty, the Road Map helps to integrate Russian concerns into the Process. In 2010 the strategic document the Road Map was adopted orientating Process to the 2014. It encompassed areas linked to promotion of the Process, transit, trade, investment promotion and protection, and etc. Two different modernization scenarios may evolve. As the Road Map which is a continuation of the Process, or as the Draft Convention which is determined as an alternative view [7]. The Road Map states The Energy Charter Treaty's investment provisions should remain untouched in their fundamentals. However, the assessment of the investment provisions must be made examining the effect of climate change and the possibility in promotion of low-carbon investments. Russian proposed Draft Convention intended to maintain an optimal sustainable balance between energy supply and demand in accordance with the model of development chosen by them. This idea of self-determination indicates Russia's willingness do not implement free market rules in their own economy. Notwithstanding different approach is taken in terms of trading in order to ensure non-discriminatory access to international energy markets, their openness and the development of their competitiveness.

4. INTERNATIONAL COOPERATION

One of the ways to improve the Process efficiency aiming at the objectives is for Secretariat to engage in closer cooperation between international organizations. Prof. Peter Cameron suggested that soft non-legal role by closer cooperation between international organization settings common grounds can play a significant part contributing to transit issues [1]. It may take cooperation and coordination in the form of joint events and reports with international organizations [13]. Mutual benefit can be identified in solving energy trade and investment issues. Substantial consideration should be dedicated to internal efficiency of the Process in terms of maximizing the potential by rescinding duplication of functions or supplementing functions of another international organization – International Energy Agency (IEA), World Trade Organization (WTO), United Nations Economic Commission for Europe (UNECE) and the Energy Community.

In this case, cooperation between WTO and the Process present one of the possible beneficial outcomes. The WTO target to develop an open, rule-based, predictable, non-discriminatory trading system corresponds to the Process objective creating the free market for energy products [31]. The Process objective to create free energy market coincides to WTO objective above. First steps were made when WTO rules regarding trade were implemented in the Treaty. Next steps should be to put more emphasis on investment issues, in particular, to promote general principles as non-discrimination, predictability and etc. for member states in form of creating general body that would monitor investment treatment practices. This approach would provide more data in terms of reviewing more countries and acquaint the states, investors and other legal persons with worst practices. Also such measure would attract or repel investment in any sector of the state's economy due to it's bad record of investment treatment. States would be more aware of possible consequences for failing to establish a level playing field.

The IEA is more engaged in energy issues as well as the Process. One of the main IEA areas of concern is economic development in terms of promoting free market and a secure framework for investment [27]. It's close co-operation with Brazil, China, India, Indonesia, Mexico, Russia and the Republic of South Africa covers activities like jointly holding topical workshops on energy efficiency and energy market regulation [28]. Combining policies

between these organizations is of great value, especially, when IEA has one of the biggest consuming and producing nations on board. At present, Russia has opt out it's membership in the Process leaving herself as in an observer status. This joint platform may play in the interests of creating free market. On the other hand it may be a tool to put more pressure on Russia to obey to international law by implementing general law principles regarding trade and investment.

New organizations and bodies were established addressing energy issues. Although, distinguish must be made in respect to the UNECE. The UNECE was mandated to assist governments and gas companies in Central and Eastern Europe in creation of free energy market. In pursuance to this goal the program called Gas Centre was initiated that focuses on developing more decentralized and market-based gas industries, in particular, interchange of information and data between the member companies on the gas markets and gas industry [29]. The UNECE and the Process cooperation in terms of information sharing compose favourable framework helping to identify major free market impediments that national governments may compose implementing their policies. Another benefit relates to the UNECE research and expertise on East and Central Europe's energy security risks, renewable energy and energy efficiency.

5. CONCLUSIONS

1. The growing number of investor-state disputes shows that the Process encounters new challenges. Lack of legal certainty in national legal systems is of great concern and emphasis should be put on the permanence of rules and norms. Due to the long term investments in the energy sector additional legal commitments should be put in place in pursuance to mitigate these risks in the form of international agreements. In addition to this more definitions of terms would bring more clarity. The positive measure to set common legal practice and to discipline states regarding their policies is the official publication of arbitration cases and decisions.

2. FDI in energy resources should have different legal framework then in other business sectors. Most energy exporting countries are not ready to open their energy resources based on free market principles. Reserving some rights by national governments over energy market is inevitable at this stage as it constitutes the foundation of the economical welfare and in most cases directly linked to politics. Therefore different policies should be implemented determining the market structure with no illusion to achieve free market performance in the states with major economical reliance on the income from energy resources. Actual regulations with regard to direct investment in natural resources and trading issues should be determined on case-by-case bases on the national level.

3. The positive outcomes of cooperation between international organizations are identified that might have significant impact on the Process evolvement. First, creation of the joint body that more efficiently and more widely monitors the practices of member states in the field of energy. Second, avoid duplication in promoting free market ideas and improve their policy effectiveness. Lastly, create a joint framework that all major actors would be impelled to participate in order to sell and buy products on the international energy market.

REFERENCES

1. Annual Report, 2011. [Referred on the 28th of February in 2014 y.]. Link to the internet < http://www.encharter.org/fileadmin/user_upload/Publications/AR_2011_ENG.pdf >
2. Annual Report, 2012. [Referred on the 28th of February in 2014 y.]. Link to the internet < http://www.encharter.org/fileadmin/user_upload/Publications/AR_2012_ENG.pdf >
3. Article 2, Convention on ensuring international energy security (draft). [Referred on the 28th of February in 2014 y.]. Link to the internet <<http://ua-energy.org/upload/files/Convention-engl1.pdf>>
4. Article 3. The Energy Charter Treaty. [Referred on the 28th of February in 2014 y.]. Link to the internet < http://www.encharter.org/fileadmin/user_upload/document/EN.pdf >
5. Article 18 para.1 The Energy Charter Treaty. [Referred on the 28th of February in 2014 y.]. Link to the internet < http://www.encharter.org/fileadmin/user_upload/document/EN.pdf >
6. Article 34(7). The Energy Charter Treaty. [Referred on the 28th of February in 2014]. Link to the internet < http://www.encharter.org/fileadmin/user_upload/document/EN.pdf>
7. BELYI, A., NAPPERT, S., POGORETSKY V. Modernising the Energy Charter Process? The Energy Charter Conference Road Map and the Russian Draft Convention on Energy Security. Energy and Natural Resources Journal, 2011 Vol. 29.
8. Conceptual Approach to the New Legal Framework for Energy Cooperation (Goals and Principles). 2009. [Referred on the 28th of February in 2014 y.]. Link to the internet < <http://archive.kremlin.ru/eng/text/docs/2009/04/215305.shtml> >
9. Conclusions of the Review conducted under Article 34(7) of the Energy Charter Treaty. 2004. [Referred on the 28th of February in 2014 y.]. Link to the internet < http://www.encharter.org/fileadmin/user_upload/document/Final_Review_Conclusions.pdf >
10. GRACHEV, I., GURIEV S., Russian's oil: luck or curse? Russia and India report, 2012. [Referred on the 28th of February in 2014 y.]. Link to the internet < http://indrus.in/articles/2012/10/26/russias_oilLuck_or_curse_18655.html >
11. GRIGORIADIS, T. N. State responsibility and antitrust in the Energy Charter Treaty: Socialization v. Liberalization in bilateral investment relations. Tex. International Law Journal, 2008-2009, Vol. 44.
12. Moscow Energy Charter Forum: Cross - Border Trade and Investment Flows as the Backbone of International Energy Security. 2014. [Referred on the 28th of February in 2014 y.]. Link to the internet < http://www.encharter.org/fileadmin/user_upload/Conferences/2014_April_3/Moscow_Forum_Programme_ENG.pdf >
13. Report of the Chairman of the Ad hoc Energy Charter Strategy Group. 2008. [referred on the 28th of February in 2014 y.]. Link to the internet <http://www.encharter.org/fileadmin/user_upload/2009_Review/Ad_Hoc_Strategy_Group_Report_2008_ENG.pdf >
14. Road Map for the Modernization of the Energy Charter Process. 2010. [referred on the 28th of February in 2014 y.]. Link to the internet < http://www.encharter.org/fileadmin/user_upload/document/Road_Map_ENG.pdf >
15. RUSNAK, U. Modernization of the Energy Charter. 2013. [Referred on the 28th of February in 2014 y.]. Link to the internet <http://www.encharter.org/fileadmin/user_upload/document/Modernisation_of_the_Energy_Charter_-_Russia_in_Global_Affairs_-_27_Dec_2013.pdf >



16. Russian Energy Minister Novak Positive about Latest Achievements and Trends in Energy Charter Process Development. 2014. [Referred on the 28th of February in 2014 y.]. Link to the internet
<http://www.encharter.org/index.php?id=21&id_article=454&L=0>
17. WALSTAD, A. Why the Energy Charter still matters. Energy Policy weekly, 2014. [Referred on the 28th of February in 2014 y.]. Link to the internet <<http://interfaxenergy.com/natural-gas-news-analysis/european/why-the-energy-charter-treaty-still-matters/>>
18. BALA-GBOGBO, E. Nigeria's Oil Revenue Rose 46% to \$59 Billion in 2010 on Improved Security <http://www.bloomberg.com/news/2011-04-14/nigeria-s-oil-revenue-rose-46-to-59-billion-in-2010-on-improved-security.html>
19. Top World Oil Net Exporters, 2012 <http://www.eia.gov/countries/index.cfm?topL=exp>
20. Article 10 Para. 5(a), The Energy Charter Treaty,
21. Article 18 para.4 The Energy Charter Treaty.
22. Article 22 para.1 The Energy Charter Treaty
23. The Energy Charter, <http://www.encharter.org/index.php?id=213>
24. Antin Infrastructure Services Luxembourg S.à.r.l. and Antin Energia Termosolar B.V. v. Spain, ICSID Case No. ARB/13/31.
25. KHAN RESOURCES B.V. (the Netherlands) v. Mongolia, Ad hoc UNCITRAL Arbitration Rules.
26. Article 10 para. 12, The Energy Charter Treaty
27. The "Shared Goals" were adopted by IEA Ministers at their 4 June 1993 meeting in Paris. IEA Ministerial meeting 2013,
<http://www.iea.org/newsroomandevents/ieaministerialmeetingphotos2013/>
28. Agenda of 2014 activities, <http://www.gascentre.unece.org/>
29. Three pillars, <http://www.apec.org/About-Us/How-APEC-Operates/Scope-of-Work.aspx>
30. United Nations Millennium Development Goals, <http://www.un.org/millenniumgoals/>

EU ENERGY: SECURITY IN UNITY

J. Lunytė

*Mykolas Romeris University
Ateities str. 20, LT-08303 Vilnius – Lithuania*

ABSTRACT

Energy security is the threshold issue in the European Union policy. Due to geopolitical approach, market-based approach, different energy strategies of member states, the current situation of Europe's energy security is challenging.

The paper is divided into several parts. First, the impact of Europe's energy system is represented on the global scene; therefore, the EU's international influence and the EU dependence on the non-EU countries are analyzed. Second, the main problems are emphasized the EU faces regarding energy security as following: the external security of supply, the coherence of internal and external EU policies, cross-cutting energy markets. Third, the measures are suggested to deal with these issues. Specific forms of cooperation with neighbourhood, shifting towards a proactive engagement with other regional countries could help to achieve the objectives regarding energy security. In addition, national measures, such as the development of infrastructure and networks, are essential for the EU unity and supply guarantee.

To conclude, one of the main pillars of the EU policy - the EU energy security – could be achieved with the measures of coordination and coherence between two dimensions: internal and external.

Keywords: energy security, internal and external dimensions, energy supply, energy transition

1. INTRODUCTION

Energy security has become a top policy priority for the European Union (EU). The EU imports about 50% of its energy needs. The global energy demand is rising and the imports are expecting to rise by 65% over the next 20 years [1]. Similarly, about half of the EU's natural gas imports come from Russia. In January 2009 the EU faced gas supply disruption. This gas crisis exposed Europe's dependency on gas imports and increased concern about Europe's reliance on Russian's energy.

The recent political events and global energy system led to forge the Energy Policy for Europe: strengthening the external dimension of the EU energy market as well as providing Energy Security through An Internal Energy Market.

The article reviews the key issues addressed the energy situation in Europe today and analyzes future actions towards the EU energy: security in unity. The major issues, such as the liberalisation of energy markets, the investments in infrastructures and the EU energy competitiveness are discussed. The aim of the article is to identify the EU energy security challenges and provide EU efforts to implement the measures of a common European Energy Strategy. The overview of broader energy security cooperation and EU neighbouring countries is included.

Energy Commissioner Gunther Oettinger outlined in 'EU Energy 2020 Strategy' that over the next 10 years the EU needs to create a single European energy market and secure its energy supplies [2]. It is obvious that the EU is on the threshold of an unprecedented period for energy policy. There is urgent need for changes in energy regulation.

1.1. Research methodology

The research is fulfilled using such research methods as descriptive method, comparative method, legal method and scientific method.

The descriptive method. This research method is used to present the research instruments and to define the main concepts of the article.

Comparative method. Comparative method is used to compare the data and to assess the EU energy dependency.

Legal method. International legal framework – strategies, policies, directives, regulations – is explored.

Scientific method. The research has been undertaken using the scientific method. This method allows forming the conclusions based on the reliable data.

2. EUROPEAN ENERGY ON THE GLOBAL SCENE

The EU has the world's largest regional energy market – 500 million people – and accounts for one-fifth of the world's energy use [3].

As one of the world's largest importers of fossil fuels – oil, gas and coal – the EU is considered to be the major player on the international energy market. But the EU still needs to exploit its geopolitical strength. Under the Lisbon Treaty most foreign and security policy decisions are taken by unanimity – all member states have to agree on the decision [4]. As a result, the EU faces a challenge to speak with one voice in order to keep leadership position in global energy market. European Commissioner for Energy Gunther H. Oettinger emphasises that the EU should take action, in particular, to integrate energy aspects into relations with third countries [2]. Otherwise, according to the Commission Green Paper “A 2030 framework for climate and energy policies” (March 2013), EU energy dependency will reach 70% in 2030 [5]. The growing EU dependence on imports from third countries is a matter of great concern, in particular for oil (81%) and gas (65%). All these challenges must be addressed and require strong action [6].

The present and predicted situations for the main imported fossil fuels are provided in Fig. 1.

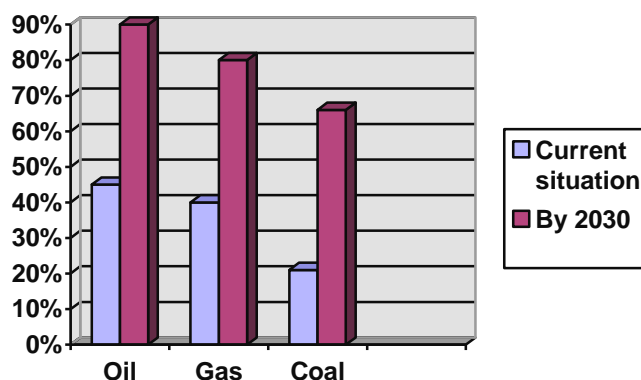


Fig. 1. Fossil fuels imports. Eurostat, May 2011

According to the Fig. 1 data, oil originates from the Middle East; gas is imported from Russia, Algeria and Norway.

The Fig. 2 represents the world's energy self-sufficiency [7].

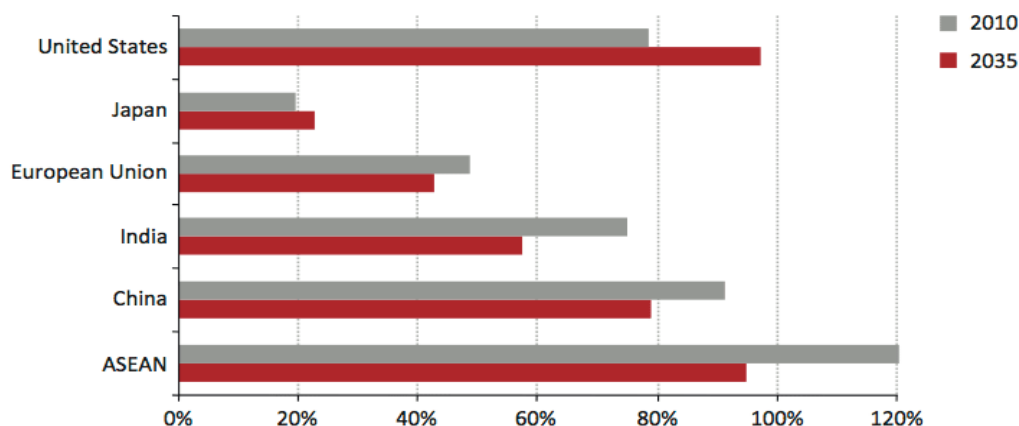


Fig. 2. Energy self-sufficiency

The reserves of oil and gas are distributed around the globe – the largest ones are situated in the Middle-East, Russia and North Sea. The EU inevitably stays dependent on non-EU countries. To ensure future energy supply and EU energy security itself, it is essential to expand and strengthen the EU's international energy relations, in particular, to develop a more proactive and cooperative engagement with Russia, Caspian and Black Sea region, OPEC, Middle-East, South-East European, Norway, US, China.

3. THE EXTERNAL DIMENSION OF THE EU ENERGY MARKET

The external challenge, the European Union has been facing, deals with the role of the EU in the world economy. It is important to develop a coherent external energy policy in order to ensue energy security. Despite the fact that the EU member states endorse to develop a collective international energy policy and represent energy interests of the EU as a whole, member states still independently pursue external relations to secure energy supplies. Member states view energy security as a national policy. They already have signed bilateral agreements, for instance, the South Stream pipeline contracts between Italy, Bulgaria and Gazprom, LNG contracts signed between Spain, France and Algeria. This practice of states should not continue because of a simple reason that it does not support long-term EU energy security. Here the principle of solidarity plays a key role. According to the Energy Strategy for Europe 2020, International agreements proposals should be made to set required regulatory framework between the EU and third countries to develop strategic routes from new suppliers. Supply issues, network development, supply arrangements and regulatory aspects concerning the transit and investment security must comply with EU *acquis communautaire*.

The second problem the EU face is the coherence of internal and external dimensions. The increasing dependency of member states has caused inner competition for supply diversification between states. The provision in the Lisbon Treaty Article 194 of the TFEU, which outlines the competence for energy policy, recognise that the energy mix – the states choice of energy sources-remains a national competence and for Member States to decide [8]. It was noted, that there is EU legislation relating to renewable energy, market liberalisation and emissions reductions which do affect the choice of Member States [8]. For example, the Renewable Energy Directive [9] sets a minimum level of energy to be derived from renewable sources. Most EU member states have involved in unprecedented diversification strategies of energy sources and resources, which undermined the principle of energy solidarity. Various competing and controversial projects for oil and gas pipelines to diversify

the supply routes have emerged as a result. Examples include Nord Stream, Nabucco and South Stream. It occurs because the EU has not developed a unified approach to the large external suppliers.

Nevertheless, the EU is still seeking to define a coherent and collective diversification strategy for supplies and international partnerships on the external dimension of European energy policy [10]. Though energy solidarity is not specifically mentioned, this principle is recommended to be included in order to have more influence in international negotiations with supplier countries as part of a European strategy for diversification of supplies.

On the contrary, the private operators in the energy sector show reluctance to the EU cooperation. They do not want any interference in their commercial activities. On the other hand, the Europeans citizens are in favour of a EU coordinated approach of energy policies above national measures. According to the European Parliament's Eurobarometer on energy of 2011, almost 80% of European citizens supports solidarity between member states in the event of supply difficulties [10].

4. THE SECOND PILLAR OF THE EU ENERGY SECURITY: INTERNAL DIMENSION

4.1. Providing Energy Security through an Internal Energy Market

The European Commission (EC) has long argued that member states could substantially increase energy supply security and network and cost efficiency by integrating national gas and electricity markets into the EU's single European market [11]. The EC began to create a competitive EU-wide gas and electricity market in the 1990s by issuing the Directives focused on four primary objectives: (1) to implement the single market for energy by promoting competition and efficiency in the production and delivery of electricity and gas; (2) to lower prices and give all EU customers the opportunity to choose their energy supplier by 2007; (3) to help improve the environment; (4) to enhance energy security [11]. To conclude, the creation of internal energy market promotes EU competition and energy efficiency, ensures customers rights and enhances energy security.

Today we see the results of the progress towards the Internal Energy Market. The pilot project for EU wide electricity trade was launched in February, 2014. Fourteen EU Member States (Belgium, Denmark, Estonia, Finland, France, Germany, Austria, UK, Latvia, Lithuania, Luxembourg, the Netherlands, Poland and Sweden) and non-EU state Norway have inaugurated the project for joint electricity trading. The project, which is a milestone on the way towards a European Electricity Market, had been jointly initiated by the EU Commission, regulators, grid operators and power exchanges in North-Western Europe (NWE) [23]. EU Energy Commissioner Oettinger said: "The start of the NWE market coupling proves that the Internal Energy Market 2014 is not just lip service. Fragmented European energy markets will soon be history, which is certainly good news for European customers". NWE market coupling combines all bids and offers in a region and creates a large integrated electricity market in the area concerned, combining 75% of today's electricity consumption in the EU [12]. Similar cross-border cooperation on other regional levels could also benefit from such developments. Furthermore, The European Council insisted that by 2015, all Member States should be integrated into the European internal market.

4.2. Establishing the European Infrastructure

The infrastructure development plays a key role in order to have a functioning internal market and guarantee security of supply. The European Commission has proposed strategic

infrastructure priorities and implemented new methods for defining the essential infrastructures for the EU as a whole in terms of competitive energy provision and access to renewables as well as security of supply [13]. The construction of the intra-EU projects should receive the same attention as new interconnections at EU borders. The development of infrastructure is a commercial matter, so the right financing framework provision is significant. Despite the fact that infrastructure investments mainly are financed from tariffs paid by the users, for projects ‘European interest’ which have no or poor commercial viability, funding mechanisms will be proposed for maximum leverage of public support to improve the investment climate and to speed up project implementation. The development of energy infrastructure requires new funding instruments (both political and private) as well as the mobilisation of additional resources under the multi-annual financial framework [13].

Recently, in February 2014 the Council of the European Union adopted regulation on notification of investment projects in energy infrastructure. The law sets out a common framework for the notification to the Commission of data and information on investment projects in energy infrastructure in the sectors of oil, natural gas, electricity (including electricity from renewable sources, electricity from coal and lignite, and cogeneration of electricity and useful heat) as well as on investment projects related to bio-fuel production and the capture, transport and storage of carbon dioxide produced by these sectors. The Commission will be notified by the member states or their delegated entities of investment projects on which construction or decommissioning work has started or on which a final investment decision has been taken [14].

The second major progress was made when the new Regulation on European energy infrastructure was adopted in 2013, and the financial instrument ‘The Connecting Europe Facility’ for the Multi-Annual Financial Framework for the period 2014–2020 [10].

The EU Regulation on energy infrastructure 2013 sets out rules for developing the interoperability of European energy networks, mainly to ensure the functioning of the internal energy market and to promote the interconnection of energy networks. More specifically, the Regulation aims to ensure security of supply and solidarity between member states, in particular by ensuring that no member state remains isolated from the European network [15].

The Regulation lists a number of energy infrastructure priority corridors and areas for 2020 and beyond, covering electricity and gas networks and requiring the most urgent EU action. These corridors (see Table 1) are going to be analysed in more details as following. Before, it is worth to mention that this Regulation also applies to the trans-European energy infrastructure corridors and areas. Since both trans-European and intra-EU infrastructures are related, the their analysis is provided under this section of internal energy dimension.

Table 1. Trans-European priority corridors and areas. Source: own elaboration on European Commission (2012)

Priority Corridors
Northern Seas offshore grid
North-South electricity interconnections in Western Europe
North-South electricity interconnections in Central Eastern and South Eastern Europe
BEMIP electricity
North-South gas interconnections in Western Europe
North-South gas interconnections in Central Eastern and South Eastern Europe
Southern Gas Corridor
BEMIP gas
Oil supply connections in Central Eastern Europe
Priority thematic areas
Smart grids deployment
Electricity highways
Cross-border carbon dioxide network

4.3. Competitive and Secure Europe: Energy Mix of Supply and Energy Prices

The energy mix of supply in EU member states is determined by national governments or energy companies. As a result, energy mix varies across the EU. For instance, in France nuclear power accounts for over 70% of all electrical generation, while Germany and Spain have legislated laws not to use nuclear power. The coal is the dominant fuel in Poland and the Czech Republic [11]. Natural gas is an essential element of the EU energy mix. It accounts for about 25% of the total primary energy supply [16] and its growing. There are two predictions regarding gas consumption and costs in future. The first that the imported gas will meet EU needs. The second, that price will increase due to the surplus of gas supply in terms of excess capacity of the infrastructures. Below the Figure 3 shows the possible changes in the EU mix [16].

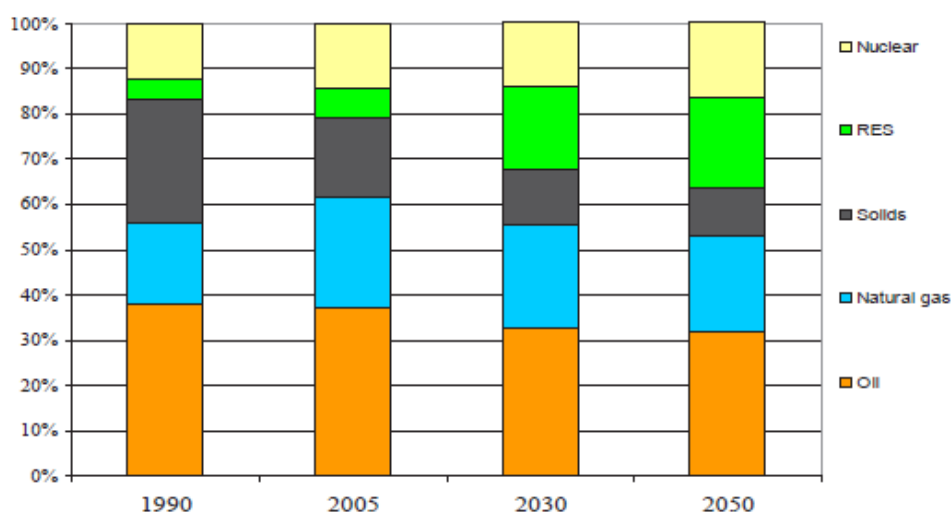


Fig. 3. Possible changes in European mix in 2030 and 2050

Furthermore, a common energy policy is a guarantee for European citizens to have stable energy prices and to maintain EU industrial competitiveness. During the Greek presidency the Council held a public policy debate on the Commission communication on energy prices and costs in Europe, focusing on actions proposed by Commission to reduce energy costs. The communication, which was presented on 22 January, provides the analysis of the composition and drivers of energy prices and costs; therefore, it helps policy makers understand the context of recent prices rises, their impact on energy consumers and the political implications [17].

The communication focuses on electricity and gas prices and costs, including their impact on citizens' access to stable and affordable energy prices and on the EU's industrial competitiveness. According to the communication, the consumer price for electricity and gas is composed of the following three elements: energy price (wholesale and retail price), network costs (transmission and distribution costs) and taxes/levies (general and targeted). The communication points out that prices, and especially costs, continued to rise overall for both households and industry despite falling or stable consumption [18].

5. SUGGESTED MEASURES AND RESULTS OF THE RESEARCH

5.1. Internal measures

The measures are suggested to deal with the external and internal challenges described above. Specific forms of cooperation with neighbourhood, shifting towards a proactive engagement with other regional countries could help to achieve the objectives regarding energy security. In addition, dealing with internal challenges, national tools, such as the development of infrastructure and networks, are essential for the EU unity and supply guarantee.

There are several measures to take in order to strengthen internal dimension. First of all, the creation of a coherent and integrated single regulatory energy market within Europe. The single energy market also requires a number of acts to take. The market liberalisation process must be built on a suitable Europe energy network. The role of infrastructure is fundamental because it interconnects markets and so leads to international solidarity. Secondly, price mechanisms must be put in place to correct the market when it proves incapable of acceptable energy price. Private operators should be allowed to make necessary investments in the network [19].

To ensure the security of energy supply, the diversification of Europe's energy mix must be determined by national governments with a strong recommendation or legal binding act from EU institutions. The EU energy mix must be supported by researchers and developers of new green technologies. The diversification must be encouraged by greater reliance on renewable energies. The EU should invest more in new technologies and create incentives, such as to levy the taxes on certain types of production.

In energy supply crises, common reserves must be available and distributed throughout Europe in the essence of the principle of solidarity. 'Solidarity' is introduced in a general context by the Lisbon Treaty Article 1a. [20]. There is no legal obligation on the member states to provide mutual support to one other.

Europe needs to complete policy tools, set binding legal regulatory framework and ensure the compliance with internal market rules. For instance, despite the fact that most of the states failed to correctly implement the two previous Internal Market Packages, the Third Energy Internal Market Package is an example of regulatory framework to make market opening fully effective and liberalize markets of gas and electricity.

5.2. External measures

The European Union must present a single interface in its relations with its external partners. Now Europe is an easy target for divide-and-rule policies by third parties. Although the Lisbon Treaty improved the EU's external representation, the EU needs to take initiative over the member states and to become the main actor on the international energy scene. To be more specific, external dependency must be taken collectively – at European level – member states should not have the right to conduct relations with third-country oil and gas suppliers and governments. Without an effective common policy, Europe risks remaining dependent on external energy sources. Member states should no longer be in privileged bilateral relations with external suppliers, contrary, international cooperation is the best defence of states national interests.

There is a need to give powers to someone in terms of co-ordination of the Union's external action on energy [21]. The High Representative for the Union in Foreign Affairs and Security Policy is responsible for ensuring coherence across external action policies, but The

High Representative will not have competence over EU environment and energy policies. There is open question who should have the competence to negotiate with third parties.

5.3. Legal measures

The European energy policy could be delivered by various legal tools. The independent think tank “Notre Europe” suggests four options [22]:

- 1) The New Energy Policy under the Lisbon Treaty;
- 2) Differentiated Integration within the Union Structures: Enhanced Cooperation and Others;
- 3) A New European Energy Treaty;
- 4) Functional and Regional Arrangements: Schengen(s) for Energy.

Under the first option, The Lisbon Treaty has entered into force and provides a new legal basis for Union to act in the field of energy. Directives and Regulations are adopted on the basis of the Article 194 TFEU. It follows that the New Energy Policy under the Lisbon Treaty does not make a relevant change from the present situation.

The second option also is not promising. It is based on the Article 20 TEU what states the opportunity of cooperation between the more ambitious members, making use of the institutional structures of the Union. The enhanced cooperation is open for all member states that wish to participate and does not exclude those that stay behind since they have the right to participate in its deliberations [22].

The third option is more radical. It aims to create a new energy-specific Treaty – European Energy Community. The member states would be no longer to exercise their powers regarding energy.

The last option is more negotiable instrument than The Energy Treaty. Whereas Energy Treaty is ‘a fully fledged Treaty’, in a case of Schengen(s) for Energy, groups of member states could decide to cooperate in certain areas on a functional or regional basis. Such agreements could supplement the EU where specific topics and competences of member states are not governed by the EU law or are not under the EU competence.

6. CONCLUSIONS

Today Europe needs to deal with such challenges as, security of supply, affordable access energy, sustainable development of energy production and energy transport, global energy competitiveness.

The goal to achieve energy security in unity should be ambitious and can be achieved by adapting these measures:

- Europe is increasingly dependent on importing energy from third countries. A well functioning internal energy market could promote EU competition. As a result, the North-Western European Price Coupling (NWE) has been launched in 2014;
- An integrated and smart network support the internal market and guarantee security of supply. Recently, the legal framework and funding instruments for the development of the EU energy infrastructure have been adopted;
- A common energy policy – as a price stabilisation measure – is a guarantee for European citizens to have stable energy prices and to maintain EU industrial competitiveness. The Commission communication on energy prices and costs in Europe, focusing on actions has been proposed by Commission to reduce energy costs in January. The communication, helps policy makers understand the context of recent prices rises, their impact on energy consumers;

- A diversified European energy portfolio and the use of renewable sources must be determined by national governments or legal binding act from the EU institutions in order to ensure the security of energy supply. The diversification must be encouraged by greater reliance on renewable energies. So far, the Renewable Energy Directive sets a minimum level of energy to be derived from renewable sources;
- External powers to deal on the international scene have to be strengthened. The European Union must present a single interface in its relations with its external partners;
- It is recommended to have the most effective legal instrument for the European Energy Policy.

In conclusion, much has been achieved in the last decade, specifically, the internal energy market has been pursued through a Third packages of Directives and Regulations, the creation of a specialised energy regulatory agency (ACER) and the regional market initiative the North-Western Europe.

Security in unity remains the main pillar of the EU policy. Freedom from energy insecurity reduces the risk of conflicts between states. And peace is what Europe is all about.

REFERENCES

1. BELKIN, P. *The European Union's Energy Security Challenges*. CRS Report for Congress, 2008 January, 2 p.
2. The European Commission, Directorate – General for Energy, *Energy 2020: A Strategy for Competitive, Sustainable and Secure Energy*. Luxembourg: Publications Office of the European Union, 2011. 2 p. ISBN 978-92-79-18869-5.
3. The European Council Press Office. *EU Energy Policy*. [Referred on the 18th of February in 2014 y.] Link to the internet < http://www.european-council.europa.eu/media/171257/ec04.02.2011-factsheet-energy-pol_finaldg.en.pdf >
4. Official website of the European Union. [Referred on the 18th of February in 2014 y.] Link to the internet < http://europa.eu/pol/cfsp/index_en.htm >
5. Green Paper. *A 2030 framework for climate and energy policies*. [Referred on the 18th of February in 2014 y.] Link to the internet < <http://eur-lex.europa.eu/legal-content/EN/ALL/?uri=CELEX:52013DC0169> >
6. Europe Infos. [Referred on the 18th of February in 2014 y.] Link to the internet < <http://www.comece.eu/europeinfos/en/archive/issue143/article/4299.html> >
7. International Energy Agency. *World Energy Outlook*. 2012 Figure 2.15. 75 p.
8. Official page of the UK Parliament. [Referred on the 18th of February in 2014 y.] Link to the internet < <http://www.publications.parliament.uk/pa/ld201213/ldselect/ldeucom/161/161/16106.htm#note92> >
9. The Renewable Energy Directive 2009/28/EC. [Referred on the 18th of February in 2014 y.] Link to the internet < http://europa.eu/legislation_summaries/energy/renewable_energy/en0009_en.htm >.
10. ANDOURA, S. *Energy Solidarity in Europe: from Independence to Interdependence*. Paris: Notre Europe – Jacques Delors Institute, 2013 June, 25–33; 44 p.
11. BELKIN, P. *The European Union's Energy Security Challenges*. CRS Report for Congress, 2008 January. 21–24 p.
12. The European Council Press Office. [Referred on the 18th of February in 2014 y.] Link to the internet < http://europa.eu/rapid/press-release_MEX-14-0204_en.htm >

13. The European Commission, Directorate – General for Energy, *Energy 2020: A Strategy for Competitive, Sustainable and Secure Energy*. Luxembourg: Publications Office of the European Union, 2011. 14 p. ISBN 978-92-79-18869-5.
14. The European Council Press Office. *EU Energy Policy*. [Referred on the 18th of February in 2014 y.] Link to the internet <<http://gr2014.eu/sites/default/files/Council%20adopts%20regulation%20on%20notification%20of%20investment%20projects%20in%20energy%20infrastructure.pdf>>
15. The EU Regulation on energy infrastructure 2013. [Referred on the 18th of February in 2014 y.] Link to the internet <<http://eur-lex.europa.eu/LexUriServ/LexUriServ.do?uri=OJ:L:2013:115:0039:0075:EN:PDF>>.
16. ANDOURA, S. *Energy Solidarity in Europe: from Independence to Interdependence*. Paris: Notre Europe – Jacques Delors Institute, 2013 June. 55 p.
17. The European Council Press Office. *EU Energy Policy*. [Referred on the 18th of February in 2014 y.] Link to the internet <http://www.consilium.europa.eu/uedocs/cms_Data/docs/pressdata/en/trans/141221.pdf>
18. The communication (5599/1/14 REV 1). [Referred on the 18th of February in 2014 y.] Link to the internet <<http://register.consilium.europa.eu/doc/srv?l=EN&t=PDF&gc=true&sc=false&f=ST+5599+2014+REV+1>>
19. ANDOURA, S.; HANCER, L.; VAN DER WOUDE, M. *Towards A European Energy Community: A Policy Proposal*. Paris: Notre Europe – Jacques Delors Institute, 2010 March. 29 p.
20. Treaty of Lisbon). [Referred on the 18th of February in 2014 y.] Link to the internet <<http://eur-lex.europa.eu/JOHtml.do?uri=OJ:C:2007:306:SOM:EN:HTML>>
21. FABRY, E. *Think Global – Act European IV Thinking Strategically About The EU's External Action*. Paris: Notre Europe – Jacques Delors Institute, 2013 April. 15 p.
22. ANDOURA, S.; HANCER, L.; VAN DER WOUDE, M. *Towards A European Energy Community: A Policy Proposal*. Paris: Notre Europe – Jacques Delors Institute, 2010 March. 100 p.
23. DE JONG J.; GROOT K. A Regional EU Energy Policy? Energy Paper. The Hague: Clingendael International Energy Programme. 2013 June. 42 p.

STRATEGIC PLANNING OF SUSTAINABLE ENERGY DEVELOPMENT FOR GEORGIA

Z. Gachechiladze,

*Technical University of Georgia
Kostava str. 77, 0175 Tbilisi – Georgia*

I. Pirveli

*International School of Economics at TSU (ISET)
Zandukeli Street 16, 0108 Tbilisi – Georgia*

N. Sumbadze

*Tbilisi State University
University Street 2, 0186 Tbilisi – Georgia*

ABSTRACT

Proposed paper aims to research sustainable development options for Georgian energy sector. Improving energy saving, utilization of renewable energy and energy efficiency potential is important challenge for Georgia. Currently, 2/3 of Georgia's energy needs are met from imported energy resources that have negative effect on current account balance, energy security and political stability. At the same time supersede of imported energy by domestic resources is limited and in many cases is impossible without abnormal environmental damage. On the other hand one has also to evaluate the social impact of potential energy projects, since social equity together with environmental protection and economic growth is the main precondition of the country's development. Sustainable energy development is the main challenge for every nation and is especially crucial for the developing countries, such as Georgia. Meanwhile, unfortunately that is still unexplored topic for Georgia.

The paper describes sustainable energy development policy and strategy options and alternatives for Georgia obtained using computer software LEAP (Long range Energy Alternatives Planning System). The two main areas that combine sustainable supply and consumption of energy resources are: renewable energy and energy efficiency. Since Georgia is rich in renewable energy resources, mainly hydropower, it is crucial to design successful and effective policies for utilization of renewable energy. Very often successful emissions reduction policies require not only supply side intervention but also coherent demand side management. The latter can be achieved through energy efficiency and energy conservation. Therefore, paper analyzes renewable energy development and energy efficiency improvement potentials for Georgia and examines their impacts on reducing energy import dependency and on sustainable development.

Keywords: Energy policy, Sustainable Energy Development, Renewable Energy, Energy Efficiency, Energy Demand

1. INTRODUCTION

It was several decades ago when mankind observed that country's development is no more function of only economic growth and technological innovation, but also environmental stability, healthy ecosystem and human life, hence the term sustainable development emerged. Sustainability concepts are important for energy sector as well, since this sector is one of the most pollutants for the earth and at the same time engine of the economic growth and technological innovation. Energy needs today should be met without compromising the ability of next generations to meet them in the future.

Sustainable energy development policies and strategies vary across countries referring different sources of energies, market structures, integration, resources, geographical location

and etc. Therefore, it is important to analyze Georgian energy sector from various aspects to outline most reasonable sustainable development strategies.

Georgian economy is heavily dependent on import. Export constituting 1/5 of total import (Table 1) creates a significant current account deficit and hinders economic growth. Even though export was increasing in past years steadily, this did not result in reducing trade deficit because of rapidly increasing imports. In 2012 Georgia imported more than 5 billion USD worth of goods and services than exported.

Table 1. Macroeconomic and Energy Parameters

Variable/Date ¹	2008	2009	2010	2011	2012
Population (thousands)	4382.1	4385.4	4436.4	4469.2	4497.6
Real GDP (at constant 2003 prices), mil. USD	8382.5	7195.4	7164.4	8118.1	8801.5
Real GDP growth, percent	2.3	-3.8	6.3	7.2	6.2
Exchange rate GEL/USD	1.5	1.7	1.8	1.7	1.7
Export (FOB), Mil USD	1495	1134	1677	2189	2377
Import (CIF), Mil USD	6302	4500	5257	7058	7842
Unemployment rate, percentage	16.5	16.9	16.3	15.1	15
Annual average inflation (CPI), percent	9.2	10.0	1.7	7.1	8.5
Total Final Energy Consumption, Ktoe	2702	2616	2663	3033	3495
Share of Renewables in Electricity Generation	85%	88%	93%	78%	74%

Unfortunately, contribution of the energy sector in this gap is high: 2/3 of energy demand is met with imported energy resources (Fig. 1). At the same time, country has potential and unutilized capacity of clean, environmentally friendly renewable sources of energy. For instance, only 18% of yearly available 40 billion kWh economically feasible hydropower energy is utilized so far. Also, Georgia has a significant potential for exploitation wind energy that is practically untapped. Estimating the contribution of renewable energy utilization in reducing import dependency is one of the goals of the research.

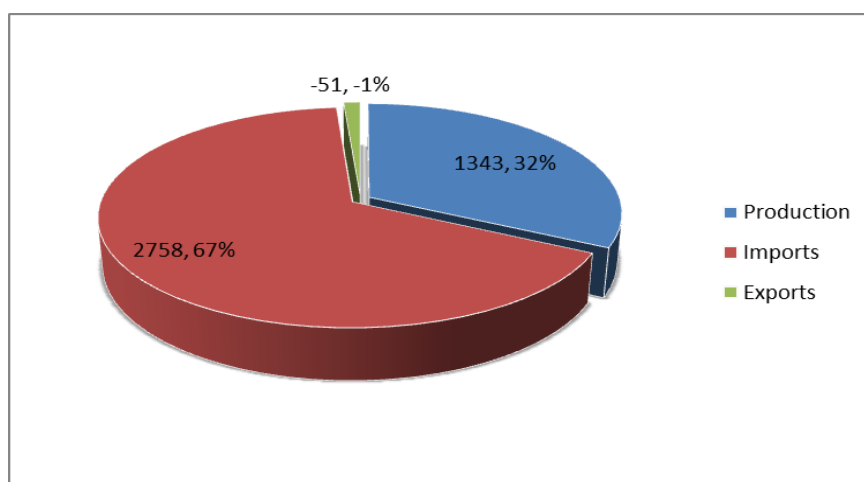


Fig. 1. Formation of Total Primary Energy Supply (TPES) of Georgia in 2012, in absolute (ktoe) and relative (percentage) terms

¹ Source: Geostat, ESCO, NBG

Besides, the Georgian post-soviet transitional economy lacks energy efficient technologies. For example, energy intensity per GDP in Georgia is more than two times higher than average intensity for OECD countries and the trend has not changed during past years. Though, compared to the neighboring Armenia and Azerbaijan, Georgia has lower energy intensity, still this indicator is very high compared to the more developed neighboring country – Turkey (Fig. 2).

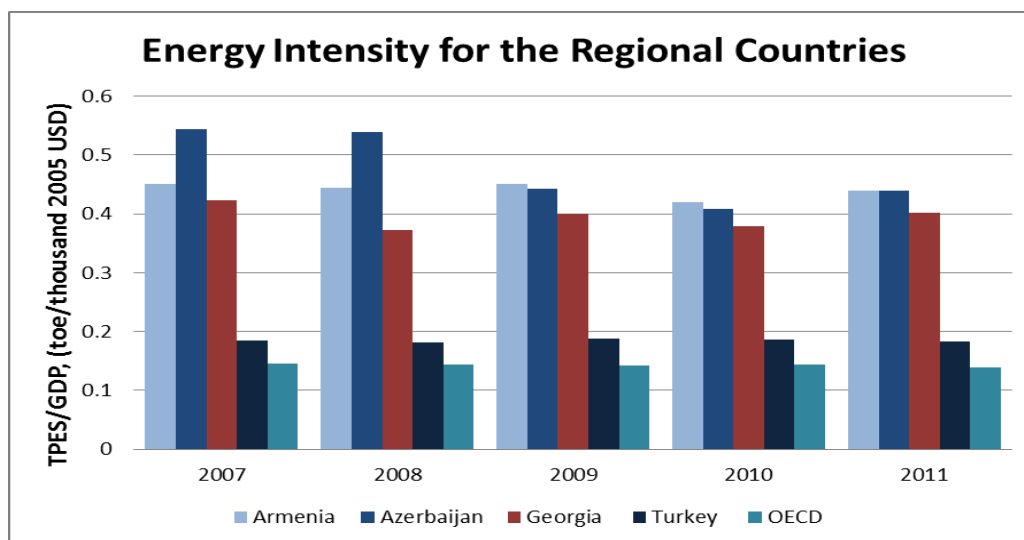


Fig. 2. Energy intensity for the regional countries

Brief analysis of current economic structure illustrate that Georgian economy is not based on energy intensive industries. Therefore, the difference in energy intensity must be due to much lower energy efficiency. Accordingly another goal of the paper is to estimate energy efficiency potential of Georgia and its role on reducing energy import dependency and contributing sustainable development.

After analyzing Georgian energy sector statistics and reviewing various research and studies [3, 4], the two most important areas that can contribute sustainable energy development of Georgia were identified: renewable energy and energy efficiency. Therefore the research is focused to examine the long term impact of improving energy efficiency and renewable energy development scenarios.

2. METHODOLOGY

Analyzing literature on sustainable energy development modelling and planning [1, 2, 5], it can be concluded that there exist four types of approach to model sustainable energy development on national level. These are:

- Optimisation Models – typically used to identify least-cost configurations of energy systems based on various constraints and selects among technologies based on their relative costs;
- Simulation Models – simulating behavior of consumers and producers under various signals and circumstances. It typically uses iterative approach to find market clearing demand-supply equilibrium.
- Accounting Frameworks – rather than simulating behavior of a system in which outcomes are unknown, instead asks user to explicitly specify outcomes. Main function of these tools is to manage data and results.
- Hybrid Models combining elements of each approach.

While selecting appropriate modelling tool, the following specifics were taken into account. Georgia lacks energy statistics on a national level and consistent time-series data on final energy consumption. Therefore, Long-range Energy Alternatives Planning System (LEAP) model was chosen to model sustainable energy development of Georgia. It is simple and flexible software tool with lower data requirements which does not assume perfect competition. It is capable to examine issues that go beyond the technology choice. As an integrated energy planning model LEAP covers both the demand and supply sides of the energy system.

The model follows the accounting framework approach to generate a consistent view of energy demand and supply based on the physical description of the energy system. Given that LEAP model uses what-if analysis, it mainly relies on the scenario development to describe a consistent storyline of the possible paths of energy system evolution. The LEAP platform was utilized to depict current Georgian energy system structure. To measure impact of energy efficiency programs and development of renewable energy, the reference energy system scenario² (REF) was constructed and compared against to the energy efficiency (EEF) and renewable energy (RES) utilization scenarios.

Physical process of energy supply and demand is depicted on Fig. 3 in order to capture the chain of activities described in the sustainable development model. The Figure is a graphical representation of general modelling approach in LEAP to describe Georgian energy sector and to generate current (year of 2012) and forecasted energy balances (year of 2030).

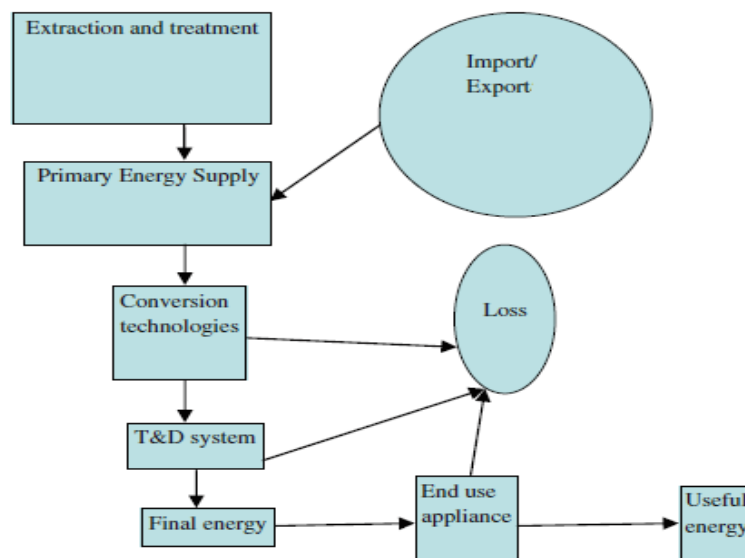


Fig. 3. Energy supply chain

Due to the lack of statistical data, model is built in combination of bottom-up (more data intensive) and top-down (less data intensive) approaches. The model uses mixed bottom-up and top-down demand modelling methodologies in different sectors – typically the choice is dictated by the availability of data. This means that the strengths or limitations of each approach will apply more specifically to each of demand sectors, rather than to the model as a whole.

² Sometimes referred as Business as Usual (BAU) scenario

The main variables and processes of the model are organized in four sections: key assumptions, demand, transformation and resources. Interactions between key assumptions and demand branches generate energy demand that should be satisfied by resources and transformation module. The LEAP-Georgia is based on accounting framework approach and applies what-if analysis to construct different Georgian energy sector development scenarios in order to track energy consumption, production, import and export and resource extraction in all sectors of the economy.

1) Key Assumptions section: under key assumptions there are given those macroeconomic and demographic variables that drives country's total energy demand. Total population, number of households, household size, urbanization, real GDP, value added of real GDP from each sectors and income are the main exogenous variables of the model which drive energy demand within different sectors.

2) Demand section: final energy demanded is normally useful energy consumption by end-users who cannot sell or transfer the energy to others. To reflect the energy sector structure of Georgia, the end-users were grouped into 5 categories: households, industry, transport, services and agriculture. Besides, separate branches were created to illustrate that energy is also used as feedstock in production processes or for non-energy purposes. The analysis is carried out at a disaggregated level. The disaggregated structure of energy consumption is organized as a “hierarchical tree” where the total or overall activity is presented at the top level and the lowest level reflects the fuels and devices used. The socio-economic drivers of energy demand are identified. Generally, the product of activity and the energy intensity (i.e. demand per unit of the activity) determines the demand at the disaggregated level. At the end-use level, useful energy is considered to forecast the energy demand.

Average historical elasticity of energy demand to real GDP for a given subsectors were calculated to link future sectorial energy demands to real GDP projection. Household energy demand was linked to number of households, urbanization level, saturation level of energy end-use devices and energy intensity. In the transport subsector, energy demand was linked with population growth and income.

3) Transformation section: in this module, energy conversion structure is defined, which is rather simple for Georgia than for developed countries. Georgia is poor with energy resources except hydropower. On average 80% of electricity is produced by Hydro Power Plants (HPP) and remaining 20% comes from Thermal Power Plants (TPP), which generate base power during winter when there is lack of water inflow. During spring and summer Georgia is exporting electricity to neighboring countries. To model renewable energy resources development scenario for meeting sustainable energy development targets and meeting long term electricity demand, the most efficient HPPs and wind farm projects were selected in terms of location, connection to transmission system, construction cost and capacity usage factor. None of them are large reservoir HPPs.

Under current and near term electricity wholesale price signals, new Georgian HPPs are mainly build for exporting electricity into regional markets, mainly in Turkey. That is why in LEAP-Georgia model, reductions in energy demand from energy efficiency policies do not dictate less generating capacity. At the same time, new CCGT power plant construction is envisaged with efficiency over 50% in 2016 while old TPP is planned to decommission with 32% efficiency in 2025.

Table 2. Capacity addition according to scenarios

Technology/Scenario	Number of plant			Capacity MW			Generation GWh		
	REF	RES	EFF	REF	RES	EFF	REF	RES	EFF
Enguri and Vardnili HPPs	0	0	0	0	0	0	0	0	0
Other Regulated HPPs	0	0	0	0	0	0	0	0	0
Large Run of River HPPs	5	10	5	497	1327	497	1973	4707	1793
Small Run of River HPPs	7	21	7	86	125	86	346	466	346
Large Reservoir HPPs	0	3	0	0	1362	0	0	3663	0
Natural Gas TPPs	0	0	0	0	0	0	0	0	0
Energy Invest Gas Turbine	0	0	0	0	0	0	0	0	0
Coal TPP	0	0	0	0	0	0	0	0	0
CCGT	1	1	1	230	230	230	1821	1821	1821
Wind	1	4	1	20	300	20	92	1050	92
Solar	0	2	0	0	100	0	0	262	0

4) Resources module: In this module data on the availability of primary resources, including both fossil and renewable energy resources, as well as information on the costs of local production, imports and exports of both primary resources and secondary fuels are inserted and analysed. The data on domestic coal, oil and gas reserves, as well on wind, biomass, geothermal, solar and hydropower potential were obtained from expert evaluations [3, 4] and were inserted in the model. As for LEAP-Georgia model, estimations on maximum economically feasible potential for fossil and renewable resources of Georgia were used.

3. RESULTS

Reference energy system development, renewable energy development and energy efficiency scenarios were developed and compared for evaluating the policy impacts on import reduction and sustainability measures.

Scenarios are story-lines of how the energy system might evolve in future in a particular socio-economic setting and under a particular set of policy conditions. All scenarios share a common set of data for a single Base Year which is the year of 2012. Each scenario runs from the first scenario year (year of 2013) to the end year of the scenario (year of 2030).

3.1 Reference Energy System Development Scenario

REF was constructed under numerous assumptions that were based on the historical statistical data analyses, already approved policy directions and expert evaluations. Without any new energy policies in place, REF scenario projects that total energy demand of Georgia increases by 60% in 2030 compared to the base 2012 year, constituting 5810 ktoe. This increased demand is satisfied mainly from increased energy imports thus increasing energy import dependency of Georgia. Overall increase of imports comprised 52% in 2030 compared to 2012. The main contributors of total energy import increase are electricity and natural gas imports, due to rising demand on the services supplied from that energy sources.

In the REF, share of natural gas fired TPP generation is increasing due to increased electricity consumption and also, to satisfy seasonal electricity demand when there is low level of hydropower generation because of low water inflow seasons. In reference scenario no construction of large reservoir HPPs are envisaged. The scenario illustrates building those new Run-off River and seasonal HPPs that are already under construction or final feasibility

study stage depending on the dates indicated in the signed Memorandum of Understandings between Government of Georgia and rewarded investors.

Projected electricity generation from different energy sources are calculated and presented in the Fig. 4.

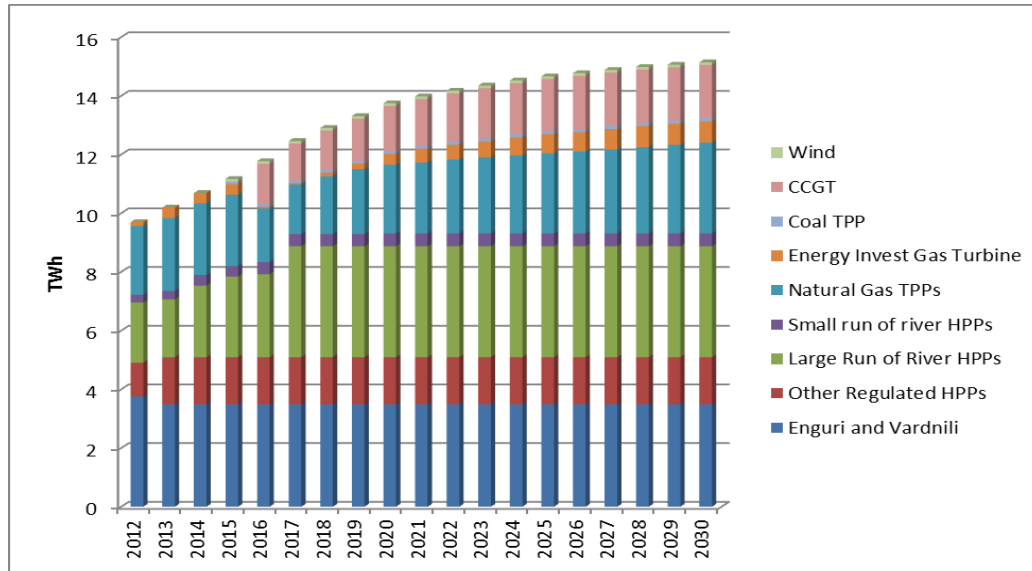


Fig. 4. Projected electricity generation in the reference scenario

Other REF projections and results will be presented below in the context of deviations from baseline energy sector development path as a result of implementation of renewable energy development scenario and energy efficiency scenario.

3.2 Renewable Energy Development Scenario

RES scenario depicts the option to satisfy increased energy demand through utilizing hydro, wind and solar energy. Consequently this scenario illustrates additional electricity production from domestic hydro power, wind and solar energy (small share of solar energy is directly inserted in the model to satisfy useful energy demand on water heating).

Fig. 5 below illustrates yearly increase of electricity production and evolution of the electricity supply mix under renewable energy development scenario, stressing significant increase of electricity generation from large and seasonal HPPs, utilization of wind and solar power and decreasing electricity generation from imported natural gas.

Model results show that as a consequence of increased electricity generation from domestic renewable energy resources, energy import dependence of Georgia is reducing from 77% to the 65% in 2030. On Fig. 6 is compared formation of TPES under reference and renewable energy scenarios at the end year of the study.

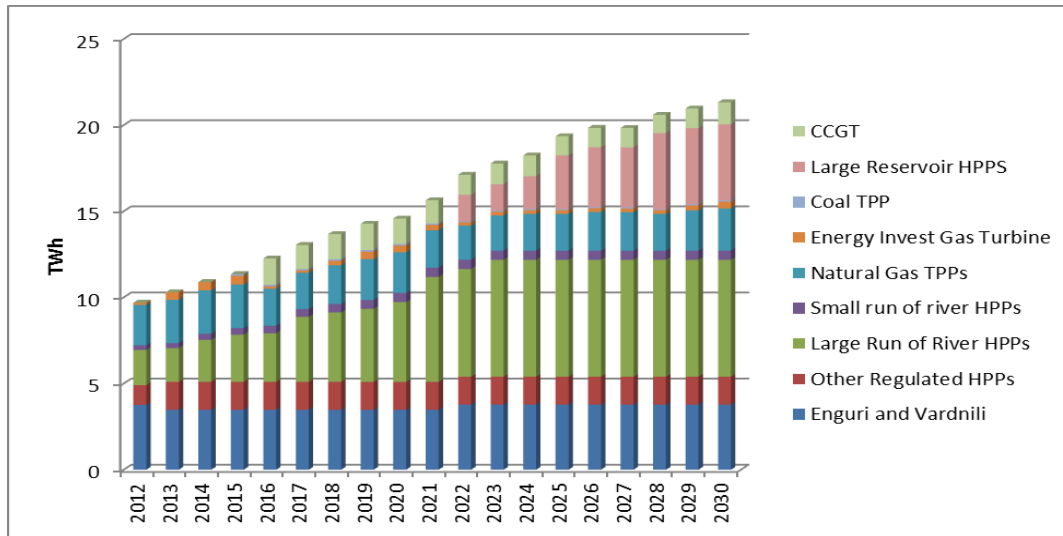


Fig. 5. Projected electricity generation in the renewable scenario

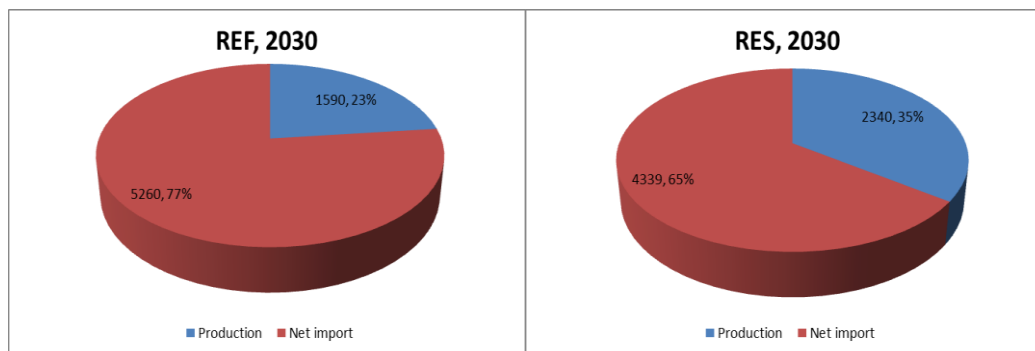


Fig. 6. Formation of TPES for different scenarios in absolute (ktoe) and relative (percentage) terms

However the study also analysed that without any fuel switching policy (for instance at least partially switching from natural gas devices to electric devices for space/water heating or cooking in households) renewable energy development scenario does not have a significant effect on import reductions.

3.3 Energy Efficiency Scenario

Currently, Georgia does not have law on energy efficiency and therefore any energy efficiency targets. However, there are positive ongoing negotiations between Government of Georgia and EU Energy Community to become Georgia energy community member country from being as an observer. Therefore general target of EU to increase energy efficiency by 20% till year 2020 was used for modelling energy efficiency scenario. However assumption is that 20% target for Georgia should be achieved till 2030. Improving energy efficiency by 20% is modelled to be achieved from estimated economic and technical potentials for energy efficiency in different economic sectors based on studies conducted for post-communist EU member countries³.

Energy efficiency scenario was calculated separately for all demand branches. In household sector energy efficiency is envisaged to be achieved via improving performance of

³ Data Base on Energy Saving Potentials, www.eepotential.eu/esd.php

dwelling, installing more efficient light bulbs, using more energy efficient technologies for cooking, cooling, refrigeration, water and space heating. In the commercial sector energy efficiency is achieved through improving building insulations and lightning technologies; in industrial and agricultural sector via improving technological process and reducing energy intensity; in transport sector fuel switching from oil products to natural gas and electricity (mainly for public transport).

According to results, in 2030 total energy demand due to energy efficiency measures is projected to be reduced by 1151 ktoe that is 20% of the demand under REF. Import is decreasing by 1184 ktoe. Relative shares of reduced energy by sectors and total energy demand reductions compared to REF is presented in Fig. 7.

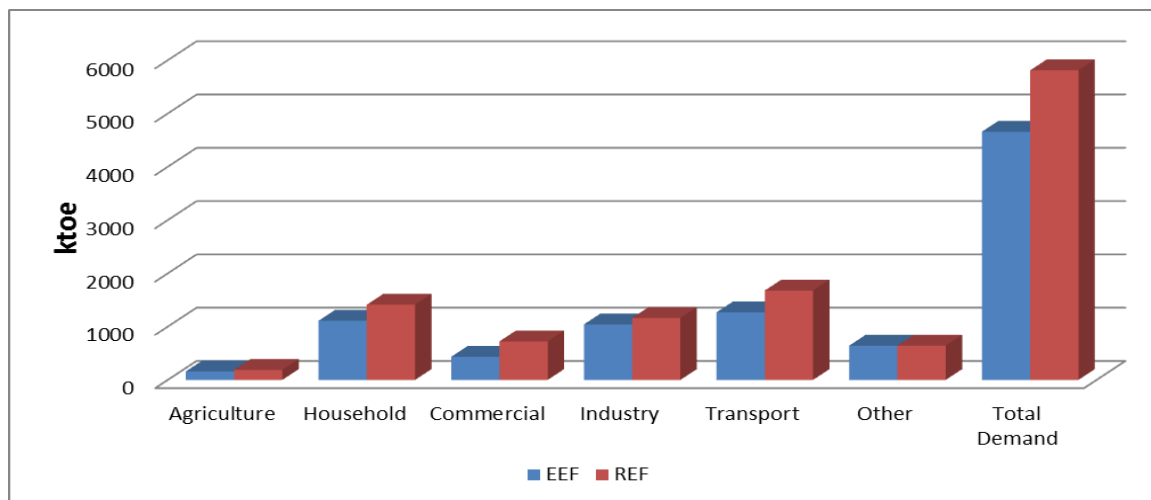


Fig. 7. Total energy demand reduction comparison

4. CONCLUSION

Analyzing Georgian energy sector characteristics and energy resources potential the paper concludes that energy efficiency and renewable energy are two important policies that can contribute energy import reduction and the country's sustainable development. The paper stresses low level of utilization of renewable energy resources and untapped energy efficiency potential. At the same time, Georgia is energy import dependent country and if no targeted renewable energy policy or energy efficiency measures are taken, in the future the energy import dependency will further increase, from existing 67% to 77% for the year of 2030.

Taking into consideration the negative impact of heavy import dependency on the economy, currency stability and energy security, two alternative policies were estimated. The expected reduction of imports is significant in both – renewable and energy efficiency scenarios.

There are other important benefits associated with implementing energy efficiency and renewable energy policies, such as reducing GHG emissions and cleaner environment but those topics are beyond to the discussion of the paper and are suggested to be explored in future.



REFERENCE

1. PIRVELI, Ivane; SUMBADZE, Nikoloz; GALDAVA, Irakli; KELBAKIANI, Giorgi. *The Political Economy of Sustainable Energy*. Tbilisi: Grigol Robakidze University, 2013. ISBN 978-9941-0-5771-7.
2. PIRVELI, Ivane; SUMBADZE, Nikoloz; GALDAVA, Irakli; KELBAKIANI, Giorgi, MUKHIGULISHVILI, Giorgi. *Electricity Policy Modeling and Analysis*. Tbilisi: Universal, 2013. ISBN 978-9941-0-5771-7.
3. GOCHITASHVILI, Teimuraz; JAVAKHISHVILI, Teimuraz. *Georgian Oil and Gas Trunk Pipelines*. Tbilisi: Meridiani, 2012. ISBN 978-9941-10-557-9.
4. GOCHITASHVILI, Teimuraz; Georgian energy sector: main priorities of gas sector development. Tbilisi: Publishing House “Meridiani”, 2012. ISBN 978-9941-10-665-1.
5. BHATTACHARYYA, Subhes; Energy Economics. New York: Springer, 2011. 673 p. ISBN 978-0-85729-267-4.

ELECTRICITY MARKET INTEGRATION AND MONITORING

O. Ruksans, I. Oleinikova

Riga Technical University

Faculty of Power and Electrical Engineering

1 Kronvalda Blvd., Riga, LV-1010, Latvia

ABSTRACT

The power markets in Baltic States were liberalized recently and they are relatively young. That is the reason why the market monitoring is not yet regularly implemented in the Baltics and none of monitoring tools are used. The target of this paper is to evaluate the electricity market by market power indices estimation in the Baltic States. General principles and methodology with the most common market power estimation indicators are given in this paper.

Keywords: electricity market, energy policy, market power

1. INTRODUCTION

The Market Monitoring is an essential part of a well-functioning energy market. The objective of market monitoring is to detect and to deter market manipulation by making the market more transparent and oriented on consumer benefit. It provides tools that help to evaluate the energy market efficiency, to identify investment gaps in cross border capacities, to ensure greater transparency regarding the use of entire electricity transmission network. After the EU regulation 1227/2011 on wholesale energy market integrity and transparency has been entered on 28 December 2011, the market participants and persons professionally arranging transaction are obliged to fulfill the obligation [1]. Obligations require market players to publish all the relevant trading, generation and consumption data.

The power markets in Baltic States were liberalized recently and they are relatively young. That is the reason why the market monitoring is not yet implemented in the Baltics and none of monitoring tools are used in the Baltics. The target of this paper is to evaluate the market power in the Baltics. However, detecting and proving the existence of market power in electricity markets is complex task, there is a need to estimate four key factors affecting market outcomes:

- Demand;
- Total available supply;
- Large suppliers' capacity share and contract position;
- Decision making development.

Generally, each market is establishing its own, optimum mix of power producing solutions based on geography, weather conditions, market acceptance, public supports schemes, existing and planned industrial capabilities and pricing conditions. The purpose of this research is to assist to regulatory bodies to consider the all relevant key factors to facilitate the harmonization, integration and efficiency of the European electricity market including grid requirement [2].

2. MARKET POWER ESTIMATION

The focus of this paper is on the detection of market power. This includes the detection of the *potential* for market power as well as the actual *exercise* of market power. We will not, however, be examining the broader role of market monitoring which includes identifying and

analyzing the market rules that may have efficiency effects outside of those related to market power.

Under term *market power* is assumed as a company's ability to manipulate the prices by influencing supply, demand or both. However, in order to hit immediate target on a market such as profit maximizing, the definition of a company's market power may be abridged as the ability to raise the market price of product above the marginal costs of production or, in other words, the ability of a company to maximize the profit margin on the market without losing the market share [6].

Various methods can be implemented for detecting market power, a useful distinction is between techniques that are applied ex ante - looking for the potential for market power - and those that are applied ex-post - usually looking for the actual exercise of market power [2, 3], Table 1.

Table. 1. Applications of Market Power Mitigation Systems

	Ex-Ante	Ex-Post
Long-Term	<ul style="list-style-type: none"> – Structural indices, e.g. Market share, the Lerner index, HHI, RSI – Simulation models of strategic behaviors. 	<ul style="list-style-type: none"> – Competitive benchmark analysis based on historical costs; – Comparison of market bids with profit maximizing bids.
Short-Term	<ul style="list-style-type: none"> – Spot market bid mitigation – Must-run activation & other system operator contracting. 	<ul style="list-style-type: none"> – Short term price recalculations – Penalties for withholding.

For market power estimation several techniques can be implemented.

2.1. The Lerner index:

$$L = \frac{p - C_m}{p} (\%), \quad (1)$$

where p is the price charged by the company and C_m is its marginal cost. In perfect competition, $L = 0$ if $L > 0$ this can indicate the possibility for the company to charge, for various reasons, a price above its marginal cost.

2.2 The reference to structure of the industry: the Herfindahl–Hirschman Index (HHI) index:

Economic theory suggests that, all other thing being equal, the level of competition in a given sector is related to the number of companies active in that sector.

$$HHI = \sum_{i=1}^n s_i^2. \quad (2)$$

Where S_i is the market share of company i expressed as a %. If $i = 1$ (monopoly), HHI reaches a maximum value of 10 000. Its value decreases when the number of companies increases.

2.3. The pivotal indexes:

A supplier is referred to as pivotal if the combined capacity of all its competitors is not sufficient to meet total demand. Then the two indexes is defined:

- the PSI index (Pivotal Supplier Index) established per supplier and which has a value of 1 if the supplier is pivotal and 0 if otherwise;
- the RSI index (Residual Supply Index) established for supplier k and which is a continuous measurement calculated by means of:

$$RSI = \frac{\sum_{i=1}^n C_i - C_x}{Total\ demand}. \quad (3)$$

In this study a RSI index is chosen as a market power evaluation tool to show “potential” market power, while HHI index will be used in order to compare the obtained results.

3. RSI INDEX

The RSI Index is a simple and effective tool that can be used to monitor market power in the power markets. The results of this research will provide the support to the regulatory bodies in the Baltic countries to monitor market players for the market manipulating opportunities and will help to operate for the benefit of the final consumers [4, 5, 3].

Residual Supply Index specification can be summarized as measures (continuous variable) the extent to which a generator’s capacity is necessary to supply demand after taking into account other generators’ capacity. It’s takes into account the demand side of market, suited for dynamic analysis on an hour-by-hour basis and local market power analysis with empirical support of ability to predict actual market power.

The application of RSI can be fourfold as follows:

1. Simple Screening Rule for Market Competitiveness;
2. For market-based rate screening - Individual supplier’s market power;
3. To evaluate new transmission Investment – Compare market power impact with and without transmission upgrade based on RSI simulation;
4. Capacity reserve required for competitive market – Using RSI simulation to evaluate system with different reserve level.

The RSI has been formulated specially for the market power estimation in the electric power industry. This index estimates the pivotality of supplier C_x and shows the position of pivotal supplier C_x in a particular situation (Fig. 4). This latter index shows the residual supply to demand ratio calculated by the following equation as:

$$RSI = \frac{\sum_{i=1}^n C_i - C_x}{Total\ demand}, \quad (3)$$

where $\sum_{i=1}^n C_i$ is the capacity of all suppliers including C_x plus the total net import;

C_x is the capacity of the largest supplier or of the examined supplier (which in a power market might be different for every hour) reduced by the (pro)portion already contracted to a particular load;

Total demand of the system is determined as a metered load including purchased ancillary services.

Generally, the lower is RSI of the analyzed market with examined supplier C_x the higher is the market power of this supplier (Fig. 1).

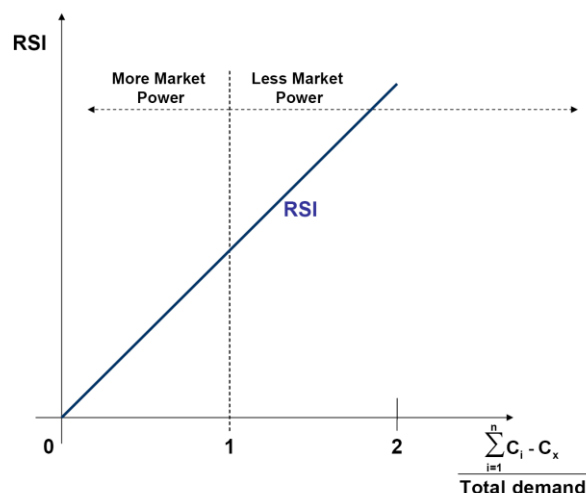


Fig. 1. Market power estimation via RSI

In practical RSI estimations on the electricity market (performed taking the demand on the hourly basis) the values of available supply can be assumed as weekly averaged (including planned outages). In order to obtain a descriptive RSI value on a particular market for the entire year, the hourly acquired values of this index are averaged.

As achievements of the RSI analysis can be considered the percentage obtained for the year when the major supplier is pivotal as well as the maximum and minimum load covered by the remained supply during the year.

4. MARKET POWER ESTIMATION IN THE BALTIC ELECTRICITY MARKET

The power system of Baltic States includes power plants that are located in all three Baltic countries with total installed capacity of 9 123 MW (see Table 2). The generation structure in each Baltic country is totally different (Fig. 2).



Fig. 2. Power system of Baltic countries

Not all of the generation capacity is used to produce electricity daily for the final customers because of the high marginal costs of old power plants, which are mostly used to ensure the secure and stable operation of the power system. If the generation structure in Latvia is commonly based on hydro with 1553 MW installed hydropower, then the Estonian generation structure is based on the oil shale – the domestic energy source. In the Lithuania power plants mostly uses gas to produce electricity at the peak hours (Table 2).

Table 2. Net Generation Capacity in Baltics, Source: ENTSOE-E 2012

Net Generation Capacity, MW	LV	EE	LT
Hydro	1553	4	877
Nuclear	0	0	0
Renewable	110	343	337
of which wind	58	266	275
of which solar	0		8
of which biomass	52		54
Fossil fuels	905	2303	2691
Total:	2568	2650	3905
Consumption, GWh	5 581	10 462	3 775
Utilization factor, %	25%	45%	11%

In the Table 2 the installed generation capacity is given are given the installed generation capacities in the Baltic countries, with Lithuania being the country with the biggest installed generation capacity, but this does not mean that the Lithuania is a major power producer in Baltics. Because of the high marginal cost of Latvian and Lithuanian power plants the power plants are used to produce electricity only in case of emergency when the safety of power system is threatened or in periods of high spot market prices. The high marginal costs in Latvian and Lithuanian power plants is the reason for generation capacities are not being utilized for higher quantity of hours. With the opposite situation in Estonia, where power plants with oil shale as a fuel have significantly lower marginal costs and can be operated for higher number of hours.

5. THE RSI CALCULATION RESULTS AND EVALUATION

The RSI index was estimated for the year 2013 for all three Baltic countries on the hourly basis. The calculation results are shown in the Fig. 3.

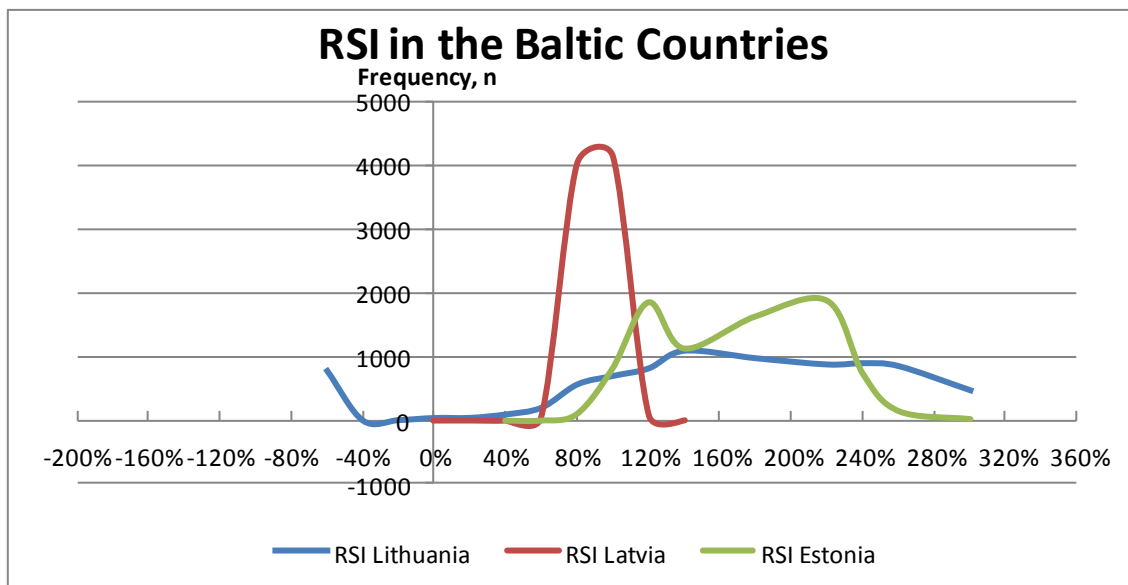


Fig. 3. RSI in the Baltic countries

The distribution of the RSI index is not even. As it can be concluded from the graph above the most competitive market of all three Baltic countries is in Estonia where the average RSI index was 105%, then followed by Latvia with average RSI of 20% and the Lithuania with the RSI averaging at 55%. These numbers show that the competition in the Baltic countries is insufficient at any time of the year with just only several hours with the RSI index above 120%. The low level of RSI index says not only about the low level of competition on the market but means that the market players cannot set the market price or manipulate with market and they are only “price takers” in the power market observed.

In order to compare the obtained results, the HHI index for the Latvian power market was calculated (Fig. 4).

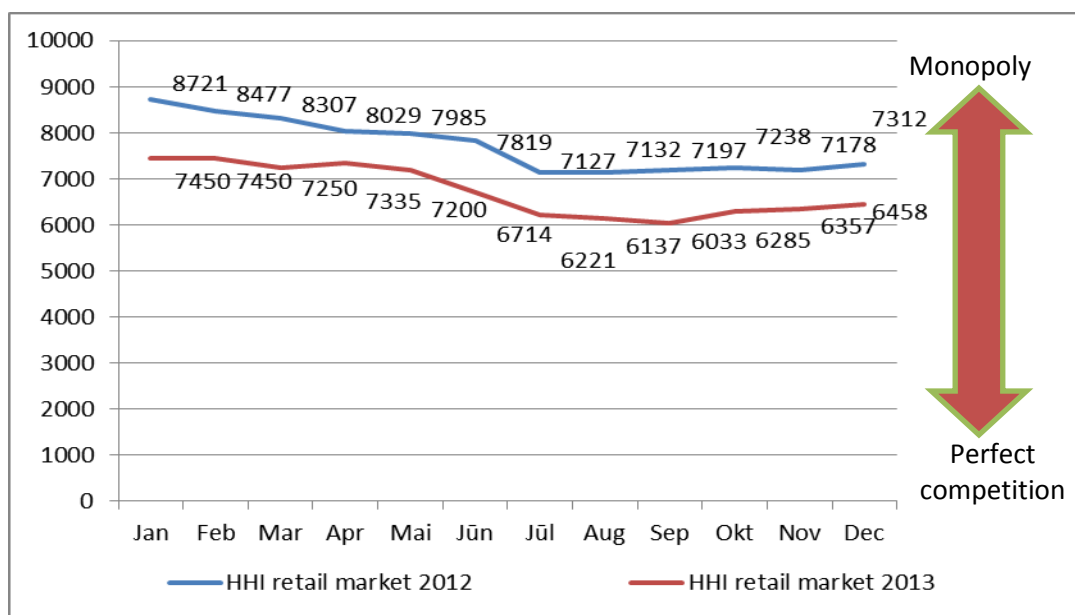


Fig. 4. HHI index distribution in Latvian retail power market

The graph above confirms the result obtained with the RSI index estimation. The competition on the Latvian power market is insufficient at all times with average 7710 points in year 2012 and with 6741 on average in the year 2013. The HHI index above 6000 points suggests that the competition on the given market is insufficient.

CONCLUSIONS AND FURTHER STEPS

Research described in this paper proved the market power monitoring and estimation results in Baltic. With the Baltic power market suffering from the lack of competition, where the market price can be influenced easily by the biggest market players what is not acceptable in modern power market where the consumer benefit is put on the first place.

To conclude the first phase of market monitoring the following inferences can be summarized:

1. As much data as possible should be published to allow independent analysis to refine techniques for the detection, and hence the deterrence of market power.
2. Several techniques need to be implemented of market power detecting to achieve valuable results that may considerably influence further decisions regarding power system operation and development.
3. To avoid market manipulations it is important to make the actual exercise of market power more transparent and regular.

Moreover, electricity market monitoring in regional level can contribute to cost-effective balancing and the reliability of supply, improve market efficiency and harmonized processes in intraday, day-ahead, forward markets.

REFERENCES:

1. European Commission (2011) Regulation No 1227/2011 of the European Parliament and of The Council (Online). Available: <http://eur-lex.europa.eu/LexUriServ/LexUriServ.do?uri=OJ:L:2011:326:0001:0016:en:PDF>
2. TWOMEY, P., GREEN, R., NEUHOFF, K., NEWBERY, D. A Review of the Monitoring of Market Power. University of Cambridge.
3. TURCIK, M., OLENIKOVA, I., JUNGHANS, G., KOLCUN, M. Market Power Estimation Techniques with Application in Electric Power Industry. Latvian Journal of Physics and Technical Sciences, 2012, No 2, P.14-23. DOI: 10.2478/v10047-012-0008-2.
4. SHEFRIN, A. (2002). Predicting Market Power Using the Residual Supply Index. Presented to FERC Market Monitoring Workshop, Dec. 3-4
5. BLUMSACK, S., & LAVE, L.B. Mitigating Market Power in Deregulated Electricity Markets. Carnegie Mellon University. <http://www.personal.psu.edu/sab51/usaee.pdf>
<http://www.personal.psu.edu/~sab51/usaee.pdf>
6. A review of the monitoring of Market Power: the possible roles of Transmission System Operators in monitoring for market power issuer in the Congested transmission systems. Available: http://web.mit.edu/ceepr/www/publications/reprints/Reprint_209_WC.pdf

STUDY ON CUSTOMER COSTS OF RELIABILITY AS KEY PREREQUISITE FOR POWER SUPPLY RELIABILITY LEVEL PERFORMANCE-BASED REGULATION

A. Lvovs

*Institute of Physical Energetics
Aizkraukles str. 21, LV-1006 Riga – Latvia*

ABSTRACT

The paper presents concept of methodology for Distribution System Operator power supply reliability level performance-based regulation (PBR) that includes customer costs of reliability study and enable to achieve optimal reliability level. PBR methodology is based on the author's studies and research, as well as on analysis of existing PBR practices that are in use at European countries. The main difference between proposed regulation and existing regulation approaches is in reliability optimality criterion that is used in proposed approach.

The paper also presents results of study on customer costs of reliability that has been performed in Latvia in years 2012 and 2013 by Institute of Physical Energetics. The study has been carried out on request of Ministry of Economics of the Republic of Latvia. Survey based method involving ~3000 end users classified as the largest energy users in Latvia have been used in the study. Customer Damage Functions and functions of costs deviations depending on interruption occurrence time have been created, as well as other power supply reliability related information has been obtained.

The last known similar type study in Latvia until year 2012 has been performed in 1976. Such studies, despite their relative popularity in Europe, are quite rare not only for Latvia, but also for the whole region of Baltic States. Electricity usage patterns, as well as economical situation in Baltic States are comparable and due to aforementioned facts, the results of the study could be of high interest not only for Latvian scientists, policy makers and Distribution/Transmission System Operators, but also for neighbouring countries.

Keywords: Customer costs of reliability, Performance-based regulation (PBR), Survey

1. INTRODUCTION

Quality of electrical energy mainly depends on electricity network. Nowadays, taking into account activities in the field of electricity market liberalization, national regulatory authorities develop and implement performance-based regulation for distribution and transmission system operators with the aim to improve power supply reliability.

Taking into account that improvement of the power supply reliability level asks for bigger investments in network, it is important to develop such performance-based regulation, that would be both easy to use and that would represent right indicators for system operators to reach optimal level of power supply reliability. This is possible only in case if customer costs of reliability of respective country are known. Due to the facts, this paper focuses on the aforementioned topics, proposes methodology for power supply reliability level performance-based regulation and gives results and shares experience on the performed study of customer costs of reliability.

2. METHODOLOGY FOR POWER SUPPLY RELIABILITY LEVEL PERFORMANCE-BASED REGULATION

Usually the main goal of implemented Performance-Based Regulation (PBR) is to maintain or raise existing power supply reliability level by using economic incentives. Regulative system, in essence, creates artificial market conditions for system operators.

Incentives used in regulation can be split into bonuses and penalties and their values have to be determined on the basis of information about customer costs of reliability. Respective penalties and bonuses are applied depending on correspondence of actual reliability indices to defined target values of indices.

Number of power supply interruptions and their durations, i.e. SAIFI (system average interruption frequency index) and SAIDI (system average interruption duration index) indices, usually are used as technical parameters of network reliability. Depending on threshold values of reliability indices, three zones can be identified: 1) bonus zone; 2) dead zone; and 3) penalty zone (see Fig.1). In case if actual reliability level is better than bonus threshold value, Distribution System Operator (DSO) receives bonus. In case, if actual reliability level is between bonus and penalty thresholds (in dead zone), no penalties and bonuses apply. In turn, if reliability index value is worse than penalty threshold value, DSO shall be punished with penalty [1, 2].

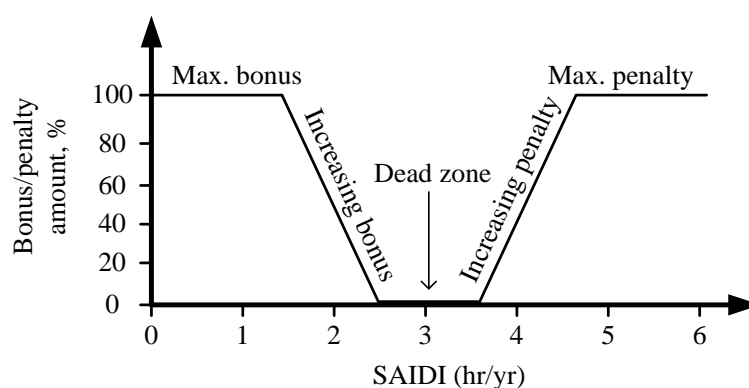


Fig. 1. Bonus and penalty system in performance-based regulation system

It is important to identify such reliability indices' threshold values for dead zone, that would correspond to optimal reliability level or zone of optimal reliability level.

The paper identifies optimal reliability level as such reliability level, at which sum of customer costs of reliability and costs of DSO, related with reliability of power supply, has minimal value.

Obviously, the theoretical basis of reliability level performance-based regulation methodology is relatively simple. However, the practical implementation of the regulation could face a number of challenges, such as the appropriate bonus/penalty amount identification and changes depending on the level of reliability, thresholds of reliability indices for regions of country (network regions), defining separate country regions (network regions) and etc. Regardless of several previously mentioned challenges, there could be one major barrier for implementation such PBR scheme that could ensure optimal reliability level. The barrier is – insufficient or incorrect usage of customer costs of reliability in PBR.

2.1. Performance-based regulation practices in Europe

According to the report of Council of European Energy Regulators (CEER), PBR is applied in at least 15 European countries [3].

Approaches of PBR application of the 16 European countries have been analysed: Denmark, Finland, France, Great Britain, Hungary, Ireland, Italy, Netherlands, Norway, etc. The analysis was based on information on existing regulations from state regulators, as well as from individual experts [3–7].

Analyzing national regulation approaches, author of the paper concluded, that at present there is no common approach for implementation of regulation that would be focused on the achievement of optimal power supply reliability. At the moment, most of the methods of PBR approaches objectively unable to provide optimal reliability level, at least because of the fact that the required level of power supply reliability for a country is determined on the basis of power network reliability levels of neighbouring countries, rather than on costs of system operators operating in the country and customer costs of reliability. Some countries use historical values of power supply reliability of their countries as reliability level target values. In the most countries there are also problems with identification of right bonus/penalty levels, as no studies on customer costs of reliability have been performed, or they have not been performed frequently.

In such situation optimal power supply reliability level cannot be reached, as it depends on actual topology and structure of specific country or region, costs related with network improvement, as well as customer costs of reliability of the country.

Literature study on the topic of improvement of power supply reliability showed that studies mainly concentrate on some specific reliability improvement techniques and their costs, like [17] concentrating on storage systems, [18] concentrating on distribution network structure, [19] on optimal placement of automation devices, or [20] on smart distribution grids reliability evaluation. But any of the reviewed literature didn't propose any methodology or approach for optimal power supply reliability finding.

Taking into account previously mentioned, paper proposes methodology for PBR that could help to reach optimal reliability level and therefore decrease costs related with power supply.

2.2. Description of proposed regulation methodology

In order to implement reliability level PBR that would facilitate the optimal reliability level achievement and maintenance, there have to be set and economically justified reliability level targets for different region in the country, at least for urban and rural areas. To determine target values of power supply reliability indices, it is proposed to carry out several activities as reflected in flowchart at Fig. 2. The flowchart represents proposed methodology.

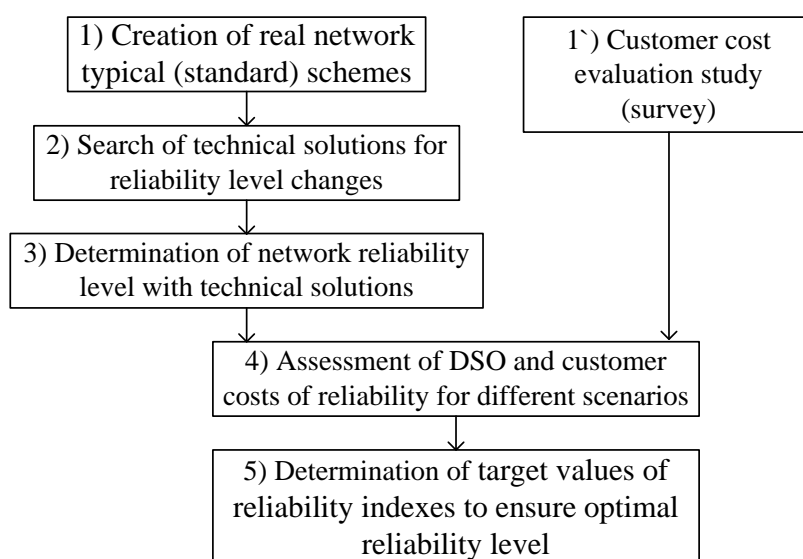


Fig. 2. Determination of power supply reliability indexes' target values as regulate of power supply reliability

As can be seen from the proposed flowchart, the primary activities of regulation implementation are: 1) creation of network typical (standard) schemes; and 2) carrying out of customer cost evaluation study (survey).

Carrying out customer cost assessment study is the crucial prerequisite for the introduction of performance-based regulation n, because it allows identifying appropriate amount of bonus/penalty.

Creation of network typical schemes allows setting appropriate target reliability values for regions of a country with different network structure, e.g. typical schemes for urban and rural networks.

Taking into account differences in network schemes, different technical solutions for reliability improvement should be proposed.

At the third step there should be evaluated effect of each reliability improvement solution, as well as their possible combinations. Implementation of each improvement solution or combination of solutions creates network development scenario.

Economical effect of network development scenarios on DSO and customers should be performed after all possible scenarios have been created (the fourth step).

Reliability level of the scenario (or group of scenarios) that ensure minimal total DSO and customer costs should be defined as reliability level target value (the fifth step). In this case national regulatory authority (NRA) has to approve network development strategy and set adequate tariff that would allow implementing chosen network development scenario. It is important to have clear vision of network development towards optimal reliability level both for DSO and NRA. Implementation of such regulation means, that NRA has not only approve tariff if it corresponds to network maintenance and operation costs, but it should also check if the tariff and large scale investment activities of DSO correspond to approved network development strategy. Otherwise it is possible to come to situation when DSO invests money in projects with low reliability-efficiency and has to pay high penalties for not fulfilling reliability target criteria. Taking into account that DSO has regulated tariff and relatively low possibilities for having profit (actually DSOs should't have profit), in some cases DSO could have problems with penalty payments. In case if tariff is approved on the basis of "right" investment program, situation of not fulfilment reliability level target values is barely possible. In proposed regulation scheme DSOs can have bonuses for fulfilling reliability targets as tariff increase by few percent.

As it was stated previously, defining correct value of customer costs of reliability is at the basis of definition of PBR. In further sections paper presents results of customer cost evaluation study in Latvia.

3. STUDY ON THE CUSTOMER COSTS OF RELIABILITY IN LATVIA

The aim of the study was to find out customer costs that are caused by power supply interruptions. Incidents with power supply reliability in Latvia during the recent years (2010 to 2012) caused power supply interruptions for big amount of customers and formed the basis for inclusion of customer cost of reliability and compensation mechanisms topics in Latvian Government Action plan for the year 2012. Implementation of the study was planned because the last known similar study in Latvia until year 2012 have been performed in 1976. Such studies, despite their relative popularity in Europe, are quite rare not only for Latvia, but also for the whole region of Baltic States. Author of the paper know only one more study on customer costs of reliability in Baltic States – it has been performed by scientists of Tallinn University of Technology about decade ago [8].

3.1. Description of the study and survey design

The study was performed in Latvia with informational support of major Latvian DSO – JSC “Sadales tīkls” during summer/autumn period of year 2012 (major study) and beginning of year 2013 (additional study). Results of major study have already been published in Latvian Journal of Physics and Technical Sciences [9], but in this paper results have been supplemented with additional results of study from year 2013.

Survey based methods – Direct worth method and Contingent valuation method (WTP and WTA method) – have been chosen for the study as they are the most common methods of estimating costs in commercial and industry sectors (the total share of usability of these methods is respectively 62% and 60%) [10, 11]. One more reason for usage of these methods is their relatively high accuracy, because users themselves are more aware of the costs of power supply interruptions.

The survey was conducted using postal (e-mail) method with telephone and web assistance and covered about (a little bit more than) 3000 respondents that have the biggest annual energy consumption and representing Industry, Commercial services, Public services, Agriculture and Logistics sectors. Survey has been performed by sending 2 mails to respondents during year 2012. The first e-mail contained questionnaire and information for successful filling of questionnaire, but the second e-mail has been used as reminder. Usage of reminder e-mail allowed raising response rate significantly. During year 2013 there were send e-mails to those respondents, which have not provided any answer during 2012 year survey.

Questionnaires for the study have been created on the basis of recommendations of Council of European Energy Regulators (CEER), study made by SINTEF, as well as using survey experience of Helsinki University of Technology and Tampere University of Technology and taking into account some local factors [10–12]. Questionnaire used in the study have been created for Latvian conditions and consist of 20 questions, 12 of which to be filled in test form, where respondents have to choose one of proposed answers, but the rest questions require personal input by providing particular indices of organization. Such design makes trade-off between response rate and information details. Created questionnaire is presented in the following paper [13].

The first questions are aimed to specify location of electricity (region of the country, as well as city/suburban/rural territory). Respondents have also been asked specify their field of activity according to NACE classification (Statistical Classification of Economic Activities in the European Community). Further questions ask for information about power supply connection parameters and annual energy consumption. Questionnaire also included a couple of questions related to power supply reservation possibilities and level of power supply reliability. The last questions addressed to costs of power supply interruption at one scenario – when interruption occur at 10 a.m. on working day in autumn, as well as the changes of costs in case if interruption occurs at another time, day and year season.

3.2. Data processing

Received data were processed according to NACE classification of respondents. For usability improvement of processed data, it has been normalized with following normalization factors:

- Annual electrical energy consumption (for long interruptions > 3 min) [kWh];
- Maximum allowed load (for short interruptions < 3 min) [kW];
- Interrupted load at reference time (for short interruptions < 3 min) [kW];

- Energy not supplied (ENS), i.e. the estimated energy that would have been supplied if the interruption did not occur (for long interruptions > 3 min) [kWh].

Data for normalization factors have been obtained from questions included in questionnaires (annual energy consumption and maximum allowed load), as well as using real load diagrams of end users and typical load diagrams (hourly average load functions) from data base of Latvian DSO – JSC “Sadales tīkls” [14].

On the basis of processed and normalized data, Customer Damage Functions (CDFs) for different customer sectors have been composed.

Normalized costs of a respondent for given scenario have been calculated using (1) [10, 15]:

$$c_{N,i}(r,t) = \frac{C_i(r,t)}{N_i(r,t)}. \quad (1)$$

Where

$c_{N,i}(r,t)$ – Normalized costs for respondent i for an interruption with duration r occurring at time t [monetary unit/kWh or kW];

$C_i(r,t)$ – Monetary value of respondent i (from the survey) for an interruption of duration r occurring at time t [monetary unit];

$N_i(r,t)$ – Normalization factor for respondent i for an interruption of duration r occurring at time t in [kWh] or [kW] (depending on interruption duration r).

For calculation of Sector's CDF (also known as SCDF), normalized costs for certain respondents from one sector for given scenario are used. Equation (2) has been used for calculation of SCDF [10, 15].

$$c_{SCDF,s}(r,t) = \frac{1}{m} \sum_{i=1}^m c_{N,i}(r,t). \quad (2)$$

Where

$c_{SCDF,s}(r,t)$ – costs for sector s customers for an interruption with duration r occurring at time t [monetary unit/kWh or kW]; m – Number of respondents in sector s .

3.3. Results of the study

During the major study in year 2012 author received 240 questionnaires that means – response rate was 8%. But it should be mentioned that only 111 questionnaires had enough data about customer costs of reliability and it means that final response rate was 3.7%. During the additional study in year 2013, additional questionnaires have been gathered, resulting in total 143 usable questionnaires and total response rate 4.8%.

Absence of obligation to fill in the questionnaire explains relatively low response rate. Author concludes, that to raise customers' interest to participate in such studies there should be defined well grounded reasons for this. For example, customers should have awareness that the data obtained from the study will be used to define compensations for power supply interruptions.

When performing the study, there should be information on concrete objects of customers and their consumption. Otherwise there could be some problems with identifying appropriate load diagram and therefore energy not supply (ENS) during power supply interruption. The fact is important, because respondents (enterprises) can have several objects that are consuming energy. Typical example is chain of shops or municipal organisations. To

overcome barrier of insufficient information there should be strong cooperation between research organizations and DSO with the aim to make precise selection of respondents, dividing them in corresponding sectors.

Data from the questionnaires after their processing and usage of equations (1) and (2) form sector customer damage functions that are given at Fig. 3, 4 and 5.

Fig. 3 represents customer costs due to short power supply interruption. These costs occur due to interruptions with duration shorter than 3 minutes and are usually normalized with interrupted power [16].

Fig. 4 represents SCDF for long unplanned power supply interruptions – starting with interruptions with duration of 20 minutes and ending with interruptions that have duration of 24 hours. Costs represented at the figure have been normalized with energy not supplied (energy that could be supplied) during interruption.

Fig. 5 represents SCDF for long planned power supply interruptions and, similarly to results represented at Fig. 4, they have been normalized with energy not supplied during interruption.

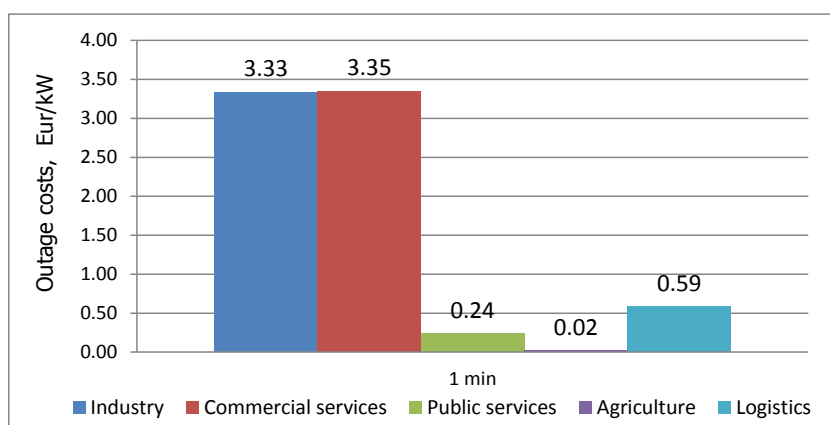


Fig. 3. Momentary outage costs normalized with load interrupted at reference time

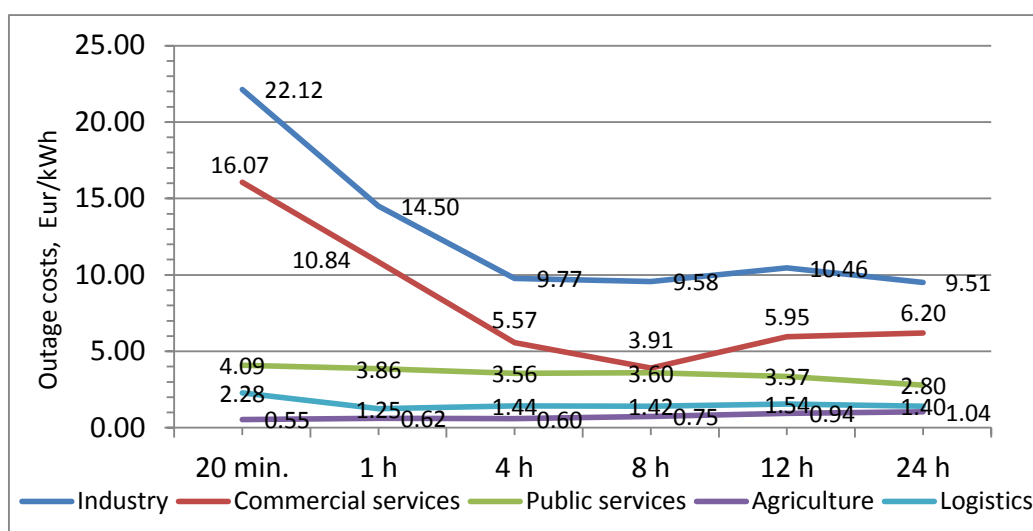


Fig. 4. Outage costs, normalized by ENS, caused by unplanned power supply interruptions

As can be seen from the figures, Industry sector representatives have the highest outage costs, followed by representatives of Commercial and Public services sectors. Expectations on the costs of Agriculture and Logistics sectors approved – these sectors showed the lowest level of costs irrespective of interruption duration. But it should be mentioned, that

representatives of the last two sectors have been extremely inactive in the survey and costs presented here may not represent real situation of outage costs in these sectors. Relatively interesting seems situation with Public services sector that showed high level of outage costs. Such situation could be partly explained with possible costs overestimation.

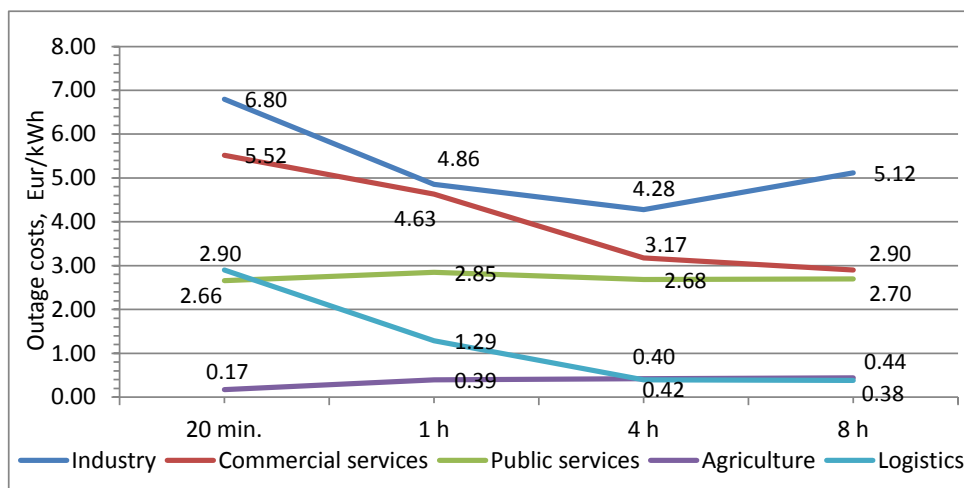


Fig. 5. Outage costs, normalized by ENS, caused by planned power supply interruptions

Comparison of results showed at Figs. 4 and 5 show importance of timely informing customers on interruptions – costs due to interruptions reduce by average 60% in Industry sector, 48% in Commercial services sector and 28% in Public services sector.

As information on changes of customer costs due to time of occurrence of interruption is also important for PBR, appropriate questions have been also included in questionnaire. Information on variations of customer costs depending on time of outage occurrence are given at Fig. 6–8 and represent changes of costs in percent comparing to the basic scenario – unplanned interruption at 10 a.m. of autumn working day.

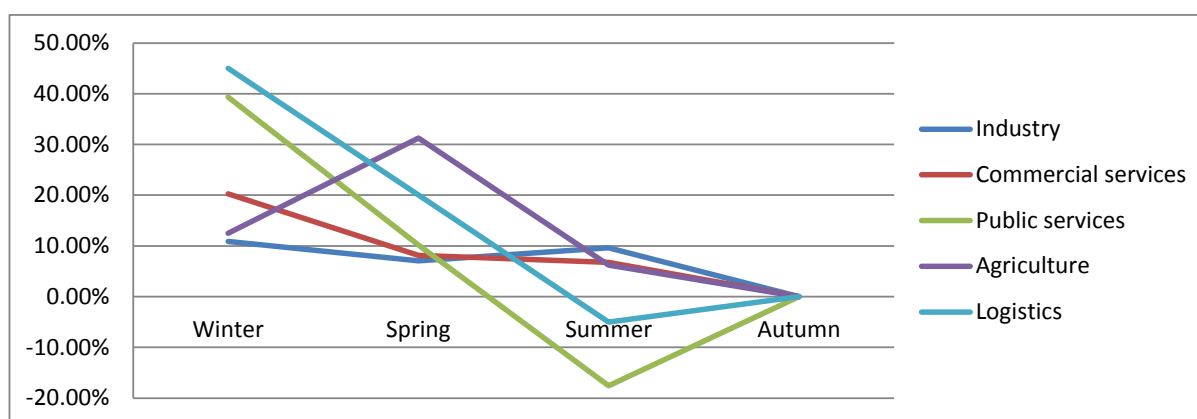


Fig. 6. Variation of outage costs due to season

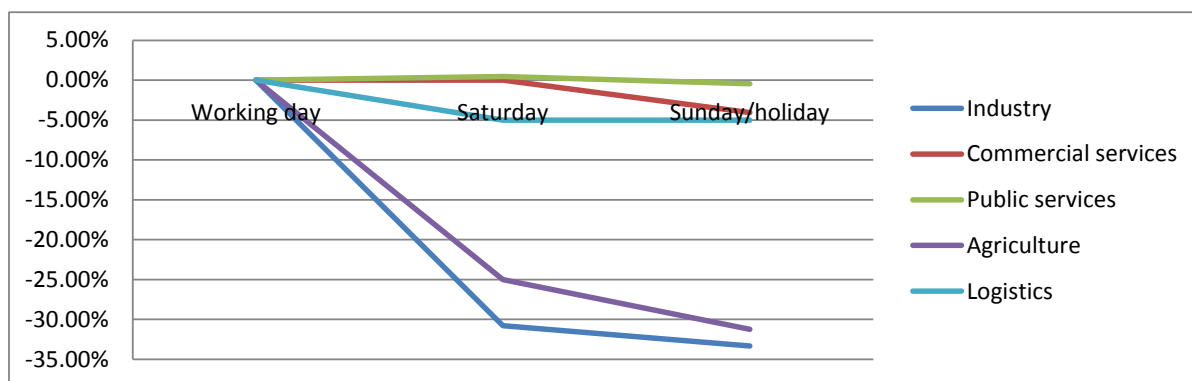


Fig. 7. Variation of outage costs due to day of week

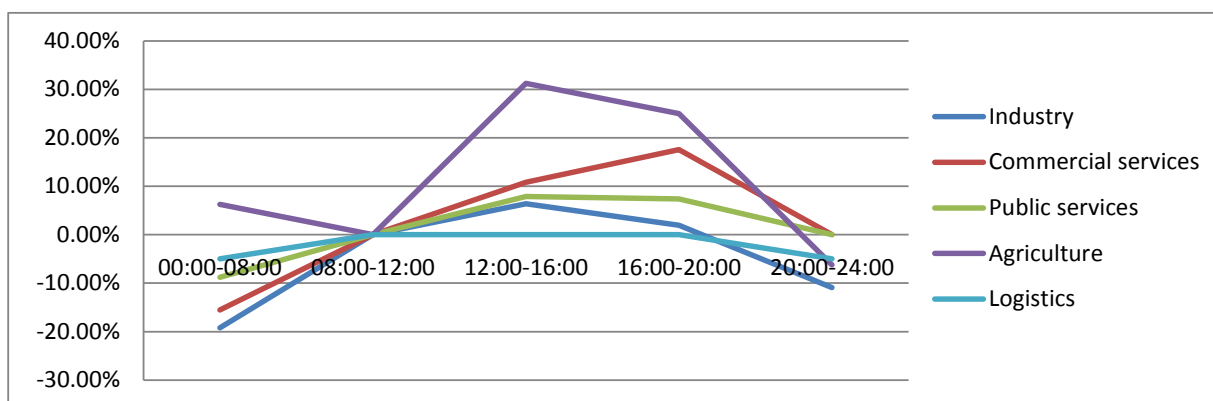


Fig. 8. Changes due to day hour

4. CONCLUSIONS

On the basis of analysis of modern performance-based regulation techniques and practices of European countries, it is concluded that there is no common vision of regulation in Europe regarding achieving optimal level of power supply reliability.

Power supply reliability level performance-based regulation has been proposed in the paper. Proposed methodology is strongly based on customer costs of reliability and aims to achieving optimal level of power supply reliability. The proposed methodology could be used as a base for performance-based regulation introduction in the countries where PBR is not introduced yet, as well as it can be used as a model for making changes in existing PBR practices.

The paper also presents the outcome of the study on customer costs of reliability that can be used for introduction of PBR in Latvia.

Taking into account that the data have been normalized by widely used normalization factors, they can have high usability not only for PBR, but also for development of load shedding schemes.

Taking into account that such type studies are rare in the Baltics, the results and experience of the study can also be used as reference point for neighboring countries with similar structure of consumption.

The experience gained during the study is extremely valuable for performing further customer cost estimation studies to actualize data and introduce corresponding corrections in PBR.

REFERENCES

1. BROWN, R.E. *Electric power distribution reliability*. New York, Basel: Marcel Dekker, Inc. 2002, 365 p.
2. CHOWDHURY, A.A., KOVAL, D.O. *Power distribution system reliability. Practical methods and applications*. New Jersey: John Wiley & Sons, Inc. 2009. 531 p.
3. „5th Benchmarking Report on Quality of Electricity Supply 2011”. Brussels: Council of European Energy Regulators. 2011, 260 p. [referred on the 10 of May in 2012 y.]. Link to the internet:
http://www.ceer.eu/portal/page/portal/EER_HOME/EER_PUBLICATIONS/NEWSLETTERS/Tab/April%202012
4. “Economic regulation of electricity grids in Nordic countries”. Copenhagen: NordREG Nordic Energy Regulators. 2011, 116 p.
5. WALLNERSTRÖM, C.J., BERTLING, L. *Laws and regulations of Swedish power distribution system*. 1996-2012. CIRED Workshop. Lyon. 2010. 4 p.
6. RIVIER J. *Critical analysis of Spanish power quality regulation design*. Proceedings of Market Design Conference. Stockholm. 2003, p. 29–38.
7. KAROTAMM, M. *Quality Regulation Through Pricing (Estonia)*. Presentation from Joint ERRA Licensing/Competition & ERRA Tariff/Pricing Committees’ Meeting. Bratislava. 2009.
8. RAESAAR, P., TIIGIMAGI, E., VALTIN, J. Assessment of electricity supply interruption costs in Estonian Power System. *Estonian Academy Publishers, Oil Shale*, 2005, Vol. 22. No. 2, p. 217–231.
9. ĻVOVS, A.; MUTULE, A. Estimation Of Power Supply Interruption Costs For Latvian Customers, *Latvian Journal of Physics and Technical Sciences*, 2013, Vol. 50, Nr. 3, p. 24–34.
10. HOFMANN, M.; SELJESETH, H.; VOLDEN, G.H.; KJØLLE, G.H. *Study on Estimation of Costs due to Electricity Interruptions and Voltage Disturbances*. SINTEF Energi AS, SINTEF Energy Research, 2010, 146 p.
11. *Guidelines of Good Practice on Estimation of Costs due to Electricity Interruptions and Voltage Disturbances*. Council of European Energy Regulators. 2010, 72 p. [Referred on the 01 of February in 2012 y.]. Link to the internet:
http://www.ceer.eu/portal/page/portal/EER_HOME/EER_PUBLICATIONS/CEER_PAPERS/Electricity/2010
12. SILVAST, A., HEINE, P., LEHTONEN, M., KIVIKKO, K., MÄKINEN, A., JÄRVENTAUSTA, P. *Sähkönjakelun keskeytyksestä aiheutuva haitta*. Helsinki University of Technology and Tampere University of Technology. 2005, 175 p.
13. ĻVOVS, A., MUTULE, A. *Estimation of power supply interruption related costs. Methodology, survey questionnaire and received data normalization*. CYSENI 2012. Proceedings of annual conference of young scientists on energy issues. [CD]. Kaunas: Lithuanian Energy Institute. 2012 May 24–25.
14. *Typical load diagrams*. Web page of Latvian DSO “Sadales tikls”. [referred on the 20 of February in 2012 y.]. Link to the internet:
http://www.st.latvenergo.lv/portal/page/portal/Latvian/Sad_tikls/Tipveida+grafiki_jauns.htm
15. SAMDAL, K., KJØLLE, G.H., SINGH, B., KVITASTEIN, O. *Interruption Costs and Consumer Valuation of Reliability of Service in a Liberalised Power Market*. Proceedings

- of the 9th International Conference on Probabilistic Methods Applied to Power System. 2006, p. 1–7.
16. KJØLLE, G., SAMDAL, K., SINGH, B., TRENGEREID, F. *Customers' interruption costs - what's the problem?* 17th International Conference on Electricity Distribution. Barcelona. 2003, 12-15 May, p. 1-4.
 17. AMING, D., RAJAPAKSE, A., MOLINSKI, T., INNES, E. *A Technique for Evaluating the Reliability Improvement due to Energy Storage Systems*. Canadian Conference on Electrical and Computer Engineering, 2007. CCECE 2007. Vancouver, BC. 2007, 22–26 April, p. 413–416.
 18. LÅGLAND, H., KAUHANIEMI, K. *Outage cost comparison of different medium voltage networks*. 19 th International Conference on Electricity Distribution, CIRED2007. Vienna. 2007, 21–24 May, p. 1–4.
 19. NOCE, C. *Optimal placement of automation devices in ENEL distribution network*. 20th International Conference on Electricity Distribution, CIRED2009. Prague. 2009, 8–11 June, p. 1–4.
 20. KAZEMI, S. *Reliability Evaluation of Smart Distribution Grids*. Doctoral dissertation. Aalto University publication series. Helsinki. 2011, p. 1–150.

TRANSMISSION EXPANSION PLANNING CONSIDERING ELECTRICITY MARKET AND INTEGRATION OF RENEWABLE GENERATION

A. Obushevs, I. Oleinikova

Institute of Physical Energetics

Laboratory of Power System Mathematical Modelling

Aizkraukles 21, Riga, LV-1006 – Latvia

ABSTRACT

To foster climate targets and estimate the technical and economic impact of renewable energy sources accommodation to transmission networks, several theories based on the social impact of the investments in competitive markets and marginal pricing are created by different authors [1]. Electricity market and Smart Grid Technology's integration in energy sector brings completely new problem setup in many countries and many recent studies are addressing this problem from different perspectives. The great majorities of studies describe only one-time static problems investment models and do not consider additional factors that can affect the network expansion in future years [1–3]. A new network operation conditions creates new requirements for transmission planning which include electricity market figures and considerable integration of renewable generation.

The main point of this paper is to demonstrate the new deterministic concept for transmission planning based on technical regulation and market – economic regulation principals. Traditional approach is taken as starting point in presented research. In the next stage, the expansion/development plan is checked for other operational constraints. For this purpose AC or DC models can be implemented, both of them have pros and cons regarding load flows power losses and stability analysis etc. However, power system operation in market condition introduce new terms such as: capacity allocation and congestion management, which will significantly affect previous modeling techniques. A coordinated approach for capacity calculation including optimal power flow implementation will show the best use of the electricity transmission lines as well as it will open additional opportunities for development planning with social welfare and market power estimation.

For the proposed concept validation the Garvers's 6-bus transmission grid was used. The simulation and validation results show the possibility of the AC/DC models implementation to transmission planning tasks solution.

Keywords: electricity market, optimal power flow, power system development, renewable generation

1. INTRODUCTION

Liberalised electricity market effects the power system development. It is determined by the condition that electricity generators are independent from transmission and distribution operators and their interests differ. This fact creates higher uncertainty conditions for the perspective forecasts than before and power system development planning and optimisation is hampered. In this connection in development tasks necessary to consider price formation mechanisms, for a more detailed definition of benefits and costs with the introduction of new or liquidation of old power system elements.

This paper provides the base for the transmission planning methodology according to the needs for new methods and tools for planning of the future power system with considerable integration of renewable generation, that takes into account liberalised electricity market. In order to achieve these targets sustainable development planning concept with OPF techniques was proposed and AC and DC OPF algorithms with planning approach was created. Determination of optimal expansion planning plan/strategy will ensure adequacy of the grid, generation and demand in the future.

2. LONG-TERM DEVELOPMENT PLANNING

Development planning is a process to determine an optimal strategy to expand the existing power system transmission network to meet the demand of the possible load growth and the proposed generators, while maintaining reliability and security performance of the power system. The general objective of the power system transmission network development planning task is to determine ‘where’, ‘how many’ and ‘when’ new element/devices must be added to a network in order to make its operation viable for a pre-defined horizon of development planning, with a costs minimization and social welfare maximization for optimal expansion/development plan determination.

Main concepts of development planning based on: Development Action (D-action); Development Step (D-step); Development Plan (D-plan) [4]. The essences of the parameters are explained on Fig. 1.

$$\overbrace{e(t-1)}^{\text{Existing state}} + \overbrace{(\dots \dots \dots)}^{\text{Realized D-action}(s)} = \overbrace{e(t)}^{\text{New state}}$$

Fig. 1. Development state formation

Development plan formation is complicated process that requires extensive studies to determine many new network elements. Creation of the optimal development plan will ensure adequacy of the grid, generation and demand in the future.

Electricity market effects not only power system operation as whole but also its development practices. It is determined by default that electricity generators are independent from transmission and distribution operators and their interests differ. This fact creates higher uncertainty conditions and time resolutions accuracy for the perspective forecasts than before and power system development planning and optimization is hampered. For sustainable development solutions of the network, estimation period must be assumed longer than economic life cycle period – advisable up to 30 years (see Fig. 2). The selection of optimal development plans under uncertainty require: information package set, representing information credibility range – prognosis, credibility estimation criteria and comparable development plans.

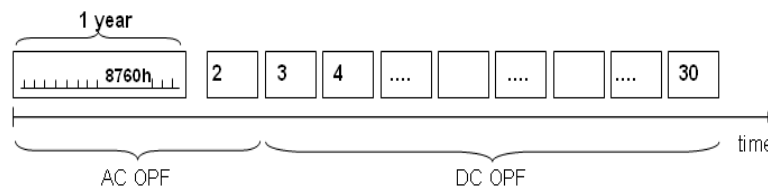


Fig. 2. Time frames within sustainable development

If the compromise between network estimation problems and development aggregated results has not been reached, the quality of the planning results will be impaired. The solution to compile both models AC and DC:

For short-term analysis, to include intermitted generation and market conditions, of several years and subject to initial information availability can be used the full AC model.

Considering the complexity and dimension of development and optimization tasks, as well as information uncertainty conditions, appropriate method for the steepest calculating of OPF to define criteria is simplified by DC method.

In real tasks the number of comparable development plans attains astronomic quantity; therefore it is required to apply specialized dynamic optimization methods. Objective function for network development plan displays and integrates technical, economic, power supply

reliability, ecological etc. parameters. The objective function in (1) represents the social welfare, where the welfare is expressed as the aggregate demand utility bid function minus the aggregate generator offer function, minus the investment cost in new lines. Objective function is a network development plan g quality criterion, denoted as $F(T, g)$ is calculated by a formula:

$$\max F(T, g) = \max_{g \in \{G\}} \sum_{t=1}^T (SW(t, e(t)) - IC(t, e(t))), \quad (1)$$

where: t – development step serial number; T – number of development steps in estimation period; $SW(t, e(t))$ – social welfare criterion in development step t and development state $e(t)$; $IC(t, e(t))$ – investment costs in development step t and development state $e(t)$; g – development process; $\{G\}$ – set of all possible development plans.

Given that the assumed conditions are observed, $SW(t, e(t))$ is not dependent on development plan up to development state $e(t)$. Thus, the objective function (1) allows application of dynamic programming.

To consider the impact of liberalized electricity market to technical and economic criteria each development state should be observed at hourly base. Application of hourly calculation based on OPF allows taking into account the major trends of production and consumption during the day, taking into account consumption time shifting when considering multiple time zones, demand response, distributed generation, etc.

3. DEVELOPMENT MODEL

Development modeling should include network dynamic behaviors and represent the network real processes as much as possible. Based on main functioning factors proposed in chapter II the following development model was created (Fig. 3).

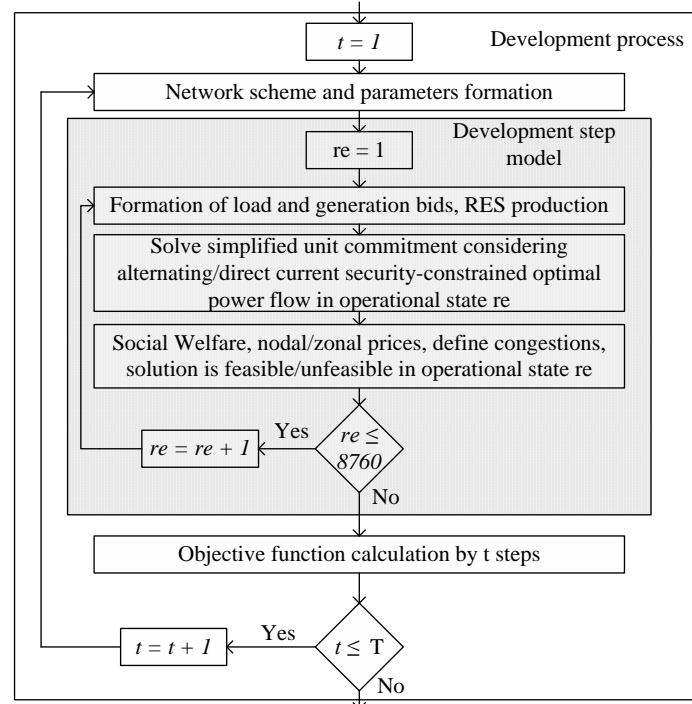


Fig. 3. Development process

4. THE AC/DC SCOPF FORMULATIONS

The optimal power flow is a very large and difficult mathematical programming problem. The main aim of the OPF is to determine the optimal steady-state operation of a power system, which simultaneously minimizes or maximizes the value of a chosen objective function and satisfies certain physical and operating constraints. To provide complex solutions for the network operation problem analysis and its consideration in development the following mathematical formulations can be implemented.

4.1. Formulation of OPF

OPF is a technique that has been used in the electricity industry for several decades. The objective function of an OPF problem may take many different forms according to the different applications. The general objective in OPF is to maximize social welfare which comprises producers' and consumers' surpluses or minimize costs of production. The costs and benefits may be defined as polynomials or as piecewise-linear functions [6]. The problem can be formulated schematically as:

$$\max_x SW(x) \quad (3)$$

subject to

$$g(x) = 0 \quad (4)$$

$$h(x) \leq 0 \quad (5)$$

$$x_{\min} \leq x \leq x_{\max}, \quad (6)$$

where $f(x)$ objective function of social welfare; $g(x)$ equality constraints of active and reactive power balance; $h(x)$ inequality constraints of power flow limit of line, bus voltage limits; x_{\min}, x_{\max} active and reactive power generation limits. One of the nodes is assigned a zero phase angle by setting its phase angle upper and lower limits to zero (slack bus).

4.2. Alternating Current and Direct current OPF

The AC version of the standard OPF problem is a general non-linear constrained optimization problem, with both nonlinear costs and constraints. In a system with nb buses, ng generators, nl branches and nc consumers, the optimization variable x is defined as follows:

$$x = [\Theta; V; P_G; Q_G; P_L; Q_L]. \quad (7)$$

The objective function (3) is a consumers' utility minus producers' cost (represented by function $B_L^i(P_L^i)$ and $C_G^j(P_G^j)$, respectively) shall be maximised subject to equality and inequality constraints:

$$SW(P_G, P_L) = \left\{ \sum_{i=1}^{nc} B_p^i(P_L^i) - \sum_{j=1}^{ng} C_G^j(P_G^j) \right\} \rightarrow \max_{\Theta, V, P_G, Q_G, P_L, Q_L} \quad (8)$$

The equality constraints (4) consist of two sets of nb nonlinear nodal power balance equations, one for real power and one for reactive power.

$$g_P(\Theta, V, P_G, Q_G, P_L, Q_L) = 0 \quad (9)$$

$$g_Q(\Theta, V, P_G, Q_G, P_L, Q_L) = 0 \quad (10)$$

The inequality constraints (5) consist of two sets of nl branch flow limits as non-linear functions of the bus voltage angles and magnitudes, one for the from end and one for the to end of each branch.

$$h_f(\Theta, V, P_G, Q_G, P_L, Q_L) \leq 0, \quad (11)$$

$$h_t(\Theta, V, P_G, Q_G, P_L, Q_L) \leq 0. \quad (12)$$

The variable limits (6) include an equality limited reference bus angle and upper and lower limits on all bus voltage magnitudes, real and reactive generator and consumption injections.

$$\theta_{ref} \leq \theta_i \leq \theta_{ref}, \quad l = l_{ref}, \quad (13)$$

$$v_i^{\min} \leq v_i \leq v_i^{\max}, \quad l = 1 \dots n_b, \quad (14)$$

$$P_{G,\min}^j \leq P_G^j \leq P_{G,\max}^j, \quad j = 1 \dots n_g, \quad (15)$$

$$Q_{G,\min}^j \leq Q_G^j \leq Q_{G,\max}^j, \quad j = 1 \dots n_g, \quad (16)$$

$$0 \leq P_L^i \leq P_{L,\max}^i, \quad i = 1 \dots n_c, \quad (17)$$

$$0 \leq Q_L^i \leq Q_{L,\max}^i, \quad i = 1 \dots n_c. \quad (18)$$

Here l_{ref} denotes the index of the slack bus and θ_{ref} is the slack angle.

When using DC network modelling assumptions, the standard OPF problem above simplified to a quadratic program, with linear constraints. In this case the DC power flow greatly simplifies the power flow by making a number of approximations including 1) completely ignoring the reactive power balance Equations, 2) assuming all voltage magnitudes are identically one per unit, 3) ignoring line losses and 4) ignoring tap dependence in the transformer reactance [7]. The optimization variable is:

$$x = [\Theta; P_G; P_L] \quad (19)$$

and the overall problem reduces to the following form:

$$SW(P_G, P_L) = \left\{ \sum_{i=1}^{n_l} B_p^i(P_L^i) - \sum_{j=1}^{n_g} C_p^j(P_G^j) \right\} \rightarrow \max_{\Theta, P_G, P_L} \quad (20)$$

subject to (9) – (18) without V, Q_G, Q_L variables.

OPF development has been carried out following the progress in numerical optimization techniques and computer technology. Many different approaches have been proposed to solve the OPF problem. These techniques include nonlinear programming, quadratic programming, linear programming, mixed programming, as well as interior point and artificial intelligence algorithms. The most successful interior point methods are based on using a primal–dual formulation and applying Newton’s method to the system of equations arising from the barrier method. This method has been widely used in power system optimization problems because of its favorable convergence, robustness, and insensitivity to infeasible starting points. The primal-dual interior point method (PDIPM) has become the algorithms of choice for long-term development planning strategies [8, 9].

4.3. Security-Constrained OPF

SCOPF problem is an extension of the OPF problem and contains important features of reliability in the optimization model. It guarantees stable work of the whole power system, without changing active power generation, when some predetermined contingencies occur (such as outages of transmission line).

Fig. 4 provides the flowchart of the iterative SCOPF algorithm, which starts by solving an OPF with (N-0) constraints. When it has solved the contingency analysis starts to identify the critical group of lines and selected according to these criteria:

$$K_{L, re}^* = \chi_L \cdot Ps_{L, re}, \quad (21)$$

where L transmission line ordinal number; $Ps_{L, re}$ transmission line flow in operational state; χ_L interruption probability of transmission line L ;

In development planning tasks for optimal steady-state operation determination only 10% of electric transmission lines should be taken into consideration in which transmission line flow, transmission line interruption probability and therefore criteria K^* are the highest values. This criterion is necessary in order to select critical group of lines and thus reducing size of optimization problem and calculation time.

4.4. Simplified Unit commitment

The UC problem in traditional form involves determining the start-up and shut down schedules of thermal units to be used to meet forecasted demand over a future short term period [9]. Due to the fact that UC problem is a complex mathematical optimization problem and significantly increases development planning tasks complexity was made some assumptions to simplify problem: not assume start-up and shut-down cost, system reserve requirements, ramp rates (each hourly base steady-state operation is independent from other hours).

Fig. 5 provides the flowchart of the iterative simplified UC-SCOPF algorithm, which starts by solving an SCOPF without units' low MW limits. When it has solved, compilation of power plants group starts with generation less than ε (in calculation ε assumed 10%) to identify the group of power plants which should be switched off.

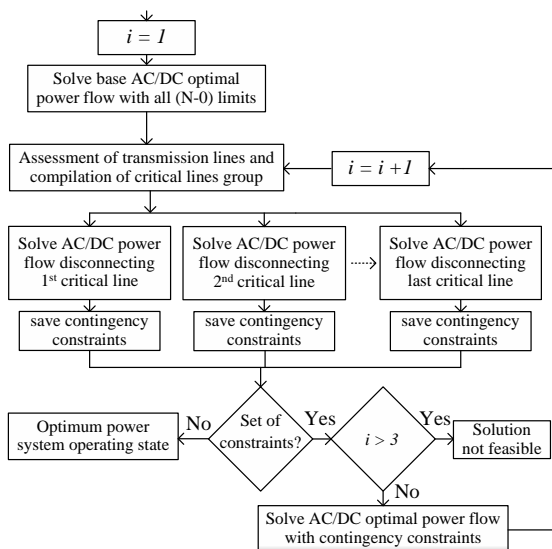


Fig. 4. Security-constrained OPF

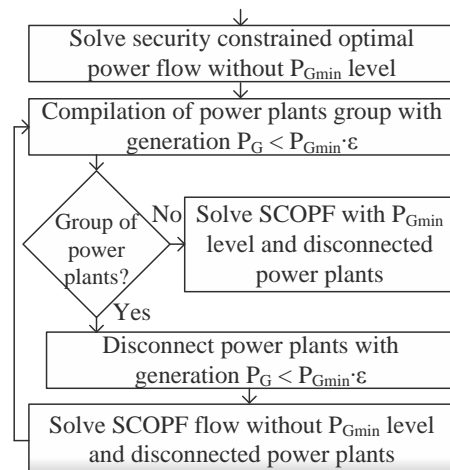


Fig. 5. Simplified Unit Commitment

Obtained steady-state operation, social welfare and nodal prices reflects the network real processes and taken for development modeling.

5. CASE STUDIES

In this section, modified Garver's 6-bus (Fig. 6) transmission grid systems are studied and the simulation results are demonstrated. Calculations were made in the MATLAB software.

5.1. Modified Garver's 6-Bus System

Basis for calculations of the modified scheme is taken from source [10]. Modified Garver's 6-bus system has 14 existing lines, 5 loads and 4 generators. The system parameters are listed in Tables I, II and III.

Table I. Generator and Load Data for Garver's 6-Bus System

Bus No.		Load parameters		Generator parameters			
		P_D MW	Q_D MVA	P_G^{MAX} MW	P_G^{MIN} MW	Q_G^{MAX} MVA	Q_G^{MIN} MVA
1	P0	80	16	160	0	65	-10
2	PQ	240	48	100	0	0	0
3	PV	40	8	370	0	150	-10
4	PQ	160	32	-	-	-	-
5	PQ	240	48	-	-	-	-
6	PV	-	-	610	0	200	-10

Table II. Line Data for Garver's 6-Bus System

Branch	r_{ij} , p.u	x_{ij} , p.u	b_{ij} , p.u	Capacity	
				MW	MVA
1 – 2	0.04	0.4	0.04	100	120
1 – 4	0.06	0.6	0.06	80	100
1 – 5	0.02	0.2	0.02	100	120
2 – 3 x 2	0.02	0.2	0.02	100	120
2 – 4	0.04	0.4	0.04	100	120
2 – 6 x 2	0.03	0.3	0.03	100	120
3 – 5 x 3	0.02	0.2	0.02	100	120
4 – 6 x 3	0.03	0.3	0.03	100	120

Table III. Generator costs and demand benefits

Node	Generators			Demands	
	Fuel source	a_j (EUR/MW ² h)	b_j (EUR/MWh)	c_i (EUR/MW ² h)	d_i (EUR/MWh)
1	Gas	0.0298	83.9	0	200
2	Wind	0	0	0	200
3	Coal	0.0081	58	0	200
4	-	-	-	0	200
5	-	-	-	0	200
6	Coal	0.0035	69.71	-	-

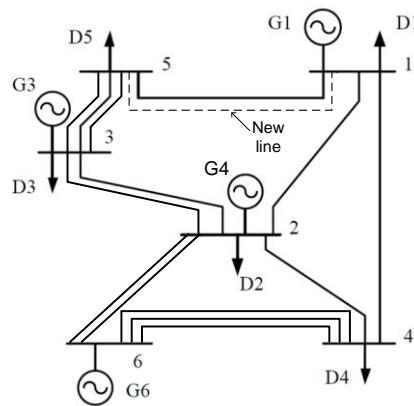


Fig. 6. Modified Garver's 6-bus system with 100MW wind PP

For the present structure of the network are considered following four case strategies of development:

- without wind PP and investments;
- without wind PP and with investments for construction of a new line 1–5;
- with wind PP and investments;
- with wind PP and investments for construction of a new line 1–5.

For development modeling calculation we make the following assumptions:

1. We consider a time horizon of ten years. For this time scale we estimate the demand, the generation offers and the demand bids. Therefore, our model represents a “Dynamic Transmission Expansion Planning” problem, for which the net social welfare is maximized.

2. Each development step is calculated in accordance with the present algorithm in Fig. 3 (AC and DC models of the network are used).

3. Generator costs changed for all the periods of study, such that gas price grow each year by 1% and coal price by 2%. We considering perfect competition strategy, generators offer at their marginal costs.

4. Each load defined by individual demand pattern and grow up each year by 0.5% (Fig. 7).

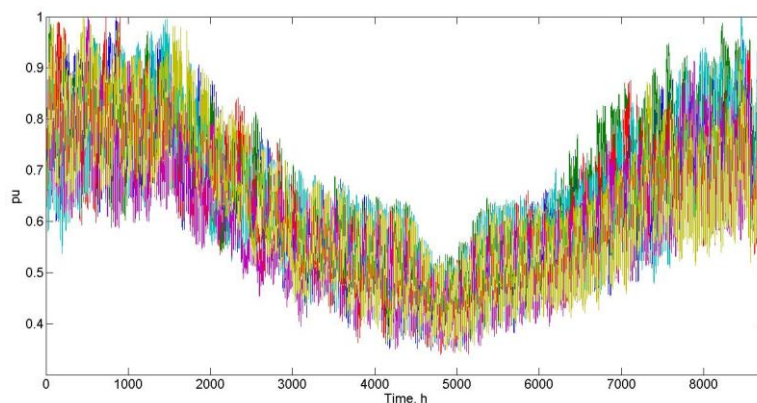


Fig. 7. Demand pattern for first development step

5. Fig. 8 represent annual wind production curve for 100 MW power plant obtained from wind production curve simulation algorithm provided in [5]. Production curve is fixed for each development step and not participate in automatic generation control.

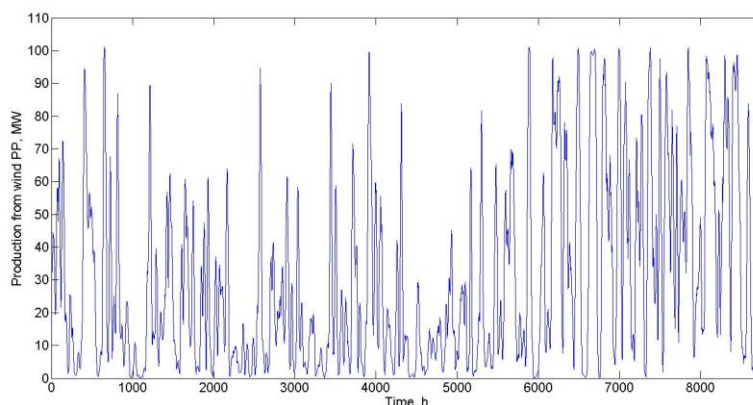


Fig. 8. Annual wind production curve for 100MW power plant

5.1.1. Analysis of results

Fig. 9 provides one year results of social welfare for first and last development steps without investing. Table IV and V represent changes of annual SW values of OPF and SCOPF problems for different development strategies. Integration of wind production significantly increase annual SW values and reduce need of most expensive conventional plants which can lead to lower average prices for electricity, however expansion of power production capacities with low marginal costs of production have negative impact to the conventional generators, mostly reducing ability sufficiently cover total production costs. Effects of renewable generation integration into generating portfolio could be evaluated as positive, regarding to improved generation and transmission adequacy as well as system reliability.

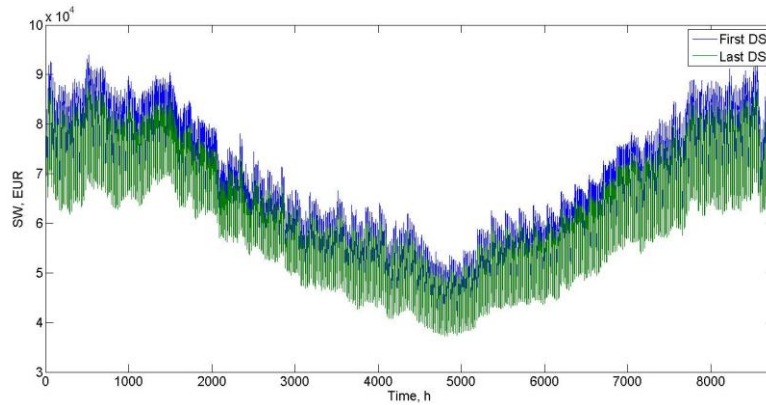


Fig. 9. First and last development step SW patterns

Table IV. SW values for the case study without wind PP

Step	Without investment		With investment	
	SW OPF, MEUR	SW SCOPF, MEUR	SW OPF, MEUR	SW SCOPF, MEUR
1	578.664	574.939	578.664	575.525
2	576.030	572.247	576.030	572.847
3	573.241	569.405	573.241	570.021
4	570.292	566.408	570.293	567.042
5	567.180	563.252	567.180	563.905
6	563.899	559.932	563.899	560.605
7	560.445	556.444	560.445	557.137
8	556.812	552.782	556.812	553.496
9	552.996	548.943	552.996	549.678
10	548.992	544.922	548.992	545.678
Total	5648.551	5609.274	5648.553	5615.934

Table V. SW values for the case study with wind PP

Step	Without investment		With investment	
	SW OPF, MEUR	SW SCOPF, MEUR	SW OPF, MEUR	SW SCOPF, MEUR
1	649.103	644.525	649.175	645.317
2	646.845	642.193	646.919	643.000
3	644.440	639.715	644.514	640.538
4	641.884	637.087	641.958	637.927
5	639.171	634.303	639.247	635.162
6	636.299	631.360	636.375	632.238
7	633.261	628.252	633.338	629.151
8	630.054	624.977	630.131	625.896
9	626.672	621.528	626.750	622.469
10	623.110	617.902	623.189	618.865
Total	6370.839	6321.842	6371.596	6330.563

The presented results clearly show the behavior and changes in the power system which subsequently must be considered with decision making theory for the future sustainable development of transmission networks.

6. CONCLUSIONS

This paper provides the base for the transmission planning methodology according to the needs for new methods and tools for planning of the future power system with considerable integration of renewable generation. In order to achieve these targets sustainable development planning concept with OPF techniques was proposed and AC and DC OPF algorithms with planning approach was created. Determination of optimal expansion planning plan/strategy will ensure adequacy of the grid, generation and demand in the future.

As well as, to fulfill transmission planning targets the forward-looking research should be supplemented with decision making theory and included to the long-term development planning simulation software.

ACKNOWLEDGMENT

This work has been supported by the European Social Fund within the project «Support for the implementation of doctoral studies at Riga Technical University», Nr. 2009/0144/1DP/1.1.2.1.2/09/IPIA/VIAA/005.

REFERENCES

1. TORRE S. DE LA, CONEJO A.J., CONTRERAS J. “Transmission expansion planning in electricity markets,” IEEE Trans. Power Syst., Vol. 23, No. 1, p. 238–248, Feb. 2008.
2. RIDER M.J., GARCIA A.V., ROMERO R. “Power system transmission network expansion planning using AC model,” IET Gener. Transm. Distrib., Vol. 1, No. 5, p. 731–742, Sep. 2007.
3. LATORE G., DARIO CRUZ R., MAURICIO AREIZA J., VILLEGAS A. “Classification of Publication and Models on Transmission Expansion Planning,” IEEE Trans. Power Syst., Vol. 18, No. 2, p. 938–946, May 2003.
4. KRISHANS Z., MUTULE A., MERKURYEV Y., OLENIKOVA I. “Dynamic management of Sustainable Development: Methods for Large Technical Systems”, in Hardcover, 1st ed., London, Springer, 2010.
5. TURCIK M., OLENIKOVA I., OBUSEVS A., KOLCUN M. “Probabilistic Method for Wind Production Forecasting and Energy Markets Trades Optimization in Power System with Large Wind Specific Gravity” Proceedings of the 12th International Conference on Probabilistic Methods Applied to Power Systems, Turkey, Stambula, 10–14. June, 2012. – p. 134–139.
6. ZIMMERMAN R.D., MURILLO-SÁNCHEZ C.E., THOMAS R.J. “MATPOWER: Steady-State Operations, Planning, and Analysis Tools for Power Systems Research and Education” IEEE Trans. Power Syst., Vol. 26, No. 1, p. 12–19, Feb. 2011.
7. THOMAS J. OVERBYE, XU CHENG, YAN SUN, “A Comparison of the AC and DC Power Flow Models for LMP Calculations”. Proceedings of the 37th Hawaii International Conference on System Sciences – 2004.
8. XI-FAN WANG, YONGHUA SONG, MALCOLM IRVING. “Modern Power Systems Analysis”. Springer, 2008, 559 p. ISBN 978-0-387-72852-0.
9. A. J. WOOD AND B.F. WOLLENBERG, “Power Generation, Operation, and Control, 2nd Edition”. New York: Wiley, 1996, 592 p. ISBN 978-81-265-0838-9.
10. ROMERO, R., MONTICELLI, A., GARCIA, A., AND HAFFNER, S. ‘Test systems and mathematical models for transmission network expansion planning’, IEE Proc., Gen. Trans. Distrib., 2002, 149, (1), p. 27–36.

MINIMUM OF EFFECTIVE THERMAL CONDUCTIVITY COEFFICIENT IN FIBROUS MATERIALS AT HIGH TEMPERATURES: THEORETICAL EXPLANATION OF EXPERIMENTAL RESULTS

P.S. Grinchuk, N.I. Stetukevich

A.V. Luikov Heat- and Mass Transfer Institute

P. Brovka Str., 15, 220072 – Belarus

ABSTRACT

A mathematical model for calculating the effective heat conductivity of fibrous materials at high temperatures and variable density has been suggested and substantiated. The main consideration is focused on accounting for heat conduction in the solid phase of a fibrous material. The calculated results were compared with experimental data that demonstrated a good accuracy of the proposed model. The effective heat conductivity of a fibrous heat-insulating material has been calculated as a function of density for a number of temperatures within the range from 200 to 1000°C.

Keywords: fibrous materials, thermal conductivity, contact heat exchange, Hertz problem.

1. INTRODUCTION

Fibrous heat insulation is one of the most technologically effective materials used for thermal insulation of high-temperature power-engineering equipment and for thermal protection of landing space craft. This stipulates the importance of the problem of measuring the parameters and describing the properties of fibrous materials. The present paper is concerned with the description of the effective heat conductivity coefficient of fibrous materials at high temperatures. The work has been motivated by experimental investigations of the effective heat conductivity of high-temperature fibrous materials on change in their density, with the results presented in [1].

2. EXPERIMENTAL RESULTS

Dependence of the effective heat conductivity coefficient on the temperature and density of a material was investigated by the special test equipment (Fig. 1). The method of measurements is based on the use of the Fourier law on condition that a steady thermal state was reached. The main parts of the experimental equipment are: a measuring cell (3), that provides transverse compression of a sample by means of a pressure plate (4) and screws (5), and an SNOL 1,6.2,5.1/11-I2 (1) laboratory heating electric furnace for thermal loading of samples. The temperature of the hot wall of the measuring cell could vary from 50 to 100°C. In the working space the temperature of the furnace was maintained by an automatic control system. The density of samples was determined by measuring their thickness and preliminary weighing.

A fibrous heat-insulating material Cerablanket, manufactured by Thermal Ceramics, with a classified temperature of 1260°C and apparent density of 128 kg/m³ was chosen as the subject of investigation [2]. At the present time this is the most widespread material used for lining heat-treating furnaces. According to the specifications, the material consists of: 50–56% SiO₂, 35–44% Al₂O₃, and slight amounts of CaO, MgO, Na₂O – hundredths of a percent. The mean diameter of the material fiber is 3.5 μm [2].

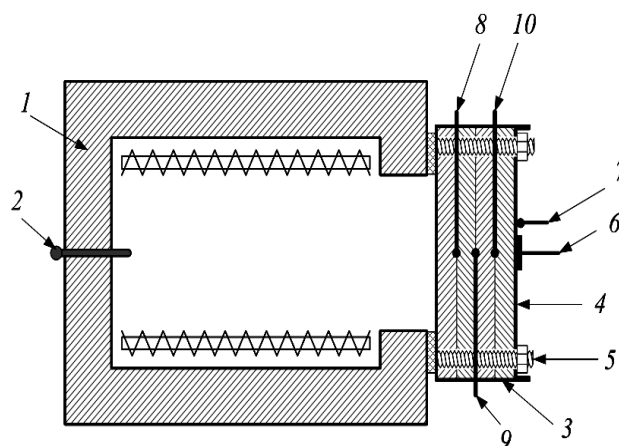


Fig. 1. Sketch of test setup for investigation the effective thermal conductivity coefficient of fibrous materials: 1) laboratory electric furnace; 2) control thermocouple of the furnace; 3) measuring cell with tested fibrous material; 4) pressing metal plate; 5) screw studs for compression of samples; 6) heat flux probe; 7) thermocouple for measuring the outer surface temperature; 8, 9, 10) thermocouples for measuring the temperature between the material layers

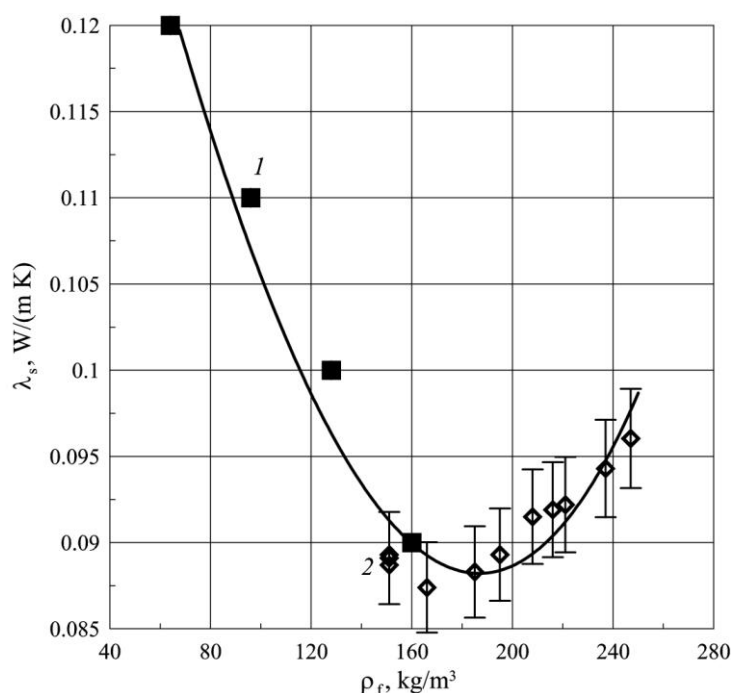


Fig. 2. Experimentally measured dependence of the effective heat conductivity coefficient of a fibrous high-temperature material Cerablanket on the material density: 1) reference data provided by the manufacturer for the material at 400°C (measurements according to the ENV 1094-7 standard); 2) experimental results for a hot wall temperature of 800°C [1]

The dependence of the effective heat conductivity of a fibrous material on its density is presented in Fig. 2. In all of the experiments the temperature of the interior surface of the material was maintained at 800°C, whereas the temperature of the exterior surface under conditions of natural convection was varied within the limits 70–90°C. To get a more detailed

picture, the measurement data was supplemented with the manufacturer data for the same material with a density of 64, 96, 128, and 160 kg/m³ at a temperature of 400°C [2]. These data correspond to the average temperature maintained in the tests with the samples described in the present work. As can be seen, the effective heat conductivity coefficient of a fibrous material at the considered characteristic temperatures varies nonmonotonically. For the studied temperature conditions and material, the minimum of the effective heat conductivity coefficient is reached at a density of 186 kg/m³ and amounts to 0.089 W/(m·K). It is important to point out that for a density of 64 kg/m³ the heat conductivity coefficient of this same material is 0.12 W/(m·K). The experimentally revealed effect of the decrease in the effective heat conductivity coefficient with change in the fibrous material density accounts for about 25% in relative terms within the limits considered.

The analysis of this problem has allowed to make following assumption: at high temperatures there are three competing mechanisms of heat transfer in a highly porous fibrous material. As the material density decreases, the contribution of heat transfer to the gas phase and of radiative heat transfer to the pore space increases with simultaneous decrease in conductive heat transfer in the fibers and in their mutual contacts. Generally, competing mechanisms of heat transfer have to lead to the minimum value of the effective heat conductivity coefficient of the fibrous material at its certain density, which was in the case of made experiments.

3. MATHEMATICAL MODEL

In order to correctly describe the effective heat conductivity coefficient of a fibrous material in wide ranges of parameters (primarily of temperatures and densities), it is necessary to construct a mathematical model that would account for all the above-listed heat transfer mechanisms. The approaches used for describing the radiative component and heat conduction in the gas phase of fibrous materials have been developed in sufficient detail at the present time [3–5]. Here, only empirical relations are used to describe heat conduction in the fibrous skeleton. In the present work, an analytical expression is suggested and justified for the conductive component of the heat conductivity coefficient of a fibrous material for describing heat transfer in its solid skeleton. This formula can to describe the experimentally observed behavior of the heat conductivity coefficient.

Various mechanisms of heat transfer allow to present the effective heat conductivity as an additive quantity:

$$\lambda_{eff} = \lambda_r + \lambda_g + \lambda_s, \quad (1)$$

where λ_r is an effective heat conductivity coefficient due to thermal radiation transfer over the pore space of a fibrous material; λ_g is the heat conductivity coefficient of gas phase; λ_s is the coefficient of effective heat conduction along the fibers and their contacts.

According to estimates, the natural convection in the fibrous material can be neglected in the considered parameter ranges.

Practically important fibrous materials can be considered as optically thick ones [3]. In this case the radiative component of the effective heat conductivity coefficient can be determined according to the following equation:

$$\lambda_r = \frac{16}{3} \frac{n^2}{\beta} \sigma_0 T^3, \quad (2)$$

were n is the refraction index of the for a fibrous material; β is the coefficient of radiation attenuation; σ_0 is the Stefan-Boltzmann constant. In [6], for the radiative component of heat conductivity the following formula was suggested, which had been adapted for fibrous materials:

$$\lambda_r = \frac{4\sigma_0 T^3}{\beta} \tilde{l}. \quad (3)$$

Here \tilde{l} is a characteristic dimension of a pore in a fibrous material. In the absence of experimental data, this formula allows to estimate the thermal conductivity in the most arbitrary conditions [6]. To compare with experimental results, let us make use of the formula for the attenuation coefficient β (mullite-silicic fiber) which is also given in [6]:

$$\beta_{mk} = 25\varepsilon dT + \frac{5000(1-\varepsilon)^2}{T}, \quad (4)$$

where ε is the material porosity and d is the average diameter of fibers. In the given case, for the characteristic size \tilde{l} of the problem we take the expression derived for fibers randomly oriented in space [7]:

$$\tilde{l} \approx 0.524 \frac{d}{1-\varepsilon}. \quad (5)$$

With Eq. (5) taken into account, we finally obtain an expression for the radiative component of heat conductivity:

$$\lambda_r \approx 2.1 \frac{d\sigma_0}{\beta_{mk}(1-\varepsilon)} T^3 \quad (6)$$

Under normal conditions, the heat conductivity coefficient of gases is independent of pressure. However, in porous bodies such dependence may also occur at a normal ambient pressure. The reason is pore sizes comparability with the molecular mean free path. The heat conductivity coefficient of gas phases in the fibrous material can be calculated using the equation below [5]:

$$\lambda_g = \frac{\lambda_{g0}}{1 + \frac{4c_p}{c_p + c_v} \frac{Kn}{Pr}} = \frac{\lambda_{g0}}{1 + \frac{4\gamma}{1+\gamma} \frac{Kn}{Pr}}, \quad (7)$$

$$Kn = \frac{l_{fp}}{\tilde{l}}, \quad (8)$$

$$l_{fp} = \frac{k_b T}{\sqrt{2\pi} d_m^2 p_g}. \quad (9)$$

Here λ_{g0} is the conductivity coefficient of a gas at normal pressure ($Kn \rightarrow 0$); c_p, c_v are the specific heats of gas at constant pressure and volume, respectively; γ is the adiabatic index (the adiabatic index for dry air at 400°C is equal to $\gamma = 1.393$); Kn is Knudsen number; l_{fp} is mean free path of gas molecules in a fibrous material; k_b is the Boltzmann constant; d_m is diameter of gas molecules; p_g is the gas pressure. In (7) the accommodation coefficient is taken to be unity. In the present work, as a gas medium we consider air. This does not impose

basic limitations on the proposed model but makes it possible to carry out rather a detailed comparison with experimental results. In our calculations, for the size of nitrogen molecules in (9) we used $d_m = 0.32$ nm ($d_m = 0.30$ nm for oxygen molecules).

In the literature, the conductive heat transfer in a solid phase is described only by empirical relations [8–12]. The most frequently used dependence has the form

$$\lambda_s = B_s (1 - \varepsilon)^b \lambda_{s,0}. \quad (10)$$

The empirical coefficients B_s and b are determined by processing experimental data for each specific material. The exponent b usually lies within the range from 1 to 3. The value of this index is not substantiated by any physical models. This, in [8] use was made of a model with $b = 1$, in [9] $b = 1.4$, in [10, 11] $b = 2$, and in [12] $b = 3$. It can be also noted that the same authors use different empirical coefficients in their various publications without adequate justifications [9, 10].

Let us construct a mathematical model that would validate the analytical form of the expression for the conductive component of the effective heat conductivity coefficient of fibrous materials. We consider a bunch of fibers with mean diameter d . Let N fibers pertain to unit area of the material cross section. The conductive heat transfer can be divided into two components: heat transfer in the fibers and the thermal resistance of the mutual contacts of fibers. Let us assume that the average distance between two successive mutual contacts of fibers be equal to the characteristic dimension of pores \tilde{l} . Then, the heat flux propagating along the fibers can be estimated as

$$q_{s,1} \approx \lambda_{s,0} \frac{\pi d^2}{4\tilde{l}} \Delta T N \approx \lambda_{s,0} \frac{\pi d(1-\varepsilon)}{2} \Delta T N, \quad (11)$$

and the corresponding thermal resistance as

$$R_f = \frac{\Delta T}{q_{s,1}} \approx \frac{2}{\pi d \lambda_{s,0} (1-\varepsilon) N} = \frac{f_{s1}}{\lambda_{s,0} (1-\varepsilon)}. \quad (12)$$

We must simultaneously take into account the thermal resistance of the contacts between various fibers. The thermal resistance of one contact can be estimated as

$$R_{t,0} \approx \frac{K_t}{\lambda_{s,0} a^2}, \quad (13)$$

where K_t is the proportionality factor. We assume that the contact conductivity is proportional to the area of the spot of contact between two fibers and to their heat conductivity. In turn this area depends on the compressive force, i.e. on the outer loading. The characteristic dimension of the contact spot of compression of two fibers can be estimated by obtaining an exact analytical solution of the Hertz problem for two cylinders [13]:

$$a = \left(\frac{4}{\pi} \frac{1-\sigma^2}{E} F d \right)^{1/2}. \quad (14)$$

Here F is the compressive force, σ, E are the Poisson coefficient and modulus of the stretching of fiber material respectively. Next, it is necessary to go over from the relationship between the characteristic dimension of the contact area and the compressive force to the relationship between the dimension and the density of the material. The dependence needed for this purpose has been obtained in the present work experimentally (Fig. 3). The

compression pressure P_F was defined as the ratio of the compressive force F to the area S of a sample. Approximation of experimental data has made it possible to establish a single analytical correlation between the increment in the fibrous material density and the compressive force:

$$\rho_f \approx \rho_{f,0} + K_f \sqrt{F}. \quad (15)$$

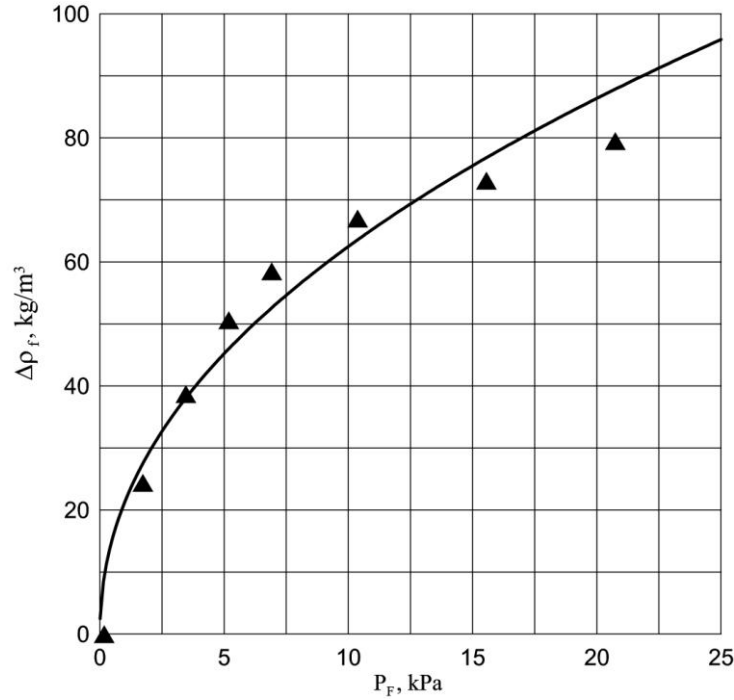


Fig. 3. Experimentally measured increment in the density $\Delta\rho_f$ of the fibrous material Cerablanket 128 as a function of the pressure applied. Symbols, the results of measurements; the line, approximation of the measurement results

Then, based on Eq. (15), for a change in the material density we may write

$$\begin{aligned} \varepsilon_0 - \varepsilon &= \frac{\Delta\rho_f}{\rho_s} \approx \frac{K_f}{\rho_s} \sqrt{F}. \\ F &\approx \left[\frac{\rho_s}{K_f} (\varepsilon_0 - \varepsilon) \right]^2 \approx \left[\frac{\rho_s}{K_f} (1 - \varepsilon) \right]^2. \end{aligned} \quad (16)$$

Based on Eq. (16) we can obtain an important relationship between the characteristic dimension a of the region of contact of two fibers and the material porosity:

$$a \approx K_a (1 - \varepsilon). \quad (17)$$

The estimate for the thermal resistance of the material can then be written in the form

$$R_t \approx \frac{R_{t,0}}{2N} \approx \frac{K_t}{2N\lambda_{s,0}a^2} \approx \frac{f_{s2}}{\lambda_{s,0}(1-\varepsilon)^2}. \quad (18)$$

In the problem considered, the resistance of fibers and that of the contact must be added up as being located in tandem. Then for the effective heat conductivity of the solid skeleton we may write the resultant estimating relation:

$$\lambda_s = \frac{1}{R_f + R_t} \approx \frac{\lambda_{s,0}}{\frac{f_{s1}}{(1-\varepsilon)} + \frac{f_{s2}}{(1-\varepsilon)^2}} \quad (19)$$

We will expand this relation into a series with respect to the small parameter $(1 - \varepsilon)$ (the fibrous material porosity lies within the range $\varepsilon = 0.9\text{--}0.97$), retaining only the first term:

$$\lambda_s \approx \lambda_{s,0} B_{s2} (1 - \varepsilon)^2 \left(1 + \frac{f_{s1}}{f_{s2}} (1 - \varepsilon) \right)^{-1} \approx \lambda_{s,0} B_{s2} (1 - \varepsilon)^2 - \lambda_{s,0} B_{s3} (1 - \varepsilon)^3 \quad (20)$$

This relation coincides in form with expression (10) at $b = 2$. Note that account for only the heat conductivity of fibers [with only R_f remaining in Eq. (19)] would have led to an analytical expression of the form of Eq. (10) with the coefficient $b = 1$.

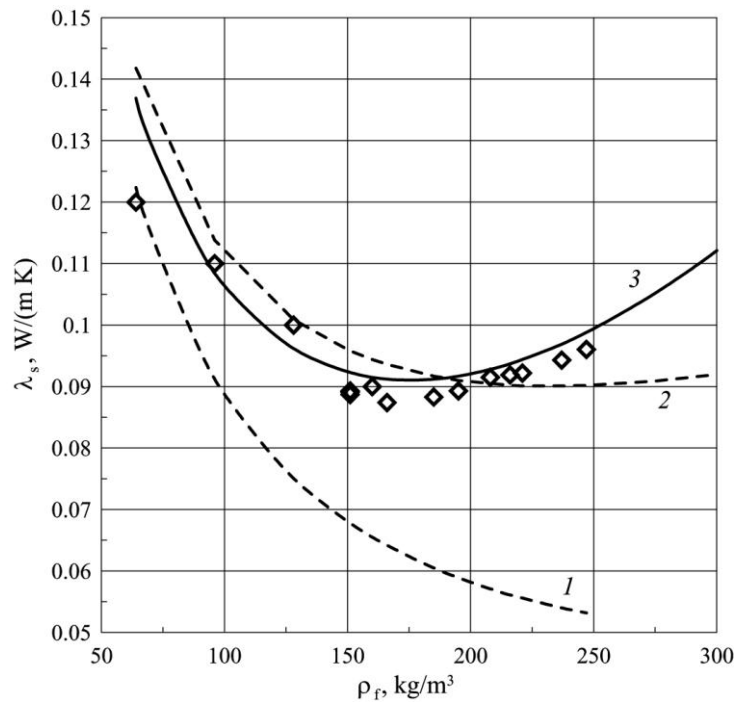


Fig. 4. The effective heat conductivity of fibrous material Cerablanket 128 vs. its density at 400°C. Symbols, experimental results of [1]: 1) calculation by relations (1), (4)–(7), (21) (“lower estimate”); 2) calculation by relations (1), (4)–(6), (10) for $b = 1$ ($B_s = 0.124$ on condition of the best approximation of experimental data); 3) calculation by the model [Eqs. (1), (4)–(7), (20)] suggested in the present work ($B_{s2} = 1.3$ on condition of the best approximation of experimental data)

The effective heat conductivity of the gas phase and skeleton without account for the radiative component can be obtained in considering a system consisting of alternating plane layers of solid skeleton (fibers) and a gas. The layers can be located both normally to the heat flux direction, which allows one to obtain the lower estimate, and in parallel with this direction (the upper estimate) [5, 14]:

$$\lambda_{eff,min} = \lambda_r + \frac{\lambda_s \lambda_g}{\varepsilon \lambda_s + (1 - \varepsilon) \lambda_g}, \quad (21)$$

$$\lambda_{eff,max} = \lambda_r + \varepsilon \lambda_g + (1 - \varepsilon) \lambda_s. \quad (22)$$

To test whether the developed approach is suitable for describing the heat conductivity of the real fibrous material, the effective heat conductivity was calculated (Fig. 4) in three different approximations: finding a lower estimate based on Eq. (21) and Eqs. (4)–(6) for the radiative component of conductivity, calculation with account for the conductive component in linear approximation with respect to density [$b = 1$ in (10)], and calculation based on the model suggested in the present work [Eqs. (1), (4)–(7), (20)]. All the calculations were compared with the experimental data of [1]. As can be seen from Fig. 4, the lower estimate performs adequately only at low densities of the material (less than 100 kg/m^3). The material density linear approximation resulting when only the conductive component of heat flux along fibers is taken into account is more accurate, but already at densities exceeding 250 kg/m^3 a considerable deviation from the experiment occurs. Only the approach suggested in the present work describes the behavior of the effective heat conductivity of a fibrous material with acceptable accuracy (7–10% for $200\text{--}600^\circ\text{C}$, 10–15% for $800\text{--}1000^\circ\text{C}$) in the entire range of densities. It should be noted that the divergence between curves 2 and 3 in Fig. 4 is substantial in the region where the external compressive force and the role of the contact heat conduction in fibers are significant.

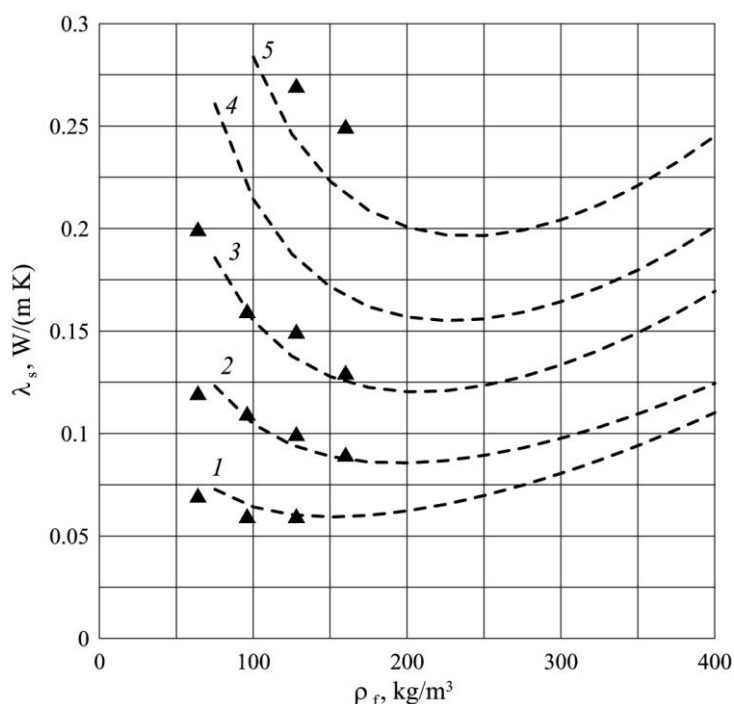


Fig. 5. The dependence of effective heat conductivity coefficient of a fibrous material on its density for various temperatures calculated by the model proposed in the present work: 1 – 200°C ; 2 – 400°C ; 3 – 600°C ; 4 – 800°C ; 5 – 1000°C . Markers are the results of measurements provided by the manufacturer [2]

Based on the approach suggested in the present work, the effective heat conductivity of a fibrous material was calculated for temperatures from 200 to 1000°C within the density range from 75 to 400 kg/m^3 (Fig. 5). In these calculations the only empirical coefficient $B_{s2} = 1.3$

was used. This coefficient was obtained from the experimental results at 400°C. The thermal conductivity of the material of fibers on change in their temperature was calculated by Eq. (4.17) from [6] for a mullite-silicic material. The calculated data was compared with measured values of the heat conductivity coefficient obtained by the manufacturer using the technique of the European standard ENV 1094-7 [2]. It is obvious that calculated results are closed to experimental results. Analyzing the results of calculations, we may note that the existence of the minimum of the effective heat conductivity coefficient of fibrous materials is observed at all the temperatures. With increase in temperature this maximum is displaced to the region of higher densities of material — from 150 kg/m³ at 200°C to 250 kg/m³ at 1000°C.

CONCLUSIONS

A mathematical model for calculating the effective heat conductivity of fibrous materials at high temperatures on change in their density has been suggested and substantiated. A comparison of the results of calculations with experimental data has shown a good accuracy of the proposed approach in a wide range of densities (from 75 to 400 kg/m³) and temperatures (up to 1000°C).

REFERENCES

1. GRINCHUK P.S., STETYUKEVICH N.I., SHEVTSOV V.F., AND CHERNUKHO E.V. The effective heat conductivity coefficient of fibrous heat-insulating materials with a variable density. *Heat- and Mass Transfer–2013*. Proceedings of the A.V. Luikov Heat and Mass Transfer Institute, Minsk (2013), p. 290–295.
2. *Product Data Brochure. P. 7 Blanket products. Morgan Crucible. Thermal Ceramics. Datasheet Code 5-5-01 R*. (URL <http://www.morganthermalceramics.com/files/datasheets/cerablanketcerachemcerachromeblanketrussian.pdf>).
3. DUL'NEV G.N., NOVIKOV V.N. *Transfer Processes in Inhomogeneous Media* [in Russian], Énergoatomizdat, Leningrad (1991).
4. FRICKE J., CAPS R. Heat transfer in thermal insulations - recent progress in analysis. *Int. J. Thermophys.* 1988. Vol. 9, Iss. 5, p. 885–895.
5. PAVLYUKEVICH N. V. *Introduction to the Theory of Heat and Mass Transfer in Porous Media* [in Russian], Izd. ITMO NANB, Minsk (2002).
6. GUTMAN M.B. (Ed.) *Materials for Electrothermal Plants: Handbook* [in Russian], Énergoatomizdat, Moscow (1987).
7. KELLER K., BLUMENBERG J. and TOMSIK J. Fibre orientation and the conduction of heat by a gas enclosed in ceramic layers. *Zeitschrift für Flugwissenschaften und Weltraumforschung*. 1988. Vol. 12, p. 258–260.
8. KOLIENKO V.P. Modeling of the thermal properties of energy-saving fibrous heat-insulating materials. *Heat- and Mass Transfer–2012*. Proceedings of the A.V. Luikov Heat and Mass Transfer Institute, Minsk (2013), p. 300–304.
9. DARYABEIGI K. Heat transfer in high-temperature fibrous insulation, *AIAA*, Paper 2002–3332.
10. DARYABEIGI K. Thermal analysis and design of multi-layer insulation for re-entry aerodynamic heating, *AIAA*, Paper 2001–2834.
11. ZHAO S., ZHANG B., and HE X. Temperature and pressure dependent effective thermal conductivity of fibrous insulation. *Int. J. Thermal Sci.* 2009. Vol. 48, p. 440–448.
12. HAGER N.E., STEERE R.C. Radiant heat transfer in fibrous thermal insulation. *J. Appl. Phys.* 1967. Vol. 38, Iss. 12, p. 4663–4668.
13. LANDAU L.D. and LIFSHITS E.M. *Elasticity Theory* [in Russian], Vol. 7, 4th revised edn., Nauka, Moscow (1987).
14. KAVIANY M. *Principles of Heat Transfer in Porous Media*, Springer-Verlag, New York (1991).

STRUCTURAL AND ELECTRICAL PROPERTIES OF P-TYPE NiO THIN FILMS DEPOSITED BY SPRAY PYROLYSIS

R.Vessart, T.Unt, A. Mere, M.Krunka

*Department of Materials Science, Tallinn University of Technology
Ehitajate tee 5, 19086 Tallinn – Estonia*

ABSTRACT

NiO semiconductor is one of the proposed materials to be incorporated as a transparent conductive oxide (TCO) layer in thin film solar cells. High optical transparency and conductivity is needed as NiO layer will function as a window layer and electrode for thin film solar cell. In our research NiO thin films were prepared by chemical spray pyrolysis method. Aqueous and alcohol based solutions were made out of Ni chloride and Ni acetate salts. The solutions were sprayed on glass substrates at growth temperatures from 350°C to 500°C. The SEM images comparison showed that solutions made out of Ni chloride salt resulted in thin films with uneven thickness, rough and porous structure. Thin films made from Ni acetate solutions resulted in uniform thickness and smooth surface. XRD studies show that using NiCl as a salt for both water and alcohol based solutions results in crystallites with plane (111) preferentially parallel to substrate in thin films. Thin films sprayed by using Ni acetate source, both water and alcohol, based solutions do not show any preferential orientation what so ever. Increasing thin film growth temperature results in increase of crystallite size and decrease of thin film thickness. The resistivity of undoped NiO is in the order of 300 Ωcm . Therefore NiO was doped with LiCl or LiNO₃ and conductive p-type thin films were achieved showing resistivity around 6 Ωcm . XRD confirmed the Lithium atoms presence in NiO lattice by the decrease of NiO lattice parameters in case of increasing Lithium concentration in precursor. Investigated NiO is promising material for solar cell application.

Keywords: NiO thin films, electrical properties, chemical spray pyrolysis, NiO:Li

1. INTRODUCTION

Nickel oxide (NiO) exhibits p-type conductivity. It is a promising candidate for transparent conductive oxide, having a wide band gap varying from 3.6 to 4.0 eV [1]. Undoped NiO shows high electrical resistivity in the order of 10^{13} Ωcm at room temperature [2]. NiO can be doped with monovalent Li ions resulting increase of p-type conductivity due to appearance of nickel vacancies and/or interstitial oxygen in crystallites. NiO films are being used in different applications such as solar thermal absorber, catalyst for O₂ evolution, electrochromic material in smart windows [3], active material in chemical sensors [4], photocathode in dye sensitized solar cells, component of p-n junction diode, component of random access memory devices [5], an anode interfacial layer in polymer solar cells, anode in oxygen fuel cells and as buffer layer in organic solar cells. NiO thin films can be prepared by different methods including atomic layer deposition, pulsed laser deposition, chemical spray deposition, sol-gel, magnetron sputtering, chemical bath deposition. Currently the most studied and production usable method is sputtering [6]. On the other hand, chemical spray pyrolysis promises to be a cost effective alternative. Due to the absence of vacuum systems, CSP used in this study, is a simple and feasible method to fabricate large area coatings [6], [7]. NiO films can be made by spray using various solutions of nickel chloride [8], [9], nickel nitrate [7], [8], [10], nickel acetate [11], [12] or nickel acetylacetonate. Lowest resistivities in the order of 1 Ωcm obtained were by spraying Ni(NO₃)₂ solutions using LiCl or LiNO₃ as dopant sources [7], [10].

First aim of this study is to focus on the comparison of structural and morphological properties of NiO films grown at different temperatures from Ni chloride and Ni acetate solutions. Second aim is to study the effect of Li-doping on the structure and electrical properties of sprayed NiO films. Only few studies have been made on these topics.

2. METHODOLOGY

Nickel acetate tetrahydrate ($\text{Ni}(\text{CH}_3\text{COO})_2 \cdot 4\text{H}_2\text{O}$, $\geq 99.0\%$, Aldrich) and nickel chloride hexahydrate ($\text{NiCl}_2 \cdot 6\text{H}_2\text{O}$, 99.95%, Alfa Aesar) were used as nickel sources dissolved in deionised water. The concentration of a nickel salt was 0.05 mol/L in an aqueous spray solution, and 0.1 mol/L in an alcoholic spray solution (isopropanol: H_2O =3:2, by volume). LiCl (99%, Sigma Aldrich) and LiNO_3 (99%, Alfa Aesar) were used as dopant sources added into the spray solution, the concentration of Li ions ($([\text{Li}^+]/([\text{Li}^+]+[\text{Ni}^{2+}]))$) in a solution was 10 and 25 at.%. The volume of the solution for each deposition was 50 mL and the solution deposition rate was 2 mL/min.

NiO films were deposited on microscopic glass substrate with the size of 20x15x1 mm by chemical spray pyrolysis (CSP), the setup is discussed elsewhere [13]. The substrates were placed onto molten tin bath, the bath temperature ranged from 350 to 500 °C with step of 50 °C. Volume of the solution for deposition was 50ml and the rate of spray was ~1ml/min.

The characterization of the sprayed NiO films were done by using Rigaku Ultima IV diffractometer (XRD) with monochromatic Cu K α radiation ($\lambda = 0.15406$ nm, 40 kV at 40 mA). Data was acquired in the 2θ range of 20°–80° with scan speed 5°/min and scan step 0.02° using the silicon strip detector D/teX Ultra. Analyzation of the diffractograms was done using the PDXL 1.4.0.3 software made for the Rigaku Ultima IV diffractometer. The surface morphology and the thickness of the sprayed films were analyzed by using a scanning electron microscope (Zeiss HR FESEM Ultra 55). Electrical properties such as electrical resistivity, charge carrier mobility and charge carrier concentration were measured by using a standard 4-probe method at room temperature using van der Pauw, Hall Controller H-50 from MMR. The contacts for electrical measurements were made from graphite conductive adhesive.

3. RESULTS AND DISCUSSION

3.1. Structure and morphology of NiO films obtained by spray of NiCl_2 and $\text{Ni}(\text{CH}_3\text{COO})_2$ solutions

The XRD patterns of thin films deposited from NiCl_2 and $\text{Ni}(\text{CH}_3\text{COO})_2$ (further marked as $\text{Ni}(\text{ac})_2$) aqueous solutions at substrate temperatures (T_s) in the interval of 350–500 °C are presented in Fig. 1 and Fig. 2, respectively. According to XRD study all the diffraction peaks are belonging to NiO with cubic structure (JCPDS 00-047-1049) [14], no other crystalline phases were detected. NiO films from chloride precursor exhibit the (111) reflection as the strongest peak on the diffractogram (Fig. 1). The ratio of the intensities of the (111) and (200) diffraction peaks ($I_{(111)}/I_{(200)}$) decreases from 16 to 2 increasing the substrate temperature from 350 to 500°C. A comparison with the intensity of XRD reference lines of NiO powder ($I_{(111)}/I_{(200)} = 0.6$) refers that all the films grown from chloride solution show preferential growth of the crystallites along the (111) plane parallel to the substrate. This result corresponds to that reported in literature [8], [9]. According to the results of present study, the preferred orientation along the (111) plane weakens with temperature. Reguig *et al.* [9] and Cattin *et al.* [8] observed weakening of the (111) orientation by spraying more concentrated solutions ($C > 0.3$ M) at fixed temperature. Full width at half maximum

(FWHM) of the diffraction peaks decreases with temperature and indicates the growth of crystallites. The mean crystallite size (calculated according to the Scherrer formula from the FWHM of the (111) reflection) increases from 16 to 26 nm (Table 1).

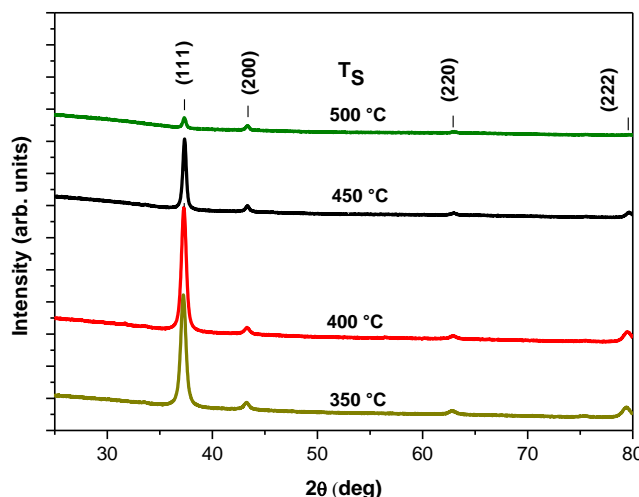


Fig. 1. XRD patterns of NiO film grown by spray of NiCl_2 0.05 mol/L aqueous solutions at different substrate temperatures in the range of 350–500 °C

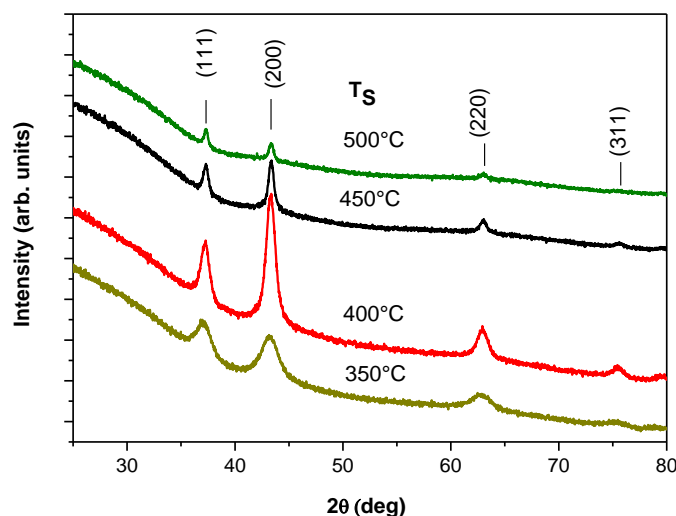


Fig. 2. XRD patterns of NiO film grown by spray of $\text{Ni}(\text{CH}_3\text{COO})_2$ 0.05 mol/L aqueous solutions at different substrate temperatures in the range of 350–500 °C

Fig. 2 shows that the crystallinity of NiO films from $\text{Ni}(\text{ac})_2$ solutions is lower compared to the films from NiCl_2 solution as the diffraction peaks are significantly wider. The crystallites do not show preferential growth as the $I_{(111)}/I_{(200)}$ varies between 0.5 and 0.7 which is close to that of powder reference 0.61 [14]. The crystallite size (calculated from the FWHM of the strongest (200) diffraction peak) changes from 6 nm to 10 nm increasing the T_s from 400 °C to 500 °C (Table 1).

Table 1. Effect of the growth temperature on the film thickness, crystallite size and orientation of NiO films grown by spray of 50 mL nickel chloride and nickel acetate 0.05 mol/L aqueous solutions

Ni salt	Ts, °C	Thickness, nm	Cryst. orientation	Crys.size, nm
NiCl ₂	400	~590	(111)	16
	450	~400	(111)	20
	500	~50	(111)	26
Ni(ac) ₂	400	1000	-	6
	450	600	-	10
	500	75	-	10

Thinner films are obtained at higher Ts, the film thickness decreases from ~ 600 nm to ~ 50 nm and from 1000 nm to 75 nm increasing the Ts from 400 °C to 500 °C when spraying NiCl₂ or Ni(ac)₂ solutions, respectively (Table 1). Much lower film thicknesses at higher growth temperatures is a commonly known characteristic of the spray process as the solution droplets are repelled from the reaction zone at higher temperatures and less precursor material reaches the substrate [15].

The SEM images reported in Fig. 3 clearly show remarkable different characteristics between the NiO films prepared from chloride and acetate solutions. NiO films from NiCl₂ solution exhibit uneven thickness, irregular rough surface and porous microstructure (Fig. 3a). Coarse grained surface of NiO films grown from Ni chloride solutions has been reported also in literature [8], [9]. The films fabricated from acetate solution are relatively smooth and dense (Fig. 3b) as also reported by Desai *et al.* [11]. It is well-known that spraying of alcohol based solutions may result in much smoother films due to smaller solution droplet size [15].

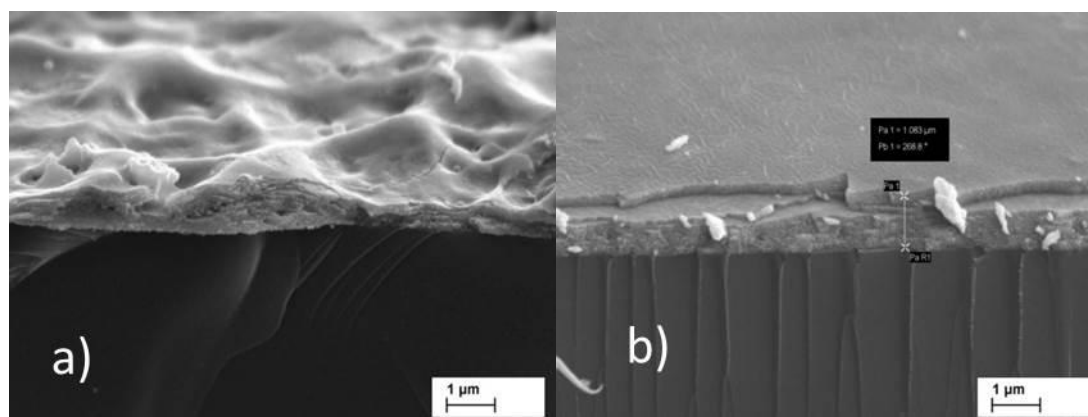


Fig. 3. SEM cross-sectional images of NiO films grown at 400 °C from (a) NiCl₂ and (b) Ni(CH₃COO)₂ aqueous solutions. Concentration of Ni salts in the spray solution 0.05 mol/L, solution volume 50 mL

XRD study of NiO films fabricated by spray of alcohol based solutions (isopropanol: H₂O) shows that the solvent has no effect on the orientation of crystallites (XRD patterns not presented), the growth of crystallites is similar to that observed in case of NiCl₂ and Ni(ac)₂ aqueous solutions. SEM images presented in Fig. 4 exhibit that much thinner films are obtained using alcohol based solutions instead of aqueous ones. For example, the thickness of NiO film is ca. 150 and 1000 nm deposited from Ni(ac)₂ alcoholic and aqueous solutions, respectively. NiO films from acetate solutions are smooth and uniform in thickness (Fig. 4b)

but those obtained by spray of NiCl_2 solution are uneven, ca. 200–250 nm thick in flat areas while the height of bumps is up to 2 microns or more (Fig.4a). Thus, the high roughness and porosity of NiO films from NiCl_2 cannot be avoided spraying alcohol based solutions at Ts in the interval of 350–450 °C.

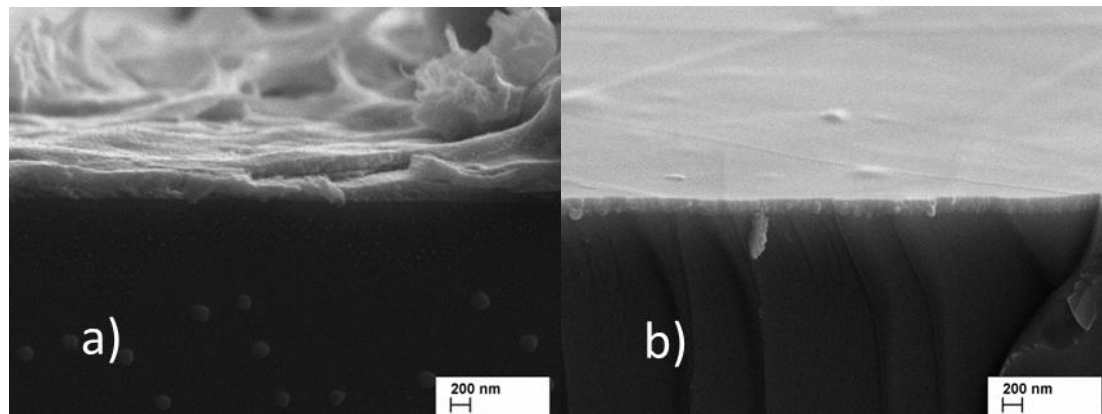


Fig. 4. SEM cross-sectional images of NiO films grown at 400 °C from (a) NiCl_2 and (b) $\text{Ni}(\text{CH}_3\text{COO})_2$ alcohol based (H_2O : 2propanol=2:3, by volume) solutions. Concentration of Ni salts in the spray solution 0.1 mol/L, solution volume 50 mL

Our study shows that the NiO film morphology is mainly controlled by the precursor while other deposition variables such as temperature and solvent have minor effect. It is likely that there are differences in the thermal decomposition reactions of $\text{NiCl}_2 \cdot 6\text{H}_2\text{O}$ and $\text{Ni}(\text{CH}_3\text{COO})_2 \cdot 4\text{H}_2\text{O}$, and because of this the chemical routes for NiO formation can be different, and may also result in various morphologies of sprayed films.

3.2. Effect of Li doping on the structural and electrical properties of NiO films obtained by spray of $\text{Ni}(\text{CH}_3\text{COO})_2$ aqueous solutions

Effect of doping with Li was studied using $\text{Ni}(\text{ac})_2$ as Ni source due to the fact that relatively uniform NiO films were obtained from this precursor. Figure 5 presents the XRD patterns of NiO films fabricated at Ts of 400 °C by spraying of $\text{Ni}(\text{ac})_2$ aqueous solutions with LiCl and LiNO_3 as Li-sources. According to XRD, the films are polycrystalline and composed of cubic NiO phase, no other phases were detected. The careful inspection of the diffractograms shows that the addition Li salt into the spray solution causes the shift of NiO diffraction peaks to higher 2θ values. For example, the (200) diffraction peak at 2θ of 43.28° in undoped NiO film [14] is shifted to 43.34° when using 25 at.% of Li (LiCl) in the spray solution (Fig. 5).

The shift of XRD peaks toward higher 2θ value by lithium addition has been observed for $\text{Ni}_{1-x}\text{Li}_x\text{O}$ thin films [7]. It has been reported that $\text{Ni}_{1-x}\text{Li}_x\text{O}$, where Li^+ ions occupy substitutional positions, has smaller lattice parameter than NiO. A decrease in NiO lattice constant by Li-doping was observed in sprayed films (Table 2).

The XRD results obtained in this study suggest that the incorporation of Li ions occurs into the NiO lattice, and it was independent from the Li salt (LiCl or LiNO_3) used for NiO doping.

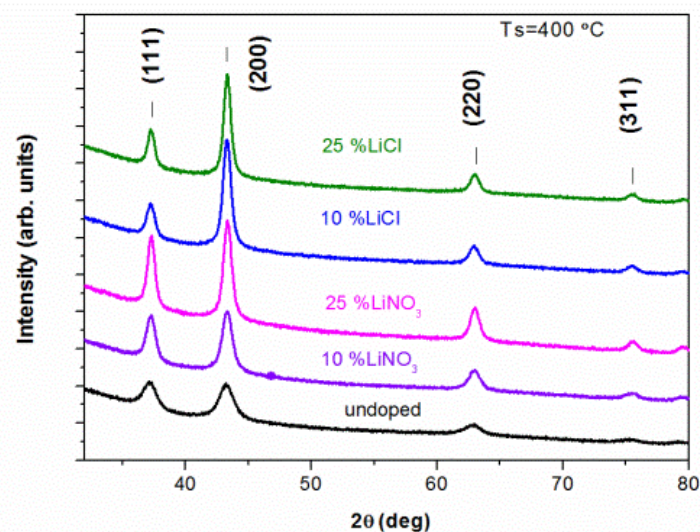


Fig. 5. XRD patterns of undoped and Li-doped NiO films grown by spray at Ts of 400 °C from 50 mL of 0.05 M $\text{Ni}(\text{CH}_3\text{COO})_2$ aqueous solutions. LiCl and LiNO_3 are used as dopant sources added into the spray solution, $[\text{Li}^+]$ in solution 10 and 25 at. %

Doping with LiNO_3 does not affect the orientation of crystallites (Fig. 5) compared to un-doped NiO film where the crystallites do not show preferential growth (see also Fig. 2). Addition of LiCl increases the relative intensity of the (200) diffraction peak with respect to the (111) peak (Fig. 5). The peak intensities ratio ($I_{(111)}/I_{(200)}$) of ca. 0.3 indicates that the crystallites in NiO:Li films obtained by spray of Ni acetate solution with LiCl are grown the (200) plane parallel to the substrate. Our results on doping of NiO films from acetate solutions are different compared to the films obtained from nickel nitrate. In case of NiNO_3 doping with LiCl promotes the growth of crystallites along the (111) plane [10] and doping with LiNO_3 along the (200) plane [7]. Results of present study show that the preferred orientation of crystallites in NiO:Li film depends on both Ni and Li sources.

Table 2 Crystallite size, lattice parameter and electrical properties (carrier type, electrical resistivity, carriers' mobility and density) of NiO films depend on Li source and concentration in the spray solution. NiO films are grown by spray of 50 ml nickel acetate 0.05 mol/L aqueous solutions at Ts of 400 °C and 450 °C

Technology			Structural properties		Electrical properties			
Growth temp., °C	Li source	$[\text{Li}^+]$ in solution, at. %	Crys. size, nm	Lattice parameter, Å	Carrier type	Resistivity, Ωcm	Mobility, $\text{cm}^2\text{V}^{-1}\text{s}^{-1}$	Carrier density, cm^{-3}
400	undoped	0	6	4.181	p	355	0.34	5.2×10^{16}
	LiCl	25	14	4.176	p	87	0.18	4.1×10^{17}
	LiNO_3	10	9	4.174	p	130	0.03	1.4×10^{18}
		25	12	4.173	p	22	0.23	1.3×10^{18}
450	undoped	0	10	4.176	p	259	1.2	2.0×10^{16}
	LiCl	25	22	4.172	p	89	0.43	1.6×10^{17}
	LiNO_3	10	15	4.173	p	41	0.15	1.2×10^{18}
		25	16	4.172	p	6.5	0.39	2.6×10^{18}

According to XRD, the dopant concentration has notable effect on the size of crystallites. For example, the crystallite size in undoped NiO film grown at Ts of 400 °C is ca. 6 nm and increases up to ca. 14 nm by 25 at.% of Li (LiCl) doping. LiNO₃ dopant has similar effect and the crystallite size is ca. 12 nm at 25 at.% of Li doping (Table 2). The growth of crystallites by Li doping has also been reported previously [7], [10].

Electrical resistivity, concentration and mobility of charge carriers in NiO and NiO:Li films are presented in Table 2. All the NiO films exhibited p-type conductivity as determined by hot probe technique and verified by the sign of the Hall coefficient. Resistivity of undoped NiO films is in the order of 300 Ωcm which is comparable to that of undoped NiO films from NiNO₃ [8], [9] but two orders of magnitude lower than that reported for NiO films from NiCl₂ solutions [15]. Doping with Li (LiNO₃) increases the concentration of carriers from ca. 10¹⁶ cm⁻³ (undoped) to 10¹⁸ cm⁻³ using [Li⁺] of 10 or 25 at.% in the solution. Lower resistivities at higher doping rates of 25 at.% of Li (Table 2) could be due to slightly higher mobilities, probably caused by some larger crystallite size. Using LiCl as dopant source, the resistivities are higher than in case of LiNO₃, mainly due to lower concentration of carriers (in the order of 10¹⁷ cm⁻³). The Cl is possible candidate for donor dopant in NiO decreasing the concentration of holes as main charge carriers. The lowest resistivity of ca 6.5 Ωcm is measured for NiO:Li films grown at 450 °C with [Li⁺] of 25 at.% (LiNO₃) in the spray solution. The carrier concentrations of ca. 10¹⁸ cm⁻³ are similar to that recorded for the most conductive NiO:Li films made by spray using NiNO₃ as nickel source [7], [10]. Doping with Li (LiNO₃, LiCl) reduces the mobility of carriers. This can be countered with higher growth temperature where increased crystallite size provides higher mobility of carriers but not better than in undoped NiO film.

4. CONCLUSIONS

Spray deposition of aqueous and alcoholic solutions of nickel chloride and nickel acetate at temperatures of 350–500 °C results in films of cubic NiO phase. Crystallites in NiO films from chloride solution show preferential growth along the (111) plane parallel to the substrate while deposition of nickel acetate solutions results in films where the crystallites are not orientated. The crystallite size increases and the film thickness decreases with the growth temperature. Results of the present study confirm that NiO films obtained by spray of Ni chloride aqueous or alcohol based solutions have uneven thickness, rough surface and porous microstructure while films with uniform thickness and smooth surface can be obtained spraying Ni acetate solutions. The difference in the thermal decomposition of starting chemicals and formation of NiO are the main causes leading to different microstructures. Porous films with rough surfaces could be useful for some applications where high open surface area is an important characteristic (gas sensors) while smooth films with uniform and controlled thickness are required for various electronic and optoelectronic applications.

Li-doped NiO films were obtained by spraying Ni acetate aqueous solutions with additions of LiCl or LiNO₃. According to XRD, sprayed NiO:Li films are of NiO phase where the lattice parameter decreases increasing the Li concentration in the spray solution indicating the insertion of Li atoms into the lattice of nickel oxide. Li-doping supports the growth of crystallites and decreases electrical resistivity. Resistivity decreases from ca 300 to 6.5 Ωcm as the concentration of main charge carriers (holes) increases from ca. 10¹⁶ cm⁻³ to 10¹⁸ cm⁻³ using [Li⁺] of 25 at.% (LiNO₃) in the spray solution. LiCl has been found to be less efficient dopant source as lower carrier densities, in the order of 10¹⁷ cm⁻³, have been recorded using similar deposition conditions. Results of this study show that nickel acetate is potential

starting chemical to make NiO films by spray pyrolysis as no evolution of toxic NO_x gases occurs during precursor thermal decomposition.

ACKNOWLEDGMENTS

This study was financially supported by the Estonian Ministry of Education and Research (IUT19-4) and the Estonian Science Foundation under grant ETF9081 and TK114 "Mesosystems:Theory and Applications" (3.2.0101.11-0029).

REFERENCES

1. BOSCHLOO, G., HAGFELDT, A. Spectroelectrochemistry of Nanostructured NiO. *Journal of Physical Chemistry B*, 2001, Vol. 105, No. 15, p. 3039–3044.
2. ADLER, D., FEINLEIB, J., J. Electrical and Optical Properties of. Narrow-Band Materials. *Physical Review B*, 1970, Vol. 2, No. 8, p. 3112–3134.
3. SVENSSON, J.S., E.,M., GRANQVIST, C.,G. Electrochromic hydrated nickel oxide coatings for energy efficient windows: Optical properties and coloration mechanism. *Applied Physics Letters*, 1986, Vol. 49, No. 23, p. 1566.
4. HOTOVY I., HURAN J., SICILIANO, P., CAPONE, S., SPIESS, L., REHACEK, V. Enhancement of H₂ sensing properties of NiO-based thin films with a Pt surface modification. *Sensors and Actuators B: Chemistry*, 2004, Vol. 103, No. 1–2, p. 300–311.
5. AKINAGA, H., SHIMA, H. Resistive Random Access Memory (ReRAM) Based on Metal Oxides. *Proceedings of the IEEE*, 2010, Vol. 98, No. 12, p. 2237–2251.
6. GILLASPIE, D.,T., TENENT, R.,C., DILLON, A.,C. Metal-oxide films for electrochromic applications: present technology and future directions. *Journal of Materials Chemistry*, 2010, Vol. 20, No. 43, p. 9585.
7. CHIA-CHING, W., CHENG-FU, Y. Investigation of the properties of nanostructured Li-doped NiO films using the modified spray pyrolysis method. *Nanoscale Research Letters*, 2013, Vol. 8, No. 1, p. 33.
8. CATTIN, L., REGUIG, A., B., KHELIL, A., MORSLI, M., BENCHOUK, K., BERNÈDE, J.,C. Properties of NiO thin films deposited by chemical spray pyrolysis using different precursor solutions. *Applied Surface Science*, 2008, Vol. 254, No. 18, p. 5814–5821.
9. REGUIG, B.,A., REGRAGUI, M., MORSLI, M., KHELIL, A.,M. ADDOU, BERNÈDE, J.,C. Effect of the precursor solution concentration on the NiO thin film properties deposited by spray pyrolysis. *Solar Energy Materials and Solar Cells*, 2006, Vol. 90, No. 10, p. 1381–1392.
10. JUYBARI, H., A., BAGHERI-MOHAGHEGHI, M.-M., SHOKOOH-SAREMI, M. Nickel – lithium oxide alloy transparent conducting films deposited by spray pyrolysis technique. *J. Alloys and Compounds*, 2011, Vol. 509, No. 6, p. 2770–2775.
11. DESAI, J., D., MIN, S., -K., JUNG, K., -D., JOO, O., -S. Spray pyrolytic synthesis of large area NiOx thin films from aqueous nickel acetate solutions. *Applied Surface Science*, 2006, Vol. 253, No. 4, p. 1781–1786.
12. ROMERO, R., MARTIN, F., RAMOS-BARRADO, J., R., LEINEN, D. Synthesis and characterization of nanostructured nickel oxide thin films prepared with chemical spray pyrolysis. *Thin Solid Films*, 2010, Vol. 518, No. 16, p. 4499–4502.
13. OTTO, K., KATERSKI, A., MERE, A., VOLOBUJEVA, O., KRUNKS, M. Spray pyrolysis deposition of indium sulphide thin films. *Thin Solid Films*, 2011, Vol. 519, No. 10, p. 3055–3060.
14. PDF 00-047-1049. ICDD PDF–2 Release 2008.
15. PATIL, P., KADAM, L. Preparation and characterization of spray pyrolyzed nickel oxide (NiO) thin films. *Applied Surface Science*, 2002, Vol. 199, No. 1–4, p. 211–221.



ZINC OXIDE RODS ON DIFFERENT TCO SUBSTRATES AND SEED LAYERS BY ELECTROCHEMICAL DEPOSITION

I. Gromyko, T. Dedova, M. Krunkas, V. Mikli, T. Unt, I. Oja Acik, A. Mere

*Tallinn University of Technology
Ehitajate str. 5, 19086 Tallinn – Estonia*

ABSTRACT

For hybrid organic/inorganic solar cells with “ITO/blocking layer/ZnO nanorod/absorber layer” structure, it is highly important to synthesize series of ITO/blocking layer/ZnO nanorod structures by simple, inexpensive and low temperature technique. In order to increase the solar cell performance, it is desired to obtain high aspect ratio relatively conductive ZnO nanorods. In this study we present results on growth of ZnO nanorod on different seed layers, such as ZnO with different morphologies, ZnS, TiO₂ compact thin films produced by spray pyrolysis on TCO (transparent conductive oxide) substrates. Also blocking layer could be deposited on a top of ZnO nanorods grown onto TCO directly, therefore in this work we also deposited ZnO nanorods by electrochemical deposition method directly on some chosen TCO substrates. All ZnO nanorod layers were grown electrochemically using ZnCl₂ aqueous solutions ($c=2$ mmol/l) at the bath temperature of 80°C during one hour. Depending on the seed layer morphology, ZnO rods with different dimension, density were obtained. The structural, optical properties and morphology of seed layers and ZnO nanorod layers grown on them were studied by scanning electron microscopy (SEM), x-ray diffraction spectroscopy (XRD).

The dimensions, orientation, shape and density of the rods depends strongly on the properties of the used substrate or seed layer on a substrate.

Morphology and conductivity of the initial substrate plays an important role in ZnO nanorods dimensions, orientations and shape. For instance, larger rods ($d=170$ nm, $L=700$ nm) were obtained on conductive substrates, such as ITO and ZnO:In substrates/ITO glass substrates and FTO substrates ($d=250$ nm, $L=600$ nm). Smaller rods ($d\approx 60$ nm, $L=400$ nm) were obtained on nonconductive smooth, uniform and fine-grained substrates, such as ZnS and TiO₂. Various ZnO seed layers resulted in ZnO nanorods with different shapes, sizes and distribution on the substrate.

Keywords: Zinc oxide, nanorods, electrodeposition, seed layer, SEM, UV-VIS, XRD

INTRODUCTION

Zinc oxide (ZnO) is n-type II-VI semiconductor with a direct band gap (3.37 eV) and large excitation binding energy of 60 meV [1, 2]. ZnO have attracted research interest in recent years due to its potential applications in various nanodevices such as lasers and light emitting diodes [3, 4, 5], gas sensors [1,4], field emissions [1, 4] or solar cells [6].

It has been shown that ZnO nanostructures can be prepared by several techniques such as chemical vapor and metal-organic chemical vapor depositions, vapor-liquid- solid deposition and pulsed laser deposition. There are also solution methods such as chemical bath deposition, spray pyrolysis and electrodeposition can be used to produce ZnO nanostructured layers. Among them, electrodeposition is a promising approach for growing ZnO nanorods, because of its simplicity, low cost, low temperature and easily scalable to large-area deposition [6, 7, 8].

Morphology of the substrate has a particular significance in nanorods growth. In many studies to contribute the rods growth or improve their vertical alignment, a seed layer (ZnO thin film) is required prior to the electrodeposition of the ZnO nanorods [1, 9, 10]. For some applications (emitting diodes, solar cells), it is required to grow ZnO nanorod directly on a transparent conductive oxide [11, 12]. In this paper, we present the study on growth of ZnO nanorods by electrodeposition on various substrates: 1) commercially available indium tin

oxide (ITO) and fluorine doped tin oxide (FTO) coated glass substrates, 2) set of ZnO seed layers with various morphologies prepared by spray pyrolysis onto ITO/glass substrates and 3) ZnS and TiO₂ thin films deposited by spray on ITO/glass substrates. We study the relationship between the initial morphology of the substrate and final morphology of the ZnO nanorod layer. The morphology and structural properties of the substrates and ZnO nanorods deposited on them, respectively, are studied by means of high resolution SEM and XRD.

1. EXPERIMENTAL

1.1. Synthesis details

Prior the deposition, ITO and FTO covered glass substrates were washed thoroughly with soap, ethanol and sulphuric acid. The samples were rinsed with deionised water after each cleaning step. On some chosen ITO and FTO substrates ZnO nanorods were deposited directly on the substrate, but for seed layers deposition commercially available ITO substrates have been chosen.

ZnO seed layers, ZnS and TiO₂ thin films were prepared using spray pyrolysis method as described in details earlier [13, 14].

Electrodeposition of ZnO nanorods was carried out potentiostatically in a three-electrode glass cell. The counter electrode – platinum (Pt) wire, the reference electrode – silver/silver chloride (Ag/AgCl) and the working electrode – ITO/glass. Solution in amount of 50 ml contained 0.2 mmol ZnCl₂ (Sigma-Aldrich) and 0.1M KCl as a supporting electrolyte was utilized. The growth temperature was kept at 80 °C using temperature controlled circulator bath and deposition time was fixed to 1 hour. Electrochemical deposition was done under -1.0V potential, using a Radiometer Analytical potentiostat PGP201.

1.2. Characterization

The morphology of the TCO substrates and ZnO layers was studied by a high resolution scanning electron microscope Zeiss EVO-MA15 at an operating voltage of 10 kV. The crystal structure of the nanorods was characterized by using X-ray diffraction on a Rigaku Ultima IV diffractometer using CuK α radiation ($\lambda=1.5406\text{\AA}$, 40 kV at 40 mA).

2. RESULTS AND DISCUSSION

2.1. Deposition of ZnO rods on TCO electrodes

In this study two different types of conducting electrodes were used: commercially available ITO (In₂O₃:Sn) and FTO (SnO₂:F) coated glass substrates.

The SEM images of the electrodeposited layers of ZnO directly grown on different transparent conductive oxides (TCO) are presented in Fig. 1b, d. Corresponding morphologies of TCO layers are shown in Fig. 1a from ITO and Fig. 1c from FTO. As can be seen from the figures, the final shape of the ZnO nanorods differs depending on the substrate. In case of ITO, the rods are thinner (diameter $d \sim$ ca. 170 nm, length $L \sim$ ca. 700 nm) and (002) top plane is not flat. Rods grown on FTO substrate are thicker ($d \sim$ ca. 300 nm, $L \sim$ ca. 600 nm) and have flat (002) terminations. Such difference can be explained by the difference in the morphology of the substrate as well as in the different conductivity of the substrate. Higher density of the grains on the FTO morphology provoke large amount of nuclei that can further coalesce and promote the lateral growth of the crystal. Same behaviour has already reported for spray pyrolysis deposited nanorods on ITO and FTO substrates [15, 16].

The resistivity of the substrates might be also a reason of such difference in final shape of the ZnO crystals. In our case, the ITO has lower resistivity ($\rho \sim 15\text{--}20 \text{ } \Omega \cdot \text{cm}$) than resistivity of the FTO substrate ($\rho \sim 150 \text{ } \Omega \cdot \text{cm}$). It was reported earlier by Kim et al., that conductive substrates greatly affect on the structural and optical properties of ZnO nanorods [17].

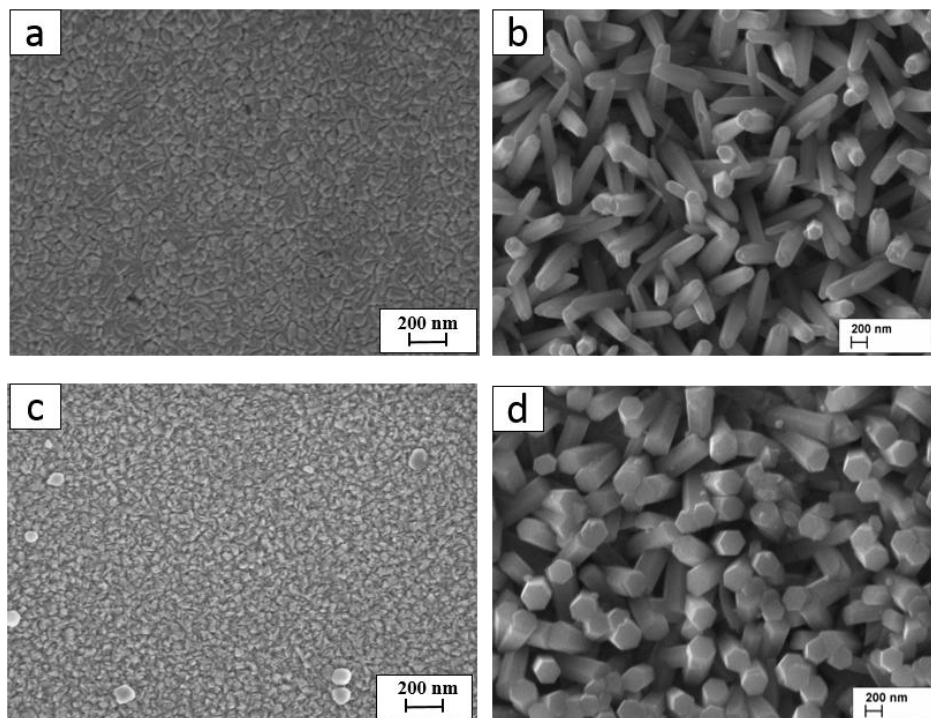


Fig. 1. SEM images of: a) ITO substrate, b) ZnO nanorods grown onto ITO, c) FTO substrate, d) ZnO nanorods grown onto FTO

2.2. Deposition of ZnO nanorods on ZnO seed layers obtained by spray pyrolysis

From previous works on ZnO thin films by spray pyrolysis [18, 19, 20], it was shown that temperature, concentration of the precursor solution (zinc acetate), dopant type and amount are the most important technological parameters that influence the morphology of the film. Here we prepared ZnO seed layers by spray pyrolysis on ITO/glass substrates using concentration of precursor $c=0.05 \text{ mol/l}$ and 0.1 mol/l and temperatures of 320 and $420 \text{ } ^\circ\text{C}$. Also ZnO seed layer doped with indium (3 at%) was deposited from $c=0.2 \text{ mol/l}$ at $T_s=420 \text{ } ^\circ\text{C}$ (ZnO:In). The morphology of ZnO seed layers from $c=0.05 \text{ mol/l}$ and $T_s=320 \text{ } ^\circ\text{C}$ is shown in Fig. 2a, from $c=0.1 \text{ mol/l}$ and $T_s=320 \text{ } ^\circ\text{C}$ in Fig. 2c, from $c=0.1 \text{ mol/l}$ and $T_s=420 \text{ } ^\circ\text{C}$ are presented in Fig. 2e and ZnO:In in Fig. 2g. The SEM images of ZnO nanostructures grown on those seed layers are presented in Fig. 2b, 2d, 2f, 2h, correspondingly.

ZnO seed layer obtained at $320 \text{ } ^\circ\text{C}$ and $c=0.05 \text{ mol/l}$ is compact and flat, composed of densely packed fine grains. As a result, ZnO nanorods grown on this substrate have a diameter of 80 nm and length of ca. 270 nm , and show uniform dense coverage (Fig. 2b). Seed layers from solution with higher concentration ($c=0.1 \text{ mol/l}$) at the same temperature $T_s=320 \text{ } ^\circ\text{C}$ have highly structured surface, reminding ranges, that composed of grains with different sizes (Fig. 2c). Because of such nonuniformity in the dimensions of the grains on this substrate, the sizes of the ZnO rods vary greatly. ZnO nanorods layers compose of smaller crystals ($d \approx 80 \text{ nm}$) and much more larger tilted crystals ($d \approx 300 \text{ nm}$) (Fig. 2d). Seed layers from $c=0.1 \text{ mol/l}$ and higher deposition temperature of $420 \text{ } ^\circ\text{C}$ is also composed

of grains with different shapes including platelets and nanoneedles (Fig. 2e). The ZnO nanostructures grown on this seed layer are mixture of fat and thin compactly standing ZnO rods-like crystals (Fig. 2 d and 2f).

Also the ZnO nanorods have been deposited onto ZnO doped with 3 at% of indium (ZnO:In) seed layer previously grown on ITO. SEM image is presented in Fig. 2g for ZnO:In seed layer and for the resultant ZnO nanorods crystals in Fig. 2h. Rods have uniform dimensions ($d \sim 200$ nm, $L \sim 700$ nm) comparable to those grown on bare ITO layer. Rods grown on ZnO:In are markedly larger, than those grown on ZnO undoped layers, that might be explained with difference in conductivity. ZnO:In layers are much more conductive compared to undoped ZnO films [21, 22].

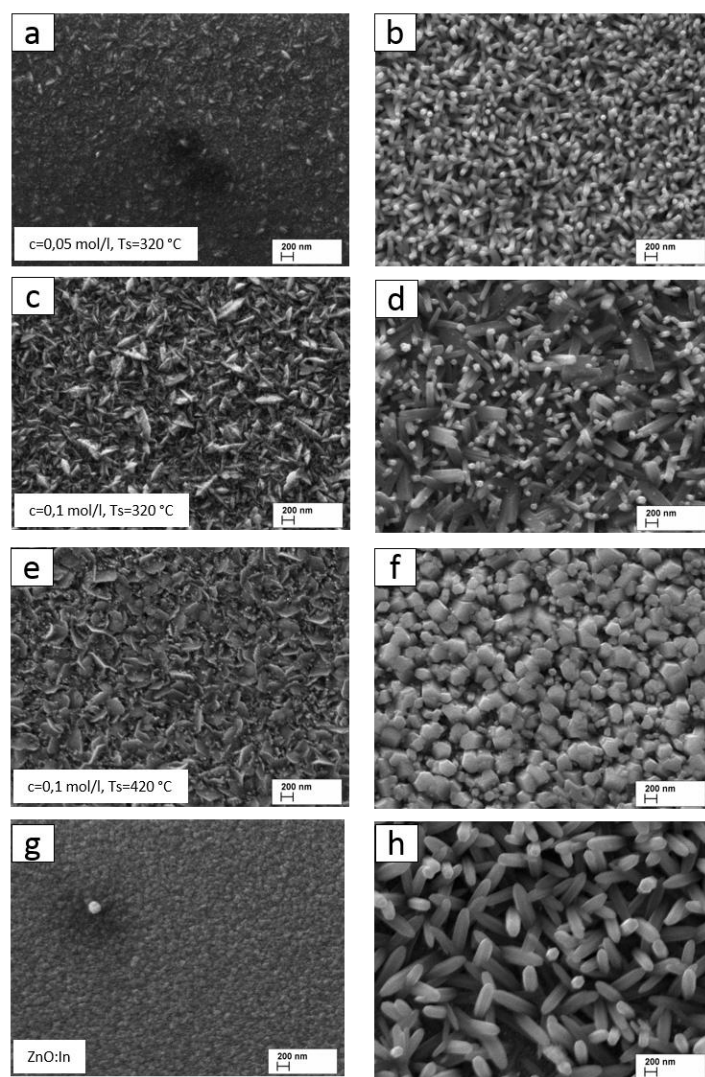


Fig. 2. SEM images of: a) ZnO seed layers by spray of zinc acetate solution with concentration $c=0.05$ mol/l grown at $T_s = 320$ °C; b) ZnO nanorods by electrodeposition on seed layer (a); c) ZnO seed layers by spray of zinc acetate solution with concentration $c=0.1$ mol/l grown at $T_s = 320$ °C; d) ZnO nanorods by electrodeposition on seed layer (c); e) ZnO seed layers by spray of zinc acetate solution with concentration $c=0.1$ mol/l grown at $T_s = 420$ °C; f) ZnO nanorods by electrodeposition on seed layer (e)

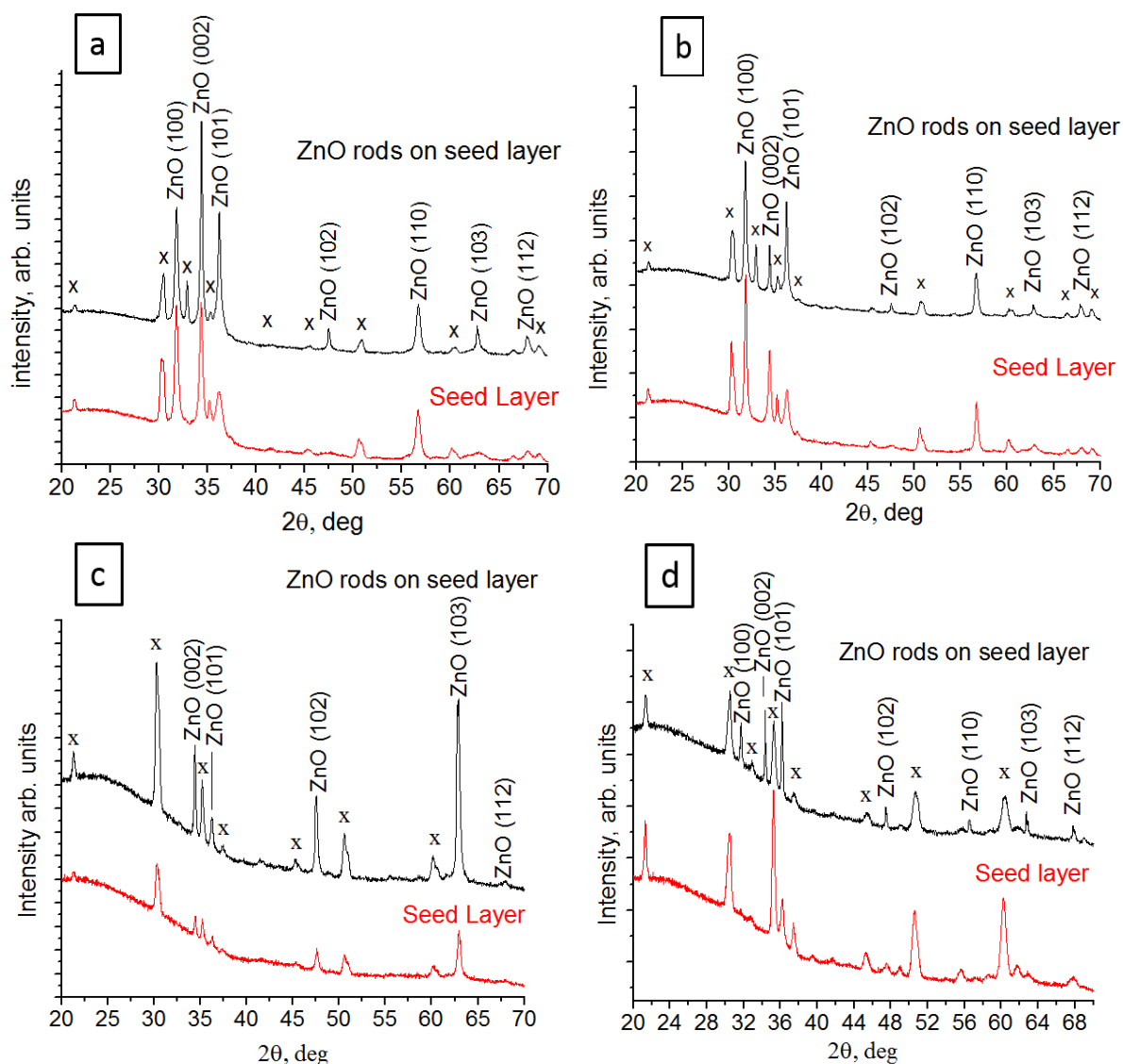


Fig. 3. XRD patterns of the ZnO nanorods deposited on seed layer grown from (a) $c=0.05$ mol/l and $T_s=320$ °C; (b) $c=0.1$ mol/l and $T_s=320$ °C; (c) $c=0.1$ mol/l solution and $T_s=420$ °C. d) ZnO:In; x- reflection from ITO substrate

According to the XRD patterns presented in Fig. 3, all the ZnO seed layers have different crystallographic orientations. For instance, ZnO layer from $c=0.05$ mol/l and $T_s=320$ °C (Fig. 3a) have two main reflections at 2θ of 30.92° and 34.38° corresponding to (100) and (002) planes, respectively with their relative intensity of $I(100)/I(002)=0.9$. The $I(100)/I(002)$ for ZnO layer from $c=0.1$ mol/l and $T_s=320$ °C is nearly two times higher being ca. 1.9 (Fig. 3b). Intensity of (103) plane is very weak for both these layers ($I(103)/I(002)=0.06$ for $c=0.05$, $T_s=320$ °C film, and $I(103)/I(002)=0.1$ for $c=0.1$, $T_s=320$ °C film). Oppositely to the films obtained at $T_s=320$ °C, the (103) reflection is dominant for the ZnO film produced at $T_s=420$ °C ($c=0.1$ mol/l) (Fig. 3c), having the $I(103)/I(002)=\text{ca. } 2.0$. According to XRD pattern of ZnO:In film (Fig. 3d), the intensity of (002) reflection is negligible, which is in a good correspondence to earlier studies [21, 22, 23].

Thus, according to XRD analysis, all ZnO nanorods layer belong to ZnO and direct dependence between the crystallographic orientation of the seed layers and resultant ZnO nanorods was not found.

2.3. Deposition of ZnO nanorods on ZnS and TiO₂ grown by spray on ITO/glass substrates.

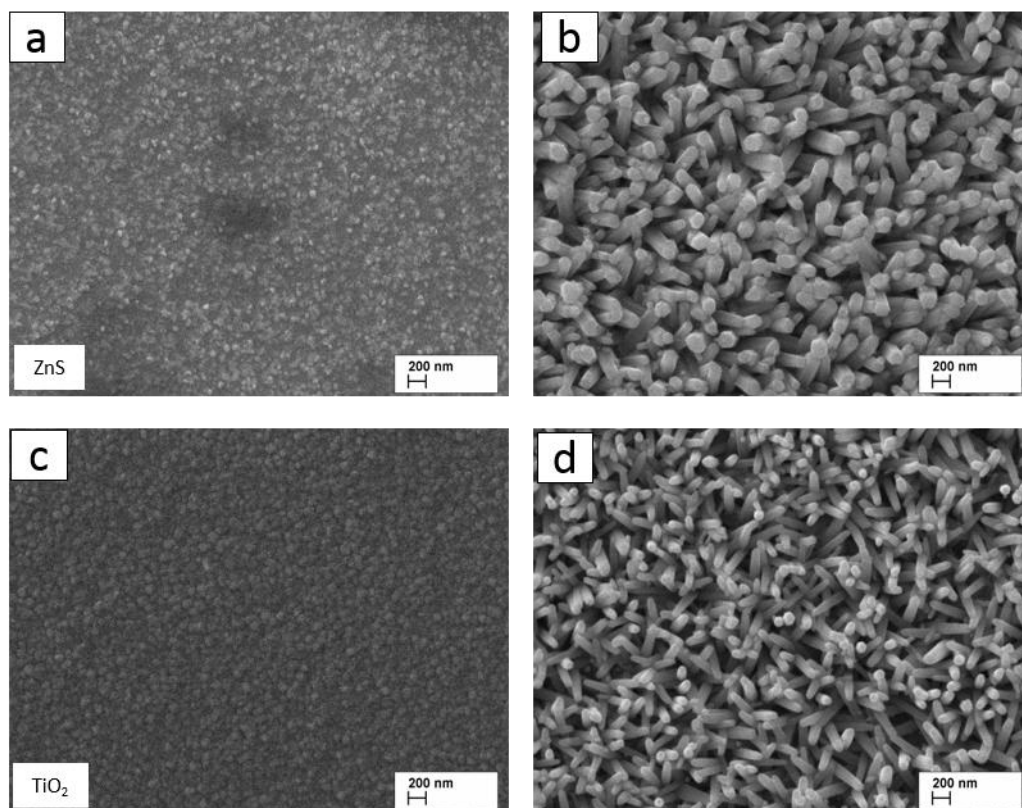


Fig. 4. SEM images of the a) ZnS seed layer; b) ZnO nanorods deposited on seed layer (a); c) TiO₂ seed layer; d) ZnO nanorods deposited on seed layer (c)

For some purposes (dye-synthesized solar cell etc.) it is important to have a nonconductive thin barrier layer between TCO and ZnO nanorods, therefore it is important to found out technological parameters in order to grow nanorods on such types of the substrate. Here we prepared ZnS thin film by spray pyrolysis according to earlier studies on ZnS by spray [24] and TiO₂ by spray [25]. Both ZnS and TiO₂ have smooth morphologies according to SEM images (see Figs. 4a and 4c). Both substrates resulted in very uniform, dense coverage well-shaped hexagonal nanorods. The dimension of the rods grown onto ZnS are slightly larger, than those grown on TiO₂, being $d=150$ nm, $L=450$ nm for ZnS and $d=60$ nm and $L=370$ nm for TiO₂. The difference in rods dimensions could be explained with different surface roughness on ZnS and TiO₂ seed layers. To study the surface roughness of the samples, additional AFM measurements are needed.

CONCLUSIONS

Herein we presented the study on growth of ZnO nanorods by electrodeposition on various substrates: 1 commercially available ITO, FTO substrates on glass, 2 set of ZnO seed layers on ITO/glass substrates prepared by spray pyrolysis with various morphologies and 3 ZnS and TiO₂ thin films deposited by spray on ITO/glass substrates. The dimensions, orientation, shape and density of the rods depends strongly on the properties of the used substrate or seed layer on a substrate.

Morphology and conductivity of the substrate plays an important role in ZnO nanorods dimensions, orientations and shape. For instance, larger rods ($d \sim$ ca.170 nm, $L \sim$ ca.700 nm) were obtained on conductive substrates, such as ITO and ZnO:In buffer/ITO glass substrates and FTO substrates ($d \sim$ ca.250 nm, $L \sim$ ca.600 nm). Thinner and shorter rods ($d \sim$ ca.60 nm, $L \sim$ ca. 400 nm) were obtained on smooth, uniform and fine-grained seed layers, such as ZnS, TiO₂ and ZnO layer grown by spray of 0.05 mol/l zinc acetate solution at $T_s=320$ °C.

ACKNOWLEDGEMENTS

This work is financially supported by the Estonian Ministry of Education and Research (IUT 19-4), TUT base financing project B24 and European Regional Development Fund through the projects: Centre of Excellence “Mesosystems: Theory and Applications” (MESO) TK114, 3.2.0101.11-0029 and project “Efficient plasmonic absorbers for solar cells” 3.2.1101.12-0023.

REFERENCES:

1. YI, G.-C., WANG, C., PARK, W.I. ZnO nanorods: synthesis, characterization and applications. *Semiconductor Science and Technology*, 2005, Vol. 20, No. 4, p. 22–34.
2. WANG, Z.L., Zinc oxide nanostructures: growth, properties and Applications. *Jornal of Physics: Condensed Matter*, 2004, Vol. 16, No. 25, p. 829–858.
3. FAN, J.C., CHANG, S.L., XIE, Z. ZnO-Based Light-Emitting Diodes. InTech, 2013. 485 p. ISB 978-953-51-0922-8.
4. WEINTRAUB, B., ZHOU, B., LI, Y., DENG, Y. Solution synthesis of one-dimensional ZnO nanomaterials and their applications. *Nanoscale*, 2010, Vol. 2, No. 9, p. 1573–1587.
5. YIN, Z., WU, S., ZHOU, X., HUANG, X., ZHANG, Q., BOEY, F., ZHANG, H. Electrochemical Deposition of ZnO Nanorods on Transparent Reduced Graphene Oxide Electrodes for Hybrid Solar Cells. *Small*, 2010, Vol. 6, No. 2, p. 307–312.
6. ELIAS, J., CLAUDE, L.-C., BECHELANY, M., MICHLER, J., WANG, G.-Y., WANG, Z., PHILIPPE, L. Hollow Urchin-like ZnO thin films by Electrochemical Deposition. *Advanced Materials*, 2010, Vol. 22, No. 14, p. 1607–1612.
7. PAUPORTE, T., BATAILLE, G., JOULAUD, L., VERMERSCH, F.J. Well-Aligned ZnO Nanowire Arrays Prepared by Seed-Layer-Free Electrodeposition and Their Cassie–Wenzel Transition after Hydrophobization. *The Journal of Physical Chemistry C*, Vol. 114, No. 1, p. 194–202.
8. KIM, H., MOON, J.Y., LEE, H.S. Temperature Dependence of the Growth of ZnO Nanorod Arrays by Electrochemical Deposition. *Electronic Materials Letters*, 2011, Vol. 7, No. 1, p. 59–62.
9. KIM, D.C., HYUN KONG, B., CHO, H.K. Morphology control of 1D ZnO nanostructures grown by metal-organic chemical vapor deposition. *Journal of Materials Science: Materials in Electronics*, 2008, Vol. 19, p. 760–763.
10. YIN, Y.T., QUE, W.X., KAM, C.H. ZnO nanorods on ZnO seed layer derived by sol–gel process. *Journal of Sol-Gel Science and Technology*, 2010, Vol. 53, No. 3, p. 605–612.
11. LEE, H.K., KIM, M.S., YU, J.S. Effect of AZO seed layer on electrochemical growth and optical properties of ZnO nanorod arrays on ITO glass. *Nanotechnology*, 2011, Vol. 22, No. 44, 445602.
12. MASYDA, Y., KATO, K. Aqueous Synthesis of ZnO Rod Arrays for Molecular Sensor. *Crystal Growth & Design*, 2009, Vol. 9, No. 7, p. 3083–3088.

13. DEDOVA, T., KRUNKS, M., OJA ACIK, I., KLAUSON, D., VOLOBUJEVA, O., MERE, A. Hierarchical nanostructures of ZnO obtained by spray pyrolysis. *Materials Chemistry and Physics*, 2013, Vol. 141, No. 1, p. 69–75.
14. KRUNKS, M., DEDOVA, T., OJA ACIK, I. Spray pyrolysis deposition of zinc oxide nanostructured layers. *Thin Solid Films*, 2006, Vol. 515, No. 3, p. 1157–1160.
15. DEDOVA, T., OJA ACIK, I., KRUNKS, M., MIKLI, V., VOLOBUJEVA, O. Effect of substrate morphology on the nucleation and growth of ZnO nanorods prepared by spray pyrolysis. *Thin Solid Films*, 2012, Vol. 520, No. 14, p. 4650–4653.
16. DEDOVA, T., VOLOBUJEVA, O., KRUNKS, M., MIKLI, V., GROMYKO, I., KATERSKI, A., MERE, A. Growth of Zinc Oxide Rods on FTO Electrodes by Spray Pyrolysis. IOP Conference 2013. International conference on functional materials and nanotechnologies. Estonia: University of Tartu, Institute of Physics, 2013 April 21–24.
17. KIM, H., MOON, J. Y., LEE, H.S. Growth of ZnO Nanorods on Various Substrates by Electrodeposition. *Electronic Materials Letters*, 2009, Vol. 5, No. 3, p. 135–138.
18. KRUNKS, M., MELLIKOV, E. Zinc oxide thin films by the spray pyrolysis method. *Thin Solid Films*, 1995, Vol. 270, No. 1–2, p. 33–36.
19. DEDOVA, T., KLAUSON, J., C. BADRE, C., PAUORTE, Th., NISUMAA, R., MERE, A., VOLOBUJEVA, O., KRUNKS, M. Chemical spray deposition of zinc oxide nanostructured layers from zinc acetate solutions. *Physica Status Solidi A*, 2008, Vol. 205, No. 10, p. 2355–2359.
20. KRIISA, M., KARBER, E., KRUNKS, M., MIKLI, V., UNT, T., KUKK, M., MERE, A. Growth and properties of ZnO films on polymeric substrate by spray pyrolysis method. *Thin Solid Films*, 2014, Vol. 555, p. 87–92.
21. KRIISA, M., KRUNKS, M., KARBER, E., KUKK, M., MIKLI, V., MERE, A. Effect of Solution Spray Rate on the Properties of Chemically Sprayed ZnO:In Thin Films. *Journal of Nanomaterials*, 2013, Vol. 2013, p. 1–9.
22. WIENKE, J., BOOIJ, A. S. ZnO. In deposition by spray pyrolysis – Influence of the growth conditions on the electrical and optical properties. *Thin Solid Films*, 2008, Vol. 516, No. 14, p. 4508–4512.
23. SONG, J., LIM, S. Effect of Seed Layer on the Growth of ZnO Nanorods. *The Journal of Physical Chemistry C*, 2007, Vol. 111, No. 2, p. 596–600.
24. DEDOVA, T., KRUNKS, M., GROMYKO, I., MIKLI, V., SILDOS, I., UNT, T. Effect of Zn:S molar ratio in solution on the properties of ZnS thin films and the formation of ZnS nanorods by spray pyrolysis. *Physica status solidi A*, 2014, Vol. 211, No. 2, p. 514–521.
25. OJA ACIK, I., JUNOLAINEN, A., MIKLI, V., DANILSON, M., KRUNKS, M. Growth of ultra-thin TiO₂ films by spray pyrolysis on different substrates. *Applied Surface Science*, 2009, Vol. 256, No. 5, p. 1391–1394.

FORCE CHAINS AS THE MAIN MECHANISM OF THERMAL CONDUCTIVITY OF GRANULAR MATTER UNDER STRESS

P.S. Grinchuk, S.M. Danilova-Tretiak, N.I. Stetukevich

A.V. Luikov Heat- and Mass Transfer Institute

P. Brovka str., 15, 220072, Belarus

ABSTRACT

The hypothesis is made about the force chains in granular media under external mechanical loads (namely compression) influence on heat transfer in such media, in particular, on their effective thermal conductivity. To verify this suggestion the experimental setup was constructed. Its principle of operation is based on the analogy between electric conductance and thermal conductance. The tablets of activated carbon were used to form two-dimensional heterogenic bed as they are characterized with appropriate combination of physical properties. The force chains in such system appear when electric current is conducted through it under mechanical load. The thermal pattern formed during the process was registered by high accuracy thermal camera. Force chains were observed even in regular particulate beds. For the first time the experimental proof of force chains influence on heat transfer in particulate beds is obtained.

Keywords: granular matter, force chains, thermal conductivity

1. INTRODUCTION

In nature and in technics there is a large number of heterogeneous media, for example porous soils, filling for heat exchangers, thermal insulation etc. [1]. Many applications of heterogeneous media are closely associated with heat transfer in such materials. Heat can be transferred through heterogeneous media due to three mechanisms. Radiative heat transfer from particle to particle by the pore space dominates at high temperatures [2]. Convective heat transfer is realized in the case of forced filtration of gas in the pore space or in high-porous media [3]. Conductive heat transfer is implemented always through the solid skeleton of porous body. The aim of this paper is studying of peculiarities of contact heat exchange in heterogeneous unconsolidated backfill. It should be noted that contact heat exchange play an important role in energetics. It determines the intensity of heat removal from reactor fuel elements. The same mechanism of heat exchange influences on efficiency of thermal insulation in the form of beds which is used both in hot-water or steam boilers and high-temperature units of metallurgical works.

There are a lot of papers in which the problem of the effective thermal conductivity of granular media and fillings was studied experimentally and theoretically [4–8]. The method of averaging over the representative volume is used for description the heat transfer in such media due to the complex geometry of their internal space. A large number of empirical coefficients are used for description of the experimental results. Recent trends in this area of research related to obtaining a large volume of information about the microstructure of a heterogeneous media [7]. In traditional models of heat transfer processes in heterogeneous media it is supposed that in average all particles of the system are included in the process of conductive heat transfer in heterogeneous backfilling. However, recent results about the mechanics of granular media [8] show that the process of conductive heat transfer in granular media is different from this point of view.

The contact spot between two particles plays an important role in conductive heat transfer through granular medium. This process limits conductive heat transfer in most cases.

Contact thermal resistance strongly depends on the compression force applied to two contact surfaces [9]. We can assume that in the granular backfill of identical balls pairwise contact forces are distributed uniformly. Then contact heat transfer must be the same in all parts of the system. This is not true however. It has been shown that mechanical stress in the fillings is distributed nonuniformly [8]. Force chains are formed in the medium under external load [8, 10, 11] (Fig. 1). Physical explanation of these structures is quite simple. The load-bearing skeleton of particles is formed inside filling under external load. Significant part of particles plays a role of ballast in terms of force transmission. The preferred direction of force chains is correlated with direction of external load vector. All the foregoing allows authors to make the following assumption. *The conductive heat transfer through the solid phase of granular backfill should take place primarily along force chains arising under the external load and also under the action of own gravity of particles.* The main objective of the work is to find experimental proof of such mechanism domination in the process of conductive heat transfer in granular unconsolidated media.

2. BACKGROUND

Let us briefly examine the history of the problem of force chains in granular media. The first experimental observation of force chains we found in the article [8]. Observation technique is described in [8, 10]. Two-dimensional filling of the disks on the plane is considered. An important aspect of the experiments is application of disks made of optically transparent photoelastic plastic. Optical anisotropy and birefringence occur in the disks under mechanical stresses. We can observe the particles subjected to mechanical stress under transillumination of the system using polarized light (Fig. 1).

We can try to fix the heat distribution correlated with the force chains by heating of the system at the boundary. This approach encounters the principal problem. The heating of even one disk requires a large time. The heating time is $\tau \sim d^2 \rho c_p / (4\lambda) \approx 100 \text{ s}$ ($\lambda \approx 0.1 \text{ W/(m K)}$, $\rho \approx 1000 \text{ kg/m}^3$, $c_p \approx 1500 \text{ J/(kg K)}$) for a plastic disk with a typical diameter of 5 mm. The heating time is only 1 s for similar steel disc. But heat propagation from disc to disc is determined by thermal contact resistance, which is 30–50 times higher than thermal resistance of the steel disc itself. This is confirmed by experimental results [12]. Therefore, the heating of the steel disks array will be slow also. 10–15 disks should be heated in order to force chain revealed. That is to say that characteristic heating time should be about 10–20 minutes excluding the effect of heat loss. Necessity of detection and visualization of force chains will not allow the application of two-side thermal insulation. Inevitably existing heat losses in two-dimensional system negate the thermal pattern of force chains and it is difficult to evaluate their role in heat transfer. We can expect that in three-dimensional system due to the local environment of the particle the qualitative picture of heat propagation will be different.

We found in the literature the mention of interrelation of force chains with thermal conductivity of granular media only in two articles [12, 13]. In those works authors used the term "stress chains". They have suggested that heterogeneity in the contact and contact forces distribution is expected to play an important role in heat conduction in granular material.

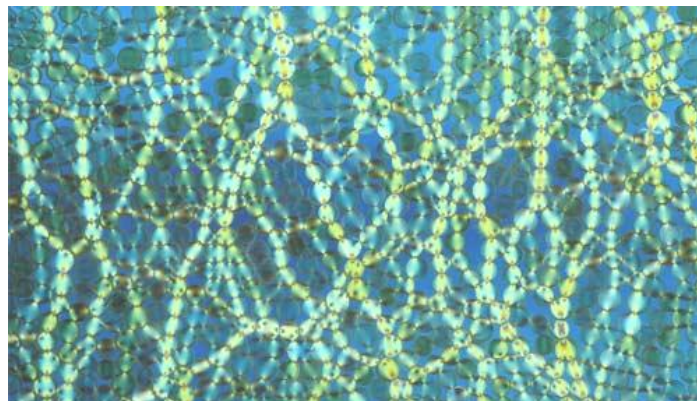


Fig. 1. The example of experimental visualization of force chains arising in granular media under an external force [11]

The influence of compression on the effective conductivity of granular medium was investigated in the same paper. That is the only experiment which is relevant to our work. The authors of [12] regarded a monolayer of steel disks, which were compressed in one direction. Directions of applied stress and gravity force were perpendicular to each other. Two opposite walls of the system could be heated due to hot water pumping. The disks were covered with liquid-crystal plate for optical registration of temperature field of the system. The system was loaded mechanically by calibrated springs and heated from one side during 2 hours after removing of several disks. The authors have observed weak disturbance of temperature field (position of isotherms differs from straight line by 5–10% after 2-hour heating) and submitted it as an argument of force chains influence on heat transfer. But in our opinion this disturbance can have a few reasons and the results obtained in [12] can't prove the influence of force chains on thermal conductivity of granular medium under stress. They just confirm our assumption that direct observing of heat transfer along force chain is impeded even if the system is characterized with free convection outward heat losses ($\alpha \approx 1\text{--}2 \text{ W/m}^2\cdot\text{K}$).

The theoretical model of force chains influence on effective thermal conductivity of granular beds was suggested in [13]. Calculated dependence of effective thermal conductivity on external stress was obtained. The authors supposed about correlation between force chains and transfer processes also. But unfortunately, there are no any theoretical or experimental results which could clear state about significant input of force chains into heat transfer.

So, the question about correlation between force chains and heat transfer in granular beds remains open.

3. METHODOLOGY

The clear experimental demonstration is absent for influence of force chains on thermal conductivity of granular media. For experimental validation of correlation between force chains and thermal conductivity in granular medium we propose the original experimental technique.

The object under investigation is two-dimensional system of disks as well. The main differences of our work are in following. For the first, to prove the influence of force chains on heat transfer we use the analogy between thermal and electrical conductivity [9, 14–16]. For example, in stationary state the temperature distribution and distribution of the electric charge in the system is described with Poisson equation. A number of models of contact thermal conductivity are based on analogy with electrical contacts [9]. But the main argument to this analogy is Wiedemann-Franz law [16]. This law connects thermal conductivity and electrical conductivity of solid bodies. According to this law the ratio of thermal conductivity λ to the electrical conductivity σ of conductor is proportional to the temperature T (1).

Proportionality factor depends on fundamental physical constants only – Boltzmann's constant k and electron charge e .

$$\frac{\lambda}{\sigma} = KT = \frac{\pi^2}{3} \left(\frac{k}{e} \right)^2 T \quad (1)$$

In [10] the disks were made from photoelastic plastic which is good electrical isolator (specific resistance $\sim 10^{14}$ Ohm·m) and has low thermal conductivity (~ 0.2 W/(m·K)). In [12] the system consisted of metallic disks which have high thermal conductivity (~ 30 W/(m·K)) and high electrical conductivity (specific resistance $\sim 1.5 \cdot 10^{-7}$ Ohm·m). In our work we used activated carbon to form heterogeneous two-dimensional bed. This material is characterized with intermediate physical properties between metal and plastic ones. The value of electrical conductivity of activated carbon determines its considerable resistive heating while current passing. At the same time the velocity of heat propagation in activated carbon tablets is not as high as in metal. It allows observe the evolution of temperature field in time.

The next distinction of our work is using of resistive electrical heating. The current passes directly through the disks system. The system must conduct preferentially through the ways of least resistance that is along force chains. The contacts between tablets are the places of highest resistance in the force chain itself. So, most intensive heat release will occur in these places. Temperature field registration by high-accuracy thermal camera allows visualizing force chains in two-dimensional granular system. On the basis of mentioned analogy we can consider the ways of preferential current passing as the ways of more probable heat flux propagation in the system. We suppose that force chains for current passing in beds of thermal conductive and electrical conductive particles are the force chains for heat transfer also.

The experimental setup for hypothesis test is shown in Fig. 2. Acrylic-plastic base is fixed rigidly to the support under some slope to hold the tablets on the plane. Four bars bound the system. Vertical bars are fixed rigidly and have electrical isolated spacers. Horizontal ones are made from copper. Due to oval holes they are movable within 3–4 mm that is comparable with disks (tablets) radius. Electric potential is applied to horizontal bars and due to this the electric current passes through the system. Simultaneously screws allow creating controlled mechanical load. Load value is measured with electronic balance which is placed between lower movable copper bar and the support (the accuracy of measurements is 1 g). To provide more uniform electrical contact and mechanical load distribution the resin spacer covered with aluminium foil is placed between upper bar and disks.

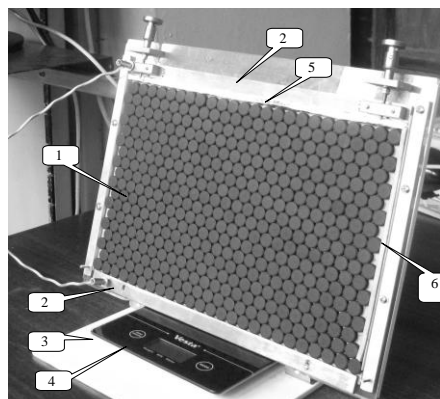


Fig. 2. The experimental setup: 1 – two-dimensional regular heterogeneous bed; 2 – copper movable bars-electrodes; 3 – setup base which is fixed rigidly to the support for disks; 4 – electronic balance; 5 – resin spacer covered with aluminium foil; 6 – resin spacer for working space dimensions correction

The size of setup working space is 280×180 mm. Initially all disks were packed as regular hexagonal system to prevent the influence of structure defects on the process under investigation. The system contained 18 rows of 24 disks (Fig. 3a). The tablets are 11 mm in diameter and 4 mm in height. The mass of one tablet is 0.33 g, total tablets mass is 143 g. Current is within 100...350 mA, potential difference is 20...60 V. The value of mechanical load is 10...600 g that is 4 times higher than all disks mass.

Under high loads the deformations of the structure (tablets ejection) or tablets destruction could occur. The electric current passed through the system during about 1 min. That led to heating of local places characterized with highest contact resistance. These places belong to force chains. Temperature field of the system registered with high accuracy thermal camera IRTIS 2000 (Russia). It's sensitivity is 0.05°C . The room temperature during the experiment was 19°C .

Aside from regular hexagonal system we considered the system with defect – polypropylene ring which is excellent electrical insulator. It should be noted that the ring was cut to place it toughly to “empty” hexagon.

4. RESULTS AND DISCUSSION

The experimental results visualized force chains which are involved in energy transfer in two-dimensional bed of identical carbon disks of the system are shown in Fig. 3. If mechanical load was distributed uniformly through all disks, the resistance of all contacts in the system would be the same because of symmetry. In this case we would observe the uniform temperature field over the system. However it is seen that under stress even in ordered system the current passes through definite chains but not through all possible pairwise contacts. That are force chains we emphasize. The results of our experiments proved that increase of external mechanical load doesn't lead to formation of new force chains but leads just to change in existing chains resistance and current value passing through them. The thermograms were placed on visible pictures of initial structure for better visualization of force chains (Fig. 3e, f). The current value for mentioned case is 250 mA, external mechanical load is 360 g, potential difference is 41 V, system resistance under stress is 194 Ohm. It is seen clearly that most intensive heating is observed in particles contacts. As follows from the Ohm law the current will pass preferentially through subcircuits with least resistance. The heating-up value of such chains is inversely proportional to its resistance as $\Delta T \sim 1/R$. The values of ΔT registered by thermal camera were equal to $5\text{--}7^{\circ}\text{C}$ during 1 min. At the same time adjacent areas temperature increased by 0.5°C . This allows us to evaluate force chains resistance as by one order of magnitude less than resistance of adjacent areas that don't belong to force chains we have observed.

The system with artificial defect is shown in Fig. 3b. In this case current value is 250 mA, external mechanical load is 300 g, potential difference is 53 V, system resistance under stress is 197 Ohm. Deformation of the ring caused additional elastic force that pressed the tablets one to another. Additional source of mechanical loads leads to redistribution of force chains structure and consequently to change of thermal image during electric current passing (Fig. 3d, f).

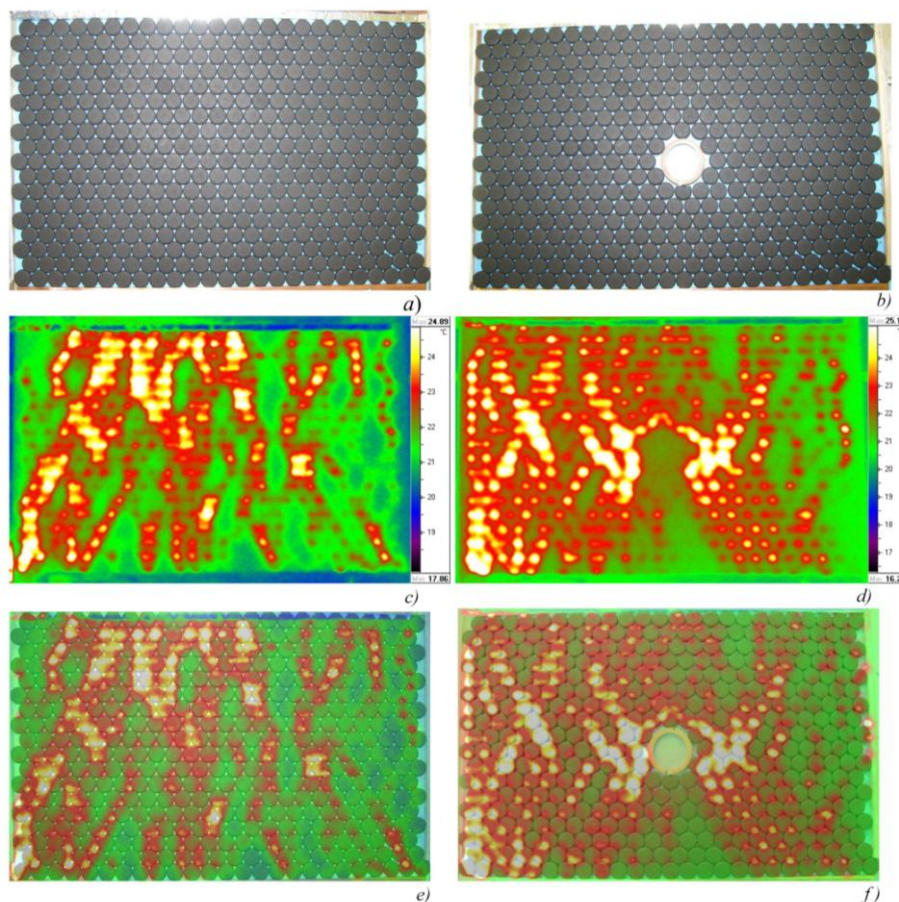


Fig. 3. Force chains vizualization: a) initial hexagonal two-dimensional structure of activated carbon tablets; b) initial structure with artificial defect; c) thermogram of the initial structure during current passing; d) thermogram of the structure with defect during current passing; e), f) thermograms placed on visible pictures of initial structure

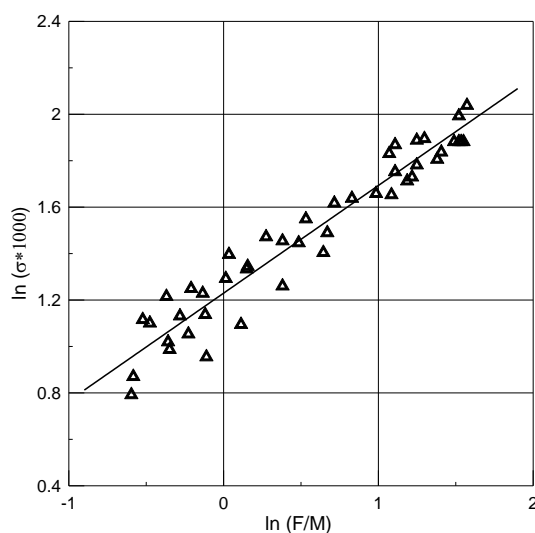


Fig. 4. Measured electrical conductivity σ (S) of the system versus external mechanical load in log-log plot. Mechanical load is normalized to own weight of all carbon disks, which is taken into account while load calculation

The correlation between conductivity and external load is important for understanding of common mechanism of energy transfer in granular medium under stress. We measured the electric conductivity of the system in hand under different external loads. The results are presented in Fig. 4. Conductivity is in inverse proportion to resistance. Load is normalized to own weight of all disks. In log-log plot the dependence of conductivity on load is linear (Fig. 4). It means that correlation between load and conductivity should have exponential character, and exponent can be found from curve slope. We received the next functional dependence:

$$\sigma \sim F^{0,46} \quad (2)$$

The next fact is worth to say. It can be expected that contact conductivity is proportional to contact spot square of two bodies. The square depends on external load. In a first approximation the correlation between contact spot square and external load could be found from the solution of Hertz problem - the problem of the theory of elasticity [17]. This problem has precise solutions. During spheres compression with effort F the radius of contact spot square depends on force as $a \sim F^{1/3}$ and spot square correlate with force as $S \sim F^{2/3}$. During cylinders compression (that corresponds to our model system) the width of contact belt depends on force as $\delta \sim F^{1/2}$. The cylinder height is constant, so contact belt square also depends on force as $S \sim F^{1/2}$, that is to say in a first approximation that $\sigma \sim F^{1/2}$. Experimentally obtained correlation between model system conductivity and external load (2) fits forecited qualitative conclusions. So we can suppose that conductivity of granular bed under stress is determined by force chains in the system. Force influence is defined, for the first, by change of contact square between particles. The experimental results allow to conclude that change (increase in the range described above) of external load in static bed doesn't lead to creation of new force chains in the system but causes just change of intensity of transfer processes along already existing chains.

5. CONCLUSIONS

So, conductive heat transfer through granular medium under stress occurs with varied intensity through different particles. There are chains of particles (force chains) which serve as prevailing ways of heat transfer. The first experimental observation of force chains influence on conductive heat transfer in granular medium under stress is presented in this paper.

ACKNOWLEDGMENTS

The authors gratefully acknowledge the assistance of Chernukho E.V., Prohorov A.N., Roschin Yu.Yu. (collaborators of radiative-convective heat exchange laboratory of A.V. Luikov Heat&Mass Transfer Institute of the National Academy of Sciences of Belarus).

REFERENCES

1. JAEGER, H.M., NAGEL, S.R., BEHRINGER, R.P. Granular solids, liquids, and gases. *Reviews of Modern Physic*, 1996, Vol. 68, No. 4, p. 1259–1273.
2. CHENG, G.J., YU, A.B. Particle Scale Evaluation of the Effective Thermal Conductivity from the Structure of a Packed Bed: Radiation Heat Transfer. *Industrial and Engineering Chemistry Research*, 2013, Vol. 52, No. 34, p. 12202–12211.



3. PAVLYUKEVICH, N.V. *Introduction into the Theory of Heat- and Mass Transfer in Porous Media*. Minsk. A.V. Luikov Heat- and Mass Transfer Institute, 2002. 140 p. (in Russian).
4. WIDENFELD, G., WEISS, Y., KALMAN, H. The effect of compression and preconsolidation on the effective thermal conductivity (ETC) of particulate beds. *Powder Technol.*, 2002, Vol. 133, p. 15–22.
5. BAHRAMI, M., YOVANOVICH, M.M., CULHAM, J.R. Effective thermal conductivity of rough spherical packed beds. *Int. J. Heat Mass Transfer*, 2006, Vol. 49, p. 3691–3701.
6. JAGOTA, A., HUI, C.Y. The effective thermal conductivity of a packing of spheres. *J. Appl. Mech.*, 1990, Vol. 57, p. 789–791.
7. WEIDENFELD, G., WEISS, Y., KALMAN, H. A theoretical model for effective thermal conductivity (ETC) of particulate beds under compression. *Granular Matter*, 2004, Vol. 6, p. 121–129.
8. LIU, C.-H., NAGEL, S. R., SCHECTER, D. A., et all. Force Fluctuations in Bead Packs. *Science*, 1995, Vol. 269, No. 5223, p. 513–515.
9. MESNYANKIN, S.YU., VIKULOV, A.G., VIKULOV, D.G. Solid-solid thermal contact problems: current understanding. *Physics Uspekhi*, 2009, Vol. 52, p. 891–914.
10. MAJMUDAR, T.S., BEHRINGER, R.P. Contact force measurements and stress-induced anisotropy in granular materials. *Nature*, 2005, Vol. 435, p. 1079–1082.
11. Official site of the American Physical Society. Section “Physics Images [referred on the 25th of February in 2014 y.]. Link to the internet <<http://www.aps.org/about/physics-images/archive/chains.cfm>>
12. LIU, C.-H., NAGEL, S. R. Sound in a granular material: Disorder and nonlinearity. *Phys. Rev. B.*, 1993, Vol. 48, No. 21, p. 15646–15650.
13. VARGAS, W.L., MCCARTHY, J.J. Stress effects on the conductivity of particulate beds. *Chemical Engineering Science*, 2002, Vol. 57, No. 15, p. 3119–3131.
14. ZHANG, H.W., ZHOU, Q., XING, H.L., MUHLHAUS, H. A. DEM study on the effective thermal conductivity of granular assemblies. *Powder Technology*, 2011, Vol. 205, p. 172–183.
15. BATCHELOR G.K. Thermal or Electrical Conduction Through a Granular Material. *Proceedings of the Royal Society of London. Series A. Mathematical and Physical Sciences*, 1977, Vol. 355, No. 1682, p. 313–333.
16. NIELSEN, L.E. The Thermal and Electrical Conductivity of Two-Phase Systems. *Industrial and Engineering Chemistry Fundamental*, 1974, Vol. 13, No. 1, p. 17–20.
17. ASHCROFT, N.W., MERMIN, N.D. *Solid State Physics*. New York: Holt, Rinehart and Winston, 1976. 826 p.
18. LANDAU, L.D., PITAEVSKII, L. P., KOSEVICH, A.M., LIFSHITZ, E.M. *Theory of Elasticity*. Third Edition: Vol. 7 (Theoretical Physics) 1984. 195 p. ISBN 9780750626330.

THERMAL TRANSFORMATION AND RAMAN STRUCTURAL INVESTIGATION OF THE NANOPOROUS TIN OXIDE

D.V. Solovei, E.V. Batirev, S.A. Filatov, G.S. Kuczynski

A.V. Luikov Heat and Mass Transfer Institute NAS Belarus

P. Brovka str. 15, 220072 Minsk – Belarus

ABSTRACT

Nanoporous tin oxide was synthesized via electrochemical oxidation process of the sputtered metallic tin films at room temperatures. Transformation of nanoporous tin oxide by SEM, Raman scattering and EDX analysis was investigated during thermal annealing from 20 up to 700 °C. After anodization procedure nanoporous oxide layers have nonstoichiometry amorphous structures with average pore diameters about 35–40 nm. Thermal annealing at 400 °C in air atmosphere adduct to the transition from amorphous to crystalline state with Raman peak at 211 cm⁻¹ corresponding to the stannous oxide phase SnO. Increasing of the annealing temperature till 700 °C gives transformation of the crystal lattice from stannous to stannic oxide phase SnO₂ due to final oxidation of tin. This transition from one oxide phase to another is accompanied by appearance of three Raman peaks at 638 cm⁻¹, 476 cm⁻¹ and 780 cm⁻¹. Also thermal annealing enhances the optical transparency of the tin oxide matrices.

Keywords: Nanoporous tin oxide, Thermal annealing, Electrochemical oxidation, Raman scattering

1. INTRODUCTION

Tin oxide is one of the most common materials used in microelectronics, optoelectronics and electronic industry [1]. Transparent electrodes [2, 3], electrodes for lithium battery [4, 5], chemical gas sensors [6–10] are manufactured on the basis of tin oxide; also it is used as a catalyst [11, 12]. Furthermore nanocomposite materials based on tin oxide and carbon allotropic forms are prospective elements for energy storage systems [13, 14]. To improve the electrical, optical and sensory characteristics nanostructured tin oxide increasingly being applied in the shape of thin films [15, 16], nanopowders [17], nanoplates [18, 19], nanocrystals [20, 21], nanowires [22] and nanorods [23, 24]. As is known, because of possessing two metal oxidation states (II and IV) tin may form two oxide phases: stannous oxide – SnO and stannic oxide – SnO₂ [1]. Furthermore, such oxide forms have not only different values of the band gap: $\Delta E(\text{SnO}) = 2.7\text{--}3\text{ eV}$, $\Delta E(\text{SnO}_2) = 3.6\text{ eV}$, but also different types of conductivity: p-type for SnO and n-type for SnO₂ [25, 26]. For the synthesis of nanostructured tin oxide chemical, sol-gel, magnetron sputtering, thermal oxidation of metallic tin, as well as physical – plasma methods are used [15, 17 and 27]. Growing interest of researchers is beginning to acquire an electrochemical method of forming nanoporous tin oxide matrix having a number of advantages: low temperature process, ease of control of geometric parameters of the matrix, the relative safety of the environment [28–31]. However most papers are described the process of a porous tin oxide producing by electrochemical treatment of tin foil or tin, electrochemically deposited on the surface of conductive materials [3, 4, 28–31]. But for practical applications, when tin oxide used as functional material, it is necessary to carry out the electrochemical oxidation of tin metal films sputtered on a dielectric substrate [8].

This paper presents the results of formation of nanoporous tin oxide matrixes obtained by electrochemical anodization of a tin metallic thin films deposited on the dielectric substrate. The investigations of morphology and chemical composition of porous tin oxide

matrixes have been done; temperature conditions for the synthesis of both tin oxide types were determined.

2. EXPERIMENTAL

The thin film layers of tin were formed by thermal vacuum evaporation on a previously cleaned glass substrate with size 26×76 mm. Chemically clean granulated tin were used as the metal source. Thermal sputtering was performed by using vacuum chamber providing vacuum $3 \cdot 10^{-3}$ Pa and using a tungsten boat for evaporation. The thickness of the deposited tin layers was about 1 μm . To improve adhesion to the glass substrate vacuum annealing was applied at 200° C for 2 hours.

Nanoporous tin oxide matrixes were formed by one-step electrochemical anodization process of deposited thin-film layers. The process carried out in aqueous solutions of oxalic acid at a concentration of 0.4 M by potentiostatic mode at ambient temperature. A 5 V anodizing potential was applied, while 6 mA/cm² current densities was measured in an electrochemical system. The platinum foil comparable in size with the anode was used as the counter electrode. After the anodization process obtained films were thoroughly washed by distilled water and dried in a stream of a hot air. For obtaining of stoichiometric porous tin oxide matrixes thermal annealing in air atmosphere was applied. The temperature range 200–700° C was used with increments to 100° C and duration of annealing procedure at each step was about 2 hours.

Surface morphology and cross section of the porous matrix was investigated by the scanning electron microscope Supra 55 at accelerating voltage 3 kV. Microanalysis of the obtained materials was carried out by using energy dispersive x-ray spectroscopy system (EDX-analysis) Inca 350 based on the electron microscope described above. Detailed analysis of the structural changes was performed using FT-IR spectrometer Nicolet Nexus with an attachment for registration Raman scattering (RS), equipped with a liquid nitrogen cooled detector, a laser with 0.5 mm diameter spot size and 0.5 W of 1064 nm laser excitation. IR-filter was used for reducing of the fluorescence and thermal radiation effect from the substrate.

3. RESULTS AND DISCUSSION

3.1. Electron microscopy and EDX-analysis investigations

Fig. 1 shows the scanning electron microscopy (SEM) image of the surface (Fig. 1 a) and cross section (Fig. 1 b) of porous tin oxide matrixes obtained after electrochemical process at room temperatures. As seen from the Fig. 1 a, nanopores are not strictly rounded shapes, but are regularly arranged on the surface of the glass substrate. The average diameter of the nanopores is about 35–40 nm, a minimum diameter of about 15 nm and the maximum around 60 nm. The pores have a parallel arrangement relative to each other and perpendicular relative to the substrate (see Fig. 1 b), which is also defined by the direction of the electric field during the electrochemical process. It is also seen that the outer nanopores diameter is narrower than diameters at the deeper part of the porous oxide. So the average pore diameter inside the matrix is about 80 nm, which is more than twice than on the surface. Pore walls thickness in the range of 5–10 nm. Such thickness is smaller compared with the porous matrixes obtained for the other valve metals (Al, Ti, W) [32, 33]. This phenomenon may be due to increased migration of oxygen atoms within the pores, which is visually expressed in substantial separation of the gas bubbles from the surface of the anode during the anodizing process [34]. The oxygen atoms appears from the oxygen ions which are did not participate in

the oxidation of tin, accumulate in the pores, creating excessive pressure, which leads to expansion of the inner of the pores diameter. Furthermore, excessive release of oxygen encourages the formation of additional nanocracks arising on the surface of the porous matrix, which leads to the formation of the more developed surface area (see Fig. 1 c). The thickness of the porous matrix of tin oxide was about 2.5 μm .

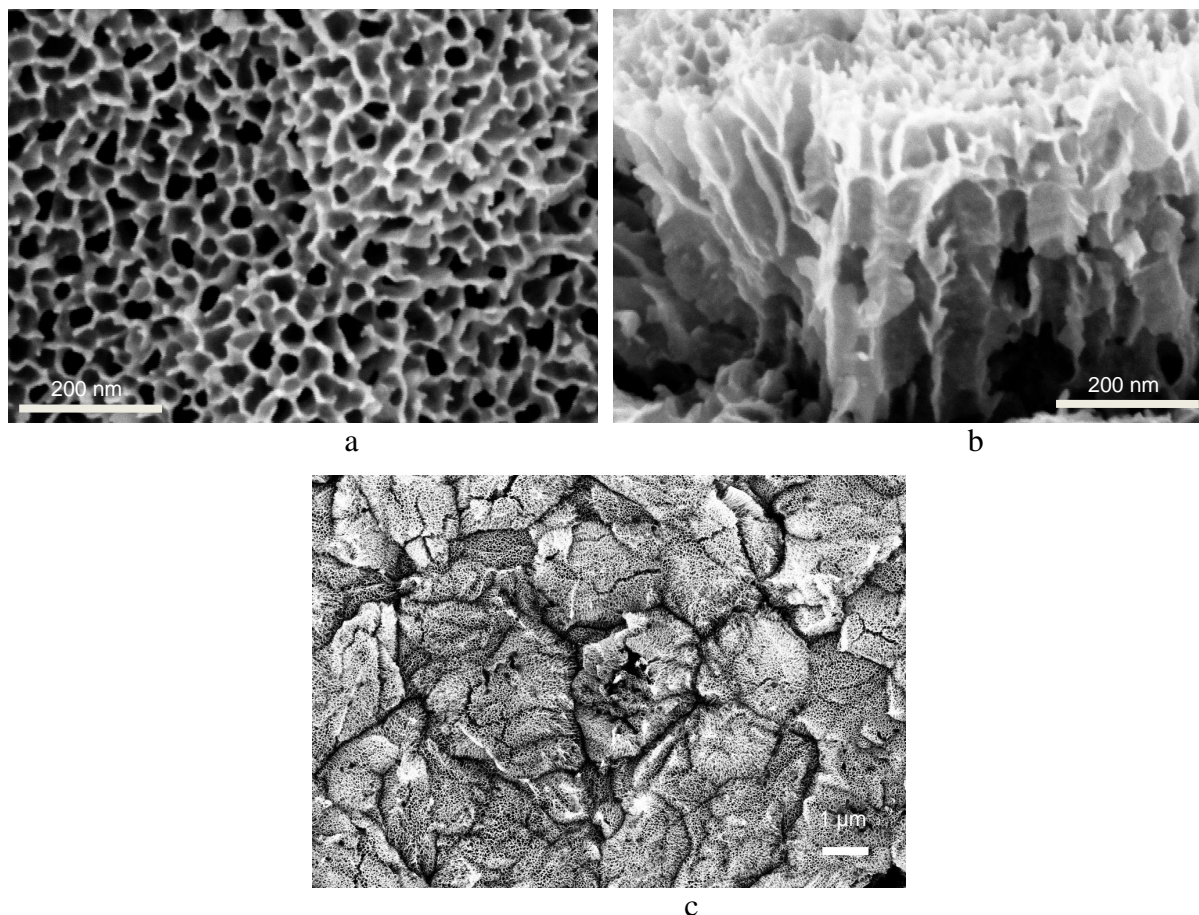


Fig. 1. SEM images of the tin oxide nanoporous matrix fabricated by electrochemical anodizing process at room temperatures: a – detailed view of the surface, b – cross section view, c – panoramic surface view

For the elemental analysis of the anodized nanoporous tin oxide films EDX measurements were performed. The measurement depth of the film was in range 0.5–1.5 μm . This observation revealed that oxide is composed of tin and oxygen. The weight percent ratio of tin and oxygen was found to be about 30% of the oxygen content and the amount of tin – 70%. Atomic ratio of tin and oxygen was determined in the 1:3. In this case two oxygen atoms belong to tin dioxide, and one oxygen atom belongs to the water embedded in the porous matrix structure. As a result a formation of nonstoichiometric nanoporous hydrated tin dioxide ($\text{SnO}_2 \cdot n\text{H}_2\text{O}$) were done.

3.2. Raman scattering chemical composition analysis

Fig. 2 shows Raman spectra of a nanoporous tin oxide films obtained after the electrochemical process without thermal annealing and annealed at various temperatures in an air atmosphere. As can be seen from the figure, in the spectra of not annealed film (curve after

anodizing) any peaks are absent, indicating what the amorphous oxide structure with a nonstoichiometric composition. After annealing at 200 °C the spectra form hardly changed, so this temperature is not sufficient to initiate the crystallization of the porous film. The further increasing of the annealing temperature till 300 °C resulted in a small broad peak in the region of 200 cm^{-1} and the next temperature increase till 400 °C yielded a spectrum line with a clearly defined peak having a maximum at 211 cm^{-1} . This value corresponds to the fundamental vibrations A_{1g} stoichiometric phase tin monoxide SnO [1]. Consequently, annealing at a temperature of 400 °C ensured the transformation of amorphous nanoporous nonstoichiometric tin oxide obtained after the electrochemical anodization in the single-phase stoichiometric SnO . Subsequent increasing of the annealing temperature was aimed on determination of the transition moment from tin monoxide phase to tin dioxide SnO_2 phase.

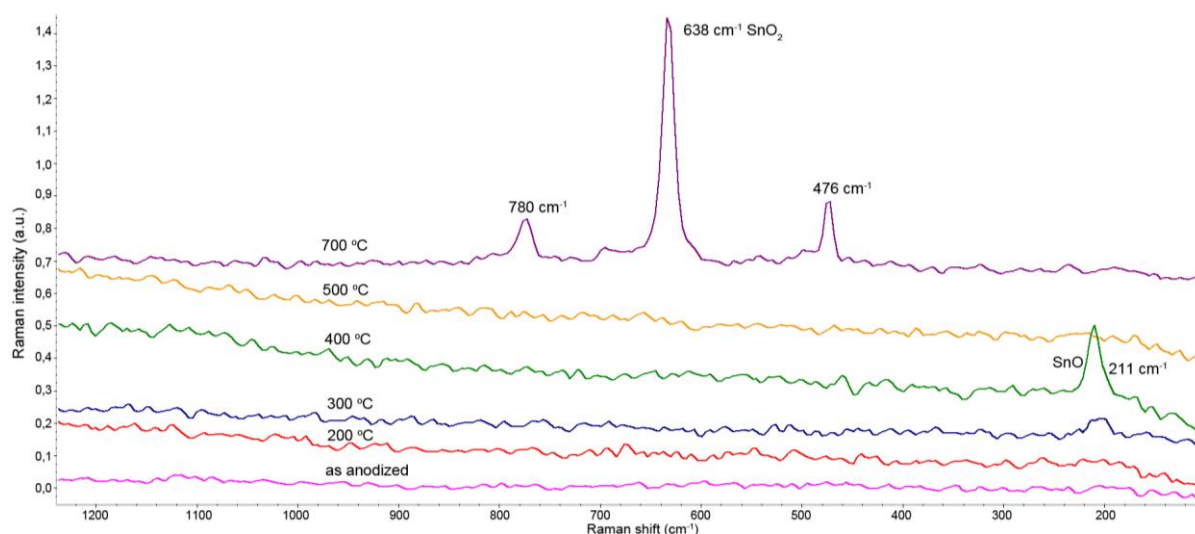


Fig. 2. Raman spectra of tin oxide nanoporous films obtained by electrochemical anodization, without thermal annealing (curve as anodized) and annealed at temperatures from 200 till 700 °C

During heating to the temperature of 500 °C peak 211 cm^{-1} , belonging to vibrations SnO , disappears completely (see Fig. 2), what indicates about the beginning of the oxidation process of monoxide phase. This process is advancing, with the formation of interoxide compounds Sn_2O_3 and Sn_3O_4 [1, 15]. Raman spectra of annealed at 500 °C tin oxide (Fig. 2) devoid of any peak, the same result was obtained for the sample annealed at 600 °C (in Fig. 2 not shown). Complete transformation of tin monoxide SnO to tin dioxide SnO_2 is performed at an annealing temperature of 700 °C, which is confirmed by the Raman spectrum of the nanoporous film. So in the spectrum (Fig. 2 line 700 °C) appear three peaks belonging to tin dioxide. The major peak with a maximum value of 638 cm^{-1} corresponds to vibrations A_{1g} of rutile atomic oxide configuration and two minor peaks with a maximum value of 476 cm^{-1} and 780 cm^{-1} , which corresponds to a phonon vibrations E_g and B_{2g} . The presence of two vibrational modes A_{1g} and B_{2g} indicates preferential vibration of tin and oxygen atoms perpendicular to the x -axis, while E_g mode indicates partial vibration of the atoms along the x -axis [1]. This is due to the orientation of the matrix pore walls which is directed perpendicularly to the substrate, and hence the greatest amount of the material in the nanoporous structure also has a vertical orientation. In this case the vibration along the x axis can carry atoms included in the barrier oxide layer at the bottom of pores and defects caused by the imperfection of the nanoporous structure of the film.

The change of phase composition of nanoporous tin oxide leads to increasing of the optical transparency of the films. On Fig. 3 the optical photos of the glass substrates with an electrochemically formed porous tin oxide matrixes obtained immediately after anodization (Fig. 3 a), after annealing at 400 °C (Fig. 3 b) and after annealing at 700 °C (Fig. 3 c) are shown. As can see from the photos, after electrochemical anodization film already has some transparency and it is possible to recognize the shape of some printed characters of the text placed behind the sample. After annealing at 400 °C when tin oxide has phase SnO, transparency film acquires allowing fully distinguish of the printed text behind the sample, but the film had a gray color. After 700 °C anneal tin oxide transform to SnO₂ phase, wherein the film becomes completely transparent, and its color changes to white. Thus, the changes in the phase composition of the nanoporous tin oxide films can be monitored by determining of the color and transparency of the resulting nanostructured layer.

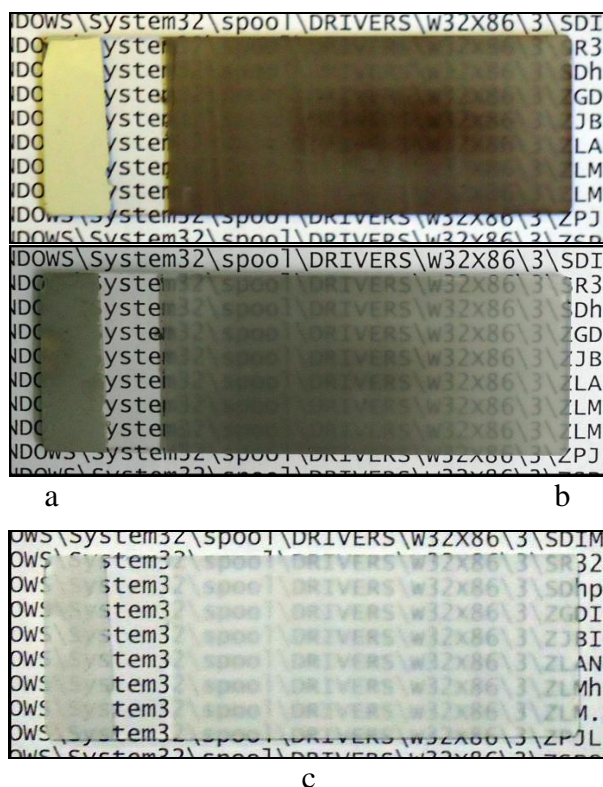


Fig. 3. The optical photo of the nanoporous tin oxide films surface obtained by the digital camera: a – after electrochemical anodization process, b – after annealing for 2 hours at 400 °C, c – after annealing for 2 hours at a temperature of 700 °C

4. CONCLUSION

The results of the electrochemical anodization process of a metallic tin films deposited on a glass substrates with formation of tin oxide nanoporous matrixes having an average pore diameter of 35–40 nm have been shown. After electrochemical process, the porous oxide matrix has a nonstoichiometric composition and an amorphous structure of hydrated tin dioxide (SnO₂·*n*H₂O). Thermal annealing in air at 400 °C provides transformation of an amorphous tin oxide to a stoichiometric phase SnO, which resulted in the detection of Raman peak at 211 cm⁻¹. Increasing of the annealing temperature till 700 °C leads to the oxidation of the SnO monoxide phase and transition of the resulting nanoporous oxide film to dioxide phase SnO₂ with atomic rutile configuration, as evidenced by the appearance of the Raman

peak at 638 cm^{-1} , 476 cm^{-1} and 780 cm^{-1} , what corresponds to the phonon vibrations A_{1g} , E_g and B_{2g} mods. Also thermal annealing enhances the optical transparency of the nanoporous tin oxide matrixes through a change in the crystal structure of tin oxide and increasing of the oxygen content.

Thus, the used methods allow to fabricate a nanoporous tin oxide films on dielectric substrates and to control their stoichiometry. The obtained nanoporous matrixes may be applied in micro- nano and -optoelectronics for creation electrochemical energy sources, transparent nanostructured electrodes, chemical sensors and photovoltaic devices.

REFERENCES

1. BATZILL, M., DIEBOLD, U. The surface and materials science of tin oxide. *Progress in Surface Science*, 2005, Vol. 79, p. 47–154.
2. WAGNER, J.F. Transparent electronics. *Science*, 2003, Vol. 300, p. 1245.
3. YAMAGUCHI, A., IIMURA, T., HOTTA, K., TERAMAE, N. Transparent nanoporous tin-oxide film electrode fabricated by anodization. *Thin Solid Films*, 2011, Vol. 519, p. 2415–2420.
4. ORTIZ, G.F., LAVELA P., KNAUTH P., DJENIZIAN, T., ALCANTARA, R., TIRADO, J.L. Tin-Based composite Materials Fabricated by Anodic Oxidation for the Negative Electrode of Li-Ion Batteries. *Journal of the Electrochemical Society*, 2011, Vol. 158 (10), p. A1094-A1099.
5. MEDURI, P., PENDYALA, C., KUMAR, V., SUMANASEKERA, G.U., SUNKARA, M.K. Hybrid Tin Oxide Nanowires as Stable and High Capacity Anodes for Li-Ion Batteries. *Nano Lett.*, 2009, Vol. 9, No. 2, p. 612–616.
6. ZHANG, Y.-Z., PANG, H., SUN, Y., LAI, W.-Y., WEI, A., HUANG, W. Porous Tin Oxide Nanoplatelets as Excellent-Efficiency Photoelectrodes and Gas Sensors. *Int. J. Electrochem. Sci.*, 2013, Vol. 8, p. 3371–3378.
7. ANDREEVA, E.V., ZILBERMAN, A.B., IL'IN, YU.L., MAHIN, A.V., MOSHNIKOV, V.A., YASKOV, D.A. Influence of ethanol on the electrophysical properties of tin dioxide. *Physics and Technics of Semiconductors*, 1993. Vol. 27, No 7, p. 1095–1100.
8. JEUN, J.-H., RYU, H.-S., HONG S.-H. Nanoporous SnO_2 Film Gas Sensor Formed by Anodic Oxidation. *Journal of the Electrochemical Society*, 2009, Vol. 156 (9), p. J263–J266.
9. BESTAEV, M.V., DIMITROV, D.TS., IL'IN, A.YU., MOSHNIKOV, V.A., TRÄGER, F., STEITZ, F. Study of the surface structure of tin dioxide layers for gas sensors by atomic-force microscopy. *Semiconductors*, 1998. Vol. 32, Iss. 6, p. 587–589.
10. SEVASTYANOV, E.Y., MAKSIMOVA, N.K., NOVIKOV, V.A., RUDOV, F.V., SERGEYCHENKO, N.V., CHERNIKOV, E.V. Effect of Pt, Pd, Au additives on the surface and in the bulk of tin dioxide thin films on the electrical and gas-sensitive properties. *Semiconductors*, 2012, Vol. 46, Iss. 6, p. 801–809.
11. FULLER, M.J., WARWICK, M.E. The catalytic oxidation of carbon monoxide on tin(IV) oxide, *J. of Catalysis*, 1973, Vol. 29, p. 441.
12. HARRISON, P.G., BAILEY, C., AZELEE, W. Modified tin(IV) oxide (M/SnO_2 M = Cr, La, Pr, Nd, Sm, Gd) catalysts for oxidation of carbon monoxide and propane, *J. of Catalysis*, 1999, Vol. 186, p. 147.
13. MU, J., CHEN, B., GUO, Z., ZHANG, M., ZHANG, Z., SHAO, C., LIU, Y. Tin oxide (SnO_2) nanoparticles/electrospun carbon nanofibers (CNFs) heterostructures: Controlled fabrication and high capacitive behavior *J. Colloid interface Sci.* 2011, Vol. 356, p. 706–712.

14. YAO, J., SHEN, X., WANG, B., LIU, H., WANG, G. *In situ* chemical synthesis of SnO₂–graphene nanocomposite as anode materials for lithium-ion batteries. *Electrochem. Commun.*, 2009, Vol. 11, p. 1849–1852.
15. ZHURBINA, I.A., TSETLIN, O.I., TIMOSHENKO, V.YU. Optical generation of free charge carriers in thin films of tin oxide. *Semiconductors*, 2011, Vol. 45, Iss. 2, p. 236–240.
16. MORAZZONI, F., CANEVALI, C., CHIODINI, N., MARI, C., RUFFO, R., SCOTTI, R., ARMELAO, L., TONDELLO, E., DEPERO, L., BONTEMPI, E. Surface reactivity of nanostructured tin oxide and Pt-doped tin oxide as studied by EPR and XPS spectroscopies. *Materials Science and Engineering: C*, 2001, Vol. 15, Iss. 1–2, p. 167–169.
17. IVANOV, V.V., SIDORAK, I.A., SHUBIN, A.A., DENISOVA, L.T. Synthesis of SnO₂ powders by decomposition of the thermally unstable compounds. *Journal of Siberian Federal University. Engineering & Technologies*, 2010, Vol. 2, p. 189–213.
18. WAGHMARE, S.D., SHINDE, D.V., ZATE, M.K., KONDA, R., MANE, R.S., HAN, S.-H. Enhanced gas sensitivity in TiO₂ nanoneedles grown on upright SnO₂ nanoplates. *Scripta Materialia*, 2013, Vol. 68, Iss. 9, p. 735–738.
19. LI, Z., CHANG, T., YUN, G., GUO, J., YANG, B. 2D tin dioxide nanoplatelets decorated graphene with enhanced performance supercapacitor. *Journal of Alloys and Compounds*, 2014, Vol. 586, p. 353–359.
20. LEE, E.J.H., RIBEIRO, C., LONGO, E., LEITE, E. R. Growth kinetics of tin oxide nanocrystals in colloidal suspensions under hydrothermal conditions. *Chemical Physics*, 2006, Vol. 328, Iss. 1–3, p. 229–235.
21. ZHOU, G.X., XIONG, S.J., WU, X.L., LIU, L.Z., LI, T.H., CHU, P. K. N-doped SnO₂ nanocrystals with green emission dependent upon mutual effects of nitrogen dopant and oxygen vacancy. *Acta Materialia*, 2013, Vol. 61, Iss. 19, p. 7342–7347.
22. DAI, Z. R., GOLE, J. L., STOUT, J. D. Tin oxide nanowires, nanoribbons, and nanotubes. *The Journal of Physical Chemistry B*, 2002, Vol. 106(6), p. 1274–1279.
23. FORLEO, A., FRANCIOSO, L., CAPONE, S., CASINO, F., SICILIANO, P., TAN, O.K., HUI, H. Wafer-Level Fabrication and Gas Sensing Properties of miniaturized gas sensors based on Inductively Coupled Plasma Deposited Tin Oxide Nanorods. *Procedia Chemistry*, 2009, Vol. 1, Iss. 1, p. 196–199.
24. JANG, H.S., KIM, D.-H., LEE, H.-R., LEE, S.-Y. Field emission from cone-like single crystalline indium tin oxide nanorods. *Materials Letters*, 2005, Vol. 59, Iss. 12, p. 1526–1529.
25. OGO, Y., HIRAMATSU, H., NOMURA, K., YANAGI, H., KAMIYA, T., HIRANO, M. and HOSONO, H. P-channel thin-film transistor using p-type oxide semiconductor SnO. *Appl. Phys. Lett.*, 2008, Vol. 93, p. 032113.
26. PAN, X.Q. and FU, L. Tin oxide thin films grown on the (1012) sapphire substrate. *J. Electroceram.*, 2001, Vol. 7, p. 35–46.
27. CHEN, Z.-W., SHEK, C.-H., LAWRENCE, C.M., AND LAI, J.K.L. Recent research situation in tin dioxide nanomaterials: synthesis, microstructures, and properties. *Front. Mater. Sci*, 2013, Vol. 7 (3), p. 203–226.
28. WANG, M., LIU, Y., XUE, D., ZHANG, D., YANG, H. Preparation of nanoporous tin oxide by electrochemical anodization in alkaline electrolytes. *Electrochimica Acta*, 2011, Vol. 56, p. 8797–8801.

29. ZARASKA, L., CZOPIK, N., BOBRUK, M., SULKA, G. D., MECH, J., JASKUŁA, M. Synthesis of nanoporous tin oxide layers by electrochemical anodization. *Electrochimica Acta*, 2013, Vol. 104, p. 549–557.
30. CHEN, H., ZHU, W., ZHOU, X., ZHU, J., FAN, LI, CHEN, X. Formation of porous SnO₂ by anodic oxidation and their optical properties. *Chemical Physics Letters*, 2011, Vol. 515, p. 269–273.
31. SHIN, H.-C., DONG, J., LIU, M. Porous tin oxides prepared using anodic oxidation process. *Adv. Mater.*, 2004. Vol. 16, No 3, p. 237 – 240.
32. SHINGUBARA, S. Fabrication of nanomaterials using porous alumina templates. *Journal of Nanoparticle Research*, 2003, Vol. 5, p. 17–30.
33. DE TACCONI, N.R., CHENTHAMARAKSHAN, C.R., YOGEEESWARAN, G., WATCHARENWONG, A., DE ZOYSA, R.S., BASIT, N.A. and RAJESHWAR, K. Nanoporous TiO₂ and WO₃ films by anodization of titanium and tungsten substrates: influence of process variables on morphology and photoelectrochemical response. *J. Phys. Chem. B*, 2006, Vol. 110 (50), p. 25347–25355.
34. KHATKO, V., MOZALEV, A., GOROKH, G., SOLOVEI, D., GUIRADO, F., LLOBET, E. and CORREIG, X. Evolution of surface morphology, crystallite size and texture of WO₃ layers sputtered onto Si-supported nanoporous alumina templates. *Journal of the Electrochemical Society*, 2008, Vol. 155 (7), p. K116-K123.



PREPARATION AND PROPERTIES OF POLYETHYLENE OXIDE COMPOSITES

A. Kiyanitsa, S. Gaidukov, E. Zukulis

*Institute of Polymer Materials, Riga Technical University,
Azenes street 14/24, 1048 – Latvia*

I. Juhnevica

*Institute of Silicate Materials, Riga Technical University,
Azenes street 14/24, 1048 – Latvia,*

ABSTRACT

Polymer nanocomposite materials caused attention because of the properties of the pure material properties can be extremely improved by adding a nano-sized fillers. This paper consists of two parts. The first one is theoretical part and it is about nanocomposites and fillers (such as carbon nanotubes, montmorillonite, silica) their structure and application. The experimental part of this paper is about novel designed polymer composite samples with different filler percentage composition, using Polyethylene Oxide as matrix and the fillers – tetraethylorthosilicate and silica nanoparticles as $C_8H_{20}O_4Si$, carbon nanotubes, montmorillonite and Lithium perchlorate. A composite polymer solution was prepared by dissolving PEO in ethanol. The effect of nanocomposite's preparation method's and filler concentrations onto polymer nanocomposites was evaluated by Fourier transform infrared spectroscopy (FTIR), Vickers hardness, tensile strength and electrical conductivity analysis. It was observed, that addition of silica nanoparticles to PEO composite increase Vickers hardness, at the same time addition of Lithium perchlorate decrease Vickers hardness and tensile test Young's modules. FTIR transmittance results confirm, that all of our SiO_2 -, TEOS- and MMT-containing nanocomposites are injected amorphous SiO_2 nanoparticles. Young's module increases with MMT, CNT, SiO_2 and TEOS fillers addition. Electric conductivity increased with respect to the enhancement of the filler, however excessive amount of these additives caused the conductivity to decrease.

Keywords: Nanocomposites, Polyethylene Oxide, Tetraethylorthosilicate, Carbon Nanotubes, Montmorillonite, Silica, Lithium perchlorate

1. INTRODUCTION

Polymeric nano-composites (PNC) are a new class of composite materials. The main attraction of PNC is these very high operation properties, such as flexibility, elasticity, recycling, hardness, resistance to abrasion, optical and electrical transmission. Preparation of PNC with finely controlled structure, especially, at nano-scale, is still one of the most perspective modification ways of the properties of polymeric composites [1].

If two or more kinds of different material will mix up, and treat in define condition (varying with temperature, pressure and other chemically-physically processes) will be obtained composite material with a clear interfacial boundary. If major part of produced composite consist of polymer, than it should be called polymeric composite. A polymeric composite material is one of the most developed areas of modern science and technology. In addition to composite materials, in modern science and technology use nano-sized fillers, therefore such composites call as nano-composites. These composite materials are widely used in different industries, such as packaging industry, medicine, electronics and mechanical engineering, building and agriculture.

This paper is dedicated on polyethylene oxide composites (PEO), because of their popular and practical applications in portable telecommunication devices, computers and in hybrid electric vehicles and for the possibility of using them in compact, light weight, high

energy density lithium rechargeable batteries. PEO is a semicrystalline polymer at room temperature and has an exceptional property to dissolve with high concentration of a wide variety of dopants [2, 3].

PEO is mostly studied as a host for ions, i.e. lithium ions from LiX salts, because of its flexible macromolecular structure and good ability of the ion dissociation. It should be noted, that lithium salt exhibits great charge delocalization favorable to ionic dissociation in solvating polymers such as PEO. Besides, LiX presents several significant advantages in PEO-LiX composite such as good mechanical stability and “plasticizing” effect (decreases the crystallinity of the host polymer and facilitates the transportation capability of ions) [4].

However, these polymer-LiX composites, which mainly use as polymer electrolyte for lithium rechargeable batteries, composites have still some unsolved problems, i.e. bad interface property and a conductivity which remains at practical levels only at medium-high temperature, i.e. 60-70°C. These disadvantages may be solved, by addition to the system inorganic fillers, such as SiO₂, MMT and CNT, with high surface area. The second aim of nano-filler addition is the reducing the crystallizing ability of the polymer without reducing the mechanical properties of the PEO composite [5, 6].

MMT structure has a net negative charge that is compensated with sodium cations. In the presence of water, the compensating Na⁺ cations on the clay layer surfaces can be easily exchanged for other cations when available in excess amount in solution [7]. CNT with its exceptional electrical properties has become one of the most potential materials to be used as conductive filler in polymer composites. The CNTs network-polymer composite exhibits electron tunneling conductivity, that show that the CNTs network offers a promising application as filler material for creating super conductive composite [8]. Among the many potential applications of CNT, its usage to strengthen polymers has been paid considerable attention due to the exceptional stiffness, excellent strength, and the low density of CNT. Dispersion of CNT within the polymer matrix, effective filler–matrix interfacial interactions, and alignment/orientation of polymer chains/CNT, contribute to the composite fibers’ superior properties. Composites incorporating CNT have received a great deal of attention in both academia and industry for their potential replacement of carbon fibers in polymer-based reinforced materials. CNT have been heralded as a game changer for producing next-generation high-performance materials [9, 10]. Additionally, due to the unique combination of properties, usage of CNT in polymer composites not only improves strength and modulus but can also result in enhancements in chemical resistance, thermal conductivity, electrical conductivity, and dimensional stability [11]. With polymer-SiO₂ nanocomposites have been extensively used in various fields such as aerospace industries, automobiles, marine, and defense industries. Their main advantages are good corrosion resistance, lightweight, dielectric characteristics and better damping characteristics than metals [12]. The nano-sized filler particles such as SiO₂ in polymer nanocomposite increase the mechanical strength and enhanced the ionic conductivity [13].

In addition, Lewis acid-base interactions between the polar surface groups of the inorganic oxide filler and the electrolyte ionic species yield a better extent of salt dissociation through formation of ion-inorganic oxide complex. Due to the heavy mass of the ion-inorganic oxide complex, the conductivity in this composite is not likely to be contributed directly from the movement of these complexes. Instead, the major conducting path is still originated from the local diffusion within the amorphous polymer matrix and the ion transport is realized through sequential replacement of ion to adjacent vacancy. Due to its large surface area, inorganic fillers prevent local PEO chain reorganization with the result of locking in at ambient temperature a higher degree of disorder which in turn favours fast ionic transport. At the same time, obtained results from [14] demonstrate that smaller filler particles show

insignificant influence in the improvement of the conductivity. This phenomenon is probably due to the immobilization of the long polymer chains. Addition of fine (nano-sized) fillers into the PEO-LiX composite film may cause the filler grains getting closer to each other that the blocking effect imposed by the more abundant filler grains could make the long polymer chains more immobilized, leading to the decrease in conductivity. However, the mechanism by which these inorganic particles influence the properties of the native materials are still not satisfactory understood [14, 15, 16, 17].

Thereof the PEO PNC material matrix that consist of nulldimensional (0D), zero-dimensional (1D), two-dimensional (2D) and three-dimensional (3D) filler were investigated. As a result of novel designed polymer composite samples with different filler composition, preparation method's and filler concentrations showed influence onto PNC spectral effects, microhardness, tensile strength and electrical conductivity properties.

2. METHODOLOGY

2.1. Sample preparations

Polyethylene oxide (Scientific Polymer Products inc., molecular weight 100 000 g/mol, density 1.21 g/cm³, glass transition temperature -67°C) as matrix of polymeric composite are chosen, lithium perchlorate (LiCl·H₂O) (ChemPure, Poland, molecular weight 60.41 g/mol) for electrolyte system, but as nano-scale reinforcing additives were chosen: 0D – Tetraethylorthosilicate (TEOS) and 3D – Silica nanoparticles (SiO₂) from C₈H₂₀O₄Si (Sigma-Aldrich ltd., molecular weight 208.33 g/mol), 1D – Carbon nanotubes (CNT) (Nanocyl NC7000, relative density 1.3–2 g/cm³, Jung module 1 TPa, stress at break 10–60 GPa, strain at break 10%, thermal conductivity >3000 W/m·K, electrical conductivity 106–107 Sm/m), 2D - Montmorillonite clay (MMT) (Dellite LVF clays, LAViosa Chemica Mineraria, white powder, 4–8% humidity degree, average particle size 7–9 μm in dry type, average particle size in dispersion 1-500 nm, relative density 2.2 g/cm³).

The tetraethoxysilan (TEOS) have been used as SiO₂ sources. TEOS before its use was subjected to full gelation in ethanol (EtOH) for 24 h, wherein the catalyst used hydrofluoric acid (HF). SiO₂ nano-particle were obtained by TEOS gel drying in the temperature controlled oven at 60°C and then at 600°C, and following grinding.

The composites were prepared by solution casting technique, by dissolving PEO in ethanol, and then by solution mixing with mechanical and magnetic mixing (5 minutes) and additional dispersion with ultrasound (20 minutes). 6% polymer solution in ethanol was prepared. The polymer solution was cast as film and solvent was allowed to evaporate at 25°C temperature for 48 h and dried by annealing them under vacuum at 60°C, for 24 h.

Preparations of the composites are schematically illustrated in Fig. 1.

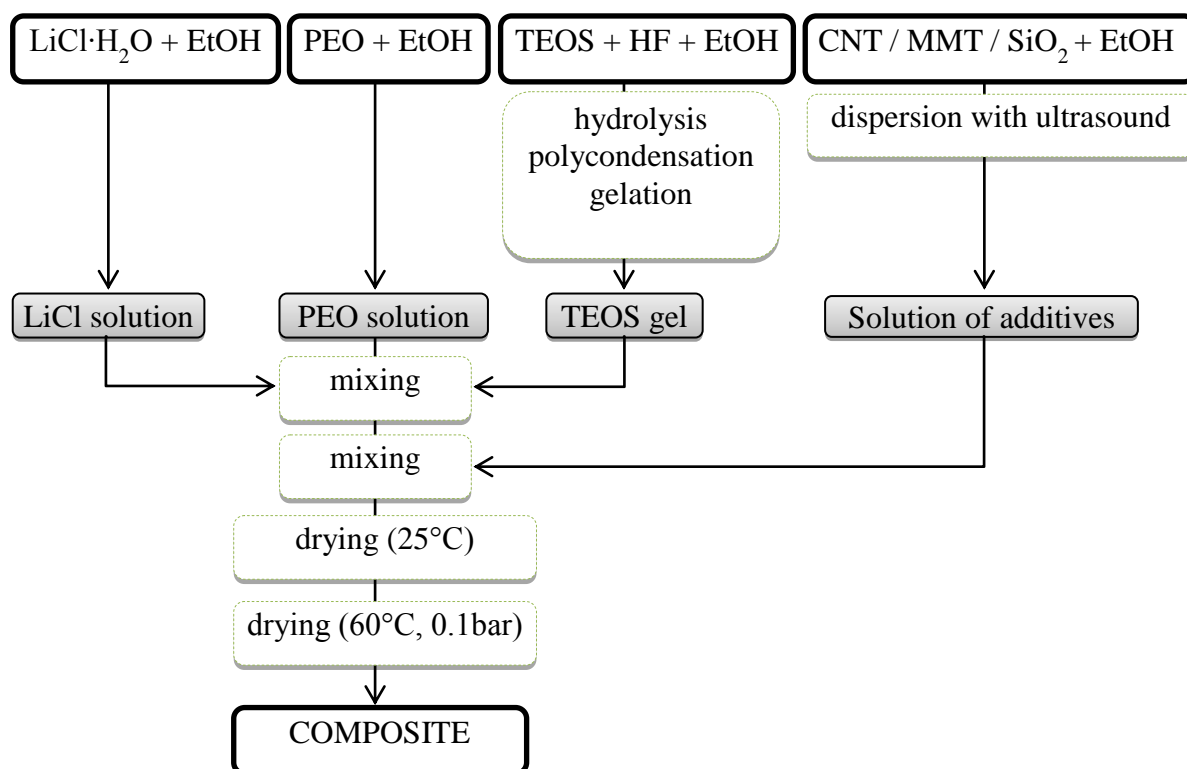


Fig. 1. The schematic representation of the overall strategy for producing PEO composites

The composite samples were prepared by the heat-pressing method, which was carried out at 90°C (6 minutes). Prepared film thickness is 150 µm.

The compositions of prepared composites are illustrated in Fig. 2. Fig. 2 presents the experimental compositions of prepared composites. The total weight of polymer and filler is equal to 100% when preparing the films of various filler and polymer ratio.

Nr	PEO, %	TEOS, %
1	99	1
2	97	3
3	95	5
4	90	10
5	80	20
6	50	50

Nr	PEO, %	CNT, %	TEOS, %
1	99,975	0,025	-
2	99,95	0,05 (2)	-
3	99,9	0,1	-
4	99,5	0,5	-
5	99	1	-
6	96,9	0,1	3
7	94,9	0,1	5
8	89,9	0,1	10

Nr	PEO, %	MMT, %	TEOS, %
1	97	3	-
2	96	3	1
3	94	3	3
4	92	3	5
5	87	3	10
6	77	3	20
7	47	3	50

Nr	PEO, %	SiO ₂ , %	TEOS, %	Li ⁺ , %
1	99,5	0,5	-	-
2	99	1	-	-
3	97	3	-	-
4	95	5	-	-
5	96	3	1	-
6	94	3	3	-
7	92	3	5	-
8	87	3	10	-
9	77	3	20	-
10	47	3	50	-
11	97	-	-	3
12	93	3	1	3
13	91	3	3	3
14	89	3	5	3
15	84	3	10	3
16	74	3	20	3
17	44	3	50	3

Fig. 2. The compositions of prepared composites

2.2. Fourier transform infrared spectroscopy analysis

Fourier transform infrared (FTIR) spectra (4000–400 cm^{-1}) we obtained on a “21 Prestige, Shimadzu Corp.” FTIR spectrometer. The specimen's transmittance spectra are produced. The resulting FTIR spectral pattern is then analyzed and matched with known signatures of identified materials in the FTIR library.

2.3. Vickers hardness studies

Micro hardness testing was performed using a Vickers indenter with a diamond square pyramid shape (the angle between the edge 136°), by using a “Vickers machine M412”.

The hardness was determined by square pyramid pushing (with a force of 100 mN) on sample's surface and measuring the diagonal length of rhombic imprint. Vickers hardness by computing the ratio of the applied load P and imprint surface S are evaluated using the following equation:

$$H_v = \frac{P}{S} = \frac{2 \cdot P \cdot \sin \frac{\alpha}{2}}{d^2} = \frac{18544 \cdot P}{d^2} = \frac{18544 \cdot P}{d^2}, \left[\frac{\text{kg}}{\text{mm}^2} \right] \quad (1)$$

P – is on pyramid applied force (5, 10, 20, 30, 50, 100, 120), [kg];

α – is the angle between the edge, $[\circ]$;

d – is an average diagonal length, [mm].

2.4. Tensile strength properties

Mechanical testing used to determine the Young's module and maximum elongation (%) and stress (MPa) at break was performed using a computer-controlled micro-force tester “ZWICK BDO-FB 020TN”. The composite film sample in the form of film “dogbone” strip (20 mm x 5 mm) was clamped between the holders of the tensometer. The speed for the elongation test was maintained at 5 mm/min for each sample under test at room temperature (at 24°C).

2.5. Electrical conductivity measurements

The electrical conductivity of the sample was measured by sandwiching the samples between two copper electrodes discs of diameter 5 cm (Fig. 3). The measurements were performed using a “Wavetek Meterman 27XT” digital multimeter (in the 50–60 Hz frequency range) at room temperature for 1–2 minutes.



Fig. 3. “Wavetek Meterman 27XT” digital multimeter with two electrodes

To assure good contacts between the film sample and the electrode surface, a constant 65 kg force were applied. DC conductivity measurements on prepared film sample thickness is 150 μm at room temperature (at 24°C) are measured. It should be noted that the electrical conductivity of solid material by full volume conductivity ρ_v and surface conductivity ρ_s may be characterized. We have only able to explore the volume electric conductivity ρ_v and specific volume conductivity γ . Volume electrical conductivity for the thin sample should be calculated using the following equation:

$$\rho_v = R_v \cdot \frac{S}{h}, [\Omega \cdot m] \quad (2)$$

R – volume resistance of the sample, $[\Omega]$;

S – surface area of the electrode, $[\text{m}^2]$;

h – thickness of the sample, $[\text{m}]$.

And using specific volume conductivity should be calculated using the following equation

$$\gamma = \frac{1}{\rho_v} = \frac{1}{R_v \cdot \frac{S}{h}}, \left[\frac{\text{Sm}}{\text{m}} \right]. \quad (3)$$

3. RESULTS AND DISCUSSIONS

3.1. Fourier transform infrared spectroscopy analysis

FTIR transmittance analysis was performed to observe the functional group and interaction that occur between the polymer host and fillers. Infrared spectra show, that the most significant changes were observed between 1600 and 800 cm^{-1} . In the pure PEO matrix spectrum a large the characteristic vibrational modes appears at 1470–1430 cm^{-1} (CH_2 scissoring mode), 1248–950 cm^{-1} (C-O-C stretching mode), 960 cm^{-1} (CH_2 twisting) and 848 cm^{-1} (CH_2 wagging). The CH_2 rocking modes observed in the ranges of 1000–700 cm^{-1} are sensitive vibrational modes in the conformational arrangements for pure PEO.

The FTIR transmittance spectra observed for PEO/TEOS, PEO/ SiO_2 , PEO/ SiO_2 (3%)/ Li^+ (3%)/TEOS, PEO/MMT, PEO/MMT(3%)/TEOS, PEO/CNT(0.1%)/TEOS, and PEO/ SiO_2 (3%)/TEOS. Fig. 4 shows the FTIR spectra results for PEO/ SiO_2 (3%)/TEOS and PEO/CNT.

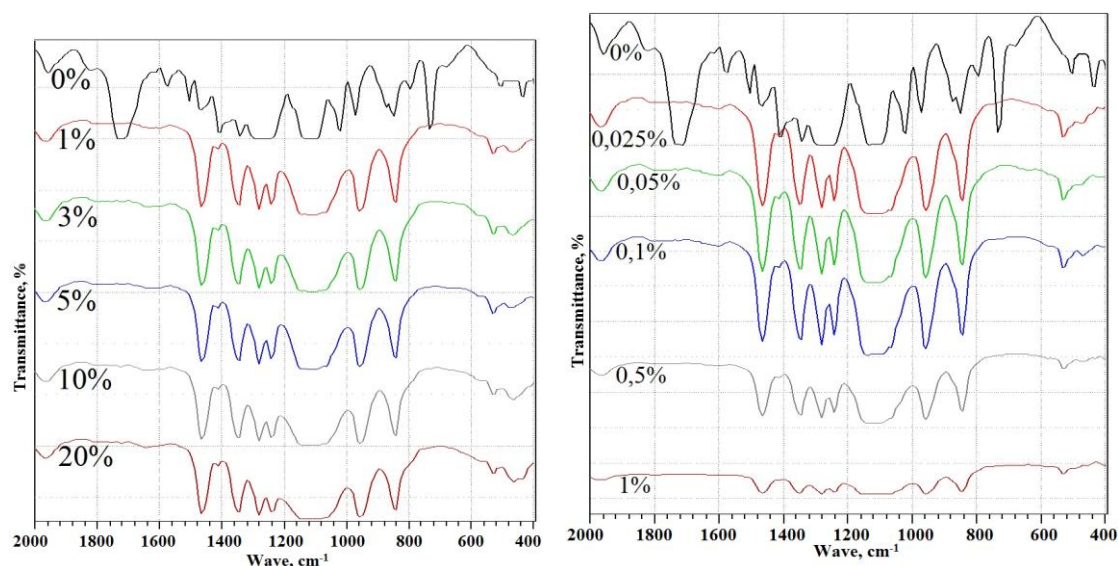


Fig. 4. The FTIR transmittance spectra results for (a) PEO/SiO₂(3%)/TEOS and (b) PEO/CNT by changing the (a) TEOS and (b) CNT content

It suggests that area and intensity of the PEO band regions increased as a result of Si-O, CO and CH bonds characteristic maximums overlapping. However several maximum compared to pure PEO range shifted to lower frequency, for example at 450 and 740 cm⁻¹. As a result, we obtained the Si-O bond corresponding oscillation frequency at 550–450, 900–800 and 1200–1050 cm⁻¹. It should be noted that the last peak frequency (1200–1250 cm⁻¹) shows that all of our SiO₂-, TEOS- and MMT-containing nanocomposites are injected amorphous SiO₂ nanoparticles, because of peak rounded shape.

The FTIR transmittance spectra of the PEO/CNT show that increasing of CNT decrease the PEO characteristic maximums intensity, as a result of CNT better infrared absorbance. However in PEO/CNT(0,1%)/TEOS increase wasn't noticed. It may be supposed, that between matrix and CNT nanoparticles is formed TEOS protective layer, which densely cover the surface of the CNT.

3.2. Vickers hardness studies

It was evaluated, that adding of 3% SiO₂ nanoparticles to PEO/TEOS(10%) composite increase microhardness by 75% comparing to pure PEO, and by 9% comparing to PEO/TEOS(10%) composite. This effect can be explained by the fact that SiO₂ is like reinforcing component, which use TEOS as linking agent, as a result we obtain more dense, well organized and harder composite system. Obtained results show, that with adding 3% Li⁺ to PEO/SiO₂(3%)/TEOS, microhardness decreases by 26%, because of Li⁺ ion hidrophility.

It was observed, that PEO/CNT microhardness values are higher than in PEO/SiO₂, PEO/MMT and PEO/Li⁺. Results show, that adding 1% CNT to PEO increase microhardness by 71%, but MMT and SiO₂ by 65% un 56% respectively, but addition of 3% Li⁺ ion only by 7%.

Fig. 5 shows the microhardness comparison between PEO and various nanocomposites.

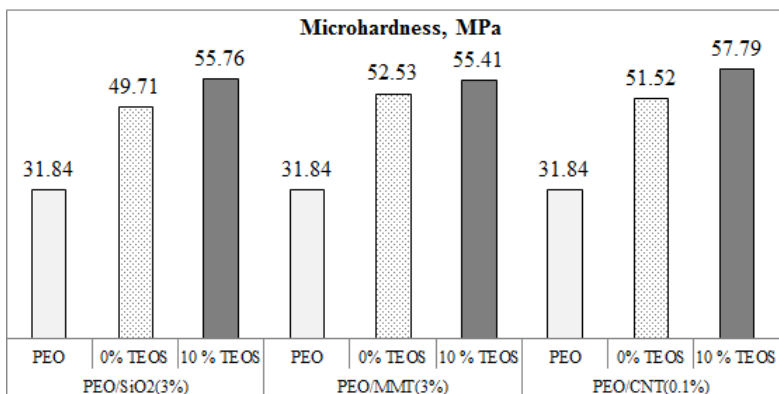


Fig. 5. Vickers hardness test results for PEO and its nanocomposites

3.3. Tensile strength properties

The tensile test Young's module values as a function of TEOS content for PEO/TEOS, PEO/SiO₂(3%)/TEOS un PEO/SiO₂(3%)/Li⁺(3%)/TEOS composites illustrated in Fig. 6.

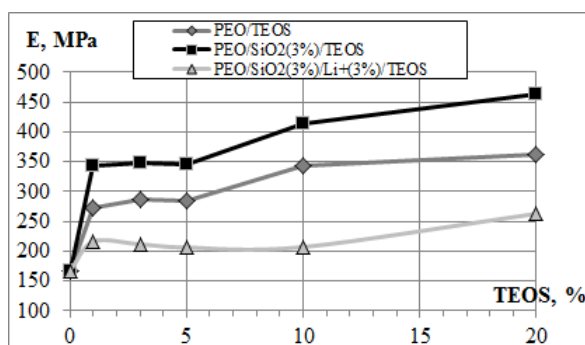


Fig. 6. The tensile test Young's module as a function of TEOS content for various nanocomposites

From Fig. 6 was observed, that addition of SiO₂ nanoparticles to PEO/TEOS(10%) composite, Young's module value increase by 134% comparing to pure PEO, and by 23% comparing to PEO/TEOS(10%) composite. On the other hand, with adding 3% Li⁺ to PEO/SiO₂(3%)/TEOS(10%) Young's module value decreases by 43% comparing to PEO/SiO₂(3%)/TEOS, at the same time increases by 33% comparing to pure PEO.

The results of PEO composite's Young's module and filler type show, that 1% CNT increase Young's module by 115%, but addition of 3% TEOS or 3% SiO₂ or 3% MMT increase by 73%, 108% and 100% respectively. In addition Young's module for PEO/Li⁺ composite increased by 23%, due to changes in PEO hightmolecular structure and dense packing formation with addition of Li⁺ ion.

From the results of PEO/SiO₂(3%)/TEOS, PEO/MMT(3%)/TEOS un PEO/CNT(0.1%)/TEOS as a function of TEOS content may conclude, that adding of CNT (in case of 10% TEOS) increase Young's module by 148% comparing to pure PEO, but for SiO₂ and MMT filler it increased by 134% and 118% respectively.

3.4. Electrical conductivity measurements

Dielectric (SiO₂ and TEOS) and electrically conductive (CNT and Li⁺) filler materials were used in composite, which electric conductivity was obtained.

The electrical conductivity results of the PEO/SiO₂ and PEO/SiO₂(3%)/TEOS show, that TEOS and SiO₂ exhibit dielectric properties. It was observed, that increase of filler content up to 5% cause rise in conductivity as a result of filler influence, supramolecular structure modification and following free ion higher mobility. On the other hand, results obtained at the quartz content (both from SiO₂ and TEOS filler) more than 23%, little by little decrease conductivity values, for the reason that the filler concentration is getting very high and the inorganic phase begins to act as a protective dielectric.

It is worth to say, that the SiO₂, MMT and CNT nano-fillers we have used in this work have particle lie in the nano-size particle range. Due to their ultra-fine structure, these nano-fillers are expected to provide effectively a large surface area with a large number of surface groups for surface interactions to take place. In the case of nanocomposite polymer films filled with SiO₂, MMT and CNT it may be suggested that, the dependence of the conductivity enhancemtn on the nature of the filler surfacegroup may be satisfactorily explained in terms of the Lewis acid-base type interactions involving surface groups. The presence of filler particles enhances the electric conductivity substantially [3, 14].

Electrical conductivity comparison results between PEO and various nanocomposites are listed in Table 1.

Table 1. Electric conductivity (at 24 °C) of the pure PEO and PEO | based polymer composite films

	PEO/SiO ₂ (3%)		PEO/MMT(3%)		PEO/CNT(0,1%)	
	Conductivity, Sm/m	Increase compare to pure PEO, %	Conductivity, Sm/m	Increase compare to pure PEO, %	Conductivity, Sm/m	Increase compare to pure PEO, %
Pure PEO	$2.57 \cdot 10^{-10}$	-	$2.57 \cdot 10^{-10}$	-	$2.57 \cdot 10^{-10}$	-
0% TEOS	$1.67 \cdot 10^{-09}$	648	$1.83 \cdot 10^{-09}$	710	$2.55 \cdot 10^{-08}$	9910
10% TEOS	$1.71 \cdot 10^{-09}$	666	$1.42 \cdot 10^{-09}$	553	$1.11 \cdot 10^{-09}$	431

4. CONCLUSIONS

Films with different filler percentage, using PEO as matrix and the fillers – tetraethylorthosilicate, carbon nanotubes, montmorillonite and silica nanoparticles and lithium chloryde nanocompositions were prepared. It was observed influence onto nanocomposites spectral effects, tensil strength, hardness and electrical properties. It was found that TEOS interact favorably with the polymer host as polyethylene oxide. Hybrid organic-inorganic nanocomposites produced by dispersing TEOS and addition of SiO₂ into a polymer matrix exhibit enhanced physical and chemical properties in relation to the neat polymer matrices. The addition of a few weight percent of SiO₂ increased the tensile test Young's modulus and the strength by over 100% for some prepared hybrid systems. Considered dependency of overall properties on the microstructural features of studied hybrid materials of polymers mixed with layered silicates were also examined. FTIR spectra of the TEOS and SiO₂ nanoparticles containing samples confirmed the presence of amorphous silica glass. Use of TEOS link-agent greatly increases the mechanical performance of samples, caused can be formed the polymer matrix, TEOS and fillers links. The Young's modulus of nano-composites increases proportionally with TEOS, SiO₂, MMT and CNT concentration increased by more than 70%, which is caused with high mechanical properties nano-scale objects were entered into PEO. The presence of lithium ions impairs the mechanical properties of prepared due to

plastification effect. It is accepted, that TEOS forms dielectric shield around the filler particles, which impairs the conductivity of samples. MMT, CNT and Li^+ adding to a polymer increases the composite conductivity. CNT content up to 1% significantly increase the electrical conductivity of nanocomposites. PEO based polymer composite's electric conductivity increased with respect to the enhancement of the MMT, CNT and SiO_2 without TEOS, however 10% amount of TEOS caused the conductivity to decrease.

REFERENCES

1. Klaus F.; Stoyko F.; Zhong Zh. *Polymer Composites: From Nano- to Macro-Scale*. New York: Springer Science, 2005. 389 p. ISBN 0-387-24176-0.
2. CHATTERJEE, T., LORENZO, A.T., KRISHNAMOORTI, R.. Poly(ethylene oxide) crystallization in single walled carbon nanotube based nanocomposites: Kinetics and structural consequences. *Polymer*, 2011, Vol. 52, No. 21, p. 4938–4946.
3. JAYATHILAKA, P.A.R.D., DISSANAYAKE, M.A.K.L., ALBINOSSON, I., MELLANDER, B.-E. Ionic conductivity of $(\text{PEO})_9\text{LiTFSI}:\text{Al}_2\text{O}_3$ nano-composite polymer electrolyte prepared by solvent-free route. *Ceylon J. of Science: Physical Sciences*, 2002, Vol. 9, No. 1, p. 9–15.
4. YANG, R., ZHANG, Sh., ZHANG, L., LIU, W. Electrical properties of composite polymer electrolytes based on PEO-SN- LiCF_3SO_3 . *Int. J. Electrochem. Sci.*, 2013, Vol. 8, p. 10163–0169.
5. PANERO, S., SCROSATI, B., SUMATHIPALA, H.H., Wieczorek, W. Dual-composite polymer electrolytes with enhanced transport properties. *J. of Power Sources*, 2007, Vol. 167, p. 510–514.
6. WANG, L., LI, Xi., YANG, W.. Enhancement of electrochemical properties of hot-pressed PEO-based nanocomposite polymer electrolyte films for all-solid-state lithium polymer batteries. *Electrochimica Acta*, 2010, Vol. 55, p. 1895–1899.
7. KURIANA, M., GALVINA, M.E., TRAPAB, P.E., SADOWAYB, D.R., MAYES, A.M. Single-ion conducting polymer–silicate nanocomposite electrolytes for lithium battery applications. *Electrochimica Acta*, 2005, Vol. 50, p. 2125–2134.
8. YUNG, K.P., WEI, J., WANG, Z.F., TAY, B.K. Carbon Nanotubes (CNTs) as conductive filler for polymer composite. Nanoelectronics Conference. INEC 2008. 2nd IEEE International. 24–27 March 2008, p. 1198–1201.
9. SONG, K., ZHANG, Y., MENG, J., GREEN, E.C., TAJADDOD, N., Li, H., MINUS, M.L.. Structural Polymer-Based Carbon Nanotube Composite Fibers: Understanding the Processing-Structure-Performance Relationship. *Materials*, 2013, Vol. 6, p. 2543–2577.
10. ANDREWS, R., WEISENBERGER, M.C. Carbon nanotube polymer composites. *Current Opinion in Solid State and Materials Science*, 2004, Vol. 8, p. 31–37.
11. BAUGHMAN. R.H., ZAKHIDOV. A.A., de HEER. W.A.. Carbon nanotubes – The route toward applications. *Science*, 2002, Vol. 297, p. 787–792.
12. RAJU, B.R., SWAMY, R.P., SURESHA, B., BHARATH, K.N. The Effect of SiO_2 Filler on the wear resistance of glass fabric reinforced epoxy composites. *Advances in Polymer Science and Technology: An Int. J.*, 2012, Vol. 2, No. 4, p. 51–57.
13. CHEW, K.W., TAN, K.W. The Effects of ceramic fillers on PMMA-based polymer electrolyte salted with lithium triflate, LiCF_3SO_3 . *Int. J. Electrochem. Sci.*, 2011, Vol. 6, p. 5792–5801.



14. YAP, Y.L., YOU, A.H., TEO, L.L., HANAPEI, H. Inorganic filler sizes effect on ionic conductivity in PEO composite polymer electrolyte. *Int. J. Electrochem. Sci.*, 2013, Vol. 8, p. 2154–2163.
15. Li, Q., SUN, H.Y., TAKEDA, Y., IMANISHI, N., YANG, J., YAMAMOTO, O. Interface properties between a lithium metal electrode and a PEO based composite polymer electrolyte. *J. Power Sources*, 2001, Vol. 94, No. 2, p. 201–205.
16. CROCE, F., SCROSATI, B. PEO-Based Nanocomposite Polymer Electrolytes. 205th Meeting of The Electrochem. Soc. – Meeting Abs. 364. Scotland, 2003 October 12–16.
17. CROCE, F., SETTIMI, L., SCROSATI, B., ZANE, D. Nanocomposite, PEO-LiBOB polymer electrolytes for low temperature, lithium rechargeable batteries, *J. New. Mat. Electrochem. Systems*, 2006, Vol. 9, p. 3–9.

AGEING AND SURFACE CHARACTERISTICS INVESTIGATION OF EXPANDED POLYSTYRENE TREATED IN AIR AND ARGON PLASMA

Š. Varnagiris, D. Milčius

Lithuanian Energy Institute

Breslaujos str. 3, LT-44403 Kaunas – Lithuania

ABSTRACT

The article presents the results obtained during investigation of surface modification of structural expanded polystyrene (EPS 70). Expanded polystyrene were treated with air and argon plasmas, which were generated using pulsed DC generator. Pressure of plasma treatment process was 1×10^{-1} mbar. These plasmas were used to modify surface of polystyrene. The samples of polystyrene were processed at different plasma voltage (300 V, 350 V, 400 V) and treatment times. The surface modification of polystyrene was evaluated by measuring water contact angle before and after plasma treatment. Hydrophobic characteristics were observed before plasma treatment ($\sim 104^\circ$ of water contact angle). It was found, that after increased plasma treatment voltage or / and time, water contact angle decreased. Samples were produced with hydrophilic surfaces (about 10° of water contact angle) at different voltage of plasmas. These samples were used to observe ageing process in samples surfaces. It was found, that samples which were treated in argon plasma have better hydrophilic characteristics. These samples kept surface hydrophilic characteristics about 48 hours. Samples which were treated in air plasma had the same hydrophilic characteristics only about 24 hours.

Also it was found, that vacuum has a very big influence in volumetric changes of polystyrene. Velocity of geometry changes in stable 1.5×10^{-5} mbar pressure is about $v = 0.1$ [% / min.].

Keywords: polystyrene, plasma, ageing, contact angle

1. INTRODUCTION

Polystyrene materials are used for wide variety of products. Thermal insulation of buildings is very important field of expanded polystyrene utilization [1]. Modified polystyrene with a coating on a surface or with introduced nanoparticles inside grains can improve thermal insulation characteristics and resistance to fire [2–3]. However, polystyrene has a low surface energy [4]. Because of this deposition on a surface of polystyrene is complicated. A polystyrene surface energy can be changed by a process of plasma activation [5–6].

Plasma activation is used to improve surface hydrophilic characteristics of polystyrene [7]. Treatment of plasma depends on the interaction between plasma and surface of polystyrene. It leads to different bonds formation [8]. Such process modifies chemical structures at few monolayers (about 10 nm depth) on polystyrene surface [9–10]. The surface modification after plasma treatment depends on the chemical structure of the polystyrene and the plasma gas [11]. Also plasma treatment process leads to formation of chemical groups on a surface. Because of this, wear characteristics can be improved [7].

It was investigated changes in surface properties of structural expanded polystyrene (EPS 70) after air and argon plasma treatments. Hydrophilic characteristics and ageing processes of polystyrene were investigated using water contact angle measurements.

Change in geometry of polystyrene in vacuum was also observed. Measurements of alteration were performed using scanning electron microscope (SEM) with observing geometry changes of polystyrene grains.

2. METHODOLOGY

2.1. Preparation of polystyrene

Experiments were performed with structural expanded polystyrene foam – EPS 70 (compressive stress at 10% deformation is ≥ 70 kPa) produced by UAB “Baltijos polistirenas”. The foam was cut into small pieces of about $15 \times 30 \times 5$ mm for water contact angle and ageing measurements. Samples which were used for change in geometry measurement were cut in $49 \times 50 \times 25$ mm pieces.

2.2. Plasma treatment

Samples were treated in the system of physical vapour deposition (KJLC, PVD 75). The system was pumped with oil rotary pump. Pressure of plasma treatment process was 1×10^{-1} mbar. Plasma was generated using pulsed DC generator. Voltage of plasma treatment process was 300 V, 350 V, 400 V (respectively powers of treatment process 60W, 84W, 110 W). Distance between samples and the plasma plate was about 40 mm. Expanded polystyrene were treated with air and argon (99.99%) plasma. The effect of surface treatment was performed by changing plasma voltage and treatment time.

2.3. Water contact angle measurements

Water contact angle was measured before and after plasma treatment using house-constructed apparatus with camera and a PC computer was used for taking high resolution pictures of the water drop on the sample surface [8]. The deionised water was used. After plasma treatment, samples were extracted into an ambient atmosphere. Measurements of water contact angle were immediately done (waiting time lower than 5 min.). Four drops were dropped at various places on surface of polystyrene. A syringe was used for this reason. Four drops were used in order to obtain an average value of the contact angle. The estimated errors of water contact angle measurements were less than 7° .

2.4. Ageing conditions

Polystyrene samples treated in air and argon plasmas were stored in conditions of ambient atmosphere. Samples were stored at room temperature (22 ± 4 °C), with an average relative humidity value ($50 \pm 10\%$). Ageing measurements were performed in every 24 hours.

2.5. Measurements of geometry changes in vacuum

Geometry changes of expanded polystyrene were observed using scanning electron microscope (SEM Hitachi S-3400N) in a stable 1.5×10^{-5} mbar vacuum. Vacuum was achieved using rotary and turbomolecular pumps. Dimensions of polystyrene grain were measured immediately after pumping process. Further measurements of dimensions were performed in every 10 min.

Observation of polystyrene volumetric changes was done using vacuum chamber. Samples were placed into a vacuum chamber with different pumping time. Pressure of vacuum was about 6.3×10^{-2} mbar.

3. RESULTS AND DISCUSSIONS

3.1. Water contact angle measurements

Water contact angle measurements were done on surface of polystyrene after plasma treatment. Fig. 1 shows water contact angle dependence on treatment time at different voltage.

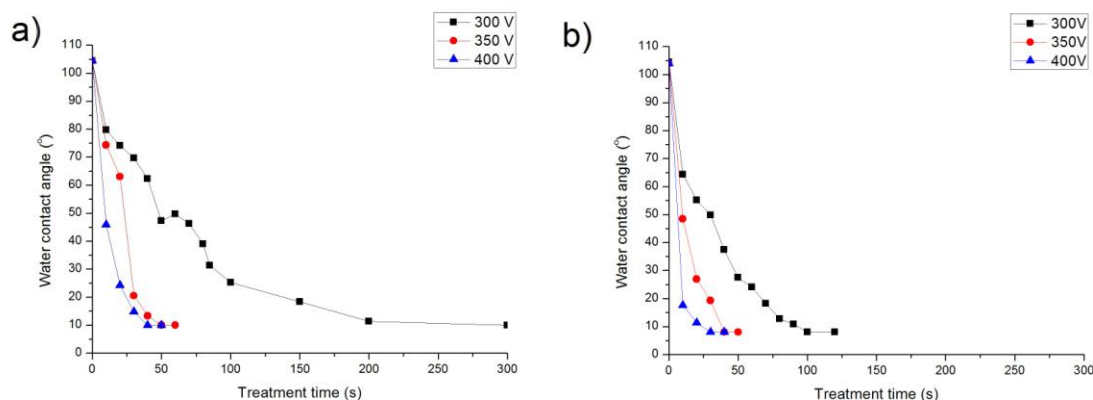


Fig. 1. Water contact angle measurements: a) air plasma treatment, b) argon plasma treatment

Measurements of water contact angle shows that voltage is very important parameter of plasma treatment process. Water contact angle of non-treated polystyrene is about 104° . It means that surface of polystyrene is hydrophobic. Higher voltage of plasma treatment process leads to reduce time in order to achieve hydrophilic characteristic of polystyrene surface.

Hydrophilic characteristic (about 10° of water contact angle) is achieved after 100 s treatment time using argon gas (voltage 300 V). The same result is obtained with air gas after 250 s. Different voltage leads to change value of water contact angle using the same treatment time. Difference between values of water contact angle is about 50° after 10 s of argon plasma treatment with 300 V and 400 V.

Stream of plasma ions depends on voltage of plasma treatment process. Irradiation of argon plasma produces the highly crosslinked layer on the surface of polystyrene [12]. The crosslinked layer leads to formation of free radical sites. These free radical sites provide high surface energy [13]. This is one of the main reasons, why polystyrene surface become hydrophilic from hydrophobic after process of plasma treatment.

3.2. Surface ageing phenomena

Ageing phenomena of polystyrene surface can be described using the term of hydrophilicity. It shows hydrophilic characteristics of polystyrene surface in percents using adopted equation from [9]:

$$\Delta = ((\Theta_{un} - \Theta_{tr}) / \Theta_{un}) \times 100\%, \quad (1)$$

where Θ_{un} – water contact angle of untreated polystyrene ($\sim 104^\circ$), Θ_{tr} – water contact angle of treated polystyrene.

Fig. 2 shows that hydrophilic characteristics decrease in time. However, changing of hydrophilic characteristics is negligible from a certain moment of ageing time (about 200 h after air plasma treatment and 100 h after argon plasma treatment). It means that loss of hydrophilic characteristics gain partial saturation. Hydrophilic characteristics in a point of partial saturation are about 5% better after argon plasma treatment. 85–88 % of hydrophilic

characteristics can be kept till 48 hours after argon plasma treatment. After air plasma treatment about 83% of hydrophilic characteristics can be kept in the same time. Also it was measured, that vacuum without plasma treatment doesn't have significant influence on hydrophilicity and ageing process.

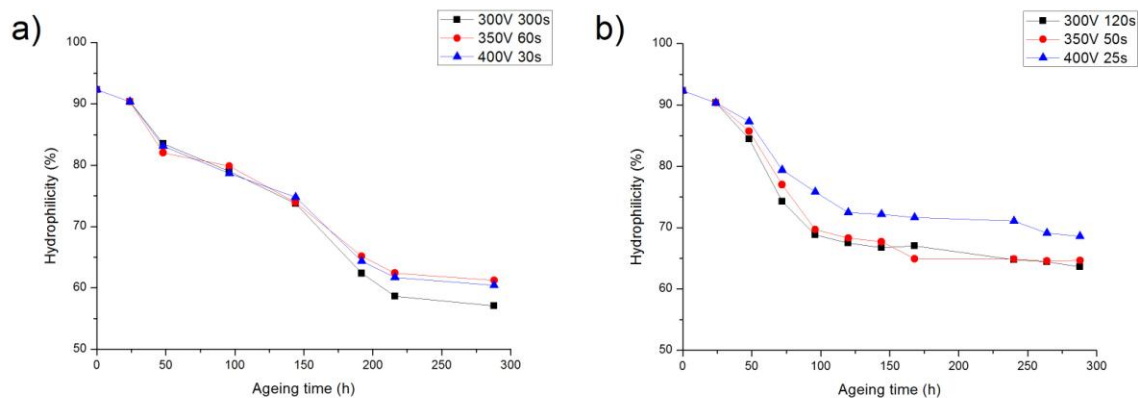


Fig. 2. Surface ageing: a) air plasma treatment, b) argon plasma treatment

Loss of hydrophilic characteristics through the ageing time is mainly due to combination of few processes. The free surface energy is reduced linked to the reorientation of polar chemical functions into the polymer bulk. Other process is polymer chains diffusion into the matrix [9]. Also adsorption of atmospheric particles has influence on the loss of hydrophilic characteristics.

3.3. Analysis of geometry changes in vacuum

Fig. 3 shows that vacuum has an influence on dimensions of polystyrene. Three pieces of expanded polystyrene were placed into a vacuum chamber. Time of vacuum impact was different.



Fig. 3. Impact of vacuum: A – untreated polystyrene, B – after 10 min., C – after 20min., D – after 30 min.

It was observed that geometry changes of polystyrene depend on time in vacuum. Alteration of polystyrene dimensions was minimal after 10 min. in vacuum chamber. However, after 30 min. it was observed significant alteration of dimensions. Dimensions were

47.5×48×24 mm after 30 min. in vacuum chamber (dimensions of untreated polystyrene were 49×50×25 mm). Alteration of dimensions is equal or more than 1 mm in each dimension.

Other measurement of polystyrene change in geometry was performed using observation of polystyrene grain in scanning electron microscope.

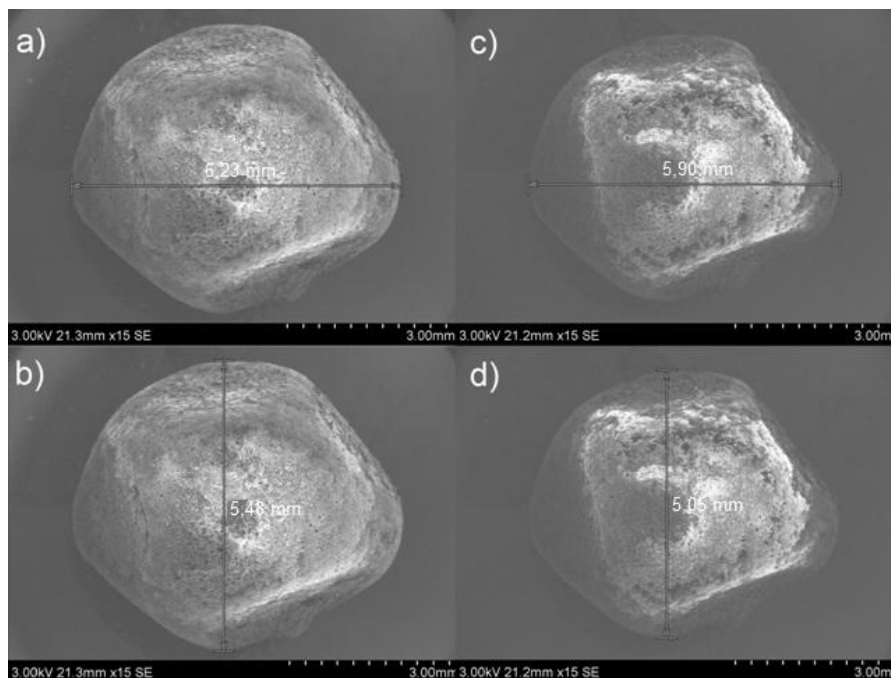


Fig. 4. Alteration of polystyrene grain: a) x dimension after 5 min.; b) y dimension after 5min.; c) x dimension after 60 min. in vacuum; d) y dimension after 60 min. in vacuum

Difference in x dimension between 5 and 60 min. in vacuum was 0.33 mm. Difference in y dimension was 0.43 mm (Fig. 4). Geometry changes of polystyrene grain is respectively 5.29% and 7.84% in each dimension. Difference between 5 min. and 10 min. is respectively 0.64% and 1.09%.

Geometry changes of polystyrene are similar in each direction. These changes gain saturation after 60 min. in vacuum. Further changes are minimal. Velocity of geometry changes (in first 60 min. in vacuum) was measured after polystyrene observation in vacuum. It is $v = 0.113$ [%/min.] in stable 1.5×10^{-5} mbar pressure.

Expanded polystyrene grains have an air inside. When grains are placed into a vacuum, air is extracted from grains because of entropy. Grains of polystyrene lose stability of volume. This loss of stability is the reason of polystyrene change in geometry.

4. CONCLUSIONS

It was found that plasma treatment of polystyrene with air and argon plasmas is an effective tool to improve the wettability. Higher voltage of plasma treatment process leads to reduce time of plasma treatment in order to achieve hydrophilic characteristic of polystyrene surface. Hydrophilic characteristic is achieved with a shorter time of treatment using argon plasma. Surface of polystyrene can keep hydrophilic characteristics (more than 85%) about 48 hours after argon plasma treatment. Change in geometry of polystyrene depends on pressure and time in vacuum. Velocity of geometry changes in stable 1.5×10^{-5} mbar pressure is about $v = 0.1$ [%/min.].

5. ACKNOWLEDGMENTS

This research was funded by a grant (Nr. VP1-3.1-ŠMM-10-V-02-019) from the project “nanoPUTPLAST”.

REFERENCES

1. DOROUDIANI S., OMIDIAN H. Environmental, health and safety concerns of decorative mouldings made of expanded polystyrene in buildings. *Building and Environment*, 2009, Vol. 8, No. 1, p. 647–654.
2. KATANCIC Z., TRAVAS-SEJDIC J., HRNJAK-MURGIC Z. Study of flammability and thermal properties of high-impact polystyrene nanocomposites. *Polymer Degradation and Stability*. 2011, Vol. 8, No. 1, p. 2104–2111.
3. DEVECI H., AHMETLI G., ERSOZB M., KURBANLI R. Modified polystyrenes: Corrosion, physicomechanical and thermal properties evaluation. *Organic Coatings*, 2012, Vol. 7, No. 1, p. 1–7.
4. LEE J.H., KWON J.S., KIM Y.H., CHOI E.H. The effects of enhancing the surface energy of a polystyrene plate by air atmospheric pressure plasma jet on early attachment of fibroblast under moving incubation. *Thin solid films*, 2013, Vol. 7, No. 1–4, p. 99–105.
5. GESCHE R., KOVACS R., SCHERER J. Mobile plasma activation of polymers using the plasma gun. *Surface and Coatings Technology*, 2005, Vol. 4, No. 1, p. 544–547.
6. KUO Y.L., CHANG K.H., HUNG T.S. Atmospheric-pressure plasma treatment on polystyrene for the photo-induced grafting polymerization of N-isopropylacrylamide. *Thin solid films*, 2010, Vol. 6, No. 1, p. 7568–7573.
7. DAVIES J., NUNNERLEY C. S., BRISLEY A. C., SUNDERLAND R.F., EDWARDS J.C. Argon plasma treatment of polystyrene microtiter wells. Chemical and physical characterisation by contact angle, ToF-SIMS, XPS and STM. *Colloids and Surfaces A*, 2000, Vol. 9, No. 2, p. 287–295.
8. VESSEL A. Modification of polystyrene with a highly reactive cold oxygen plasma. *Surface and Coatings Technology*, 2010, Vol. 8, No. 1–2, p. 490–497.
9. LARIEU J., HELD B., MARTINEZ H., TISON Y. Ageing of atactic and isotactic polystyrene thin films treated by oxygen DC pulsed plasma. *Surface and Coatings Technology*, 2005, Vol. 7, No. 1–2, p. 2310–2316.
10. GURUVENKET S., MOHAN RAO G., KOMATH M., RAICHUR A.M. Plasma surface modification of polystyrene and polyethylene. *Applied Surface Science*, 2004, Vol. 7, No 1, p. 278–284.
11. DHAYAL M., ALEXANDER M.R., BRADLEY J.W. The surface chemistry resulting from low-pressure plasma treatment of polystyrene: The effect of residual vessel bound oxygen. *Applied Surface Science*, 2006, Vol. 7, No. 1–2, p. 7957–7963.
12. SASAI Y., MATSUZAKI N., KONDO S., KUZUYA M. Introduction of carboxyl group onto polystyrene surface using plasma techniques. *Surface and Coatings Technology*, 2008, Vol. 4, No. 2, p. 5724–5727.
13. ZEKONYTE J., ERICHSEN J., ZAPOROJTCHENKO V., FAUPEL F. Mechanisms of argon ion-beam surface modification of polystyrene. *Surface science*, 2003, Vol. 5, No. 2, p. 7568–7573.

PLASMA SYSTEM FOR ASH RESIDUES PROCESSING

V.V. Sauchyn, A.V. Lozhachnik, Hr.V. Dalholenka, D.V. Skamarokhau

A.V. Luikov Heat and Mass Transfer Institute

National Academy of Sciences of Belarus

15 P. Brovka Str. Minsk, 220072, Belarus

ABSTRACT

The combustion of fossil fuel is one of the main sources of environmental pollution. Fly ash can be mentioned as an example of such harmful pollutants.

Laboratory plasma set was developed and manufactured for adjusting the modes for different types of fly ash processing. The capacity of the set is 10–20 kg/hour. The set was equipped with a plasma torch with a capacity of up to 40–80 kW.

The average chemical composition of the ash that was used in the experiments was as follows: 90 % of carbonates and oxides of sodium, calcium, magnesium, iron, and 10 % of other substances, including non-burned carbon and organic compounds. In order to receive a homogeneous compound we propose to add SiO_2 (sand) to the ash.

As a result of the experiment organic components of fly ash were completely burned out and an inorganic part was melted into a monolith. The chemical resistance of vitrified samples was tested by their leaching in deionized water. The leaching rate of macro components from the vitrified sample for the investigated elements was less than $1 \cdot 10^{-7} \text{ g}/(\text{cm}^2 \cdot \text{day})$.

Obtained results show that arc plasma technology can be used for toxic fly ash processing into chemically stable and environmentally friendly material.

Keywords: arc plasma, plasma set, fly ash processing, ash vitrification

1 INTRODUCTION

The combustion of fossil fuel for heat and/or electricity as a part of central power supply systems is a basis of the economy and modern society in general. On the other hand, the combustion of fossil fuel is one of the main sources of environmental pollution. Fly ash is an example of such harmful pollutants. This shows that modern society faces a great problem of toxic waste management and processing.

Accumulation of heavy metals and radionuclides is one of the most dangerous aspects of fly ash. Due to its high dispersion and ability to partially dissolve in water fly ash can easily spread in the environment, atmosphere, rivers, lakes and ground water. As a result of transboundary transport, pollutants can travel a long distance.

In cases in which fly ash contains toxic substances that exceed maximum permissible concentrations, special methods are required for its management and processing. Special attention should be paid to decreasing the amount of ash and transforming it into forms suitable for transportation and storage.

Considering the large volume of generated ash, stringent requirements for its safe handling and ever increasing costs of disposal it is obvious that we have to minimize the amount of waste and convert toxic substances into safe non-leachable forms. In addition, this material should be environmentally friendly.

The main requirements for the products of recycled fly ash are listed below:

- high chemical stability;
- low water solubility;
- thermal and radiation stability with no emitted toxic and radioactive gases;
- mechanical stability and chemical resistance must not change during the storage;

- maximum number of toxic elements immobilized in the final products;
 - hardware and technological layout accessible and providing secure process control.
- Nowadays many toxic ash immobilization methods are known, among them:
- Cementation [1];
 - Bituminization [2];
 - Solidification in polymer matrix [3];
 - Vitrification, including plasma vitrification [4–9].

2 CLASSIFICATION OF FLY ASH FROM FUEL-BURNING FURNACES

In general, fly ash is a material that is formed as a result of cooling exhaust gas on a power plant and collected by electrostatic precipitators or bag filters. The particles of fly ash are formed from the particles suspended in gas. As a rule, they are spherical in shape and their dimensions are 0.5 μm to 100 μm . As a rule fly ash mainly consists of silicon dioxide (SiO_2) in two forms: amorphous, whose particles are rounded and smooth; and crystalline, whose particles are sharp. Other macro components such as aluminum oxide (Al_2O_3), ferric oxide (Fe_2O_3) and calcium oxide (CaO) can be found, too. Generally fly ash is highly heterogeneous and contains different crystalline inclusions, for example, quartz, mullite and different ferric oxides.

Fly ash also contains toxic substances including arsenic, beryllium, boron, cadmium, chromium, cobalt, lead, manganese, mercury, molybdenum, selenium, strontium, thallium and vanadium with concentration up to hundreds ppm. Standard ASTM C618 defines two classes of fly ash: Class C and Class F. The main difference between these classes is the amount of calcium, silicon, aluminum and iron in ash. The chemical properties of fly ash depend on the chemical properties of the combusted coal (e.g. see Table 1).

Table 1. Typical composition of fly ash from combustion of different fuels, %

Component \ Fuel	Bituminous coal	Subbituminous coal	Brown coal (Lignite)
SiO_2	20-60	40-60	15-45
Al_2O_3	5-35	20-30	20-25
Fe_2O_3	10-40	4-10	4-15
CaO	1-12	5-30	15-40
LOI (loses of ignition)	0-15	0-3	0-5

2.1 Class F fly ash

The combustion of anthracite and mineral carbon results in the production of class F fly ash in general. This fly ash is pozzolatic in nature and contains less than 10% of lime (CaO). Because of pozzolatic properties of some components, such as vitreous silica and argil, Class F fly ash requires binding materials, such as cement, lime or slaked lime and water to enable cement compound formation.

2.2 Class C fly ash

Fly ash that is produced when burning brown coal or black lignite, in addition to pozzolatic properties, is self-cementing. After adding water, Class C fly ash hardens with time. Class C fly ash normally contains more than 20% of lime (CaO). As a rule, Class C fly ash contains more alkali and sulfate (SO_4).

3 ASH VITRIFICATION

One of the most promising methods of treating fly ash is its vitrification under high temperature. This method allows receiving a solid product with a low level of leaching during long term storage.

Technologies with molten glass are widely used for hazardous waste treatment and immobilization of toxic substances. However, in order to start the process of melting ash we have to heat the material to more than 1400°C. It is very difficult to reach this temperature in fuel burning facilities, but easily achieved in plasma units. The heart of a plasma plant is a plasma torch that can generate plasma flow with temperatures ranging from 4000°C to 7000°C.

Plasma technology for the vitrification of fly ash has many advantages compared with traditional methods:

- Due to high temperature and high energy density, the high intensity of the process allows treating heat-resistant materials (such as ash) and obtaining a chemically stable form with a low level of leaching;
- Gas medium in the reaction zone can be controlled easily;
- Plasma torches require significantly less gas for the process compared with fuel technologies. This results in the dispersed material saving and decreased utilization of the gas cleaning system;
- Plasma reactors and furnaces are of compact size;
- The use of plasma torches minimizes the emission of CO₂ and other green house gases into the atmosphere that takes place when fossil fuel burners are used;
- High temperature of the plasma flow allows higher thermal efficiency compared with fuel burners. It compensates for the higher cost of electricity compared with the thermal energy derived from burning fossil fuel.

4 DEVELOPMENT OF A LABORATORY SCALE PLASMA PLANT

An experimental plasma plant was developed and manufactured, aiming to provide different modes of treating fly ash. The experimental plasma reactor is shown in Fig. 1. The plant was equipped with a transferred arc plasma torch with a capacity of 40–80 kW; current strength is 150–300 A; temperature of arc 10 000–15 000 °C. It is possible to use different plasma forming gases, such as nitrogen, argon or compressed air. The capacity of the plant is 10–20 kg/hour of ash [10, 11]. Compressed air is used as transport gas for dispersed material loading to reaction chamber. The reaction chamber has a fireproof brick lining and removable water-cooling cover. The bulk temperature in reaction chamber can be varied from 1400 to 2000 °C. It depends on material to be melted. The framework was manufactured for adjustable reaction chamber volume. Volume of reaction chamber is 6 liters. The layout of the experimental plasma plant is presented in Fig. 2. The reactor is connected to cooling water supply system, gas supply system and control system.

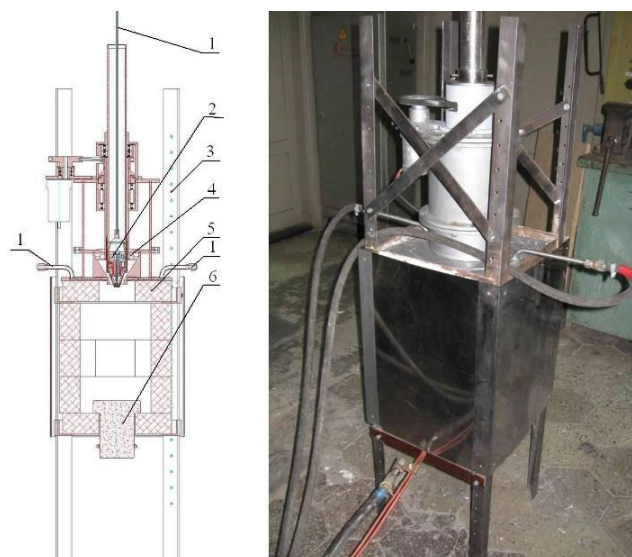


Fig. 1. Experimental plasma reactor for treating fly ash (1 – cooling water supply; 2 – plasma torch; 3 – framework; 4 – ash loading system; 5 – fire-proof brick lining; 6 –bottom electrode)

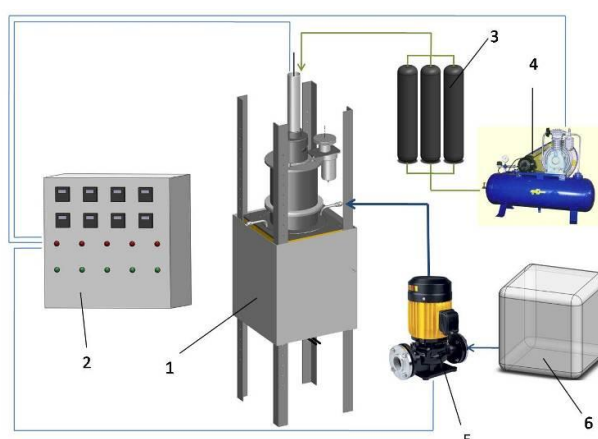


Fig. 2. Layout of the experimental plasma plant (1 – plasma reactor; 2 – control panel; 3 – receiver; 4 – compressor; 5 – water cooling system pump; 6 – water cooling system tank)

5 CHEMICAL COMPOSITION AND MORPHOLOGY OF ASH SAMPLES INVESTIGATION

In this project [12], we received some samples of ash from heavy oil combustion at power plant. The study of the composition of ash samples and its structure was carried out using a scanning electron microscope with an energy-dispersing X-ray fluorescent spectrometer channel. The chemical composition of macro components and the morphology of substances were determined with this method. The analysis shows that about 75–80% of the material has spheroidal form with dimensions from 10 to 130 μm . Two images made by the scanning electron microscope are shown in Fig. 3.

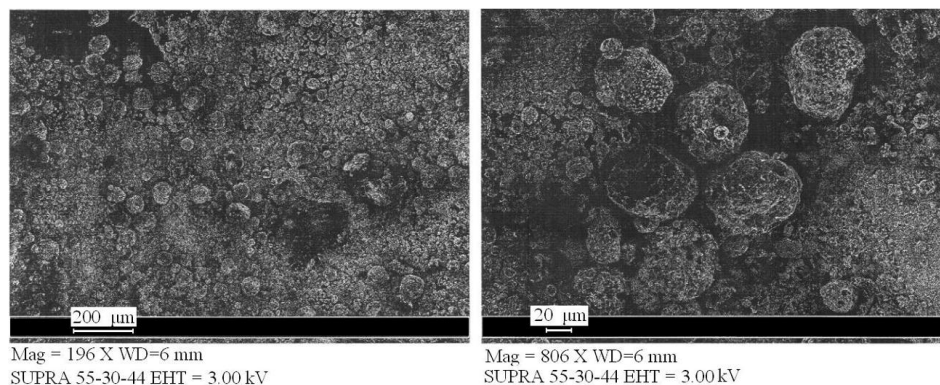


Fig. 3. Images of a fly ash sample received with a scanning electron microscope

For the preliminary estimation of the chemical composition, we chose an area of 70x50 µm where characteristic X-ray emission was excited with an electron beam of 200 keV in the mode of scanning the selected area. The secondary radiation was analyzed with an energy-dispersion silicon detector with liquid nitrogen cooling and energy resolution of 134 eV. It should be noted that the relative error of the method may be 5%. The results of the preliminary analysis show that carbon constitutes about 85% of the mass fraction of the material (Table 2). High rate of underburning takes place in the technological process at power plant.

Table 2. Elemental composition of macro components of the fly ash
(X-ray fluorescent analysis method)

Element	% atomic
C	85.97
O	9.98
S	3.12
Mg	0.32
V	0.29
Si	0.19
Al	0.13

In order to obtain complete and detailed information about the thermal properties of the samples, derivatography investigations were conducted. The results of the measurements in the modes of DTA (differential thermal analysis) and TG (thermogravimetry) are presented in Fig. 4. The analysis of the results confirms that more than 90% of the mass fraction of the material was transferred to volatile state during thermal annealing up to 1000°C. The characteristic peak in the DTA curve appears at 450°C due to the oxidation of carbon. Mass reduction at 860°C can be explained by the conversion of sulfur compounds into volatile substances.

Solid-phase microextraction and chromatography/mass spectroscopy were used to determine organic toxins. The results of the analyses show that the concentration of toxins is lower than specified by environmental requirements.

The analysis of heavy metals was carried out by Inductively Coupled Plasma Optical Emission Spectroscopy (ICP-OES Analysis). This method allows identifying up to 73 chemical elements with sensitivity up to ppb. In this method samples are introduced into plasma in the form of solutions. Since the graphitic carbon component is almost insoluble using conventional methods of sample preparation, we had to develop a special method that allows dissolving graphite without losing heavy metals.

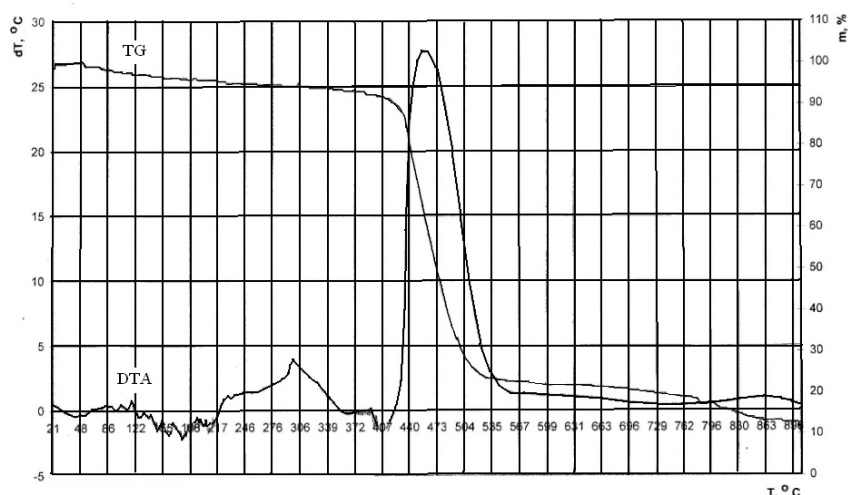


Fig. 4. The results of the derivatography analysis of ash

Following the developed method, three grams of dry sample were weighed in a glass flask for decomposition. Sixty milliliters of sulfuric acid and fifty milliliters of concentrated perchloric acid were added into the flask. In addition, a special condenser was used to collect volatile components. Thirty milligrams of vanadium pentoxide were added to the solution as a catalyst for the process. We used only pure reagents in order to avoid uncontrolled pollution of the sample by impurities. Experiments show the applicability of the method even in case of wood and coal.

After the sample was dissolved it was filtered and poured into a flask. The volume was adjusted to 200 ml. This sample was used for the analysis of heavy metals by the ICP-OES. Analytical wavelengths which provide measurements with minimum potential spectral interferences and maximum sensitivity were selected. The results of the analysis are presented in Table 3.

6 RESULTS OF EXPERIMENTS

We used ash from wood burning as a model in preliminary tests. The average chemical composition of the ash was 90 % of carbonates and oxides of sodium, calcium, magnesium, iron, and 10 % of other substances, including non-burned carbon and organic compounds. After the plasma processing the chemical composition of the product material was: CaO – 45%, SiO₂ – 32%, Al₂O₃ – 8%, Fe₂O₃ – 8%, MgO – 4%, K₂O – 2%, Na₂O – 1%.

In order to produce a homogeneous compound we have to add SiO₂ (sand) to the ash. The results of the experiments are shown in Fig. 5–6.



Fig. 5. Melted ash



Fig. 6. Vitrified material

Table 3. Micro-component composition of ash

Element	Wavelength, nm	Conc.	Units	Element	Wavelength, nm	Conc.	Units
Ag	328.068	3	ppm	Na	589.592	0.23	%
Al	396.152	0.30	%	Ni	216.555	0.34	%
As	188.98	24	ppm	P	213.618	2751	ppm
Au	242.794		ppm	Pb	220.353	18	ppm
B	249.772		ppm	Pd	340.458		ppm
Ba	493.408	28	ppm	Pt	214.424		ppm
Be	234.861		ppm	Rb	780.026	21	ppm
Bi	223.061		ppm	S	181.972		ppm
Ca	396.847	0.02	%	Sb	206.834		ppm
Cd	226.502	1	ppm	Sc	335.372	9	ppm
Co	228.615	7	ppm	Se	196.026		ppm
Cr	267.716	272	ppm	Si	250.69	587	ppm
Cu	327.395	74	ppm	Sn	189.927		ppm
Fe	259.94	0.11	%	Sr	421.552	26	ppm
Hg	184.887		ppm	Te	214.282	286	ppm
K	766.491	322	ppm	Ti	336.122	118	ppm
La	333.749		ppm	Tl	190.796		ppm
Li	610.365	18	ppm	V	292.401	0.58	%
Mg	279.553	0.17	%	W	207.912	8	ppm
Mn	259.372	122	ppm	Zn	213.857	384	ppm
Mo	202.032	480	ppm	Zr	343.823	12	ppm

In addition, a number of experiments were conducted with ash from an oil refinery. In this case, the raw material contains high concentration of carbon. Experiments on treating the ash were conducted using the laboratory plasma reactor at 60–80 kW. A water cooled rheostat with section resistivity of 0.11 Ω was used for the plasma arc current stabilization. To prevent the leakage of waste gases we had to lower the pressure in the reaction chamber with the help of the exhaust venting system by 50–80 Pa compared to the atmospheric pressure.

As a result of the experiment, organic components of ash were completely burned out and the inorganic part was melted into a monolith (see Fig. 7). The chemical resistance of vitrified samples was tested by their leaching in deionized water. A vitrified monolithic fragment with a surface area of 5.6 cm² was placed into a container made of polypropylene of analytical purity. Then, the container was filled with deionized water (> 18 M Ω /cm). The resistance time was 14 days. The concentration of macro components was analyzed by ICP-OES (Table 4). The leaching rate of investigated elements from the vitrified sample was less than 1·10⁻⁷ g/(cm²·day).

The obtained results show high efficiency of the plasma technology for the waste ash vitrification. The result of the treatment is a vitrified compound with a low level of leaching.

Table 4. Results of the test on leaching from the vitrified sample

Element	Concentration in the contact solution, mg/dm ³
Ca	0.0230±0.0021
Fe	0.0010±0.0002
Mg	0.0010±0.0002
Na	0.0020±0.0003
K	0.0020±0.0003

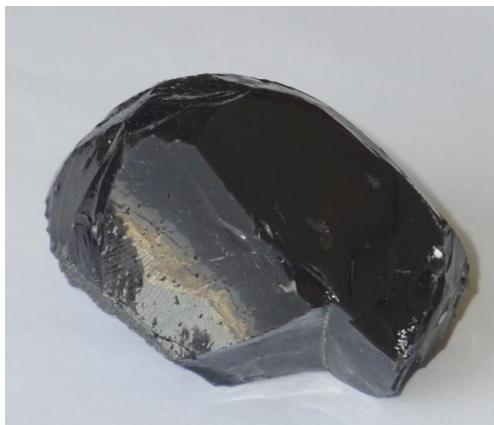


Fig. 7. Fragment of the vitrified product

7 CONCLUSION

As a result of fossil fuels combustion, a lot of ash is produced. Generally, ash accumulates heavy metals and radionuclides. Due to its high dispersion and ability to partially dissolve in water, fly ash can easily spread in the environment. Taking into account the large volume of generated ash, stringent requirements for its safe handling, and ever increasing cost of disposal, it is obvious that we have to minimize the amount of waste and convert toxic substances into safe non-leachable forms.

We propose arc plasma technology for toxic ash vitrification. We developed a laboratory-scale plasma plant of 40–80 kW for the implementation of the process. A plasma torch is the heart of the plasma plant. Bulk temperature in the reaction chamber is 1400–2000°C. As a result of the conducted experiments, we produced a homogeneous vitrified compound with a low rate of leaching. The developed method allows converting toxic ash into a solid product for long-term storage.

REFERENCES

1. *Proceedings of World of Coal Ash*. LIVINGSTON, R.A. and BUMRONGJAROEN, W. Optimization of silica fume, fly ash and cement mixes for high performance concrete, 2005, [referred on the 28th of February in 2014 y] Link to the internet <www.flyash.info/2005/79liv.pdf>
2. SHON, J., LEE, S., PARK, H., KIM, K., MIN, D. The improvement of the mechanical stability and leachability of bituminized waste form of radioactive ash by addition of reused polyethylene, *Korean Journal of Chemical Engineering*, 2001, Vol. 18, № 5, p. 668–672.
3. MASSARDIER, V, MOSZKOWICZ, P., TAHA, M. Fly ash stabilization-solidification using polymer-concrete double matrices. *European Polymer Journal*, 1997, Vol. 33, № 7, p. 1081–1086.
4. GHILOUFI, I. Simulation of radioelement volatility during the vitrification of radioactive wastes by arc plasma. *Journal of Hazardous Materials*, 2009, Vol. 163, p. 136–142.
5. KIM, H. and PARK, D. Characteristics of fly ash/sludge slags vitrified by thermal plasma. *Journal of Industrial and Engineering Chemistry*, 2004, Vol. 10, № 2, p. 234–238.



6. KINOSHITA, K., HAYASHI, A., AKAHIDE, K., YAMAZAKI T. High power plasma arc melting process for incinerated ash contraction. *Pure and Applied Chemistry*, 1994, Vol. 66, №. 6, p. 1295–1300.
7. MIN, B., KANG, Y., SONG, P., CHOI, W., JUNG, Ch., OH, W. Study on the vitrification of mixed radioactive waste by plasma arc melting. *Journal of Industrial and Engineering Chemistry*, 2007, Vol. 13, № 1, p. 57–64, 2007.
8. PARK, Y., HEOB, J. Vitrification of fly ash from municipal solid waste incinerator. *Journal of Hazardous Materials*, 2002, Vol. B91, p. 83–93.
9. BAUR, I., LUDWIG, Ch., JOHNSON, C.A., The leaching behavior of cement stabilized air pollution control residues: A comparison of field and laboratory investigations. *Environmental Science Technologies*, 2001, Vol. 35, p. 2817–2822.
10. SAUCHYN V., KHVEDCHYN I., MOSSE A., DALHOLENKA Hr., OLENOVICH A. Arc plasma application for toxic ash processing. VII International conference Plasma physics and plasma technology. Minsk, Belarus. 2012 September 17–21, Contributed papers, Vol. 2, p. 620–623.
11. SAUCHYN V., KHVEDCHYN I., MOSSE A., DALHOLENKA Hr., OLENOVICH A. Plasma technology application for ash residues processing. 25-th Symposium on Plasma Physics and Technology. Prague, Czech Republic. 2012 June 18–21, p. 63–64.
12. SAUCHYN V., KHVEDCHYN I., AL-MAYMAN S., AL-ABBADI N., AL-JUHANI M., AL-ENAZI K. Plasma technology for vitrification of ash from power plants. *High Temperature Material Processes*, 2012, Vol. 16 (1), p. 1–13.



DIAGNOSTICS OF THE ATMOSPHERIC PRESSURE THERMAL ARC PLASMA BY ENTHALPY PROBE METHOD

A. Tamošiūnas, P. Valatkevičius, V. Grigaitienė, V. Valinčius

Lithuanian Energy Institute

Plasma Processing Laboratory

Breslaujos str. 3, LT-44403 Kaunas – Lithuania

ABSTRACT

Enthalpy probe diagnostic method used for the atmospheric pressure thermal arc plasma is presented in the paper. An experimental direct current (DC) arc plasma torch was used as a source for plasma generation at atmospheric pressure. Overheated water vapor was employed as a plasma-forming gas with admixture of argon as a shielding-gas. Enthalpy probe measurements were performed in order to measure the local temperature and the velocity lengthwise and crosswise the generated plasma stream. It enabled to determine the temperature and the velocity profiles, which will help to better understand the behavior of the plasma. It was measured that at the axial distance of 0 mm the highest local temperature of water vapor plasma was 3300 ± 100 K, and the velocity was 560 ± 30 m/s, respectively. The obtained experimental results were compared to the same design plasma torch stabilized by air stream.

Keywords: plasma torch, thermal plasma diagnostics, DC thermal arc plasma, waste treatment

1. INTRODUCTION

Atmospheric pressure thermal plasmas generated by electrical discharges present considerable interest for a wide range of industrial, material science and environmental applications, such as plasma welding-cutting, material and surface treatment and plasma spraying, as well as for the utilization of hazardous organic materials with simultaneous recovery of energy from waste etc [1–4]. The good properties of thermal plasma, such as the high energy density and temperature, the treatment of a wide range of waste, and high chemical reactivity, as well as an environmental friendly alternative to conventional waste treatment methods, such as landfill or incineration, render this technology more and more attractive.

In a variety of gases used to form thermal plasma one of the most promising is water vapor due to the following unique advantages: generation of active radicals (OH, O, H), ecological cleanness, much higher enthalpy compared to air, nitrogen or other noble gases, ability to be directly involved in the chemical reactions as a reagent and heat carrier simultaneously.

In order to understand the mechanism and behaviour of outflow plasma, it is necessary to investigate plasma parameters such as enthalpy, temperature and velocity. Since the diagnostics of the DC thermal arc plasma is complicated due to very high temperatures, only very few methods could be used. The enthalpy probe measurements could be applied as a reliable diagnostic tool for the arc plasma diagnostics. It enables to determine the gas temperature and velocity profiles in the outflow plasma stream [5–8].

The present study deals with the diagnostics of the DC thermal arc plasma in a mixture of argon-water vapor at atmospheric pressure by intrusive enthalpy probe measurements. The obtained results will help to better understand the behavior of generated water vapor plasma and apply it for hazardous waste treatment.

2. EXPERIMENTAL SETUP AND METHODOLOGY

The sketch of experimental system used in the research is shown in Fig. 1. A non-transferred direct current thermal arc plasma torch of a linear design operates at atmospheric pressure. The torch consists of the following major parts: a cylindrically shaped copper cathode with inserted 2.5 mm in diameter tungsten rod, which emits electrons initiating gas ionization; a confusor type stair-shaped anode used to fix the mean arc length; and neutral section with insulating rings used for the arc stabilization in the discharge chamber by tangentially supplying plasma forming gas. Sudden expansion of the anode channel helps to minimize a large-scale shunting of the arc [9].

Noble gas argon, with flow rate of $0.52 \cdot 10^{-3} \text{ kg} \cdot \text{s}^{-1}$, was used to protect the tungsten cathode from erosion, whereas water vapor as main plasma forming gas with flow rates in range of 2.63 to $4.48 \cdot 10^{-3} \text{ kg} \cdot \text{s}^{-1}$. Dry saturated water vapor was produced by 5-bar pressure steam generator GAK-50. It was overheated to 450 K by a superheater in order to prevent the condensation on the walls of the discharge chamber of the torch. Condensation determines the shorter life-time of the copper anode and initiates the pulsations of the plasma flow asserted by the shunting of the arc.

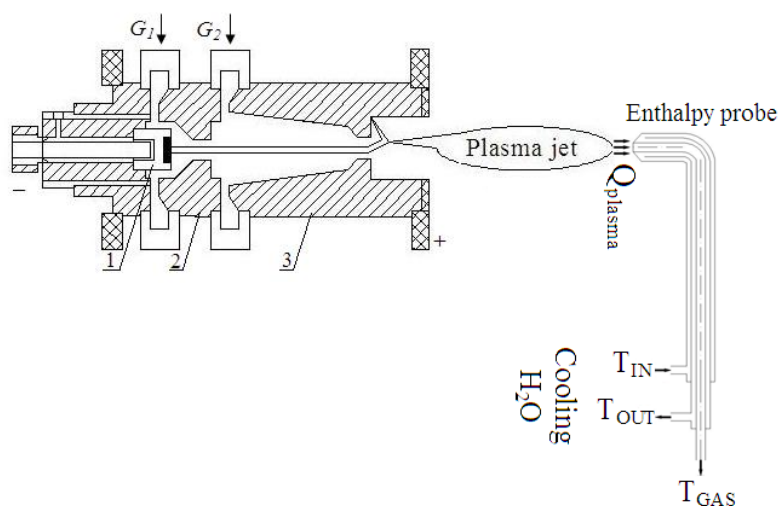


Fig. 1. Scheme of the enthalpy probe measurement system: 1 – cathode, 2 – neutral section, 3 – anode. G_1 , G_2 – gas supply, T_{IN} , T_{OUT} , T_{gas} – thermocouples measuring temperature difference of cooling agent and temperature of gas

The probe made of stainless steel consisted of the triple wall tubing, which was cooled by a high-pressure water circuit (Fig. 1). The outer diameter of the probe tube was 4 mm and the inner 0.5 mm. All measurements were performed close to isokinetic conditions. This means that the gas velocity at the probe entrance was kept similar to the free stream velocity by adjusting the sample rate.

The enthalpy of the gas was determined by calorimetric measurements in the application of stationary method based on two measurements. The first measurement makes it possible to find the heat flow on the probe without sucking the gas through the internal tube of the probe. The result on the second measurement is the heat flow on the probe with sucking the gas through the probe when it is in a contact with the high-temperature flow on both the outer and inner surfaces.

The temperature of gas could be expressed as a function of enthalpy $T_f = f(H_f)$, therefore, it was simple to determine the distribution of the gas temperature. The high

temperature flow velocity was determined from the measurement of the static pressure of the flow, using the probe as a Pitot tube. The heat flows were recorded by thermocouples.

The measurements were performed directly at the nozzle exit of the plasma torch at an axial distance of 0 mm to 100 mm, because the sufficient cooling of the probe let to avoid thermal overload of the probe tip by excessive local heat flux.

3. RESULTS AND DISCUSSION

Fig. 2 shows the temperatures of water vapor plasma in axial and radial directions measured at the torch power of 57.4 kW, the current intensity 200 A, the voltage 287 V, and the water vapor flow rate $3.71 \cdot 10^{-3} \text{ kg} \cdot \text{s}^{-1}$. The temperature and velocity profiles were compared to the same design plasma torch stabilized by the air stream ($P = 46 \text{ kW}$, $I = 190 \text{ A}$, 240 V , $G_{\text{air}} = 5 \cdot 10^{-3} \text{ kg} \cdot \text{s}^{-1}$). One can see that at the axial distance of 0 mm the temperature of water vapor plasma was much lower than the temperature of air plasma, $3300 \pm 100 \text{ K}$ and $4000 \pm 150 \text{ K}$, respectively. This could be explained by different chemical composition of water and air molecules, as well as different physical properties. At such temperatures water vapor and air were dissociated into their elemental composition. However, the mass enthalpy of water vapor plasma at such temperatures was three times higher compared to the air mass enthalpy. It means, that the probe tip observed three times higher energy flux from heated water vapor stream. The higher enthalpy of the water vapor plasma could be explained by presence of hydrogen, whereas lower temperature because of undissociated vapors which cooled down the plasma stream. The higher temperature of the air plasma was obtained in respect of high temperature oxidation (above 1870 K) of the diatomic nitrogen found in combustion air.

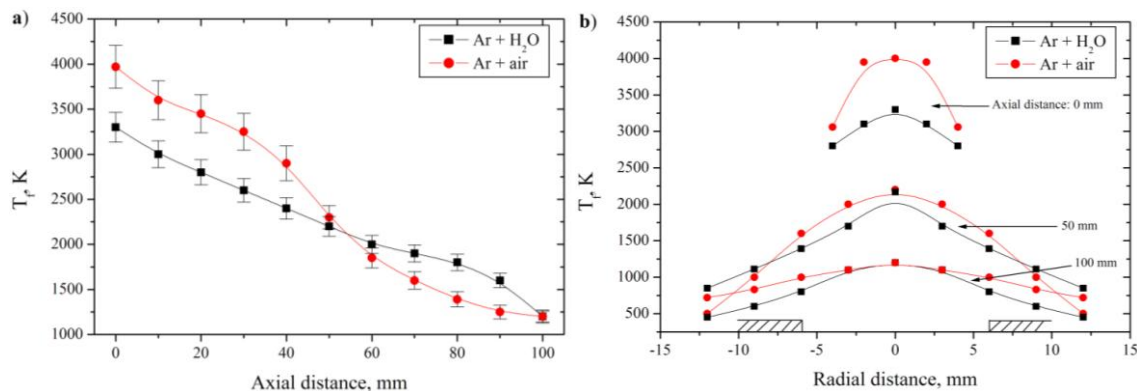


Fig. 2. Axial (a) and radial (b) distribution of the measured plasma gas temperature (T_f)

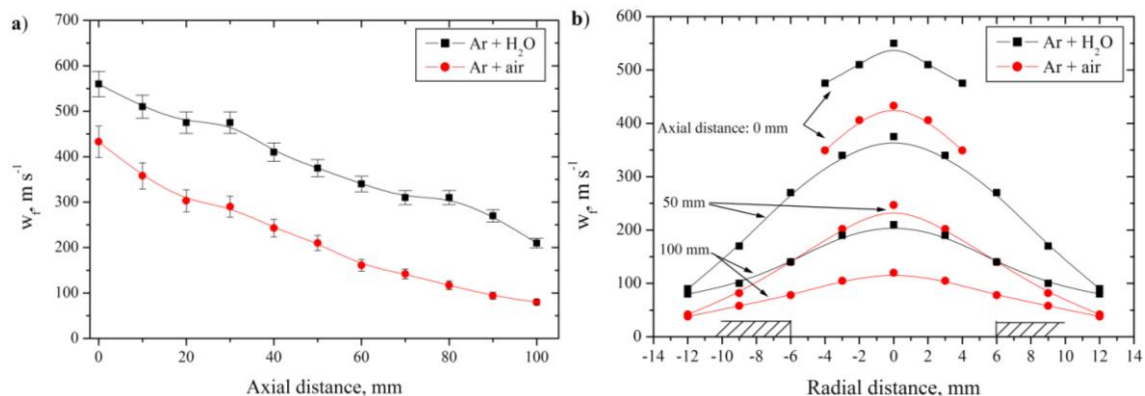


Fig. 3. Axial (a) and radial (b) distribution of the measured plasma gas velocity (w_f)

The measured velocity distributions both in the water vapor and air plasmas showed identical evolutions than the temperatures Fig 3a and Fig. 3b. The highest velocities at a nozzle distance of 0 mm in the water vapor and air plasmas were $560 \pm 30 \text{ m} \cdot \text{s}^{-1}$ and $430 \pm 25 \text{ m} \cdot \text{s}^{-1}$, respectively. The lower velocity of air used as plasma forming gas could be explained by its physical properties, such as density, viscosity. Moreover, high quenching rate of the plasma, fast recombination of excited species and mixing with the colder ambient air determined lower velocities of the flow. At an axial distance of 50 and 100 mm no significant differences between the temperature and velocity profiles had been observed. The same tendency was seen in radial direction.

Despite the fact that the mean temperature of water vapor plasma was measured to be lower and the velocity was higher compared to the air used as plasma forming gas, but, in all cases, the mean mass enthalpy of water vapor plasma was around three times higher the mean mass enthalpy of air plasma (Fig. 4).

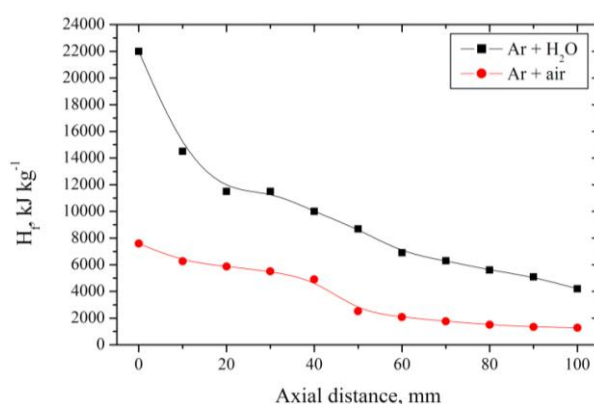


Fig. 4. The mean mass enthalpies (H_f) of water vapor and air plasma at an axial distance

It's very important factor in hazardous waste treatment to keep the treated materials in the reaction zone as longer as possible (usually 1–2 s for solid phase). But, because of the higher velocity of water vapor plasma flow, the residence time of treated materials inside the plasma-chemical reactor would be lower. Thus, it could affect lower conversion efficiency. On the other hand, due to the three times higher enthalpy of water vapor plasma, treated hazardous materials would absorb three times higher energy flux from the flow. It means that it could be decomposed into non-hazardous substances much faster and the neutralization process would be more effective than air plasma used. Moreover, due to the chemical composition of water vapor, no undesirable compounds, such as nitrogen oxides, would be produced as it is using air as plasma forming gas.

4. CONCLUSIONS

In this experimental research diagnostics of the atmospheric pressure thermal arc water vapor plasma by intrusive enthalpy probe measurements were performed.

The temperature and velocity profiles determined by means of the enthalpy probe in the water vapor and air plasma showed different results. At an axial distance of 0 mm the temperature and velocity of water vapor plasma were $3300 \pm 100 \text{ K}$ and $560 \pm 30 \text{ m} \cdot \text{s}^{-1}$, while in case of air used, $4000 \pm 150 \text{ K}$ and $430 \pm 25 \text{ m} \cdot \text{s}^{-1}$, respectively. The mean mass enthalpy of water vapor plasma was around three times higher the mean mass enthalpy of air plasma. Knowing the distribution of the temperature and velocity profiles it is possible to improve the design of a plasma-chemical reactor used for the organic waste treatment.



ACKNOWLEDGEMENTS

This research was funded by the grant (No. ATE-10/2012) from the Research Council of Lithuania.

REFERENCES

1. TENDERO, C., TIXIER, C., DESMAISON, P.T.J., LEPRINCE, P. Atmospheric pressure plasmas: A review. *Spectrochimica Acta Part B: Atomic spectroscopy*, 2006, Vol. 61, p. 2–30.
2. MOUSTAKAS, K., FATTA, D., MALAMIS, S., HARALAMBOUS, K., LOIZIDOU, M. Demonstration plasma gasification/vitrification system for effective hazardous waste treatment. *Journal of Hazardous Materials*, 2005, Vol. B123, p. 120–126.
3. BYUN, Y., CHAO, M., CHUNG, J.W., NAMKUNG, W., LEE, H.D., JANG, S.D., KIM, Y.S., LEE, J.H., LEE, C.R., HWANG, S.M. Hydrogen recovery from the thermal plasma gasification of solid waste. *Journal of Hazardous Materials*, 2011, Vol. 190, p. 317–323.
4. VAIDYANATHAN, A., MULHOLLAND, J., RYU, J., SMITH, S.M., CIRCEO, L.J. Characterization of fuel gas products from the treatment of solid waste streams with a plasma arc torch. *Journal of Environmental Management*, 2007, Vol. 82, p. 77–82.
5. MAUER, G., GUINARD, A., STOVER, D. Process diagnostics in suspension plasma spraying. *Surface and Coatings Technology*, 2010, Vol. 205, p. 961–966.
6. FINCKE, J.R., SNYDER, S.C., SWANK, W.D. Comparison of enthalpy probe and laser light scattering measurement of thermal plasma temperature and velocities. *Review of Scientific Instruments*, 1993, Vol. 64, p. 711–718.
7. GAO, Y., AN, L.T., SUN, CH.Q., YAN, Z.J. Measurement of a low power plasma jet by the enthalpy probe. *Proceedings of the International Thermal Spray Conference* 10–12 May 2004, Osaka, Japan.
8. RAHMANE, M., SOUCY, G., BOULOS, M. Analysis of the enthalpy probe technique for thermal plasma diagnostics. *Review of Scientific Instruments*, 1995, Vol. 66, p. 3424–3431.
9. ZHUKOV, M.F., ZASYPKIN, I.M. *Thermal Plasma Torches: Design, Characteristics, Applications*. Cambridge International Science Publishing Ltd, 2007. 600 p. ISBN-13: 978-1-904602-02-6.

SPECTROSCOPIC ANALYSIS OF SYNGAS GENERATED FROM WOODEN PELLETS ADDITION TO NATURAL GAS COMBUSTION

A. Saliamonas, N. Striūgas, R. Navakas

Lithuanian Energy Institute

Laboratory of Combustion Processes

Breslaujos str. 3, LT-44403 Kaunas – Lithuania

ABSTRACT

The analysis of flame chemiluminescence is known as a good non-intrusive method for combustion process monitoring and control. Currently there are more than one way to analyse chemiluminescence. Main methods are emission or absorption spectroscopy, Planar Laser Induced Fluorescence (PLIF) method, flame tomography. All these methods can give decent information about the combustion process.

This article presents results of flame analysis by using emission spectroscopy method for registering chemiluminescent species OH^* , CH^* and C_2^* . These radical species are known as main indicators of chemical reactions and namely – hydrocarbon decomposition. It is known that it is possible to analyse and compare chemical kinetics between different fuel mixtures combustion by measuring spatial distribution of these species around the burner.

The aim of this research is to determine the differences of chemiluminescent emissions between pure natural gas and mixture of natural gas and syngas from wooden pellet gasification process. The influence of syngas to combustion process is important topic because it is mostly related to use of renewable energy sources.

Keywords: Syngas, combustion, chemiluminescence, renewable energy sources, spectroscopy

1. INTRODUCTION

In past decade the use of in creation of active combustion process management systems made a great progress. During this time main methods of analysis were developed for processing data which was acquired by non-intrusive optical monitoring by using chemiluminescence effect. Most common tools for such research are casegrain optics, flame reconstruction by using Abel transformation or 3d topography algorithms and use of Planar Laser Induced Fluorescence (PLIF) [1]. These tools have their cons and pros. For example PLIF is most successfully applied in small particle tracking but it is also applicable for chemiluminescence research. The downside of this technique is that equipment is expensive and applicable mostly for laboratory research. Also it is known that ground state OH radicals which are abundant in the post flame gas reaction zone can be excited by PLIF and this can give errors in research. This problem doesn't apply when using casegrain (CS) optics, because it detects only the natural chemiluminescence in the reaction zone. [2]. The Abel transform and 3d topography methods are cheapest way for analyzing data, but it requires very steady and symmetrical flame, because this mathematical method gives best results when input data has cylindrical symmetry [3]. By Using these tools some major steps were done in research of relation between flame chemiluminescence and combustion process control.

Hardalupas and Orain et al. [4] used natural gas with 94% methane and air that were premixed and subsequently injected with a symmetrical flow in opposing jets through four pipes, parallel to the axis of the burner. The paper results stated that intensities of chemiluminescence from OH and CH and background intensity from CO_2 are able to indicate the heat release rate, whereas that from C_2 is not. It was also found that the intensity ratio OH/CH has a monotonic decrease with equivalence ratio for lean and stoichiometric mixtures, while remaining independent of flame strain rate that means that it is possible to measure

equivalence ratio of the reacting mixture using intensity of chemiluminescence. Veríssimo and Rocha et al. [5] based on the OH* images reported that as excess air coefficient increases the main reaction zone moves progressively closer to the burner presumably due to the increase in the central jet momentum, which leads to a faster entrainment of fuel and burnt gases, and due to the increase in the oxygen concentration in the recirculated flue-gas. Bouvet and Chauveau et al. [6] commented that the volumetric heat loss and collisions of active radical species are dependent of the burner tube diameter and increases with increase of diameter. This is why syngas flames in their research with % H₂ < 20% could not be sustained at the open end of the 4 mm diameter tube while stable flames could be obtained on the 12 mm burner for the same mixture compositions. They also noted that the flame stability regions can be considerably extended towards lower equivalence when using a methane/air pilot flame. Higgins and McQuay [7] added that OH emission decreased significantly with increasing pressure. In their research the OH emission also monotonically increased with the equivalence ratio and a linear relationship was observed between increasing mass flow and increasing chemiluminescence as in [4]. So it was concluded that suitable resolution and dynamic range exist for a high-pressure flame to be adequately controlled to minimize both NO_x and CO emissions.

Table 1. Main kinetic reaction pathways and the wavelengths representing the chemical reaction [8]

Radical	Reactions		Wavelength(nm)
OH*	R1:	$\text{CH} + \text{O}_2 \rightarrow \text{CO} + \text{OH}^*$	282.9, 308.9
CH*	R4:	$\text{C}_2\text{H} + \text{O}_2 \rightarrow \text{CO}_2 + \text{CH}^*$	387.1, 431.4
C ₂ *	R6	$\text{CH}_2 + \text{C} \rightarrow \text{C}_2^* + \text{H}_2$	513, 516.5

Ballester and Garcí'a-Armingol et al. [8] concluded that the chemiluminescent light emitted is directly proportional to the concentration of the excited radical, which is a result of its formation and destruction rates. The concluded main kinetic reaction pathways and the wavelengths representing the chemical reaction where presented in Table 1. For example based to Higgins and McQuay et al. [9] the CH chemiluminescence near 430 nm is from excited state CH (i.e. CH(A²Δ)) produced primarily through the reaction of C₂H with molecular oxygen. The resulting excited CH either loses its energy through spontaneous fluorescence (i.e. chemiluminescence) or through physical quenching (i.e. collisions). According to this information for experiments in this paper where used filters, that represent R1, R4 and R6 reactions because they are considered to be leading reactions of combustion process.

The aim of this article is to investigate how mixing syngas with the natural gas flow changes spectral characteristics of flame at OH, CO and C₂ wavelength ranges. The results of this research are necessary for determining if already existing tendencies for air equivalence ratio determination can be applied for gas that was produced from renewable energy sources like woodchips gasification.

2. METHODOLOGY

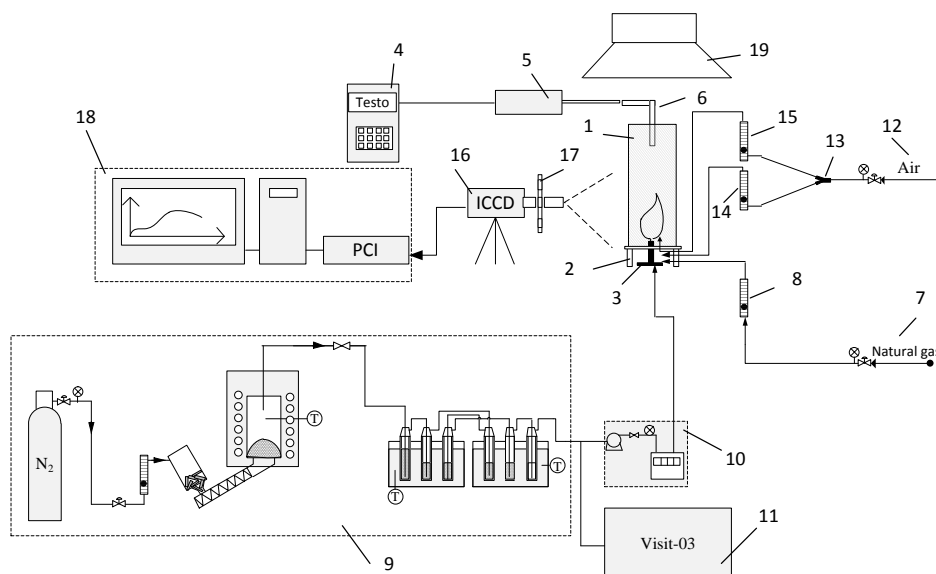


Fig 1. Experimental stand: 1) Quartz pipe; 2) Combustion chamber stand; 3) Bunsen burner 4) Flue gas analyzer; 5) Analizatoriaus zondas; 6) Copper tube; 7) Natural gas source; 8) Gas rotameter; 9) Gasification reactor system; 10) Aspirators; 11) Syngas composition analyzer; 12) Air source; 13) „Y“ shaped elbow ; 14) Primary air rotameter; 15) Secondary air rotameter; 16) ICCD camera; 17) Optic filters 18) Computer with PCI board; 19) Duct

Research was carried by using experimental stand built in Lithuanian Energy institute combustion process laboratory chemiluminescent species spatial distribution in laminar flame at atmospheric pressure (Fig. 1). Combustion chamber was made of 56 cm height and 6 cm diameter transparent quartz glass pipe (1). The pipe was mounted on metal stand (2) which connects combustion chamber and Bunsen burner (3). There was a gap between Bunsen burner and metal stand, to let secondary air in to the chamber. For flue gas analysis TESTO analyzer was used (4). Flue gas analyzer data is given in Table 1

Table 2. Flue gas analyzer data

Mixture	Excess ratio	O ₂ , %	CO, %	CO ₂ , %	NOX, mgm ³	SO ₂ , mgm ³	T, °C
Pure natural gas	1	0.116	16904	10.68	124.6	0	41.04
	1.1	0.496	153	11.418	149.4	1	41.34
	1.3	3.496	4.2	9.798	198.8	7.2	47.78
Natural gas 65%, Syngas 35%	1	1.74	2612.4	11.268	118.2	38	39.82
	1.1	2.214	43	11.07	141.4	4.2	41.08
	1.3	4.702	9	9.72	146	8	36.78

The probe was inserted in to chamber with 50 cm distance from the burner. To protect from ambient leakage whole combustion chamber was set under ventilated duct (19).

During experiment mixtures from table 1 were used. Natural gas was supplied at constant 0.3 MPa pressure. For each measurement a precalculated (Table 2) volumetric flow was set with rotameter. Rotameter's measuring range was 0.5–5 l/min, error ± 0.1 , maximum pressure 14.1 kg/cm².

Table 3. Precalculated air and fuel flow

Amount of fuel in the mixture		Fuel flow and power		Air flow l/min		
		Natural gas flow	Syngas flow.	ER=1.0	ER=1.1	ER=1.3
Natural gas.	Syngas.	l/min				
1	0	1.08	0	10.3	11.33	13.4
0.65	0.35	0.7	1.4	9.67	10.63	12.57

Syngas was generated by using lab scale gasification reactor (9). It consists of biomass pyrolysis reactor and tar condensers. Syngas were generated by doing following procedures:

Nitrogen flow (1.8 l/min) for pyrolysis gas transportation was supplied in to a container filled with fuel pellets. For experiments a pine and spruce wood pellets where used. Pellets properties are given in Table 3.

Table 4. Properties of wood pellets used in experiment

Ash, % of mass	Moisture content, % of mass	Lower calorific value, MJ/kg	Dry wood composition, % of mas				
			C	H	O (difference)	N	S
0.35	5.20	19.00	49.20	6.20	44.46	0.08	0.06

Pellets where supplied by constant 5g/min flow in to a pyrolysis reactor. The temperature of reactor was set to 850 °C. There was a syngas cleaning system for removing tar from gas. This system consists of 6 bottles filled with isopropanol (99.5% “sigma aldrich). The bottles where put in to two bats with different temperatures. First condenser was filled with 150 ml isopropanol, four remaining where filed with 100 ml isopropanol and the last one was filled with 6 mm diameter glass balls. Gas cleaning (rinsing) was proceeded in all bottles with different temperatures. First bottle (+40°C) → 2 – (+40°C) → 3 – (-16°C) → 4 – (+40°C) → 5 – (-16°C). Last bottle collected remaining drops of tar, that where carried by the flow after rinsing. Prepared syngas where then supplied trough separate channel in to the burner. The flow was controlled by aspirimeter „Zambelli ZB1“ (10), (flow 0–6 L/min, error ± 0.1), (10). Syngas composition was monitored with analyzer “Visit-03” (11). Syngas composition is given in Table 4.

Table 5. Average composition of syngas during the experiment

Mixture	ER	O ₂ , %	H ₂ , %	CO, %	CH ₄ , %	CO ₂ , %
Natural gas 65%, syngas 35%	1	0.08	16.2	15.4	10.68	7.22
	1.1	0.14	13.36	12.74	10.9	6.44

Air flow was supplied by two channels. The channels where separate by “Y” shaped elbow (13). Primary and secondary air flows were controlled by rotameters (Primary air 0–10 L/min (21.1 °C), error ±2, max pressure 1379 kPa; Secondary air (15), 1–20 L/min, error ±1). Primary air was mixed in to the gas flow inside the burner. Secondary air was flowing in to the burning chamber trough a gap between burner ant metal stand. This way the

“ambient air” was simulated and the flame was stabilized. Experiments were performed for ER 1.0, 1.1 and 1.3 with maintaining same calorific value for the mixture

The flame was monitored with “andor iStar” ICCD camera (16). It is ccd (charge coupled device) with 18 mm sensor. Sensor consists of 1024x1024 pixels sensitive to 200 – 800 nm wavelength light.

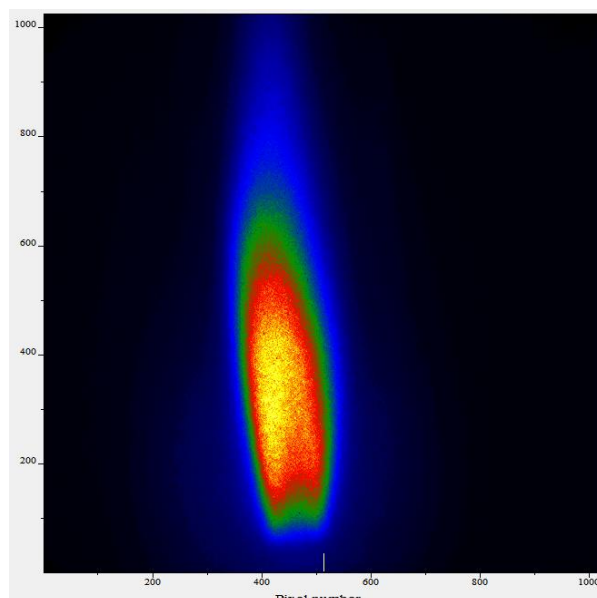


Fig 2. Example of flame image

Distance between camera and burner was 2.78 m. Resolution achieved was 6.6 pixel/mm. The ICCD camera operated with “Solis” software. Exposure was set to 01.s. 300 frames were accumulated in to single frame for each flame condition and each optical filter. Single accumulation cycle time was set to 1.266.

For registering individual species five optical filter were used (17). Filter parameters are given in Table 6.

Table 6. Optical filter parameters

Filter	Wavelength	Transparency	CWL*	FWHM**
CH*	431.1 nm	>95%	427 ± 1 nm	6 ± 1 nm
C ₂ *	514 nm	>65%	514.5 ± 2 nm	10 ± 2 nm
OH*	308.9 nm	>15%	310 ± 2 nm	10 ± 2 nm
CH*	387.1 nm	>90%	387 ± 1 nm	6.5 ± 1 nm
OH*	282.9 nm	>65%	285 ± 2 nm	8 ± 2 nm

*CWL – center wavelength;

**FWHM-full width at half maximum

3. DATA PROCESSING:

To reduce flame instability for each flame condition and each filter 300 frames were put together with “Solis” software resulting in single image representing mean values of species spatial distribution. To filter out the camera inter noise dark frame was taken and the values of the frame were subtracted from main image. The dark frame was taken in dark and the camera was covered with cloth to prevent accidental light leaks during exposure. Post processed data were exported via Flexible Image Transport System (FITS) files. Later FITS

files were imported in to MATLAB environment for further processing. To determine how light intensity changes along the flame every image was converted in to the single column of mean horizontal values representing chemiluminescent species spatial distribution along burner axis. Parallel there were calculated total mean values of each image to compare how chemiluminescence changes when changing ER.

4. RESULTS AND DISCUSSION

Results show that spectral intensity along flame has similar profile shape at 431.4 nm, (CH*), 514 nm (C²*), and 282.9 nm (OH) wavelengths. Similar results are obtained by other authors who used same or similar experimental methodology [10], [3]. Two peaks were observed at 1 cm and 3–5 cm distance from the burner. According to Hardalupas et al [2] only maximum intensity values are important when deciding about chemical reaction at defined point in space. Area before and after peaks are considered as reaction beginning and ending zones.

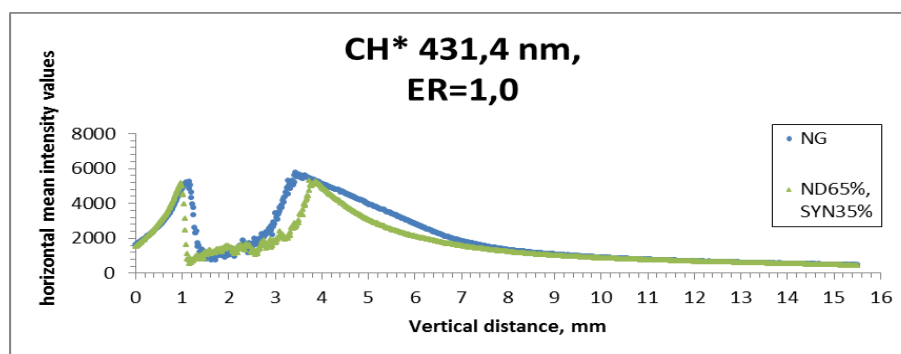


Fig. 3. Spectral intensity along flame

Stable increasing and decreasing of intensity was observed at two wavelengths (308.9 and 387.1 nm). It was assumed that this effect was due to quenching in the zone between 1 and 3 cm from burner. This assumption is based on observation of 514 nm wavelength peaks. When burning natural gas at ER=1 two peaks disappear and only one extended peak can be observed. It is related to high C²* concentration. In that case flue gas analyzer also shows high CO concentration that is related to C²* existence in combustion zone [11].

NO_x reduction was observed when using gas mixture instead of pure natural gas. The reason of this effect relates with hydrogen existence in the mixture. There are more than few researches stating that hydrogen addition to lean natural gas mixture lowers the NO_x emissions [12, 13].

Hydrogen existence in the mixture also explains the reason why in most of current work results faster peak maximum was observed (when peak is closer to burner it means that reaction occurred faster) when using mixtures. Hydrogen reacts faster than methane and increases temperature in reaction zone. That boosts reactions and they end faster and closer to the burner's end [14]. This theory can also be supported with VISIT analyser data of syngas composition compared with chemiluminescence results.

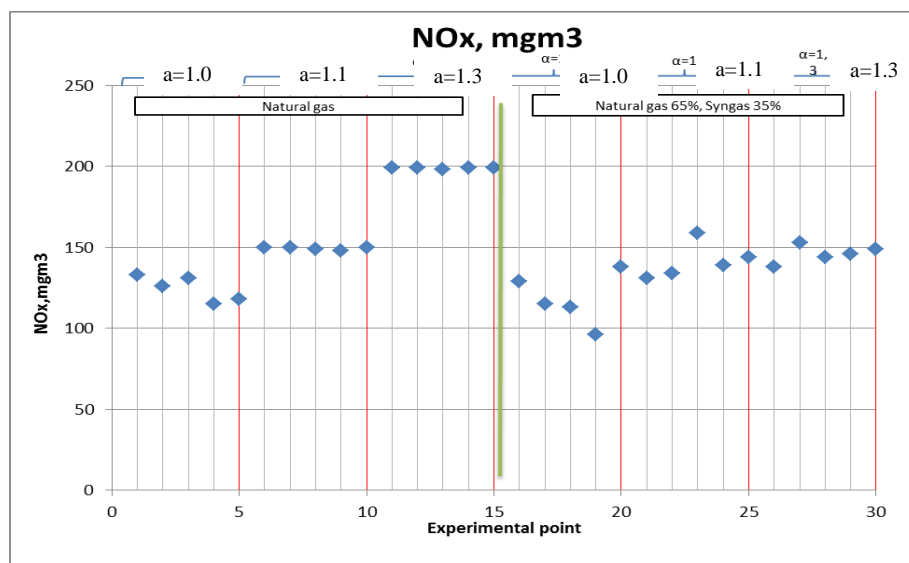


Fig. 4. Gas analyzer data

Multiple articles report of ER relation with chemiluminescence intensity [1, 2, 15, 16]. This relation also can be seen in current research. This tendency also remains not only for pure natural gas but for the mixtures with syngas to (Fig. 5).

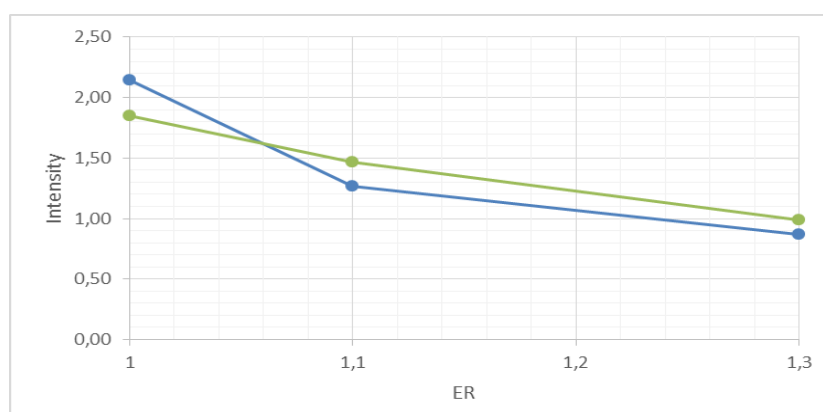


Fig. 5 The dependence between Intensity and ER. Blue line – natural gas only.
Green line – natural gas +35% syngas

5. CONCLUSIONS

Due to quenching in the zone between 1 and 3 cm from burner a stable increasing and decreasing of chemiluminescent species intensity was observed only at 308.9 and 387.1 nm wavelength.

Hydrogen existence in gas mixture resulted in decreased NO_x emissions when burning natural gas with syngas addition.

A chemiluminescence maximum intensity peak shift towards burner was due to hydrogen in the syngas. Hydrogen resulted higher temperature and chemical reactions developed faster.

Excess ratio can be expressed as function of OH/CH not only for natural gas but also for the mixture of natural gas and syngas.

REFERENCES

1. DOCQUIER, N.; CANDEL, S. Combustion control and sensors: a review. *Prog. Energy Combust. Sci.* Vol. 28, No. 2, p. 107–150.
2. HARDALUPAS, Y.; ORAIN, M., PANOUTSOS, C.S. Chemiluminescence sensor for local equivalence ratio of reacting mixtures of fuel and air (FLAMESEEK). *Appl. Therm. Eng.* Vol. 24, No. 11–12, p. 1619–1632.
3. DRIBINSKI, V., OSSADTCHI, A., MANDELSHTAM, V. Reconstruction of Abel-transformable images: The Gaussian basis-set expansion Abel transform method. *Review of Scientific Instruments.* Vol. 73, 2634 p.
4. HARDALUPAS, Y.; ORAIN, M. Local measurements of the time-dependent heat release rate and equivalence ratio using chemiluminescent emission from a flame. *Combustion and Flame.* Vol. 139, p. 188–207.
5. VERÍSSIMO, A.S.; ROCHA, A.M.A.; COSTA, M. Operational, Combustion, and Emission Characteristics of a Small-Scale Combustor. *Energy Fuels*, Vol., p. 2469–2480.
6. BOUVET, N.; CHAUVEAU, C. Characterization of syngas laminar flames using the Bunsen burner configuration. *International Journal of Hydrogen Energy.* Vol. 36 p. 992–1005.
7. HIGGINS, B.; MCQUAY, M.Q. Systematic measurements of OH chemiluminescence for fuel-lean, high-pressure, premixed, laminar flames. *Fuel*, Vol. 80, p. 67–74.
8. BALLESTER, J.; ARMINGOL, T.G. Diagnostic techniques for the monitoring and control of practical flames. *Progress in Energy and Combustion Science.* Vol. 36, p. 375–411.
9. HIGGINS, B.; MCQUAY, M.Q. An experimental study on the effect of pressure and strain rate on CH chemiluminescence of premixed fuel-lean methane /air flames. *Fuel.* Vol. 80, p. 1583–1591.
10. HERNÁNDEZ, J.J.; LAPUERTA, M.; BARBA, J. Flame stability and OH and CH radical emissions from mixtures of natural gas with biomass gasification gas, *Appl. Therm. Eng.* Vol. 55, p. 133–139.
11. KATHROTIA, T. *Reaction Kinetics Modeling of OH*, CH*, and C₂* Chemiluminescence*. Ruprecht-Karls-Universität at Heidelberg Vorgelegt, 2011.
12. NABHANI, N.; SHARIFI, V. Investigation on the Combustion of Hydrocarbon Fuel Enriched by Hydrogen for a Cleaner Environment. Proceedings of International Conference on Chemical, Environmental Science and Engineering (ICEEBS'2012) July 28–29, 2012 Pattaya (Thailand).
13. ANDERSSON, T. Hydrogen Addition for Improved Lean Burn Capability on Natural Gas Engine. *Rapport SGC.* Vol. 134, p. 1102–7371.
14. GASUNIE, N. V. N.; ENGINEERING, G.; DARMEVEIL, H. “Should we add hydrogen to the natural gas grid to reduce CO₂ emissions? (Consequences for gas utilization equipment). 23rd World Gas Conference, Amsterdam 2006.
15. TUNESTÅL, P.; CHRISTENSEN, M.; EINEWALL, P.; ANDERSSON. Hydrogen Addition for Improved Lean Burn Capability of Slow and Fast Burning Natural Gas Combustion Chambers. *SAE Technical Paper* 2002-01-2686.
16. HARDALUPAS, Y.; PANOUTSOS, CS.; SKEVIS, G. Numerical evaluation of equivalence ratio measurement using OH* and CH* chemiluminescence in premixed iso-octane/air flames. Proceedings of the 2nd European Combustion Meeting, Louvain-la-Neuve, Belgium, 2005.

CARBON BLACK PRODUCTION FROM DIFFERENT TYPES OF RAW MATERIAL: EXPERIMENTS AND MATHEMATICAL MODELLING

S.I. Dmitriev, P.S. Grinchuk, N.V. Pavljukevich

*A.V. Luikov Heat&Mass Transfer Institute of NAS of Belarus
Brovki str., 15, Minsk 220072, Belarus*

ABSTRACT

Carbon black (CB) is widely used in industry as reinforcing filler for rubber production. All manufactures need CB with strictly formulated characteristics and quality. That is why it is important to investigate and to modernize regimes of carbon black production.

Experimental results on obtaining CB in a high temperature flow reactor after evaporation of liquid hydrocarbonic (HC) raw material of two types are given. Important physicochemical values of this process such as temperature, pressure, composition of gas mixture (H_2 , CO, CO_2 , CH_4 concentrations) are compared in terms of using of HC fuel of different types.

Hydrodynamic and kinetic models of evaporation of HC fuel droplets are formulated. A comparative analysis of modeling and experimental results concludes, that kinetic model describes the process of HC droplet evaporation in the high temperature flow reactor more precisely.

Keywords: carbon black, furnace black, pyrolysis reaction, flow reactor

1. INTRODUCTION

Carbon black (furnace black, commercial soot, further in text this term is abbreviated as CB) is fine-grained carbonic material. It is widely used in industry as reinforcing filler in rubber products and tires as well as a black pigment for paints and toners [1]. There are number of CB types that characterize its properties (e.g. average particle diameter, structure, surface-area-to-volume ratio and surface activity) according to common standards. These properties influence on physical and chemical properties of final good that consists CB. For instance, CB with the sizes of its particles of 18–30 nm makes high strength and excellent abrasion resistance for a tire protector (this type of CB is known as “Super Abrasion Furnace” [2]). At the same time carcass of tire consists CB with the particle diameter of 40–60 nm that gives softness with losses of strength effect [3].

Carbon black is produced with the thermal decomposition method or the partial combustion method using hydrocarbons (HC) such as oil (a furnace black process) or natural gas (a thermal black process) as raw material. The furnace black process forms CB by blowing petroleum oil or coal oil as raw material (feedstock oil) into high-temperature gases to combust them partially. This method is suitable for mass production due to its high yield, and allows wide control over its properties such as particle size or structure. This is currently the most common method used for manufacturing carbon black for various applications from rubber reinforcement to coloring.

With an increasing aromaticity of used feedstock oil with the same other conditions of furnace method following characteristics of obtained CB are enlarged: structuredness (i.e. degree of particles coalescence), degree of dispersion, CB yield, etc. [3]

In this article, chemical and physical values of CB obtaining process by furnace method with using of two different HC raw material are studied. Obtained CB was compared in terms of the surface-area-to-volume ratio measured by BET (Brunauer–Emmett–Teller) and Langmuir methods. Working installation design involves modern technologies as described

further and this aspect gives novelty for experiments carried out. Another purpose is an investigation of obtained CB species for discovering the proper producing technology in the future.

For precise understanding of physicochemical processes that occur during formation of CB particles a mathematical model is formulated and presented in this paper. The model allows estimating a contribution of some key factors (e.g. the rate of HC droplet evaporation in a reactor) by means of hydrodynamics and kinetics approaches. It gives understanding about scales of HC material evaporation in comparison with the length of horizontal reactor. Such estimations help us to be sure that with given parameters (the diameter and concentration of HC droplets, temperatures in the reactor chamber, etc.) feedstock oil evaporates quickly without grit formation that negatively affects on CB quality. These estimations can be further expanded to the global model of CB particles formations in the furnace reactor.

As there is no generally accepted theory of CB formation today it can be a subject for investigation. Existing theories only agree that CB is formed from liquid phase but they differ in describing the mechanism of its formation [4].

2. EXPERIMENTS ON CB PRODUCTION

2.1. Installation for CB production

During last three years at the A.V. Luikov Heat and Mass Transfer Institute of NAS of Belarus an experimental installation for investigation of regimes of CB producing by furnace method was modernized. The modernization based on solution of some technical problems on CB catching system, liquid feedstock material spraying and methods of automated measuring of temperatures and gas concentrations.

This experimental installation works on basis of thermal pyrolysis of HC fuel in a flow-type reactor. A principle diagram of the installation is shown in Fig. 1. Natural gas and air with controlled flow rates are supplied at the gas burner (1 in Fig. 1) established at the beginning of the reactor from refractory ceramics. A burning of natural gas / air mixture results in creation of high-temperature smoke fumes containing a certain amount of uncombined oxygen. Obtained gas mixture flows in the reactor prechamber 3. A liquid HC fuel is scattered from a water-cooled centrifugal nozzle 2 into the reactor prechamber which has the temperature of about 1400–1500°C. Fine-dispersed droplets of HC fuel evaporate quickly (see sub-section 3.3 on the velocity of evaporation). The fact that CB is formed only from vapour phase is a proven fact [3]. If the liquid fuel begins to decompose quicker than it evaporates, grit particles are created. They are often a contamination agents for finally obtained CB. Therefore, the major feature of the installation design at this stage is a spraying into fine-dispersed droplets which evaporate quickly. After the reactor prechamber the gas mixture comes to the reaction channel 4. Its draft at the entrance leads to the better mixing of complete combustion gas products with HC raw material. A vapor of HC fuel is decomposed by thermal pyrolysis into less heavy molecules and chemical elements. Leaving prechamber gases still contain a certain amount of uncombined oxygen. It can react with a portion of HC fuel vapor with releasing additional energy for decomposing of the main portion of raw material. In such a manner the gas flow composition is strongly saturated with carbon vapor. Then this flow is cooled in a scrubber 10 by scattering of water. This water impact stops the thermal-oxidative reaction and cools the reaction gases as well as created by pyrolysis CB before a bag filter 11 catching solid carbon particles at the surface of cloth sleeves (bags). Refined gases are released via smoke stack and CB is gathered at the filter.

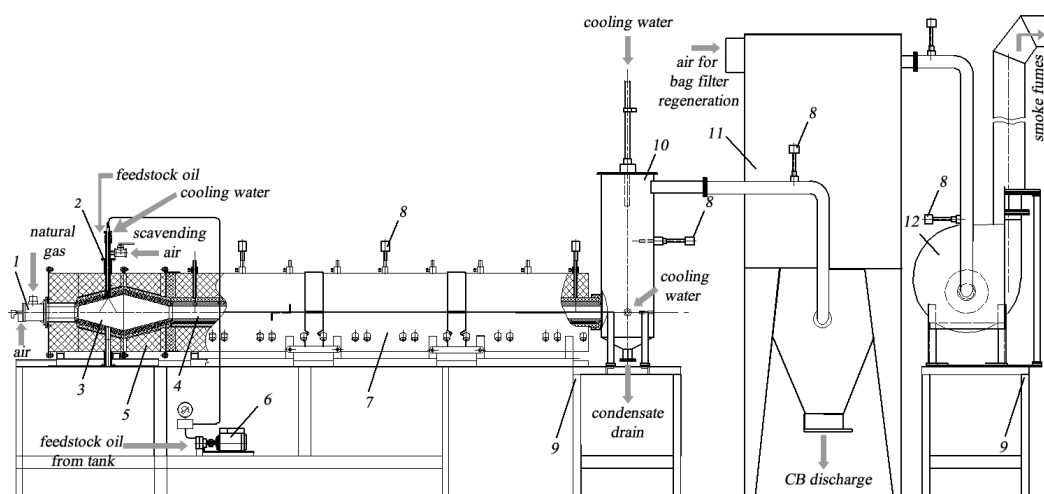


Fig. 1. Layout of the installation: 1 – gas burner, 2 – water cooled nozzle for spraying HC feedstock oil, 3 – reactor prechamber, 4 – reactor channel, 5 – fibrous insulation, 6 – pump for feedstock oil supply, 7 – steel protective cover, 8 – thermocouple, 9 – supporting metalwork, 10 – scrubber, 11 – bag filter for CB catching, 12 – exhaust fan

In the Fig. 2, *a* the reactor prechamber and channel in a steel protection cover are shown. Fig. 2, *b* is a photo of the bag filter insulated to prevent inside water condensation. For the filter bags shaking (regeneration) a sequence of compressed air impulse is applied.

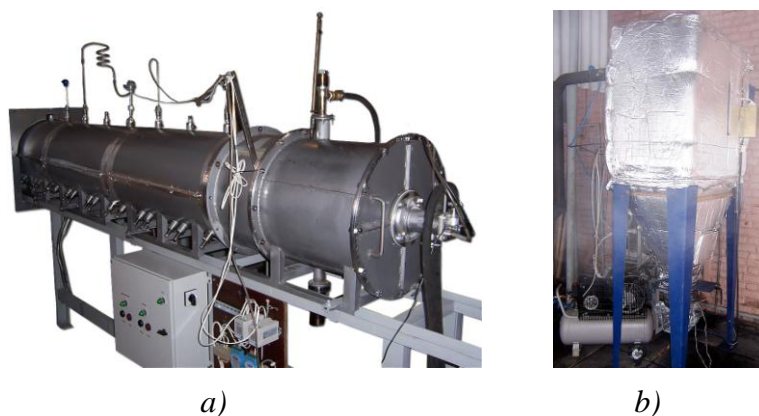


Fig. 2. Installation units: *a* – reactor under steel cover, *b* – bag filter

Table 1 shows a technical data of the installation. It is equipped with an automation system, which allows to register a number of parameters (temperatures, pressures, flow rates of operating environments) and to control the technical process.

Table 1. Technical data on the experimental installation for CB obtaining

Diameter of reactor channel, mm	80
Length of reactor prechamber and channel, m	3400
Natural gas at burner inlet flow rate, nm ³ /h	up to 8
Air flow rate, nm ³ /h	up to 90
Liquid HC fuel flow rate, kg/h	5–7
Temperature at the reaction zone, °C	~1450–1500
Productivity of CB, kg/h	1.9

Temperature of the gas mixture flow in the reactor is registered by thermocouples $Tc1$ – $Tc4$ that are sequentially set over the reactor channel (Fig. 3). Thermocouple $Tc5$ detects the temperature of a point between the outer surface of ceramics reactor channel and the beginning of insulation cover. The intake channel supplies probes for gas analyzer.

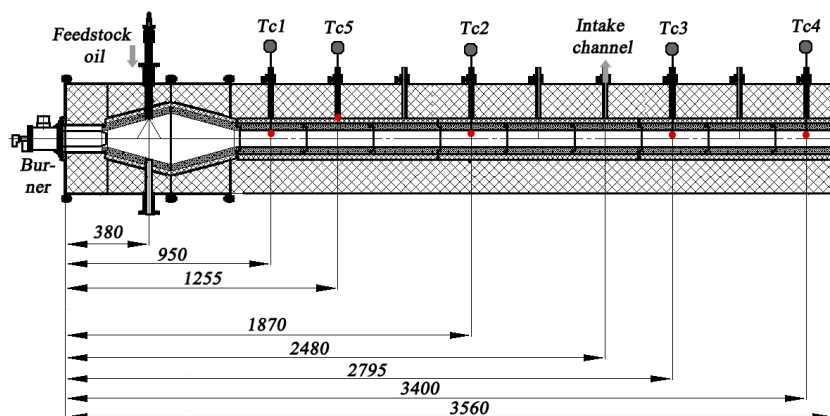


Fig. 3. Cross section of the reactor channel (dimensions are given in mm):
 $Tc1$ – $Tc5$ – high temperature thermocouples (red dots show the measuring area);
intake channels are used for gas analysis

2.2. HC feedstock material

To see the influence of HC fuel type on the obtained by furnace method CB two types of feedstock material were used: diesel fuel (density $\rho_{DF} = 790$ flow rate through the nozzle $G_{DF} = 5.0$ l/h) in an experiment #1 and high-aromaticity HC oil ($\rho_{HAO} = 970$ g/l, $G_{HAO} = 7.2$ l/h) in an experiment #2. The last one is widely used in industry for obtaining the majority CB types. As the degree of spraying depends on nozzle properties and the viscosity of fuel [5], the flow rate varies for different type of fuel (for optimal fine-dispersed spraying).

2.3. Experimental data

Two experiments of carbon black production were carried out (#1 and #2). Some physicochemical values of this process such as temperature, pressure, composition of gas mixture (H_2 , CO, CO_2 , CH_4 concentrations with accuracy of measurements ± 1 vol.% for H_2 and ± 2 vol.% for CO_2 and CO.) were registered.

Temperatures and gas concentrations for regimes of liquid HC fuel spraying and filter regeneration in experiment #1 (Fig. 4, 5 a) and #2 (Fig. 5 b) respectively are shown below. Temperature profiles (distributions) for the time moments t_1 – t_5 in the exp. #1 are given in the Fig. 5, a (each moment of time is grouped by dashed line).

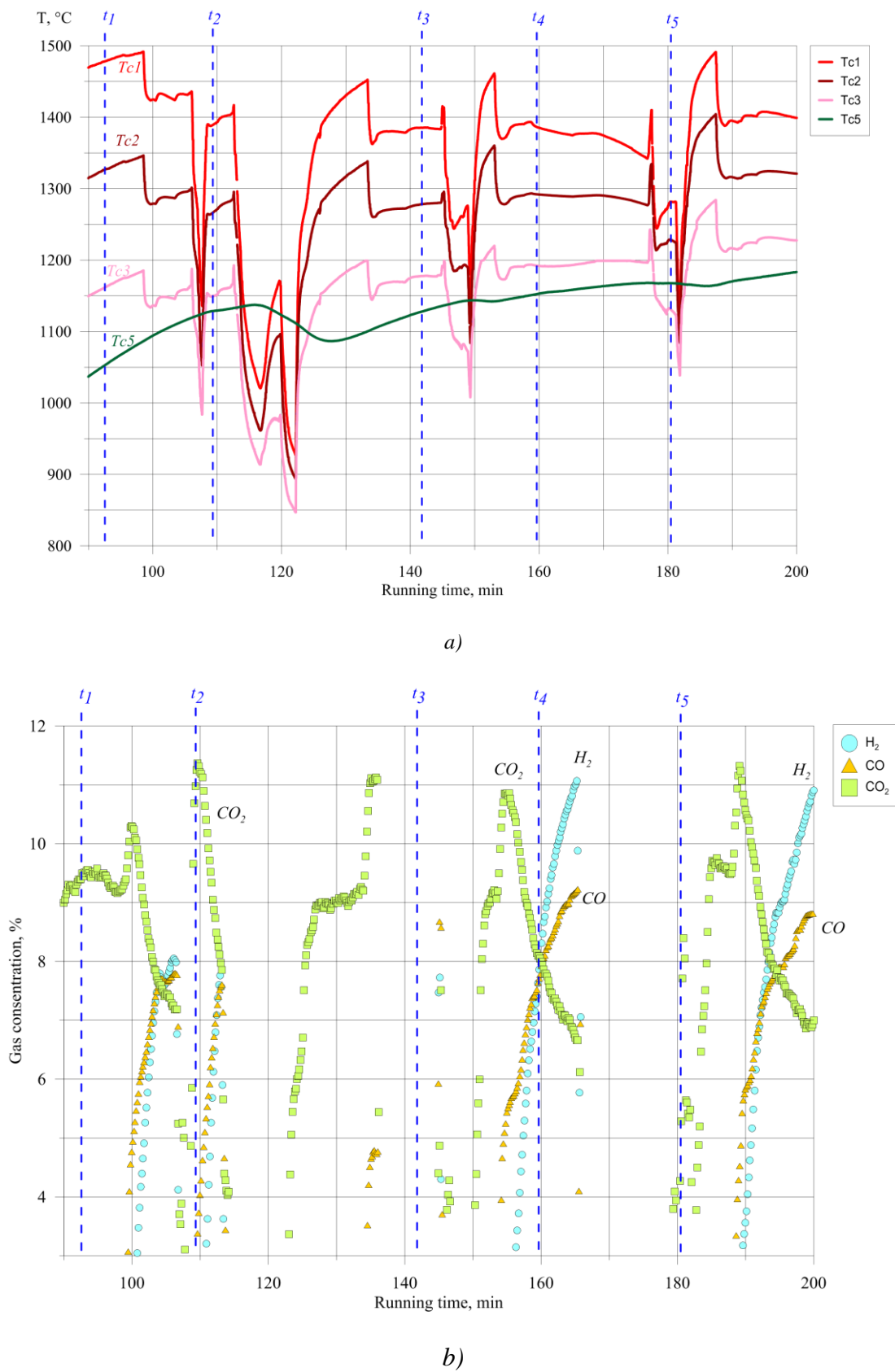
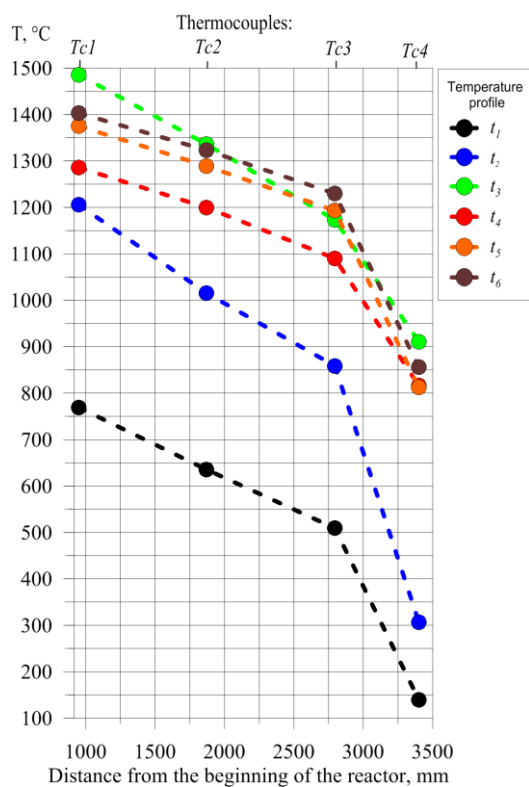
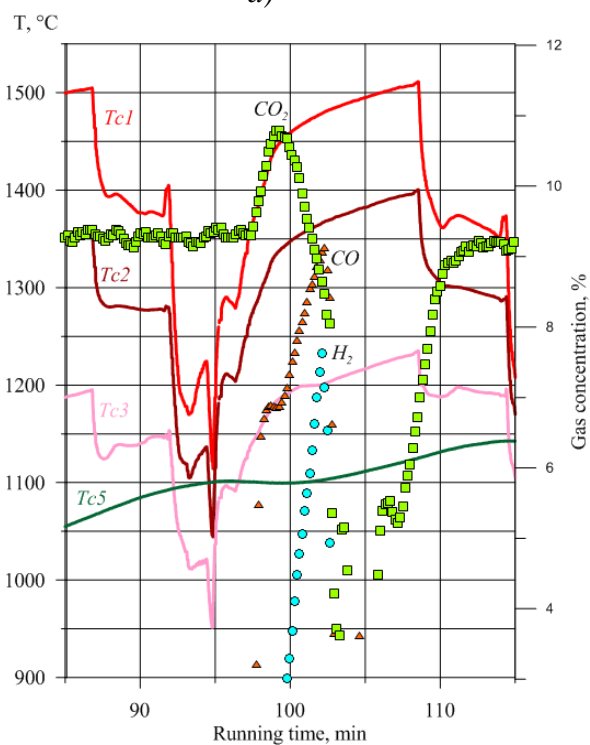


Fig. 4. Data of temperatures (a) and gas concentrations (b) for experiment #1



a)



b)

Fig. 5. Experimental data:
a – temperature profiles, exp. #1,
b – temperatures and gas concentrations, exp. #2

2.4. Characteristics of obtained CB

A SEM image of CB obtained in the experiment #1 is shown in Fig. 6. The CB specimens of exp. #2 have the same view. All obtained CB particles have globe structure and compound conglomerates. The surface-area-to-volume ratios measured by “ASAP 2020” Physisorption Analyzer and processed by BET method are following: 108 m²/g (exp. #1) and 82 m²/g (exp. #2), by Langmuir method: 167 m²/g (exp. #1) and 132 m²/g (exp. #2).

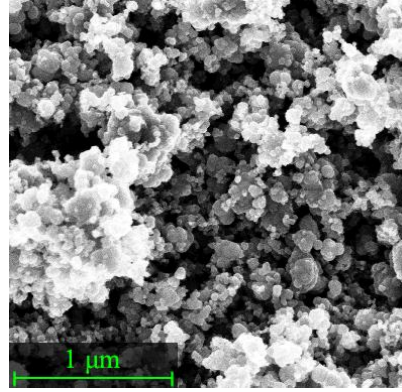


Fig. 6. SEM image of CB obtained in the exp. #1

2.5. Mathematical model of HC droplets evaporation in flow reactor

Another aspect of the problem of CB obtaining is the right choice of design parameters for the reactor. The main question is also determining the stage that is limitative for the entire process of CB production. The idea is to consider the evaporation of the HC droplets, as some researchers believe that it is the limitative stage of such a process [6]. Taking into account the processes of diffusion and convection while the droplet of HC fuel is evaporating a hydrodynamic model of its evaporation was formulated:

$$\frac{1}{2} \rho_f v_{fz} \frac{dd_f}{dZ} = - \frac{ShD}{d_f} (\rho_{ev} - \rho_v) \cdot \frac{1}{1 - \frac{\rho_v}{\rho_g}} \equiv j, \quad d_f|_{Z=0} = d_{f0}; \quad (1)$$

$$u \frac{d\rho_v}{dZ} = \pi d_f^2 n_f \frac{ShD}{d_f} (\rho_{ev} - \rho_v) \frac{1}{1 - \frac{\rho_v}{\rho_g}} \equiv \pi d_f^2 n_f j, \quad \rho_v|_{Z=0} = \rho_v|_{300K}; \quad (2)$$

$$\frac{dv_{fz}}{dZ} = - \frac{3}{4} C(Re_f) \frac{\rho_g (v_{fz} - u)^2}{\rho_f d_f v_{fz}}, \quad v_{fz}|_{Z=0} = 0.1 \text{ m/s}; \quad (3)$$

$$c_{pf} \rho_f v_{fz} \frac{dT_f}{dZ} = \frac{6}{d_f} \left[\alpha (T - T_f) - (Q_v + Q_l) \frac{ShD}{d_f} (\rho_{ev} - \rho_v) \frac{1}{1 - \frac{\rho_v}{\rho_g}} \right], \quad T_f|_{Z=0} = 300 \text{ K}, \quad (4)$$

$$T(Z) = 1700 - \frac{1}{3} \cdot 200Z \quad (5)$$

Equation (1) describes changing of droplet diameter d_f , (2) – a change in the density ρ_v of HC fuel vapor in the channel during the evaporation of cloud of droplets ($n_f = 10^{10} \text{ 1/m}^3$) and (3) – change of velocity v_{fz} of the particle moving along the channel, the drag coefficient here is $C(\text{Re}) = \frac{24}{\text{Re}_f} \left(1 + \frac{1}{6} \text{Re}_f^{\frac{2}{3}} \right)$. In the balance equation (4) for the temperature droplet T_f the first term on the right describes the convective heat transfer, and the second – the cooling of droplet due to both the phase transition and the heat of HC molecules bond breaking [7]. Even though the breaking of molecules of HC droplet vapor into individual atoms of H_2 and C occurs in the flow of gas mixture, this loss of heat is included in the equation for T_f because the heat transition in gas flow is not considered in this model (the distribution of the gas mixture (5) is taken from the experiments). Another assumption is that all HC droplets have the same diameter $d_{f0} = 100 \text{ }\mu\text{m}$ and they presence in the reactor with given concentration $n_f = 0.4 \cdot 10^{10}$. In the equations (1)–(4) $\rho_g = \rho_B + \rho_v$, $\text{Sh} = 2 + 0.6 \text{Re}_f^{\frac{1}{2}} \text{Sc}^{\frac{1}{3}}$, $\text{Sc} = \frac{\nu}{D}$, $\text{Re}_f = \frac{d_f \sqrt{(v_{fz} - v)^2}}{\nu_g}$, $\alpha = \frac{\lambda}{d_f} \text{Nu}$, $\text{Nu} = \frac{\ln(1 + B_T)}{B_f} \left(2 + 0.6 \text{Re}_f^{\frac{1}{2}} \text{Pr}^{\frac{1}{3}} \right)$ and $B_T = \frac{c_{pv}(T - T_f)}{Q_v}$ – Spalding number for heat transfer which takes into account the influence of blowing more cold vapor (with $B_T > 1$ number Nu decreases). The pressure of saturated vapor of HC fuel P_{ev} is calculated from the known empirical formulas [8]. In the equations (1)–(4) the term $\alpha_m = \frac{\text{Sh}D}{d_f}$ is used for mass-transfer [9], a factor $\left(1 - \frac{\rho_v}{\rho_g} \right)$ indicates a consideration of Stefan flow during the droplets evaporation [10], i.e. the density of mass flow of hydrocarbon vapour that is equal to

$$j \equiv \frac{\text{Sh}D}{d_f} (\rho_{ev} - \rho_v) \frac{1}{1 - \frac{\rho_v}{\rho_g}} \quad (6)$$

This model can be improved by considering of the velocity of vaporization (kinetic approach).

In this case for j a Herzt-Knudsen condition is used

$$j = \frac{2\beta}{2 - \beta} \left(\frac{P_{ev}(T_f) - P_v}{\sqrt{2\pi \frac{R}{M_v} T_f}} \right) \quad (7)$$

3. RESULTS AND DISCUSSION

3.1. Experimental results

The sharp decreasing of the temperatures T_{c1} – T_{c3} (for example, before time moment t_2 in exp. #1) is explained by beginning of liquid HC fuel spraying (unsteady state when a colder fuel is impacted into a high temperature flow). Temperature before the cover insulation (T_{c5}) reacts on the regimes changing more smoothly and gives important data for future developing of mathematical model describing the reactor heating.

Temperature profiles in Fig. 4, *b* are given as an example of temperature regimes in the reactor channel that are important for CB producing. They characterize uniformity of reactor heating and gives important information for technological control of CB producing regimes that require steady state heating, temperature gradient along the reactor channel for finishing pyrolysis of HC material and initializing CB particles forming.

Shown concentrations in Fig. 4 *a*, *c* characterize the intensity of the pyrolysis of raw materials and the process of CB formation. The higher degree of HC fuel decomposition corresponds to the higher level of hydrogen concentration. Each time when the concentration of H_2 raised up to 11 vol.% the pressure fall at the bag filter became too high due to of its contamination with obtained CB. This required stopping of feed oil supply as well as gas burner working. After regeneration of the bag filter (1–3 min.) the works of the installation continued. That explains the periodic character of the experimental data (temperatures and gas concentrations peaks and falls repeat as result of changing two regimes: the liquid fuel supply and the filter regeneration).

For two experiments carried out the type of liquid fuel and its flow rate were different (see subsection 2.2). Other parameters (temperatures, the flow rates of flow rates, etc.) were in the same range. It gives the basement for a comparison of obtained CB properties.

3.2. Calculation on formulated models

The results of calculation for dependence of d_f , ρ_v , v_{fz} and T_f on the channel length (its maximum value is $L = 3$ m) with velocity of flow $v = 16$ m/s by these two models are in Fig. 7. It is obvious that HC droplets evaporate too quickly and do not limit the entire process.

There is an analysis of results of the application (instead of α_m) the expressions for the flow of steam on the basis of the molecular-kinetic theory in [9]. It is noted, that the kinetic effect on diesel fuel droplet evaporation are always noticeable despite the fact that evaporation takes place at high pressures. Kinetic models predict a longer evaporation time and higher temperature drop compared to a hydrodynamic model for tiny droplet sizes (about 5 microns) [11]. However, this applies to the case of single drop, a constant vapor density in the environment and the lack of gas flow. In our case the kinetic approach accelerate the droplet evaporation.

From the Fig. 7 one can see that in two-phase stream both of gas and hydrocarbon droplets the droplet temperature T_f does not exceed 480°K and smal depends on the droplet diameter.

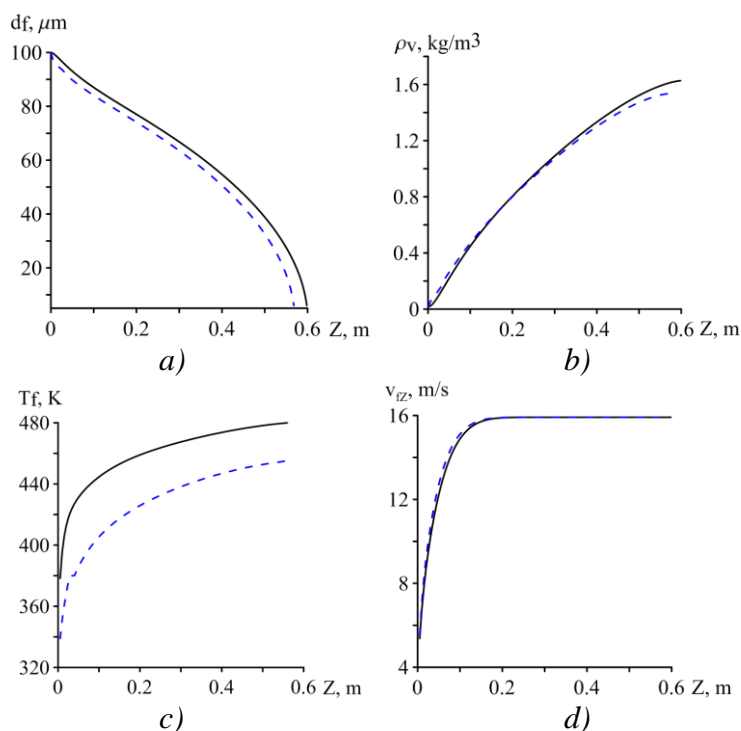


Fig. 7. Results of calculations on formulated models: *a* – droplet diameter d_f , *b* – density of vapor ρ_v , *c* – temperature of HC droplet T_f , *d* – velocity v_{fz} . Solid line – result for hydrodynamic approach, dashed line – result for kinetic model

4. CONCLUSIONS

The possibilities of controlling a set of technological parameters (temperature gradient in the reactor channel, flow rates of operating agents, gas concentration) that are available on described installation are important for adjusting technologies for CB producing by furnace method. Using two different type of feedstock oil two species of CB were obtained. In the SEM images they looks to be the same but the characteristics of the surface-area-to-volume ratios are different. In consequence, the type of HC raw material can be chosen for obtaining the resulting CB with planned properties.

The results of experimental research will be used for the verification of mathematical models describing the complex physical and chemical processes occurring in the reactor channel while producing CB including mechanisms of CB particles formation that are the subject of nowadays investigation.

Estimation based on given model proves that HC droplets evaporate too quickly and do not limit the entire process. A comparative analysis of hydrodynamic and kinetic approaches to the problem of HC fuel droplet evaporation shows that the model can be more specific with velocity of evaporation. The formulated model can be expanded for obtaining more rigorous view of involved processes. The goal of such research is intimate understanding of the processes taking place in the synthesis of nanoparticles of CB and look for opportunities to control the properties of the resulting product. As the evaporation is the occurs before carbon black formation the model helps to appreciate of the latter taking into account such key factors as gas temperature and coordinate in the reactor.

Competition between manufacturers of CB as well as of any other raw materials on the world market requires continuous improvement of production technology, aimed not only at the output with improved performance, but also to reducing of the production cost. And



applied by us technologies and the approach are an apparent leap toward modern science development and viable manufacturing.

DESIGNATIONS

Z – coordinate on the axis of reactor channel in longitudinal direction with the beginning in the point of HC fuel injection, m;
 d_{f0} – initial diameter of HC droplet, m;
 d_f – diameter of HC droplet, m;
 n_f – concentration of HC droplets, $1/\text{m}^3$;
 T – temperature of the smoke fumes in the reactor channel, K;
 ν – gas mixture viscosity, m/s;
 v_{fz} – velocity of moving HC droplets in towards Z-axis, m/s;
 T_f – temperature of HC droplet, K;
 ρ_{ev} – density of saturated vapor of HC fuel, kg/m^3 ;
 ρ_v – density of mixture of smoke fumes and HC fuel vapor, kg/m^3 ;
 ρ_f – density of liquid HC fuel, kg/m^3 ;
 ν – kinematic viscosity coefficient of the gas mixture, kg/m^3 ;
 Sh – Sherwood number;
 ρ_B – density of smoke fumes without HC fuel vapor, kg/m^3 ;
 Re – Reynolds number;
 Sc – Schmidt number;
 Nu – Nusselt number;
 Pr – Prandtl number;
 B_T – dimensionless criteria;
 D – diffusion coefficient, m^2/s ;
 Q_1 – specific bond energy of HC fuel molecule, $842 \cdot 10^3 \text{ J/kg}$;
 Q_v – heat of vaporization of HC fuel, $254 \cdot 10^3 \text{ J/kg}$;
 α – heat-transfer coefficient for HC fuel, $\text{W}/(\text{m}^2 \cdot \text{K})$;
 c_{pv} – heat capacity of HC vapor, J/K;
 c_{pf} – heat capacity of liquid HC fuel, J/K;
 λ – molecular heat conductivity of smoke fumes, $0.16 \text{ W}/(\text{m} \cdot \text{K})$;
 β – evaporation coefficient.

REFERENCES

1. *Application Examples of Carbon Black*. Mitsubishi Chemical. Link to the internet <<http://www.carbonblack.jp/en/cb/index.html>>
2. PATNAIK, T., BROWN B. Carbon black: why quality matters. Rubber and plastic news. Dec. 13, 2010. Link to the internet <<http://hmicronpowder.com/carbonblackmatters.pdf>>
3. IVANOVSKI V.I. *Tekhnicheskii uglerod. Processy i apparaty: Uchebnoe posobie. (Carbon black. Processes and devices: tutorial)*. Omsk: JSC “Tehuglerod”, 2004, 228 p.
4. PROBST, N. carbon black: processes and production. Carbon Black World Conference 1999. April of 1999.



5. GIUL`MISARIAN T.G., GILIAZETDINOV L. P. Sy`r`e dlia proizvodstva uglerodny`kh pechny`kh sazh. (Feedstock material for producing furnace black of different types). Moscow: "Himiya", 1975.
6. BASS YU.P., GILYAZETDINOV L.P. K raschetu dliny reaktora dlya proizvodstva saji. (For calculation of reactor length for carbon black production) // *Journal of Engineering Physics and Thermophysics*, 1964. Vol. 7, No. 8, p.114–120.
7. KEL'CEV V.V., TESNER P.A. *Saja: svoistva, proizvodstvo i primeneniye. (Carbon black: properties, manufacture and appliance)* M.-L.: Gostoptehizdat, 1952.
8. SAZHIN S.S. Advanced models of fuel droplet heating and evaporation // *Progress in energy and combustion science*, 2006. Vol. 32, p. 162–214.
9. FISENKO S.P., BRIN A.A., PETRUCHIK A.I. Evaporative cooling of water in a mechanical draft cooling tower // *Int. Journal of Heat and Mass transfer*. 2004. Vol. 47, p. 165–177.
10. LY`KOV A.V. Teoriia sushki. (Drying theory) — M.: E`nergiia, 1968 – 472 p.
11. KRYKOV A.P., LEVASHOV V.Yu., Sazhin S.S. Evaporation of diesel fuel droplets: kinetics versus hydrodynamic models // *Int. Journal of Heat and Mass transfer*. 2004. Vol. 47, p. 2541–2549.

EXPERIMENTAL INVESTIGATION OF WOOD PELLET SHRINKING DURING PYROLYSIS

R. Paulauskas, A. Džiugys, N. Striūgas

Lithuanian Energy Institute

Breslaujos str. 3, LT-44403 Kaunas – Lithuania

ABSTRACT

Pyrolysis is important part in combustion and gasification. During pyrolysis wood pellets are decomposed into gases, tar and char. Thermal degradation causes shrinking of pellets, which affects particles size and has important influence on particles dynamics, pyrolysis time, mixing and segregation. Gathered pellet shrinking parameters during pyrolysis can greatly assist in the build of numerical model for more extensive analysis of shrinkage.

Experimental approach was applied for investigation of wood pellet shrinking. The experimental study of feedstock shrinkage was made with ultra-zoom video camera recording of pyrolysis process in special reactor and parameters such as temperature, feedstock radius and mass, pyrolysis time, gas flow were collected for analysis. Data of experiments showed structure, density, radius and volume changes during pyrolysis at different temperatures (300–1100 °C).

Moreover, recorded video analysis revealed expansion of wood pellet at low temperatures (300–830 °C) in the beginning of pyrolysis. Expansion of feedstock influenced pyrolysis time and residual wood pellet's diameter.

According to the results the wood pellets diameter reduces by 20% from 1000 to 830 °C temperature during pyrolysis. When expansion of feedstock take place, pellets diameter grows up by 10–15% and after that, pellets diameter reduces only 10%. Process of expansion depends of pyrolysis temperature. The lower is the temperature, the lower expansion and vice versa up to 830 °C temperature.

It can be concluded that experimental study revealed wood pellets expansion which affects pyrolysis process. Also collected data is important for numerical model development.

Keywords: shrinkage, wood pellet, pyrolysis, expansion

1. INTRODUCTION

Renewable fuel resources are increasingly used for electricity and heat production. With the growing demand for these stocks and their price, looking for ways to use low-quality biofuels. One of the ways - gasification [1]. During this process, it is possible to get a higher quality gaseous fuel that can be used in industry. Using granulated fuel for gasification process, there are created conditions in which the wood pellets clump together moving from the pyrolysis reactor zone to the gasification zone and clog the reactor resulting in inhibition of the gasification process. One of the reasons influencing adhesive bond of the fuel particles are changes of wood pellets at high temperatures when the fuel particle shrinks due to the chemical reactions taking place inside, caused by high temperatures. Thermal deformations of the wood pellets affect the fuel movement, mixing and the gasification process time. In order to avoid clogging of the reactor needs to know the regularities of this phenomenon, which are investigated by experimental study on the fuel particles changes at high temperatures during pyrolysis, combustion and gasification processes.

The experimental study of wood pellet changes by inserting the sample to the perpendicular pyrolysis reactor is presented in the paper [2]. Experiments were carried out between 650 °C and 850 °C temperature. The published results show that a 10 mm diameter sample shrunked by 10.9% of its initial diameter at 650 °C temperature and by 14.7% at 850 °C temperature. Other authors [3] provide the results of wood pellets changes obtained from 365 to 700 °C temperature. The 8 mm diameter wood pellets were used for experimental

study. Authors [3] published results differ from these in the article [2]: wood pellet shrinks by 20 in 365 °C, by 30% in 600 °C and by 24% in 700 °C temperature. Mostly ambient temperature fuel falls into the gasification reactor and gasification reactor temperature field (the drying zone temperature up to 100 °C, the pyrolysis zone – up to 500–700 °C and the combustion zone - up to 1000–1400 °C) varies within wider than the works mentioned due to the processes of chemical reactions and heat transfer. During granular biomass gasification the combustion zone temperature is only 1000 °C due to the high aerodynamic drag of the granular layer. In order to describe the thermal deformation of the fuel particles is necessary to determine phenomena occurring in pelleted fuel in the gasification process temperature range. This paper presents experimental study of wood pellets changes due to the thermal deformation in the pyrolysis reactor at a constant temperature in the range from 300 to 1000 °C

2. RESEARCH METHODOLOGY

Experimental studies were performed by measuring thermal deformation of wood pellet during pyrolysis in the electrical furnace from 300 to 1000 °C temperature. Quartz tube (length 1 m, diameter 0.05 m, wall thickness 0.003 m) was inserted in the electrical furnace SUOL-025.1/12.5-II. One end of the quartz tube is supplied by the heated nitrogen, which flows through the tube to other end of the pipe which stick out from the oven. Nitrogen flow is controlled by rotameter (Fig. 1).

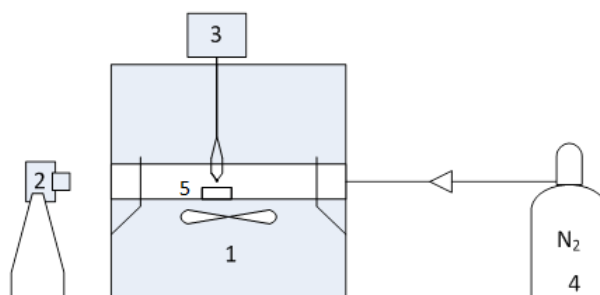


Fig. 1. Small test facility: 1 – pyrolysis reactor; 2 – digital camera; 3 – thermocouple; 4 – nitrogen; 5 – sample (wood pellet)

The wood pellet is placed in the middle of quartz tube when furnace and nitrogen is heated to the desired temperature (temperature is measured by K-type thermocouple). After that the sample is filmed with a photo camera Canon PowerShot SX30 IS. The photo camera has integrated wide-angle (24–840 mm) lens, which focuses automatically on the sample. Before the experiment, the sample is weighed with KERN EW scales which accuracy is 0.01 g. The wood pellets diameter is measured with Vernier caliper which provides a precision to 0.05 mm.

Nitrogen flow rate, according to the sample size, is an important value for the wood pellet changes recording quality. If nitrogen flow is too low, the capturing sample changes are out of the sight due to the slow diffusion of gas evolution from wood pellets. Therefore nitrogen flow is supplied from 4 to 10 l/min. according to the size and weight of sample. If the particle diameter is up to 6.5 mm and weight up to 0.3 g, supplied nitrogen flow is from 4 to 6 l/min. Where particle mass is up to 0.6 g, the nitrogen flow is increased to 8 l/min. Nitrogen flow of 10 l/min. is used for larger than 6.5 mm diameter particles.

At the end of the pyrolysis process, the recording is stopped and the wood pellet is moved closer to the quartz tube end where it is left to cool to ambient temperature (20 °C). The cooled wood pellet is pulled out to measure its diameter and mass.

The measurements were performed from 300 to 1000 °C temperature by 100 °C step. The high-resolution (1280x720 pixels) recorded videos of wood pellet changes were analyzed using graphics editing program GIMP. Each 150th recorded video frame was converted into a photo and the wood pellet diameter was measured with digital ruler, which provides the size in pixels. The value of measured sample diameter with digital ruler was compared with value of measured sample diameter with Vernier caliper at the initial time. The compared values were expressed in millimeters by the principle of proportion. In order to reduce errors due to occurrence of digital processing, the measurements of the wood pellet diameter were repeated 3 times in GIMP program.

3. RESULTS AND DISCUSSIONS

In the end of the experiment measured wood pellet mass and diameter changes at different temperatures are shown in Fig. 2.

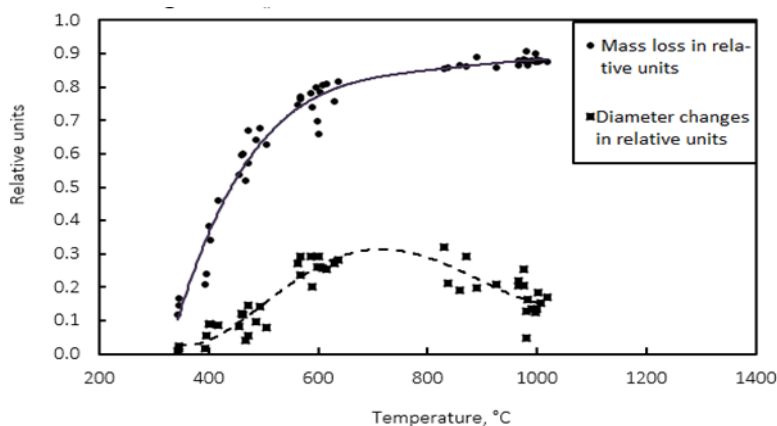


Fig. 2. Residual pellet mass $((m_0 - m_g)/m_0)$ and diameter $((D_0 - D_g)/D_0)$ changes at different heating temperatures

As it can be seen, the final mass of the pellets monotonically increases growing the heating temperature by equation (1):

$$(m_0 - m_f)/m_0 = 0.1 + 0.9 \cdot \left(1 - e^{-4 \frac{T-300}{700-300}}\right), \quad (1)$$

where m_0 is initial sample mass, mg, m_f – residual mass, mg, T – heating temperature, °C.

Changes of pellets diameter are nonmonotonous by Eq. (2). It depends on the heating temperature: shrinkage is increasing till 700 °C, but it is decreasing when the heating temperature grows over 700 °C temperature till 1000 °C. Final diameter of pellets can be described as follows:

$$(D_0 - D_f)/D_0 = (T - 200)^2 \cdot e^{-(T-400)/200}, \quad (2)$$

where D_0 – initial sample diameter, mm, D_f – residual sample diameter, mm.

When wood pellet is placed in the pyrolysis reactor, the thermal deformation of sample proceeded for 100 seconds in 300–400 °C temperature range. The particle expanded to 2.7% of the initial diameter at the beginning of pyrolysis process. The expanded particle started to

shrink after 300 seconds and it decreased 12.5% of the initial diameter. The diameter changes versus time at different temperatures are shown in Fig. 3.

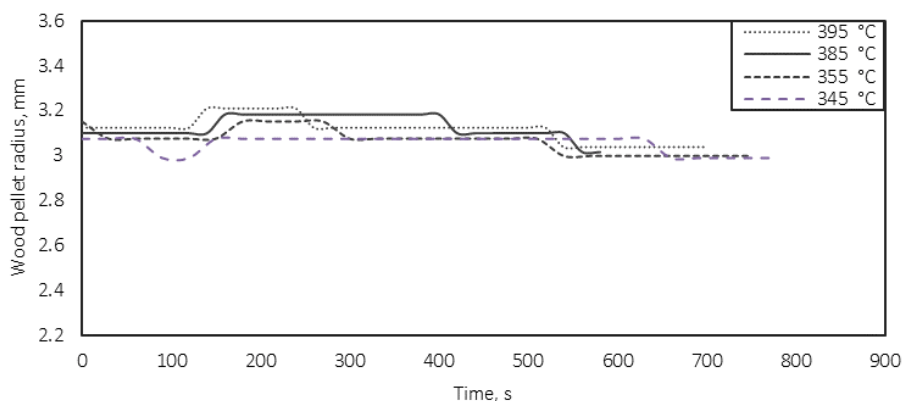


Fig. 3. Wood pellet changes during time from 300 to 400 °C temperature

The experiment lasted 800 seconds in 300–400 °C temperature range till the changes of wood pellet were invisible by photo camera. In this temperature range the particle mass loss was up to 14% (Fig. 2).

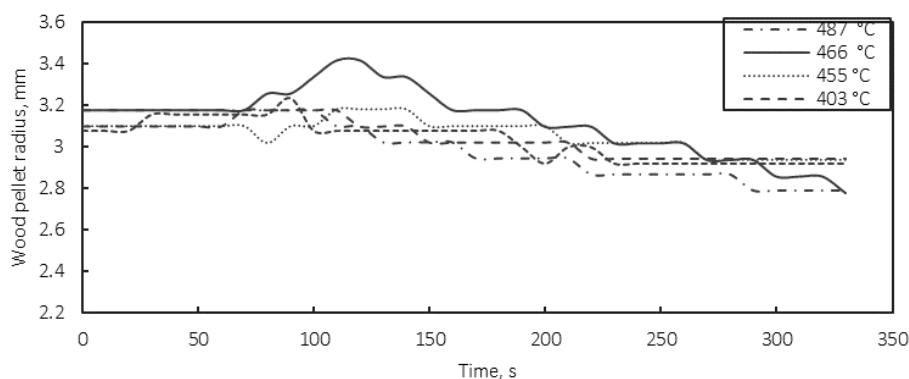


Fig. 4. Wood pellet changes during time from 400 to 500 °C temperature

When pyrolysis temperature was grown from 400 to 500 °C, the expansion of wood pellets became more intensive (Fig. 4). The pellet radius increased to 3.1% in 400 °C and 7% in 460 °C temperature. Along with the intensifying changes of the particle size increases mass loss (Fig. 2).

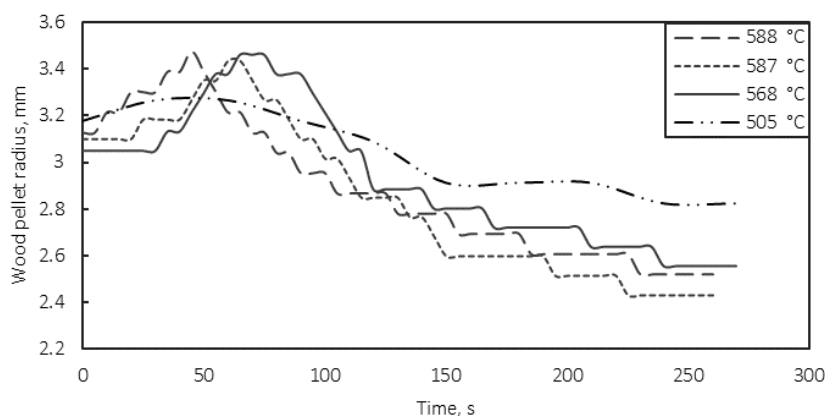


Fig. 5. Wood pellet changes during time from 500 to 600 °C temperature

The thermal deformation of wood pellet occurred in 500–600 °C temperature range are presented in Fig. 5. The expansion of pellets was also noticeable in this temperature range. Due to increased temperature up to 570 °C, the pellet radius expanded to 11% of the initial radius.

The expansion of pellet increased to 20% of the initial pellet radius when the heating temperature was raised to 600–700 °C temperature. At this temperature the pellet began to expand in the first 50 seconds after the placement into the pyrolysis reactor. The expanded pellet started to shrink after 50 s of expansion process. The wood pellet expansion and shrinkage is displayed in Fig. 6.

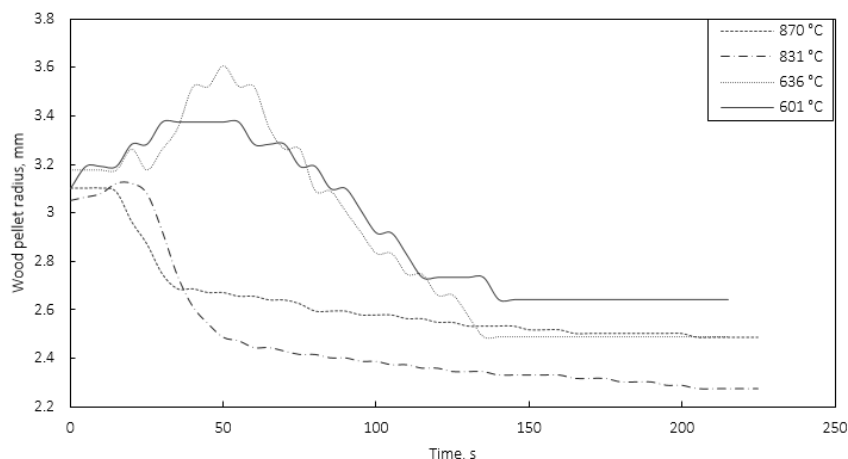


Fig. 6. Wood pellet changes during time from 600 to 900 °C temperature

Pellet stopped to exchange after 125 seconds. Experiment results of 800–1000 °C temperature range are also shown in Fig. 6. The expansion of wood started to decrease when heating temperature was above 800 °C. The sample grew only to 10% of the initial radius. Also the pellet expansion observed after 10 s from the beginning of the experiment and lasted only 10 seconds. In this temperature range mass loss was 90% of initial mass (Fig. 2).

The experimental results received in 900–1000 °C temperature range are shown in Fig. 7. In this temperature range, the wood pellet expansion was no longer visible. The wood pellet shrank from 15 to 20% depending on heating temperature after 100 seconds from the start of the experiment. The changes of pellet stabilized after 100 s of shrinkage. According to the given mass loss and the pellet shrinkage it is seen that the pellet volume decreased from 15 to 20% when temperature raised from 500 to 1000 °C.

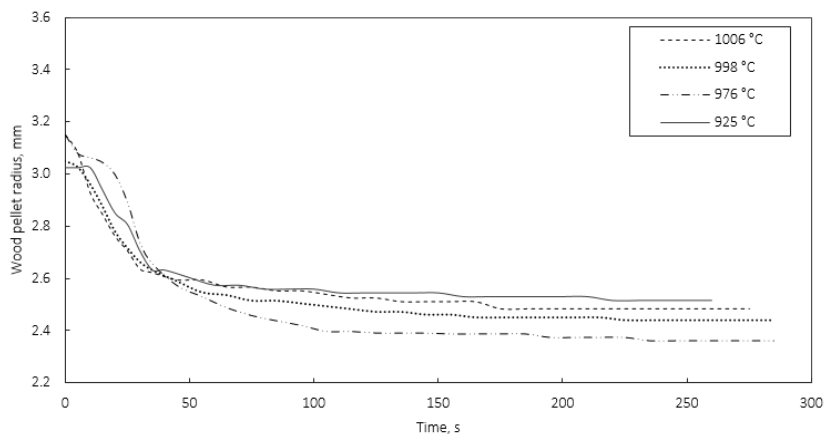


Fig. 7. Wood pellet changes during time from 900 to 1000 °C temperature

The results show that the pellet diameter changes depends on the pyrolysis temperature and heat transfer in the particles. The heat flow is higher from the reactor environment to the particle and volatile release mechanism also is different at higher temperatures. We believe that the expansion of the pellets is due to a slow heat transfer which influences volatiles release from pellets. When the particle heats evenly at low temperatures (till 300 °C), the pressure of water vapor and volatiles compounds do not reach a critical value inside the particles and the pellets surface is not destructed by water and volatile diffusion from it. The higher heating temperature (over 300 °C) causes the pellets quickly overheat resulting in failure of water and volatiles diffusion from pellet. In this way, water vapor and volatiles accumulate inside the pellet and internal pressure is growing near the pellet surface. When the internal pressure is too high, it destroys the surface structure of the pellets by expanding pellet and freeing accumulated water vapor and volatiles. Shrinkage of pellets begins after volatiles evaporation.

However, the pellets expansion decreases above 700 °C temperature, what maybe it is due to the faster particle heating. The particle overheats so quickly that emitted compounds from the surface layer decompose by high temperatures and the way for volatiles evaporation is open from the deeper layers. The expansion phenomenon is no longer detected after 800 °C temperature.

4. CONCLUSIONS

Experimental investigation of wood pellet shrinkage during pyrolysis can be concluded by these statements:

- The experimental study during pyrolysis between 300 and 800 °C temperature showed that the wood pellet expands at the beginning of pyrolysis and only after that it begins to shrink. The particles expand up to 20% of its initial size depending from the pyrolysis temperature.
- The particles expansion affects the duration of pyrolysis process and the size of residual pellets.
- The collected data from experimental investigation is important for numerical model development.

REFERENCES

1. GURSKIENĖ, V., ŠLANČIAUSKAS, A. *Medienos anglies likučio dujųofikacijos spartinimas didinant CO₂ dujų generavimą*. Energetika 58, 2012, p. 213–218.
2. PARKA, W. ATREYA Ch., BAUMB A., R.H. *Experimental and theoretical investigation of heat and mass transfer processes*. Combustion and Flame 157, 2010, p. 481–494.
3. KUMAR, R.R. KOLAR, A.K. LECKNER B. *Shrinkage characteristics of Casuarina wood during devolatilization in a fluidized bed combustor*. Biomass and Bioenergy 30, 2006, p. 153–165.
4. SREEKANTH, M., KOLAR KUMAR, A. *Progress of conversion in a shrinking wet cylindrical wood particle pyrolyzing in a hot fluidized bed*. Journal of Analytical and Applied Pyrolysis 84, 2009, p. 53–67.
5. LAM, K.L., OYEDUN, A.O., HUI, C.W. *Experimental and Modelling Studies on Biomass Pyrolysis*. Chinese Journal of Chemical Engineering 20(3), 2012, p. 543–550.
ZHOU, Ch., ZHANG, Q., ARNOLD, L., YANG, W., BLASIAK, W. *A study of the pyrolysis behaviours of pelletized recovered municipal solid waste fuels*. Applied Energy 107, 2013, p. 173–182.



EXPERIMENTAL INVESTIGATION OF ADDITIONAL REFORMING PROCESS OF SYNGAS USING BIOMASS CHAR

K. Zakarauskas, N. Striūgas

Lithuanian Energy Institute

Laboratory of Combustion Processes

Breslaujos str. 3, LT-44403 Kaunas – Lithuania

ABSTRACT

Biomass gasification is one of alternatives in heat and electricity production, when developing local renewable energy resources. This technology has not been fully developed yet, and there is a number of problems, which prevent from mass spread of gasification technologies in industry. The present paper focuses on the following two issues: reduction of char residues after gasification and reduction of carbon dioxide concentrations in synthesis gas. One of the methods to use char is secondary gasification of char, at the same time passing syngas with tar from wood gasifier. Thus, not only char is used, tar concentration in gas is reduced, but also the total gas yield and calorific value is increased. The article presents the results of charcoal gasification experiments, considering the air flux and the influence of syngas in the process on quality parameters of syngas. What is more, the analysis of obtained results was carried out, and the generalization of results enables to define the optimum parameters at which the cleaning of syngas is the most effective and the gas yield is the best.

Keywords: Biomass, gasification, tars, syngas, char

1. INTRODUCTION

Currently, one of the most promising renewable energy sources is different types of bioenergy. It includes timber, firewood, wood chips, sawdust, briquettes, logging and wood processing residues, as well as straw. Different types of biomass can be used to produce syngas. Biomass energy potential is the fourth after char, oil and natural gas, according to primary energy sources [1]. Gasification is one of the alternatives, seeking to expand the use of biomass potential, in comparison with direct combustion.

Gasification is a complex thermochemical process where biomass is converted into the following main gaseous components: CO, H₂, CO₂, CH₄ and N₂, and tar [2, 3]. This process consists of two main stages: biomass gasification, and gasification of residual char. Biomass consists of ~ 80% of volatile substances, while the remaining part consists of char and ash. After the process of pyrolysis the volatile substances and moisture evaporate, only char remains. Char gasification duration is several tens of times longer than the release of volatile substances [4]. Intensification of decomposition of residual char requires high temperature, time, and an oxidizer. Three types of oxidizing agents, i.e., oxygen, water vapour and CO₂, are used for char gasification.

Residual char can be used for direct combustion as a fuel. However, in order to optimize the gasification process, it is looked for ways for efficient use of char, and one of them is thermal gasification, where char reacts with carbon dioxide (CO₂) and/or water vapour, and hydrocarbons, present in syngas, if there are appropriate conditions. Thus, not only char, remaining after gasification, is used, but also the concentration of tar and carbon dioxide (CO₂) in gas is reduced, which in turn increases the total gas output. The aim of this paper is to determine the optimal conditions for gasification of residual char and the influence of introduction of syngas on this process.

2. METHODOLOGY

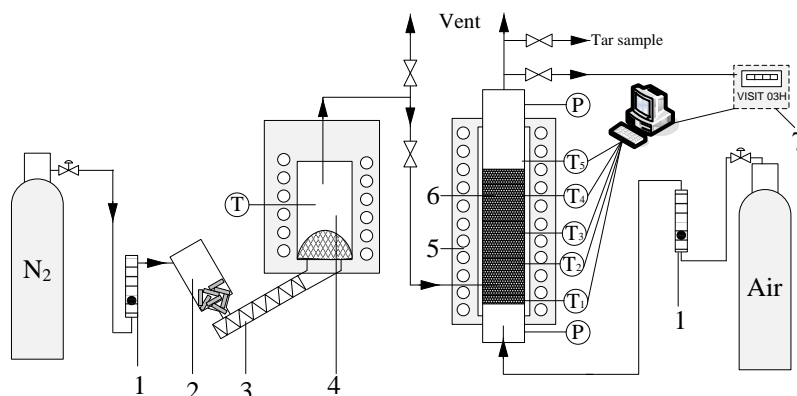


Fig. 1. Scheme of the experimental rig

1 – rotameter; 2 – biomass pellet container; 3 – screw conveyer; 4 – biomass pyrolysis reactor; 5 –char gasification reactor; 6 – char bed; 8 – gas analyzer (VISIT 03H)

Experimental stand (Fig. 1) consists of the following two parts: biomass char gasification reactor and biomass pyrolysis reactor. Char gasification reactor is made of stainless steel tube of 1000 mm length and 37 mm diameter, where char load of 470 mm height (~500 ml, char mass 110 g) is placed. The main characteristics of char are given in Table 1.

Table 1. Properties of wood char pellets

Parameter	Unit	Value
Moisture content	%	0.9
Ash content	%	2.2
Fixed carbon	%	83.6
Volatile organics	%	13.3
Higher heating value	kJ/kg	33768

Before introducing the air, char gasification reactor with char is heated up to 800 °C. Heating guarantees the initial temperature, required for char gasification, in order the self-gasification of char would be started upon introduction of air. Just before air introduction, electrical heating of char gasification reactor is turned off. Air is supplied from compressed air receiver, which is controlled by rotameter. What is more, pyrolysis syngas flow of 6 l/min. is supplied to the hottest area of gasification reactor from biomass pyrolysis reactor. The composition of pyrolysis syngas is presented in Table 2.

Table 2. Composition of syngas from pyrolysis reactor

Compound	Unit	
H ₂	%	11.2
CO	%	16.3
CO ₂	%	19.1
CH ₄	%	9.1
N ₂	%	44.3
Tar	g/m ³	21.1

Pyrolysis syngas is obtained in the following way: nitrogen (99.6 % purity AB “Achema”) is supplied to container with fuel pellets at constant pressure and flow of 1,8 l/min. Screw conveyer supplies a constant quantity of fuel pellets at 5 g/min from container to pyrolysis reactor. Commercially available wood pellets made from softwood, mainly spruce and pine (UAB “Baltwood” (Ltd.)), were used in experiments. A constant temperature of 850 °C is maintained in pyrolysis reactor. Six type K (NiCr-Ni) thermocouples are installed in char gasification chamber. The readings of these thermocouples are transferred and collected in computer by using the data collection system TC-08 (Pico). The composition of syngas from char gasification reactor is determined by gas analyzer Visit 03H, the readings of which are also transferred to computer. Gas analyzer shows the composition of H₂, CO, CH₄, and CO₂. Tar concentration in gas is determined, following the method of „cold trap“ [5, 6]

3. RESULTS AND DISCUSSION

First, experiments were carried out at different air fluxes, seeking to determine the temperature profile of char reactor and composition of syngas (from char). Air flux is calculated in the following way:

$$D = \frac{V}{A}; \quad (1)$$

where: V – air flow rate to reactor (kg/s), A – grate area m².

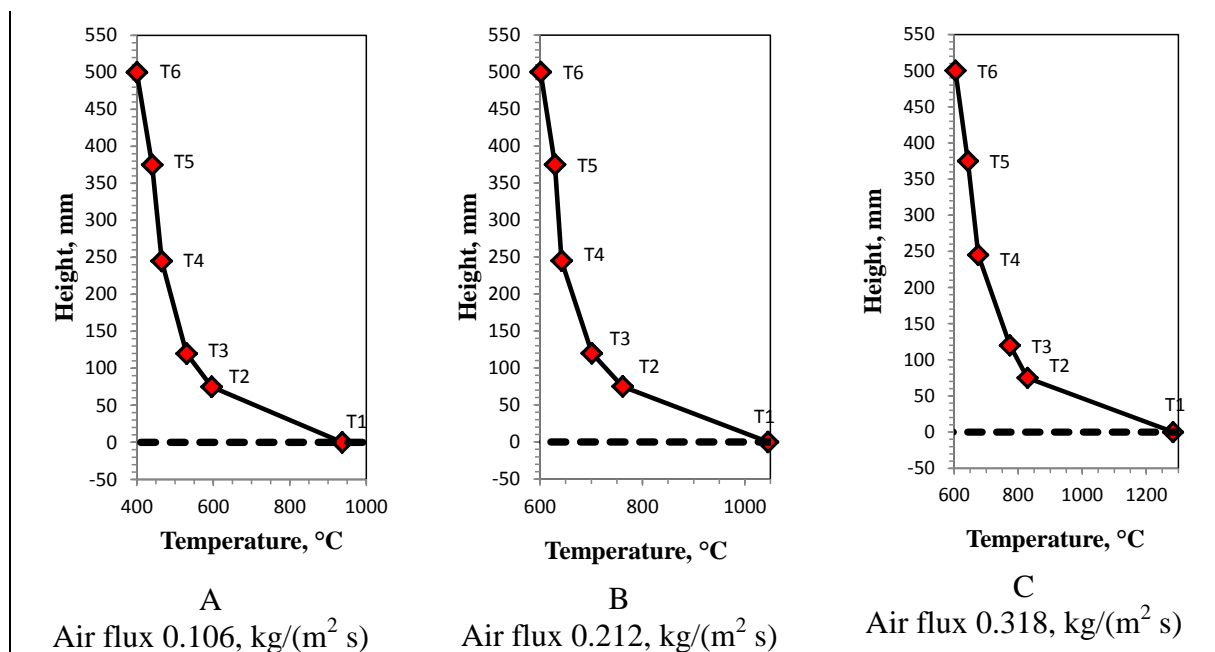


Fig. 2. Temperature profiles of wood char reactor at different air fluxes

The results of temperature values are presented in Fig. 2. It might be observed that at air flux of 0.106, kg/(m² s) the maximum temperature is 937 °C (T1), and it decreased to 596 °C (T2). Previous research [6] has demonstrated that the best temperature for cleaning the pyrolysis syngas from tar is 900 °C and higher, and in this case, the temperature in point of introduction of syngas (from wood gasifier) is ~600 °C. Seeking to increase the temperature, experiments with two air fluxes of 0.212 and 0.318, kg/(m² s) were carried out. In this case, the temperature values T1 were 1045 and 1284 °C, respectively. Increase of air flux and the resulting growth in temperature Bonduar reaction, leading to decrease of CO₂ and increase of CO concentrations in syngas (from char) (Fig. 3).

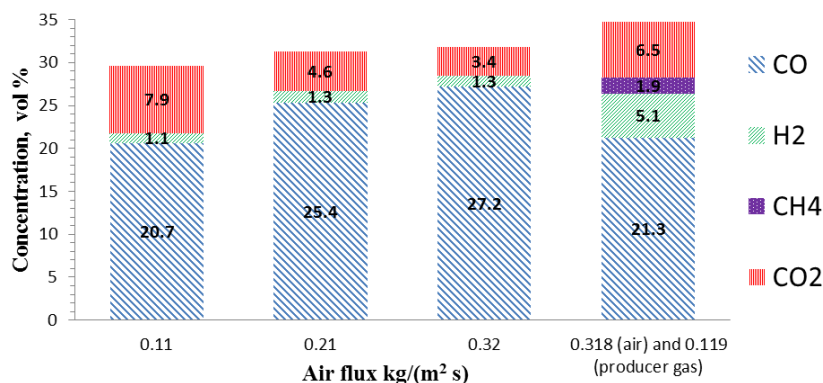


Fig. 3. Syngas composition under different conditions

In the next stage, at air flux of $0.318 \text{ kg}/(\text{m}^2 \text{ s})$, syngas from biomass pyrolysis reactor with tar was introduced into char gasifier. Only the aforementioned air flux was selected by taking into account that in this case the temperature in point of syngas introduction (from wood gasifier) was $\sim 1000^\circ\text{C}$ and after 210 mm decreased to $\sim 700^\circ\text{C}$, at which tar decomposition efficiency could be up to 81% [6].

While comparing the influence of syngas, it might be observed that temperature T1 decreased from 1284°C to 1137°C , and temperature T2 and T3 decreased by $\sim 50^\circ\text{C}$, whereas temperature values in other areas (T4–T6) remained similar. This change in process conditions is affected by partial gas pressure over char load: while char gasification to CO takes place only in CO₂ environment, the partial pressure of this gas is the highest and only carbon dioxide reforming takes place. Upon introduction of gas mixture, the concentrations of active compounds of mixture change, thus, changing the mechanism of reactions: several oxidation – water vapour reactions, carbon dioxide and methane reforming take place simultaneously, the speed of which depend on concentration of their materials towards char surface.

Studies on tar concentrations revealed that its concentration decreased from 21.1 to $0.9 \text{ g}/\text{m}^3$. Tar decomposition efficiency was equal to 95.7%, although in comparison to catalytic tar decomposition efficiency of up to 100% [6], it is less effective. However, in this case, external heat source is not required.

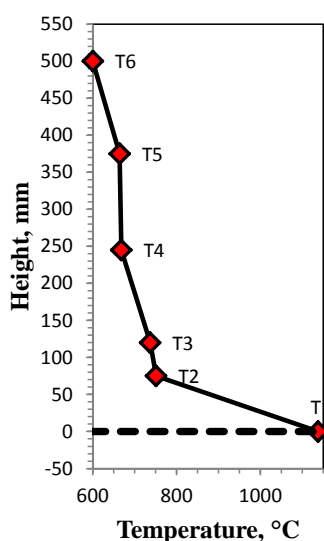


Fig. 4. Temperature profile of wood char reactor at air flux of $0.318 \text{ kg}/(\text{m}^2 \text{ s})$ and with additional syngas flow of $0.119 \text{ kg}/(\text{m}^2 \text{ s})$

4. CONCLUSIONS

1. The experiments showed that during char gasification the highest temperature of 1284 °C is achieved at air flux of 0.318 kg/(m² s). At the same time, gas of the highest calorific value is obtained, where the lowest CO₂ concentration is 3%, and the highest CO concentration is 27%.
2. Additional introduction of syngas (from wood pyrolysis reactor) into char gasifier changed the process conditions; the change in concentrations of mixture compounds resulted in change of reaction mechanism: several oxidation – water vapour reactions, carbon dioxide and methane reforming take place simultaneously. It triggered the reduction of temperature from 1284 to 1137 °C. Tar decomposition efficiency was equal to 95.7 % during this process.

REFERENCES

1. DEMIRBAS, A. Yields of hydrogen-rich gaseous products via pyrolysis from selected biomass samples. *Fuel*, 2001, Vol. 80, p. 1885–1891.
2. LIM, M.T., ZAINAL, Z.A. Bubbling fluidized bed biomass gasification-performance, process findings and energy analysis. *Renewable Energy. Fuel*, 2008, Vol. 33, p. 2339–2343.
3. GIL, J., CORELLA, J., AZNAR, M.P. CABALLERO, M.A. Biomass gasification in atmospheric and bubbling fluidized bed: effect of the type of gasifying agent on the product distribution. *Biomass and Bioenergy*, 1999, Vol. 17, p. 389–403.
4. CETIN. E., MOGHTADERI, B., GUPTA R., WALL, T.F. Influence of pyrolysis conditions on the structure and gasification reactivity of biomass chars. *Fuel*, 2004, Vol. 83, p. 2139–2150.
5. Sampling and analysis of tar and particles in biomass producer gases. Technical report prepared under CEN BT/TF 143 „Organic contaminants („tar“) in biomass producer gases“. July 2005.
6. ZAKARAUSKAS K., STRIŪGAS N., STRAVINSKAS G. Investigation of thermal cracking of syngas tar from biomass gasification by catalytic steam reforming. CYSENI 2012. Proceedings of annual conference of young scientists on energy issues. [CD]. Kaunas: Lithuanian Energy Institute. 2012 May 24–25.

GENERATION OF A TYPICAL METEOROLOGICAL YEAR FOR ALŪKSNE, LATVIA

M. Ruduks, A. Lešinskis

*Department of Architecture and Building
Latvia University of Agriculture
Akadēmijas str.19, LV-3001 Jelgava – Latvia*

ABSTRACT

Meteorological conditions vary significantly from year to year. By this reason, there is a need to create typical meteorological year (TMY) data model, to represent the long term weather conditions over a year. TMY data is one of the main sources for successful building energy simulations. Two different typical meteorological data models were generated and compared TMY and TMY-2. Both models were created by analysing every 3-hour weather data of a 27-year period (1986–2012) in Alūksne, Latvia, provided by Latvian Environment Geology and Meteorology Centre (LEGMC). TMY model was created using statistical approach, but to create second model – TMY-2, 27 year average data were applied. In TMY model creation representative typical meteorological months (TMM) were selected. TMM for each of the 12 calendar months, were selected by choosing the one with the smallest deviation from the long-term average weather data. The 12 TMMs, selected from the different years, were used to create a TMY for Alūksne. Gathered data from TMY and TMY-2 models were compared with climate data from Latvian Cabinet of Ministers regulation No. 379, Regulations Regarding Latvian Building Code LBN 003-01. Average monthly temperature values in LBN 003-01 were lower than the TMY and TMY-2 values. TMY selection process should include the most recent meteorological observations, and should be periodically renewed to reflect the long term climate change.

Keywords: Typical meteorological year; building energy simulations

1. INTRODUCTION

In Latvian legislation long-term climate data is reflected in the Latvian Building Code (LBN) 003-01 „Būvklimatoloģija” (23.08.2001, Riga), where various climatic indicators are shown that represents the climatic situation in the territory of Latvia, providing information about the average monthly and yearly meteorological parameters. But this information is not enough to fully describe the regions climatic conditions, because there is necessity to define every day and every hour meteorological data values.

The need of such meteorological data worldwide led to the development of methodologies for generating the typical meteorological year (TMY). TMY is data set that contains a sequence of 8760 hourly values of chosen meteorological quantities. The requirement of TMY is that it has to correspond to an average year [1]. TMY provides every hour climatic parameter values, enabling to use these parameters for heating, ventilation and air conditioning (HVAC) device management and capacity optimisation.

Creation of TMY was introduced in 1978 by Hall et al. [2]. For a network of stations in the United States, a representative database consisting of weather data was created. Hall's method has been used to successfully generate TMYs for a number of locations across the globe [1–12].

LBN 003-01 describes climate parameters for ten cities of Latvia. These parameters have been calculated using data from 1961–1990. The aim of this research is to generate a representative climate database for one of these cities – Alūksne, by employing the method

that has been proposed by Hall et.al. [2] and adapted in Latvia by Zariņš [3]. Generation of TMY of Alūksne would provide with hourly climate data that LBN 003-01 does not provide.

Geographical data for Alūksne: latitude 57°26' N; longitude 27°02' E; on relatively flat surface, elevated 193 m above sea level. Located 160 km from Gulf of Riga (Fig. 1). Average temperature 4.5 °C.

The TMY is generated using the available weather data obtained from the station of Alūksne by the Latvian Environment Geology and Meteorology Centre (LEGMC), covering the period from 1986–2012. Limitation of 27 year period is related to the availability of the necessary data from LEGMAC database. This database provides with 3-hour weather data values for the temperature and relative humidity.



Fig. 1. Location of Alūksne

2. METHODOLOGY

TMY models were created applying two different TMY creation methods. TMY model was created by using method that was described by Hall et.al. [2] and adapted in Latvia by Zariņš [3]. The second TMY model – TMY-2 was created by applying average meteorological year method [4]. TMY model consists of weather data that have been observed in one of the 27 year period. This method includes temperature peaks that can be used to determine the appropriate power for HVAC systems. TMY-2 model consists of averaged 27 year weather data, this method does not show the temperature peaks, but it shows the most precise average monthly temperatures. TMY-2 model is best used for calculating average long-term building energy consumptions for HVAC systems.

2.1. TMY creation

Climate data for TMY creation were obtained from LEGMC database from 1986–2012. LEGMC provides climate data with 3 hour interval, but TMY needs hourly climate data. The necessary data for TMY were calculated by linear interpolation.

In February there may be 28 or 29 days, and it is not possible to compare years with different count of days, the 29. February was excluded from TMY creation. The rest of the days were rearranged in ascending order starting with the first hour of January till the last hour of December (8760 values).

For each month temperature distribution was calculated – how many hours per month each of the temperature (in range from -35 °C till 35 °C) was observed. This action was used for each month of the 27 year period. Each month can be included in TMY, but before it is determined it is called candidate month.

Adapted Halls TMY creation method [2] tries to find the most typical month – typical meteorological month (TMM), for each of the 12 months (January–December), from the observed time period (1986–2012).

To determine the TMM for each of the 12 calendar months, each month's temperature distribution was compared with temperature distribution from 27 year period. Sum of square error (SSE) parameter was used (equation 1) to compare months. Where x_i is the temperature distribution value in candidate month and \bar{x}_i is distribution value from 27 year average data. When all 27 year SSE values were compared the month that had the lowest value of SSE (equation 2) was chosen as the TMM and was included in TMY. This action was applied for all 12 calendar months.

$$SSE = \sum_{i=1}^n (x_i - \bar{x}_i)^2 \quad (1)$$

$$SSE = \sum_{i=1}^n (x_i - \bar{x}_i)^2 \rightarrow \min . \quad (2)$$

All TMM were combined and TMY was generated, but as TMM were from different years and there was mismatch of values at the connecting point of two TMM. Last 6 hours of the preceding month and the first 6 hours of the following month were smoothened by replacing them with the average values.

TMY model includes temperature and relative humidity values, temperature values are selected as described, but relative humidity values for TMY are determined according to the selected TMM. Relative humidity values are smoothened at the connecting point of two TMM like with the temperature.

2.2. TMY-2 creation

TMY-2 model was created with average meteorological year method [4]. In this method the same climate data were used as it was in TMY model creation. And they were arranged starting from first hour of January till the last hour of December. Each of the TMY-2 model 8760 temperature and relative humidity values were calculated by averaging this value from 27 year data.

3. RESULTS AND DISCUSSIONS

TMY was created combining TMMs that are determined based on their ability to follow the long term distribution. Selected month/year combinations from which the TMY was created are shown in Fig. 2. Three months (March, May and November) were selected from one year (2003), but other months were selected from different years. That displays that TMMs are selected from all range of the observed period.

After TMMs were connected and TMY was created, temperature fluctuation (Fig. 3), temperature distribution (Fig. 5), relative humidity fluctuation (Fig. 4) and relative humidity distribution (Fig. 6) was displayed.

When TMY and TMY-2 temperature distribution values are compared with 27 year average data (long term data) (Fig. 5), TMY shows good agreement with the long term data. TMY value deviation from long term data is maximum 90 hours per year at 2 °C, but TMY-2 deviation at –5 °C is more than 400 hours per year. The difference between TMY and TMY-2 models can be explained by the fact that TMY-2 is made averaging climate data and it does not contain maximum and minimum temperature values.

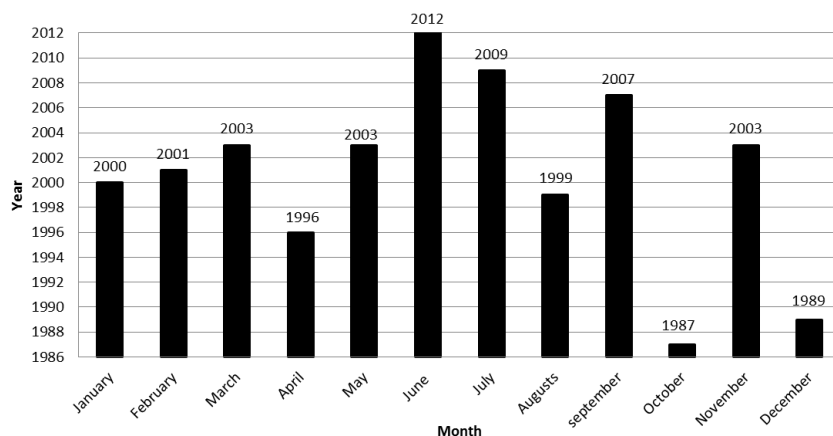


Fig. 2. The Month/Year combinations for the composition of TMY

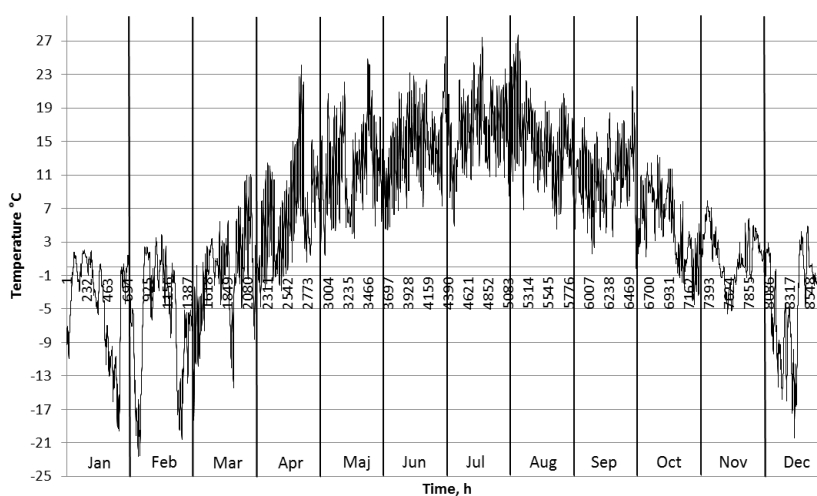


Fig. 3. Temperature fluctuation in TMY

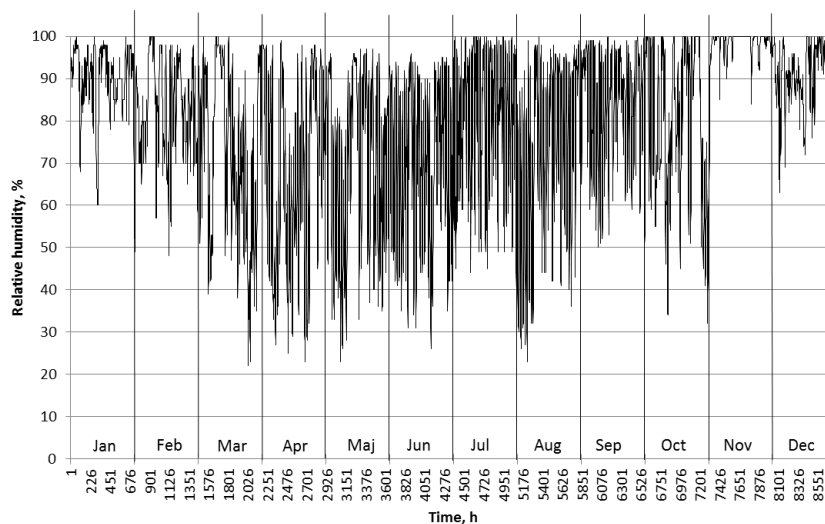


Fig. 4. Relative humidity fluctuation in TMY

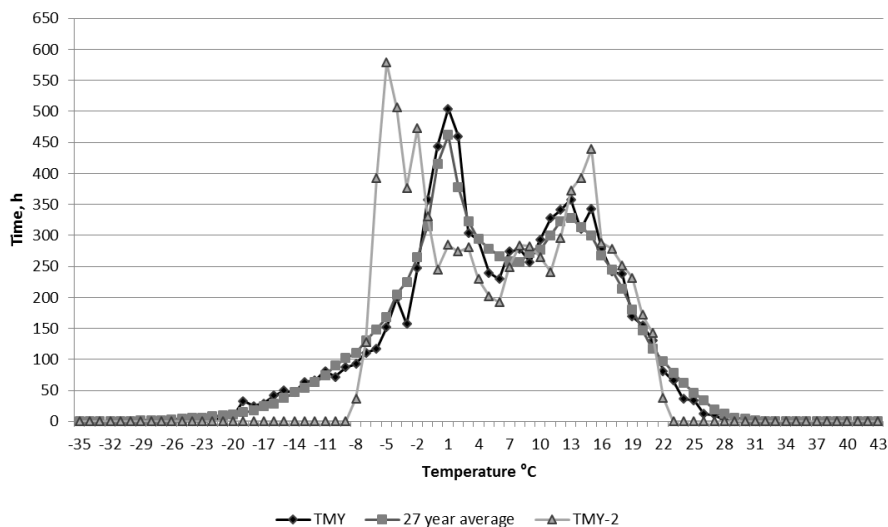


Fig. 5. Hourly temperature distribution for TMY, TMY-2 and 27 year average data

One of the most important result that can be obtained from TMY are shown in Fig. 7 and 8. These Figures show how many hours per year each temperature and content of moisture combination can be observed. Most typical content of moisture and temperature combination in TMY model is 4g/kg at 2 °C, respectively. This combination can be observed for 335 hours. These results can be used for HVAC system analysis and building energy simulations. Data from Fig. 7 gives ability to calculate how long it will be necessary to use heating and cooling devices for buildings in this region, and choose optimal capacity for these devices.

TMY-2 most typical content of moisture and temperature combination is 2g/kg at -5 °C (Fig. 8), respectively. This combination can be observed for 616 hours.

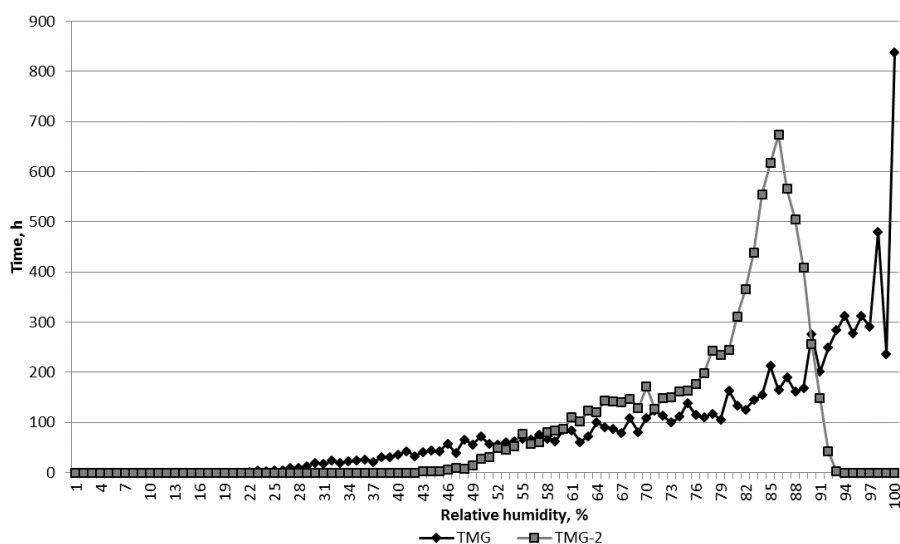


Fig. 6. Relative humidity distribution for TMY and TMY-2

Table 1. Average monthly temperature values (°C)

Month	Jan	Feb	Mar	Apr	May	Jun	Jul
27 year average	−5.1	−5.7	−1.2	5.5	11.1	14.9	17.4
TMY	−4.2	−6.2	−1.1	5.7	11.9	13.9	16.7
TMY-2	−5.1	−5.7	−1.2	5.5	11.1	14.9	17.4
LBN 003-01	−7.6	−6.8	−2.5	4.0	11.0	14.8	16.1
Month	Aug	Sep	Oct	Nov	Dec	Average	
27 year average	15.6	10.6	5.2	−0.2	−4.0	5.3	
TMY	15.3	10.9	4.8	1.2	−4.6	5.4	
TMY-2	15.6	10.6	5.2	−0.2	−4.0	5.3	
LBN 003-01	15.0	10.2	5.2	−0.4	−4.9	4.5	

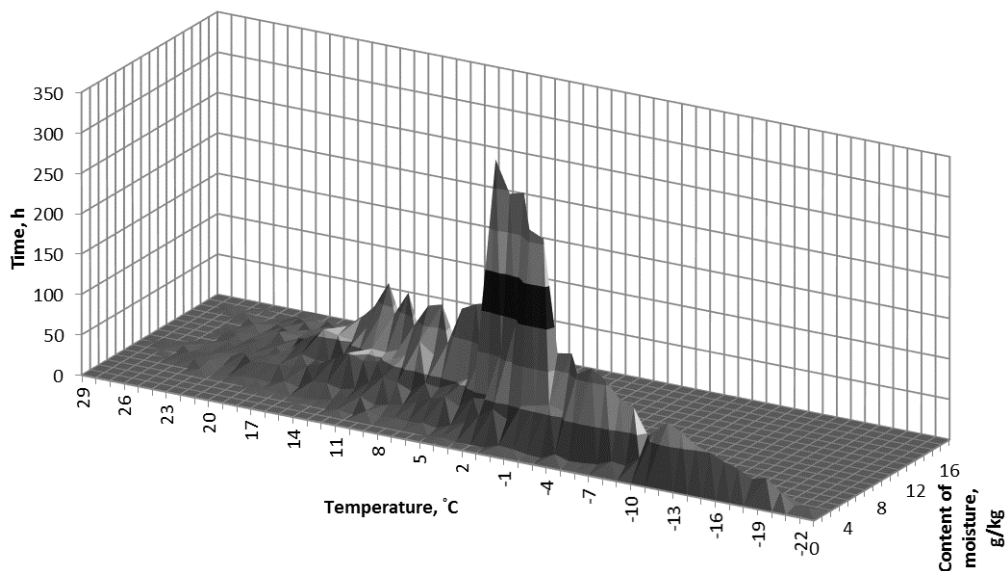


Fig. 7. Combination of temperature and content of moisture for TMY

TMY and TMY-2 average year temperature value difference is 0.1 °C, but difference with LBN 003-01 value are 0.9 and 0.8 °C, respectively (Table 1). The difference with LBN 003-01 values can be explained by the fact that they have been obtained from 1961–1990, but TMY and TMY-2 values were obtained from 1986–2012. The climate change can be the factor for the difference.

TMT and TMY-2 average year relative humidity value difference is 1% (Table 2), but difference with LBN 003-01 value for TMY-2 is 1% but TMY has the same value.

Comparing TMY, TMY-2, long term average and LBN 003-01 values (Table 3) LBN 003-01 has the highest and lowest fixed temperature, it has the longest duration of heating period, the lowest average temperature in heating period and also it has the most number of degree days.

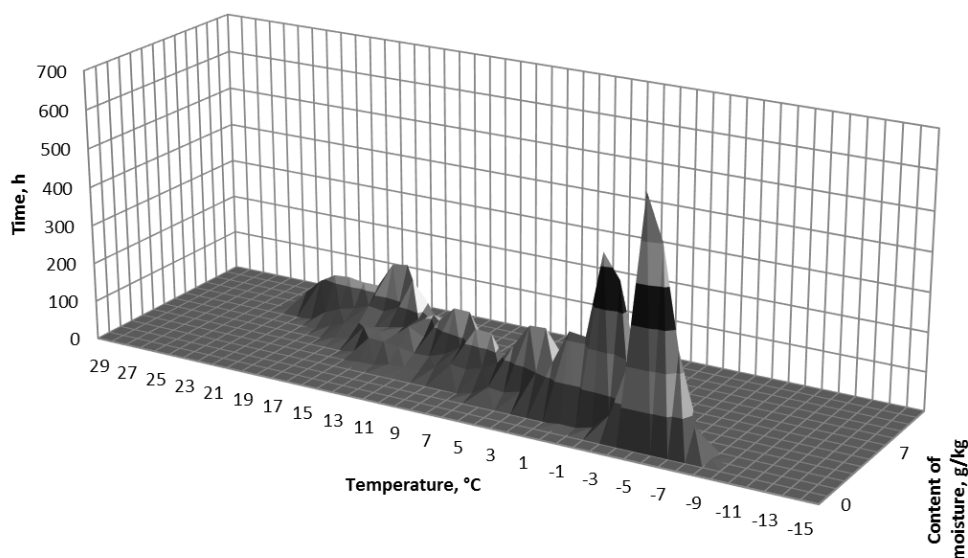


Fig. 8. Combination of temperature and content of moisture for TMY-2

Comparing results in table 1 with results that were obtained by Zariņš [3] for city Riga, they show similar tendency that average monthly temperatures in LBN 003-01 are lower than the TMY values. Results can be explained by the fact that data in LBN 003-01 are obtained from 1961–1990, but for TMY from 1986–2012. Due to the global changes the average monthly temperatures have risen.

Table 2. Average monthly relative humidity value (%) comparison from January till December

Month	Jan	Feb	Mar	Apr	May	Jun	Jul	Aug	Sep	Oct	Nov	Dec	Average
27 year average	90	87	79	69	67	74	76	80	84	87	91	92	81
TMY	89	84	72	69	70	70	80	72	84	81	98	92	80
TMY-2	90	87	79	69	67	74	76	80	84	87	91	92	81
LBN 003-01	87	84	78	71	68	71	75	79	84	87	90	90	80

Table 3. Summary of climate parameters

Parameter	TMY	TMY-2	27 year average	LBN 003-01
Maximum temperature, °C	27.7	21.9	32	31.1
Minimum temperature, °C	−22.6	−8.6	−32	−32.7
Duration of heating period, days	199	204	-	214
Average temperature in heating period, °C	−1.1	0.2	-	−1.9
Number of degree days	3796	3624	-	4259

4. CONCLUSIONS

The aim of this research was to generate TMY for Alūksne and it was generated based on the most recent 27 year (1986–2012) climate data. The generation of a TMY is very useful

for optimal HVAC system design and building energy simulations. TMY provides a reliable database for engineers who are engaged in design, installation and maintenance of HVAC systems. With data provided by TMY it is possible to make building energy simulations and make calculations to determine the necessary power for devices.

Comparing TMY and TMY-2 model values with LBN 003-01 values showed deviation of some weather parameters that can be explained with climate changes. These differences show that there is need for TMY creation and the newest possible climate data should be used. In this paper TMY is created for one city of Latvia, but results suggest that research needs to be continued, and TMY models needs to be generated for all 10 cities that are described in LBN 003-01.

REFERENCES

1. SKEIKER, K. Generation of a typical meteorological year for Damascus zone using the Filkenstein–Schafer statistical method. *Energy Conversion and Management*, 2004, Vol. 45, p. 99–112.
2. HALL, I.J., PRAIRIE, R.R., ANDERSON, H.E., BOES, E.C. Generation of a typical meteorological year. Denver 1978. Proceedings of the 1978 Annual Meeting of the American Section of the International Solar Energy Society. Denver: Sandia Laboratories. 1978.
3. ZARIŅŠ, M. *Klimata datu izvēle gaisa kondicionēšanas jaudas aprēķinam*. Jelgava: Latvia University of Agriculture, 2001. 59 p.
4. SKEIKER, K. Comparison of methodologies for TMY generation using 10 years data for Damascus, Syria. *Energy Conversion and Management*, 2007, Vol. 48, p. 2090–2102.
5. CHAN, A.L.S., CHOW, T.T., FONG, S.K.F., LIN, J.Z. Generation of a typical meteorological year for Hong Kong. *Energy Conversion and Management*, 2006, Vol. 47, p. 87–96.
6. GUGGENBERGER, J.D., ELMORE, A.C., CROW, M.L. Predicting performance of a renewable energy-powered microgrid throughout the United States using typical meteorological year 3 data. *Renewable Energy*, 2013, Vol. 55, p. 189–195.
7. JIANG, Y. Generation of typical meteorological year for different climates of China. *Energy*, 2010, Vol. 35, p. 1946–1953.
8. KALOGIROU, S.A. Generation of typical meteorological year (TMY-2) for Nicosia, Cyprus. *Renewable Energy*, 2003, Vol. 28, p. 2317–2334.
9. LEE, K., YOO, H., LEVERMORE, G.J. Generation of typical weather data using the ISO Test Reference Year (TRY) method for major cities of South Korea. *Building and Environment*, 2010, Vol. 45, p. 956–963.
10. YANG, L., LAM, J.C., LIU, J. Analysis of typical meteorological years in different climates of China. *Energy Conversion and Management*, 2007, Vol. 48, p. 654–668.
11. ZANG, H., XU, Q., BIAN, H. Generation of typical solar radiation data for different climates of China. *Energy*, 2012, Vol. 38, p. 236–248.
12. ZHANG, Q. Development of the typical meteorological database for Chinese locations. *Energy and Buildings*, 2006, Vol. 38, p. 1320–1327.



NEW NUCLEAR ADVANCED FACILITIES AT CVREZ

X.C. Arnoult, M.Zychova, E. Krecanova, J. Berka, F. Di Gabriele, O. Srba

Centrum Výzkumu Řež

Hlavní 130, 250 68 Husinec-Rez – Czech Republic

ABSTRACT

The SUSEN program is divided in four sub-programs and teams: Technological Experimental Loops (TEL), Structural and System Diagnostics (SSD), Material Research (MAT) and Material Fuel Cycle (JPC). TEL team is in charge of the development large-scale experimental loops to improve the quality and quantity of data about the behavior of coolants used in the primary circuit and the corrosion of steel in contact with coolants. The coolants investigated are: supercritical water, helium and lead-bismuth. The SSD team is in charge to perform in hot-cells various kinds of mechanical tests on irradiated materials in the range from room temperature to 800°C (tensile test, creep test, tension-torsion test and fatigue test in different type of loading) and microstructure investigation with SEM and TEM. The goal of this paper is to present the facilities designed and built in the frame of the SUSEN program in the Centrum Výzkumu Řež, allowing research and development in the area of Generation IV and nuclear fusion reactors.

Keywords: mechanical test, high temperature, corrosion, loops

1. INTRODUCTION

Centrum Výzkumu Řež (CVREZ) is a research and development institute in the field of power engineering (mainly in the nuclear field). CVREZ is 100% a subsidiary of the UJV group; they both are located in the Czech Republic. Fundamental research in natural sciences using neutrons, research and development in nuclear energy related fields as corrosion processes, radiation induced damages in construction materials and research of development of radio-pharmaceuticals prepared by using nuclear reactors and design of new treatment procedures using neutrons are the different research activities at CVREZ. CVREZ is a nonprofit organization and its activities are restricted only for fundamental research and development.

With the support of the European Commission and the Ministry of Education, Youth and Sports of the Czech Republic, the implementation of the SUSTainable ENergy (SUSEN) project allows to build a strong infrastructure for sustainable research and development activities. The SUSEN project permits the participation of the Czech Republic on the European effort in the investigations in the life extension for Generation II and Generation III technologies (Gen II and Gen III) and the investigation of materials which will be used for Generation IV (Gen IV) reactor concepts and fusion [1]. Material candidates for both technologies are similar. The SUSEN project is organized around four research programs: Technological Experimental Loops (TEL), Structural and System Diagnostics (SSD), Nuclear Fuel Cycle (JPC) and Material Research (MAT) [1]. In this paper MAT program is not presented because this research program is mainly linked to the TEL and SSD teams in the area of testing of non-irradiated materials for high temperatures applications and the development of new technologies for fusion welding of advanced materials for conventional and nuclear energy.

2. TECHNOLOGICAL EXPERIMENTAL LOOPS (TEL)

The Generation IV international forum (GIF) defined eight technology goals to select the new reactor concept. These goals are gathered in four broad areas: sustainability, economics, safety and reliability, and proliferation resistance and physical protections [2]. Very-High-Temperature reactor (VHTR), Supercritical water-cooled reactor (SCWR), Molten-salt reactor (MSR), Gas-cooled fast reactor (GFR), Sodium-cooled fast reactor (SFR) and Lead-cooled fast reactor (LFR) are the reactor concepts meeting the eight technology goals. The TEL program in CVREZ is mainly focused on the construction of large-scale experimental facilities allowing research in the field of media present in Gen IV reactors and Fusion reactor. The following media are studied at CVREZ: supercritical water as medium for the primary circuit of SCWR, helium as medium for the primary circuit of VHTR and as coolant for the first wall of a fusion reactor [1]. Lead and lead-bismuth media are also studied in CVREZ for research on materials.

2.1. Supercritical Critical Water Loop (SCWL)

The SCWL (Fig. 1) was designed for materials and water chemistry investigation. The system is composed in two functional parts: irradiation channel and auxiliary circuits. The operational parameters in the irradiation channel are 600°C and 25 MPa respectively. The irradiation channel was designed to be plugged into one rig of the research reactor LVR-15 in Řež, Czech Republic.

The primary circuit, the dosing system, measuring system, the purification system and cooling circuits compose the auxiliary circuits. The dosing system performs dosing of chemicals in gas and fluid form. The measuring circuits provide the chemical conditions in primary circuit. They monitor conductivity, electrochemical corrosion potential, various chemical concentrations, temperature and pressure in various parts of the facility. It is important to monitor these chemical parameters to ensure the proper chemical properties in the loop and its safe operation. The purification system is composed by a system of mechanical and ionex filters. The purification system cleans partially the medium circulating in the loop.

In the past, the basement of the building of the reactor LVR-15 was designed for some weight limit. Actually, this limit was already reached, so it is not possible to place the loop in the reactor building. Nowadays, in the frame of SUSEN project, a new building is under construction. In 2015, when the building will be finished, the in-pile testing will begin. At the moment the loop operates in out-off-pile regime.



Fig. 1. Supercritical-Water Loop and its flowchart [3]

2.2. High Temperature Helium Loop (HTHL)

The goals of HTHL (Fig. 2) are simulation of physical and chemical conditions of the GFR and VHTR simulation of clean up of the medium in operation mode of the reactor. HTHL is designed for testing of interaction of materials and gaseous atmosphere at high temperature, experiments aimed to helium coolant chemistry and purification are also possible. HTHL consists of two parts: active channel and helium purification, purity control and dosing system. Main projected parameters of the device are: maximum temperature in test section: 900°C, maximum gas pressure: 7 MPa, maximum gas flow rate: 0.01042 kg.s⁻¹. To minimize loss of helium during experiments, gas pressure during operation is usually maintained lower, typically 4–5 MPa.

The active channel was originally designed to be placed to the core of test reactor LVR-15, but later the decision was to use HTHL only for out-of-pile experiments. The section for specimens is approximately 500 mm long with diameter about 30 mm. Currently, the new loop for in-pile operation is built within the SUSEN project.

The purification system is similar to the real HTR reactor, the design was inspired by helium purification system of Chinese test reactor HTR-10 [4, 5]

The experimental system is composed of five flow meters, eighteen pressure sensors and twenty nine thermocouples located in different loop sections. The loop is also composed of monitoring system of chemical composition of the gaseous medium, a hygrometer, and dosing device of gaseous additions.

Gas chromatograph with a helium ionization detector (GC-HID) is used to monitor the chemical substances present inside the helium gas. The following chemical substances are checked: CO, CO₂, H₂O, CH₄. HID detector principle: helium goes in the space between two electrodes; helium atoms are brought into excited state and form the helium plasma. When the helium returns in the gas state, photons are radiated and they ionize the sample. The ionized substances are those having a lower ionization potential than 17.7 eV. After the ionized molecules are attracted to the collecting electrode [6], GC-HID, with special chromatographic columns, allows a very low detection limits for gaseous substances determination.

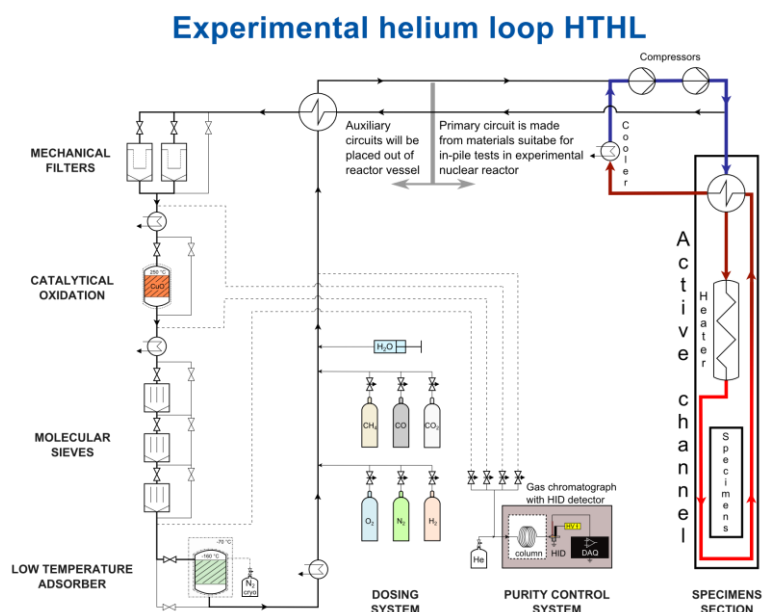


Fig. 2. Experimental helium loop

To check humidity, an optical hygrometer Bartec 5673 is used; three sensors are placed in the loop. Locations of sensors are at the input and output of the purification circuit and behind the absorbers with molecular sieves. The principle of measuring the wavelength change of beam of infrared light is used by this type of hygrometer. This method is particularly accurate for determination of low humidity concentration (units, tens vppm). The low detection limit is 1 vppm. The hygrometer records and stores the experimental data every 10 minutes.

A dosing container is used for gaseous additions. Its vessel has a volume of 500 ml; it is filled with a gas or a gas compound. The composition and the pressure are defined. The content is flushed into the gas circuit of loop. First experimental results have been already published about the purification system and the behavior of impurities [5, 7]. The first experience with dosing system during test operation of HTHL is not very good; the improvement of the system is under development.

2.3. Lead/Lead-Bismuth loops

COLONRI I and II loops allow the monitoring of corrosion of material in lead-bismuth (Pb-Bi) and lead (Pb) respectively. They both are natural convection loops. Their design is based on convection loops allowing the measurement of corrosion evolution of structural materials in heavy and alkaline liquid metals [8]. Both loops are identical and have a mirror structure. The loops are made of an upper expansion tank, a high- (HT) and low-temperature sections (L), a heating (h) and cooling (c) legs (Fig. 3). The loops are wrapped by resistance wires to heating the system. During the test, the temperature is maintained constant and controlled by thermocouple with an accuracy of $\pm 1^\circ\text{C}$ for experimental sections and $\pm 3^\circ\text{C}$ in the expansion tank. The two experimental sections work at different temperature, with a temperature difference up to $\Delta T=150^\circ\text{C}$.

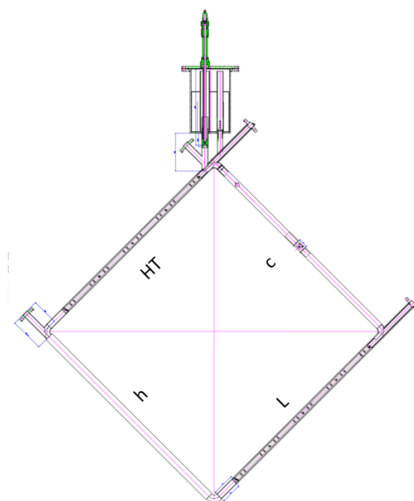


Fig. 3. Lead/Lead-Bismuth loop sketch

The loops were manufactured from austenitic stainless steel AISI 321. The inner surface of the tube working at the highest temperature (h) was covered with a molybdenum plate. Specimen holders, four for each leg, have a capacity of three rows of specimens, for a total length of around 2000 mm (Fig. 4). The upper expansion tank allows a partial derivation of fluid and as well to have a chemistry controlled of the medium. The chemistry of liquid metal is controlled by dosing gases (Ar , ArO_2 , ArH_2 , H_2) and monitored by electrochemical oxygen

sensor. Up to five oxygen sensors can be placed in each loop. Sensors are electrochemical galvanic cells and manufactured in the CVREZ laboratories. The sensor is an yttrium stabilized zirconium ceramic tube, which is the solid electrolyte, and the reference system used is Bi/Bi₂O₃ [9]. The maximum operating temperature for Pb-Bi and Pb are respectively 550°C and 650°C, for a flow rate of 2 cm.s⁻¹ and each loops contains about 1.7l of liquid metal.

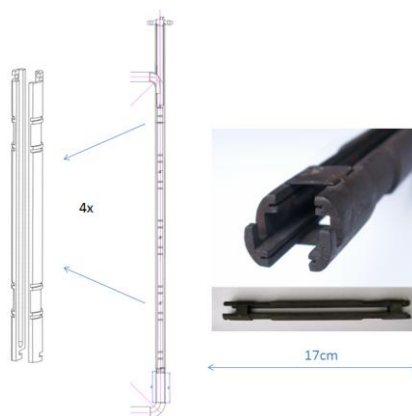


Fig. 4. Holder and test section

Several types of materials were tested in the COLONRI loops. Ferritic/martensitic steel T91 and austenitic 316 L were extensively tested in the loops [10], because they were selected as candidate materials for LFR construction materials. However, a large amount of work was also focused on ODS materials, coatings and other stainless steels evaluated for applications in Heavy Liquid Metals environments.

3. STRUCTURAL AND SYSTEM DIAGNOSTIC (SSD)

This program is focused on structural and system diagnostics of Gen II, Gen III and Gen IV nuclear power plant. The following tests will be performed in hot-cells at CVREZ, tensile testing, impact testing, fracture toughness testing, crack growth rate testing at cyclic loading, small-cycle fatigue testing, creeping tests for irradiated materials from room temperature to 800°C [1].

3.1. Static and dynamic confinement

Preparation and testing of irradiated materials require a confined area to be manipulated and protect persons working with these active materials. Thank to the program SUSEN ten hot-cells and one semi-hot-cell are under construction (Fig. 5). The Hot-cells Hall is divided in 4 spaces, as show on Fig. 6. There are hot-cells in blue, operator hall, basement and ceiling. The maximum source activity from hot-cells will be up to 300 TBq ⁶⁰Co. Dose equivalent rate (DER) received in operator hall, basement and ceiling will be 1.38 μSv/h, 2950 μSv/h and 54 μSv/h, respectively.

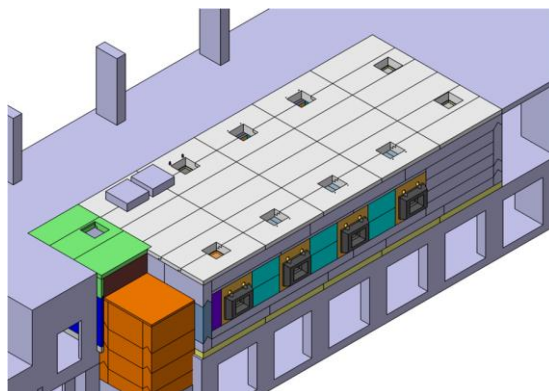


Fig. 5. Hot-cells overview



Fig. 6. Cross section of Hot-cells Hall

The level of dose received determines the thickness of shielding. Stainless steel was chosen to be the shielding material. The thickness of side wall, wall between hot-cells, the ceiling shielding and floor shielding are 500 mm, 300 mm, 300 mm respectively. All hot-cells will be equipped by a hermetic, removable box made in stainless steel (Fig. 7). This approach of facility management allows at CVREZ, for any reason, to change the instrumentation inside the box and simply pull out the box and put new inside with new instrumentation without any delay.

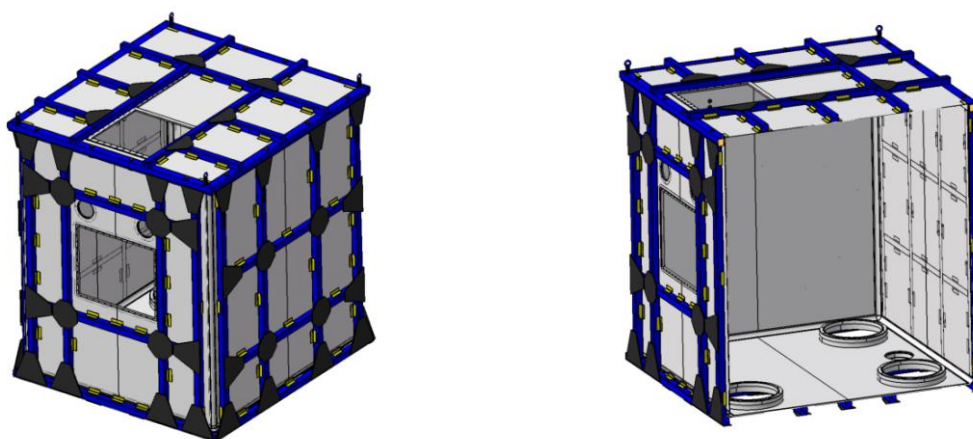


Fig. 7. Steel box with holes for windows, manipulator and entrance for specimens

The shielding of the hot-cells and the steel box are the static confinement part. The dynamic confinement is made by ventilation. The air from hot-cells passes through three sets of filter before to go in the air. Also inside the box will be active waste piping, LED light system for illumination of work space, numerous sensors (temperature, pressure, radiation

level, etc.) and cameras for better control of the device inside. Each hot-cell will equip of set of manipulator to handle the sample, preparation machines, testing machines etc.

3.2. Equipment inside Hot-cell

Electrical discharge machine (EDM) is used to manufacture sample (cutting and machining) at the desired shape without thermal and mechanical damage in the surrounding area of the cut. The maximum weight of work piece is 30 kg and the dimension of traversing table is 600 x 400 mm.

Electron beam welding machine (EBW) uses a high-velocity electrons beam which melts and flow two materials together under vacuum. The maximum dimension of work piece is 170 x 170 x 230 mm, the accelerating voltage is 20–60 kV and vacuum condition is 10^{-5} Pa.

Computer numerical control (CNC) is numerical machine to perform grinding, machining and drilling. The maximum weight of work piece is 15 kg for a maximum length of 200 mm.

For tensile test, fracture toughness test, low cycle fatigue and combined loading a universal tensile machine will be used. The loading cell is 250 kN maximum for a range of temperature from -150°C to 1000°C.

High frequency resonance pulsator is a device to test mechanical properties at high frequencies. Combination of static and dynamic loading is 50 kN maximum for a frequency of 250 Hz maximum for a range of temperature from room temperature to 800°C. CVREZ will use this machine for high cycle fatigue and pre-cracking of compact tensile sample.

Electromechanical creep machine will test the creep behavior in static and fatigue regimes at elevated temperatures. The loading cell is 50 kN maximum.

Autoclave with water loop is device for testing materials in control environment (water, high pressure, and high temperature). The loading cell is 50 kN maximum with maximum testing temperature at 350°C with control of chemical composition of water. With this device, it is possible to test the mechanical properties and corrosion resistance properties.

For the microscopy investigation a scanning electron microscope and light optical microscope will be present in a hot-cell.

4. CONCLUSION

SUSEN project allows at CVREZ to develop the facilities and instrumentations that institute has already had. This project allows also developing new facilities, buying new experimental machines and gives a wide range of investigation in different field in the research and development of Gen IV reactor. The different types of loops study the impact of media on the properties of structural materials. The behavior of media and the different type of mechanical tests in static and fatigue regime at different temperatures enable to extend the limit of knowledge about mechanisms of corrosion, mechanisms of degradations and improve the design and safety in nuclear power plant.

The presented work was financially supported by the SUSEN Project CZ.1.05/2.1.00/03.0108 realized in the framework of the European Regional Development Fund (ERDF).

REFERENCES

1. <http://susen2020.cz/>.
2. https://www.gen-4.org/gif/jcms/c_9260/public.
3. ZYCHOVA, M., et al. *New research infrastructure for SCWR in Centrum Vyzkumu Rez.* in *The 6th International Symposium on Supercritical Water-Cooled Reactors* 2013. Shenzhen, Guangdong, China.
4. BERKA, J., et al. *New experimental device for VHTR structural material testing and helium coolant chemistry investigation at High Temperature Helium Loop in NRI Řež.* Nuclear Engineering and Design, 2012. 251(0), p. 203–207.
5. MATĚCHA, J., et al. *Testing of analytical and purification methods for HTR helium coolant.* Nuclear Engineering and Design, 2012. 251(0), p. 208–215.
6. <http://www.srigc.com/HIDman.pdf>.
7. BERKA, J., VÍDEN I., KOZMÍK V. *Organické látky detegované vheliovém okruhu experimentální výzkumné aparatury k simulaci chlazení jaderného reaktoru při zahájení provozu.* Chemnické listy 2012. 106(10), p. 980–987.
8. ILINČEV, G. *15 years of research in structural material corrosion resistance in liquid metals at State Research Institute for Protection of Materials in Prague.* Nuclear Energy, 1977. 23(85).
9. BRISSONNEAU, L., et al. *Oxygen control systems and impurity purification in LBE: Learning from DEMETRA project.* Journal of Nuclear Materials, 2011. 415(3), p. 348–360.
10. DOUBKOVÁ, et al. *Corrosion behavior of steels in flowing leadâ“bismuth under abnormal conditions.* Journal of Nuclear Materials, 2008. 376(3), p. 260–264.

THE DEFINITION OF MAXIMUM TEMPERATURE IN VENTILATED CONTAINER WITH SPENT NUCLEAR FUEL

S. Alyokhina, A. Feshchenko

*National Technical University, “Kharkiv Polytechnical Institute”
21 Frunse str., Kharkiv, UA-61002 – Ukraine*

ABSTRACT

The spent nuclear fuel of six reactors of Zaporizhska NPP is storing by dry method on open platform which is placed on the site. The storage technology is based on usage of ventilated containers which withdraw decay heat from spent nuclear fuel by passive ventilated system with natural convection.

The safety of the Dry Spent Nuclear Fuel Storage Facility consists of three main components – Nuclear safety, Radiation safety and Safe thermal condition. For last field the main problem is the definition of thermal state of containers and spent fuel assemblies inside container. These results will be especially important at stage of Dry Spent Nuclear Fuel Storage Facility operating and modernization for predicting thermal state of fuel during whole period of storage.

The main goal of this investigation is numerical definition of the maximum temperature inside containers in different conditions (i.e. normal and accident conditions). For the first time the detailed structure of container was considered and a couple of numerical studies allow to determine the distribution of maximal temperature vs decay heat.

Keywords: spent nuclear fuel, temperature field, conjugate heat transfer

1. INTRODUCTION

One of popular strategies of spent nuclear fuel (SNF) handling in countries employed open fuel cycle is temporary dry storage. The advantages of this technology are safety, low level of radioactive contamination, simplicity of realization and modification, the low-cost construction and operation.

In Ukraine where open nuclear fuel cycle was realized about 50% of all energy supply come from nuclear industry. Each year Ukrainian nuclear energy industry produces about 270 tons of spent nuclear fuel. So SNF handling is very important issue for Ukraine.

The strategy of dry spent nuclear fuel storage has been chosen in Ukraine as temporary method of SNF handling before making the final decision about SNF disposal or reprocessing [1].

The spent nuclear fuel of six reactors of Zaporizhska NPP is storing by dry method on open platform which is placed on the site. The safety of the Dry Spent Nuclear Fuel Storage Facility is based on three main components – Nuclear safety, Radiation safety and Safe thermal condition. For last field the main problem is the definition of thermal state of containers and spent fuel assemblies inside container. These results will be especially important at stage of Dry Spent Nuclear Fuel Storage Facility operating and modernization for predicting thermal state of fuel during whole period of storage.

2. PROBLEM DEFINITION

The biggest NPP in Ukraine is Zaporizhska Nuclear Power Plant. Every year this station produces about half of all SNF in Ukraine.

From August 2001 the spent nuclear fuel of six reactors of Zaporizhska NPP is stored by a dry method on the open area in Dry Spent Nuclear Fuel Storage Facility, which is

designed for the placement of 380 ventilated containers, each of which contains 24 spent fuel assemblies.

For Dry Spent Nuclear Fuel Facility was chosen USA technology of dry storage in ventilated containers (Fig. 1) [2]. The container was designed on base of containers of Sierra Nuclear Corporation (USA) with changes of inner structure of storage basket.

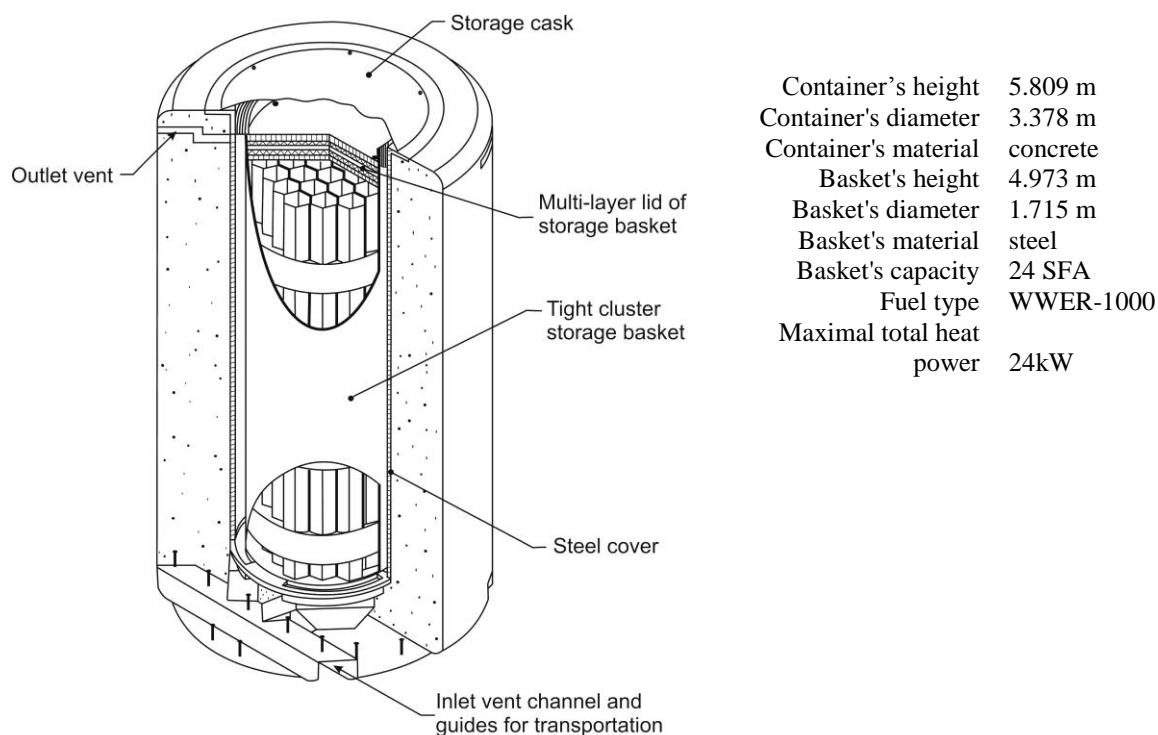


Fig. 1. Ventilated container

The twenty four spent fuel assemblies (SFA) was placed into tight cluster storage basket, which is filled with inert gas – helium. Helium circulates in the inner space of the basket due to natural convection caused by temperature difference between hot SFA and cold basket casing.

The passive cooling system is organized in storage containers, so cooling by atmospheric air take place only. The thermal safety criteria limited maximum temperature of 350 °C for the temperature of spent nuclear fuel cladding inside storage basket [3]. The ventilating air on an exit from channels should not be heated more than on 61 degrees. The temperature measurements are carrying out only on exit of ventilation channels.

The safety of Dry Spent Nuclear Fuel Storage Facility is based of three main components – Nuclear safety, Radiation safety and Safe thermal condition. Therefore the problem of determination of safe thermal condition for the storage facility is one of main problems at operation.

3. METHODOLOGY

The SNF storage facility is the complex system especially from thermal point of view. Firstly in this system three main heat transfer mechanisms are used: conduction, convection, radiation heat exchange. Secondly all these heat transfer processes take place inside the system which has complex space form. And finally there are couple of factors which have internal and external influence on this system: initial decay heat which depends of assembly

storage time, decay heat variations during storage, influence of external factors (ambient temperature, wind and solar influences, precipitation etc.). So for definition of thermal state of containers with spent nuclear fuel it is reasonable to solve the conjugate heat transfer problem. It means to consider mutual influence of thermal processes in solid body and fluid environment with taking into account flow structure [4].

Static 3D case was investigated in this study. The mathematical model is described in [2, 5] in detail and consists of the next equations in partial derivatives:

– continuity

$$\frac{\partial}{\partial x}(\rho u) + \frac{\partial}{\partial y}(\rho v) + \frac{\partial}{\partial z}(\rho w) = 0, \quad (1)$$

where ρ – density; u, v, w – component of velocity vector $\mathbf{v} = (u, v, w)$;

– motion of viscous fluid

$$\begin{aligned} \rho u \frac{\partial u}{\partial x} + \rho v \frac{\partial u}{\partial y} + \rho w \frac{\partial u}{\partial z} = & -\frac{\partial p}{\partial x} + 2 \frac{\partial}{\partial x} \left(\mu_{\text{eff}} \frac{\partial u}{\partial x} \right) + \\ & + \frac{\partial}{\partial y} \left(\mu_{\text{eff}} \left(\frac{\partial u}{\partial y} + \frac{\partial v}{\partial x} \right) \right) + \frac{\partial}{\partial z} \left(\mu_{\text{eff}} \left(\frac{\partial u}{\partial z} + \frac{\partial w}{\partial x} \right) \right) - \frac{2}{3} \frac{\partial}{\partial x} \left(\mu_{\text{eff}} \left(\frac{\partial u}{\partial x} + \frac{\partial v}{\partial y} + \frac{\partial w}{\partial z} \right) \right), \\ \rho u \frac{\partial v}{\partial x} + \rho v \frac{\partial v}{\partial y} + \rho w \frac{\partial v}{\partial z} = & -\frac{\partial p}{\partial y} + 2 \frac{\partial}{\partial y} \left(\mu_{\text{eff}} \frac{\partial v}{\partial y} \right) + \\ & + \frac{\partial}{\partial x} \left(\mu_{\text{eff}} \left(\frac{\partial u}{\partial y} + \frac{\partial v}{\partial x} \right) \right) + \frac{\partial}{\partial z} \left(\mu_{\text{eff}} \left(\frac{\partial v}{\partial z} + \frac{\partial w}{\partial y} \right) \right) - \frac{2}{3} \frac{\partial}{\partial y} \left(\mu_{\text{eff}} \left(\frac{\partial u}{\partial x} + \frac{\partial v}{\partial y} + \frac{\partial w}{\partial z} \right) \right), \\ \rho u \frac{\partial w}{\partial x} + \rho v \frac{\partial w}{\partial y} + \rho w \frac{\partial w}{\partial z} = & -\rho g - \frac{\partial p}{\partial z} + 2 \frac{\partial}{\partial z} \left(\mu_{\text{eff}} \frac{\partial w}{\partial z} \right) + \\ & + \frac{\partial}{\partial x} \left(\mu_{\text{eff}} \left(\frac{\partial u}{\partial z} + \frac{\partial w}{\partial x} \right) \right) + \frac{\partial}{\partial y} \left(\mu_{\text{eff}} \left(\frac{\partial v}{\partial z} + \frac{\partial w}{\partial y} \right) \right) - \frac{2}{3} \frac{\partial}{\partial z} \left(\mu_{\text{eff}} \left(\frac{\partial u}{\partial x} + \frac{\partial v}{\partial y} + \frac{\partial w}{\partial z} \right) \right), \end{aligned} \quad (2)$$

where p – pressure; μ_{eff} – effective dynamical viscosity;

– energy

$$c_p \rho \left(u \frac{\partial T}{\partial x} + v \frac{\partial T}{\partial y} + w \frac{\partial T}{\partial z} \right) - \left(u \frac{\partial p}{\partial x} + v \frac{\partial p}{\partial y} + w \frac{\partial p}{\partial z} \right) = \frac{\partial}{\partial x} \left(\lambda_{\text{eff}} \frac{\partial T}{\partial x} \right) + \frac{\partial}{\partial y} \left(\lambda_{\text{eff}} \frac{\partial T}{\partial y} \right) + \frac{\partial}{\partial z} \left(\lambda_{\text{eff}} \frac{\partial T}{\partial z} \right), \quad (3)$$

where c_p – specific heat at constant pressure, λ_{eff} – effective heat conductivity, T – temperature;

– heat conductivity

$$\frac{\partial}{\partial x} \left(\lambda \frac{\partial T}{\partial x} \right) + \frac{\partial}{\partial y} \left(\lambda \frac{\partial T}{\partial y} \right) + \frac{\partial}{\partial z} \left(\lambda \frac{\partial T}{\partial z} \right) + q_v = 0, \quad (4)$$

where λ – heat conductivity, q_v – quantity of heat.

The system of differential equations is supplemented by the thermal equation of state for closure. For that the ideal gas law is acceptable for investigation. The standard k- ϵ turbulent flow model is used for the prediction of the turbulent components of coefficients in equations [6]. This model consists of two differential equations: for the turbulent kinetic power k and velocity of its dissipation ϵ .

The mathematical model is supplemented with the equation which describes heat exchange between outside surface of fuel basket and inner surface of container.

Computer programs which allow solving the equations of mathematical model (ANSYS Fluent, STAR-CD, PHOENICS, OpenFOAM etc.) can be used for definition of maximum temperature in ventilated container.

The calculation area was considered as concrete container with storage basket inside.. The simplified structure of the inlet channels in container was considered (hydraulic resistance has been maintained). Due to limited computer sources and complex structure of storage basket it was considered solid body (with homogeneous body with uniformly distributed heat source and equivalent heat conductivity which was defined by solving inverse heat transfer problem [7]).

The atmospheric pressure (101325 Pa) and the temperature of atmospheric air (40 °C) were set as boundary conditions in calculation areas.

The mathematical model was verified with results of temperature measurements on exit of ventilating channels which are taking during first week of container storage [8]. The difference between measured and calculated data was not more than 1.5 degree.

4. RESULTS

The maximum of environmental temperature on the territory of Zaporizhska NPP is 40 °C and this temperature was considered as the limiting one. Temperature fields inside the container and temperature of ventilated air in windless day (calm conditions) are shown on Fig. 2.

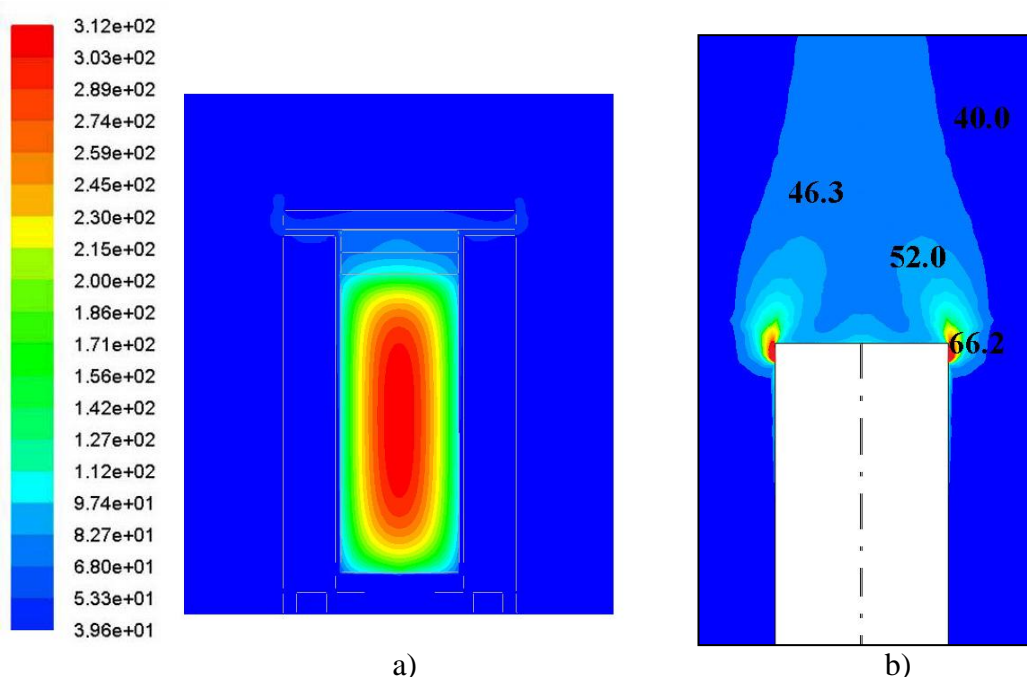


Fig. 2. Temperature fields of the container and ventilating air at 40 °C (°C):
a – temperature field of storage basket, container and ambient air; b – temperature field of ambient air which created by container

The ambient air flows into inlet channels, passes the space between a basket and a steel cover of the container, is heated up and leaves the container through the outlet channels. Heated air flows next vertically upwards above the container. At calculations the power of 1 kW was considered for each SFA as limiting value. The maximum of temperature in storage basket is 311.5 °C. Heating of air does not exceed 61 degrees, criteria of safety are observed.

The series of calculations with taking into account the time-depended changes of decay heat in storage basket (10-24 kW) allowed to define the maximum temperature inside storage basket. The Fig. 3 shown that the maximum temperature of spent nuclear fuel decreases with time of storage.

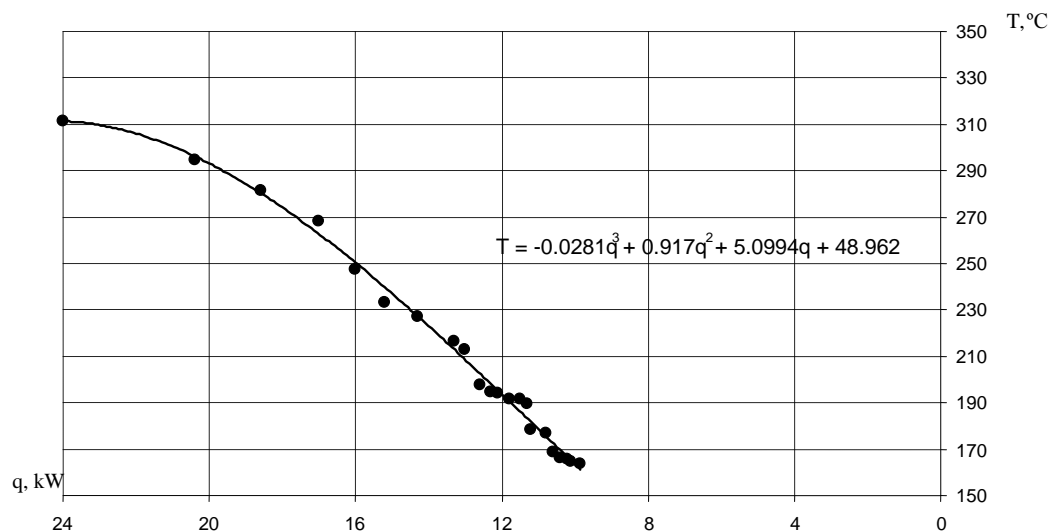


Fig. 3. Dependence the maximum temperature in storage basket from the decay heat of storage basket

5. CONCLUSIONS

The more effective methodology for calculation of the maximum temperature inside spent nuclear storage container is the conjugate heat transfer problem which do not need to define boundary conditions on each surface of elements. This methodology was used for definition of container thermal state and it allowed to obtain dependence of maximum temperature vs decay heat (it can mean the time of cooling) of spent nuclear fuel storage. The received results will be used for increasing safety of Dry Spent Nuclear Fuel Storage Facility on Zaporizhska NPP. The next stage of investigations is in finding dependence for calculating temperatures of each spent fuel rods inside storage basket in different type of storage condition.

REFERENCES

1. “Energy strategy of Ukraine till 2030” authorized by the order of Ukrainian Cabinet of Ministers No. 145, p. 15, March 2006.
2. RUDYCHEV V.G., ALYOKHINA S. V., GOLOSCHAPOV V.N. et al. Spent Nuclear Fuel Dry Storage Safety. V.N. Karazin Kharkiv National University, 2013. – 200 p. – in rus.
3. The safety analysis report for dry spent nuclear fuel storage facility of Zaporizhska NPP. Version 3.01.1, Zaporizhska NPP, Inv. No. 1526(3), Energodar, 2008 – 624 p.
4. LYKOV A.V., ALEKSASHENKO V.A., ALEKSASHENKO A.A. Conjugate problems of convective heat exchange. Minsk, 1971 – 348 p. – in rus.



5. ALYOKHINA S.V., GOLOSHCHAPOV V.N., KOSTIKOV A.O. Thermal state of ventilated containers with spent heat-generation fuel elements of reactor WWER-1000. Problems of nuclear power plants' safety and of Chornobyl, 2009, Vol.11, p. 36–41. – in rus.
6. FISCHER L.E., HOWE A. Qualification of independent spent fuel storage installation. Nuclear Engineering and Design, 1999, No. 2–3, p. 217–228.
7. ALYOKHINA S., et al. Definition of equivalent heat conductivity of the many-placed hermetic basket of storage of the spent nuclear fuel by the decision of the inverse problem. Nuclear and radiation safety, v. 12, Issue 4, Kyiv, 2009, p. 48–51 – in rus.
8. ALYOKHINA S.V. et al. Analysis of storage conditions of the spent nuclear fuel on the dry storage platform. Problems of nuclear power plants' safety and of Chornobyl – Chornobyl, 2010, Vol.13 – P.76-83 – in ukr.

ANALYSIS OF THE FUEL RODS DEGRADATION IN IGNALINA NPP SPENT FUEL POOLS IN CASE OF LOSS OF COOLANT ACCIDENT

A. Šutas

*Lithuanian Energy Institute
Breslaujos str.3, LT-44403 Kaunas*

ABSTRACT

The accident in Fukushima Daiichi NPP showed, that the loss of the coolant accident in spent fuel pools could have significant probability. Because the coolant is used for the removal of residual heat from spent fuel assemblies, if this heat removal function is not restored in a couple of days time period, overheating of fuel assemblies, damage and melting of fuel rods starts. In the nuclear power plants the spent fuel pools are equipped close to the reactor and in some of NPPs these pools are not covered by a containment. Thus, the damage of fuel assemblies in the spent fuel pools can lead to very large release of radioactive materials to the environment.

The purpose of this paper is to model the process of degradation of nuclear fuel rods in Ignalina Nuclear Power Plant spent fuel pools during loss of coolant accident and to find out modelling limitations of applying ASTEC programe package. The some inaccuracies of such a modelling will be presented. The received results of calculation can be used for the development of severe accident management guidelines in a spent fuel pools.

Keywords: spent fuel pool, fuel degradation, ASTEC computer code

1. INTRODUCTION

The significant technical aspects of spent fuel pools (SFP) are:

- Permanent cooling is necessary due to decay heat from spent fuel rods;
- Water layer in SFP is necessary due to cooling function assurance as well as plant personel protection from ionizing radiation.

The main reason for a severe accident in a spent fuel pool is loss of coolant accident. According to the NRC data, the probability of such an event is about 10^{-6} per pool per year [1]. Severe accident in SFP scenario is very similar to that in a reactor pressure vessel, except several aspects:

1. Air pressure in SFP's are at atmospheric level. This is favorable to hydrogen spreading in pool building;
2. SFP building contains air atmosphere, while reactor primary circuit has no (or limited) air. It is important when zirconium oxidation reaction is evaluated.
3. Fuel bundles in a SFP emit much less thermal energy (which is at residual heat level) compared to those in a reactor pressure vessel;
4. Water inventory in SFP is much more than in a reactor active zone;
5. Due to slower heating and higher water quantity accident scenario in a SFP is characterized by higher time margin to take accident managment actions than in an analogous accident scenario in a reactor pressure vessel.

Critical time moment in a SFP accident scenario is time when water level drops below the top of fuel bundles. This increases ionizing radiation dose to pool service personal and limits personal actions to manage an accident. For example, water levels drop in three meters induces 9-fold increase in radiation dose [2].

Recent events at Fukushima NPP after an earthquake and tsunami attack have drawn attention to an accident in a SFP's problem. During Fukushima accident water level in SFP

decreased about 7 m and only 1.5 m thickness water layer left above the top of spent fuel assemblies. Water leakage was stopped and nondesign water injection sources were used to restore the initial water level [3].

This paper describes a severe accident scenario at Ignalina NPP Unit 2 SFP due to water loss and a consequences of heating and degradation of fuel assemblies. Modelling limitations is also presented. The modelling results is difficult to compare with other author's results due to a choice to use dryout scenario without restoring water supply to the pool as it is selected in the scenarios used by other authors [4].

2. METHODOLOGY

2.1 SFP design

The whole complex of storage pools of the spent fuel storage and handling system comprises 12 pools (Fig. 1) which are detailly described in the SAFETY ANALYSIS REPORT FOR INPP UNIT 2 [5]. They are as follows:

- Two pools (Rooms 236/1, 236/2) intended to store spent fuel assemblies after they are extracted from the reactor;
- Five pools (Rooms 336, 337/1, 337/2, 339/1, 339/2) intended to store spent fuel fragmentized assemblies placed in baskets;
- Pool (Room 234) intended to accumulate spent fuel assemblies prepared to be fragmentized, to cut suspension brackets from the spent fuel assemblies, transport spent fuel assembly to the “hot” cell and full 102 placed transport baskets from the “hot” cell to the storage pools, store the 102 placed transport baskets when the storage pools hall is under repair;
- Two pools (Rooms 338/1, 338/2) intended to perform operations to load the transport baskets with the spent fuel assemblies into the transport casks and store the 102 placed transport baskets when the storage pools hall is under repair;
- Transport corridor (Room 235) intended to transport spent fuel assemblies and transport baskets loaded with spent fuel assemblies between the pools;
- Transport corridor (Room 157) intended to transport fresh fuel and reactor assemblies from the fresh fuel assembly preparation bay of Storage Pools Hall to the reactor and return spent fuel and reactor assemblies from the reactor to the storage pools.

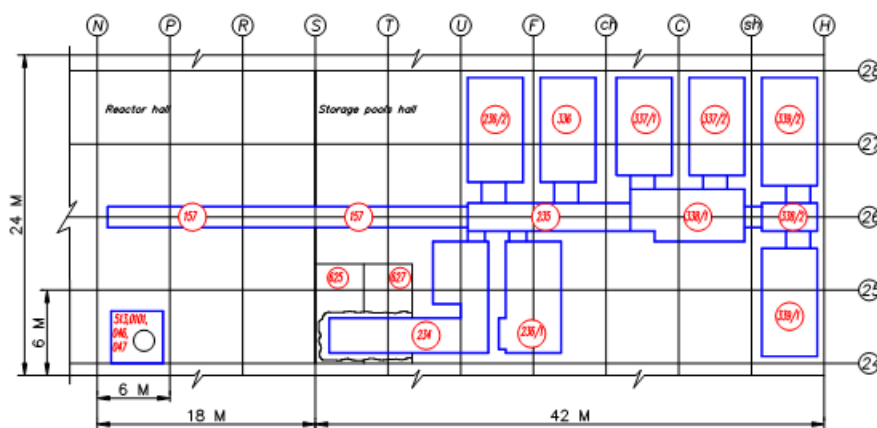


Fig. 1. Layout of buildings in storage pools hall at Ignalina NPP Unit 2

2.1. Modelling methodology

The numerical modelling was performed using ASTEC program package [6], which takes into account such a processes as:

1. Heating and ballooning of fuel rods;
2. Hydrogen generation as a result of zirconium oxidation reaction;
3. Breaching and melting of fuel elements;
4. Movement of molten material;
5. Corium accumulation on a bottom of spent fuel pool and reactions with steel and concrete;
6. Spreading, migration and discharge of fission products into the surrounding environment.

ASTEC code has a modular structure and was designed to evaluate an accident source term. The modeling was performed with ICARE module which is a part of ASTEC V2.0R2 code. The ICARE module simulates in-vessel core degradation and thermal-hydraulics. It computes behaviour of in-vessel structures, thermal-hydraulics for water, steam and non-condensable gases, chemical reactions between materials, thermal and mass transfers between components.

Table 1 presents general parameters of water, water level dynamics and pool structure, which model is presented at Fig. 2. The initial water leakage rate is 21.1 kg/s. At the time moment $t = 315\,500$ s water leakage is terminated and 45.5 m³ is left at the pool. Further no operator actions is done and SFP heating and degradation processes are modeled up to time $t = 5\,000\,000$ s.

Table 1. General modelling parameters

Total power of SFA, kW	4253
Water level, m	16.9
Water volume in SFP, m ³	5070
Water volume after leakage termination, m ³	45.5
Initial water temperature, °C	50
Water leakage rate, kg/s	21.111
Outside wall thickness, m	0.5
Cooling of outside wall of SFP	Constant heat transfer coefficient (5W/m ²)

The main data used in calculations for fuel rod models “ROD1”, “ROD2”, “ROD3” and “ROD4” is presented in Table 2.

Table 2 Parameters of groups of Spent Fuel Assemblies (SFA) in ASTEC model, according situation at 2009

Groups	Group of SFAs in ASTEC model	Assumed storage time in SFP	SFA decay heat, kW	Amount of SFAs in group	Group power, kW
SFAs in 236/2 room	ROD1	8 days	5.21	166	864.9
SFAs in 236/2 room	ROD2	137 days	1.281	1182	1514.1
SFAs in 236/1 and 234 rooms	ROD3	2 years	0.489	892	436.2
SFBs in shipping casks	ROD4	3 year	0.254	5661	1437.9
Total:				7901	4253

In ASTEC code all rooms of SFPs and fuel assemblies are modeled as a single pool with 4 different groups of spent fuel assemblies (Table 1 and Figure 2). It is assumed that heat from the pool to the environment is transferred through the walls of SFP. In the model SFP and a hall is modeled as a single element with a direct connection between SFP and the environment. Heat removal from outside of SFP to the environment is modeled through the heat structure POOLWALL using selected heat transfer coefficient. As it is mentioned above, all fuel assemblies are divided into 4 groups with different decay heat levels (Table 1). These decay values of spent fuel assemblies in the pool presents the situation at the moment of final shutdown of Ignalina NPP Unit 2 at the end of year 2009.

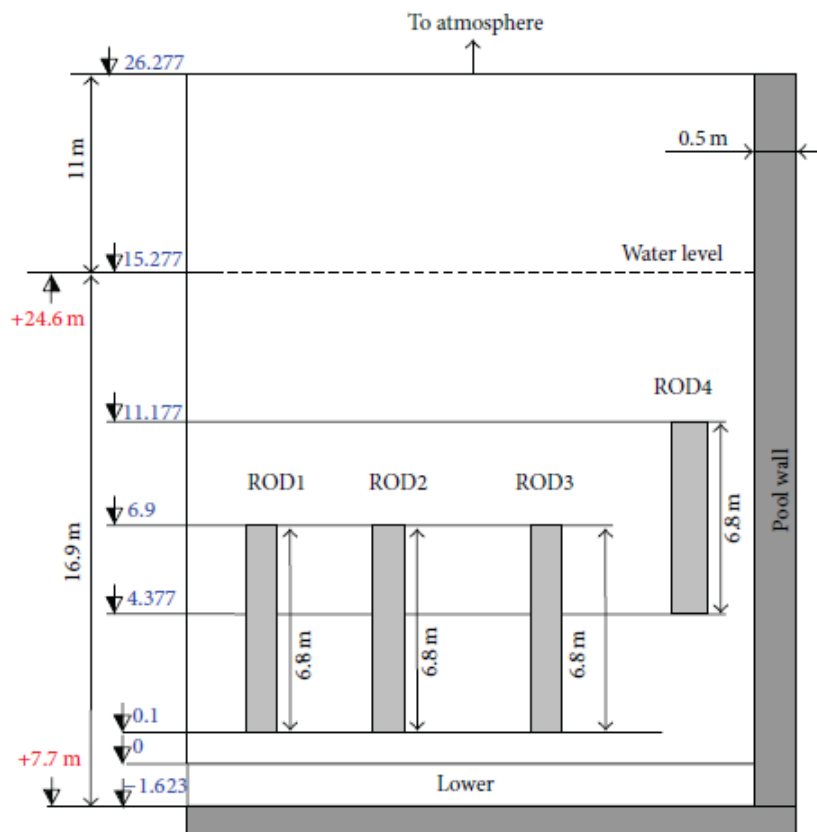


Fig. 2. SFP and SFAs nodalization scheme in ASTEC model

3. MODELLING RESULTS AND DISCUSSION

The most important moments of the severe accident scenario in Ignalina NPP Unit 2 SFP are presented in the maximum temperature dynamics (Fig. 3). 7 important time moments in the accident progression are indicated:

- “0” moment ($t = 55.000$ s): uncovering of SFA’s in ROD4 group;
- “I” moment ($t = 170.000$ s): fuel rods cladding ballooning and slow hydrogen generation;
- “II” moment ($t = 235.000$ s): all fuel assemblies in a SFP are fully uncovered;
- “III” moment ($t = 241.000$ s): fuel rod rupture, strong hydrogen generation, fission product release, molten corium occurrence;
- “IV” moment ($t = 522.000$ s): corium relocation into the bottom of SFP;
- “V” moment ($t = 640.000$ s): all water in the bottom of SFP evaporates;
- “VI” moment ($t = 790.000$ s): maximum temperature in the SFP is reached.

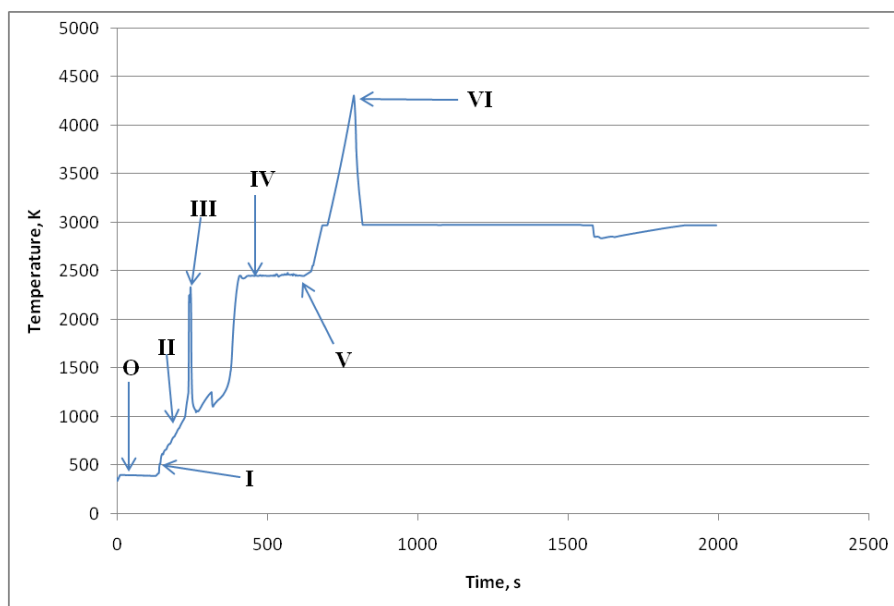


Fig. 3. Maximum temperature in the SFP

3.1. Uncovering of SFA's

Time moment “0” ($t = 55.000$ s) is important because of significant radiation exposure increase due to uncovering of the top of fuel assemblies in ROD4 group (Fig. 4). For NPP operators it is critically important to stop water leakage or to compensate the leak up to this time. Radiation dose increase after this moment and limits personal actions in managing an accident.

3.2. Fuel rods ballooning

Fuel rods cladding is produced from Zirconium alloy, which becomes soft enough at the temperatures $T > 1000$ K to start swelling. This temperature is also the start of steam starvation hydrogen generation which is a result of zirconium oxidation reaction. The start point of these processes is time moment “I” ($t = 170.000$ s).

3.3. Water level drops below a bottom of SFA's

Time moment “II” ($t = 235.000$ s) is a moment when water level drops below a bottom of fuel assemblies (ROD1, ROD2, ROD3 groups) and all fuel assemblies in a SFP becomes fully uncovered. At this time moment SFA's cooling function is lost and heating processes continues.

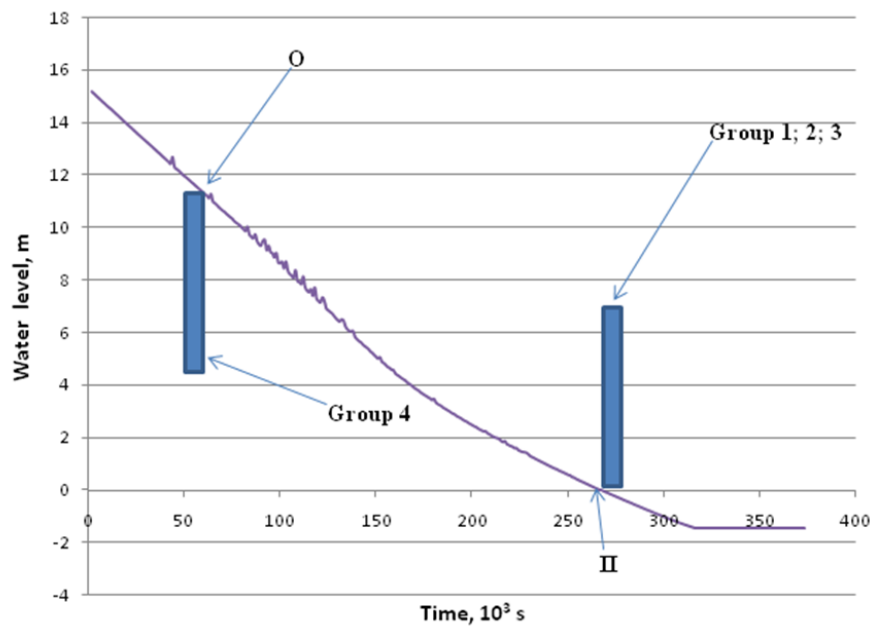
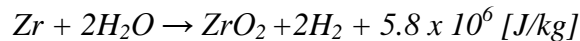


Fig. 4. Water level dynamics up to time moment $t = 375.000$ s

3.4. Several phenomena occurrence at the same time moment

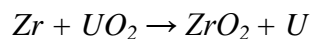
Time moment “III” ($t = 241.000$ s) is a start point when several phenomenas occursimultaneously:

- First fuel cladding ruptures occure. This induces fast and strong double sided exothermic oxidation reaction of zirconium cladding:



Sharp rise in hydrogen generation chart is presented in Fig. 5.

- The result of this reaction is sharp increase in maximum temperature in the SFP (arrow “III” in Fig. 3).
- Fuel cladding rupture causes physical contact between uranium dioxide fuel and zirconium alloy cladding. This induces uranium dioxide chemical reaction with zircalloy:



The result of this reaction is molten uranium ($T_{\text{melt (uranium)}} = 1402$ K). This means that integrity of fuel pellet is lost and molten corium generation process starts (Fig. 6).

- Fission products release in SFP starts.

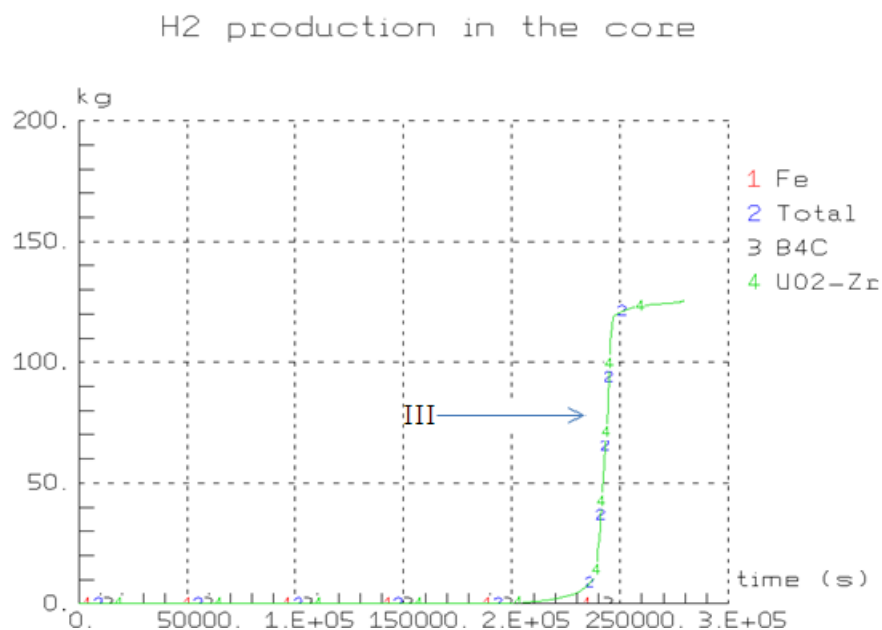


Fig. 5. Fast and strong zirconium oxidation reaction at time moment III

Because of these phenomena time moment “III” is critical in severe accident scenario. It is very important to restore SFP cooling function before the time moment $t = 241.000$ s.

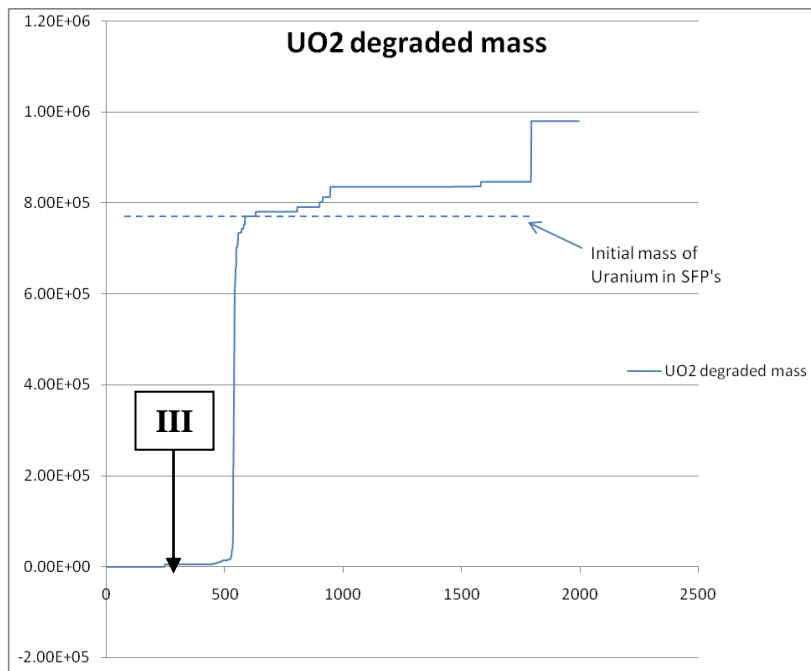


Fig. 6. Degradation of uranium at time moment “III”

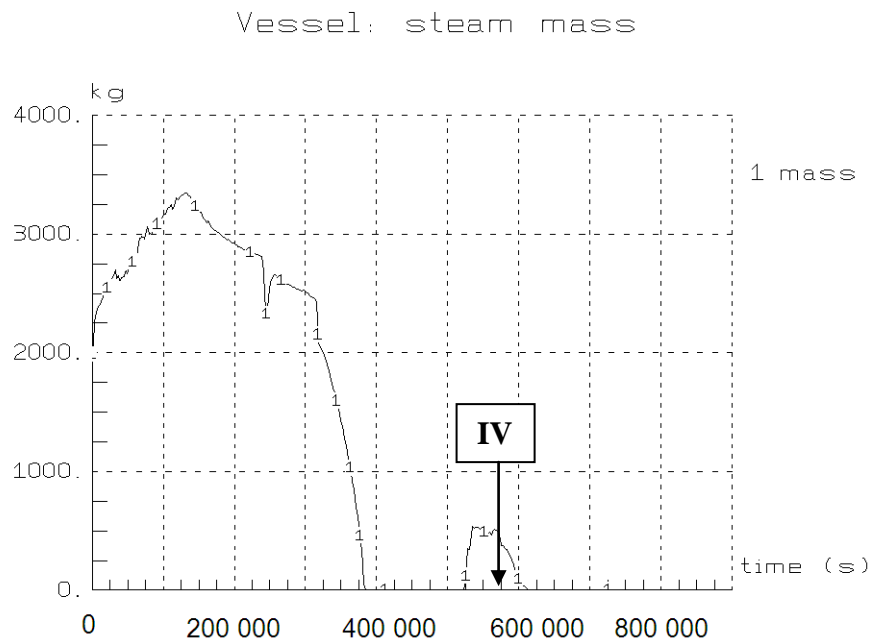


Fig. 7. Generation of steam at time moment “IV” processes

3.5. Corium relocation into the bottom of SFP

Time moment “IV” ($t = 522.000$ s) is important because of first molten corium contact with a residual of water in a bottom of SFP. This causes significant increase in vapour generation (Fig. 7) and rapid acceleration in hydrogen generation.

3.6. Water evaporation and corium heating in the bottom of SFP

Time moment “V” ($t = 640.000$ s) is a start of rapid maximum temperature increase due to evaporation of water residual in the SFP. This is a start of “ex-vessel” processes and ICARE module is not designed to evaluate these phenomenas with a desirable accuracy. Heating of corium continues and favourable conditions for corium-steel/concrete reactions originate.

3.7. Modelling limitations with ICARE module

Time moment “VI” ($t = 790.000$ s) is a moment when maximum temperature reaches it’s extremum value ($T > 4300$ K). It is obvious that such a value is unrealistic. The highest melting temperature among the materials in SFP has uranium dioxide ($T_{\text{melt}} = 3123$ K).

Moreover, uranium degradation chart (see “a” picture in Figure 6) presents the situation at $t > 580.000$ s when degraded uranium mass exceeds the initial uranium mass in SFP. It can be stated that after the time when fuel bundles melt and ex-vessel degradation occurs ICARE module is not appropriate for modelling further processes.

Such inaccuracies shows limits of desirable modelling accuracy of ICARE module when severe accident scenario at Ignalina NPP Unit 2 SFPs modeled.

4. CONCLUSIONS AND RECOMMENDATIONS

1. The most important moments that should be addressed in a severe accident management in Ignalina NPP Unit 2 SFP scenario are the following:
 - Time $t = 55.000$ s is a moment of uncovering of first fuel assemblies;
 - Time $t = 241.000$ s is a start point when first ruptures of fuel rods occur.
2. Time moment $t = 580.000$ s is the point when first modelling inaccuracies occur and ex-vessel degradation processes progress. ICARE module is not appropriate for modelling severe accident phenomena at appropriate accuracy after this time moment.

REFERENCES

1. COLLINS T.E. and HUBBARD G. "Technical study of spent fuel pool accident risk at decommissioning nuclear power plants," Tech. Rep. NUREG-1738, NRC, Washington, DC, USA, 2001.
2. Electric Power Research Institute, Vol. 2: The Physics of Accident Progression, Final Report, California, USA, October 2012.
3. YANG R. and RAHN F. "Fukushima Technical Evaluation," Final Report, EPRI, California, USA, February 2013.
4. KALIATKA A., OGNERUBOV V., VAISNORAS M., USPURAS E., TRAMBAUE K. "Analysis of Beyond Design Basis Accidents in Spent Fuel Pools of the Ignalina NPP", Proceedings of ICAPP '08 Anaheim, CA USA, June 8–12, 2008.
5. PENKOV V. "System for storing and handling of spent nuclear fuel", Safety analysis report for Ignalina NPP unit 2, system for storing and handling of spent nuclear fuel safety analysis report for inpp unit 2, chap. 16, sect. 16.5, p. 6, 2002.
6. J. van DORSSELAERE, SEROPIAN C., CHATELARD P. et al., "The ASTEC integral code for severe accident simulation," Nuclear Technology, vol. 165, No. 3, p. 293–307, 2009.